NEXT GENERATION BULK HETEROJUNCTION ORGANIC PHOTOVOLTAIC AND LIGHT EMITTING DIODE SYSTEMS OF NOVEL POLYCYCLIC AROMATIC HYDROCARBON, POLYFLUORENES AND POLYTHIOPHENES

SURU VIVIAN JOHN

BSc Honours Industrial Chemistry, University of Ado Ekiti; MSc Chemistry (*Cum Laude*), University of Johannesburg

A thesis submitted in fulfilment of the requirements for the degree of

PHILOSOPHIAE DOCTOR

In the

Department of Chemistry
Faculty of Science
University of the Western Cape, South Africa

Supervisor: Professor Emmanuel I. Iwuoha
**Co-supervisor: Professor Daniel Egbe**

January 2017

ABSTRACT

In these times of diminishing reserve of fossil fuel, the development of novel "green or renewable" technologies to meet the increasing worldwide demand for energy is of great importance. The sun is the largest carbon free source of energy and an infinite source of renewable energy. However, except for the expensive inorganic crystalline silicon photovoltaic cells, this source of energy has not been utilized. The field of organic photovoltaic cell has made impressive progress in the last few years with the tremendous efforts of researchers working tirelessly to develop organic materials for solar energy conversion. Organic conjugated materials have the advantage of low cost, light weight, process-ability and good flexibility over inorganic materials. They have attracted wide academic and industrial interest due to their promise as semiconductors for photovoltaic applications. Design of advanced organic conjugated materials with the ability to absorb light from the sun and convert it into useful and storable form has and still is one of the most important goals of researchers in the field of renewable energy. This work describes a number of novel exciting and promising materials based on polycyclic aromatic compounds (PACs) for organic photovoltaic cells and organic light emitting diodes.
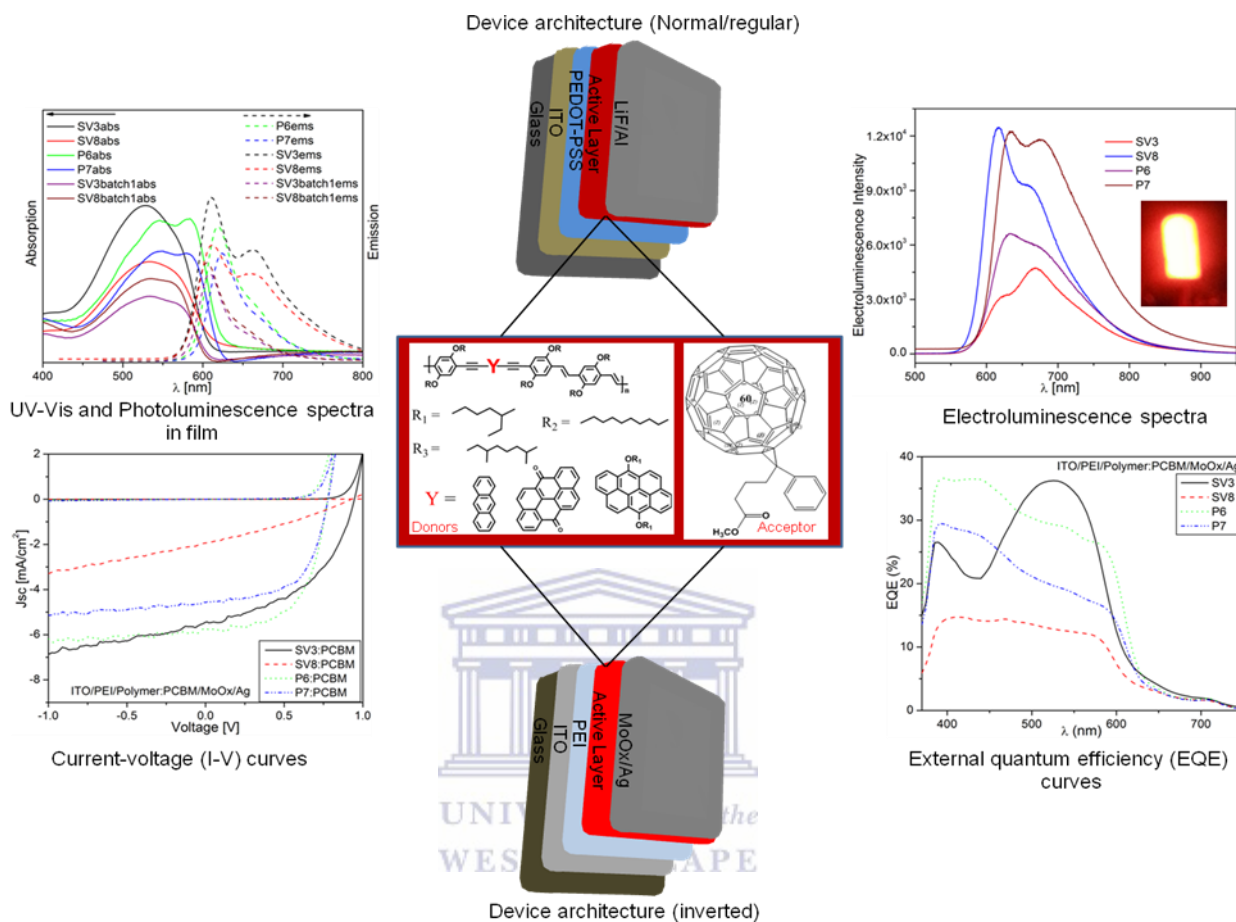
PACs are a unique class of organic compounds consisting of fused aromatic rings and planar geometries. They have the ability to stack in well-organized arrays and they exhibit good charge-transport properties in thin films while also absorbing light over the visible region of the electromagnetic spectrum. PACs, including anthracene, anthanthrone and anthanthrene were individually employed for homo-polymer synthesis via the poly(arylene ethynylene)-*alt*-poly(arylene vinylene)s (PAE-PAV) backbone. The possibilities of applications of polycyclic aromatic compounds based on anthanthrone and anthanthrene as building blocks

i

for polymer synthesis via the PAE-PAV backbone are unveiled. The influence of the type, nature and number of attached alkyloxy side chain on the photo-physical and subsequent photovoltaic properties of the homo-polymers was investigated. Un-optimized photovoltaic efficiency of over 2% was obtained for some of the anthracene homo-polymers with a maximum of 2.62%. Anthanthrene homo-polymer exhibited a short circuit current (J_{sc}) of 2.9 mV/cm^2, open-circuit voltage of (V_{oc}) of 0.76 V corresponding to efficiency of 1.17%. Solubility problems associated with anthanthrone and anthanthrene in the homo-polymers was further addressed by the incorporation of anthracene into the anthanthrone and anthanthrene polymer backbones respectively to form novel co-polymers with PAE-PAV backbone structure and varying side chains. Photo-physical and photovoltaic properties of these novel co-polymers were influenced by the ratio of anthracene component present and the type or nature of the grafted alkyloxy side chain. The observed photovoltaic parameters for anthanthrene based homo-polymer was further improved to J_{sc} (4.00 mA/cm^2), V_{oc} (0.92 V) and efficiency of 1.7% by the co-polymerization.
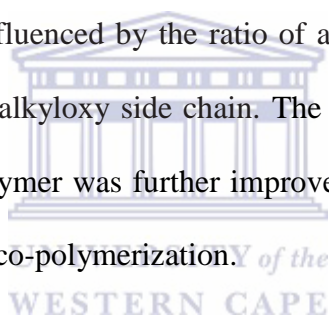
In the course of this work, fullerene (3-(benzo[b]thiophene-3yl)-5-fulleropyrrolidinepyridine) and non-fullerene (Cobalt (II) salicylaldimine metallodendrimer) based materials were also synthesized and their potential as acceptor materials for photovoltaic applications investigated. Their properties were compared with that of traditional fullerene acceptor ([6,6]-phenyl C$_{61}$ butyric acid methyl ester (PCBM)). They combine a strong absorption over a broad range of the electromagnetic spectrum with good electrical characteristics and interesting air stability. Their stability gives room for easy handling, room temperature process-ability and long shelf life. The novel conjugated polymers and acceptors synthesized and investigated in this work are promising donor and acceptor materials for the advancement of the photovoltaic energy research.

ii

GRAPHICAL ABSTRACT

Device architecture (Normal/regular)

UV-Vis and Photoluminescence spectra in film

Current-voltage (I-V) curves

Electroluminescence spectra

External quantum efficiency (EQE) curves

Device architecture (inverted)

Graphical Abstract: Poly(arylene ethynylene)-*alt*-poly(arylene vinylene)s (PAE-PAV) based polymers with varying side chains employed as donors, their photo-physical (UV-Vis and PL) and photovoltaic (I-V curves and EQE) properties, types of device architectures (normal and inverted) employed for the photovoltaic study, and electroluminescence behavior of the polymers.

KEYWORDS

Absorption

Acceptor

Current-voltage curves

Donor

Efficiency

Electroluminescence

Emission

External quantum efficiency

Fullerenes

Light emitting diodes

Photoluminescence

Photovoltaic cells

Polycyclic aromatic compounds

Renewable energy

v

LIST OF ABBREVIATIONS

AFM	Atomic force microscopy
BHJ OPV	Bulk heterojunction organic photovoltaic cells
BHJ OSC	Bulk heterojunction organic solar cells
BTFP	3-(Benzo[b]thiophene-3yl)-5-fulleropyrrolidinepyridine
BTPA	5-(Benzo[b]thiophene-3-yl)pyridinealdehyde
$CDCl_3$	Deuterated chloroform
Co-PPI	Cobalt (II) salicylaldimine metallodendrimer
CV	Cyclic voltammetry
D-A	Donor-acceptor
DMSO-d6	Deuterated dimethylsulfoxide
DP	Degree of polymerization
E_g	Band gap
EIS	Electrochemical impedance spectroscopy
EQE	Equivalent quantum efficiency
F8BT	poly[(9,9-di-*n*-octylfluorenyl-2,7-diyl)-*alt*-(benzo[2,1,3]thiadiazol-4,8-diyl)]
FF	Fill factor
F8T2	poly[(9,9-dioctylfluorenyl-2,7-diyl)-*co*-bithiophene]
FTIR	Fourier transform infrared spectroscopy
FWHM	Full width at half maximum
GPC	Gel permeation chromatography
HOMO	Highest occupied molecular orbital
HR-SEM	High resolution scanning electron microscopy

vi

ICT	Intermolecular charge transfer
I-V	Current-voltage
J_{sc}	Short circuit current
LUMO	Lowest unoccupied molecular orbital
MDMO-PPV	Poly((2-methoxy-5-(3,7-dimethyloctyloxy)-*p*-phenylene) vinylene
MS	Mass spectroscopy
NMR	Nuclear magnetic resonance spectroscopy
OPV	Organic photovoltaic cell
OSC	Organic solar cell
PA	Poly(arylene)
PAC	Polycyclic aromatic compound
PAE-PAV	Poly(arylene ethynylene)-alt-poly(arylene vinylene)
PAV	Poly(arylene vinylene)
PCBM	[6,6]-phenyl-C61-butyric acid methyl ester
PDI	Poly dispersity index
PEDOT-PSS	poly(3,4-ethylenedioxythiophene)-poly(styrenesulfonate)
PEI	Polyethylene imine
PFT	Poly(9,9-n-dihexyl-2,7-fluorenylenevinylene-alt-2,5-thienylenevinylene
P3HT	Poly(3-hexylthiophene-2,5-diyl)
PL	Photoluminescence spectroscopy
PPE	Poly(*p*-phenylene ethynylenes)
PV	Photovoltaics
SEC	Sixe exclusion chromatography
TBAPF$_6$	Tetrabutylammonium hexafluorophosphate
TGA	Thermo-gravimetric analysis

TLC   Thin layer chromatography

UV-Vis   Ultraviolet visible spectroscopy

VEH   Valence effective Halmitonian theorem

Vis-NIR   Visible near infra red

V_{oc} Open circuit voltage

DECLARATION

I declare that "**Next generation bulk heterojunction organic photovoltaic and light emitting diode systems of novel polycyclic aromatic hydrocarbon, polyfluorenes and polythiophenes**" is my own work, that it has not been submitted before for any degree or examination in any other university, and that all the sources I have used or quoted have been indicated and acknowledged as complete references.

Signature -----------------------

Suru Vivian John   **Month: January**

Year: 2017

UNIVERSITY *of the*
WESTERN CAPE

ix

DEDICATION

I dedicate this thesis to

My parents

Sunday Andrew John

Mary John

And

My late brother

Paul Abodunde John

UNIVERSITY *of the*
WESTERN CAPE

x

ACKNOWLEDGEMENTS

Unreserved thanks to my maker who formed me for a purpose and has been personally supervising my life to see that His purpose for my life is perfectly fulfilled. I thank my Lord Jesus for thus far He has led me and for giving me the strength and wisdom through the Holy Spirit to bring this work to a successful completion.

My Supervisors: - I am grateful to my supervisors Professor Emmanuel Iwuoha and Professor Daniel Egbe for their academic guidance, very helpful discussions, suggestions and kindness. Special thanks to my mentor, role model, father and supervisor, Professor Emmanuel Iwuoha. Sir, you combine all the quality any child will ever need in a father, any woman will need in a spouse, any student will need in a supervisor and any mentee will need in a mentor. You made my PhD years memorably wonderful by being not just a supervisor but a father. Thank you sir for playing such a profound role in my life, I am grateful beyond description. To Professor Daniel Egbe, thank you sir for the huge role you played in making my two visits to LIOS a success and for making it possible for me to obtain the ANSOLE scholarship for my first LIOS visit.

Family: - I thank my parents, siblings and entire members of the John's family. Thank you for believing so much in me. You guys are my strength. I love you all. To my late brother, Paul Abodunde John, who passed away in his prime and at the peak of my PhD, I miss your constant checks, love and care. The news of your sudden death came hitting like a tornado. That night, June 26th, 2015 (two days to my birthday) remains the longest night of my life. You left without saying goodbye. Your memory remains ever green.

To my in-law Engr. Chukwuemeke Agholor Osakwe, thank you for believing so much in me. You are an elder brother to me and not just an in-law. I am blessed to have you in my life.

SensorLab: Special thanks to Dr Chinwe Ikpo and Dr Fanelwa Ajayi for the checks and encouragement. To the entire SensorLab members, thank you for the cordial work relationship and conducive environment to work.

LIOS Group/Lab 205: I appreciate the encouragement and support I received from the entire members of Linz Institute for Organic Solar Cells (LIOS), Johannes Kepler University, Linz, Austria; and Organic Synthesis and Materials Research Group, Chemical Sciences Department (Lab 205), University of Padova, Italy. Special thanks to Professor Niyazi Serder Sariciftci and Professor Michele Maggini; for the opportunity given me to carry out part of my research work in their respective laboratories. Special thanks also to Patrick Denk for training/schooling me on solar cell device fabrication and for the very useful discussions at LIOS. To Simone Silvestrini, Christian C. De Filippo, Christoph Ulbricht and Herwig Heilbrunner, thank you for very helpful discussions.

Spiritual Family: Pastor Gbenga Oduniyi and Pastor Kemi Oduniyi, thank you for your spiritual guidance and support. Brother Happy Owoloko, Bro Ados, Bro Ekene, Sister Ebere, Sister Kadriye, Bro Dele (all of King of Glory Parish, Linz, Austria) and Bro Tobi (Maranatha Parish, Vienna) thank you all for your support. To Bridget Roman and family, thank you for your spiritual guidance, your interest in my progress, constant checks, support and encouragement; even after leaving South Africa for Bahrain, you have not stopped caring. I am most grateful.

Friends: – My gratitude also goes out to my friends Inyang Edet, Anthony Lawani, Nomaxabiso Tta, Agnes Musa, Dr Tijani Jimoh, Alechine Emmanuel Ameh, Chris Ademola Aluko, Daniel Adeoluwa Seun Adeniyi and Anthony Okotie. You have all proven to be more than ordinary friends. Special thanks to Alechine Emmanuel Ameh for all the support and very useful advice. You rock.

I owe a debt of gratitude to Professor Omotayo Ademola Arotiba, my daddy and mentors Professor Olorunfemi Olaofe and Dr Richard Akinyeye for giving me the lead to my academic career in South Africa. I am forever grateful.

Many thanks to Chemistry Department staff (both academic and technical) for your support in one way or the other in making this research a success. I specially thank Wilmer Jackson for always being there and willing to help even when it is not convenient.

Finally, I will like to thank the National Research Foundation (NRF) of South Africa for the award of Doctoral Scholarship through the South African Research Chair Initiative (SARChI) for NanoElectrochemistry and Sensor Technology of Prof E. Iwuoha. I am grateful for the award of a Coimbra Group of Universities Scholarship for Young African Researchers in 2014 for a research exchange visit to the University of Padova in Italy. Also I am very thankful to the International Centre for Theoretical Physics (ICTP) for the award of an Africa-North Exchange (ANEX) Fellowship through the African Network for Solar Energy (ANSOLE) for a research visit to LIOS in 2015.

LIST OF PUBLICATIONS

1. **Suru Vivian John**, Christian C. De Filippo, Simone Silvestrini, Michele Maggini, Emmanuel Iwuoha. Novel 5-(benzo[b]thiophene-3-yl)pyridinealdehyde (BTPA) functionalization framework for modulating fullerene electronics, *ChemistryOpen Commun.* (**2017**) DOI: 10.1002/open.201600174.

2. **Suru Vivian John**, Emmanuel Iwuoha. Electrochromic Polymers for Solar Cells: In Springer Handbook of Functional Polymers, *Springer books*, Mohammad Jafar Mazumder, Heather Sheardown, Toshihiro Akaike, Amir Al-Ahmed (Ed.), (**2017**).

3. **Suru Vivian John**, Noluthando Mayedwa, Chinwe Ikpo, Lerato Yvonne Molefe, Miranda Mengwi Ndipingwi, Nomxolisi Ruth Dywili, Juanita Van Wyk, Selwyn F. Mapolie, Priscilla Baker, Emmanuel Iwuoha. Photoluminescence quenching of poly (octylfluorenylbenzothiadiazole) luminophore by n-type cobalt(II) salicylaldimine metallodendrimer, *Synth. Met.* 220 (**2016**) 114–122.

4. N. Dywili, N. Njomo, C.O. Ikpo, A.L.D. Yonkeu, **S.V. John**, N.W. Hlongwa, N. Raleie and E.I. Iwuoha. Anilino-Functionalized Graphene Oxide Intercalated with Pt Metal Nanoparticles for Application as Supercapacitor Electrode Material, *J. Nano Res.* 44 (**2016**) 79–89.

5. Hlamulo R. Makelane, **Suru V. John**, Tesfaye T. Waryo, Abd Baleg, Noluthando Mayedwa,Candice Rassie, Lindsay Wilson, Priscilla Baker, Emmanuel I. Iwuoha. AC voltammetric transductions and sensor application of a novel dendritic poly(propylene

thiophenoimine)-co-poly(3-hexylthiophene) star co-polymer, *Sensors and Actuators B* 227 (**2016**) 320–327.

6.   Oluwakemi Tovide, Nazeem Jahed, Christopher E. Sunday, Keagan Pokpas,Rachel F. Ajayi, Hlamulo R. Makelane, Kerileng M. Molapo, **Suru V. John**, Priscilla G. Baker, Emmanuel I. Iwuoha. Electro-oxidation of anthracene on polyanilino-graphenecomposite electrode, *Sensors and Actuators* B 205 (**2014**) 184–192.

7.   **Suru Vivian John**, Christoph Ulbricht, Jean-Benoit Giguère, Antoine Lafleur Lambert, Jean-Francois Morin, Emmanuel Iwuoha, Daniel Mbi Egbe, Synthesis, characterization and photovoltaic investigation of poly(arylene ethynylene)-*alt*-poly(arylene vinylene)s polymers based on anthanthrone and its derivatives. Submitted to *J. Mater. Chem. A*.

8.   **Suru Vivian John**, Emmanuel I. Iwuoha. Luminescence quenching characteristics of fullerenyl systems – A Review. Prepared for *Carbon*.

9.   **Suru Vivian John**, Emmanuel I. Iwuoha. Amplification of the spectra window of polycyclic-aromatic compounds based class of donor polymers for organic photovoltaic cells – A Review. Prepared for *J. Mater. Chem. A*.

10.   **Suru Vivian John**, Christoph Ulbricht, Patrick Denk, Herwig Heilbrunner, Emmanuel Iwuoha, Daniel Mbi Egbe. Photovoltaic Cell with Remarkable Fill Factor and High Open Circuit Voltage by Side Chain Modulation of Anthracene Containing Polymeric Materials. Prepared for *Chem. Mater.*

11. **Suru Vivian John**, Patrick Denk, Christoph Ulbricht, Emmanuel Iwuoha, Daniel Ayuk Mbi Egbe. Side chain engineering of anthracene-based polymers: Applications in photovoltaics. Prepared for *Chem. Mater.*

12. **Suru Vivian John**, Patrick Denk, Christoph Ulbricht, Jean-Benoit Giguère, Antoine Lafleur Lambert, Jean-Francois Morin, Emmanuel Iwuoha, Daniel Ayuk Mbi Egbe. Enhancing the properties of poly(arylene ethynylene)-*alt*-poly(arylene vinylene)s (PAE-PAV) polymers based on anthanthrone and its derivatives by backbone modification. Prepared for *J. Mater. Chem. A*.

UNIVERSITY *of the*

WESTERN CAPE

CONFERENCES AND WORKSHOPS

<u>Conferences</u>

1. Intersolar and ees Europe, Munich, Germany, June, **2016**

2. **Suru Vivian John**, Christoph Ulbricht, Samuel Inack Ngi, Emmanuel Iwuoha, Daniel Mbi Egbe. Synthesis of anthanthrene-containing PAE-PAVs for opto-electronic applications. 5[th] Anniversary of ANSOLE (2011-2016: Int'l Conference on Renewable Energy (INCORE), February, Sharm El-Sheikh, Egypt, **2016**.

3. **Suru Vivian John**, Priscilia Baker, Emmanuel Iwuoha. Functionalization of Fullerene C_{60} with Novel 5-(Benzo[b]thiophene-3-yl)pyridinealdehyde Via the 1, 3-dipolar cycloaddition chemistry and the investigation of the photophysical and electrochemical properties. 3[rd] Intl. Symposium on Electrochemistry: Materials, Analytical and Physical Electrochemistry Today, Cape Town, South Africa, May **2015**.

4. **Suru Vivian John**, Christian Corrado De Filippo, Simone Silvestrini, Michele Maggini, Priscilla Baker, Emmanuel Iwuoha. Electrochemistry and photoluminescence of Novel 3-(Benzo[b]thiophene-3yl)-5-fulleropyrrolidinepyridine. I[st] Int'l Conference for Solar Energy (INCOSOLE), Algeria, May **2015**.

xvii

<u>Workshops</u>

1.   Youngs Forum on Supramolecular and Materials Chemistry, Padova, Italy, November, **2014**.

2.   The Abdus Salam International Centre for Theoretical Physics (ICTP) Regional Workshop on Materials Science for Solar Energy Conversion, Cape Town, South Africa, November, **2013**.

UNIVERSITY *of the*
WESTERN CAPE

TABLE OF CONTENT

LIST OF FIGURES

xxxiii

xxxv

xxxvi

LIST OF TABLES

xxxviii

xxxix

Then the LORD answered me and said, 'Record the vision and inscribe it on

tablets that the one who reads it may run. For the vision is yet

for the appointed time; it hastens toward the goal and

it will not fail. Though it tarries, wait for

it; for it will certainly come,

it will not delay

Habakkuk 2:2-3

Not slothful in business; fervent in spirit; serving the Lord

Romans 12:11

Vision not pursued is Vision Lost. Vision gives pain a purpose

xl

CHAPTER ONE

INTRODUCTION - The Need for Renewable Energy

1   Background

Energy is one of the fundamental needs of man and it is a significant factor in evaluating the standard of living/economic development of any country. Energy speeds up economic growth and lack of sustainable energy hinders development by limiting the potentials of meeting basic domestic needs, needs in agriculture, education, health care, transport services, manufacturing or trading enterprises and in mining, as well as real estate development and telecommunication [1]. Civilization has been achieved through the efficient and extensive use of energy to enhance human capabilities and skills. For continued economic growth and human development, energy is indispensible. In earlier times, all our energy needs relied on wood, and shortly after, deforestation became a regular occurrence with our planet at risk [2]. This challenge brought about the discovery of coal (first fuel of the industrial revolution), a presumed efficient alternative to wood; and thereafter, petroleum was also discovered [2]. With this discovery, it was assumed our energy challenge had been resolved forever. However, not long after that, we realized that as we mined and drilled, the quantity of extractable coal and oil kept on decreasing without replacement and gradually leading to demand surpassing availability. It was also observed that as energy is being generated from these sources, the environment gradually became unfriendly; making it clear that there is a limit to how much these sources of energy can be utilized.

1

Energy can now be gotten from a number of sources like petroleum, coal, biomass, geothermal, natural gas, propane, hydrothermal, solar, uranium, and wind. Energy from these sources can be used to generate electricity, heat up our homes, move our cars and manufacture a number of products. These sources of energy can further be classified into two forms; **renewable** and **non-renewable**. Sources that are unlimited in supply; exist in infinite amounts and can be replenished within a short period of time are termed renewable energy sources. Examples are biomass, geothermal, hydrothermal, wind and solar. It is the energy generated from natural resources that can be reproduced while non-renewable energy (petroleum, coal, natural gas, propane and uranium) is energy generated from limited sources and cannot be replenished. Unfortunately, world energy consumption relies heavily on non-renewable energy sources [3]. Over 85% of world energy consumption is from non-renewable energy sources. Global demand for energy increases as world human population grows. Increase in world population, improvement in the quality of life and industrialization of developing countries daily increases the consumption of fossil fuels leading to a diminishing reserve. Over one fourth of the global population especially the rural dwellers are faced with energy crisis as the non-renewable traditional grid from urban to rural areas is often time, not economically viable [4]. They are characterized by price volatility, operation safety, supply security and geopolitical sensitivity. The quantity of fossil fuels is not equivalent from country to country; therefore, countries with huge reserves can influence world economy. The decisions of these countries regarding price and level of production have far reaching effect on global energy consumption and production and can result in social tension. In addition to these limitations is the irreparable harm that this form of energy has done to our environment. Non-renewable sources of energy are faced with a number of challenges/concerns like water pollution, radioactive waste disposal and emission of substances like oxides of sulfur (SO_x), oxides of nitrogen (NO_x), CH_4, CFCs, Ozone and CO_2

2

contributing to acid deposition and global climate change [5-7]. The volatility of oil prices and our dependence on oil continues to grow. Our forest, wildlife, shorelines and ocean beds have been destroyed. These concerns, especially the global environmental consequences are giving a warning that sustainable development cannot be achieved from non-renewable energy sources [8].

Energy is the centre point in achieving the goal of sustainable development. Sustainable energy development promotes harmony between environmental protection and economic development. There exist a strong relationship between economic development and energy availability/sustainability; and this has been shown in the incredible economic growth in the heavily populated China when they harnessed the opportunity of sustainable energy [9]. The availability of modern energy such as electricity and liquid fuels boosted global economic development in the 20th century. However, most part of the developing world lack access to this modern energy and still relies on out-of-date energy sources like fuel wood. The desire for renewable sustainable energy is on the rise both in the developed and developing world. No one will argue with the fact that finding alternative energy source is one of our century's main goals. There is a growing need for a viable alternative energy source that is sustainable, environmentally friendly and can provide the growing population with a high standard of living [10]. A transition from fossil fuels (non-renewable energy source) to the infinite renewable energy source is inevitable.

1.1 Solar Energy Technology

The direct harvest of energy from sunlight is a major way of addressing the growing global energy challenge with a renewable resource. The entire energy required globally for a year

3

can be provided by the sun in roughly an hour. This therefore means that the transition from
from carbon based energy to solar energy is possible by tapping into a tiny proportion of this
massive solar potential. Solar technology (**Figure 1.1**), an important source of global
renewable/sustainable energy today is accessible in the form of photovoltaics (PV) and
concentrated solar power (CSP) with varying mode of design, operation and performance.
These two technologies are highly contested among industry experts and scholars on their
viability. Photovoltaic is that form of solar energy in which sunlight is directly converted into
electricity. They use solar cells to directly convert solar irradiation into electricity by
exploiting the photovoltaic effect exhibited by semiconductors while concentrated solar
power use heat provided by solar irradiation concentrated on a small area to generate
electricity [11].
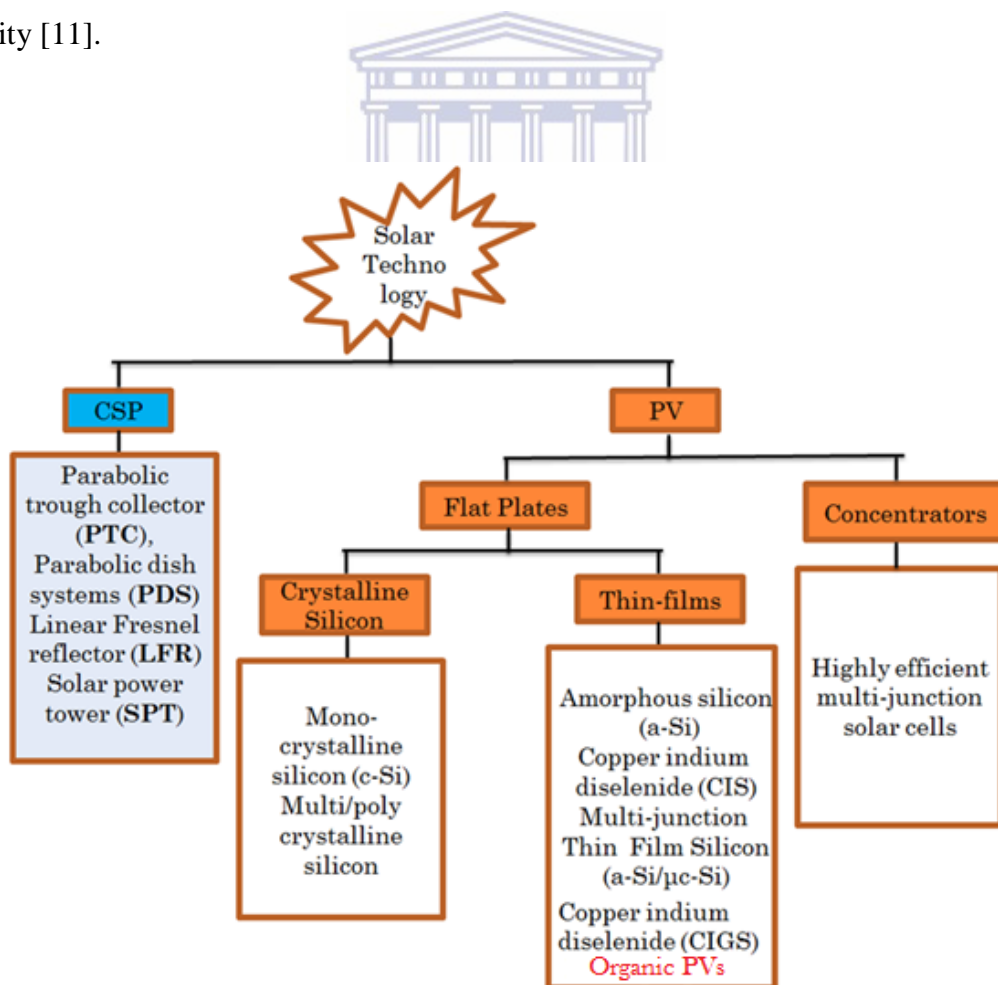
Figure 1.1: Schematic of the forms of solar energy technology.

4

Concentrated solar power (CSP) is designed based on a simple scheme – solar irradiation is captured and redirected by large tracking mirrored collectors placed around a receiver (solar boiler) which converts the captured solar irradiation into useful heat that drives a turbine to generate electricity. Although the CSP technology is faced with so many challenges, it has witnessed a growth rate of about 37% in the last few years [12].

Photovoltaics (PV) on the other hand are the fastest growing renewable solar energy technology. The CSP industry has faced increasing competition from PV in recent years as PV manufacturing costs are decreasing rapidly due to mass manufacturing and associated learning curves [13]. A prominent example of this competition is the conversion of the first 500 MW of 1000 MW Blythe solar power project of solar energy developer, Solar Trust of America (STA) from CSP to PV technology. They opted for PV technology instead of CSP technology citing PV's modularity and bankability as key reasons for the change in strategy [14]. It is therefore not surprising when Shell, the largest producer of oil stated in their recent publication that energy from solar cell may in a period of 50 years from now become the largest energy source with photovoltaics becoming the principal power source. Photovoltaics, therefore, appear to be a promising alternative to non-renewable energy sources. It is the direct conversion of sunlight into electricity/electrical energy. This is achieved by the use of devices made of semiconducting materials which are similar to those used in computer chips. Photovoltaic cells exist as inorganic or organic. Inorganic photovoltaic (IPV) cells are developed from inorganic materials such as crystalline silicon (c-Si), amorphous silicon (a-Si), cadmium telluride (CdTe), copper indium gallium diselenide (CIGS), and group III-V semiconductors like gallium-arsenide (GaAs), gallium indium arsenide (GaInAs), indium arsenide (InAs), indium phosphide (InP) [15-16]; while organic photovoltaic (OPV) cells are made from organic materials like conducting polymeric and (or) non-polymeric materials

[17]. Solar energy based on inorganic photovoltaic cells is gradually loosing attention due to the drawbacks of cost and weight. As the need for sustainable energy increases due to the rising cost of electricity, limited supply of traditional energy and their environmental impact; the research on photovoltaic cells based on organic semiconducting material is attracting more and more attention.

1.2 Problem Statement and Research Motivation

The global energy sources (non-renewable sources) in addition to being expensive and environmentally unfriendly are limited. South Africa for instance is the fourth largest coal exporting country in the world. At present, South Africa has only about 50 years of coal supply left [18] and Eskom (South Africa's electricity public utility), ranked the seventh in the world as an electricity generator is currently battling load shedding. The availability of significant amounts of extractable coal reserves for future use is therefore uncertain. If the energy supply and well being of the South African nation and the international community it provides its coal is to continue and improve, these challenges must to be addressed.

The largest carbon-free energy source is the sun. This source of energy has not been utilized except for the conventional expensive inorganic crystalline silicon (c-Si). The current photovoltaic market is dominated by inorganic c-Si which has achieved power conversion efficiency (PCE) of about 25% [19]. This form of photovoltaic is however becoming less attractive due to its drawbacks of high material cost, high cost of material purification as well as the bulky and rigid nature of the panels [20]. These drawbacks are the major motivation for the development of organic photovoltaic cells.

6

Organic photovoltaics first discovered by Heeger, Shirakawa and MacDiarmid in 1977 [21] have a variety of cheap and easy processing techniques and are light weight [22-26]. They are promising alternatives to crystalline silicon based devices. Due to their high extinction coefficient, a small quantity of material is required to capture incoming photons in photovoltaic cells based on organic semiconductors [22, 27]. By chemical synthesis, the chemical structure of these organic based materials can be fine-tuned and by extension, their optical and electrical properties [22-23, 28-29]. These semiconducting polymer based photovoltaic cells have recently made a number of advances towards commercialization. Progress in the efficiency of lab-scale photovoltaic cell has been made and the efficiency has more than doubled over the past decade [30-32]. As impressive as this progress may seem, they have not met the targeted efficiency required for broad commercialization [33]. Envisioned to be low-cost alternatives to existing c-Si photovoltaic cells, organic photovoltaic (OPVs) cells are yet to deliver their promise of broad commercialization due to persistently low efficiencies [34]. To achieve this efficiency required for broad/mainstream commercial market, new structurally related polymers must be synthesized and studied to help clearly define future rationale. This work seeks to synthesize novel organic semiconducting π-conjugated materials capable of bringing a turnaround to the photovoltaic market.

7

1.3   Aims and Objectives

1.3.1   Aims

The aim of this research work is to synthesize novel donor materials incorporating polycyclic aromatic compounds such as anthanthrone, anthracene and their derivatives; synthesize novel acceptors based on functionalized fullerene as well as investigation of other non-fullerene acceptors (dendritic materials) for the development of organic photovoltaic cells.

1.3.2   Objectives

The objectives of the study are to:

1.   Synthesize novel donors based on anthanthrone, anthanthrene and anthracene containing poly(arylene-ethynylene)-alt-poly(arylene-vinylene)s.

2.   Synthesize novel fullerene derivative by 1,3-dipolar cycloaddition of azomethine ylides to olefins.

3.   Interrogate the morphological, structural, spectroscopic, electrochemical and optical characteristics of the synthesized acceptor and donors.

4.   Understand the function/structure relationship and design organic photovoltaic cells from the synthesized materials.

1.4   The Thesis Statement

Photovoltaic cells based on organic conjugated materials have advantages of inexhaustible supply option over non-renewable sources of energy and pose potential low-cost and light weight advantages over mainstream inorganic based silicon photovoltaic cells. The design of novel acceptor and donors may bring organic photovoltaic cells to the mainstream and bring a turnaround in the energy sector by initiating a principle strategy for sustainable energy development.

1.5   Brief Overview of Chapters

This thesis is divided into ten chapters

➢   Chapter **one:** presents the background, problem statement, motivation, aims and objectives of this research

➢   Chapter **two:** presents a detailed review on amplification of the spectral window of polyaromatic compound-containing donor polymers for organic photovoltaic cell.

➢   Chapter **three:** presents a review on the luminescence quenching characteristics of fullerenyl systems

➢   Chapter **four**: this chapter features the list of materials used, describes the major reaction mechanisms employed for polymer synthesis and functionalization of fullerene, the general experimental procedures, and a detailed methodology of the research

➢   Chapter **five to nine:** discusses the experimental results obtained in the research

➢   Chapter **ten:** gives the general conclusion and recommendation for future work

Chapters two, three and five to nine each consist of a sub-abstract and conclusion.

9

1.6 References

[1]   I. M. Bugaje, "Renewable energy for sustainable development in Africa: a review," *Renewable and Sustainable Energy Rev.,* 10 (**2006**) 603 - 612.

[2]   http://www.scienceclarified.com/scitech/Energy-Alternatives/The-Development-of-Energy.html, (**25-09-2016**)

[3]   http://www.nrel.gov/learning/re_basics.html, (**01-12-2013**)

[4]   Y. S. Mohammed, M. W. Mustafa, N. Bashir and A. S. Mokhtar, "Renewable energy resources for distributed power generation in Nigeria: A review of the potential," *Renewable and Sustainable Energy Rev.,* 22 (**2013**) 257 - 268.

[5]   F. L. Toth and H.-H. Rogner, "Oil and nuclear power: Past, present, and future," *Energy Economics,* 28 (**2016**) 1 - 25.

[6]   N. L. Panwar, S. C. Kaushik and S. Kothari, "Role of renewable energy sources in environmental protection: A review," *Renewable and Sustainable Energy Rev.,* 15 (**2011**) 1513 - 1524.

[7]   R. S. Dhillon and G. von Wuehlisch, "Mitigation of global warming through renewable biomass," *Biomass and Bioenergy,* 48 (**2013**) 75 - 89.

[8]   I. Ushiyama, "Renewable energy strategy in Japan," *Renewable Energy,* 16 (**1999**) 1174 - 1179.

[9]   P. Meisen and N. Cavino, "Rural electrification, human development and the renewable energy potential of China," *China-Global Energy Network Institute (GENI),* (**2007**) 1 - 33.

[10]   "Africa's Renewable Future - The path to sustainable growth," *IRENA Int'l Renewable Energy Agency,* (**2013**)

10

[11] M. Peters, S. T. Schmidt, D. Wiederkehr and M. Schneider, "Shedding light on solar technologies—A techno-economic assessment and its policy implications," *Energy Policy,* 39 (**2011**) 6422 - 6439.

[12] K. Lewandowska, B. Barszcz, A. Graja, S. Y. Nam, Y.-S. Han, T.-D. Kim and K.-S. Lee, "Spectroscopic properties and orientation of molecules in Langmuir–Blodgett layers of selected functionalized fullerenes," *Spectrochim. Acta, Part A,* 118 (**2014**) 204 - 209.

[13] J. H. Peterseim, S. White, A. Tadros and U. Hellwig, "Concentrated solar power hybrid plants, which technologies are best suited for hybridisation?," *Renewable Energy,* 57 (**2013**) 520 - 532.

[14] http://social.csptoday.com/markets/pv-not-csp-sta%E2%80%99s-1gw-blythe-project#sthash.Xog11sVX.dpuf, (**14-11-2013**)

[15] J. Lauth, T. Strupeit, A. Kornowski and H. Weller, "A Transmetalation route for colloidal GaAs nanocrystals and additional III–V semiconductor materials," *Chem. Mater.,* 25 (**2013**) 1377 - 1383.

[16] A. Shahini, "An organic solar cell theoretical model with two concepts of excitonic and bipolar transport," *Asia-Pac. J. Chem. Eng.,* 8 (**2013**) 59 - 68.

[17] B. A. Gregg and M. C. Hanna, "Comparing organic to inorganic photovoltaic cells: Theory, experiment, and simulation," *J. Appl. Phys.,* 93 (**2003**) 3605 - 3614.

[18] http://www.energy.gov.za/files/coal_frame.html, (**11-12-2016**)

[19] H. M. Hlaing, "Integration of nanostructured semiconducting/conducting polymers in organic photovoltaic devices," *Stony Brook University,* (**2012**)

[20] M. Sathish, "Photovoltaics in : An introduction to energy sources," *National Centre for Catalysis Research Department of Chemistry Indian Instutute of Technology, Madras,* (**2006**)

11

[21]   H. Shirakawa, E. J. Louis, A. G. MacDiarmid, C. K. Chiang and A. J. Heeger, "Synthesis of electrically conducting organic polymers: halogen derivatives of polyacetylene, (CH)x," *J. Chem. Soc., Chem. Commun.,* (**1977**) 578 - 580.

[22]   G. Dennler, M. C. Scharber and C. J. Brabec, "Polymer-fullerene bulk-heterojunction solar cells," *Adv. Mater.,* 21 (**2009**) 1323 - 1338.

[23]   B. P. Lyons, N. Clarke and C. Groves, "The relative importance of domain size, domain purity and domain interfaces to the performance of bulk-heterojunction organic photovoltaics," *Energy Environ. Sci.,* 5 (**2012**) 7657 - 7663.

[24]   S. B. Darling and F. You, "The case for organic photovoltaics," *RSC Adv.,* 3 (**2013**) 17633 - 17648.

[25]   M. C. Scharber and N. S. Sariciftci, "Efficiency of bulk-heterojunction organic solar cells," *Prog. Polym. Sci.,* 38 (**2013**) 1929 – 1940.

[26]   K. A. Mazzio and C. K. Luscombe, "The future of organic photovoltaics," *Chem. Soc. Rev.,* 44 (**2014**) 78 - 90.

[27]   H. Hoppe and N. S. Sariciftci, "Organic solar cells: an overview," *J. Mater. Res.,* 19 (**2004**) 1924 - 1945.

[28]   J. D. Servaites, M. A. Ratner and T. J. Marks, "Organic solar cells: A new look at traditional models," *Energy Environ. Sci.,* 4 (**2011**) 4410 - 4422.

[29]   B. Walker, C. Kim and T-Q. Nguyen, "Small molecule solution—Processed bulk heterojunction solar cells," *Chem. Mater.,* 23 (**2011**) 470 - 482.

[30]   Y. Liu, J. Zhao, Z. Li, C. Mu, W. Ma, H. Hu, K. Jiang, H. Lin, H. Ade and H. Yan, "Aggregation and morphology control enables multiple cases of high-efficiency polymer solar cells," *Nat. Commun.,* 5 (**2014**) 1 - 8.

[31]   C.-C. Chen, W.-H. Chang, K. Yoshimura, K. Ohya, J. You, J. Gao, Z. Hong and Y. Yang, "An efficient triple-junction polymer solar cell having a power conversion efficiency exceeding 11%," *Adv. Mater.,* 26 (**2014**) 5670 - 5677.

[32]   Z. He, B. Xiao, F. Liu, H. Wu, Y. Yang, S. Xiao, C. Wang, T. P. Russell and Y. Cao, "Single-junction polymer solar cells with high efficiency and photovoltage," *Nat. Photonics,* 9 (**2015**) 174 - 179.

[33]   S. C. Price, A. C. Stuart and W. You, "Low band gap polymers based on benzo[1,2-b:4,5-b']dithiophene: Rational design of polymers leads to high photovoltaic performance," *Macromolecules,* 43 (**2010**) 4609 – 4612.

[34]   H. Zhou, L. Yang, S. Liu and W. You, "A Tale of current and voltage: Interplay of band gap and energy levels of conjugated polymers in bulk heterojunction solar cells," *Macromolecules,* 43 (**2010**) 10390 - 10396.

UNIVERSITY *of the*

WESTERN CAPE

13
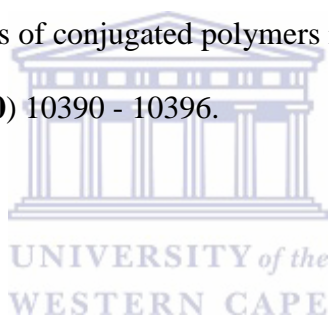
CHAPTER TWO

LITERATURE REVIEW - Amplification of the Spectral Window of Polycyclic-Aromatic Compounds Based Class of Donor Polymers for Organic Photovoltaic Cells

Abstract

Apart from the environmental effects of the limited natural sources of energy (fossil fuels), the drop in the quantity available for use globally with the associated devastating consequences for the global economy is now a concern. There is the fear that our energy resources are beginning to run out as we cannot have growing demands on limited resources without eventually running out of the resource. This concern is getting the world back on its feet as government and researchers are working to make the use of renewable resources a priority. Organic and inorganic materials have been used for the capture of renewable sunlight and conversion into useful energy through the 'photovoltaic effect'. The synthetic chemists have designed and synthesized a variety of conjugated polymers with different architectures and functional moieties to meet the requirements of organic photovoltaic devices. Conjugated polymers have attracted an increasing amount of attention for applications in photovoltaic devices due to their potential advantages over inorganic semiconductors. A number of reports and reviews are available on poly[2-methoxy,5-(2'-ethyl-hexyloxy)-p-phenylene vinylene) (MEH-PPV), poly(2-methoxy-5-(3′,7′-dimethyloctyloxy)-*p*-phenylene vinylene) (MDMO-PPV) and poly(3-hexylthiophene) (P3HT) based semiconducting polymers for photovoltaic applications. This review describes

14

emerging polycyclic aromatic compound based polymers and their spectra amplification for improved photovoltaic applications.

2   Introduction

The diminishing reserve of fossil fuels coupled with its environmental consequences calls for urgent attention. One of the most important ways to deal with the growing global energy needs and environmental concerns is the direct harvest of energy from sunlight via the photovoltaic technology. The practical and effective application of the knowledge of 'photovoltaic effect' in the generation of electricity from sunlight is a promising solution to the growing need for clean, environmentally friendly, abundant, and renewable energy sources. Unfortunately, due to the relatively high cost of silicon based solar cells, only a tiny fraction of the energy used globally comes from sunlight [1]. A promising alternative to silicon based solar cells is organic photovoltaic (OPV) cells. Organic photovoltaic cells based on polymers have emerged as an alternative promising photovoltaic technology. This is due to the potential of cost-effective production of large area of flexible devices using solution-processing techniques, versatility in organic material design, low environmental impact and lightweight platform for the clean conversion of sunlight to electricity [2-14]. Due to their high extinction coefficient, a small amount of material is required to harvest incoming photons in photovoltaic cells based on organic semiconductors [5, 7]. By chemical synthesis, the chemical structure of these organic based materials can be fine-tuned and by extension, their optical and electrical properties [8-9, 15-16]. A number of research works has focused on the design and synthesis of conjugated semiconducting polymers with new molecular structures aimed at harvesting solar irradiation in the visible part of the electromagnetic

15

spectrum and in conjunction with innovative strategies for device design, improved the efficiency of cells. The synergic efforts of researchers from various fields of science have resulted in a rapid improvement in the conversion efficiency [4, 17] which has progressed very recently to slightly above 10% [18-20]. The first polymer-based OPV device is now commercially available [21]. This shows a promise of mass production for solar cells based on OPVs. However, for improved efficiency and broad commercialization, the development of new materials and their integration into efficient device configurations have to be explored. Researchers have unfolded a number of new polymers and small molecules aiming to improve properties such as solubility, light absorption and charge transport of organic semiconductors. This review will focus on polycyclic aromatic compounds as building blocks for donor polymer in OPV cells and the effect or influence of structural deviation on the spectra window of these donor polymers.
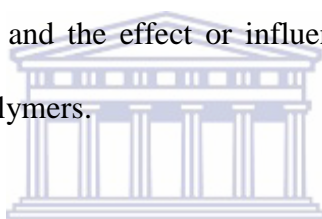
Polycyclic aromatic compounds (PACs) and their derivatives are very useful building blocks for the synthesis of organic semiconducting materials for organic electronic e.g organic light-emitting diodes (OLEDs), organic field-effect transistors (OFETs), and organic photovoltaic (OPV) cell applications [22]. They are a unique class of organic compounds with planar geometries which make them promising for optoelectronic applications. They consist of fused aromatic rings with the ability to stack in well-organized arrays and exhibit good charge-transport properties in thin films while also absorbing light over the visible region of the electromagnetic spectrum [23-29]. Their structural and electronic features such as the effective conjugation length, the overlap between π-orbitals, rigid π-conjugated backbone and the manner in which the rings are fused in these materials determine their optical and electronic properties [30]. In terms of cost and property tailoring, they are usually very cheap and possess properties that enable the introduction of new functional groups to fine-tune their

16

electronic and optical properties. They can easily be functionalized through known reactions via C-C cross couplings. A wide range of the visible region of the electromagnetic spectrum can be accessed by modification of their structural properties. Their low cost and tunable electronic and optical properties over the entire visible region provide them with many advantages for organic electronics applications. Examples of polycyclic aromatic compounds that are emerging as building blocks for donor materials in photovoltaic design are anthanthrone, anthracene (**Figure 2.1**) and their derivatives.
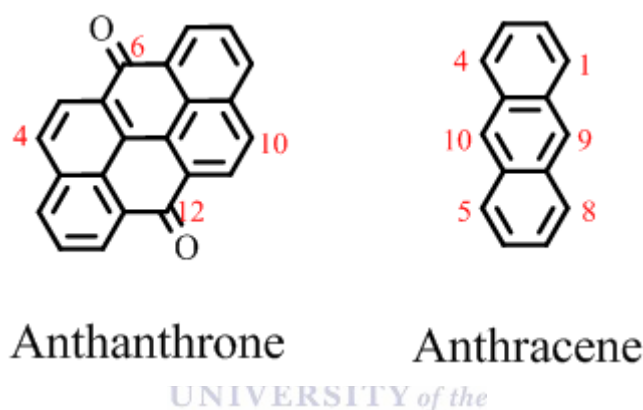
Figure 2.1: Chemical structures of polycyclic aromatic compounds (anthanthrone and anthracene) with labelled C-positions.

2.1 Anthanthrone-Containing Donor Materials

Anthanthrones are polycyclic aromatic compounds with extended conjugation and symmetric structures. They are known compounds which are used as pigments and vat dyes. Their large conjugated planar structure facilitates intermolecular interactions and their extended π-conjugation is believed to be an advantage in photovoltaics since electronic coupling increases with respect to size. They have been rarely studied as building blocks for organic semiconductors. Only very recently, Morin and co-workers synthesized a series of

17

anthanthrone and their derivatives, investigated their optoelectronic properties and photovoltaic performance of a few of them. The group reported small molecule derivatives of commercially available low-cost anthanthrone (4,10-dibromoanthanthrone) for device testing [31-32]. This particular compound possesses two bromine atoms and two ketones with a rigid and extended π-conjugated backbone which provide useful optical properties in the visible range. The presence of the bromine atoms allows the introduction of functional groups and alkyl chains to increase the solubility of the compound or polymer made from it. Electrophilicity of the carbonyl groups can serve as reactive sites for different nucleophiles to modify or tune the optical and electronic properties. The effective conjugation length can also be increased through the carbonyl end by introduction of conjugated moieties. The absorption spectra (**Figure 2.2**) of the anthanthrone derivative (6,12-bis(amino) anthanthrene)-based conjugated molecules were modulated by changing the conjugated moieties linked at the 4 and 10 positions (**Figure 2.3**) [31]. The optoelectronic properties of the derivatives show a strong dependence on the moieties attached to the nitrogen atoms at the 6 and 12 positions. The molecule with the DPP moieties attached show an optical response covering almost the entire visible region.

18
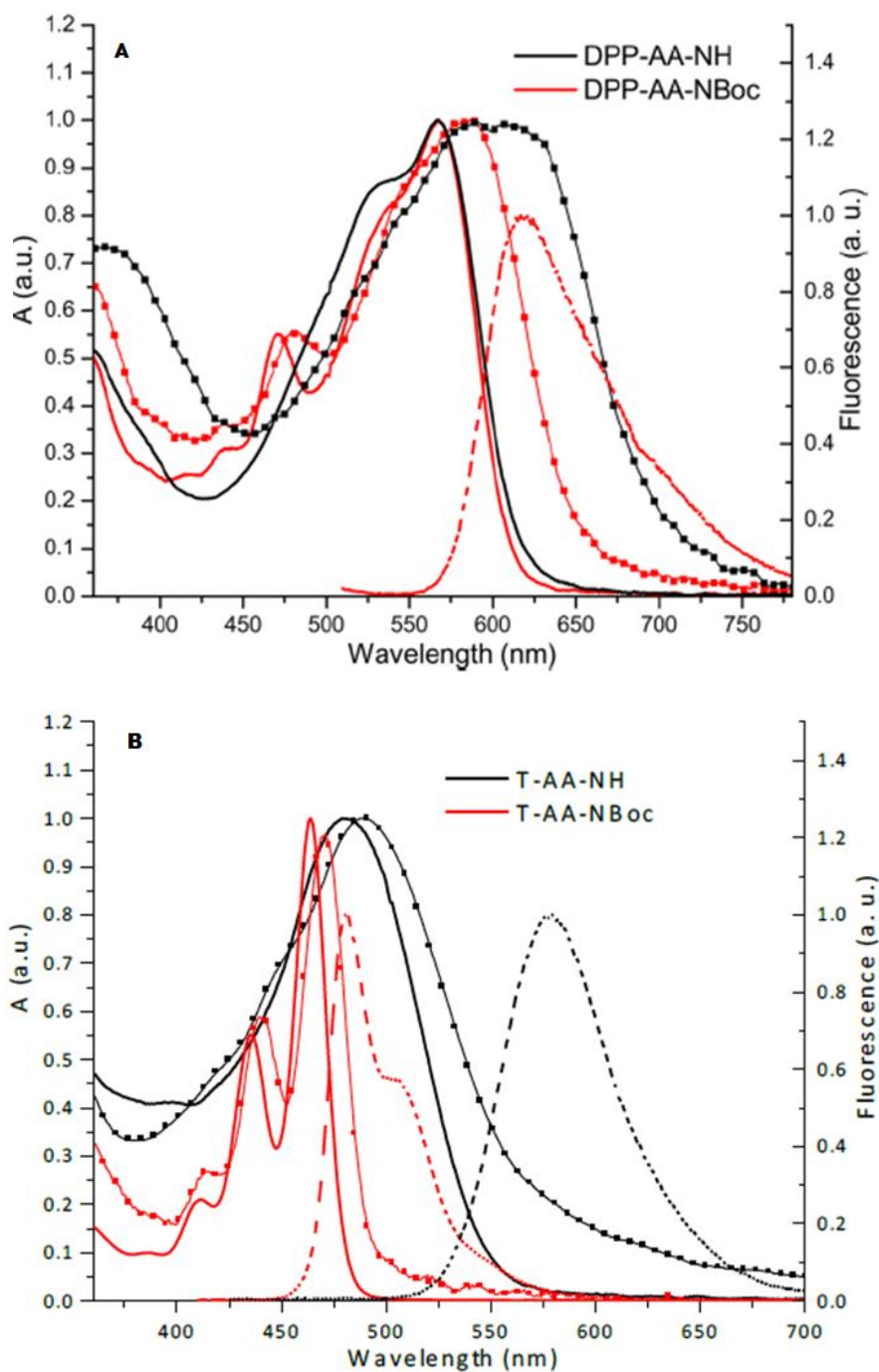
Figure 2.2: UV−Vis spectra (CHCl$_3$ (solid lines); thin films (square symbols)) and fluorescence spectra (CHCl$_3$, dashed lines) of anthanthrone derivatives A) DPP-AA and B) T-AA as shown in Figure 2.3. Reprinted (adapted) with permission from (J.-B. Giguère and J.-F. Morin, Synthesis and Optoelectronic Properties of 6,12-Bis(amino)anthanthrene Derivatives, *J. Org. Chem.,* 78 (2013) 12769 - 12778). Copyright (2013) American Chemical Society.

19
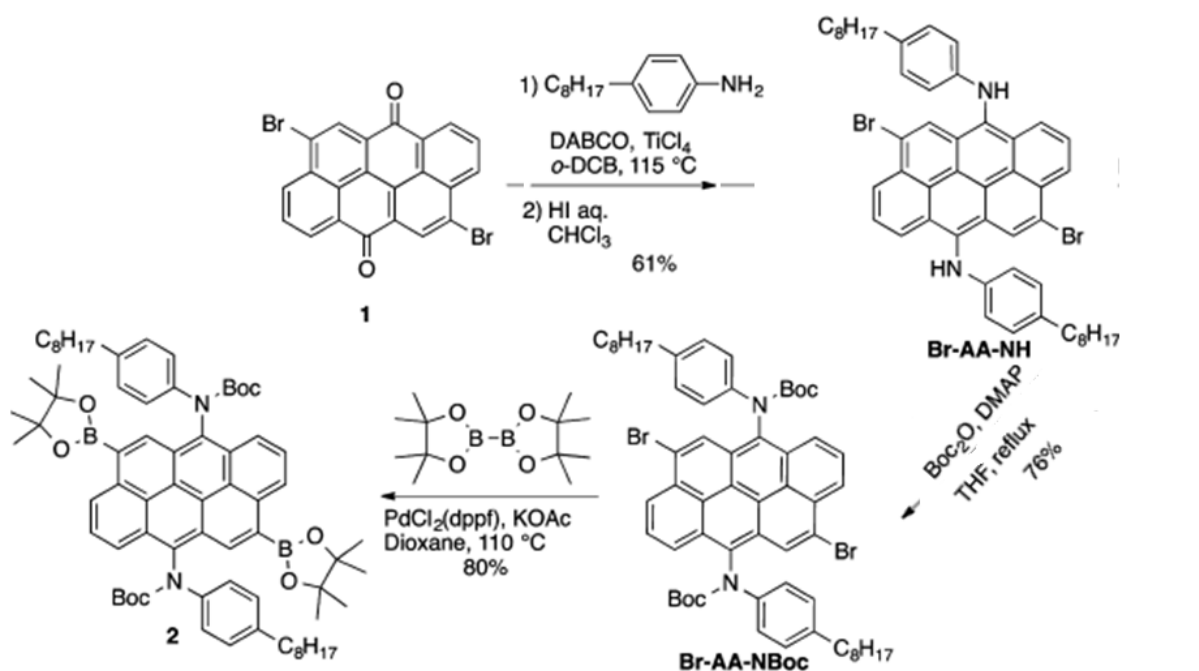
Scheme 1. Imine Condensation and Synthesis of the Starting Building Blocks Br-AA-NBoc and 2
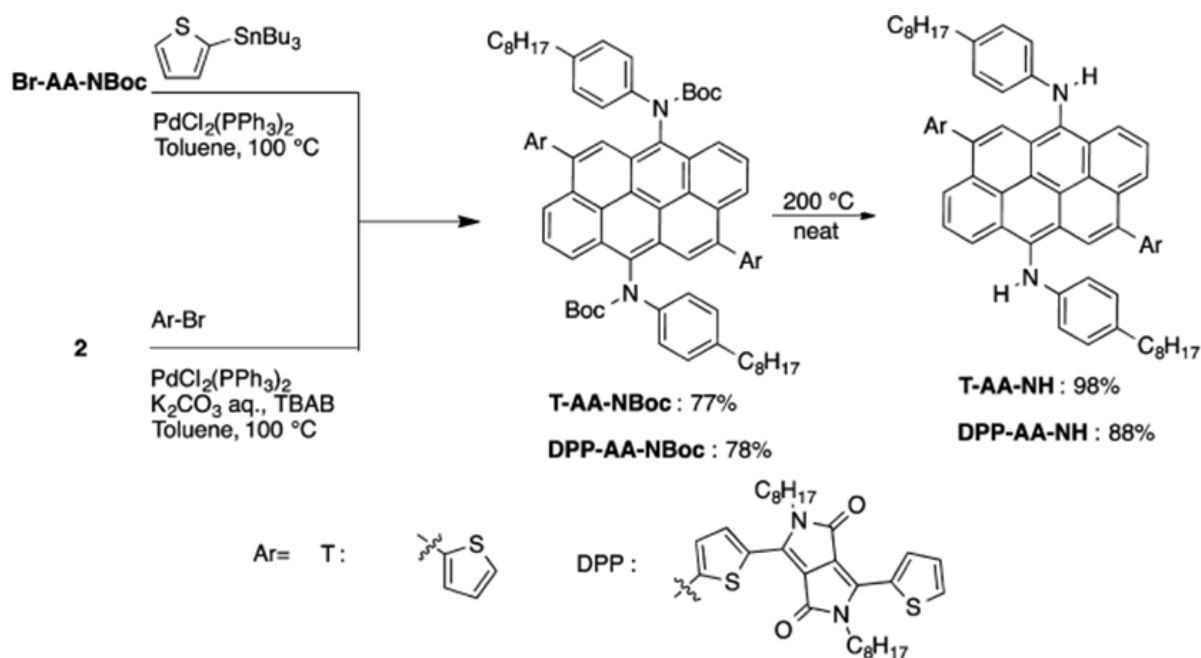
Scheme 2. Stille and Suzuki Couplings of Br-AA-NBoc and 2 with Different Aromatic Moieties and Subsequent N-Boc Thermal Deprotection

Figure 2.3: Anthanthrone modification at the 4,10-position.

Briseno *et al*. [33] reported the unique packing motif and photovoltaic performance of a small molecule based on anthanthrone. The molecule is shown to have good oxidative stability and serve as an electron donor in bulk heterojunction organic photovoltaic (BHJ OPV) cell

20

exhibiting a power conversion efficiency of ~2.0%. Apart from stability and optical tailorability, materials based on anthanthrone have shown interesting charge transport properties [34]. Anthanthrene (anthanthrone derivative) small molecules with different pendant groups as semiconductors for OPV cells have been reported [30]. Charge mobilities were greatly improved with solvent annealing and reached maximum values of 0.078 cm2 V^{-1} s^{-1} and when used as donors in conjunction with PC$_{61}$BM in bulk heterojunction OPV cells, PCE of 2.4% was achieved with good open circuit voltage (V_{oc}) and fill factor (*FF*) of 0.77 V and 59%, respectively. The study showcased the potential of the anthanthrene scaffold as a versatile building block for organic electronics. A number of anthanthrone derivatives have been investigated [30-33, 35-39], but very few have been tested as p-type or donor materials for photovoltaic cell device fabrication.

2.2   Anthracene-Containing Donor Materials

Anthracenes are very appealing as building blocks with high thermal and device stability [40]. The rigid structure can be easily functionalized at its 9,10 position. They possess high fluorescence quantum yield and their emission can be tuned during polymerization by the incorporation of other arylene-building blocks [41]. The good photoconductive behavior, high fluorescence quantum yields in thin films and high absorption coefficients around 100 000 M^{-1} cm^{-1} of anthracene based polymers make them ideal for design of organic electronic devices [42]. Anthracene and its derivatives have been investigated [43-45] and used in light emitting diodes [46] and other thin-layer-based organic electronic devices like transistors [47] and photovoltaic cells [48]. However, relatively little work has been done with this materials in areas of OPV device fabrication. The main limitation is the poor solubility of the early anthracene-containing polymers which leads to processing difficulties in thin-layer

preparation by the spin-coating technique and the high crystallinity of anthracene units which prevents the formation of stable flexible thin films.

Among organic semiconductors, two types of architectures are the most commonly used. They are the poly-arylenes (PAs), *i.e.*, polymers made up of aryl units connected together, and poly-arylene vinylenes (PAVs), *i.e.*, polymers comprising alternating aryl and vinylene units. Introduction of ethynylene unit between arylenes in poly(arylenes) results in poly-arylene ethynylene (PAE). Combination of PAE and PAV has led to a new type of conjugated system, denoted poly(arylene-ethynylene)-alt-poly(arylene-vinylene) (PAE-PAV) (polymers made up of alternating aryl, ethynylene and vinylene units), with outstanding optoelectronic properties [49-51]. In the past few years, research interest has focused on conjugated ethynylene containing polymers, PAEs and PAE-PAV, as a promising class of semiconductors. This is due to the availability of efficient protocols for palladium catalyzed alkynylation reactions and the understanding of their steric and conformational advantages [52]. Compounds of this class have been used as donor materials in photovoltaic cells and V_{oc} up to 0.95 V and 1.05 V have been recorded for polymer-fullerene heterojunction devices [53-55] and polymer-polymer bilayer devices [56-57] respectively. Photovoltaic parameters (short circuit current (J_{sc}) and fill factor (*FF*)) of devices based on these materials are largely dependent on the ethynylene-vinylene bond ratio in conjunction with the type and length of solubilizing alkyoxy side chains [58]. Different donor polymers can be achieved using the PAE-PAV backbone via structural modification by varying the aryl groups. The knowledge of poly(arylene-ethynylene)-alt-poly(arylene-vinylene)s prompted the design of poly(arylene-ethynylene)-alt-poly(arylene-vinylene)s with anthracene based arylene for photovoltaic applications [59]. Anthracene conjugated polymers that have found applications in photovoltaic cells are majorly based on PAE-PAV backbone and are abbreviated AnE-PV.

22

The problems of intractability and infusibility are well taken care of in the PAE-PAV backbone by the attachment of one or more solubilizing side chains (alkyl/alkyloxy) on the aromatic rings. Grafting of solubilizing side chains does not only aid solubility, it significantly impacts their optoelectronic and transport properties, and also enables polymer process-ability into thin films for diverse use.

Photovoltaic properties of conjugated polymers can be improved by the attached side chain and through structural modification of the conjugated polymers leading to tuning of the band gap for improved light absorption [60-67]. For instance, the presence of an electron rich and electron deficient unit within the same polymer back bone shifts the light absorption toward lower energy and results in a significant decrease in the band gap of the copolymer. Several electron deficient and electron rich functional groups have advanced in the past 20 years and they have proven to be the best instruments for the fine tuning of electronic properties of conjugated molecules [24-25, 27].
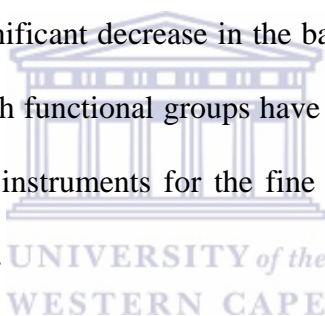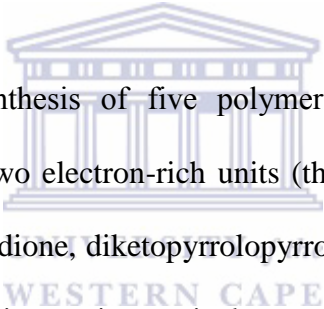
2.3 Donor-Acceptor (D-A) Strategy

The development of low band gap donor polymers with good charge carrier mobilities is of crucial importance for increasing efficiency of photovoltaic cells. Recent research advances on conjugated polymers for photovoltaic devices have therefore focused on creating low band gap polymers with good charge carrier mobilities and other interesting properties necessary for device fabrication by the D-A strategy. A D-A polymer is a polymer which contains both an electron rich and an electron deficient moiety in the polymer backbone. It is the synthesis of alternating donor (D) and acceptor (A) units to tune the energy (highest occupied molecular orbital (HOMO) and lowest unoccupied molecular orbital (LUMO)) levels,

23

thereby reducing the band gap of the resulting D-A copolymers. The energy levels of polymer can be effectively tuned in a D-A polymer and as a result, the band gap. This understanding is borne out of the fact that the HOMO is located in the donor part of the copolymer while the LUMO is located in the acceptor part of the copolymer [68] and band gap is the difference between both energy levels. Therefore a good selection of appropriate donor and acceptor for copolymerization can effectively tune the energy levels. This understanding can be applied in the control of the V_{oc} and the J_{sc} of OPV devices for improved efficiency. In principle, higher V_{oc} values are achieved with donor polymers with deep low-lying HOMO levels [69-70] while higher J_{sc} values are attained with low band gap polymers [71-73]. To maximize the V_{oc} and the J_{sc}, polymers used in BHJ OPVs should maintain a low HOMO energy level as well as a narrow band gap. Therefore suitable alignment of the HOMO and LUMO levels is a necessary requirement for an 'ideal' polymer for BHJ OPV cell. To concurrently maximize V_{oc} and J_{sc}, researchers have resorted to the synthesis of polymers containing both donor and acceptor material in the polymer backbone. Such polymers have been shown to display improved absorption i.e red-shifted absorption spectra towards the visible region in the wavelength range of $500 - 800$ nm where the solar flux is most intense [74-75]. This has proven to be an efficient strategy in tuning the band gap and tailoring the properties of conjugated semiconducting polymers for applications in organic electronics [76].

For OPV cells, important polymers from fluorene class of polymers are alternating polyfluorene copolymer. The homo polyfluorene based polymers for example show weak absorptions in the visible region and as such are not appropriate for electricity conversion. Fluorene based polymers for solar electricity conversions are usually copolymerized with other aromatic building blocks with electron deficient units. This results in a bathochromic

24

shift of the absorption of the resulting polymer. Incorporation of electron-deficient benzothiadiazole unit into fluorene based polymer backbone reduced the LUMO level and thus lowered the band gap [77]. From the report by Andersson and co-workers, broad and extended absorption with further reduction in the band-gap of the copolymer was achieved by replacing the benzothiadiazole with 4,7-dithien- 2-yl-2,1,3-benzothiadiazole (DTBT) as the electron acceptor unit in the polymer backbone [78]. The bathochromic shift can be attributed to the contribution from both the electron deficient benzothiadiazole unit, thiophene and fluorene moieties which give rise to the lowering of the band-gap. Apart from lowering of band gap, these copolymers can also be used to achieve high hole mobility and nanoscale morphology of the active layer blend in BHJ OPV cells [79-80].

Morin's group reported the synthesis of five polymers (series of PTANT) based on anthanthrone unit coupled with two electron-rich units (thiophene and carbazole) and three electron-poor units (thienopyrroledione, diketopyrrolopyrrole, and benzothiadiazole) (**Figure 2.4**) [81]. The polymers display interesting optical properties with light absorption in the visible range in both solid state and chloroform solution. The maximum wavelength in thin film ranged from 545 nm for PTANTBT to 674 nm for PTANTDPP with relatively low optical band gap values, ranging from 1.80 to 1.39 eV. The electronic properties (**Table 2.1**) show notably similar LUMO level values of all polymers irrespective of the co-monomer attached to the anthanthrone unit. The LUMO level values of these polymers range from −3.40 eV for PTANTDPP to −3.45 eV for PTANTTPD; indicating that the LUMO orbitals are mostly localized on the anthanthrone unit. The HOMO energy value of the polymers however vary in response to the attached co-monomer from −4.99 to −5.35 eV for PTANTTPD and PTANTBT, respectively. Further work by same authors on anthanthrone derivative (series of PAA) based polymers incorporating either electron rich or electron-

deficient units revealed that the electronic nature of these co-monomers had little or no influence on the overall electronic properties of the series investigated [82]. The optoelectronic properties of both series investigated were largely dictated by the anthanthrone unit. However, comparing both works from same authors, we see a striking influence of the attachment of two thiophene units on the diketopyrrolopyrrole electron deficient moiety attached to PTANT and PAA series. PTANT in this context is the anthanthrone unit with two thiophene units attached, while PAA is the anthanthrone derivative (anthanthrene) with no ring substituent. The attachment of two thiophene units to diketopyrrolopyrrole to give diketopyrrolopyrrole dithiophene (DPP $(Th)_2$) and subsequent addition to PTANT and PAA series to give PTANTDPP and PAADPP respectively, resulted in promising photovoltaic properties. PTANTDPP and PAADPP both have the lowest band gap (1.39 eV), broader absorption band, highest absorption maximum and onset, highest molecular weight and good yield in their respective series (**Table 2.1**). They both show broad absorption with full width at half maximum (FWHM) values up to 300 nm (**Figure 2.5**), which is very promising for organic photovoltaic cell application.
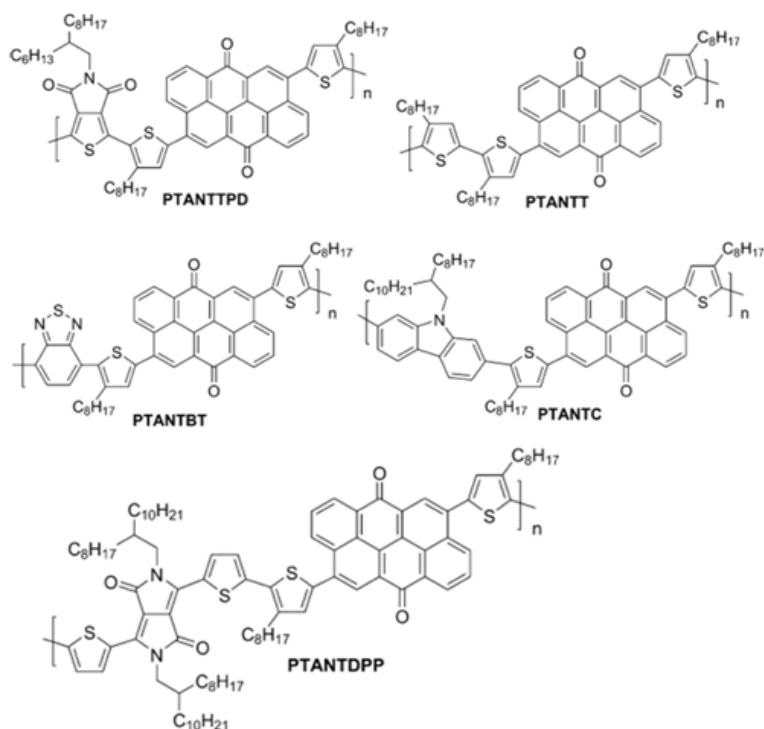
Structures of polymer PTAANT series
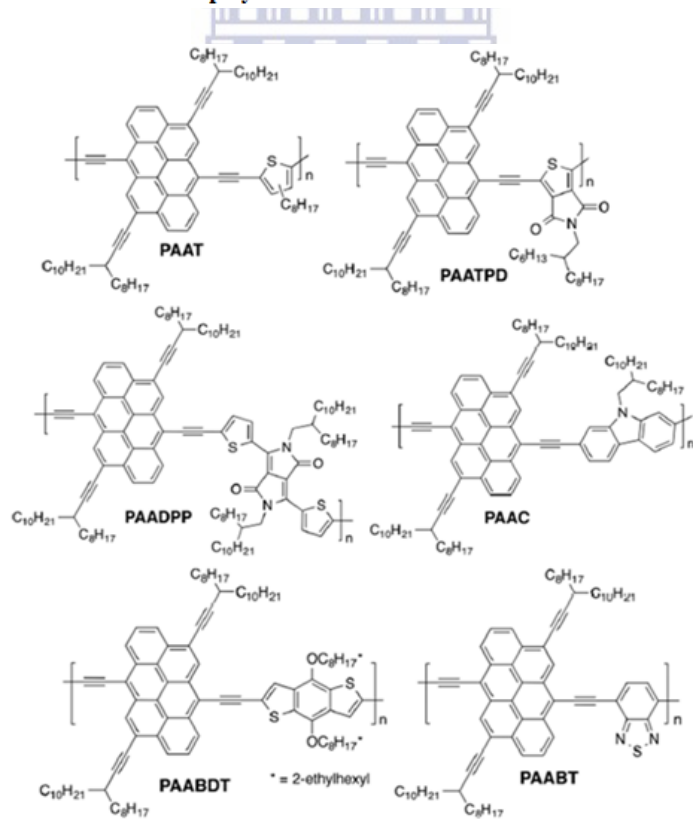
Structures of polymer PAA series

Figure 2.4: Structures of anthanthrone containing polymer.

27

Table 2.1: Optical and electrochemical properties of anthanthrone and its derivative based polymers

	Yield (%)	M_n (g/mol)	λ_{max} (nm)	E_g^{opt} (eV)	V_{ox} (V)	V_{red} (V)	E_{LUMO} (eV)	E_{HOMO} (eV)
PTANTDPP	87	11,600	674	1.39	0.81	-0.86	-3.40	-5.07
PTANTBT	24	1,700	545	1.79	1.09	-0.85	-3.41	-5.35
PTANTC	94	5,300	569	1.68	0.96	-0.85	-3.41	-5.22
PTANTT	75	4,700	578	1.59	0.76	-0.86	-3.41	-5.02
PTANTTPD	60	4,600	574	1.80	0.73	-0.82	-3.45	-4.99
PAAT	70	10,400	592	1.71	1.05	-0.88	-3.38	-5.31
PAATPD	61	5,700	569	1.68	1.06	-0.84	-3.42	-5.32
PAADPP	77	18,500	705	1.39	0.83	-0.81	-3.45	-5.09
PAAC	55	7,000	556	1.73	1.12	-0.86	-3.40	-5.38
PAABDT	33	13,000	580	1.76	0.81	-0.87	-3.39	-5.07
PAABT	13	16,200	N/D	1.59[b]	N/D[c]	-0.85	-3.41	N/D[c]

E_g film values were measured at the onset. V: onset vs Ag/AgCl, scan rate of 100 mV s^{-1}, Fc/Fc+ $E_{1/2}$ measured at 0.44 vs Ag/AgCl. [b] The value was measured from solution since a good quality film could not be obtained. [c] Reliable measurements could not be taken because of poor film forming properties.
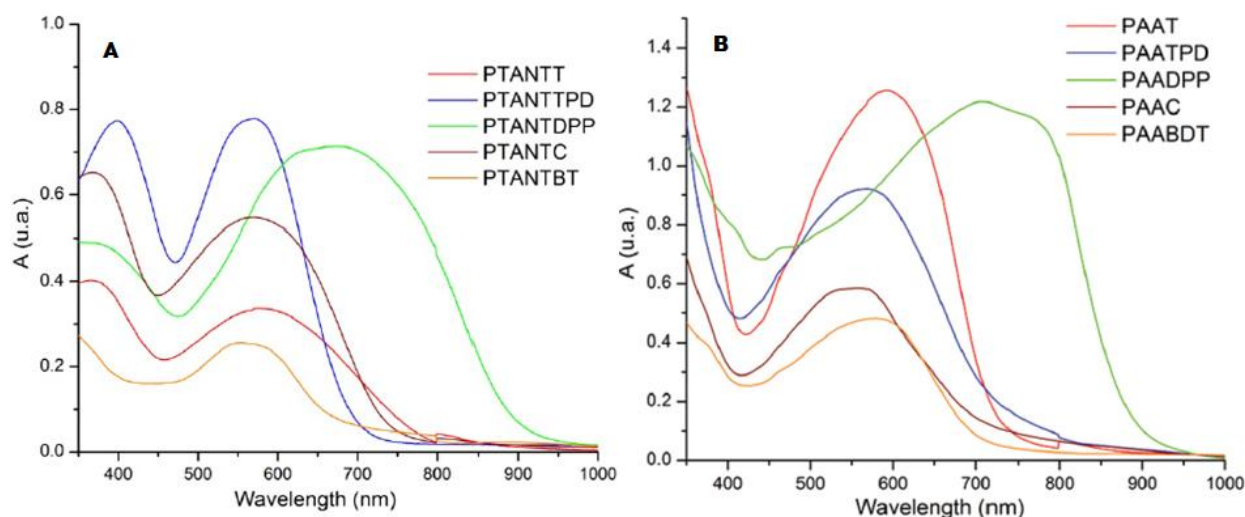
Figure 2.5: UV-Vis spectra for polymer A) PTANT and B) PAA series in solid state. A). Reprinted (adapted) with permission from (A. Lafleur-Lambert, J.-B. Giguère and J .-F. Morin, "Conjugated Polymers Based on 4,10-Bis(thiophen-2-yl)anthanthrone:Synthesis, Characterization, and Fluoride-Promoted Photoinduced Electron Transfer," *Macromolecules,* 48 (2015) 8376 - 8381). Copyright (2015) American Chemical Society. B) Reproduced ("Adapted") from {A. Lafleur-Lambert, J.-B. Giguère and J.-F. Morin, "Anthanthrene as a large PAH building block for the synthesis of conjugated polymers," *Polym. Chem.,* 6 (2015) 4859 – 4863} with permission of The Royal Society of Chemistry.

A critical goal of D-A copolymer design is to achieve extended absorption to match the solar spectrum. Donor polymers for OPV cell application can be influenced by factors like (i) side chains of the conjugated semiconducting polymer, which enhance solubility and process-ability, (ii) molecular weight and (iii) position of aromatic ring

29

2.3.1   Side Chain Effect

Side chains can be used to enhance solubility of π-conjugated molecules and subsequently influence the thin-film supramolecular ordering for various thin film applications [83-84]; permit the formation of flexible materials and offers greater tuning of molecular properties [85]. They play an important role in the ordering of molecular self assembly and contribute to both the tuning of the optical as well as electronic properties of semiconducting materials. The attachment of hexyl side chain to the back bone of polythiophene in a regio-regular manner to give poly(3-hexylthiophene) (P3HT) for example, has resulted in polythiophene exhibiting high charge carrier mobility. This is as a result of high degree of intermolecular ordering, and this behavior makes P3HT one of the best materials for the construction of high efficiency organic electronic devices like OFETs and OPVs till date [86-87]. Slight change in the attached side chains in PAE-PAV based polymers have been shown to influence the electronic and physical properties of these polymers and appreciably improve their photovoltaic performance [58, 88]. Egbe *et al* [89] reported the influence of side chains on the electrochemical properties of alkyloxy-substituted phenylene ethynylene/phenylene vinylene hybrid polymers. Longer linear octadecyl and bulky branched 2-ethylhexyl enhance the interface energy barrier due to their strong insulating nature. The solid-state photophysical properties (photoconductivity, absorption and emission spectra, fluorescence quantum yield, Stokes shift, and full width at half maximum (FWHM)) of **Daa-cc** and **D3** (**Figure 2.6**) greatly depend on the nature (linear or branched), length, and location of the grafted alkyloxy side groups as shown in the absorption and emission spectra (**Figure 2.7**) [42]. Polymer **Daa-cc** showed almost identical absorption and emission spectra in dilute chloroform solution while the FWHM value of the emission curves revealed a dependence on

30

the length of the attached side chains. This class of polymers have been shown to exhibit easy

photoconductivity with incorporation of long octadecyloxy side chains [90].
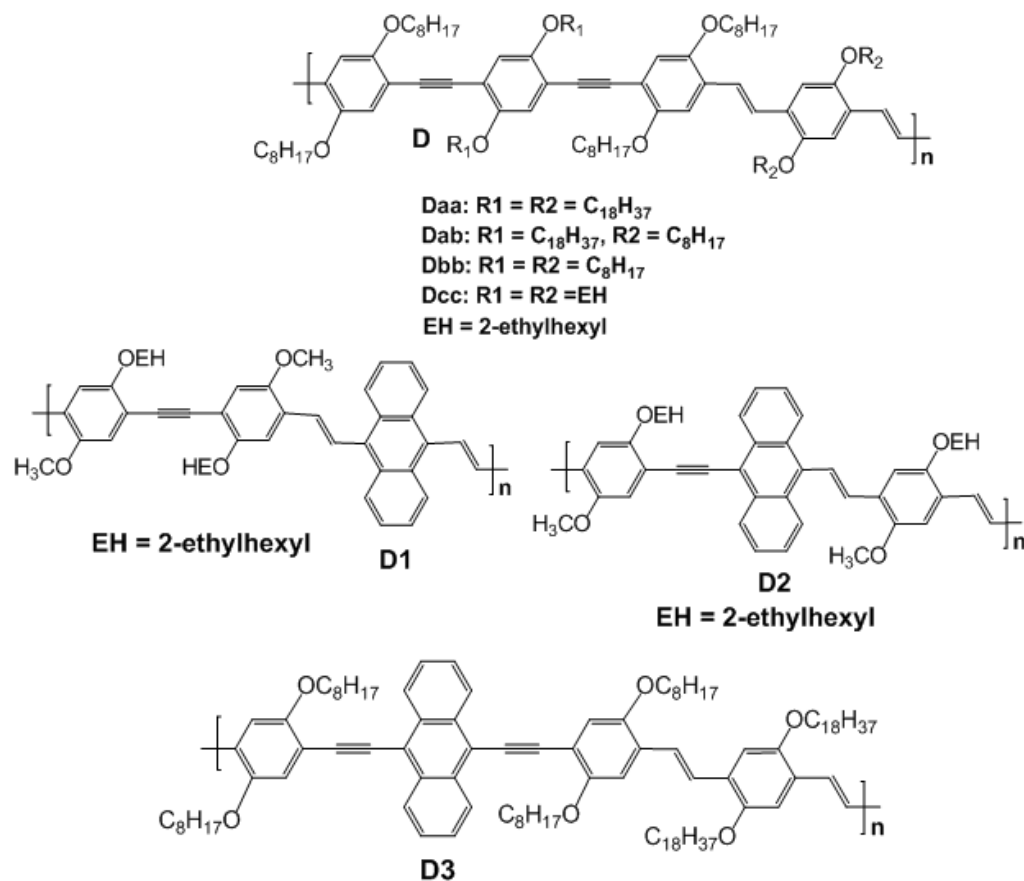
Figure 2.6: Structures of phenyl and anthracene-containing PAE-PPV polymers D-D3 with

varying side chain.

31
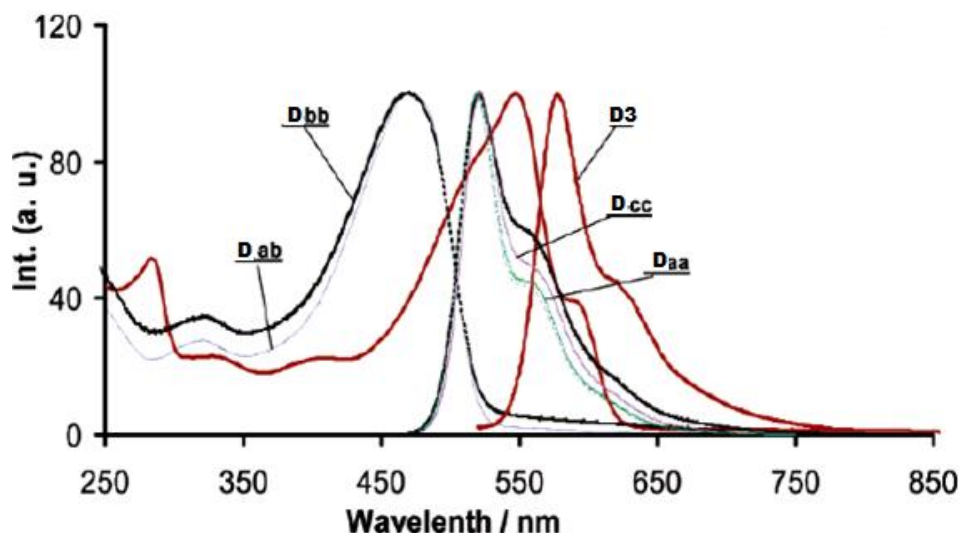
Figure 2.7: A) Absorption and emission spectra in CHCl$_3$ solution of polymers D and D3. Reprinted (adapted) with permission from (D. A. M. Egbe, Bader Cornelia, J. Nowotny, W. Gunther and E. Klemm, "Investigation of the Photophysical and Electrochemical Properties of Alkoxy-Substituted Arylene-Ethynylene/Arylene-Vinylene Hybrid Polymers," *Macromolecules*, 36 (2003) 5459 - 5469). Copyright (2003) American Chemical Society.

Photovoltaic device performance of anthracene containing polymers bearing linear octyloxy/branched 2-ethylhexyloxy side chains and methoxy/2-ethylhexyloxy side chains have been shown to be affected by length and distribution of the side chain [91]. The polymers exhibit a broad variation in their photovoltaic properties with strong dependence on the structure of the attached side chains. PAE-PAV-based anthracene polymers bearing asymmetric alkyloxy side chains were reported to display optimal interfacial contact with [6,6]-phenyl C$_{61}$ butyric acid methyl ester (PCBM) in BHJ OPV cells due to the side chains [59]. By varying the mole fractions of polymer units with different side-chain species, the photovoltaic properties can be optimized [92-93] as variations of the side chain of polymers have strong impact on the π–π stacking ability of the polymer backbone. Random distribution of linear octyloxy side chains and or branched 2-ethylhexyloxy side chains on the backbone

32

of anthracene containing polymers was used to vary the backbone π–π-stacking distance ($d_{\pi-\pi}$) and the interlayer separation (d_{inter}) of the polymer resulting in optimized photovoltaic properties [94]. The donating effect of side chains lowers the band gap of polymers and they can be used to tune the nano-morphology of the active layer of organic photovoltaic device. It is common knowledge that the performance of bulk heterojunction devices is strongly dependent on the values of the V_{oc}, J_{sc} and *FF*. The J_{sc} and *FF* in OPV devices have been shown to be greatly dependent on the type and length of the solubilizing alkyloxy side chains [58].

2.3.2 Molecular Weight Effect

Molecular weight fine-tuning can impact on the optoelectronic properties of a polymer, as well as the photovoltaic properties. One of the important parameters to be considered in the synthesis of donor materials for improved device performance is molecular weight [75, 95]. Usually, the molecular weight is analyzed in the form of weight average molecular weight (M_w) and number average molecular weight (M_n). M_n has a strong impact on the physical properties of the polymer. The relatively low molecular weight polymer PTANTBT (with M_n value of 1700 g/mol) reported by Morin's group [81], has the lowest absorption maximum and highest solid state optical band gap in the entire series investigated (**Table 2.1**). The low molecular weight may be responsible for the poor absorption of this polymer in the visible region. The effects of a moderate variation of the molecular weight on the optical, structural, morphological and transport properties of an anthracene-containing PAE-PAV copolymer, as well as their overall implication on the photovoltaic parameters of BHJ OPV was investigated by Camaioni *et al* [96]. A two-fold variation in the molecular weight of the polymer induced

33

appreciable changes in the properties of the investigated polymer films, resulting in conversion efficiency of 3.26%.

2.3.3   Position of Aromatic Ring

The position of aromatic ring on the polymer chain can also have an effect on the photophysical properties of the polymer. Mullen *et al* [97] demonstrated that placing anthracene unit between two double bonds leads to a backbone torsion of 80°. This results from the steric hindrance between the vinylene hydrogen atoms and the anthracenylene hydrogen atoms. The replacement of the vinylene units by ethynylene units displaces this steric repulsion. This explains the report by Egbe *et al* [98-99] of a bathochromic shift in absorption wavelength in their investigation based on position of aromatic ring on the backbone of anthracene-containing polymers. They observed a bathochromic shift of approximately 50 nm in the absorption maximum going from an anthracene-containing polymer of general constitutional unit (-Ph-C≡C-Ph-CH=CH-Anthracene-CH=CH)$_n$ (**D1**) (**Figure 2.6** where the anthracene unit is located between two double bonds) to the polymer of general constitutional unit (-Ph-C≡C-Anthracene-CH=CH-Ph-CH=CH)$_n$ (**D2**) in which the anthracene unit is placed at the bridge between a vinylene and an ethynylene bond. A further 50 nm bathochromic shift was observed in moving from the **D2** architecture to the architecture (-Ph-C≡C-Anthracene-C≡C-Ph-CH=CH-Ph-CH=CH)$_n$ (**D3**) (anthracene unit placed between two triple bonds). Also, going from **D1** to **D2** and through to **D3**, a decrease in the observed anthracene band around 255 nm was observed (**Figure 2.8a**). This suggests the degree of contribution of the anthracene unit to the main chain conjugation based on the position of the anthracene in the chain. Going from solution to thin film, a slight bathochromic shift is observed for **D2** and **D3** except for **D1** (**Figure 2.8b**). The

34

bathochromic shift observed in **D2** and **D3** is ascribed to enhanced planarization of the conjugated backbone while the constant absorption observed for **D1** in both solution and film is attributed to large torsion angle which does not allow enhancement of conjugation even in thin film.
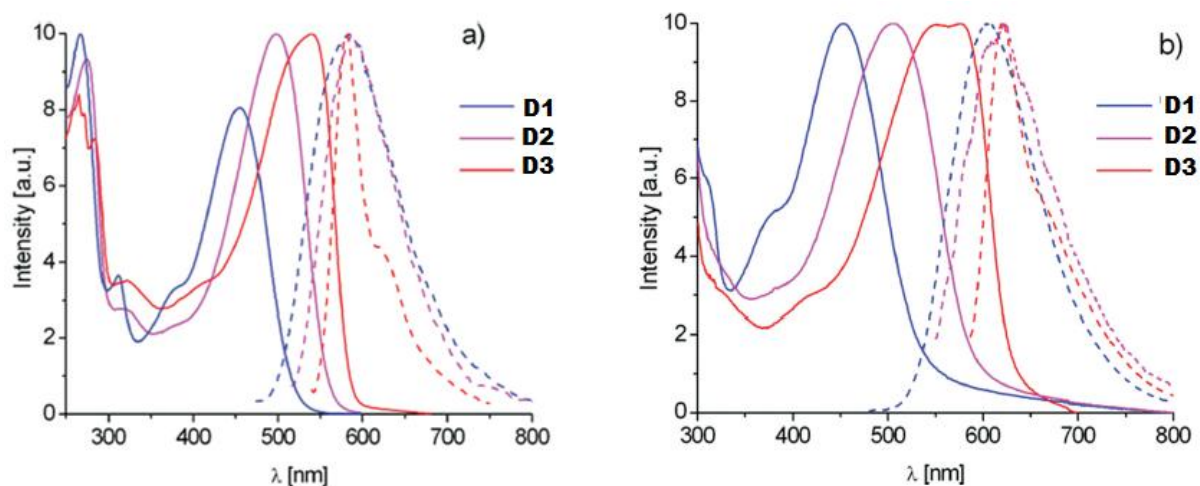
Figure 2.8: Normalized absorption (solid lines) and emission (dash lines) spectra of D1 – D3 in a) solution, b) thin film. Reprinted (adapted) with permission from Ref [98], Copyright (2009) John Wiley and Sons.

Figures 2.6, 2.9 and Table 2.2 reveals a number of reports on organic photovoltaic cells based on anthracene-containing polymers. It shows the effect of band gap, molecular weight, side chains and position of the aromatic ring on the optical properties of anthracene containing polymers. These factors are inter-dependent and as such should be considered during synthesis of materials for photovoltaic applications. For instance, the solubility, molecular weight, intermolecular interactions and charge carrier mobilities of a conjugated semiconducting polymer can be greatly influenced by the presence and type/nature of side chain. Side chains enhance the solubility of conjugated polymers and can lead to increase in molecular weight. Molecular weights on the other hand influence the intermolecular

35

interactions of polymers through changes in morphology and thereby enhance the charge carrier mobility in the device. In a very recent report by Bouguerra *et al* [100] the film properties of a set of conjugated polymers poly(1,4-arylene−ethynylene)-alt-poly(1,4-arylene−vinylene)s (PAE−PAVs) with dissymmetrical configuration of alkyloxy side chains showed a dependence on the combinatorial effects of side chain configuration and molecular weight. Certain types of substituents or side chains can red-shift the absorption thereby tuning the HOMO and the LUMO energy levels and lowering the optical band gap of a polymer. It is therefore vital to understand and account for these designing principles and balance the guiding concepts in order to achieve an 'ideal' polymer for organic photovoltaic cell applications.
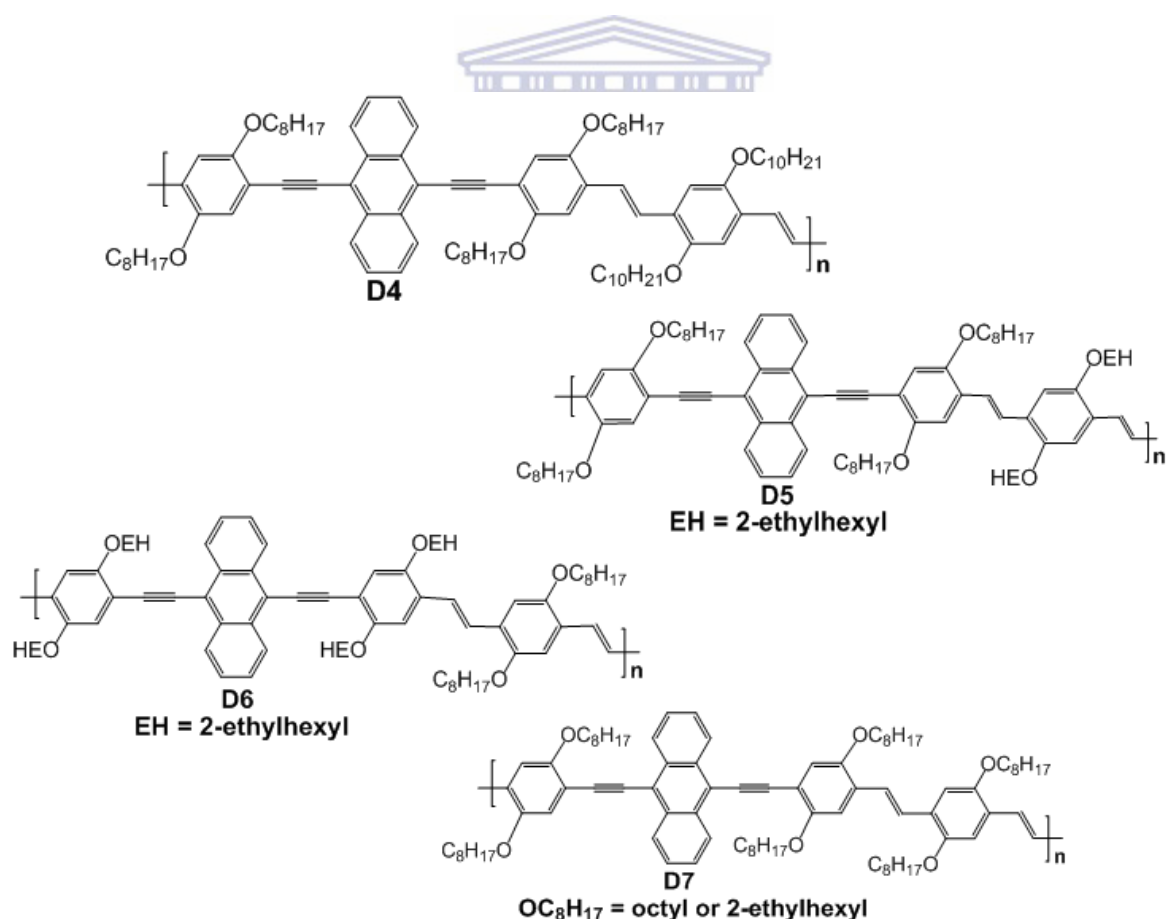
Figure 2.9: Structures of anthracene-containing PAE-PPV polymers D4-D7.

Table 2.2: Optoelectronic and photovoltaic response of anthracene-containing PAE-PPV polymers

Donor	M_n (g/mol)	λ_a (nm)	λ_f (nm)	E_g^{opt} (eV)	HOMO	LUMO	E_g^{el} (eV)	J_{sc} (mA/cm^2)	V_{oc} (mV)	FF (%)	PCE (%)	Ref.
D1	33,000	453	607	2.22	5.21	3.23	1.98					[59, 93, 98]
D2	31,000	506	621	2.05	5.23	3.35	1.88					[59, 93, 98]
D3	25,600	575	620	1.90	-	-	-					[42, 93, 98]
D4	19,300	552, 590	621	1.91	5.15	3.38	1.77	6.75	680	48.37	2.22	[92-93]
D5	40,000	508, 583	624	1.80	5.17	3.37	1.80	7.14	790	55.65	3.14	
D6	25,500	504	605	1.95	5.16	3.37	1.79	3.44	930	34.67	1.11	
D5	7,980							6.6	880	52.5	3.1	[101]
D7								8.0	826	69.2	4.6	[102]
D7								8.3	774	61	3.9	[102]
D7	6,600	577	621	-	-	-	-	6.27	828	58.42	3.03	[91]
D6	25,500	504	605	1.95	5.16	3.37	1.79	7.23	802	69.60	4.03	[92-93, 103]
D7								8.0	822	65	4.3	[104]
D5								7.05	764	67.97	3.66	[105]
D7								7.52	843	68.1	4.33	[106]

2.4   Conclusion

Although polycyclic aromatic compounds are promising for OPV applications there are very few reports in which they have been employed as building blocks for this purpose. The challenge of solubility and complex synthetic routes are most likely responsible for the lack of interest and widespread adoption of these materials for photovoltaic application. However, this challenge is being overcome by the use of solubilizing alkyl/alkyloxy side chains on the aromatic ring, extending the conjugation length and the use of electron-rich and electron-poor (D-A) units within the main chain in order to create a charge transfer complex, resulting in the lowering of the band gap. The basic optical behavior and electronic properties of a D-A conjugated polymer is determined by the electron strength and molecular geometry of the donor and acceptor as well as their interactions. As a result of this dependence, a rational design of electron donor and acceptor units is vital before combining them to develop high-performance donor-acceptor polymers. It is of great importance for researchers to understand the role of each factor and how to combine them for amplification of the optical window and subsequent enhancement of device efficiency.

38

2.5   References

[1]   S. Beaupré, P. L. Boudreault and M. Leclerc, "Solar-energy production and energy-efficient lighting: photovoltaic devices and white-light-emitting diodes using poly(2,7-fluorene), poly(2,7-carbazole), and poly(2,7-dibenzosilole) derivatives," *Adv. Mater.,* 22 (**2010**) E6 - E27.

[2]   C. J. Brabec, N. S. Sariciftci and J. C. Hummelen, "Plastic Solar Cells," *Adv. Funct. Mater.,* 11 (**2001**) 15 - 26.

[3]   K. M. Coakley and M. D. McGehee, "Conjugated Polymer Photovoltaic Cells," *Chem. Mater.,* 16 (**2004**) 4533 - 4542.

[4]   Y. J. Cheng, S. H. Yang and C. S. Hsu, "Synthesis of conjugated polymers for organic solar cell applications," *Chem. Rev.,* 109 (**2009**) 5868 - 5923.

[5]   H. Hoppe and N. S. Sariciftci, "Organic solar cells: an overview," *J. Mater. Res.,* 19 (**2004**) 1924 - 1945.

[6]   B. C. Thompson and J. M. J. Frechet, "Polymer–Fullerene Composite Solar Cells," *Angew. Chem. Int. Ed.,* 47 (**2008**) 58 – 77.

[7]   G. Dennler, M. C. Scharber and C. J. Brabec, "Polymer-Fullerene Bulk-Heterojunction Solar Cells," *Adv. Mater.,* 21 (**2009**) 1323 - 1338.

[8]   B. P. Lyons, N. Clarke and C. Groves, "The relative importance of domain size, domain purity and domain interfaces to the performance of bulk-heterojunction organic photovoltaics," *Energy Environ. Sci.,* 5 (**2012**) 7657 - 7663.

[9]   S. B. Darling and F. You, "The case for organic photovoltaics," *RSC Adv.,* 3 (**2013**) 17633 - 17648.

[10]   M. C. Scharber and N. S. Sariciftci, "Efficiency of bulk-heterojunction organic solar cells," *Prog. Polym. Sci.,* 38 (**2013**) 1929 – 1940.

[11]   K. A. Mazzio and C. K. Luscombe, "The future of organic photovoltaics," *Chem. Soc. Rev.,* 44 (**2014**) 78 - 90.

[12]   J. Peet, A. J. Heeger and G. C. Bazan, ""Plastic" solar cells: self-assembly of bulk heterojunction nanomaterials by spontaneous phase separation," *Acc. Chem. Res.,* 42 (**2009**) 1700 - 1708.

[13]   F. C. Krebs, J. Fyenbo and M. Jørgensen, "Product integration of compact roll-to-roll processed polymer solar cell modules: methods and manufacture using flexographic printing, slot-die coating and rotary screen printing," *J. Mater. Chem.,* 20 (**2010**) 8994 - 9001.

[14]   M. Helgesen, R. Søndergaard and F. C. Krebs, "Advanced materials and processes for polymer solar cell devices," *J. Mater. Chem.,* 20 (**2010**) 36 - 60.

[15]   J. D. Servaites, M. A. Ratner and T. J. Marks, "Organic solar cells: A new look at traditional models," *Energy Environ. Sci.,* 4 (**2011**) 4410 - 4422.

[16]   B. Walker, C. Kim and T-Q. Nguyen, "Small molecule solution—Processed bulk heterojunction solar cells," *Chem. Mater.,* 23 (**2011**) 470 - 482.

[17]   J. Chen and Y. Cao, "Development of novel conjugated donor polymers for high-efficiency bulk-heterojunction photovoltaic devices," *Acc. Chem. Res.,* 42 (**2009**) 1709 - 1718.

[18]   R. F. Service, "Outlook brightens for plastic solar cells. Science," *Science* 332 (**2011**) 293 - 303.

[19]   Y. Liu, J. Zhao, Z. Li, C. Mu, W. Ma, H. Hu, K. Jiang, H. Lin, H. Ade and H. Yan, "Aggregation and morphology control enables multiple cases of high-efficiency polymer solar cells," *Nat. Commun.,* 5 (**2014**) 1 - 8.

[20]   C.-C. Chen, W.-H. Chang, K. Yoshimura, K. Ohya, J. You, J. Gao, Z. Hong and Y. Yang, "An Efficient Triple-Junction Polymer Solar Cell Having a Power Conversion Effi ciency Exceeding 11%," *Adv. Mater.,* 26 (**2014**) 5670 - 5677.

[21]   http://www.photovoltaik4all.de,

[22]   X. Feng, W. Pisula and K. Müllen, "Large polycyclic aromatic hydrocarbons: Synthesis and discotic organization," *Pure Appl. Chem.,* 81 (**2009**) 2203 - 2224.

[23]   J. Wu, W. Pisula and K. Müllen, "Graphenes as potential material for electronics," *Chem. Rev.,* 107 (**2007**) 718 - 747.

[24]   A. Facchetti, "π-Conjugated Polymers for Organic Electronics and Photovoltaic Cell Applications," *Chem. Mater.,* 23 (**2011**) 733 - 758.

[25]   C. Wang, H. Dong, W. Hu, Y. Liu and D. Zhu, "Semiconducting π-conjugated systems in field-effect transistors: a material odyssey of organic electronics," *Chem. Rev.,* 112 (**2011**) 2208 - 2267.

[26]   W. Pisula, X. Feng and K. Müllen, "Charge-Carrier Transporting Graphene-Type Molecules," *Chem. Mater.,* 23 (**2011**) 554 - 567.

[27]   J. Mei, Y. Diao, A. L. Appleton, L. Fang and Z. Bao, "Integrated Materials Design of Organic Semiconductors for Field-Effect Transistors," *J. Am. Chem. Soc.,* 135 (**2013**) 6724 - 6746.

[28]   Z. Zhang, T. Lei, Q. Yan, J. Pei and D. Zhao, "Electron-transporting PAHs with dual perylenediimides: syntheses and semiconductive characterizations," *Chem. Commun.,* 49 (**2013**) 2882 - 2884.

[29]   S. Xiao, S. J. Kang, S. Zhang, A. M. Scott, A. Moscatelli, N. J. Turro, M. L. Steigerwald, H. Li and C. Nuckolls, "Controlled doping in thin-film transistors of large contorted aromatic compounds," *Angew. Chem., Int. Ed.,* 52 (**2013**) 4558 - 4562.

[30]   J.-B. Giguère, N. S. Sariciftci and J.-F. Morin, "Polycyclic anthanthrene small molecules: semiconductors for organic field-effect transistors and solar cells applications," *J. Mater. Chem. C,* 3 (**2015**) 601 - 606.

[31]   J.-B. Giguère and J.-F. Morin, "Synthesis and Optoelectronic Properties of 6,12-Bis(amino)anthanthrene Derivatives," *J. Org. Chem.,* 78 (**2013**) 12769 - 12778.

[32]   J.-B. Giguère, J. Boismenu-Lavoie and J.-F. Morin, "Cruciform Alkynylated Anthanthrene Derivatives: A Structure–Properties Relationship Case Study," *J. Org. Chem.,* 79 (**2014**) 2404 - 2418.

[33]   L. Zhang, B. Walker, F. Liu, N. S. Colella, S. C. B. Mannsfeld, J. J. Watkins, T.-Q. Nguyen and A. L. Briseno, "Triisopropylsilylethynyl-functionalized dibenzo[def,mno]chrysene: a solution-processed small molecule for bulk heterojunction solar cells," *J. Mater. Chem.,* 22 (**2012**) 4266 - 4268.

[34]   Z. Lei, F. Alexandr, Z. Yue, Z. Guangyao, C. Veaceslav, H. Wenping, P. Sean, B. Jean-Luc and A. L. Briseno, "Triisopropylsilylethynyl-Functionalized Graphene-Like Fragment Semiconductors: Synthesis, Crystal Packing, and Density Functional Theory Calculations," *Chem. Eur. J,* 19 (**2013**) 17907 - 17916.

[35]   J.-B. Giguere, Q. Verolet and J.-F. Morin, "4,10-Dibromoanthanthrone as a New Building Block for p-Type, n-Type, and Ambipolar p-Conjugated Materials," *Chem. Eur. J.,* 19 (**2013**) 372 - 381.

[36]   B. K. Shah, D. C. Neckers, J. Shi, E. W. Forsythe and D. Morton, "Photophysical Properties of Anthanthrene-Based Tunable Blue Emitters," *J. Phys. Chem. A,* 109 (**2005**) 7677 - 7681.

[37]   B. K. Shah, D. C. Neckers, J. Shi, E. W. Forsythe and D. Morton, "Anthanthrene Derivatives as Blue Emitting Materials for Organic Light-Emitting Diode Applications," *Chem. Mater.,* 18 (**2006**) 603 - 608.

[38] T. Matsuno, S. Kamata, S. Hitosugia and H. Isobe, "Bottom-up synthesis and structures of π-lengthened tubular macrocycles," *Chem. Sci.,* 4 (**2013**) 3179 - 3183.

[39] J.-B. Giguère and J .-F. o. Morin, "Superextended Tetrathiafulvalene: Synthesis, Optoelectronic Properties, Fullerenes Complexation, and Photooxidation Study," *J. Org. Chem.,* 80 (**2015**) 6767 - 6775.

[40] J.-W. Park, P. Kang, H. Park, H.-Y. Oh, J.-H. Yang, Y.-H. Kim and S.-K. Kwon, "Synthesis and properties of blue-light-emitting anthracene derivative with diphenylamino-fluorene," *Dyes Pigment,* 85 (**2010**) 93 - 98.

[41] J. Sun, J. Chen, J. Zou, S. Ren, H. Zhong, D. Zeng, J. Du, E. Xu and Q. Fang, "π-Conjugated poly(anthracene-alt-fluorene)s with X-shaped repeating units: New blue-light emitting polymers," *Polymer,* 49 (**2008**) 2282 - 2287.

[42] D. A. M. Egbe, Bader Cornelia, J. Nowotny, W. Gunther and E. Klemm, "Investigation of the Photophysical and Electrochemical Properties of Alkoxy-Substituted Arylene-Ethynylene/Arylene-Vinylene Hybrid Polymers," *Macromolecules,* 36 (**2003**) 5459 - 5469.

[43] H. Meng, F. Sun, M. B. Goldfinger, F. Gao, D. J. Londono, W. J. Marshal, G. S. Blackman, K. D. Dobbs and D. E. Keys, "2,6-Bis[2-(4-pentylphenyl)vinyl]anthracene:a stable and high charge mobility organic semiconductor with densely packed crystal structure," *J. Am. Chem. Soc.,* 128 (**2006**) 9304 - 9305.

[44] E. Gondek, I. V. Kityk and A. Danel, "Some anthracene derivatives with N,N-dimethylamine moieties as materials for photovoltaic devices," *Mater. Chem. Phys.,* 112 (**2008**) 301 - 304.

[45] R. B. Chaâbane, N. Jaballah, M. Benzarti-Ghédira, A. Chaieb, M. Majdoub and H. B. Ouada, "Synthesis and thin films characterization of new anthracene-core molecules for opto-electronic applications," *Physica B,* 404 (**2009**) 1912 - 1916.

[46] P. Raghunath, M. Ananth Reddy, C. Gouri, K. Bhanuprakash and V. Jayathirtha Rao, "Electronic properties of anthracene derivatives for blue light emitting electroluminescent layers in organic light emitting diodes: a density functional theory study," *Phys. Chem. A,* 110 (**2006**) 1152 - 1159.

[47] Y. Li, T.-H. Kim, Q. Zhao, E.-K. Kim, S.-H. Han, Y.-H. Kim, J. Jang and S.-K. Kwon, "Synthesis and Characterization of a Novel Polymer Based on Anthracene Moiety for Organic Thin Film Transistor," *J. Polym. Sci. Part A Polym. Chem.,* 46 (**2008**) 5115 - 5122.

[48] L. Valentini, D. Bagnis, A. Marrocchi, M. Seri, A. Taticchi and J. M. Kenny, "Novel Anthracene-Core Molecule for the Development of Efficient PCBM-Based Solar Cells," *Chem. Mater.,* 20 (**2008**) 32 - 34.

[49] D. A. M. Egbe, H. Tillmann, E. Birckner and E. Klemm, "Synthesis and Properties of Novel Well-Defined Alternating PPE/PPV Copolymers," *Macromol. Chem. Phys.,* 202 (**2001**) 2712 - 2726.

[50] D. A. M. Egbe, C. Ulbricht, T. Orgis, B. Carbonnier, T. Kietzke, M. Peip, M. Metzner, M. Gericke, E. Birckner, T. Pakula, D. Neher and U.-W. Grummt, "Odd-Even Effects and the Influence of Length and Specific Positioning of Alkoxy Side Chains on the Optical Properties of PPE-PPV Polymers," *Chem. Mater.,* 17 (**2005**) 6022 - 6032.

[51] E. Tekin, H. Wijlaars, E. Holder, D. A. M. Egbe and U. S. Schubert, "Film thickness dependency of the emission colors of PPE–PPVs in inkjet printed libraries " *J. Mater. Chem.,* 16 (**2006**) 4294 - 4298.

44

[52] F. Silvestri and A. Marrocchi, "Acetylene-Based Materials in Organic Photovoltaics," *Int. J. Mol. Sci.,* 11 (**2010**) 1471 - 1508.

[53] H. Hoppe, D. A. M. Egbe, D. Mühlbacher and N. S. Sariciftci, "Photovoltaic action of conjugated polymer/fullerene bulk heterojunction solar cells using novel PPE-PPV copolymers," *J. Mater. Chem.,,* 14 (**2004**) 3462 - 3467.

[54] M. Al-Ibrahim, A. Konkin, H.-K. Roth, D. A. M. Egbe, E. Klemm, U. Zhokhavets, G. Gobsch and S. Sensfuss, "PPE-PPV copolymers: optical and electrochemical characterization, comparison with MDMO-PPV and application in flexible polymer solar cells," *Thin Solid Films,* 474 (**2005**) 201 - 210.

[55] D. A. M. Egbe, L. H. Nguyen, B. Carbonnier, D. Muhlbacher and N. S. Sariciftci, "Thiophene-containing poly(arylene–ethynylene)-alt-poly(arylene–vinylene)s: Synthesis, characterisation and optical properties," *Polymer,* 46 (**2005**) 9585 - 9595.

[56] D. A. M. Egbe, T. Kietzke, B. Carbonnier, D. M. hlbacher, H.-H. Horhold, D. Neher and T. Pakula, "Synthesis, Characterization, and Photophysical, Electrochemical, Electroluminescent, and Photovoltaic Properties of Yne-Containing CN-PPVs," *Macromolecules,* 37 (**2004**) 8863 - 8873.

[57] T. Kietzke, D. A. M. Egbe, H.-H. Horhold and D. Neher, "Comparative Study of M3EH-PPV-Based Bilayer Photovoltaic Devices," *Macromolecules,* 39 (**2006**) 4018 - 4022.

[58] D. A. M. Egbe, L. H. Nguyen, K. Schmidtke, A. Wild, C. Sieber, S. Guenes and N. S. Sariciftci, "Combined fffects of fonjugation pattern and alkoxy side chains on the photovoltaic properties of thiophene- containing PPE-PPVs," *J. Polym. Sci. Part A Polym. Chem.,* 45 (**2007**) 1619 - 1631.

[59] D. A. M. Egbe, A. Wild, E. Birckner, U.-W. Grummt and U. S. Schubert, "Anthracene- and Thiophene-Containing Poly(parylene-ethynylene)/poly(p-arylene-

45

vinylene)s:Towards Optimized Structures for Photovoltaic Applications," *Macromol. Symp.,* 268 (**2008**) 25 - 27.

[60] D. Mühlbacher, M. Scharber, M. Morana, Z. Zhu, D. Waller, R. Gaudiana and C. Brabec, "High Photovoltaic Performance of a Low-Bandgap Polymer," *Adv. Mater.,* 18 (**2006**) 2884 - 2889.

[61] J. Peet, J. Y. Kim, N. E. Coates, W. L. Ma, D. Moses, A. J. Heeger and G. C. Bazan, "Efficiency enhancement in low-bandgap polymer solar cells by processing with alkane dithiols," *Nat. Mater.,* 6 (**2007**) 497 - 500.

[62] J. Hou, H.-Y. Chen, S. Zhang, G. Li and Y. Yang, "Synthesis, characterization, and photovoltaic properties of a low band gap polymer based on silole-containing polythiophenes and 2,1,3-benzothiadiazol," *J. Am. Chem. Soc.,* 130 (**2008**) 16144 - 16145.

[63] D. Veldman, O. Ipek, S. C. J. Meskers, J. Sweelssen, M. M. Koetse, S. C. Veenstra, J. M. Kroon, S. S. van Bavel, J. Loos and R. A. J. Janssen, "Compositional and electric field dependence of the dissociation of charge transfer excitons in alternating polyfluorene copolymer/fullerene blends," *J. AM. Chem. Soc.,* 130 (**2008**) 7721 - 7735.

[64] E. Wang, L. Wang, L. Lan, C. Luo, W. Zhuang, J. Peng and Y. Cao, "High-performance polymer heterojunction solar cells of a polysilafluorene derivative," *Appl. Phys. Lett.,* 92 (**2008**) 033307.

[65] S. H. Park, A. Roy, S. Beaupré, S. Cho, N. Coates, J. S. Moon, D. Moses, M. Leclerc, K. Lee and A. J. Heeger, "Bulk heterojunction solar cells with internal quantum efficiency approaching 100%," *Nat. Photonics,* 3 (**2009**) 297 - 302.

[66]   H.-Y. Chen, J. Hou, S. Zhang, Y. Liang, G. Yang, Y. Yang, L. Yu, Y. Wu and G. Li, "Polymer solar cells with enhanced open-circuit voltage and efficiency," *Nat. Photonics,* 3 (**2009**) 649 - 653.

[67]   Y. Liang, Z. Xu, J. Xia, S.-T. Tsai, Y. Wu, G. Li, C. Ray and L. Yu, "For the Bright Future—Bulk Heterojunction Polymer Solar Cells with Power Conversion Efficiency of 7.4%," *Adv. Mater.,* 22 (**2010**) E135 – E138.

[68]   Z. G. Zhang and J. Wang, "Structures and properties of conjugated Donor−Acceptor copolymers for solar cell applications," *J. Mater. Chem.,* 22 (**2012**) 4178 - 4187.

[69]   H. Zhou, L. Yang, S. Xiao, S. Liu and W. You, "Donor–acceptor polymers incorporating alkylated dithienylbenzothiadiazole for bulk heterojunction solar cells: pronounced effect of positioning alkyl chains," *Macromolecules,* 43 (**2010**) 811 - 820.

[70]   H. J. Son, W. Wang, T. Xu, Y. Liang, Y. Wu, G. Li and L. Yu, "Synthesis of fluorinated polythienothiophene-co-benzodithiophenes and effect of fluorination on the photovoltaic properties," *J. AM. Chem. Soc.,* 133 (**2011**) 1885 - 1894.

[71]   H. Zhou, L. Yang, S. Liu and W. You, "A Tale of Current and Voltage: Interplay of Band Gap and Energy Levels of Conjugated Polymers in Bulk Heterojunction Solar Cells," *Macromolecules,* 43 (**2010**) 10390 - 10396.

[72]   H. Zhou, L. Yang, S. C. Price, K. J. Knight and W. You, "Enhanced Photovoltaic Performance of Low-Bandgap Polymers with Deep LUMO Levels," *Angew. Chem. Int. Ed.,* 49 (**2010**) 7992 - 7995.

[73]   R. L. Uy, S. C. Price and W. You, "Structure-Property Optimizations in Donor Polymers via Electronics, Substituents, and Side Chains Toward High Effi ciency Solar Cells," *Macromol. Rapid Commun.,* 33 (**2012**) 1162 - 1177.

47

[74] E. E. Havinga, W. ten Hoeve and H. Wynberg, "Alternate donor–acceptor small-band-gap semiconducting polymers; polysquaraines and polycroconaines," *Synth. Met.,* 55 (**1993**) 299 - 306.

[75] P. M. Beaujuge and J. M. J. Fréchet, "Molecular design and ordering effects in pi-functional materials for transistor and solar cell applications," *J. AM. Chem. Soc.,* 133 (**2011**) 20009 - 20029.

[76] X. Guo, S. R. Puniredd, M. Baumgarten, W. Pisula and K. Müllen, "Benzotrithiophene-Based Donor–Acceptor Copolymers with Distinct Supramolecular Organizations," *J. Am. Chem. Soc.,* 134 (**2012**) 8404 - 8407.

[77] P. Herguth, X. Jiang, M. S. Liu and A. K. Y. Jen, "Highly efficient fluorene- and benzothiadiazole-based conjugated copolymers for polymer light emitting diodes," *Macromolecules,* 35 (**2002**) 6094 - 6100.

[78] M. Svensson, F. Zhang, S. C. Veenstra, W. J. H. Verhees, J. C. Hummelen, J. M. Kroon, O. Inganäs and M. R. Andersson, "High-performance polymer solar cells of an alternating polyfluorene copolymer and a fullerene derivative," *Adv. Mater.,* 15 (**2003**) 988 - 991.

[79] W. H. Tang, L. Ke, L. Tan, T. T. Lin, T. Kietzke and Z. K. Chen, "Conjugated copolymers based on fluorene-thieno[3,2-b]thiophene for light-emitting diodes and photovoltaic cells," *Macromolecules,* 40 (**2007**) 6164 - 6171.

[80] W. H. Tang, V. Chellappan, M. H. Liu, Z. K. Chen and L. Ke, "Hole transport in poly[2,7-(9,9-dihexylfluorene)-alt-biothiophene and high-efficiency polymer solar cells from its blends with PCBM," *ACS Appl. Mater. Interf.,* 1 (**2009**) 1467 - 1473.

[81] A. Lafleur-Lambert, J.-B. Giguère and J.-F. Morin, "Conjugated Polymers Based on 4,10-Bis(thiophen-2-yl)anthanthrone:Synthesis, Characterization, and Fluoride-Promoted Photoinduced Electron Transfer," *Macromolecules,* 48 (**2015**) 8376 - 8381.

48

[82] A. Lafleur-Lambert, J.-B. Giguère and J.-F. Morin, "Anthanthrene as a large PAH building block for the synthesis of conjugated polymers," *Polym. Chem.,* 6 (**2015**) 4859 - 4863.

[83] M. Moroni, J. Le Moigne, T. A. Pham and J.-Y. Bigot, "Rigid Rod Conjugated Polymers for Nonlinear Optics. 3. Intramolecular H Bond Effects on Poly(phenyleneethynylene) Chains," *Macromolecules,* 30 (**1997**) 1964 - 1972.

[84] U. H. F. Bunz, "Poly(aryleneethynylene)s: Syntheses, Properties, Structures, and Applications," *Chem. Rev.,* 100 (**2000**) 1605 - 1644.

[85] M. J. Hollamby and T. Nakanishi, "The power of branched chains: optimising functional molecular materials," *J. Mater. Chem. C,* 1 (**2013**) 6178 - 6183.

[86] C. D. Dimitrakopoulos and D. J. Mascaro, "Organic thin-film transistors: a review of recent advances," *IBM J. Res. Dev.,* 45 (**2001**) 11 - 27.

[87] F. Padinger, R. S. Rittberger and N. S. Sariciftci, "Effects of Postproduction Treatment on Plastic Solar Cells," *Adv. Funct. Mater.,* 13 (**2003**) 85 - 88.

[88] D. K. Susarova, E. A. Khakina, P. A. Troshin, A. E. Goryachev, N. S. Sariciftci, V. F. Razumov and D. A. M. Egbe, "Photovoltaic performance of PPE-PPV copolymers: effect of the fullerene component," *J. Mater. Chem.,* 21 (**2011**) 2356 - 2361.

[89] D. A. M. Egbe, L. H. Nguyen, H. Hoppe, D. Muhlbacher and N. S. Sariciftci, "Side Chain Influence on Electrochemical and Photovoltaic Properties of Yne-Containing Poly(phenylene vinylene)s," *Macromol. Rapid Commun.,* 26 (**2005**) 1389 - 1394.

[90] D. A. M. Egbe, C. P. Roll, E. Birckner, U.-W. Grummt, R. Stockmann and E. Klemm, "Side Chain Effects in Hybrid PPV/PPE Polymers," *Macromolecules,* 35 (**2002**) 3825 - 3837.

[91] O. Usluer, C. Kastner, M. Abbas, C. Ulbricht, V. Cimrova, A. Wild, E. Birckner, N. Tekin, N. S. Sariciftci, H. Hoppe, S. Rathgeber and D. A. M. Egbe, "Charge Carrier

Mobility, Photovoltaic, and Electroluminescent Properties of Anthracene-Based Conjugated Polymers Bearing Randomly Distributed " *J. Polym. Sci. Part A: Polym. Chem.,* 50 (**2012**) 3425 - 3436.

[92]   D. A. M. Egbe, S. Turk, S. Rathgeber, F. Kuhnlenz, R. Jadhav, A. Wild, E. Birckner, G. Adam, A. Pivrikas, V. Cimrova, G. Knor, N. S. Sariciftci and H. Hoppe, "Anthracene Based Conjugated Polymers: Correlation between π-π-Stacking Ability, Photophysical Properties, Charge Carrier Mobility, and Photovoltaic Performance," *Macromolecules,* 43 (**2010**) 1261 - 1269.

[93]   S. Rathgeber, D. B. de Toledo, E. Birckner, H. Hoppe and D. A. M. Egbe, "Intercorrelation between Structural Ordering and Emission Properties in Photoconducting Polymers," *Macromolecules,* 43 (**2010**) 306 - 315.

[94]   D. A. M. Egbe, G. Adam, A. Pivrikas, A. M. Ramil, E. Birckner, V. Cimrova, H. Hopped and N. S. Sariciftci, "Improvement in carrier mobility and photovoltaic performance through random distribution of segments of linear and branched side chains " *J. Mater. Chem.,* 20 (**2010**) 9726 - 9734.

[95]   J. B. Bijleveld, A. J. Zoombelt, S. G. J. Mathijssen, M. M. Wienk, M. Turbiez, D. M. de Leeuw and R. A. J. Janssen, "Poly(diketopyrrolopyrrole-terthiophene) for ambipolar logic and photovoltaics," *J. AM. Chem. Soc.,* 131 (**2009**) 16616 - 16617.

[96]   F. Tinti, F. K. Sabir, M. Gazzano, S. Righi, C. Ulbricht, Ö. Usluer, V. Pokorna, V. Cimrova, T. Yohannes, D. A. M. Egbe and N. Camaioni, "Tuning the properties of an anthracene-based PPE-PPV copolymer by fine variation of its macromolecular parameters " *RSC Adv.,* 3 (**2013**) 6972 - 6980.

[97]   R. O. Graray, H. Naarmann and K. Mullen, "Synthesis and characterization of poly(1,4-anthrylenevinylene)," *Macromolecules,* 27 (**1994**) 1922 - 1927.

50

[98] A. Wild, D. A. M. Egbe, E. Birckner, V. Cimrova, R. Baumann, U.-W. Grummt and U. S. Schubert, "Anthracene- and Thiophene-Containing MEH-PPE-PPVs: Synthesis and Study of the Effect of the Aromatic Ring Position on the Photophysical and Electrochemical Properties," *J. Polym. Sci. Part A: Polym. Chem.,* 47 (**2009**) 2243 - 2261.

[99] J. Gasiorowski, S. Boudiba, K. Hingerl, C. Ulbricht, V. Fattori, F. Tinti, N. Camaioni, R. Menon, S. Schlager, L. Boudida, N. S. Sariciftci and D. A. M. Egbe, "Anthracene-Containing Conjugated Polymer Showing Four Optical Transitions Upon Doping: A Spectroscopic Study," *J. Polym. Sci., Part B: Polym. Phys.,* 52 (**2014**) 338 - 346.

[100] N. Bouguerra, A. Růžička, C. Ulbricht, C. Enengl, S. Enengl, V. Pokorná, D. Výprachtický, E. Tordin, R. Aitout, V. r. Cimrová and D. A. M. Egbe, "Synthesis and photophysical and electroluminescent properties of poly(1,4-phenylene−ethynylene)-alt-poly(1,4-phenylene−vinylene)s with various dissymmetric substitution of alkoxy side chains," *Macromolecules,* 49 (**2016**) 455 - 464.

[101] C. Kastner, D. K. Susarova, R. Jadhav, C. Ulbricht, D. A. M. Egbe, S. Rathgeber, P. A. Troshin and H. Hoppe, "Morphology evaluation of a polymer–fullerene bulk heterojunction ensemble generated by the fullerene derivatization," *J. Mater. Chem.,* 22 (**2012**) 15987 - 15997.

[102] C. Kastner, C. Ulbricht, D. A. M. Egbe and H. Hoppe, "Polymer BHJ Solar Cell Performance Tuning by C_{60} Fullerene Derivative Alkyl Side-Chain Length," *J. Polym. Sci. Part B: Polym. Phys.,* 50 (**2012**) 1562 - 1566.

[103] C. Kastner, S. Rathgeber, D. A. M. Egbe and H. Hoppe, "Improvement of photovoltaic performance by ternary blending of amorphous and semi-crystalline polymer analogues with PCBM," *J. Mater. Chem. A,* 1 (**2013**) 3961 - 3969.

[104] S. Aazou, A. Ibral, M. S. White, M. Kaltenbrunner, E. D. Głowacki, D. A. M. Egbe, N. S. Sariciftci and E. M. Assaid, "Organic Bulk Heterojunction Solar Cells Based on P3HT and Anthracene-Containing PPE-PPV: Fabrication, Characterization and Modeling," *J. Optoelec. Adv. Mater.,* 13 (**2013**) 395 - 404.

[105] H. Mangold, A. A. Bakulin, I. A. Howard, C. Kastner, D. A. M. Egbe, H. Hoppe and F. Laquai, "Control of charge generation and recombination in ternary polymer/polymer:fullerene photovoltaic blends using amorphous and semi-crystalline copolymers as donors," *Phys.Chem.Chem.Phys.,* 16 (**2014**) 20329 - 20337.

[106] C. Kastner, D. A. M. Egbe and H. Hoppe, "Polymer aggregation control in polymer–fullerene bulk heterojunctions adapted from solution," *J. Mater. Chem. A,* 3 (**2015**) 395 - 403.

UNIVERSITY *of the*

WESTERN CAPE

CHAPTER THREE

LITERATURE REVIEW - Luminescence Quenching Characteristics of Fullerenyl Systems

Abstract

Fullerenes are semiconducting materials which have a variety of applications. Specifically, fullerenes serve as electron acceptors and electron transport materials in organic photovoltaic cells. Photo-induced charge transfer and charge separation is the basics for organic photovoltaic cells. It is the core on which the overall energy conversion efficiency of organic photovoltaic cells is based. The understanding of the working principle of photo-induced electron transfers in organic photovoltaic cells improves the capture and conversion of light energy into electrical energy. In this review, a brief overview of the photo-induced charge transfer mechanisms by fluorescence quenching of donor materials in organic photovoltaic cells involving fullerenes will be presented.

3 Introduction

Carbon, the most common organic element existed in two allotropic forms (diamond and graphite) until 1985 when a third allotrope (fullerenes) was uncovered. Fullerenes are large carbon cage molecules viewed as three-dimensional analogues of benzene with possibility of many attachments. They are the third form of carbon after graphite and diamond and the only known molecular form of carbon. They are spherical, hollow molecular allotropes of carbon

53

made of a cage of interlocking pentagons and hexagons. The first synthesized is fullerene C_{60}.

The C_{60} molecule was discovered by a group of scientists led by Richard E. Smalley in 1985

[1] in Rice University in Houston during experiments aimed at understanding the

mechanisms by which long-chain carbon molecules are formed in interstellar space and

circumstellar shells. A startling result of their effort was the coincidental discovery of the

third form of carbon. In the experiment, graphite was vaporized by laser irradiation,

producing a remarkably stable cluster consisting of 60 carbon atoms. The surface of the

graphite was vaporized into plasma containing atoms and free ions. The atoms and free ions

collided with the helium atoms and through the collision; clusters containing various numbers

of carbon atoms were formed. These clusters were dominated by 60 and 70 carbon atoms,

with most clusters having 60 carbon atoms; and now referred to as fullerene C_{60}. This newly

found molecule was named after the American architect Richard Buckminster Fuller whose

geodesic dome based on hexagons and pentagons it resembles. The discovery of fullerenes

triggered a lot of interest and excitement amongst researchers and it earned Curl, Kroto, and

Smalley the 1996 Nobel Prize in chemistry.

At the early stage of discovery, the scientists had problem with up-scaling production. They

succeeded in producing only minute quantity. This challenge was soon overcome when after

5 years, Kratschmer's group [2] and Kroto's group [3] developed new methods of synthesis

at high scale. Fullerenes have also been found to exist naturally in interstellar dust as well as

geological formations on earth though in very low quantity (ppm range). The search for

carbon in space and the fallout of fullerene has turned out to be one of the rare research

breakthroughs that basically alters traditional knowledge of carbon consisting of just two

allotropes (diamond and graphite); and activates a multidisciplinary research. Fullerenes are

interesting molecules with wide spread applications. For instance, the relatively high

superconductivity with T_c of up 33 K and above [4-6] of alkali metal intercalated fullerenes is of great interest to physicists, their mono-disperse nanostructures [7-9] is enticing to material scientists, their use in optical and switching devices [10] is fascinating to device engineers while the molecular nature of the solid phase, phase transitions and large family of new compounds [11-16] that can be prepared from them are attractive to chemists. Since its discovery, fullerenes have opened up novel research fields in chemistry, physics/engineering, material science, medicine etc. with significant potentials for broad/mainstream commercial applications in pharmaceuticals, catalysis, semiconductors, optics, organic electronic; particularly organic photovoltaic (OPV) cells [17-19]. Fullerenes are attractive and important spherical molecules with low reduction potentials and strong electron acceptor properties [20-22]. The extremely low reorganization energy of fullerenes makes them one of the most useful electron acceptor molecules in organic photovoltaic cells [23]. Their n-type semi-conductive nature makes them a good counterpart to the numerous good p-type organic semiconductors and this makes their utilization in OPV cells interesting.

The past 25 years of rapid development and successful fullerene research has resulted in thousands of novel chemical materials and breakthroughs in technology. C_{60} derivatives with special electronic and structural properties have been synthesized and investigated. In the relatively short history of fullerenes, researchers have been extraordinarily dedicated to the field and this has been repeatedly rewarded with novel reactions and mechanisms for fullerenes. A huge number of fullerene derivatives have become available through the attachment of various kinds of chemical groups. This advancement was pioneered by Wudl and his co-workers [24], opening up different kinds of applications in science and technology, and from bio-sciences to organic optoelectronic devices [25-26]. Efforts are now focussed on the most versatile and general methods to obtain derivatives of fullerenes with

attractive properties. Well-optimized and widely used synthetic methods such as the Bingel cyclopropanation [27], 1,3-dipolar additions [28-29] and Diels–Alder reactions [30-31] provided readily accessible building blocks for higher molecular architectures and optoelectronic devices. A number of reviews have provided in-depth insights into the reactions of fullerenes [32-37]. Thus, in this review, the fluorescence quenching characteristics of traditional and novel fullerenyl systems are discussed with their applications in organic photovoltaic cells.

3.1 Fullerenes in Organic Photovoltaics

Photovoltaic cells are commonly composed of a thin film made from a blend of semiconducting donor material and a soluble acceptor sandwiched between a transparent conducting electrode (the anode) and a low work-function metal cathode. Fullerenes and their derivatives with tunable shape and size are extremely promising nanostructures for the construction of novel advanced materials [32, 38], and particularly as electron acceptors in organic photovoltaic cells. They have attracted great attention for their potential applications in photovoltaic cells since two decades ago when Heeger and co-workers observed that the carrier collection efficiency (η_c) and energy conversion efficiency (η_e) of polymer photovoltaic devices were enhanced by blending of π-conjugated semiconducting polymer with C_{60} or its functionalized derivatives [39]. Blend films of poly(2-methoxy-5-(2′-ethyl-hexyloxy)-1,4-phenylene vinylene) (MEH-PPV) and fullerenes showed η_c of about 29 percent of electrons per photon and η_e of about 2.9 percent; with efficiencies that are better by over two orders of magnitude compared to devices with pure MEH-PPV. An efficient charge separation resulting from photo-induced electron transfer from the donor MEH-PPV to C_{60} (as acceptor) and a high collection efficiency resulting from a bi-continuous network of

56

internal donor-acceptor heterojunctions was also recorded. In 2001, Hummelen and his group reported the synthesis and application of a series of highly soluble fullerene derivatives (methanofullerene [6,6]-phenyl C_{61}-butyric acid methyl ester (PCBM), azafulleroid, and a ketolactam quasifullerene) with varying acceptor strengths (i.e., first reduction potentials) as electron acceptors in plastic solar cells based on MEH-PPV donor [40]. The fullerene derivatives gave a variation of almost 0.2 V in their first reduction potential with the open circuit voltage of the corresponding devices correlating directly with the acceptor strength of the fullerenes. The highest and the lowest average open circuit voltages were observed for the PCBM and ketolactam containing cells, with 760 and 560 mV, respectively. Progress in the use of MEH-PPV/C_{60} was achieved with improved photovoltaic elements of up to 3% power conversion efficiency reported [41]. Attention soon shifted to the use of P3HT:PCBM with a conversion efficiency ranging from 4–5% [42-44]. The fullerene acts as the n-type semiconductor (electron acceptor) while the polythiophene acts as the p-type polymer (electron donor). They are blended and cast as the active layer to create what is known as a bulk heterojunction. Presently, the most widely used fullerene derivative electron acceptors are [6,6]-phenyl-C_{61}-butyric acid methyl ester ([60]PCBM) and [6,6]-phenyl-C_{71}-butyric acid methyl ester ([70]PCBM). [6,6]-phenyl-C61-butyric acid methyl ester ([60]PCBM) is one of the most important electron acceptor materials currently employed in organic bulk-heterojunction photovoltaic cells. Poly (3-hexylthiophene) (P3HT) and [6,6]-phenyl-C_{61}-butyric acid methyl ester (PCBM) are the most widely used donor and acceptor materials respectively today.

One of the growing research areas primarily driven by solar energy conversion is photo-induced electron transfer in donor-acceptor systems [45-46]. Photo-induced electron transfer is basically used in the fabrication of molecular electronic and optoelectronic devices [47-48].

The discovery of photo-induced electron transfer in blends of conjugated polymers and fullerenes revealed solution processed organic photovoltaic (OPV) cells as promising form of solar cells [49]. The electron transfer processes in fullerenyl based systems are enhanced as a result of the small reorganization energy and spherical shape of fullerenes [50]. As a result, fullerenes increases the rate of forward electron transfer and slow down backward electron transfer, resulting in the formation of long-lived charge-separated states in donor-acceptor systems. This characteristic is vital in the fabrication of organic photovoltaic devices. In the first report, the solution processed bulk heterojuction organic photovoltaic (BHJ OPV) cells by Heeger *et al* [39] used a highly soluble fullerene derivative to achieve sufficient percolation of charges through both components. Remarkably, even after about twenty years of acceptor material research, fullerene derivatives are still one of the best performing acceptors, and certainly the most popular electron acceptors for OPV devices. Investigation and understanding of fullerene quenching of donor polymers by photo-induced charge transfer and separation processes can be used for the improvement of power conversion efficiencies in organic solar cells.
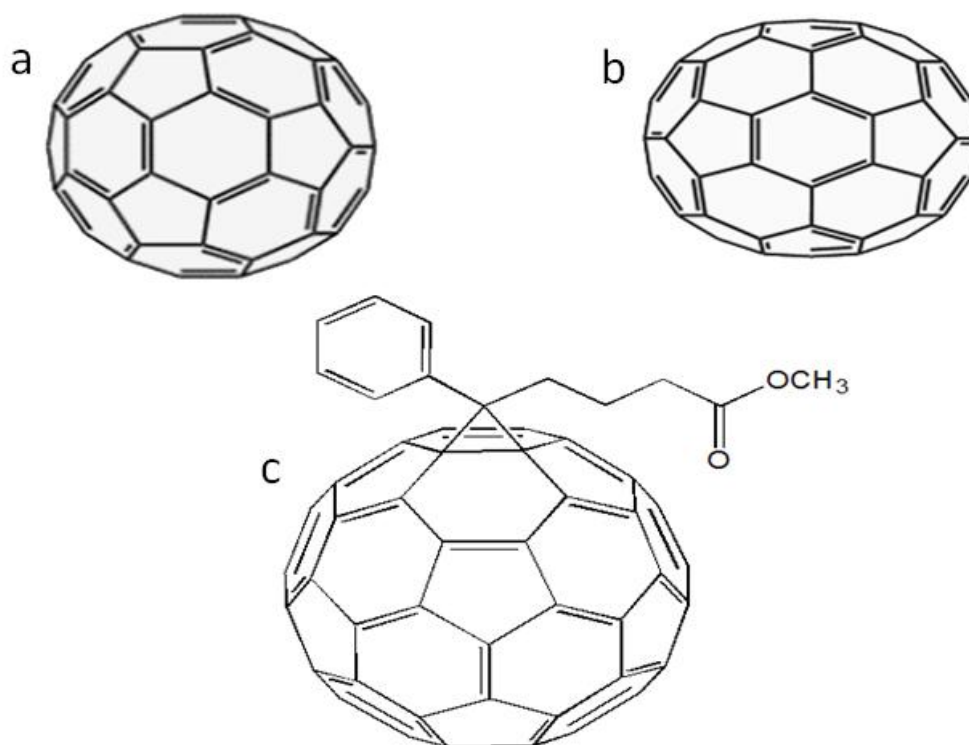
Figure 3.1: Structure of (a) fullerene C_{60}, (b) fullerene C_{70} and (c) functionalized fullerene (PCBM).
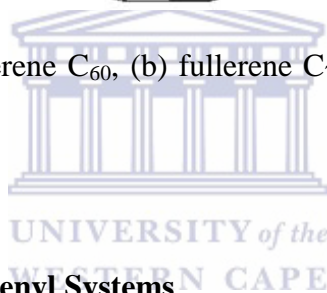
3.2 Charge Transfer in Fullerenyl Systems

A large number of the studies on charge transfer applications have been on the development of light-energy conversion systems and molecular photonic devices [51-53]. Charge transfer is an important process particularly in chemistry and biology; therefore, a good understanding of the process between a donor and an acceptor is vital. From the wide variety of donor–acceptor systems, fullerenes stands out as electron acceptor due to their unique physical properties of three-dimensional structure, delocalized π-electrons within the spherical carbon framework, small reorganization energy and low reduction potential [54-55]. These unique physical and chemical properties make the investigation of the electron transfer processes between fullerenes and donors interesting.

C_{60} fullerenes for example, readily accept up to six electrons and also form charge-transfer complexes with a variety of materials including small molecules [56-59] and polymers [60-63]. From an energetically deep lowest unoccupied molecular orbital (LUMO) level of −4.3 eV *versus* vacuum, fullerenes show a high electron affinity [55]. The high electron affinity of fullerenes favors electron transfer process from donor to fullerene when it comes in contact with organic donor having a higher lying LUMO level. The use of donors and fullerenes as acceptors in organic photovoltaic cells is appreciated not only for the affinity that exists between the donors and the surface of fullerenes but also for the capability that the donor/acceptor systems with fullerene acceptors results in photo-induced charge-separated species. The proof of photo-induced electron transfer from the excited state of a donor to fullerene C_{60} and its derivatives and the response time of charge transfer have given rise to an appreciable interest in their applications as an optical absorber or fluorescence quencher [39, 49, 64-66]. For instance, for a donor polymer blended with C_{60}, the time scale for photo-induced electron transfer is faster than the radiative or non-radiative decay of the photoexcited state [49, 66-67]. Charge transfer can be very efficient and on a faster timescale than the radiative decay in organic chromophores such as conjugated polymers with transfer rates as high as $K_{T}=10^{12}$ s^{-1} [68-70].

Photo-induced charge transfer between a donor and an acceptor can be described in six steps as follows: (i) Light absorption by the donor is followed by (ii) photo-excitation of the donor, (iii) delocalization of the excitation between the donor and acceptor, (iv) polarization of the excitation leading to partial charge transfer, (v) radical ion is formed and finally, (vi) the charge is completely separated. The donor and acceptor must be covalently bounded (intra-molecular charge transfer) or spatially very close (inter-molecular charge transfer) for electron transfer to occur. The distance between the donor and acceptor must be small enough

to permit significant coupling of their electronic wave-functions [69, 71]. Another important factor for charge separation is the energy level alignment of the participating molecules. Charge transfer is only possible if the offset between the LUMOs (for electron transfer) or the HOMOs (for hole transfer) of donor and acceptor is large enough to overcome the coulombic attraction between the charges.

A vast variety of materials like conjugated polymers [49], metal phthalocyanine [72] or porphyrins [73] undergo photo-induced electron transfer to fullerenes. The high symmetry of fullerenes which results in good contact with the donor is one of the advantages of employing fullerenes as photo-induced charge transfer acceptors. In organic photovoltaic cells for example, the photo-induced electron transfer from a donor to fullerene acceptor is followed by an efficient photo-induced hole transfer from the acceptor. This is due to the HOMO level of fullerene which is at about -6.1 eV *vs* the energy level of the vacuum [55]. The long lifetime of the charge separated state is one of the most remarkable aspects of the photo-induced charge transfer between organic donors. The photo-induced charge transfer is very fast with transfer rates above 10^{12} s^{-1} when the conditions are conducive and the back transfer that can lead to recombination is extremely slow at ambient temperature. This is believed to be as a result of instant rapid delocalization of the charges generated in the donor and acceptor π -electron systems making the possibility of recombination low [49, 74]. In the work by de la Escosura and group [75], a dyad covalently linked between Zn–phthalocyanine and a C$_{60}$ molecule was investigated. Ultrafast photo-induced charge transfer revealed by photo-induced absorption measurements and fluorescence quenching was observed. Time resolved photo-induced absorption measurements revealed the lifetime of the charge separated state to be 130 ns. Mixture of Pd–phthalocyanine compound having a strong electron accepting behavior with Zn–phthalocyanine [76] in solution resulted in a complex

61

with significantly longer lifetime of the charge separated state of 475 ns. This behavior is attributed to strong electronic coupling between the two phthalocyanine moieties, which allows photo-induced radical cation generated to move from the counter charge on the fullerene; leading to a stable charge separated state.

Very recently, Santos *et al* [77] clearly showed that efficient electron transfer takes place in *β*-substituted fullerene/donor dyad system connected through *p*-phenylenevinylene dimer. The primary component of the fullerene/donor interaction is controlled by the dispersive forces associated with π - π and weak electrostatic interaction. Predominant character of electrostatic interaction and $\pi - \pi$ interaction has been shown for the formation of supramolecular ensemble fullerene/phthalocyanine [53, 78-79]. Rate constant for charge separation, quantum yield for charge separation and different energy calculations related to electron transfer and solvent reorganization energies employed suggest photo-induced electron transfer from excited phthalocyanine to fullerene [79]. A number of works on photo-induced charge transfer from the excited state of a conducting polymer onto fullerene have been reported [49, 80-82]. Reports on ground state electron transfer between fullerenes and electron donors are also available [68]. Such electron transfer system is different from the photo-induced type that happens only upon excitation of the charge transfer donor [49, 83]. This is the reason for the interest in fullerenes for application as electron acceptors in OPVs [41, 84]. Interactions between electron donating polymers and fullerenes are particularly of importance due to the need for a fundamental understanding of the interaction mechanism of donor-acceptor components in Bulk heterojunction organic photovoltaic cell (BHJ-OPV) for improved device design and fabrication. This understanding can be achieved using photophysical and photochemical methods such as absorption, fluorescence spectral measurements and the Stern–Volmer approach for analyzing fluorescence quenching.

62

3.3   Fluorescence Quenching of Donor Polymers by C$_{60}$ Fullerene and Its Derivatives

Fluorescence quenching and decrease of luminescence lifetime for donor-acceptor when they are blended together is usually the first indication of photo-induced charge transfer. Fluorescence quenching occurs as a result of charge transfer processes from a donor to an acceptor. The decrease in fluorescence intensity of a donor with increasing fullerene concentration is associated with decrease in the quantity of free donor, which is caused by interactions between fullerene and the donor. The fluorescence intensity of a material can be reduced or quenched by a number of processes or molecular interactions. These processes or interactions can occur as a result of molecular rearrangements, during excited state reactions, energy transfer, charge transfer reactions or they may occur due to formation of complexes in the ground state. The decrease in the intensity of fluorescence is termed *fluorescence quenching*. Possible fluorescence quenching mechanisms include *collisional or dynamic quenching*, *static or complex formation quenching* or a combination of both. The process of complex formation is termed *static quenching* while quenching caused by collision of diffusion of materials is termed *collision* or *dynamic quenching*. Fluorescence quenching studies can be carried out in solution or in solid state in the form of thin film. However, for understanding of the processes taking place between a donor and acceptor during fluorescence, studies cannot be conducted in solid state since the solid state fluorescence is most often completely quenched; and as such does not give room for understanding of the interaction mechanism. It is assumed that the quenching in the solid state involve additional non-diffusional component or complex formation contributing to polymer quenching. Fluorescence quenching studies are usually carried out in solution to get an insight or understanding of the charge transfer process from the electron donor to the electron acceptor with the assumption that the same processes taking place in solution also take place in the

63

solid state. In solution, fluorescence quenching by an acceptor molecule follows the classic Stern-Volmer relationship.

$$I_o/I = 1 + K_q \tau_o [Q]$$

equation (3.1)

where I_o is the intensity of fluorescence without a quencher, I is the steady-state intensity of fluorescence at the concentration of quencher $[Q]$ [85-88], τ_o is the lifetime of the fluorophore in the absence of quencher and K_q is the quenching constant.

3.3.1 The Stern-Volmer Equation
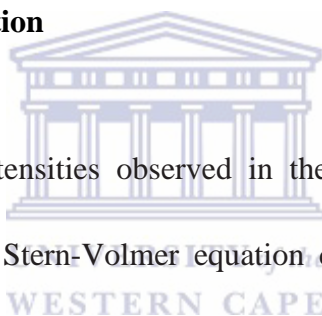
Considering the fluorescence intensities observed in the absence of quencher (I_o) and presence of quencher (I), the Stern-Volmer equation can be derived. The fluorescence intensity of a fluorophore is proportional to its concentration in the excited state $[F^*]$. Under uninterrupted light, a sustained population of excited fluorophores is formed. At this stage, $d[F^*]/dt = 0$. The differential equations describing the concentration of the fluorophore in its excited state in the absence and presence of a quencher are

$$\frac{d[F^*]}{dt} = f(t) - \gamma [F^*]_o = 0$$

equation (3.2)

$$\frac{d[F^*]}{dt} = f(t) - (\gamma + K_q [Q])[F^*] = 0$$

equation (3.3)

where $f(t)$ is the constant excitation function, $[Q]$ is quencher, and $\gamma = \tau_o^{-1}$ is the decay rate of the fluorophore in the absence of quencher

64

$$\gamma = \tau_{O}^{-1} = K_r + K_{nr}$$

$$\tau_o = \frac{1}{K_r + K_{nr}} \qquad \text{equation (3.4)}$$

where K_r is the radiative rate and K_{nr} is the non-radiative decay rate. An additional decay rate $K_q[Q]$ is observed in the presence of a quencher yielding **equation (3.5)**

$$\tau = \frac{1}{(K_r + K_{nr}) + K_q[Q]} \qquad \text{equation (3.5)}$$

Division of **equation (3.4)** by **equation (3.5)** yields the Stern-Volmer equation

$$\frac{\tau_o}{\tau} = \frac{\gamma + K_q[Q]}{\gamma} = 1 + K_q \tau_o [Q]$$

$$\tau_o / \tau = 1 + K_q \gamma^{-1} [Q]$$

$$\tau_o = \gamma^{-1}$$

$$\tau_o / \tau = 1 + K_q \tau_o [Q] \qquad \text{equation (3.6)}$$

In the case of purely dynamic quenching, $\tau_o / \tau = I_o / I$. Therefore,

$$I_o / I = 1 + K_q \tau_o [Q]$$

τ_o is the lifetime of the fluorophore in the absence of quencher, and τ is the lifetime of the fluorophore in the presence of quencher. $K_q \tau_o = K_{sv}$ is the Stern-Volmer quenching constant.

65

The constant is evaluated from the normalized plot of fluorescence intensity against the quencher concentration. Quenching data are usually presented as plots of I_o / I against $[Q]$ to yield a straight line graph with slope $= K_q \tau_o$ and intercept 1 (**Figure 3.2**). The plot is linear if either dynamic or static quenching mechanism is dominant [85-88].
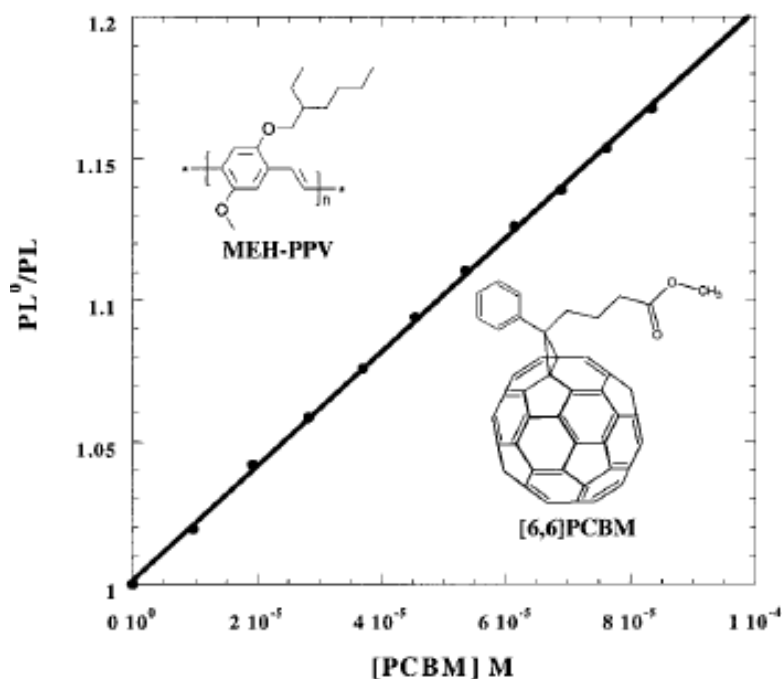
Figure 3.2: Stern–Volmer quenching plot (PL of MEH-PPV over the PL of polymer with PCBM versus the PCBM concentration). The solid line is the fit obtained from the Stern–Volmer equation. Inset: The chemical structures of MEH-PPV and PCBM. Reprinted (adapted) with permission from Ref [80], Copyright (2001) John Wiley and Sons.

3.3.2 Dynamic Quenching

Dynamic quenching occurs as a result of the diffusive encounters between the fluorophore and quencher during the lifetime of the excited state. The quencher collides with the fluorophore during the lifetime of the excited state and the quenching takes place when the

66

excited fluorophore experiences contact with an atom or molecule that can facilitate non-radiative transitions to the ground state. Upon contact with the quencher, the fluorophore returns to the ground state without emission of photon. It is a time-dependent process and usually, no permanent change or photochemical reaction occurs. In the simplest case of dynamic quenching, the Stern-Volmer equation holds according to **equation (3.7)**

$$I_o/I = 1 + K_D[Q]$$ **equation (3.7)**

The Stern-Volmer quenching constant is given by $K_D = K_q \tau_o$ for dynamic quenching.

3.3.3 Static Quenching

Static quenching, first reported by Gregorio Weber, occurs when the fluorophore forms a stable complex with the quencher. This results in quenching of the fluorescence intensity as the complex formed is non-fluorescent. It occurs as a result of the formation of a non-fluorescent ground-state complex between the fluorophore and quencher. On absorption of light, the complex immediately returns to the ground state without emission of a photon. Static quenching follows the Stern-Volmer equation according to **equation 3.8**

$$I_o/I = 1 + K_a[Q]$$ **equation (3.8)**

K_a is the association constant of the complex. The Stern-Volmer constant contains both static and dynamic components, but where static quenching is dominant, the Stern-Volmer constant is taken as the association constant, K_a, between the fluorophore and quencher [85,

67

87-88]. The Stern-Volmer quenching constant in this case is given by $K_a = K_q \tau_o$ for static quenching.

The dependence of the fluorescence on the concentration of the quencher can be derived as follows

$$F + Q = FQ \qquad \qquad \textbf{equation (3.9)}$$

$$K_a = \dfrac{FQ}{[F\,[Q\,]} \qquad \qquad \textbf{equation (3.10)}$$

$$FQ = K_a [F\,[Q\,] \qquad \qquad \textbf{equation (3.11)}$$

$$\dfrac{I_o}{I} = \dfrac{F_{tot.}}{F} = \dfrac{[F\,] + [FQ\,]}{F} = 1 + K_a [Q\,] \qquad \qquad \textbf{equation (3.12)}$$

where F is the fluorophore and Q is the quencher.

The association constant, K_a, can be used to evaluate the strength of charge transfer complex formed between fullerenes and other molecules [56, 59, 89], and fullerenes and polymers [61].

3.3.4   Differences between Dynamic and Static Quenching

In both dynamic and static quenching, molecular contact between the fluorophore and quencher is important. However, dynamic quenching only affects the excited states of the fluorophores, and as a result, no changes in the absorption spectra occur. On the other hand, static quenching results in changes in the absorption spectra. The complex as formed in static quenching is formed in the ground state resulting in perturbation of the absorption spectrum

68

of the fluorophore. Static and dynamic quenching can be distinguished from one another by various methods. It can be on the basics of their different temperature dependences, fluorescence lifetime measurement, exploring the curvature with a Stern-Volmer plot and the absorbance spectra [87, 90-93]. However, the most commonly used method to identify and differentiate between both quenching mechanisms is the fluorescence lifetime measurement [92-93]. Dynamic quenching reduces the average lifetime of the fluorophore while the fluorescence lifetime for static quenching remains unchanged with the addition of quencher [87-88]. In static quenching the complexed fluorophores are non-fluorescent, and the only observed fluorescence is from the un-complexed fluorophores. In general, for static quenching, the fluorescence lifetime remains unchanged while dynamic quenching results in decrease in the fluorescence lifetime. **Figure 3.3** [94], shows the fluorescence decay of donor protoporphyrinIX (PPIX) in the absence and presence of fullerene. The donor reveals a single exponential decay with fluorescence life-time of 11.2 ns. The fluorescence decay remained a single exponential with no change in the fluorescence lifetime as the fullerene concentration increases. This report confirmed a static quenching for the PPIX/fullerene system.

69
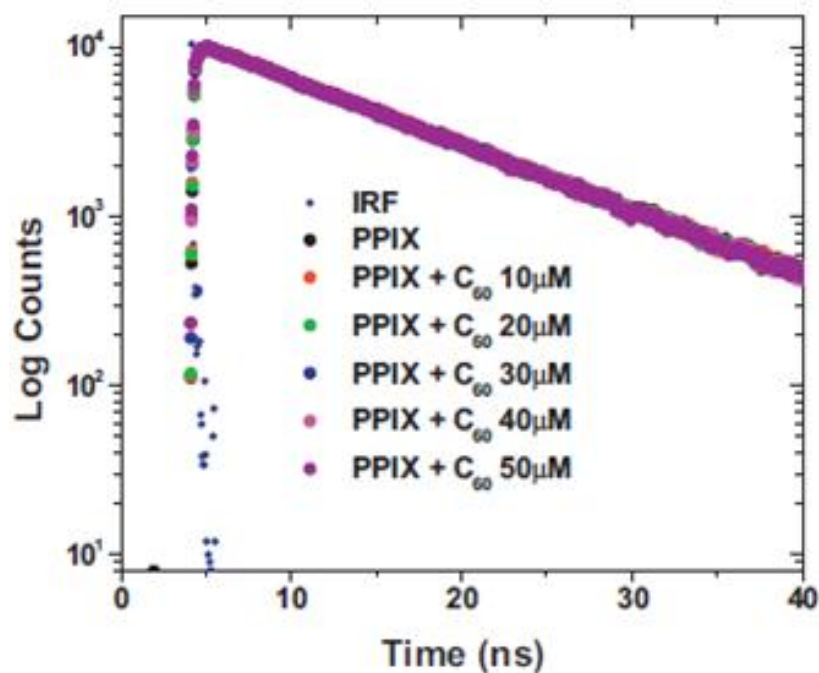
Figure 3.3: Fluorescence decay dynamics of PPIX by varying fullerene concentration. Reprinted from Synthetic Metal, 194, A. Kathiravan, Excited state electron transfer reactions of ProtoporphyrinIX with fullerene, 77 - 81, Copyright (2014), with permission from Elsevier.
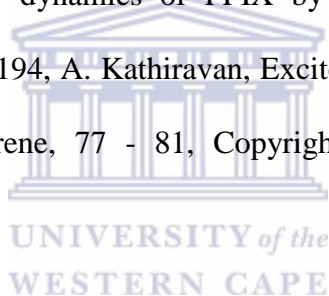
Fluorescence quenching increases with temperature for dynamic quenching while quenching decreases in static quenching. The reason for this is that diffusion rates and dynamic collision rates increase with increasing temperature, whereas; complex formation strength tends to decrease with increasing temperature. Temperature-dependant method can therefore be used to determine the exact quenching mechanism, by comparing the quenching extent at various temperatures. In most cases, both interactions are present but with one dominant. In the interaction of fullerenes with poly(*p*-phenylene ethynylene) (PPE) for example, static quenching is reportedly dominant [88].

In a system with both static and dynamic quenching simultaneously taking place, the following relation holds:

$$I_o/I = (1 + K_D[Q])(1 + K_a[Q])$$

equation (3.13)

and a plot of I_o/I against $[Q]$ yields an upward curvature due to the squared concentration of the quencher.

Figure 3.4 shows the Stern-Volmer plot for static and dynamic quenching with a slope = K intercept = 1 and quenching response to temperature.
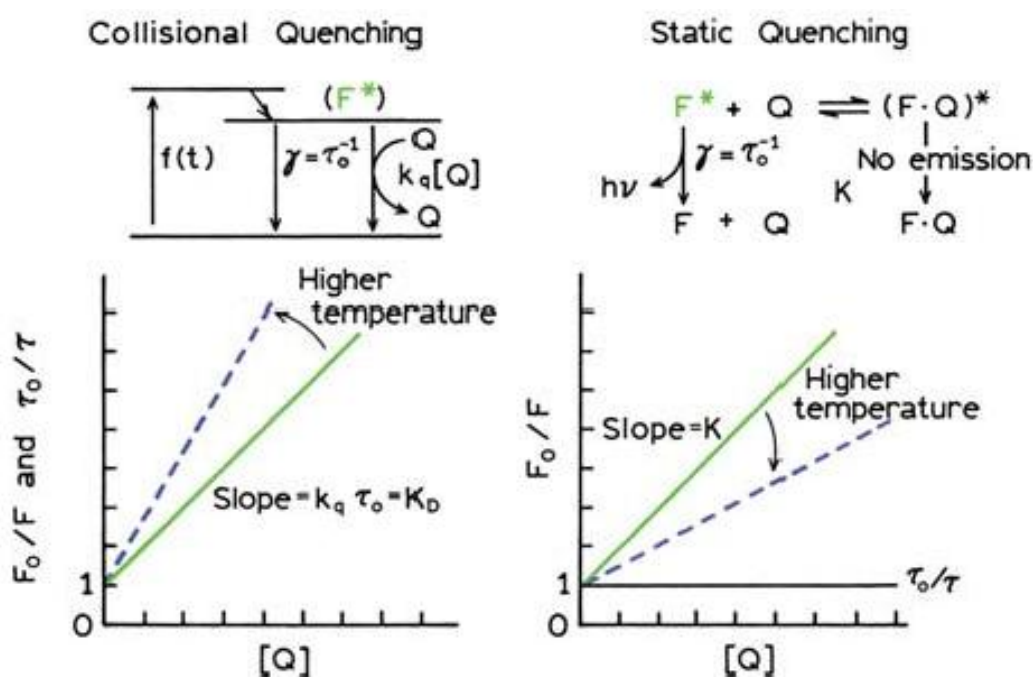
Figure 3.4: Comparison of dynamic and static quenching. Principles of fluorescence spectroscopy; quenching of fluorescence, 2006, p. 280, Joseph R. Lakowicz. "With permission of Springer".

T. Chaudhuri *et al* [95] described emission spectroscopic studies performed to study the intermolecular complexation of fullerene C_{60} and C_{70} as well as of o- and p-chloranils with meso-tetra-2-chlorophenylporphyrin(clTP) in non- interacting toluene medium. The report revealed different quenching mechanisms to be operational for these two groups of compounds. With incremental addition of the electron acceptors to a fixed concentration of the donor clTP, a progressive quenching of fluorescence intensity of the clTP was observed (**Figure 3.5**). From the report, the type of quenching mechanism operational for the two groups of acceptor on the donor clTP using temperature-dependent steady state emission studies (**Figures 3.6 A and B**) and time-resolved emission studies (**Figures 3.6 C and D**) was confirmed. From the temperature-dependent studies, the increase in temperature lowered the slope of the linear Stern-Volmer plots indicating that static quenching occurs with fullerenes (**Figure 3.6A**). This was further confirmed through the linear horizontal plot of $\tau_\circ/\tau$ against the concentration of C_{60} (**Figure 3.6D**). Chloranils on the other hand, revealed both dynamic and static quenching mechanism (**Figure 3.6B**), and the dynamic contribution was evaluated by time- resolved measurements (**Figure 3.6C**). The report by this group revealed the possibility of both quenching methods in the system and practical methods of identifying the different quenching mechanisms.
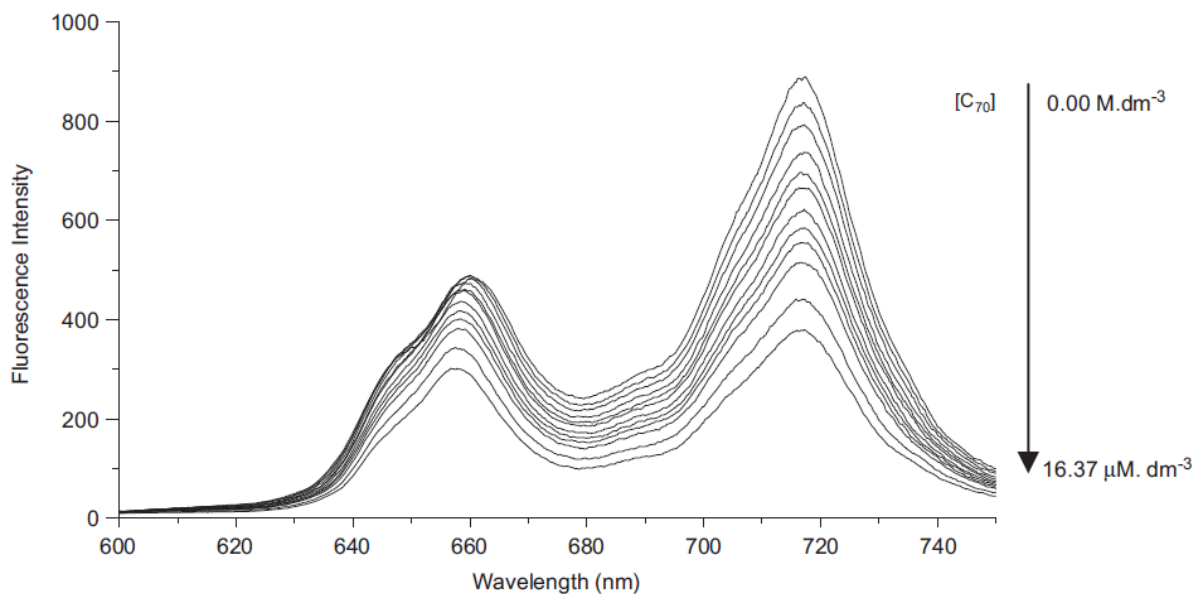
Figure 3.5: Quenching of fluorescence intensity with incremental addition of fullerene. Reprinted from J. Lumin, 130, T. Chaudhuri, S. Nath, S. Chattopadhyay, M. Banerjee and S. K. Nayak, Supramolecular interactions of meso-tetra-2-chlorophenylporphyrin with fullerenes: A luminescence study, 507 - 511., Copyright (2010), with permission from Elsevier.

73
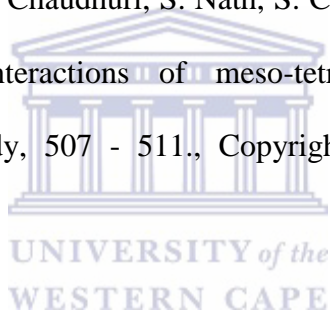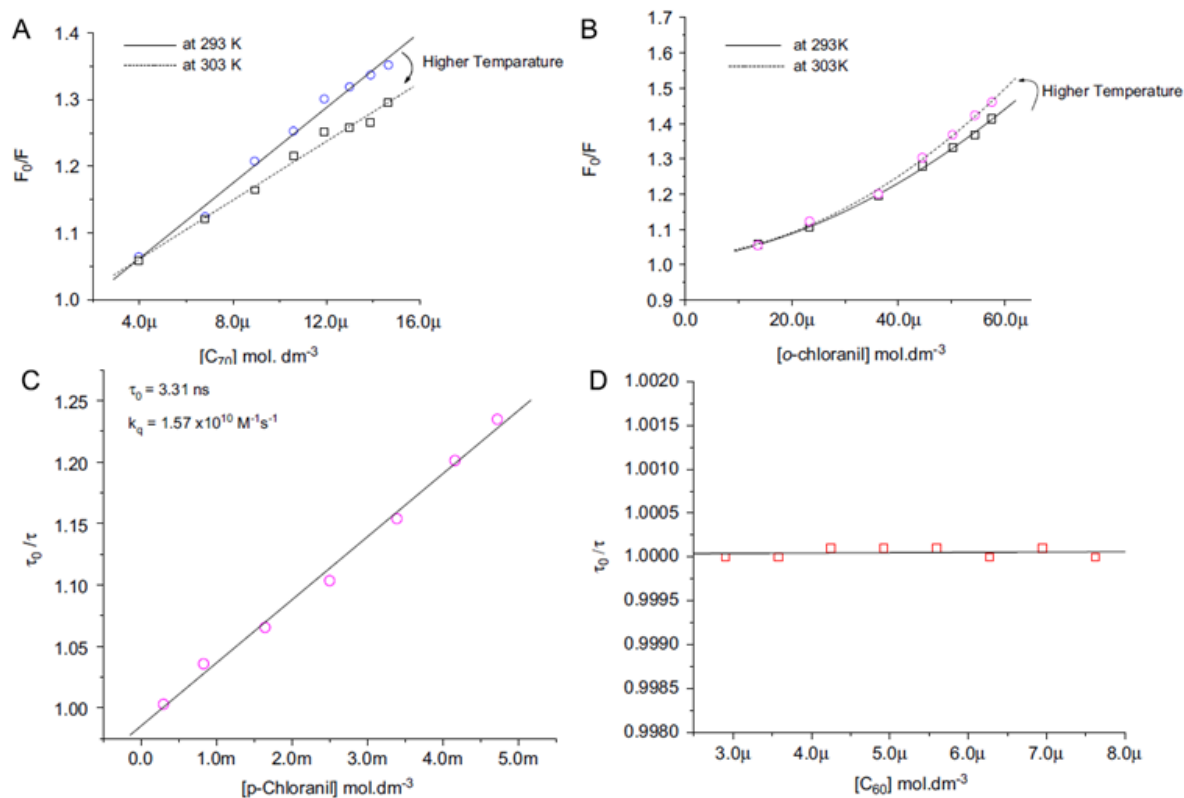
Figure 3.6: Effect of temperature on steady-state fluorescence quenching of (A) clTP/C70, (B) clTP/o-chloranil and Stern–Volmer plots of time-resolved quenching of fluorescence for (C) clTP/o-chloranil (D) clTP/C60. Reprinted from J. Lumin, 130, T. Chaudhuri, S. Nath, S. Chattopadhyay, M. Banerjee and S. K. Nayak, Supramolecular interactions of meso-tetra-2-chlorophenylporphyrin with fullerenes: A luminescence study, 507 - 511., Copyright (2010), with permission from Elsevier.

In principle, I_o/I is expected to be linearly dependent on the concentration of quencher. However, deviations from linearity may occur. The deviations can be as a result of both static and dynamic mechanisms being active in the quenching process, thereby resulting in upward curvature or positive deviation in the Stern–Volmer plot [86-87]. It can be as a result of large degree of quenching at large quencher concentrations [86-87, 96-98]. A linear Stern-Volmer plot is generally indicative of a single class of fluorophores, all equally accessible to

74

quencher. If two fluorophore or more populations are present, and one class is not accessible to quencher, then the Stern-Volmer plots deviate from linearity. Also, deviations can occur when a system contains a fluorophore in different environments, as a result of the existence of a reverse reaction or hydrogen bond complex formation with the fluorophore [97-100]. The Stern-Volmer equation can be modified to suit the deviations which results in non-linear plots [101].

3.4 Mechanism of Photo-Induced Charge Separation and Operating Principle of Organic Photovoltaic Cell

The operating principle of a photovoltaic cell is based on the ***photovoltaic effect***. The ***photovoltaic effect*** is the generation of a potential difference at the junction of two different materials in response to visible or other radiation [102]. In photovoltaic cells, the potential difference facilitates dissociation of photo-generated charge which results in light energy conversion into electrical energy. For organic photovoltaic cell to convert light energy to electrical energy, they must be able to absorb incident photons through the promotion of electrons to higher energy level and contain an internal electric field that accelerates the promoted electrons in a particular direction, resulting in an electric current. Absorption of light in the active layer results in the generation of excitons (**Figure 3.7**). Excitons consist of an electron and a hole in the LUMO and HOMO respectively [103]. The generation of exciton is followed by diffusion of the generated exciton through the material until it either decays or reaches the interface where it dissociates into electrons and holes and is transported to appropriate electrodes [104]. The hole is transported to and collected at the anode while the electron is transported to and collected at the cathode. If they are able to exit the anode and cathode before recombination, current is produced [104]. The possibility of constructing

75

donor–acceptor bulk heterojunction photodiodes from a blend of fullerene and organic semiconductor [72, 105] or even inorganic semiconductor nanoparticle [106] is the most important application of photo-induced charge transfer. The fullerene acts as the acceptor and electron transporter in the device.
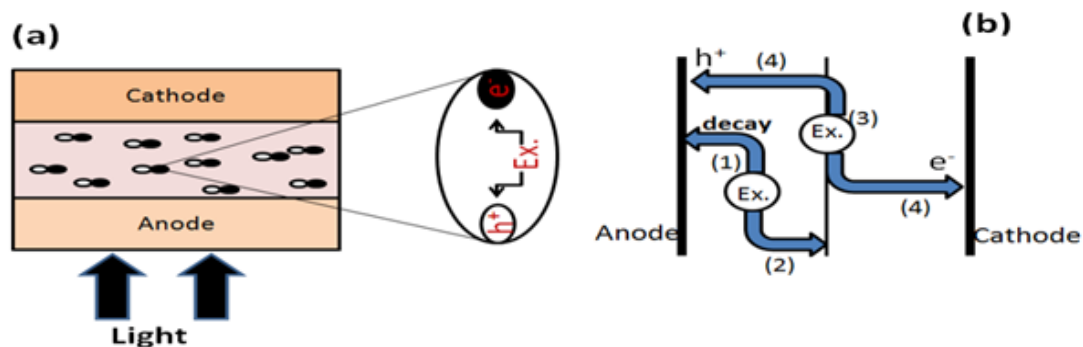
Figure 3.7: Schematic of typical organic photovoltaic cell device architecture. a. Schematic PV cell with an expanded exciton. b. Explains the main processes taking place in a. Light absorption is followed by (1) generation of excitons which can either decay if unable to reach the interface within its diffusion length or diffuse to the interface (2) diffusion of exciton to the interface, (3) dissociation of the diffused excitons at the interface into holes and electrons and (4) transfer of holes and electrons to the appropriate electrodes where they are collected and charge produced.

A donor material can transfer an electron to fullerene to generate photo-induced charge separation when the difference between the LUMO of the donor and the LUMO of fullerene is around 0.3 eV (**Figure 3.8**). This is regarded as the exciton splitting energy and it is required to guarantee the efficient charge separation at interface of donor and acceptor [107]. When a conjugated polymer absorbs light greater than π - π^* gap, it becomes excited and electron transfer to an electron deficient material is initiated [49]. Amongst all other

processes which take place during light absorption, photo-induced charge transfer is indispensible for materials to be considered for donor–acceptor bulk heterojunction solar cell application. This can be achieved by fine tuning the energy level of the donor by chemical synthesis to achieve a low band gap and an 'ideal' exciton splitting energy with a suitable acceptor. Another method or additional method of achieving unhindered photo-induced charge transfer is having an 'ideal' active layer blend morphology, solubility of the materials and cast solvent e.g the type of solvent the blend is cast from. The donor and acceptor should be properly blended by stirring since charge generation takes place at donor/acceptor interface.
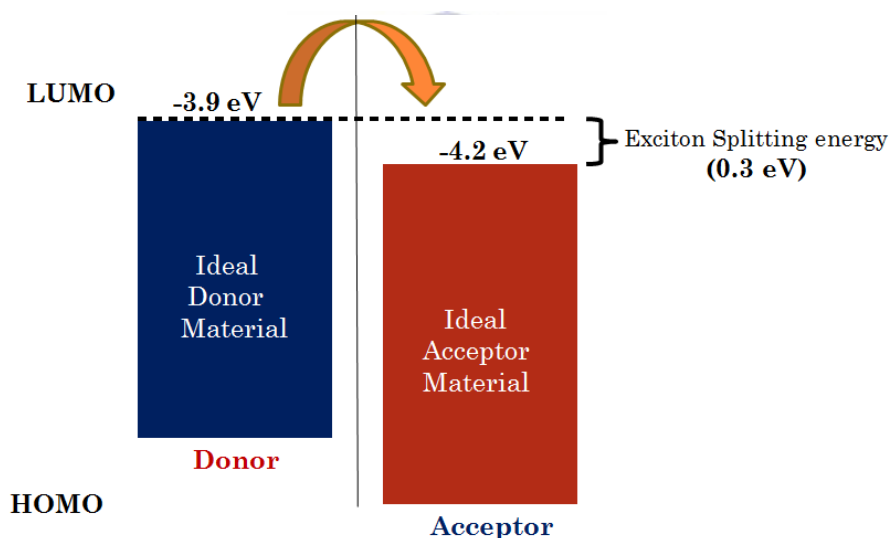
Figure 3.8: Schematic of the energy levels of an 'ideal' active layer blend.

Increase in photo-generated current and general performance was recorded in donor-acceptor BHJ OPV constructed from a blend of semiconducting polymer MDMO–PPV (poly((2-methoxy-5-(3,7-dimethyloctyloxy)-*p*-phenylene) vinylene) and PCBM by using chlorobenzene as cast solvent in place of toluene [108]. The probing of both systems via scanning electron microscopy (**Figure 3.9**) revealed a strong phase separation between the

77

two compounds in blend films cast from toluene while films cast from chlorobenzene shows a fine mixture [109-111]. The report shows that a nanoscale phase separation takes place during the film formation resulting in a nano-morphology with a significant influence on the casting conditions. Taking into account the importance of charge transfer in organic photovoltaic cells, the connection between the blend morphology and the performance of an OPV can be understood. The interfacial area where electrons and holes generated from excitations can be separated is smaller in the coarse blends casted from toluene as solvent, as shown in the photoluminescence spectra of the films (**Figure 3.10**). From the spectra, some of the PCBM in the blend cast of toluene are not available or in proximity with the donor to undergo a charge transfer. This is noticed in the strong luminescence of the PCBM in the blend cast from toluene compared to the blend cast from chlorobenzene. Therefore, the amount of charge carrier generated and the photo-generated current is lessened in the coarse phase separated blend.

78
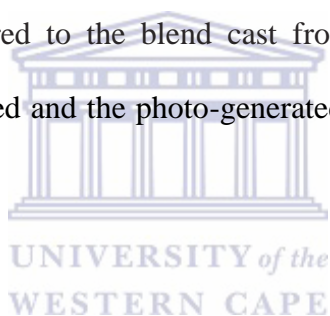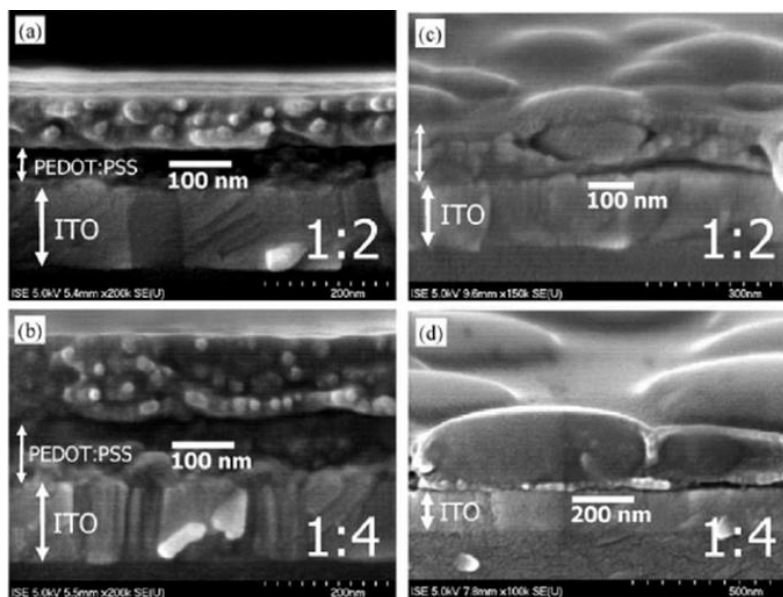
Figure 3.9: SEM cross-section images of films of MDMO–PPV:PCBM blends cast from chlorobenzene (a, b) and toluene (c, d). The blending ratio is depicted in the lower right corner. Reprinted (adapted) with permission from Ref [109], Copyright (2004) John Wiley and Sons.
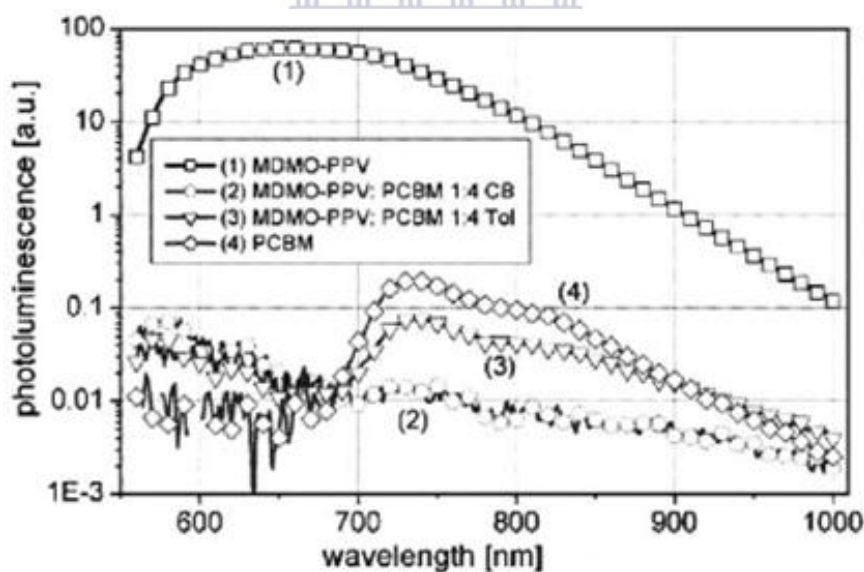
Figure 3.10: Photoluminescence spectra of thin films on glass: MDMO–PPV (1), PCBM (4) and blends of MDMO–PPV:PCBM (1:4 by weight) cast from chlorobenzene (2) and toluene (3). Reprinted (adapted) with permission from Ref [109], Copyright (2004) John Wiley and Sons.

79

3.5 Factors Responsible for Fluorescence Quenching

The factors responsible for fluorescence quenching can be summed up as concentration, side chain/molecular weight, $\pi - \pi$ interaction and effective charge transfer from donor to acceptor. The reduction in the fluorescence intensity of a donor with increasing acceptor concentration can be attributed to decrease in the quantity of free donor fluorophore. This is caused by a strong interaction between donor and acceptor. The fluorescence quenching of D-A-D-type low band gap organic dyes based on triphenylamine and benzoxadiazole/benzothiadiazole, 4,7-Bis{5-{4-{2-[4-(N,N-diphenylamino)phenyl]-1-nitrilethenyl} phenyl}-2-thienyl}-2,1,3-benzoxadiazole (BDNTBX) and 4,7-Bis{5-{4-{2-[4-(N,N-diphenylamino)phenyl]-1-nitrilethenyl}phenyl}-2-thienyl}-2,1,3-benzothiadiazole (BDNTBT) by PCBM was investigated by Zeng *et al* [112]. As the concentration of the acceptor PCBM increased, the fluorescence of both donor materials was gradually quenched, revealing a photo-induced charge transfer and separation process between the donor and acceptor. The report conformed to the linear Stern-Volmer equation at low concentration of PCBM (**Figure 3.11**).
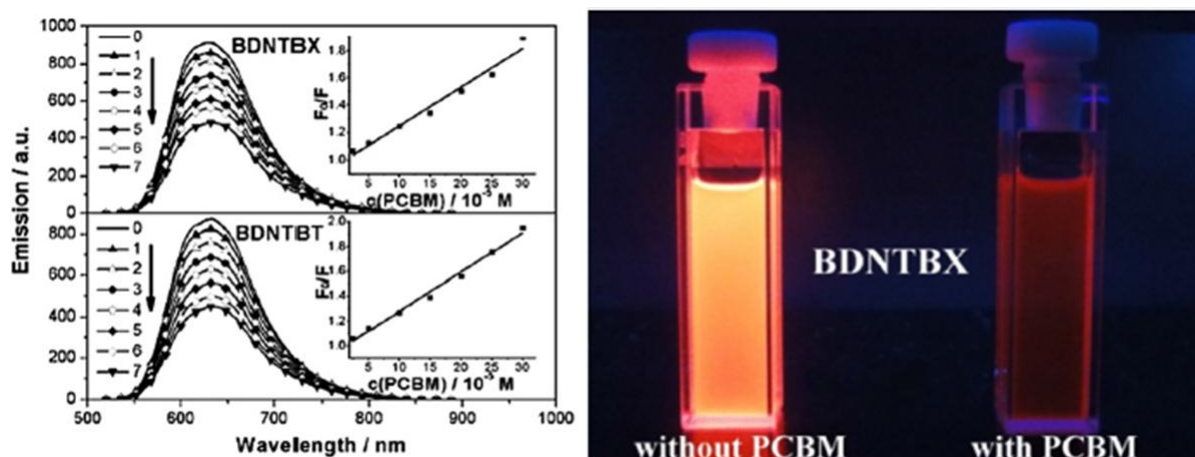
Figure 3.11: Emission spectra (left) of BDNTBX and BDNTBT ($1.0*10^{-5}$ M) in CHCl₃ with increasing concentration of PC₆₁BM ($*10^{-5}$ M): 0.0 (0), 2.5 (1), 5.0 (2), 10.0 (3), 15.0 (4), 20.0 (5), 25.0 (6), 30.0 (7). The insets are Stern-Volmer quenching plots for both compounds respectively. Fluorescence of BDNTBX without and with PCBM in CHCl₃ under irradiation (365 nm) on the setting of Panasonic DSC-TX1 camera (right). Reprinted from Dyes Pigm, 95, S. Zeng, L. Yin, X. Jiang, Y. Li and K. Li, D–A–D low band gap molecule containing triphenylamine and benzoxadiazole/benzothiadiazole units: Synthesis and photophysical properties, 229 - 235., Copyright (2012), with permission from Elsevier.

Although interactions between fullerenes and polymers can be dominated by the polymer backbone [101], side chains can play a role in the interaction of polymer and fullerene. C_{60} interactions have been shown to be stronger due to the presence of certain side chains groups [57-58, 113-116]. Also, fluorescence quenching of a donor material can be associated with molecular weight of the donor. Studies on poly(*p*-phenylene ethynylenes) (PPE) fluorescence quenching and the effects of molecular weight conducted on poly(*p*-phenylene ethynylenes) by fullerene showed constant values of Stern-Volmer constants at low molecular weight followed by an increase at higher molecular weights [101]. Generally, fullerenes interact strongly with conjugated polymers. The quenching of polymer by fullerene gives higher

81

Stern-Volmer constant values than the quenching of small molecules by fullerene. This can be ascribed to molecular weight effect where longer average diffusion lengths and increased mobility of excitons for larger molecules results in large degree of enhancement. Also, an increase in molecular weight of polymer can increase the Stern-Volmer constant if the exciton diffusion length of a polymer in solution is greater than the polymer length [117]. Quenching can also be related to the electronic properties e.g electron affinity of the acceptor. However the report by Mayorova *et al* [118] showed a series of fullerene based acceptor with similar electronic properties. These acceptors were applied individually for the quenching of MEH-PPV and revealed different quenching abilities. It can therefore be concluded that apart from electronic property like electron affinity, other factors are responsible for fluorescence quenching abilities of the acceptor materials. In the report by Campbell *et al* [101], the fluorescence quenching behavior of a series of poly(*p*-phenylene ethynylenes) of different molecular weight and side chain chemistry with C_{60} was investigated using a modified Stern–Volmer equation. The fluorescence quenching measurements showed no significant difference in the complex strength for poly(*p*-phenylene ethynylenes) with different side chains. This suggests that the interaction of C_{60} with the polymer is basically through the conjugated polymer backbone. Considering the strength of interaction and lack of side group contribution to the interaction, it is believed that π - π interactions between the C_{60} cage and PPE backbone are responsible for the comparatively strong interactions observed. The fluorescence quenching of extensively studied P3HT donor with acceptor PCBM was attributed to efficient charge transfer from P3HT to PCBM, providing a fast non-radiative decay of the excited state [119]. Alves *et al* [120] reported the fluorescence quenching of P3HT and PFT respectively by PCBM and compared the quenching observed for PCBM as acceptor with that of CdSe as acceptor both in solution and film. The Stern-Volmer constants obtained for P3HT:PCBM and PFT:PCBM were 2579 and 2711 $Lmol^{-1}$ respectively while

the constant obtained for P3HT:CdSe and PFT:CdSe are 1445 and 665 $Lmol^{-1}$ respectively. From the Stern-Volmer constant values, it is clear that PCBM have better interaction with the polymers and therefore quenches more efficiently than CdSe.

3.6   Conclusion

Fullerenes have proven to be good electron acceptors in the presence of light absorbing electron donors. Charge transfer processes are the core of the rapidly growing field of organic photovoltaic cells and the possibility of constructing donor–acceptor bulk heterojunction photodiodes from fullerenes with semiconducting materials is the most important application of photo-induced charge transfer. Amongst all other processes which take place during absorption and conversion of light energy into electrical energy, photo-induced charge transfer is crucial. The understanding of photo-induced charge transfer process is vital in the photo-physics and photochemistry of organic systems. A good understanding of this process within polymer-fullerene blend will increase the amount or quantity of absorbed photons converted into electricity. The application of fullerenes therefore, in organic photovoltaic cells as photo-induced electron acceptors and electron transport materials is indispensable. Their versatility which results from their energetic properties places them above other acceptor materials for organic photovoltaic cell applications.

3.7   References

[1]   H. W. Kroto, J. R. Heath, S. C. O'Brien, R. F. Curl and R. E. Smalley, "C_{60}: Buckminsterfullerene," *Nature,* 318 (**1985**) 162 - 163.

[2]   W. Krätschmer, L. D. Lamb, K. Fostiropoulos and D. R. Huffman, "Solid C_{60}: a new form of carbon," *Nature,* 347 (**1990**) 354 - 358.

[3]   H. W. Kroto, A. W. Allaf and S. P. Balm, "C_{60} - Buckminsterfullerene," *Chem. Revs,* 91 (**1991**) 1213-1235.

[4]   T. S. Jakubov and D. E. Mainwaring, "Interaction Between C60 Fullerene And Alkali Metals Demonstrating Superconductivity," *Procedia Chem.,* 1 (**2009**) 1584–1589.

[5]   E. J. Nicol, "Carbon-Based Superconductors," *Physics in Canada,* 67 (**2011**) 78-83.

[6]   A. Mohammad and D. A. Jyoti, "Superconductivity in Organic Materials: A Fascinating Phenomenon," *Research Journal of Chemical Sciences,* 2 (**2012**) 67-70.

[7]   M. Maria, "C_{60} Monodisperse nanoclusters - silica based thin film obtained by microemulsion technique," *ICTON-MW,* 1 (**2007**) 6-8.

[8]   G. Lee, J. H. Shim, H. Kang, K. M. Nam, H. Song and J. T. Park, "Monodisperse Pt and PtRu/C60 hybrid nanoparticles for fuel cell anode catalysts," *Chem. Commun.,* DOI: 10.1039/b911068b (**2009**) 5036–5038.

[9]   Y. Shen and T. Nakanishi, "Exotic Self-Organized Fullrene Materials Based on Uncommon Hydrophobic-Amphiphilic Approach: in Fullerenes and Other Carbon-Rich Nanostructures," *Springer,* DOI: 10.1007/430_2013_114 (**2013**) 259.

[10]   A. Mateo-Alonso, K. Iliopoulos, S. Couris and M. Prato, "Efficient Modulation of the Third Order Nonlinear Optical Properties of Fullerene Derivatives," *J. AM. Chem. Soc.,* 130 (**2008**) 1534-1535.

84

[11]   K. Lewandowska, B. Barszcz, A. Graja, A. Biadasz, B. Bursa, D. Wróbel, S.-T. Kim, T.-D. Kim and K.-S. Lee, "Molecular orientation in self-assembled layers of two functionalized fullerenes—Role of bromine atom at the end of alkyl chain," *Synth. Met.,* 162 (**2012**) 2134 – 2137.

[12]   K. Kokubo, H. Masuda, N. Ikuma, T. Mikie and T. Oshima, "Synthesis and characterization of new acetalized [60]fullerenes," *Tetrahedron Letters,* 54 (**2013**) 3510 – 3513.

[13]   K. Lewandowska, B. Barszcz, A. Graja, S. Y. Nam, Y.-S. Han, T.-D. Kim and K.-S. Lee, "Spectroscopic properties and orientation of molecules in Langmuir–Blodgett layers of selected functionalized fullerenes," *Spectrochim. Acta, Part A,* 118 (**2014**) 204–209.

[14]   S. Zottl, A. Kaiser, M. Daxner, M. Goulart, A. Mauracher, M. Probst, F. Hagelberg, S. Denifl, P. Scheier and O. Echt, "Ordered phases of ethylene adsorbed on charged fullerenes and their aggregates," *Carbon,* 69 (**2014**) 206 – 220.

[15]   M. A. lvarez-Murga and J. L. Hodeau, "Structural phase transitions of C60 under high-pressure and high-temperature," *Carbon,* 82 (**2015**) 381 - 407.

[16]   P. A. Ward, J. A. T. Jr., R. N. Compton, V. Schwartz, G. M. Veith and R. Zidan, "Evaluation of the physi- and chemisorption of hydrogen in alkali (Na, Li) doped fullerenes," *International Journal of Hydrogen Energy* 40 (**2015**) 2710 - 2716.

[17]   D. Y. Lyon, L. K. Adama, J. C. Falkner and P. J. J. Alvarez, "Antibacterial activity of fullerene water suspensions: effects of preparation method and particle size," *Environ. Sci. Tech.,* 40 (**2006**) 4360 - 4366.

[18]   Z. Mahdavifar, M. Poulad and A. Ostovan, "Electronic and stability characters of endohedral Zn@Sin and exohedral SinHn (n = 20, 30, 40, 50, 60) fullerenes: A DFT approach," *J. Mol. Liq.,* 219 (**2016**) 561 - 572.

[19]   M. Wang, L. Zhu, M. Zhou, C. Jiang and Q. Li, "High efficiency organic bulk-heterojunction solar cells applying a new system of co-additives," *Mater. Lett.,* 166 (**2016**) 227 - 230.

[20]   H. Imahori and Y. Sakata, "Fullerenes as Novel Acceptors in Photosynthetic Electron Transfer," *Eur. J. Inorg. Chem.,* 1999 (**1999**) 2445 - 2457.

[21]   D. M. Guldi, "Fullerenes: three dimensional electron acceptor materials," *Chem. Commun.,* (**2000**) 321 - 327.

[22]   E. M. Pérez and N. Martín, "Molecular tweezers for fullerenes," *Pure Appl. Chem.,* 82 (**2010**) 523 - 533.

[23]   H. Imahori and S. Fukuzumi, "Porphyrin- and Fullerene-Based Molecular Photovoltaic Devices," *Adv. Funct. Mater.,* 14 (**2004**) 525 - 536.

[24]   F. Wudl, "The Chemical Properties of Buckminsterfullerene (C_{60}) and the Birth and Infancy of Fulleroids," *Acc. Chem.Res.,* 25 (**1992**) 157 - 161.

[25]   M. Prato, "Fullerene materials," *Top. Curr. Chem.,* 199 (**1999**) 173 - 187.

[26]   S. Bosi, T. Da Ros, G. Spalluto and M. Prato, "Fullerene derivatives: an attractive tool for biological applications," *Eur. J. Med. Chem.,* 38 (**2003**) 913 - 923.

[27]   C. Bingel, *Chem. Ber./Recl.,* 126 (**1993**) 1957 - 1959.

[28]   M. Prato, T. Suzuki, H. Foroudian, Q. Li, K. Khemani, F. Wudl, J. Leonetti, R. D. Little, T. White, B. Rickborn, S. Yamago and E. Nakamura, "[3 + 2] and [4 + 2] Cycloadditions of fullerene C_{60}," *J. Am. Chem. Soc.,* 114 (**1993**) 1594 - 1595.

[29]   M. Prato, Q. Chan Li, F. Wudl and V. Lucchini, "Addition of azides to fullerene C60: synthesis of azafulleroids," *J. Am. Chem. Soc. ,* 115 (**1993**) 1148 - 1150.

[30]   T. Tago, T. Minowa, Y. Okada and J. Nishimura, "Reaction of fullerene with benzocyclobutene homologs," *Tetrahedron Lett.,* 4 (**1993**) 8461 - 8464.

[31] H. H. Wang, J. A. Schlueter, A. C. Cooper, J. L. Smart, M. E. Whitten, U. Geiser, K. D. Carlson, J. M. Williams, U. Welp, J. D. Dudek and M. A. Caleca, "Fullerene Derivatives and Fullerene Superconductors," *J. Phys. Chem. Solids,* 54 (**1993**) 1655 - 1666.

[32] M. Prato, "[60]Fullerene chemistry for materials science applications," *J. Mater. Chem.,* 7 (**1997**) 1097 - 1109.

[33] P. A. Troshin and R. N. Lyubovskaya, "Organic chemistry of fullerenes: the major reactions, types of fullerene derivatives and prospects for their practical use," *Russ. Chem. Rev.,* 77 (**2008**) 305 - 349

[34] M. D. Tzirakis and M. Orfanopoulos, "Radical Reactions of Fullerenes: From Synthetic Organic Chemistry to Materials Science and Biology," *Chem. Rev.,* 113 (**2013**) 5262−5321.

[35] N. O. Mchedlov-Petrossyan, "Fullerenes in Liquid Media: An Unsettling Intrusion into the Solution Chemistry," *Chem. Rev.,* 113 (**2013**) 5149 - 5193.

[36] O. V. Boltalina, A. A. Popov, I. V. Kuvychko, N. B. Shustova and S. H. Strauss, "Perfluoroalkylfullerene," *Chem. Rev.,* 115 (**2015**) 1051-1105.

[37] W. Yan, S. M. Seifermann, P. Pierratd and S. Bräse, "Synthesis of highly functionalized C_{60} fullerene derivatives and their applications in material and life sciences," *Org. Biomol. Chem.,* 13 (**2015**) 25 - 54.

[38] S. S. Babu, H. Möhwald and T. Nakanishi, "Recent progress in morphology control of supramolecular fullerene assemblies and its applications," *Chem. Soc. Rev.,* 39 (**2010**) 4021 - 4035.

[39] G. Yu, J. Gao, J. C. Hummelen, F. Wudl and A. J. Heeger, "Polymer photovoltaic cells: enhanced efficiencies via a network of internal donor−acceptor heterojunctions," *Science,* 270 (**1995**) 1789 - 1791.

[40]   C. J. Brabec, A. Cravino, D. Meissner, N. S. Sariciftci, T. Fromherz, M. T. Rispens, L. Sanchez and J. C. Hummelen, "Origin of the Open Circuit Voltage of Plastic Solar Cells," *Adv. Funct. Mater.,* 11 (**2001**) 374 - 380.

[41]   C. J. Brabec, N. S. Sariciftci and J. C. Hummelen, "Plastic Solar Cells," *Adv. Funct. Mater.,* 11 (**2001**) 15 - 26.

[42]   G. Li, V. Shrotriya, J. Huang, Y. Yao, T. Moriarty, K. Emery and Y. Yang, "High-efficiency solution processable polymer photovoltaic cells by self-organization of polymer blends," *Nat. Mater.,* 4 (**2005**) 864 - 868.

[43]   W. Ma, C. Yang, X. Gong, K. Lee and A. J. Heeger, "Thermally Stable, Efficient Polymer Solar Cells with Nanoscale Control of the Interpenetrating Network Morphology," *Adv. Funct. Mater.,* 15 (**2005**) 1617 - 1622.

[44]   Y. Kim, S. Cook, S. M. Tuladhar, S. A. Choulis, J. Nelson, J. R. Durrant, D. D. C. Bradley, M. Giles, I. McCulloch, C.-S. Ha and M. Ree, "A strong regioregularity effect in self-organizing conjugated polymer films and high-efficiency polythiophene:fullerene solar cells," *Nat. Mater.,* 5 (**2006**) 197 - 203.

[45]   O. Ito, "Electron-Transfer Processes of Fullerenes Studied with Time-Resolved Spectroscopies. In Fullerenes, Principles and Applications," *2nd ed.; Langa, F., Nierengarten, J.-F., Eds.; RCS Publishing: Cambridge, UK,,* Vol. 2, Chapt. 8 (**2012**) pp. 270 - 328.

[46]   L. Wang, W.-Y. Wang, X.-Y. Fang, C.-L. Zhu and Y.-Q. Qiu, "Intramolecular photo-induced electron transfer in nonlinear optical chromophores: Fullerene (C_{60}) derivatives," *Org. Electron.,* 33 (**2016**) 290 - 299.

[47]   F. D'Souza and O. Ito, "Electron Transfer in Self-assembled Supramolecular Fullerene Based Donor-Acceptor Conjugates. In Handbook of Organic Electronics

and Photonics," *Nalwa, H.R., Ed.; American Scientific Publishers: Valencia, CA, USA,* Vol. 1, Chapt. 13 (**2008**) pp. 485 - 521.

[48]   F. D'Souza and O. Ito, "Tetrapyrrole-Nanocarbon Hybrids: Self-Assembly and Photoinduced Electron Transfer. In Handbook of Porphyrin Science," *Kadish, K.M., Smith, K.M., Guilard, R., Eds.; World Scientific Publishing: Singapore,* Vol. 1 (**2010**) pp. 307 - 437.

[49]   N. S. Sariciftci, L. Smilowitz, A. J. Heeger and F. Wudl, "Photoinduced electron transfer from a conducting polymer to buckminsterfullerene," *Science,* 258 (**1992**) 1474 - 1476.

[50]   O. Ito and F. D'Souza, "Recent Advances in Photoinduced Electron Transfer Processes of Fullerene-Based Molecular Assemblies and Nanocomposites," *Molecules,* 17 (**2012**) 5816 - 5835.

[51]   D. Kreher, M. Cariou, S.-G. Liu, E. Levillain, J. Veciana, C. Rovira, A. Gorguesa and P. Hudhomme, "Rigidified tetrathiafulvalene–[60]fullerene assemblies: towards the control of through-space orientation between both electroactive units " *J. Mater. Chem.,* 12 (**2002**) 2137 - 2159.

[52]   A. Gorgues, P. Hudhomme and M. Sallé, "Highly Functionalized Tetrathiafulvalenes: Riding along the Synthetic Trail from Electrophilic Alkynes," *Chem. Rev.,* 104 (**2004**) 5151 - 5184.

[53]   M. E. El-Khouly, O. Ito, P. M. Smith and F. D'Souza, "Intermolecular and supramolecular photoinduced electron transfer processes of fullerene– porphyrin/phthalocyanine systems," *J. Photochem. Photobio. C: Photochem. Rev.,* 5 (**2004**) 79 - 104.

[54]   R. E. Haufler, J. Conceicao, L. P. F. Chibante, Y. Chai, N. E. Byrne, S. Flanagan, M. M. Haley, S. C. O'Brien, C. Pan, Z. Xiao, W. E. Billups, M. A. Ciufolini, R. H.

89

Hauge, J. L. Margrave, L. J. Wilson, R. F. Curl and R. E. Smalley, "Effcicient Produetion of C_{60} (Buckminsterfullerene), $C_{60}H_{36}$, and the Solvated Buckide Ion," *J. Phys. Chem.,* 94 (**1990**) 8634 - 8636.

[55] P. M. Allemand, A. Koch, F. Wudl, Y. Rubin, F. Diederich, M. M. Alvarez, S. J. Anz and R. L. Whetten, "Two Different Fullerenes Have the Same Cyclic Voltammetry," *J . Am. Chem. Soc,* 113 (**1991**) 1050 - 1051.

[56] Y. Wang, "Photophysical properties fo fullerenes and fullerene/N,Ndiethylaniline charge-transfer complexes," *J. Phys. Chem.,* 96 (**1992**) 764 - 767.

[57] R. D. Scurlock and P. R. Ogilby, "Excited-state charge-transfer complexes formed between C60 and substitute naphthalenes," *J. Photochem. Photobio. A: Chem.,* 91 (**1995**) 21 - 25.

[58] S. P. Sibley, Y. T. Nguyen, R. L. Campbell and H. B. Silber, "Spectrophotometric studies of complexation of C_{60} with aromatic hydrocarbons," *Spectrochim. Acta, Part A,* 53 (**1997**) 679 - 684.

[59] J. L. Qiao, Q. J. Gong, L. M. Du and W.J. Jin, "Spectroscopic study on the photoinduced reaction of fullerene C60 with aliphatic amines and its dynamics-strong short wavelength fluorescence from the adducts," *Spectrochim. Acta, Part A,* 57 (**2001**) 17 - 25.

[60] I. Sapurina, M. Mokeev, V. Lavrentev, V. Zgonnik, M. Trchova, D. Hlavata and J. Stejskail, "Polyaniline complex with fullerene C_{60}," *Eur. Polym. J.,* 36 (**2000**) 2321 - 2326.

[61] Y. Yamaguchi, S. Kobayashi, N. Amita, T. Wakamiya, Y. Matsubara, K. Sugimoto and Z. Yoshida, "Creation of nanoscale oxaarenecyclynes and their C60 complexes," *Tetrahedron Lett.,* 43 (**2002**) 3277 - 3280.

[62]   M. Gutierrez-Nava, H. Nierengarten, P. Masson, A. Van Dorsselaer and J.-F. Nierengarten, "A supramolecular oligophenylenevinylene–C60 conjugate," *Tetrahedron Lett.,* 44 (**2003**) 3043 - 3046.

[63]   A. Laiho, R. H. A. Ras, S. Valkama, J. Ruokolainen, R. Sterbacka and O. Ikkala, "Control of self-assembly by charge-transfer complexation between C60 fullerene and electron donating units of block copolymers," *Macromolecules,* 39 (**2006**) 7648 - 7653.

[64]   B. Kraabel, C. H. Lee, D. McBranch, D. Moses, N. S. Sariciftci and A. J. Heeger, "Ultrafast Photoinduced Electron Transfer in Conducting Polymer Buckminsterfullerene Composites," *Chem. Phys. Lett.,* 213 (**1993**) 389 - 394.

[65]   A. J. Heeger, F. Wudl, N. S. Sariciftci, R. A. J. Janssen and N. Martin, "Photoinduced electron transfer between conjugated polymers and a homologous series of TCNQ derivatives," *Journal De Physique,* 16 (**1996**) 2151 - 2158.

[66]   C. J. Brabec, G. Zerza, G. Cerullo, S. De Silvestri, S. Luzzati, J. C. Hummelen and S. Sariciftci, "Tracing photoinduced electron transfer process in conjugated polymer/fullerene bulk heterojunctions in real time," *Chem. Phys. Lett.,* 340 (**2001**) 232 - 236.

[67]   N. S. Sariciftci and A. J. Heeger, "Reversible, Metastable, Ultrafast Photoinduced Electron Transfer from Semiconducting Polymers to Buckminsterfullerene and in the Corresponding Donor Acceptor Heterojunctions," *Int. J. Mod. Phys. B,* 8 (**1994**) 237 - 274.

[68]   S. Morita, A. A. Zakhidov and K. Yoshino, "Doping effect of buckminsterfullerene in conducting polymer: Change of absorption spectrum and quenching of luminescence," *Solid State Communications,* 82 (**1992**) 249 - 252.

[69] M. J. Rice and Y. N. Gartstein, "Theory of photoinduced charge transfer in a molecularly doped conjugated polymer," *Phys. Rev. B,* 53 (**1996**) 10764.

[70] B. Kraabel, J. C. Hummelen, D. Vacar, D. Moses, N. S. Sariciftci, A. J. Heeger and F. Wudl, "Subpicosecond photoinduced electron transfer from conjugated polymers to functionalized fullerenes," *J. Chem. Phys.,* 104 (**1996**) 4267 - 4273.

[71] M. W. Wu and E. M. Conwell, "Theory of photoinduced charge transfer in weakly coupled donor–acceptor conjugated polymers: application to an MEH–PPV:CN–PPV pair," *Chem. Phys.,* 227 (**1998**) 11 - 17.

[72] T. Tsuzuki, Y. Shirota, J. Rostalski and D. Meissner, "The Effect of Fullerene Doping on Photoelectric Conversion Using Titanyl Phthalocyanine and a Perylene Pigment," *Sol. Energy Mater. Sol. Cells,* 61 (**2000**) 1 - 8.

[73] K. C. Hwang and D. Mauzerall, "Photoinduced electron transport across a lipid bilayer mediated by C_{70}," *Nature,* 361 (**1993**) 138 - 140.

[74] J. G. Muller, J. M. Lupton, J. Feldmann, U. Lemmer, M. C. Scharber, N. S. Sariciftci, C. J. Brabec and U. Scherf, "Ultrafast dynamics of charge carrier photogeneration and geminate recombination in conjugated polymer:fullerene solar cells," *Phys. Rev. B,* 72 (**2005**) 195208.

[75] A. de la Escosura, M. V. Martinez-Diaz, D. M. Guldi and T. Torres, "Stabilization of Charge-Separated States in Phthalocyanines–Fullerene Ensembles through Supramolecular Donor–Acceptor Interactions," *J. Am. Chem. Soc.,* 128 (**2006**) 4112 - 4118.

[76] A. de la Escosura, M. V. Martinez-Diaz, P. Thordarson, A. E. Rowan, R. J. M. Nolte and T. Torres, "Donor–acceptor phthalocyanine nanoaggregates," *J. Am. Chem. Soc.,* 125 (**2003**) 12300 - 12308.

[77]   J. Santos, B. M. Illescas, M. Wielopolski, A. M. G. Silva, A. C. Tome, D. M. Guldi and N. Martın, "Efficient electron transfer in ß-substituted porphyrin-C60 dyads connected through a p- phenylenevinylene dimer," *Tetrahedron,* 64 (**2008**) 11404 - 11408.

[78]   M. Quintiliani, A. Kahnt, T. Wölfle, W. Hieringer, P. Vázquez, A. Görling, D. M. Guldi and T. Torres, "Synthesis and Photoinduced Electron-Transfer Properties of Phthalocyanine–[60]Fullerene Conjugates," *Chem. Eur. J.,* 14 (**2008**) 3765 - 3775.

[79]   A. Ray, H. Pal and S. Bhattacharya, "Photophysical investigations on supramolecular fullerene/phthalocyanine charge transfer interactions in solution," *Spectrochim. Acta, Part A: Mol. Biomol. Spect.,* 17 (**2014**) 686 - 695.

[80]   J. Wang, D. Wang, D. Moses and A. J. Heeger, "Dynamic Quenching of 5-(2'-Ethyl-hexyloxy)-*p*-Phenylene Vinylene (MEH-PPV) by Charge Transfer to a C60 Derivative in Solution," *J. Appl. Polym. Sci.,* 82 (**2001**) 2553 - 2557.

[81]   H. Lin, Y. Weng, H. Huang, Q. He, M. Zheng and F. Bai, "Photoinduced partial charge transfer between conjugated polymer and fullerene in solutions " *Appl. Phys. Lett.,* 84 (**2004**) 2980.

[82]   D. Tenery, J. G. Worden, Z. Hu and A. J. Gesquiere, "Single particlespectroscopyoncompositeMEH-PPV/PCBMnanoparticles," *J. Lumin.,* 129 (**2009**) 423 - 429.

[83]   N. S. Sariciftci and A. J. Heeger, "Photophysics, Charge Separation and Associated Device Applications of Conjugated Polymer/Fullerene Composites, in Handbook of Organic Conductive Molecules and Polymers," *ed. H. S. Nalwa, John Wiley & Sons, New York,* vol. 1 (**1997**) pp. 413 - 455.

[84]   H. Hoppe and N. S. Sariciftci, "Organic solar cells: an overview," *J. Mater. Res.,* 19 (**2004**) 1924 - 1945.

[85]   M. F. Acquavella, M. E. Evans, S. W. Farraher, C. J. Névoret and C. J. Abelt, "Static and dynamic fluorescence quenching of a dicyanoanthracene-capped β-cyclodextrin," *J. Chem. Soc., Perkin Trans. 2,* (**1995**) 385 - 388.

[86]   C. D. Geddes, "Optical halide sensing using fluorescence quenching: theory, simulations and applications – a review," *Meas. Sci. Tech.,* 12 (**2001**) R53 - R88.

[87]   J. R. Lakowicz, *Principles of Fluorescence Spectroscopy, Third Edition, Springer, New York, USA,* (**2006**)

[88]   T. A. Skotheim and J. R. R. (Eds.), *Conjugated Polymers: Theory, Synthesis, Properties, and Characterization, Third Edition, CRC Press, Boca Raton, USA,* (**2006**)

[89]   H. A. Benesi and J. H. Hildebrand, "A spectrophotometric investigation of the interaction of iodine with aromatic hydrocarbons," *J. AM. Chem. Soc.,* 71 (**1949**) 2703 - 2707.

[90]   Y. C. Bai, F. C. Wu, C. Q. Liu, J. Y. Guo, P. Q. Fu, W. Li and B. S. Xing, "Interaction between carbamazepine and humic substances: a fluorescence spectroscopy study," *Environ. Toxicol. Chem.,* 27 (**2008**) 95 - 102.

[91]   Y. C. Bai, F. C. Wu, C. Q. Liu, W. Li, J. Y. Guo, P. Q. Fu, B. S. Xing and J. Zheng, "Ultraviolet absorbance titration for determining stability constants of humic substances with Cu(II) and Hg(II)," *Anal. Chim. Acta,* 616 (**2008**) 115 - 121.

[92]   H. M. Marwani, M. Lowry, P. Keating, I. M. Warner and R. L. Cook, "Segmented frequency-domain fluorescence lifetime measurements: minimizing the effects of photobleaching within a multi-component system," *J. Fluor.,* 17 (**2007**) 687 - 699.

[93]   H. M. Marwani, M. Lowry, B. Xing, I. M. Warner and R. L. Cook, "Frequency domain fluorescence lifetime measurements via frequency segmentation and

94

recombination as applied to pyrene with dissolved humic materials," *J. Fluor.,* 19 (**2009**) 41 - 51.

[94]   A. Kathiravan, "Excited state electron transfer reactions of ProtoporphyrinIX with fullerene," *Synth. Met.,* 194 (**2014**) 77 - 81.

[95]   T. Chaudhuri, S. Nath, S. Chattopadhyay, M. Banerjee and S. K. Nayak, "Supramolecular interactions of meso-tetra-2-chlorophenylporphyrin with fullerenes: A luminescence study," *J. Lumin.,* 130 (**2010**) 507 - 511.

[96]   J. Keizer, "Nonlinear fluorescence quenching and the origin of positive curvature in Stern–Volmer Plots," *J. AM. Chem. Soc.,* 105 (**1983**) 1494 - 1498.

[97]   J. R. Lakowicz, *Principles of Fluorescence Spectroscopy, 1st Ed., Plenum Press, New York, London,* (**1983**)

[98]   B. Valeur, *Molecular Fluorescence: Principles and Application Wiley-VCH, Weinheim,* (**2002**)

[99]   T. Htun, "A Negative Deviation from Stern–Volmer Equation in Fluorescence Quenching," *J. Fluor.,* 14 (**2004**) 217 - 222.

[100] A. B. Naik, L. R. Naik, J. S. Kadadevarmath, H. Pal and V. Jayathirtha Rao, "Fluorescence quenching of anthrylvinyl acetate by carbon tetrachloride," *J. Photochem. Photobio. A: Chem.,* 214 (**2010**) 145 - 151.

[101] K. Campbell, A. Zappas, U. Bunz, Y. S. Thio and D. G. Bucknall, "Fluorescence quenching of a poly(para-phenylene ethynylenes) by C60 fullerenes," *J. Photochem. Photobio. A: Chem.,* 249 (**2012**) 41 - 46.

[102] J. Bisquert, D. Cahen, G. Hodes, S. Rühle and A. Zaban, "Physical Chemical Principles of Photovoltaic Conversion with Nanoparticulate, Mesoporous Dye-Sensitized Solar Cells," *J. Phys. Chem. B,* 108 (**2004**) 8106 - 8118.

[103] A. I. Hochbaum and P. Yang, "Semiconductor Nanowires for Energy Conversion," *Chem. Rev.,* 110 (**2010**) 527 - 546.

[104] K. Feron, W. J. Belcher, C. J. Fell and P. C. Dastoor, "Organic Solar Cells: Understanding the Role of Förster Resonance Energy Transfer," *Int. J. Mol. Sci.,* 13 (**2012**) 17019 - 17047.

[105] N. S. Sariciftci, D. Braun, C. Zhang, V. I. Srdanov, A. J. Heeger, G. Stucky and F. Wudl, "Semiconducting polymer–buckminsterfullerene heterojunctions: Diodes, photodiodes and photovoltaic cells," *Appl. Phys. Lett.,* 62 (**1993**) 585 - 587.

[106] E. Arici, N. S. Sariciftci and D. Meissner, "Hybrid Solar Cells based on Nanoparticles of CuInS$_2$ in Organic Matrices," *Adv. Funct. Mater.,* 13 (**2003**) 165 - 171.

[107] B. C. Thompson and J. M. J. Frechet, "Polymer–Fullerene Composite Solar Cells," *Angew. Chem. Int. Ed.,* 47 (**2008**) 58 – 77.

[108] S. E. Shaheen, C. J. Brabec, N. S. Sariciftci, F. Padinger, T. Fromherz and J. C. Hummelen, "2.5% efficient organic plastic solar cells," *Appl. Phys. Lett.,* 78 (**2001**) 841 - 843.

[109] H. Hoppe, M. Niggemann, C. Winder, J. Kraut, R. Hiesgen, A. Hinsch, D. Meissner and N. S. Sariciftci, "Nanoscale morphology of conjugated polymer/fullerene based bulk-heterojunction solar cells," *Adv. Funct. Mater,* 14 (**2004**) 1005 - 1011.

[110] H. Hoppe, T. Glatzel, M. Niggemann, A. Hinsch, M. C. Lux-Steiner and N. S. Sariciftci, "Kelvin probe force microscopy study on conjugated polymer/fullerene bulk heterojunction organic solar cells," *Nano Lett.,* 5 (**2005**) 269 - 274.

[111] H. Hoppe and N. S. Sariciftci, "Morphology of polymer/fullerene bulk heterojunction solar cells," *J. Mater. Chem.,* 16 (**2006**) 45 - 61.

[112]   S. Zeng, L. Yin, X. Jiang, Y. Li and K. Li, "D-A-D low band gap molecule containing triphenylamine and benzoxadiazole/benzothiadiazole units: Synthesis and photophysical properties," *Dyes Pigm.,* 95 (**2012**) 229 - 235.

[113]   R. S. Ruoff, D. S. Tse, R. Malhotra and D. C. Lorents, "Solubilty of C_{60} in a Variety of Solvents," *J. Phys. Chem.,* 97 (**1993**) 3379 - 3383.

[114]   R. Seshadri, F. D'Souza, V. Krishnan and C. N. R. Rao, "Electron donor–acceptor complexes of the fullerenes C_{60} and C_{70} with amines," *Chem. Letts.,* (**1993**) 217 - 220.

[115]   K. M. Kadish and R. S. Ruoff (Eds.), *Fullerenes: Chemistry, Physics, and Technology, Wiley-Interscience, New York, USA,* (**2000**)

[116]   C. M. Hansen and A. L. Smith, "Using Hansen solubility parameters to correlate solubility of C60 fullerenes in organic solvents and in polymers," *Carbon,* 42 (**2004**) 1591 - 1597.

[117]   Q. Zhou and T. M. Swager, "Methodology for Enhancing the Sensitivity of Fluorescent Chemosensors: Energy Migration in Conjugated Polymers," *J. Am. Chem. Soc.,* 117 (**1995**) 7017 - 7018.

[118]   J. Y. Mayorova, S. L. Nikitenko, P. A. Troshin, S. M. Peregudova, A. S. Peregudov, M. G. Kaplunov and R. N. Lyubovskay, "Synthesis and investigation of fullerene-based acceptor materials," *Mendeleev Commun.,* 17 (**2007**) 175 - 177.

[119]   Z. Hu, D. Tenery, M. S.Bonner and A. J. Gesquiere, "Correlation between spectroscopic and morphological properties of composite P3HT/PCBM nanoparticles studied by single particle spectroscopy," *J. Lumin.,* 130 (**2010**) 771 - 780.

[120]   J. P. d.-C. Alves, J. N. d. Freitas, T. D. Z. Atvars and A. F. Nogueira, "Photophysical and photovoltaic properties of a polymer–fullerene system containing CdSe nanoparticles," *Synth. Met.,* 164 (**2013**) 69 - 77.

CHAPTER FOUR

RESEARCH MATERIALS AND METHODOLOGY

4   Introduction

This chapter gives details of the following:

- Materials: Information on all the materials used, including source and assay.

- Methodology: Research design and a general overview of all the sequential steps taken to actualize the aim of this research. It also contains the section on research mechanism. The research mechanism section give information on the types and mechanism of all the major reactions carried out in the course of this research.
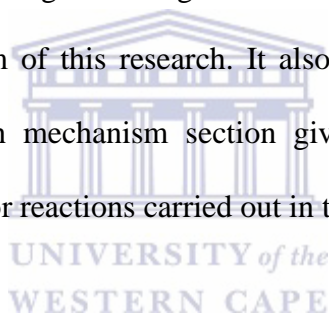
The analytical techniques employed in this study includes nuclear magnetic resonance (NMR) spectroscopy, mass spectroscopy (MS), ultrviolet-visible (UV-Vis) spectroscopy, photoluminescence (PL), electroluminescence (EL), thermogravimetric analysis (TGA), transmission electron microscopy (TEM), scanning electron microscopy (SEM), atomic force microscopy (AFM), infra red (IR) spectroscopy, cyclic voltammetry (CV), square wave voltammetry (SWV), electrochemical impedance spectroscopy (EIS), microscopy, and photovoltaics (current voltage (*I-V* curves) and external quantum efficiency (EQE)).

4.1   Materials

A list of the materials used, their source (Sigma Aldrich, Aldrich, Fluka, Alfa Aesar, Merck, VWR, etc) and purity is presented in **Table 4.1**.

Table 4.1: List, source and purity of materials used

Material	Source	Assay [%]
Benzo[b]thien-3-ylboronic acid	Sigma Aldrich	≥95
5-Bromo-3-pyridinecarboxaldehyde	Sigma Aldrich	97
Tetrakis(triphenylphosphine) palladium(0)	Sigma Aldrich	99
Bis(triphenylphosphine)palladium(II) dichloride	Sigma Aldrich	98
Chloro(2-dicyclohexylphosphino-2′,4′,6′-triisopropyl-1,1′-biphenyl)[2-(2′-amino-1,1′-biphenyl)]palladium(II)	Sigma Aldrich	-
1, 2-dimethoxyethane	Sigma Aldrich	99.9
Triphenyl phosphine	Sigma Aldrich	≥95
Fullerene C_{60}	Bulky USA	-
Sarcosine	Sigma Aldrich	≥98
Tetrabutylammonium hexafluorophosphate (TBAPF$_6$)	Sigma Aldrich	>99.0
Hydroquinone	Aldrich	≥ 99.5

99

Material	Source	Assay [%]
1,3-dimtheyloctane	Aldrich	96
Potassium carbonate, anhydrous	Alfa Aesar	99
Sodium metabisulfite	Alfa Aesar	97
Paraformaldehyde	Alfa Aesar	97
Sodium bromide	Alfa Aesar	97
(Trimethylsilyl)acetylene	Alfa Aesar	98
n-Buthyllithium, 2.5 M in hexane	Alfa Aesar	-
Diisopropylamine	Alfa Aesar	99+
Potassium tert-butoxide	Alfa Aesar	97
2-Ethylhexyl bromide	Aldrich	95
1-Bromoundecane	Aldrich	98
1-Bromotridecane	Aldrich	98
Dibromo anthracene	Alfa Aesar	98
Triethylphosphite	Aldrich	98
Diethyl ether	Sigma Aldich	≥99.0
1-Bromodecane	Sigma Aldrich	98
Potassium hydoxide	Alfa Aesar	85
N, *N*-dimethyl formamide	Alfa Aesar	99.8
Bromine	Sigma Aldrich	≥99.0
H_2SO_4	Merck	-
CH_3COOH	Merck	-
CuI	Alfa Aesar	-
Potassium fluoride	Alfa Aesar	99
Sodium sulfate	Sigma Aldrich	≥99

100

Material	Source	Assay [%]
Poly[(9,9-di-*n*-octylfluorenyl-2,7-diyl)-*alt*-(benzo[2,1,3]thiadiazol-4,8-diyl)] (F8BT)	Sigma Aldich	-
[6,6]-Phenyl C_{61} butyric acid methyl ester (PCBM)	Solene, Sigma Aldich	≥99.5
1-[3-(Methoxycarbonyl)propyl]-1-phenyl-[6.6]C_{61}, 3′*H*-Cyclopropa[1,9][5,6]fullerene-C_{60}-I*h*-3′-butanoic acid 3′-phenyl methyl ester, PCBM, [60]PCBM	Sigma Aldrich	>99.5
Silica Gel	Merck, Macherey-Nagel MN 60	0.063-0.200 mm (70–230 mesh)
Poly-(3-hexylthiophene) (P3HT)	Rieke	-
Poly(ethyleneimine) solution	Aldrich	-
Poly[[2,2′-bithiophene]-5,5′-diyl(9,9-dioctyl-9*H*-fluorene-2,7-diyl)] (F8T2)	Sigma Aldrich	99.9
Methanol	VWR Chemicals	-
Tetrahydrofuran & Toluene	VWR Chemicals	-
Dichloromethane	VWR Chemicals	Technical
Dimethyl sulfoxide	VWR Chemicals	Technical
Acetonitrile	VWR Chemicals	-
Cyclohexane	VWR Chemicals	-
Ethylacetate	VWR Chemicals	-

4.2   Methodology

4.2.1   Research Design

This thesis was designed to follow some sequential steps or cycles. Nuclear magnetic resonance (NMR) spectroscopy measurements were made after each synthesis to ascertain its conformity to proposed structure. Thereafter, purification and characterization were carried out to confirm the properties of the materials for possible application in organic electronics; particularly, organic photovoltaic cells. The broad research design can be summarised in the flow diagram below:
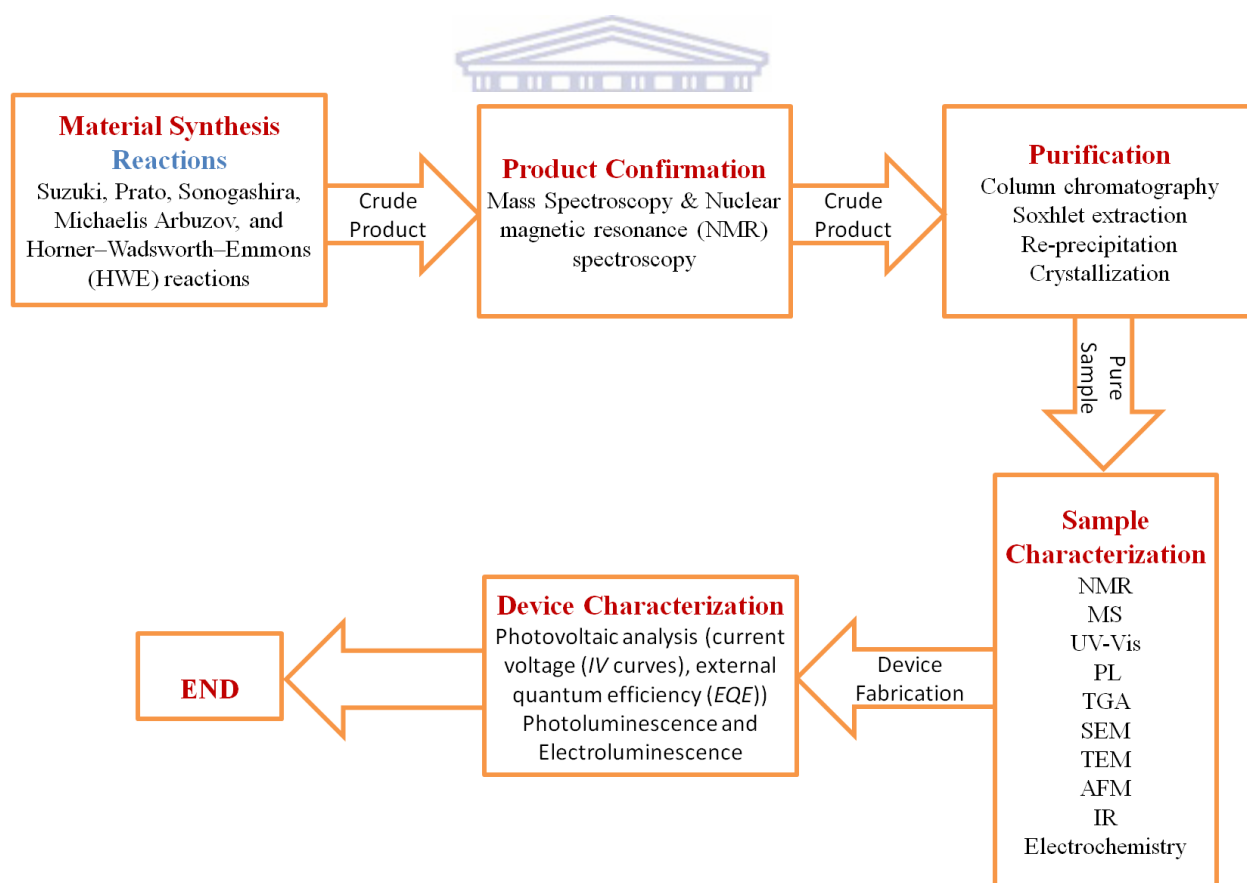
Figure 4.1: A flow chart of the research design.

102

The entire research is based on polymer synthesis and functionalization of fullerene for photovoltaic applications. The above research design follows the sequential steps below:

❖ Material synthesis: each synthetic step of the material synthesis followed a set of known reactions usually to give a crude product which is then purified. For polymerization, synthetic steps such as alkylation, bromination, formylation, alkynylation (protected), alkynylation (deprotected), **Sonogashira reaction**, **Michaelis Arbuzov reaction** and finally **Horner Wadsworth Emmons** reaction were employed. Fullerene functionalization was achieved via the **Suzuki coupling reaction** followed by the **Prato reaction**. The major reactions are in bold.

❖ Product confirmation: the crude product is usually confirmed by MS and ^{1}H NMR to ascertain the success of the synthesis.

❖ Purification: all successful reactions undergo purification either by column chromatography, Soxhlet extraction, re-precipitation, crystallization or two or all of the above purification steps to obtain the pure product.

❖ Sample Characterization: the pure sample/product is then characterized by nuclear magnetic resonance (NMR) spectroscopy, mass spectroscopy (MS), ultrviolet-visible (UV-Vis) spectroscopy, photoluminescence (PL), electroluminescence (EL), thermogravimetric analysis (TGA), transmission electron microscopy (TEM), scanning electron microscopy (SEM), atomic force microscopy (AFM), infra red (IR) spectroscopy, elemental analysis and cyclic voltammetry (CV) to ascertain its potential for device fabrication.

❖ Device Fabrication and Characterization: Samples with promising potential for device fabrication are then employed in device fabrication and characterized to obtain the current-voltage curve where the device efficiency is determined and the external quantum efficiency which gives information on the percentage of energy the device can give out from what it receives.

4.2.2   Reaction Mechanisms

This section gives a schematic representation showing all the reactions that were carried out in this work and brief illustration of the mechanisms. **Figure 4.2** shows two reaction steps based on the Suzuki coupling reaction and the Prato reaction while **Figure 4.3** consists of a series of reactions ranging from the well known Williamson synthesis to the Horner Wadsworth Emmons (HWE) reaction. However, in this section we will be dwelling on the mechanisms and discussion of the reactions of **Figure 4.2** and the three major reactions of **Figure 4.3**. Namely;

➢ Sonogashira reaction
➢ Michaelis Arbuzov reaction and
➢ Horner Wadsworth Emmons reaction

The formation of carbon-carbon (C–C) bond in chemistry is of great importance as it provides vital steps in the synthesis of bio-active molecules for medicines and agrochemicals and novel organic materials with intriguing electronic, optical or mechanical properties which are likely to play a significant role in the rapidly growing area of nanotechnology [1]. In this section, C-C bond forming reactions employed in this work will be briefly explained.
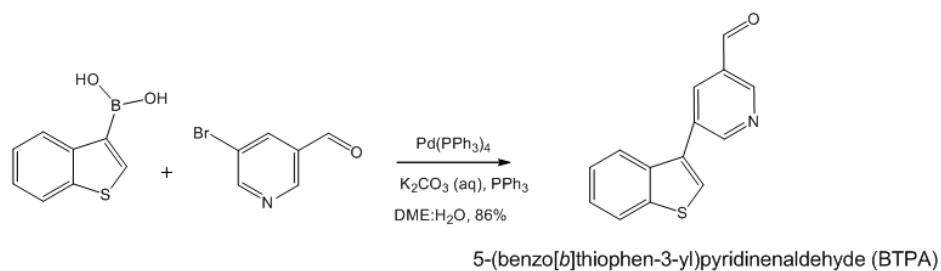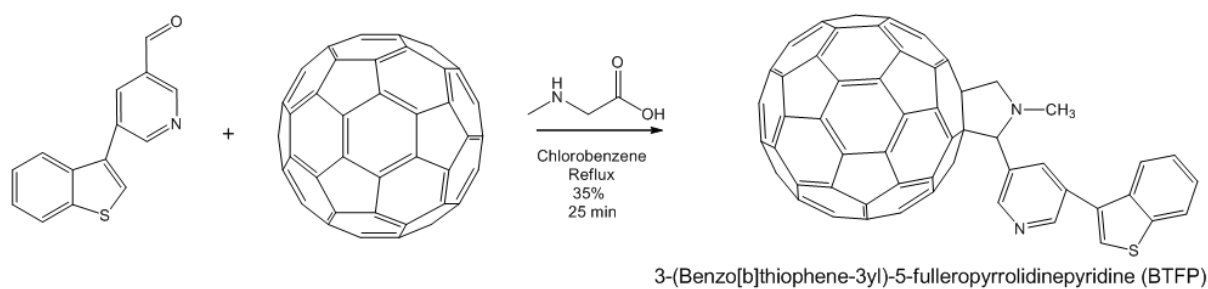
Figure 4.2: Reaction steps based on the Suzuki coupling reaction and the Prato reaction.

105
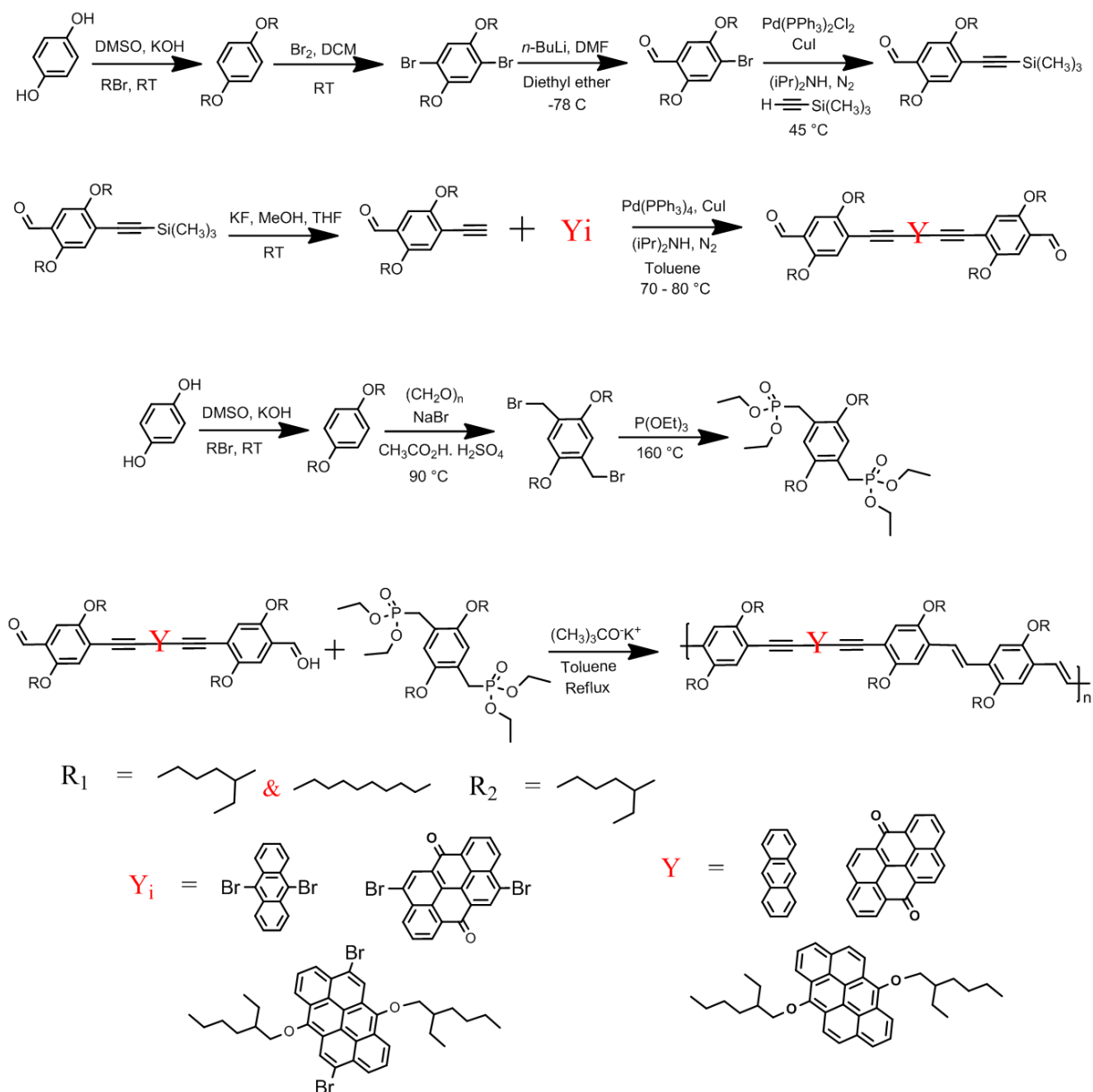
Figure 4.3: Series of reactions ranging from Williamson synthesis to Horner Wadsworth Emmons (HWE) reaction.

4.2.2.1 Suzuki Coupling Reaction

The **Suzuki coupling reaction** is the reaction between an aryl or vinyl boronic acid and an aryl or vinyl halide by a Pd (0) complex [2-4]. The coupling takes place in the presence of a base. The role of the base as reported by Duc and coworkers are basically to enhance the

106

transmetalation and the reductive elimination [5] by increasing the reactivity of the boronic acid toward the Pd-halide complex and converting it into the respective organoborate. The reaction was first reported in 1979 by Akira Suzuki's group and he shared the 2010 Nobel Prize in Chemistry with Richard F. Heck and Ei-ichi Negishi for their effort for discovery and development of palladium-catalyzed cross couplings in organic synthesis [6].

The aim of transition metal-catalysed organic synthesis is generally a C–C bond formation. The palladium-catalysed Suzuki reaction [7] is one of the most efficient methods for carbon-carbon (C–C) bond formation. Other coupling methods like Stille, Kharash, Himaya, Kumuda, Liebeskind–Srogl and Negishi can also be used to achieve same purpose [8], but the Suzuki coupling reaction has proven to be the most popular due its mild conditions of reaction, availability of the various boronic acids commercially and the environmental safety of same compared to other organometallic reagents [9-13]. The wide spread interest in applications of the Suzuki reaction, new developments and advancements in the reaction being reported constantly as described by several reviews [4, 14-16] is also due to the stability, ease of preparation and low toxicity of the boronic acid compounds. In addition, the reaction management and removal of unwanted boron-containing products is easier compared to other organometallic reagents especially during upscaling. The reaction has been used in the synthesis of many valuable compounds such as pharmaceuticals, polymers, and agrochemical.

The mechanism of the Suzuki reaction starts with the palladium catalyst. The steps as shown in **Figure 4.4** is briefly described

- The first step is the oxidative addition of palladium catalyst in the oxidation state zero to the halide (**2**) to form the organopalladium species (**3**), where palladium picks up oxidation state 2.

- (**3**) reacts with base to give the intermediate (**4**).

- (**4**) undergoes transmetalation with the boronate complex (**6**) (base activated boronic acid produced by the reaction of the boronic acid **5** with base) to form the organopalladium specie (**8**).

- (**8**) undergoes reductive elimination to give the desired product (**9**) and the catalytic cycle is completed by the restoration of the original palladium catalyst (**1**) which has an oxidation state of zero.

The oxidative addition step is believed in most cases to be the rate determining step.

108
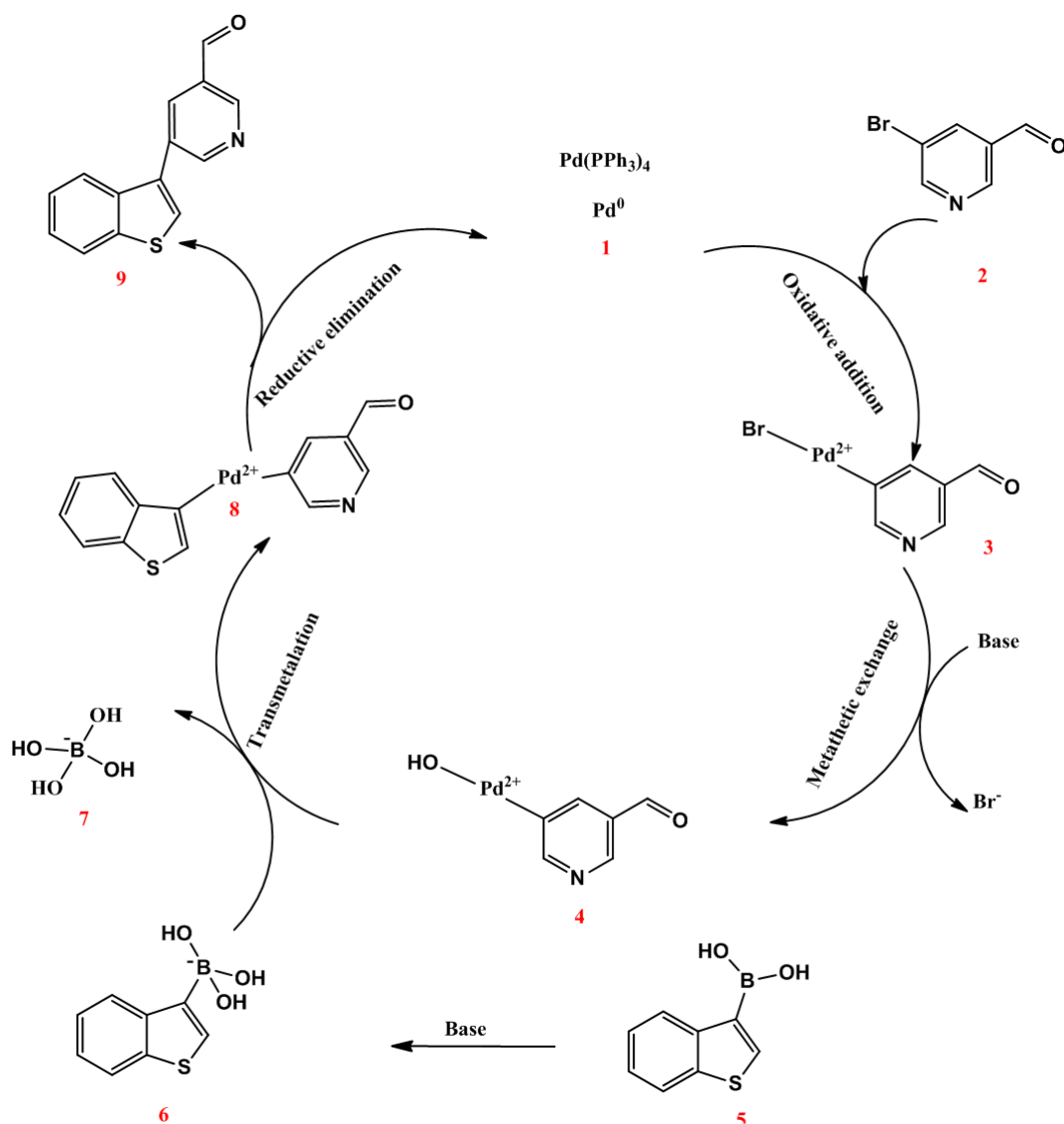
Figure 4.4: Mechanism for Suzuki coupling reaction.

4.2.2.2 Prato Reaction

The **Prato reaction** is the well-known 1,3-dipolar cycloaddition of azomethine ylides to olefins. In fullerene chemistry, this reaction is referred to as the functionalization of fullerenes and nanotubes [17]. It is a highly valued reaction for the functionalization of fullerenes and carbon nanotubes. It involves the use of amino acid (particularly *N*-methylglycine) which reacts with aldehyde when heated at reflux in toluene to generate

109

azomethine ylide which then reacts with a double bond in a 6,6 ring position in fullerene via a 1,3-dipolar cycloaddition to yield a *N*-methylpyrrolidine derivative (**Figure 4.5**).

Mechanism

The mechanism as shown in **Figure 4.5** is briefly interpreted below

- Amino acid is heated in the presence of the aldehyde (**1**) to form a 1, 3-dipolar compound (**6**) after the removal of H_2O and decarboxylation
- 1, 3-dipolar compound reacts readily with 6, 6 ring of fullerene to give the functionalized fullerene (**8**)

110
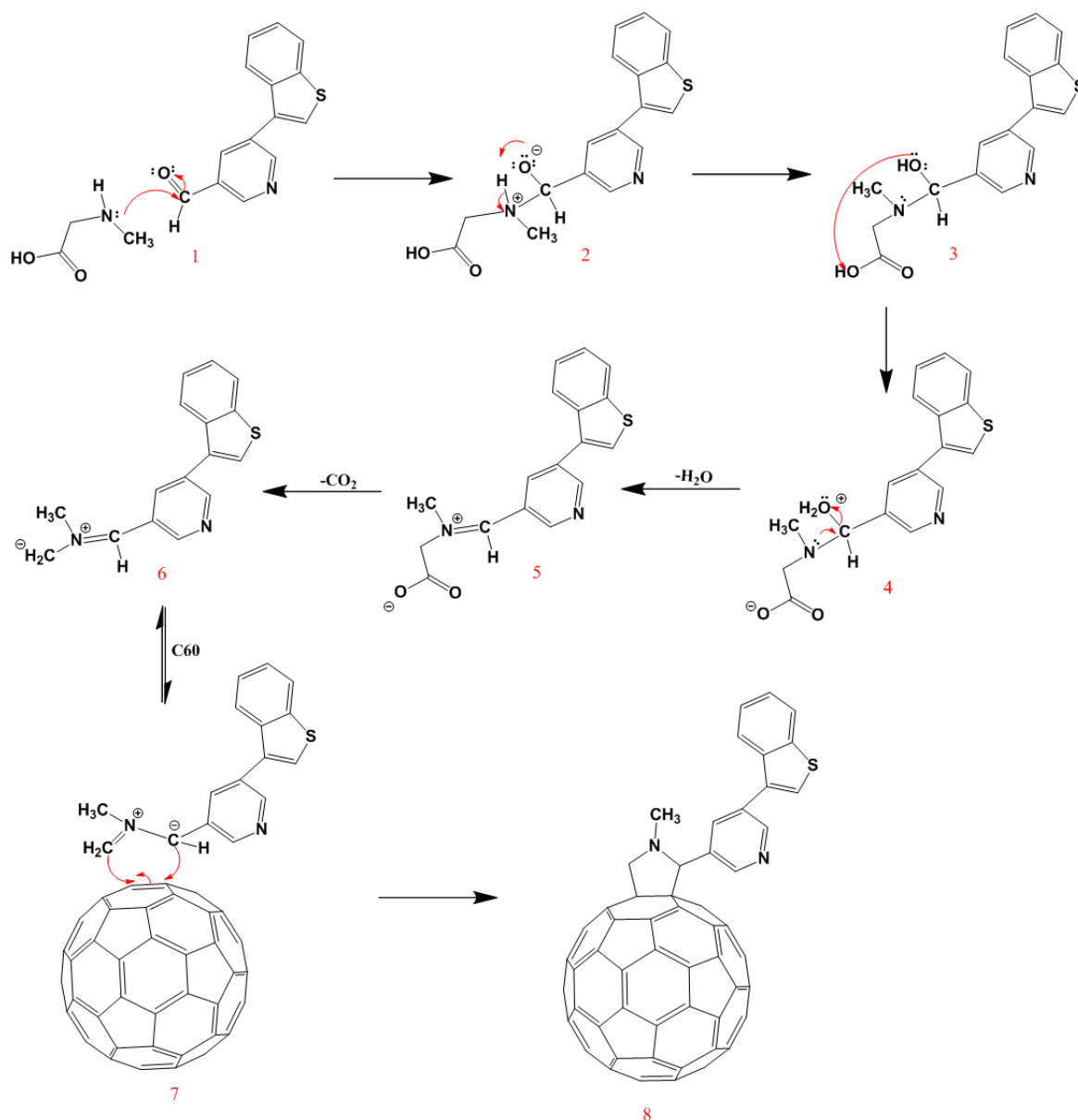
Figure 4.5: Mechanism for Prato reaction.

4.2.2.3 Sonogashira Coupling Reaction

Sonogashira coupling reaction is a useful palladium-catalyzed sp^2-sp coupling reaction of terminal alkynes with aryl or vinyl halides [18]. The reaction is performed using a palladium catalyst, a copper (I) co-catalyst and an amine base under anhydrous and anaerobic conditions. The co-catalyst which increases the rate of the reaction, react with the terminal

111

alkyne and produce a copper (I) acetylide, which acts as an activated specie for the coupling reactions (**Figure 4.6**). The inclusion of a copper co-catalyst in this coupling reaction results in increased reactivity of the reagents and makes it possible for the reaction to be carried out under mild conditions.

The procedures of the Sonogashira coupling reaction were first reported by Heck and Cassar in 1975 [19-20]. Heck's study which was based on the Mizoroki-Heck reaction for the palladium-catalyzed arylation or alkenylation of alkenes, reported the now known Sonogahira reaction employing a phosphane-palladium complex as a catalyst and triethylamine or piperidine as a base and solvent while Cassar's report involved the use of a phosphane-palladium catalyst in combination with sodium methoxide as a base and DMF as solvent. Both methods generally required harsh reaction temperature (up to 100 °C). In the same year, Sonogashira and Hagihara reported that addition of a co-catalyst (CuI) greatly accelerates the reaction, thus enabling the reaction to be carried out under milder conditions compared to earlier reports by Heck and Cassar. The cross-coupling is carried out at mild conditions with a base, typically an alkylamine base [21-22] which in most cases also acts as the solvent. The alkylamine solvent helps neutralize the hydrogen halide produced as the by-product in the coupling reaction by creating a basic medium. In addition, due to the instability of palladium (0) complexes in air, and the promotion of the formation of homocoupled acetylenes in the presence of oxygen, anaerobic conditions are advised for Sonogashira coupling reactions. Considering the pivotal role of the base in this reaction, specific amines such as piperidine, morpholine, or diisopropylamine are used for the reaction to proceed. These secondary amines can react efficiently and reversibly with *trans*-$RPdX(PPh_3)_2$ complexes by substituting one PPh_3 ligand; where the R, X, a factor for basicity, and the amine's steric hindrance are responsible for the equilibrium constant of the reaction [23]. The amine is

112

usually added in excess to prevent competition of ligand exchange between the amine and the alkyne group.

As a result of this new finding, the Sonogashira protocol became the most popular procedure for the alkynylation of aryl or alkenyl halides. The method has become the most important method to prepare arylalkynes and conjugated enynes, which are starting materials for natural products, pharmaceuticals products and molecular organic materials. A brief description of the mechanism as shown in **Figure 4.6** is given below

Mechanism

- The active palladium catalyst (**1**) reacts with the aryl or vinyl halide (**2**) in an oxidative addition to produce a Pd^{II} intermediate (**3**). This step is believed to be the rate-limiting step of the reaction.
- The Pd^{II} intermediate (**3**) reacts in a transmetallation with the copper acetylide (**4**), which is produced in the copper cycle and undergoes a trans-cis isomerization (**5**).
- Finally, **5** undergo reductive elimination to produce the alkyne (**6**), with regeneration of the palladium catalyst.

113

L = Base, Solvent, Phosphane or Alkyne
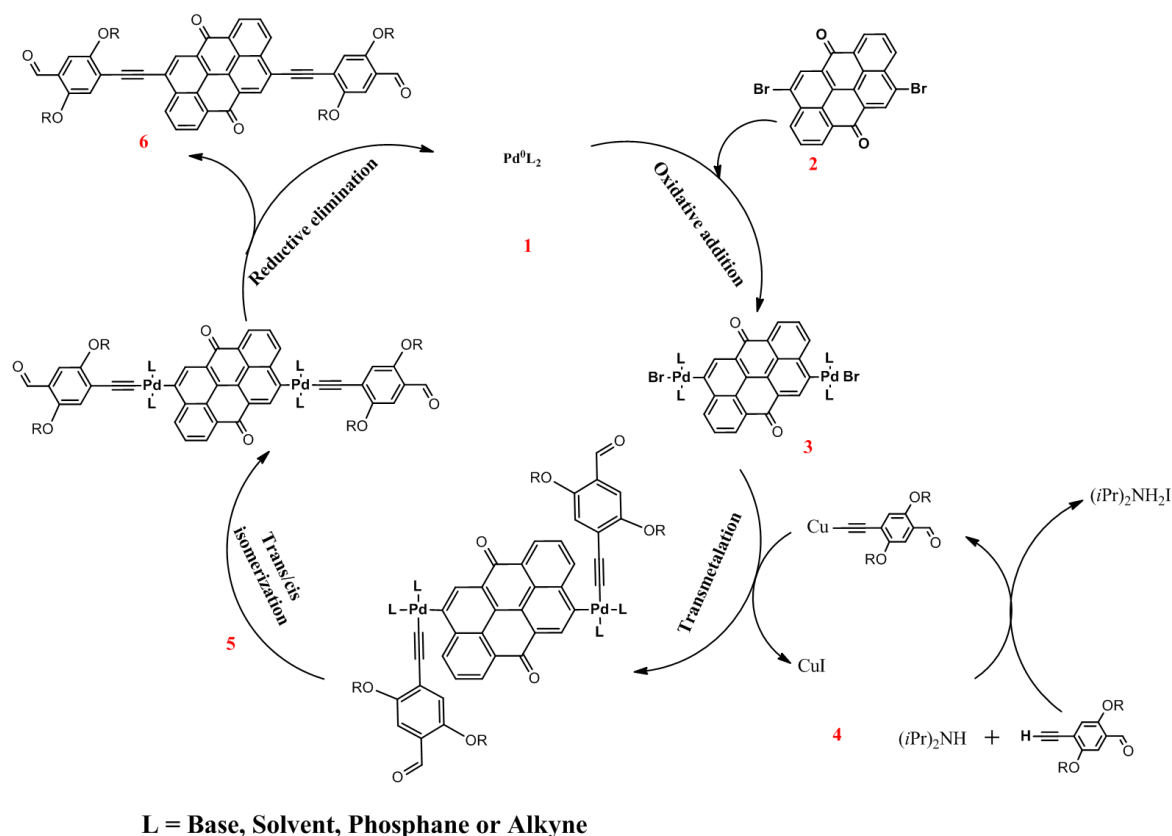
Figure 4.6: Mechanism for Sonogashira coupling reaction.

4.2.2.4 Michaelis Arbuzov Reaction

The Michaelis-Arbuzov's reaction is one of the most versatile pathways for the formation of carbon-phosphorus bonds from the reaction of a trialkyl phosphate with an aryl or alkyl halide. It involves the formation of alkyl phosphonates containing one phosphorus-carbon bond. The reaction, first discovered and reported by German chemist August Michaelis [24] in 1898, was expanded by Arbuzov in 1906 [25]. This reaction has been reported successful with or without a catalyst. Microwave assisted reaction of the synthesis of organophsophorus compounds [26-28] and phosphonylation of aromatic compounds has been reportedly realized under catalytic conditions [29-30]. The heating of highly activated benzene compounds with phosphites yield the corresponding phosphonates without a catalyst [31].

114

The reaction is one of the most thoroughly investigated among organophosphorus reactions and is widely employed for the synthesis of phosphonates, phosphinic acid esters, and phosphine oxides; and has gained industrial importance with major application in petro-chemistry and the synthesis of polymers. This reaction finds extensive application in the synthesis of phosphonate esters for use in the Horner-Wadsworth-Emmons reaction.

Mechanism

The mechanism as shown in **Figure 4.7** is briefly interpreted below

- The alkyl group of the alkyl halide (**2**) is attacked by the lone pair of electrons of the phosphite (**1**) to form the addition compound (**3**) in which the alkyl group of the alkyl halide is attached to the phosphorus.

- Next, an alkyl group of the phosphite dissociates from (**3**), resulting in the formation of the P=O bond.

- The alkyl group is eliminated as an alkyl halide and compound (**4**) is produced.
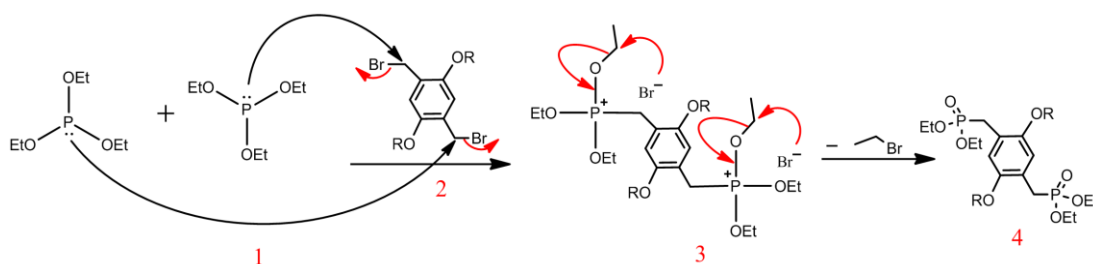
Figure 4.7: Mechanism for Micheallis Arbuzov Reaction.

115

4.2.2.5 Horner Wadsworth Emmons Reaction

The **Horner–Wadsworth–Emmons reaction** is a chemical reaction resulting in olefin formation by means of phosphonate carbanions. It is the reaction of phosphonate carbanions with aldehydes to produce mainly *E*-alkenes [32]. In 1958, Leopold Horner published a novel reaction between phosphine-oxide stabilized carbanions and carbonyl compounds known as the Wittig reaction [33-34]. This was further modified/expanded by William Wadsworth and William Emmons into the **Horner–Wadsworth–Emmons reaction** (or **HWE reaction**) by employing phosphonates [35]. It was soon discovered that as olefin forming reagents, phosphonates have certain advantages over both phosphoranes and phosphine oxides [32, 36-39]. Since then, the HWE reaction has gained popularity for C=C bond formation [36, 40-42]. The ease of workup, convenient reaction conditions and availability of reagents has attracted interest in this reaction method. The extraction of the by-product of reaction is easy and can be simply done by taking advantage of the solubility of the phosphate by-product in water. This is an important advantage over conventional Wittig reaction. The HWE reaction have become one of the most frequently employed synthetic process for polymerization employing products from the Micheallis Arbuzov reactions

Steps in the mechanism of the Horner–Wadsworth–Emmons reaction (Figure 4.8):

- The first step of the mechanism is the formation of the phosphonate carbanion by the removal of a proton at the α-carbon by a base (**1**).
- Next is the nucleophilic addition of the carbanion to a carbonyl - ketone or aldehyde (reaction with an aldehyde is shown (**2**)).

116

- This is followed by the formation of the phosphorous-oxygen bond between phosphonate and carbonyl (**3**).

- Step (**4**) is the elimination of the phosphonate to give the final product (**5**).

In this reaction, the rate-determining step is the addition of phosphonate anion to the carbonyl group (step 3), where the carbanion-stabilizing group is important for the elimination to take place. The product of the classical HWE reaction is known to be predominantly *E*-alkene favoured. Notwithstanding, reducing the size of the alkyl on the carbonyl can reduce *E*-favored products and result in a mixed yield. In the case of a strongly dissociating metallic base, this process can lead to strong *Z*- selective products. It has been shown that the stereochemical outcome of the reaction depends on the reactants (type of carbonyl compound), and the reaction medium (reaction conditions) [43]. Others include the base, solvent, and additives (such as metal salts, crown ethers, or even the deliberate exclusion of salts) [44-48].

117
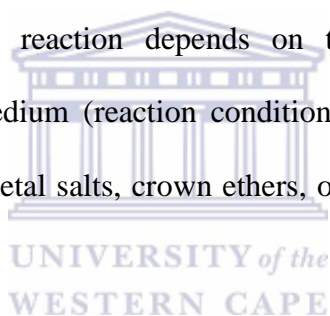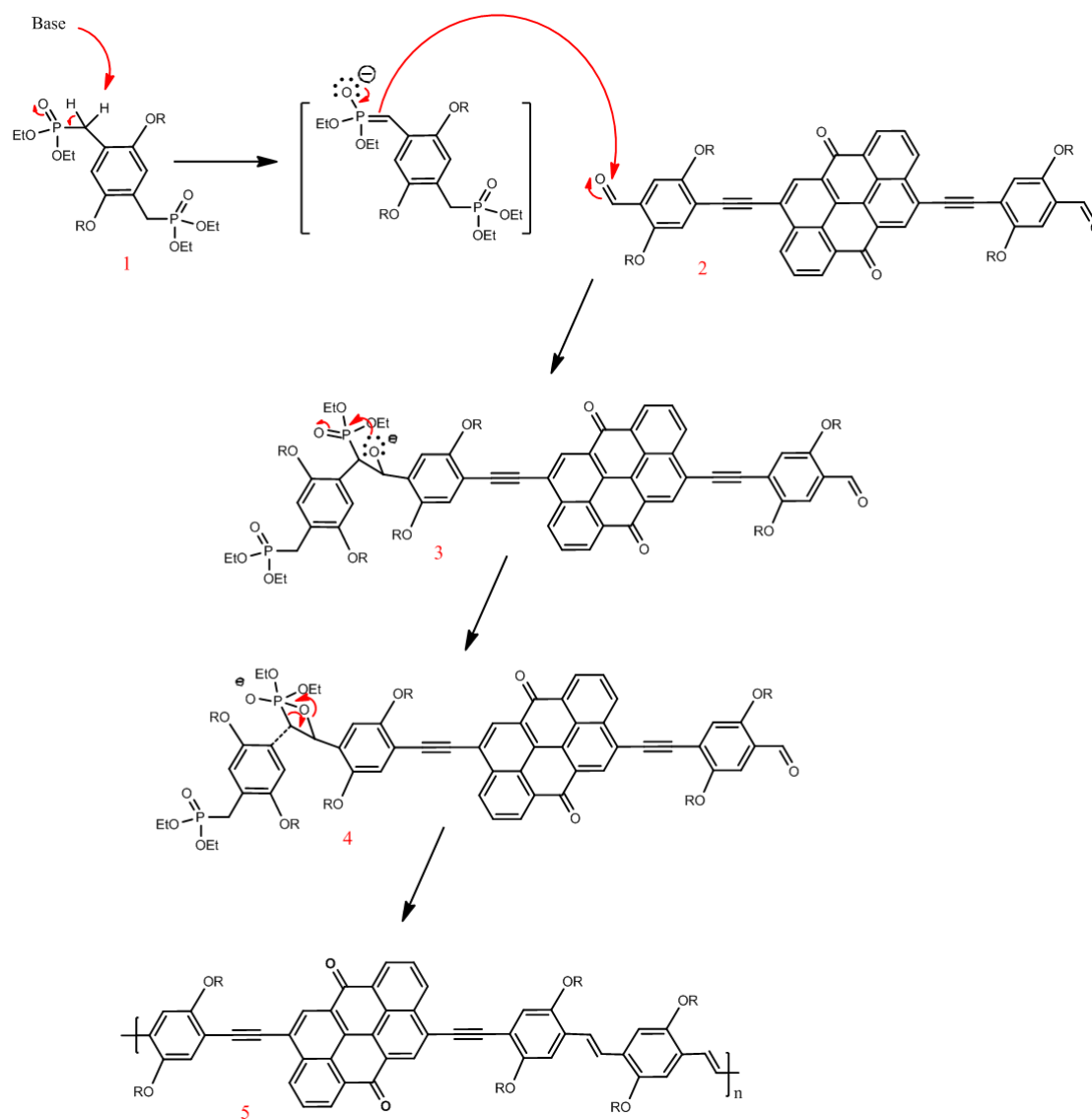
Figure 4.8: Mechanism for Horner Wadsworth Emmons reaction.

4.3   References

[1]   A. Suzuki, "Cross-Coupling Reactions of Organoboranes: An Easy Way for C-C Bonding," *Nobel Lecture,* (**2010**)

[2]   N. Miyaura, K. Yamada and A. Suzuki, "A new stereospecific cross-coupling by the palladium-catalyzed reaction of 1-alkenylboranes with 1-alkenyl or 1-alkynyl halides," *Tetrahedron Lett.,* (**1979**) 3437 - 3440.

[3]   N. Miyaura and A. Suzuki, "Stereoselective synthesis of arylated (E)-alkenes by the reaction of alk-1-enylboranes with aryl halides in the presence of palladium catalyst " *J. Chem. Soc., Chem. Commun.,* (**1979**) 866 - 867.

[4]   N. Miyaura and A. Suzuki, "Palladium-Catalyzed Cross-Coupling Reactions of Organoboron Compounds," *Chem. Rev.,* 95 (**1995**) 2457 - 2483.

[5]   C. Amatore, A. Jutand and G. L. Duc, "Kinetic Data for the Transmetalation/Reductive Elimination in Palladium-Catalyzed Suzuki-Miyaura Reactions: Unexpected Triple Role of Hydroxide Ions Used as Base," *Chem. Eur. J,* 17 (**2011**) 2492 - 2503.

[6]   Nobelprize.org., "The Nobel Prize in Chemistry 2010," *Nobel Prize Foundation,* (**Retrieved 01-02-2016**)

[7]   N. Miyaura, T. Yanagi and A. Suzuki, "The Palladium-Catalyzed Cross-Coupling Reaction of Phenylboronic Acid with Haloarenes in the Presence of Bases," *Synth. Commun.,* 11 (**1981**) 513 - 519.

[8]   S. P. Stanforth, "Catalytic Cross-coupling Reactions in Biaryl Synthesis," *Tetrahedron,* 54 (**1998**) 263 - 303.

[9]   A. Suzuki, "Organoboron compounds in new synthetic reactions," *Pure Appl. Chem.,* 57 (**1985**) 1749 - 1758.

119

[10] A. Suzuki, "Synthetic studies via the cross-coupling reaction of organoboron derivatives with organic halides," *Pure Appl. Chem.,* 63 (**1991**) 419 - 422.

[11] A. Suzuki, "New synthetic transformations via organoboron compounds," *Pure Appl. Chem.,* 66 (**1994**) 213 - 222.

[12] S. P. Stanforth, *Tetrahedron* 54 (**1998**) 263 - 303.

[13] N. Miyaura, "Advances in Metal-organic Chemistry," *Libeskind, L. S., Ed.; Jai: London,* 6 (**1998**) 187 - 243.

[14] A. R. Martin and Y. Yang, "Palladium-Catalyzed Cross-Coupling Reactions of Organoboronic Acids with Organic Electrophiles," *Acta Chem. Scand.,* 47 (**1993**) 221 - 230.

[15] A. Suzuki, "Recent advances in the cross-coupling reactions of organoboron derivatives with organic electrophiles, 1995 – 1998," *J. Organomet. Chem.,* 576 (**1999**) 147 - 168.

[16] F. Alonso, I. P. Beletskaya and M. Yus, "Non-conventional methodologies for transition-metal catalysed carbonecarbon coupling: a critical overview. Part 2: The Suzuki reaction," *Tetrahedron,* 64 (**2008**) 3047 - 3101.

[17] M. Maggini, G. Scorrano and M. Prato, "Addition of Azomethine Ylides to C_{60}: Synthesis,Characterization, and Functionalization of Fullerene Pyrrolidine," *J. Am. Chem. Soc.,* 115 (**1993**) 9798-9799.

[18] R. Chinchilla and C. Nájera, "Recent advances in Sonogashira reactions," *Chem. Soc. Rev.,* 40 (**2011**) 5084 - 5121.

[19] H. A. Diek and F. R. Heck, "Palladium catalyzed synthesis of aryl, heterocyclic and vinylic acetylene derivatives," *J. Organomet. Chem.,* 93 (**1975**) 259 - 263.

[20] L. Cassar, *J. Organomet. Chem.,* 93 (**1975**) 253 - 257.

120

[21]   K. Sonogashira, Y. Tohda and N. Hagihara, "A convenient synthesis of acetylenes: catalytic substitutions of acetylenic hydrogen with bromoalkenes, iodoarenes and bromopyridines," *Tetrahedron Lett.,* 16 (**1975**) 4467 - 4470.

[22]   A. L. Kohnen, R. L. Danheiser, S. E. Denmark and X. Liu X, "Synthesis of Terminal 1,3-Diynes Via Sonogashira Coupling of Vinylidene Chloride Followed by Elimination. Preparation of 1,3-Decadiyne," *Org. Synth. ,* 84 (**2007**) 77 - 87.

[23]   A. Jutand, S. Négri and A. Principaud, "Formation of ArPdXL(amine) Complexes by Subsitution of One Phosphane Ligand by an Amine in trans-ArPdX(PPh3)2 Complexes " *Eur. J. Inorg. Chem.,* 2005 (**2005**) 631.

[24]   A. Michaelis and R. Kaehne, *Chem. Ber.,* 31 (**1898**) 1048 - 1055.

[25]   A. E. Arbuzov, *J. Russ. Phys. Chem. Soc.,* 38 (**1906**) 687.

[26]   A. R. Sardarian and B. Kaboudin, *Synth. Commun.,* 27 (**1997**) 543 - 551.

[27]   A. R. Sardarian and B. Kaboudin, *Tetrahedron Lett.,* 38 (**1997**) 2543 - 2546.

[28]   B. J. Kaboudin, *Chem. Research (s)* (**1999**) 402 - 403.

[29]   T. M. Balthazor and R. C. Grabiak, *J. Org. Chem.,* 45 (**1980**) 5425 - 5426.

[30]   X. Lu and J. Zhu, *Synthesis,* (**1987**) 726 - 727.

[31]   T. Erker and N. Handler, *Synthesis,* (**2004**) 668 - 670.

[32]   W. S. Wadsworth Jr, "Synthetic Applications of Phosphoryl-Stabilized Anions," *Org. React.,* 25 (**1977**) 73 - 253.

[33]   L. Horner, H. M. R. Hoffmann and H. G. Wippel, "Phosphororganische Verbindungen, XII. Phosphinoxyde als Olefinierungsreagenzien," *Ber.,* 91 (**1958**) 61 - 63.

[34]   L. Horner, H. M. R. Hoffmann, H. G. Wippel and G. Klahre, "Phosphororganische Verbindungen, XX. Phosphinoxyde als Olefinierungsreagenzien," *Ber.,* 92 (**1959**) 2499 - 2505.

[35]   W. S. Wadsworth and W. D. Emmons, "The Utility of Phosphonate Carbanions in Olefin Synthesis," *J. Am. Chem. Soc.,* 83 (**1961**) 1733 - 1738.

[36]   J. Boutagy and R. Thomas, "Olefin Synthesis with Organic Phosphonate Carbanions," *Chem. Rev.,* 74 (**1974**) 87 - 99.

[37]   B. E. Maryanoff and A. B. Reitz, "The Wittig olefination reaction and modifications involving phosphoryl-stabilized carbanions. Stereochemistry, mechanism, and selected synthetic aspects," *Chem. Rev.,* 89 (**1989**) 863 - 927.

[38]   J. A. Bisceglia and L. R. Orelli, *Curr. Org. Chem.,* 16 (**2012**) 2206 - 2230.

[39]   J. A. Bisceglia and L. R. Orelli, *Curr. Org. Chem.,* 19 (**2015**) 744 - 775.

[40]   B. E. Maryanoff and A. B. Reitz, "The Wittig Olefination Reaction and Modifications Involving Phosphoryl-Stabilized Carbanions. Stereochemistry, Mechanism, and Selected Synthetic Aspects," *Chem. Rev.,* 89 (**1989**) 863 - 927.

[41]   P. J. Murphy and J. Brennan, "The Wittig olefination reaction with carbonyl compounds other than aldehydes and ketones," *Chem. Soc. Rev.,* 17 (**1988**) 1 - 30.

[42]   B. M. Trost and I. Fleming, "(Eds). Comprehensive Organic Synthesis, Vol. 1 " *Oxford: Pergamon Press,* (**1999**)

[43]   I. Gosney and A. G. Rowley, "In Organo hosphorus Reagents in Organic Synthesis," Cadogan J. I. &., Ed.; Academic Press:New York (**1979**) 17 - 153.

[44]   W. C. Still and C. Gennari, "Direct synthesis of Z-unsaturated esters. A useful modification of the Horner-Emmons olefination," *Tetrahedron Lett.,* 24 (**1983**) 4405 - 4408.

[45]   K. Ando, "Highly Selective Synthesis of Z-Unsaturated Esters by Using New Horner - Emmons Reagents, Ethyl (Diarylphosphono)acetates," *J. Org. Chem.,* 62 (**1997**) 1934 - 1939.

122

[46] K. Ando, "Z-Selective Horner-Wadsworth-Emmons Reaction of alpha-Substituted Ethyl (Diarylphosphono) acetates with Aldehydes," *J. Org. Chem.,* 63 (**1998**) 8411 - 8416.

[47] K. Ando, "Convenient Preparations of (Diphenylphosphono)acetic Acid Esters and the Comparison of the Z-Selectivities of Their Horner-Wadsworth-Emmons Reaction with Aldehydes Depending on the Ester Moiety," *J. Org. Chem.,* 64 (**1999**) 8406 - 8408.

[48] K. Ando, T. Oishi, M. Hirama and T. Ibuka, "T. Z-Selective Horner-Wadsworth-Emmons Reaction of Ethyl (Diarylphosphono)acetates Using Sodium Iodide and DBU," *J. Org. Chem.,* 65 (**2000**) 4745 - 4749.

UNIVERSITY *of the*

WESTERN CAPE

CHAPTER FIVE

RESULTS AND DISCUSSION - Synthesis, Characterization and Photovoltaic Investigation of Poly(arylene ethynylene)-*alt*-poly(arylene vinylene)s (PAE-PAV) Polymers Based On Anthanthrone and Its Derivatives

Abstract

Anthanthrone and its derivatives are large polycyclic-aromatic compounds (PACs) and pose a number of challenges for incorporation into the structure of soluble conjugated polymers. For the first time, this group of polycyclic aromatic compounds were employed as building blocks for the synthesis of polymers (P1, P2, P3, P4 and P5) based on poly(arylene ethynylene)-*alt*-poly(arylene vinylene)s (PAE-PAV) backbone by Sonogashira and Horner Wadsworth Emmons reaction. In a bid to tune the material properties, different alkyloxy side chains were incorporated. The photo-physical properties were recorded both in solution and films and the electrochemical investigations were conducted by means of cyclic voltammetry. The UV-Visible absorption spectroscopy of the un-substituted anthanthrone based polymer (P1) revealed more light absorption, a Vis-NIR region absorption. The substituted anthanthrone polymers (P2 and P3) show almost similar photo-physical response with the frontier orbital energy levels basically unaffected by the side chains. The highest occupied molecular orbital/lowest unoccupied molecular orbital energy levels of the polymers estimated from their voltammetric response are observed to be confined within the anthanthrene/anthanthrone core. The highest occupied molecular orbital (-5.3 eV) and lowest

unoccupied molecular orbital (-3.0 eV) energy values of P2 and P3 are exactly the same while deeper HOMO/LUMO is observed for P1 (HOMO -5.5 eV; LUMO -4.1 eV). P1, P2 and P3 were investigated for photovoltaic applications. Open circuit voltage over 0.9 V was observed for P1. P2 and P3 exhibited an open-circuit voltage over 0.75 V; and fill factor of 0.53 was observed for P2.

5   Introduction

Polycyclic aromatic compounds (PACs) containing several benzenoid constituents have attracted considerable attention for potential applications in supramolecular electronics [1-3] and are becoming increasingly popular for optoelectronic applications [4-8]. The large conjugated π-systems of PACs accelerate electron delocalization while the rigid flat geometry enables them to stack in well organized arrays for strong π-stacking interactions. The conjugated π-systems influence the tuning of the optoelectronic properties, while the flat geometry is enables good light emitting properties and intermolecular charge transport [9-14]. These combined features make PACs appealing building blocks for the preparation of organic semiconducting polymers.

In spite of this, a comparatively low number of conjugated polymers incorporating large PACs building blocks have been reported so far [15-23]. The lack of interest in PACs based polymers (especially for organic photovoltaic cells) is as a result of the drawbacks which is majorly relatively high band gap. Extension of the effective conjugation can be used to overcome this drawback [24-25]. However, this is often likely to be accompanied by a significant decrease in solubility, which might hinder processing into thin films suitable for photovoltaic applications. Large hexabenzocoronene PAC for example, was reportedly

incorporated in the main chain of conjugated polymers [26]. These materials, however, were insoluble in common organic solvents. The synthesis of π-conjugated small molecules based on anthanthrone is relatively simple but the preparation of polymers using anthanthrone units is challenging. Its rigidity coupled with its large and flat π surface hinders good solubility in common organic solvents [27]. Only very recently, the synthesis and characterization of the first series of soluble conjugated polymers based on anthanthrone derivative (anthanthrene) [28] and 4,10-bis(thiophen-2-yl)anthanthrone (TANT) unit were reported [27].

Herein, the application of anthanthrone and its derivative as building blocks for solution process-able π-conjugated polymer synthesis via the poly(arylene ethynylene)-*alt*-poly(arylene vinylene)s (PAE-PAV) backbone using the Horner-Wadsworth-Emmons (HWE) polycondensation reaction is reported for the first time. The new polymers were characterized in detail and their applicability as absorber materials in organic photovoltaic (OPV) devices was investigated. PAE-PAV are a class of polymeric materials that combine the intrinsic properties of poly(arylene-ethynylene) (PAE) and poly(arylene-vinylene) (PAV) into a single backbone with additional structure-specific properties [29]. The general constitutional unit of the PAE-PAV backbone in this study (-Ph-C≡C-Anth-C≡C-Ph-CH=CH-Ph-CH=CH-)$_n$ contains an anthanthrone or its analogue anthanthrene embedded between two triple bonds (**Figure 5.1b**).
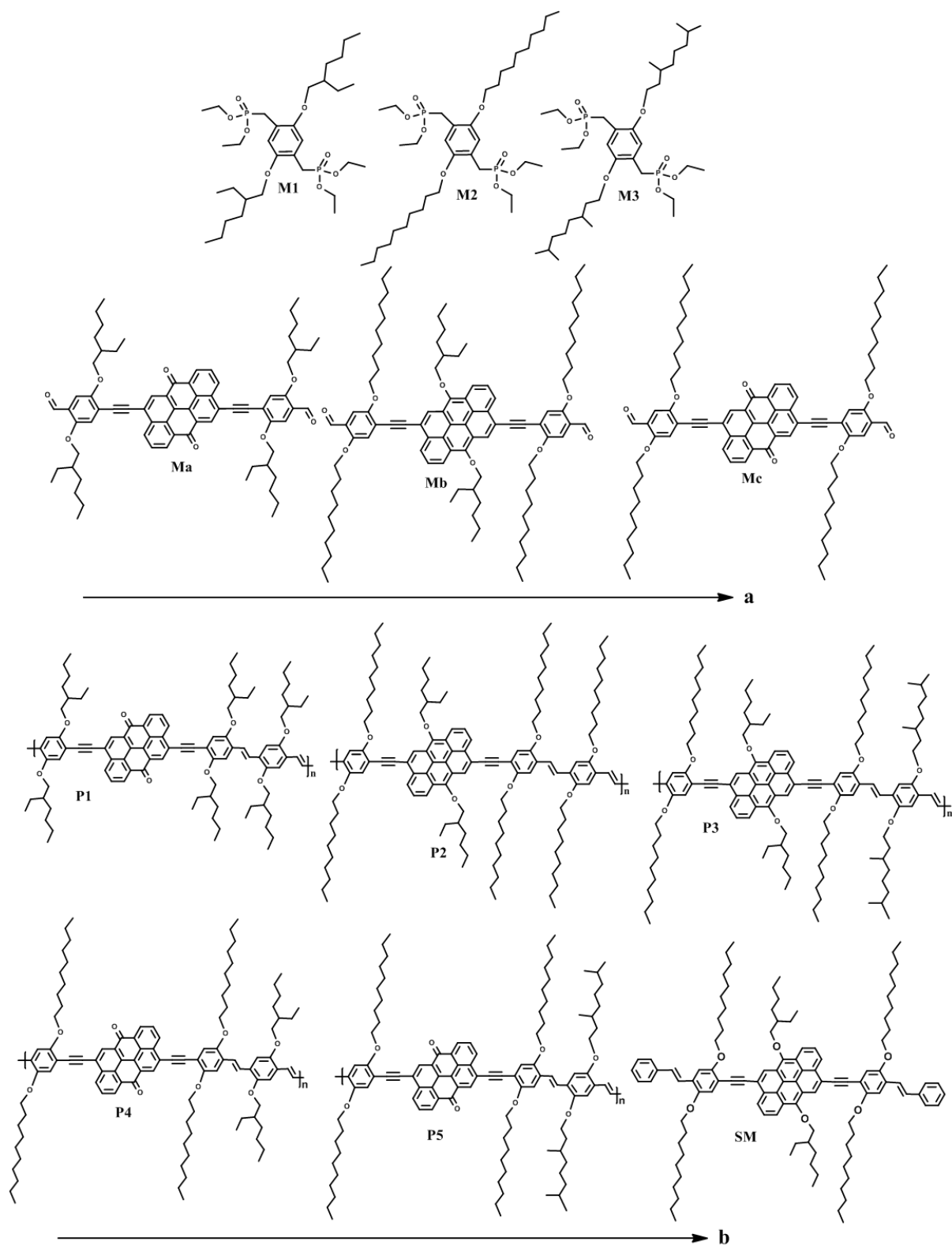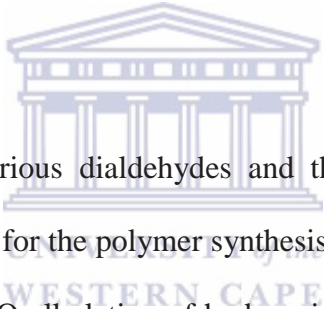
Figure 5.1: a) Synthesized monomers for polymer synthesis, b) Synthesized polymers P1 -
P5 and small molecule SM.

127

To the best of my knowledge, the use of anthanthrone and its derivative as building blocks for polymer synthesis via the PAE-PAV backbone has not been reported. PAE-PAV based on other structures such as anthracene [30-39], thiophene and phenylene core [29, 40-41] have been presented in previous works. The aim of the current study is to establish anthanthrone and its derivatives as suitable building blocks for the design of novel PAE-PAV backbones with good solubility (through side chain incorporation and variation) and to probe the suitability of the new materials in photovoltaic applications.

5.1   Experimental

5.1.1   Synthesis

The preliminary synthesis of various dialdehydes and the corresponding bisphosphonate esters (**Figure 5.1a**) is imperative for the polymer synthesis. The synthesis of the dialdehydes are 6-step reactions starting with O-alkylation of hydroquinone with the corresponding alkyl bromide; while the synthesis of the bisphosphonate derivatives are 3-step reactions starting with O-alkylation of hydroquinone with the corresponding alkyl bromide. The 6-step dialdehyde synthesis was obtained via the O-alkylation of hydroquinone, dibromination of the O-alkylated product, formylation of the new product, alkynylation via trimethyl silylacetylene, deprotection of the product by removal of the trimethylsilane cap to give an uncapped alkyne, and finally; Sonogashira cross coupling of a dibrominated compound with the uncapped alkyne (**Figure 5.2a**).
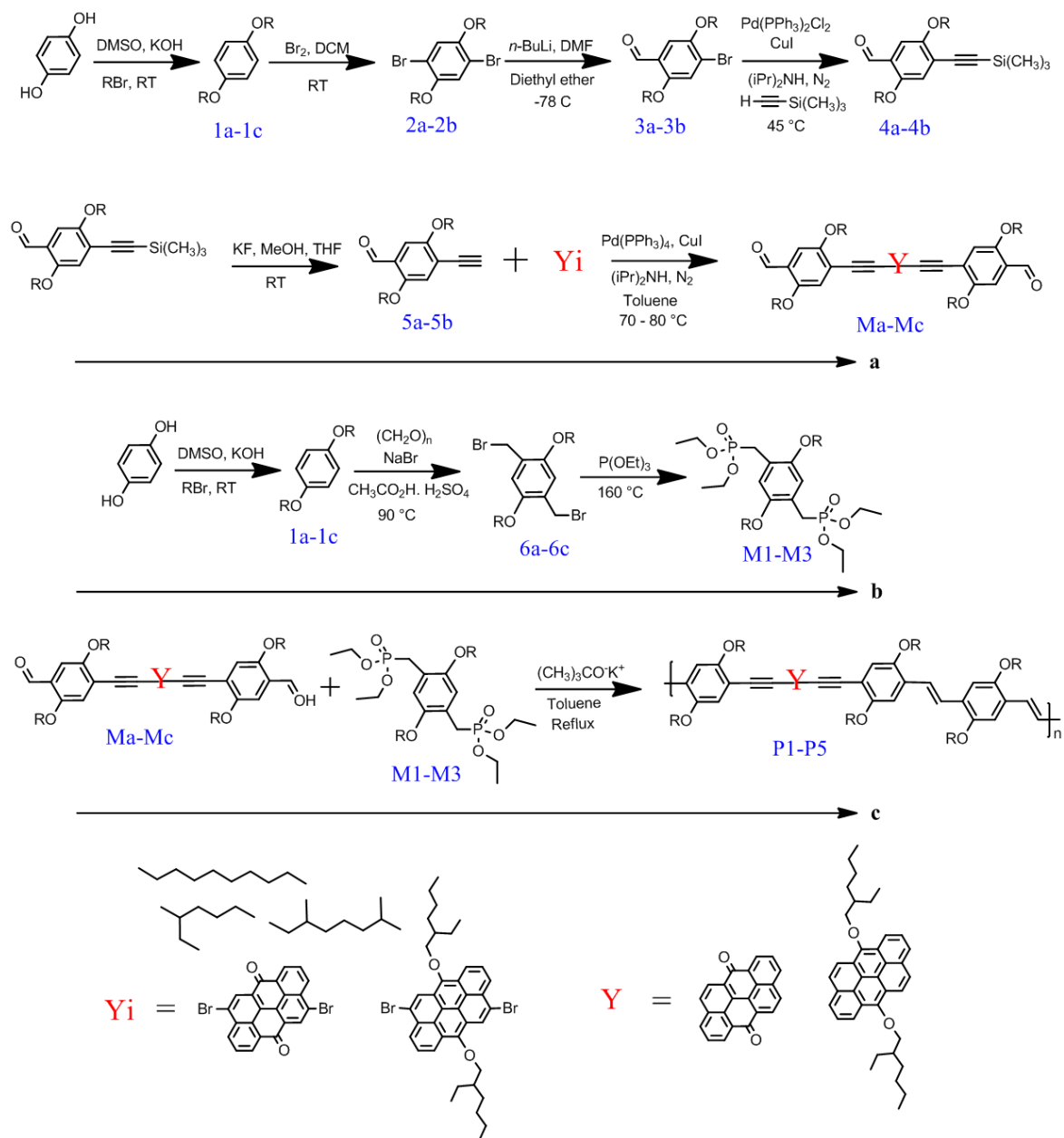
Figure 5.2: Reaction pathway leading to polymer synthesis.

The Sonogashira reactions proceed via the Pd-catalyzed and Cu-cocatalyzed cross-coupling reaction of terminal alkyne and an aryl dihalide with an amine base to form the dialdehyde [30-31, 42-43]. For the bisphosphonate derivatives, the alkyloxy derivative obtained from O-alkylation of hydroquinone was bromomethylated using NaBr, paraformaldehyde, CH_3COOH and H_2SO_4. The bromomethylated derivatives were then converted to the

129

corresponding bisphosphonate esters by the Michealis-Arbuzov reaction (**Figure 5.2b**) [30-31, 42-43]. The polymer synthesis (**Figure 5.2c**) proceeds via the Horner-Wadsworth-Emmons olefination reaction of the dialdehyde with bisphosphonate esters [29, 44-45].

5.1.1.1 Synthesis of Precursors

This section presents the synthesis procedure depicted in **Figure 5.2**.

1,4-bis(decyloxy)benzene (1a)

Dimethylsulfoxide (293 mL) was added to a flask containing hydroquinone (16.19 g, 146.3 mmol). The mixture was deaerated under vigorous stirring for 30 minutes. KOH (25 g, 380.3 mmol) was added in one portion and the deaerating was continued for 30 more mins. Thereafter, 1-bromodecane (84 mL, 0.395 mmol) was added dropwise. The reaction mixture was stirred overnight at room temperature. By pouring into cold water (600 mL) the reaction was quenched. The precipitate was filtered off and washed several times to neutrality. The raw product was re-crystallized in acetone. Filtration and drying in vacuum yielded a white solid (53.2 g, 93%). ^{1}H NMR (300 MHz, CDCl$_3$) δ 6.82 (s, 4H), 3.90 (t, J = 6.6 Hz, 4H), 1.78 (m, 4H), 1.52 – 1.14 (m, 28H), 0.89 (t, J = 6.7 Hz, 6H).

1,4-bis((2-ethylhexyl)oxy)benzene (1b)

A mixture of dimethylsulfoxide (598 mL) and hydroquinone (33.08 g, 298.8 mmol) was deaerated under vigorous stirring for 30 minutes. KOH (51 g, 777.2 mmol) was added in one portion. After another 30 minutes of deaerating 2-ethylhexyl bromide (151 mL, 807.1 mmol)

130

was added dropwise. The reaction mixture was stirred overnight at room temperature and poured into ice water. Toluene was added. The organic phase was washed with brine and water, dried over Na_2SO_4 and filtered. The solvent was evaporated using a rotary evaporator leaving a brown oil, which was subjected to flash column chromatography (silica/toluene) to yield a colourless liquid (95.03 g, 95%). ^{1}H NMR (300 MHz, CDCl$_3$) δ 6.82 (s, 4H), 3.90 (t, J = 6.6 Hz, 4H), 1.87 − 1.63 (m, 2H), 1.52 − 1.14 (m, 16H), 0.89 (m, 12H).

1,4-bis((3,7-dimethyloctyl)oxy)benzene (1c)

Dimethylsulfoxide (73 mL) and hydroquinone (4.24 g, 36.6 mmol) were deaerated for 30 minutes. KOH (6 g, 95.1 mmol) was added in one portion and the deaerating was continued for 30 more minutes. Thereafter, 3,7-dimethyloctyl bromide (22.75 g, 98.7 mmol) was added dropwise. The reaction mixture was stirred overnight at room temperature and poured into ice water. Toluene was added and the organic phase was washed with brined and water, dried over Na_2SO_4 and filtered. The solvent was removed using a rotary evaporator to leave a brown oil, which was distilled under reduced pressure to yield a brown liquid (8.89 g, 62%). ^{1}H NMR (300 MHz, CDCl$_3$) δ 6.82 (s, 4H), 3.89 (t, J = 6.6 Hz, 4H), 1.85 − 1.62 (m, 4H), 1.51 − 1.11 (m, 28H), 0.88 (t, J = 6.7 Hz, 6H).

1,4-dibromo-2,5-bis(decyloxy)benzene (2a)

To a stirred solution of 1a (13.36 g, 34.2 mmol) in dichloromethane (164 mL) bromine (4.40 mL, 85.5 mmol) was added. The mixture was stirred at room temperature overnight. Saturated aqueous K_2CO_3 was added. The organic layer was separated, and the aqueous layer was extracted with DCM. The combined organic layers were washed with aqueous solution

131

of saturated sodium metabisulphite ($Na_2S_2O_5$), dried over anhydrous Na_2SO_4, filtered, and concentrated to yield a light yellow solid (18 g, 96%). ^{1}H NMR (300 MHz, $CDCl_3$) δ 7.08 (s, 2H), 3.94 (t, J = 6.5 Hz, 4H), 1.92 – 1.62 (m, 4H), 1.53 – 1.14 (m, 28H), 0.88 (t, J = 6.7 Hz, 6H).

1,4-dibromo-2,5-bis((2-ethylhexyl)oxy)benzene (2b)

To a stirred solution of 1b (95 g, 284.1 mmol) in dichloromethane (1360 mL) bromine (37 mL, 7103 mmol) was added. After stirring at room temperature overnight saturated aqueous K_2CO_3 was added. The organic layer was separated, and the aqueous layer was extracted with dichloromethane. The combined organic layers were washed with aqueous solution of saturated sodium metabisulphite ($Na_2S_2O_5$), dried over anhydrous Na_2SO_4, filtered, and concentrated to yield a dark yellow liquid (126.3 g, 90%). ^{1}H NMR (300 MHz, $CDCl_3$) δ 7.08 (s, 2H), 3.94 (t, J = 6.5 Hz, 4H), 1.93 – 1.65 (m, 2H), 1.54 – 1.11 (m, 16H), 0.88 (m, 12H).

4-bromo-2,5-bis(decyloxy)benzaldehyde (3a)

2a (11.72 g, 21.4 mmol) was dissolved in dry diethyl ether (235 mL) and deaerated. To the stirred and cooled (-10 °C) mixture a solution of n-BuLi (8.87 mL, 22 mmol, 2.5 M in hexane) was added dropwise, followed by the addition of DMF (2.2 mL, 28.4 mmol). The cooling bath was removed and the solution left to stir overnight. The reaction was quenched by the addition of 10% aqueous HCl. The organic phase was separated and the aqueous phase washed with toluene. The combined organic phases were washed with saturated aqueous $NaHCO_3$ solution and water until neutrality. The organic phase dried over Na_2SO_4, filtered and concentrated using a rotary evaporation. The crude product was further purified by

132

column chromatography (silica; toluene:hexane (1:1)) to yield a bright yellow solid (4.34 g, 40%). ^{1}H NMR (300 MHz, CDCl$_3$) δ 10.41 (s, 1H), 7.30 (s, 1H), 7.22 (s, 1H), 4.14 – 3.89 (m, 4H), 1.91 – 1.67 (m, 4H), 1.52 – 1.08 (m, 28H), 0.88 (t, J = 6.6 Hz, 6H).

4-bromo-2,5-bis((2-ethylhexyl)oxy)benzaldehyde (3b)

2b (35.32 g, 71.7 mmol) was dissolved in dry diethyl ether (788 mL) and deaerated. To the stirred and cooled (-40 °C) mixture a solution of n-BuLi (29.55 mL, 73.9 mol, 2.5 M in hexane) was added dropwise, followed by the addition of DMF (7.4 mL, 95.4 mmol). The cooling bath was removed and the solution was stirred overnight. The reaction was quenched by the addition of 10% aqueous HCl. The organic phase was separated and the aqueous phase washed with toluene. The combined organic phases were washed with water until neutrality, dried over Na$_2$SO$_4$ and concentrated using a rotary evaporator. The crude product was further purified by column chromatography (silica; hexane:dichloromethane (1:1)) to yield a brownish liquid (21.46 g, 68%). ^{1}H NMR (300 MHz, CDCl$_3$) δ 10.42 (s, 1H), 7.31 (s, 1H), 7.23 (s, 1H), 4.00 – 3.76 (m, 4H), 1.87 – 1.62 (m, 2H), 1.62 – 1.11 (m, 16H), 1.03 – 0.77 (m, 12H).

2,5-bis(decyloxy)-4-((trimethylsilyl)ethynyl)benzaldehyde (4a)

To a 1 h deaerated solution of 3a (4.33 g, 8.7 mmol) in diisopropylamine (96 mL) were added Pd(PPh$_3$)$_4$ (0.5 g, 0.44 mmol) and CuI (0.05 g, 0.26 mmol). The resulting mixture was further deaerated for 50 minutes. Trimethylsilylacetylene (1.9 mL, 13.1 mmol) was added dropwise within 3 h to the stirred mixture. The reaction mixture changed from yellow to greenish yellow with addition of the catalyst and to dark green with addition of

133

trimethylsilylacetylene. The reaction was left to run at room temperature overnight and heat was introduced for 2 hours at 45 °C. Toluene (20 mL) was added, and the reaction mixture was filtered over celite to remove the precipitated diisopropyl ammonium bromide. Solvent was removed under reduced pressure and the residue was submitted to column chromatography (silica gel 60; toluene:hexane (1:1)) to yield a dark yellow solid (4.04 g, 90%). ^{1}H NMR (300 MHz, CDCl$_3$) δ 10.42 (s, 1H), 7.16 (s, 1H), 7.04 (s, 1H), 4.00 (m, 4H), 1.91 – 1.65 (m, 4H), 1.27 (m, 28H), 0.88 (m, 6H), 0.35 – 0.12 (s, 9H).

2,5-bis((2-ethylhexyl)oxy)-4-((trimethylsilyl)ethynyl)benzaldehyde (4b)

To a 50 min deaerated solution of 3b (13.07 g, 29.6 mmol) in diisopropylamine (325 mL) were added Pd(PPh$_3$)$_4$ (1.04 g, 1.48 mmol) and CuI (0.17 g, 0.89 mmol). The resulting mixture deaerated for another 50 minutes. Trimethylsilylacetylene (6.45 mL, 44.4 mmol) was added dropwise within 8 h to the stirred mixture. The reaction mixture changed from yellow to greenish yellow upon addition of the catalyst, turbid yellow and then to dark green with addition of trimethylsilylacetylene. The reaction was left stirring at room temperature overnight and heat was introduced for 2 hr at 45 °C. Toluene was added and the mixture was filtered over celite to remove the precipitated diisopropyl ammonium bromide. Solvents were removed under reduced pressure, and the residue was subjected to column chromatography (silica gel 60; hexane:dichloromethane (1:1) as eluent) to yield a dark brown liquid (13 g, 96%). ^{1}H NMR (300 MHz, CDCl$_3$) δ 10.44 (s, 1H), 7.26 (s, 1H), 7.07 (s, 1H), 4.00 – 3.75 (m, 4H), 1.83 – 1.64 (m, 2H), 1.48 – 1.12 (m, 16H), 0.92 (m 12H), 0.35 – 0.14 (m, 9H).

134

2,5-bis(decyloxy)-4-ethynylbenzaldehyde (5a)

4a (2.62 g, 5.1 mmol) and potassium fluoride (1 g, 17.2 mmol) were added to a deaerated solution of methanol (13 mL) and tetrahydrofuran (18 mL). The mixture was protected from light and stirred at room temperature for 3 h. The solvent was removed under reduced pressure, residue dissolved in toluene and washed with water. The organic layer was dried over Na_2SO_4, concentrated under reduced pressure and purified by flash chromatography (silica; toluene:hexane (1:1) as eluent) to yield a bright yellow solid (1.71 g, 76%). ^{1}H NMR (300 MHz, $CDCl_3$) δ 10.43 (s, 1H), 7.30 (s, 1H), 7.08 (s, 1H), 4.02 (m, 4H), 3.45 (s, 1H), 1.95 – 1.63 (m, 4H), 1.46 – 1.03 (m, 28H), 0.88 (t, J = 6.6 Hz, 6H).

2,5-bis((2-ethylhexyl)oxy)-4-ethynylbenzaldehyde (5b)

4b (12.99 g, 28.3 mmol) and potassium fluoride (5 g, 58.1 mmol) were added to a solution of methanol (72 mL) and tetrahydrofuran (102 mL). The mixture was protected from light and stirred at room temperature for 3 h. The solvent was removed under reduced pressure, the residue dissolved in toluene and washed with water. The organic layer was dried over Na_2SO_4 and, after the removal of the solvent, purified by flash chromatography (silica; hexane:dichloromethane (1:1) as eluent) to yield a dark brown oil (9.9 g, 90%). ^{1}H NMR (300 MHz, $CDCl_3$) δ 10.45 (s, 1H), 7.30 (s, 1H), 7.09 (s, 1H), 3.91 (m, 4H), 3.46 (s, 1H), 1.89 – 1.66 (m, 2H), 1.57 – 1.12 (m, 16H), 1.03 – 0.76 (m, 12H).

1,4-bis(bromomethyl)-2,5-bis(decyloxy)benzene (6a)

A suspension of 1a (4.84 g, 12.4 mmol), paraformaldehyde (5.2 g, 169 mmol), and NaBr (6.4 g, 62 mmol) in glacial acetic acid (56 ml) was heated at 70°C yielding a clear solution. To this a 1:1 mixture of concentrated sulfuric acid and glacial acetic acid was added dropwise. The temperature was increased to 90°C and kept for 7 hours. The reaction was allowed to cool to room temperature, the precipitate was filtered off and washed with water several times to a pH of 6 − 7. The precipitate was dried under vacuum and re-crystallized from hexane (50 ml) to give a white solid (6.18 g, 87% yield). ^{1}H NMR (300 MHz, CDCl$_3$) δ 6.85 (s, 2H), 4.52 (s, 4H), 4.08 − 3.85 (m, 4H), 1.92 − 1.67 (m, 4H), 1.53 − 1.15 (m, 28H), 0.88 (t, J = 6.7 Hz, 6H).

1,4-bis(bromomethyl)-2,5-bis((3,7-dimethyloctyl)oxy)benzene (6c)

A suspension of 1c (6.34 g, 16.2 mmol), paraformaldehyde (6.9 g, 221.4 mmol), and NaBr (8.4 g, 81.2 mmol) in glacial acetic acid (74 ml) was heated at 70°C. A 1:1 mixture of concentrated sulfuric acid and glacial acetic acid was added dropwise. The temperature was increased to 90°C and allowed to run for 7 h. The reaction was allowed to cool to room temperature and washed with water several times to a pH of 5 − 6. The crude product was purified by column chromatography (silica; toluene:hexane (1:1)) to yield a creamy colored solid (5.5 g, 59%). ^{1}H NMR (400 MHz, CDCl$_3$) δ 6.86 (s, 2H), 4.53 (s, 4H), 4.11 − 3.94 (m, 4H), 1.96 − 1.79 (m, 2H), 1.78 − 1.66 (m, 2H), 1.66 − 1.45 (m, 4H), 1.45 − 1.25 (m, 8H), 1.25 − 1.09 (m, 6H), 0.97 (m, 6H), 0.88 (d, J = 6.6 Hz, 12H).

136

5.1.1.2 Monomer Synthesis

Synthesis of M1

A mixture of 1,4-bis(bromomethyl)-2,5-(2-ethylhexyloxy)benzene (15.2 g, 18.97 mmol) and excess triethylphosphite (9.47 g, 57 mmol) was stirred and heated slowly to 150±160°C; simultaneously, the evolving ethyl bromide was distilled off. After 4 h, vacuum was applied for 30 mins at 180°C to distil off excess triethylphosphite. The resulting oil was allowed to cool to room temperature to form pure oily substance (14.4 g, 83% yield). ^{1}H NMR (300 MHz, CDCl$_3$) δ/ppm: 6.92 (d, J = 1.6 Hz, 2H), 4.08 – 3.89 (m, 8H), 3.79 (d, J = 5.6 Hz, 4H), 3.15 (d, J = 20.1 Hz, 4H), 1.76 – 1.59 (m, 2H), 1.55 – 1.34 (m, 10H), 1.34 – 1.11 (m, 18H), 0.99 – 0.63 (m, 12H); ^{13}C NMR (75 MHz, CDCl$_3$) δ 150.43, 119.30, 114.50, 71.17, 61.8, 39.65, 30.58, 29.09, 27.06, 25.21, 23.89, 23.00, 16.30, 14.01, 11.12.

M2 and M3 were prepared under similar reaction conditions as described for M1

Synthesis of M2

A mixture of 1,4-bis(bromomethyl)-2,5-decyloxybenzene (3.37 g, 5.85 mmol) (6a) and excess triethylphosphite (3.0 g, 17.6 mmol) was stirred and heated slowly to 150±160°C, and the evolving ethyl bromide was distilled off simultaneously. The reaction went on for 4 h, after which vacuum was applied for 1 h at 180°C to distil off any excess triethylphosphite left in the mixture. The resulting oil was allowed to cool to room temperature to form a white solid, which was recrystallized from diethyl ether (30 ml) yielding (3.9 g, 97%) of pure substance. ^{1}H NMR (400 MHz, CDCl$_3$) δ 6.89 (s, 2H), 4.00 (m, 8H), 3.90 (t, J = 6.5 Hz, 4H),

137

3.20 (d, $J = 20.3$ Hz, 4H), 1.82 – 1.65 (m, 4H), 1.41 – 1.15 (m, 40H), 0.86 (t, $J = 6.6$ Hz, 6H);

^{13}C NMR (100 MHz, CDCl$_3$) δ 150.31, 119.28, 114.70, 68.89, 61.69, 31.89, 29.61, 29.56, 29.47, 29.44, 29.32, 26.92, 26.13, 25.54, 22.67, 16.38, 16.34, 16.31, 14.10.

Synthesis of M3

A mixture of 1,4-bis(bromomethyl)-2,5-(3,7-dimethyloctyloxy)benzene (5.1 g, 8.7 mmol) (6c) and excess triethylphosphite (4.4 g, 26.1 mmol) was stirred and heated slowly to 150±160°C, and the evolving ethyl bromide was concurrently distilled off. After 4 h, vacuum was applied for 30 min at 180°C to distil off any excess triethylphosphite still present in the mixture. The resulting oil was allowed to cool to room temperature to form a pure yellowish oil (5.73 g, 96% yield). ^{1}H NMR (400 MHz, CDCl$_3$) δ 6.85 (s, 2H), 4.07 – 3.79 (m, 12H), 3.14 (d, $J = 20.4$ Hz, 4H), 1.86 – 1.37 (m, 8H), 1.32 – 1.01 (m, 24H), 0.86 (d, $J =$ Hz, 6H), 0.79 (d, $J = 6.6$ Hz, 12H); ^{13}C NMR (100 MHz, CDCl$_3$) δ 150.15, 119.18, 114.60, 67.01, 61.61, 38.99, 37.09, 36.23, 29.63, 27.72, 26.71, 25.32, 24.45, 22.45, 22.34, 19.44, 16.09.

Synthesis of Ma

4,10-Dibromoanthanthrone (408 mg, 0.88 mmol) was given to a degassed solution of 15 mL of diisopropylamine and 40 mL of tetrahydrofuran. 30 mins later, Pd(PPh$_3$)$_4$ (45.1 mg, 0.04 mmol), and CuI (7.4 mg, 0.04 mmol) were added. Mixture was allowed to stir and degas for another 30 mins and thereafter, 2,5-bis((2-ethylhexyl)oxy)-4-ethynylbenzaldehyde (750 mg, 2.0 mmol) (in a solution of degassed THF) was added drop-wisely. The reaction mixture was heated at 60 °C for 72 h in a nitrogen atmosphere and monitored with TLC. 40 mL of toluene was thereafter added and heat removed while still stirring. After cooling to room temperature,

138

the mixture was re-precipitated in cold methanol and refrigerated for 4 h. The mixture was filtered, re-dissolved in toluene and concentrated under vacuum. The residue was chromatographed on a silica gel column with toluene as eluent to yield 350 mg (37%) of a purplish black substance. ^{1}H NMR (300 MHz, CDCl$_3$) δ 10.47 (s, 2H), 8.87 – 8.66 (m, 4H), 8.60 (s, 2H), 7.95 – 7.73 (m, 2H), 7.32 (s, 2H), 7,17 (s, 2H), 4.17 – 3.82 (m, 8H), 2.03 – 1.73 (m, 4H), 1.73 – 1.16 (m, 32H), 1.1 – 0.8 (m,24H); ^{13}C NMR (100 MHz, CDCl$_3$) δ 188.98, 182.12, 155.49, 154.07, 134.07, 133.74, 131.28, 129.53, 129.30, 128.63, 127.60, 125.45, 124.11, 119.09, 117.49, 109.36, 94.20, 93.96, 71.72, 71.65, 39.57, 39.48, 30.65, 30.34, 29.71, 29.14, 29.01, 24.04, 23.77, 23.11, 23.08, 14.13, 14.07, 11.26, 11.06.

Mb and Mc were prepared under similar reaction conditions as described for Ma
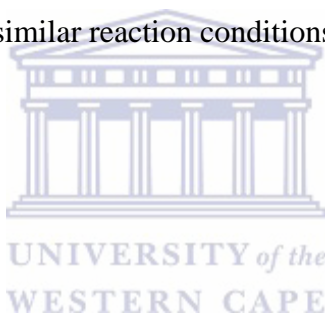
Synthesis of Mb

4,10-Dibromo-6,12-ethylhexyloxylanthanthrene (200 mg, 0.29 mmol) was given to a degassed solution of 10 mL of diisopropylamine and 20 mL of toluene. Pd(PPh$_3$)$_4$ (16.7 mg, 0.015 mmol), and CuI (2.8 mg, 0.015 mmol) were added after 30 mins of stirring and degassing and the reaction was allowed to run under same condition for 1 h. 2,5-bis(decyloxy)-4-ethynylbenzaldehyde (320 mg, 0.72 mmol) was dissolved in 15 mL of toluene and degassed for 30 mins. The degassed solution of 2,5-bis(decyloxy)-4-ethynylbenzaldehyde was added drop-wisely to the reaction mixture. The reaction mixture was heated at 70-80 °C for 24 h in a nitrogen atmosphere and monitored with TLC. 40 mL of toluene was added and heat removed while still stirring. After cooling to room temperature, the precipitated diisopropylammonium bromide was filtered off and the solvent was evaporated under vacuum. The residue was chromatographed on a silica gel column with

toluene:hexane (4:1) as eluent. 380 mg (93% yield) of a greenish substance was obtained. ^{1}H NMR (300 MHz, CDCl₃) δ 10.49 (s, 2H), 8.94 (d, J = 7.4 Hz, 2H), 8.80 (d, J = 8.1 Hz, 2H), 8.73 (s, 2H), 8.19 (m, 2H), 7.38 (s, 2H), 7.22 (s, 2H), 4.29 (d, J = 5.5 Hz, 4H), 4.21 − 4.07 (m, 8H), 2.23 − 1.68 (m, 10H), 1.68 − 1.08 (m, 78H), 1.03 (t, J = 7.0 Hz, 6H), 0.90 (t, J = 6.6 Hz, 6H), 0.77 (t, J = 6.7 Hz, 6H); ^{13}C NMR (100 MHz, CDCl₃) δ 189.13, 155.51, 153.95, 150.13, 130.72, 127.58, 125.98, 125.61, 124.88, 124.52, 123.95, 121.27, 120.54, 120.22, 119.50, 117.12, 109.28, 96.16, 90.48, 69.26, 59.55, 41.30, 38.17, 31.94, 31.86, 31.26, 30.48, 29.70, 29.62, 29.46, 29.32, 26.12, 24.03, 23.31, 22.72, 22.58, 14.32, 14.15, 14.05, 11.56.

Synthesis of Mc

4,10-Dibromo-anthanthrone (200 mg, 0.43 mmol) was given into a degassed solution of 12 mL of diisopropylamine and 20 mL of toluene. Pd(PPh₃)₄ (20.3 mg, 0.02 mmol) and CuI (3.3 mg, 0.02 mmol) were added. Degassed solution of 2,5-bis(decyloxy)-4-ethynylbenzaldehyde (390 mg, 0.88 mmol) was added drop-wisely after 30 mins. The reaction mixture was heated at 70-80 °C for 24 h in a nitrogen atmosphere. Toluene was added and reaction mixture stirred to acquire room temperature. After cooling to room temperature, the precipitated diisopropylammonium bromide was filtered off and the solvent was distilled off under vacuum. The residue was chromatographed on a silica gel column with toluene as eluent to yield 130 mg (26% yield) of a purple substance. Same reaction was conducted in THF at 60 °C for 72 h. After cooling, the mixture was re-precipitated in cold methanol (100 mL). The precipitate was recovered via filtration, and the crude residue was purified by silica gel column chromatography (toluene) to afford Mc as a purplish black solid (74% yield). ^{1}H NMR (300 MHz, CDCl₃) δ 10.44 (s, 2H), 8.72 (d,d, J = 6.9 Hz, 4H), 8.49 (s, 2H), 7.82 − 7.68 (m, 2H), 7.24 − 7.13 (m, 2H), 7.09 (s, 2H), 4.06 (t,t, J = 6.6 Hz, 8H), 2.17 (m, 4H), 1.91 (m,

8H), 1.66 − 1.08 (m, 56H), 0.87 − (t,t, *J* = 6.2 Hz, 6H, 6H). Acquisition of the ^{13}C NMR spectrum of Mc proved unsuccessful because of the poor solubility and precipitation of the product during the course of the acquisition.

5.1.1.3 Polymer Synthesis

Synthesis of P1

For the synthesis of P1, a solution of Ma (150 mg, 0.14 mmol) and M1 (89 mg, 0.14 mmol) in dry toluene (12 mL) was mechanically stirred and heated under nitrogen to reflux. The polymerization was initiated by the addition of potassium tert-butoxide (63 mg, 0.56 mmol) and an instant color change from deep pink to black was observed. Reaction mixture was stirred for 45 min and additional toluene (100 mL) was added. The reaction was quenched with aqueous HCl (10%, 10 mL). The organic phase was separated and washed with deionized water until a pH of ~ 7 was obtained. Residual water was removed from the mixture by heating to reflux in a Dean Stark apparatus. The obtained solution was concentrated under reduced pressure using a rotary evaporator. The resulting concentrated solution was precipitated in cold methanol and kept in the refrigerator for 24 h. After 24 h the precipitate was filtered off in a Soxhlet thimble and transferred into a Soxhlet extractor. Extraction was done using methanol to remove oligomers and any impurity. The extraction continued until the extract became colorless. The polymer was re-dissolved in toluene, re-precipitated in cold methanol and stored in the refrigerator. After 24 h, it was filtered and dried under air to obtain 190 mg (95% yield) of black partially soluble polymeric material. GPC (THF as eluent; polystyrene as standard): Mn 1,830 g/mol, Mw 3,570 g/mol, PDI 2. ^{1}H NMR (300 MHz, CDCl$_3$) δ 10.48 (s), 9.25 − 8.41 (m, anthanthronylene H's), 8.07 − 6.67 (m,

141

arylene vinylene H's), 4.37 – 3.20 (m, -CH2O-), 2.49 – 0.37 (m, alkyl H's). FTIR cm^{-1}: 3064 (ν(=C-H)), 2962, 2934 and 2878 (ν(C-H)), 2198 (ν(C≡C)), 1659 (ν(C=O)), 1575 (ν(C=C) vinylene linker), 1500 (ν(C=C) aromatic ring), 1464 (δ (CH$_2$)), 1380 (δ (CH$_3$)), 1203 (ν(C=C-O-C) aromatic-aliphatic).

P2 – P5 were prepared under similar reaction conditions as described for P1

Synthesis of P2

A solution of Mb (170 mg, 0.12 mmol) and M2 (83 mg, 0.12 mmol) in dry toluene (12 mL) was mechanically stirred and heated under nitrogen to reflux. Potassium tert-butoxide (54 mg, 0.48 mmol) was added at a stable temperature to initiate the reaction. A color change from bright to dark green was observed. The reaction mixture was stirred for 80 min. Thereafter, toluene (100 mL) was added, and the reaction was quenched with aqueous HCl (10%, 10 mL) to neutralize the potassium tert-butoxide. Mixture was cooled to room temperature; the organic phase separated and washed with deionized water until a pH of ~ 7 was obtained. Residual water was removed from the mixture by heating to reflux in a Dean Stark apparatus. The obtained solution was concentrated under reduced pressure using a rotary evaporator. The resulting concentrated solution was precipitated in cold methanol and kept in the refrigerator for 24 h. After 24 h the precipitate was filtered off and transferred into a Soxhlet extractor, and extracted using methanol. The polymer was re-dissolved in chloroform and re-precipitated in cold methanol. It was filtered and dried after 24 h to obtain 220 mg (95% yield) of brownish green polymeric material. GPC (THF as eluent; polystyrene as standard): Mn 3,200 g/mol, Mw 11,730 g/mol, PDI 3.7. ^{1}H NMR (300 MHz, CDCl$_3$) δ 9.05 - 8.22 (anthanthrenylene H's), 7.58 - 6.92 (arylene vinylene H's), 4.28- 3.28 (m, -CH$_2$O-), 2.41 – 0.42 (m, alkyl H's). FTIR cm^{-1}: 3064 (ν(=C-H)), 2962, 2924 and 2850 (ν(C-H)),

2180 (ν(C≡C)), 1594 (ν(C=C) vinylene linker), 1500 (ν(C=C) aromatic ring), 1464 (δ (CH$_2$)), 1203 (ν(C=C-O-C) aromatic-aliphatic).

Synthesis of P3

P3 was obtained from a solution of Mb (190 mg, 0.14 mmol) and M3 (93 mg, 0.15 mmol) in dry toluene (13 mL). Both monomers were mechanically stirred and heated to reflux under nitrogen. The polymerization was initiated by the addition of potassium tert-butoxide (60 mg, 0.56 mmol). A color change from bright green to deep green was observed. The reaction mixture was stirred for 1 h 20 mins. Chloroform (100 mL) was thereafter added, and the reaction was quenched with aqueous HCl (10%, 10 mL) to neutralize the potassium tert-butoxide. Mixture was cooled to room temperature; the organic phase was separated and washed with deionized water until a pH of ~ 7 was obtained. Residual water was removed from the mixture by heating to reflux in a Dean Stark apparatus. The obtained solution was concentrated under reduced pressure using a rotary evaporator. The resulting concentrated solution was precipitated in cold methanol and kept in the fridge for 24 h. After 24 h the precipitate was filtered off in a thimble and transferred into a Soxhlet extractor, and extracted with methanol. The polymer was re-dissolved in chloroform and re-precipitated in methanol. 24 h later, it was filtered and dried to obtain a brownish green polymeric material. Two different reactions with different temperature were conducted for this polymer synthesis. One was done at 111 °C [GPC (THF as eluent; polystyrene as standard): Mn 3,650 g/mol, Mw 11,800 g/mol, PDI 3.2] and the other at 118 °C [GPC (THF as eluent; polystyrene as standard): Mn 2,880 g/mol, Mw 7,820 g/mol, PDI 2.7]. The reaction conducted at 111 °C is soluble in common organic solvents and yielded 180 mg (73% yield) while that conducted at 118 °C (33% yield) is only partially soluble at heated temperatures. ^{1}H NMR (300 MHz,

143

CDCl$_3$) δ 8.73 (dd, *J* = 126.1, 116.0 Hz, (anthanthreneylene H's)), 7.65 -6.90 (m, arylene vinylene H's), 4.61 – 3.48 (m, -CH$_2$O-), 2.38 – 0.42 (m, alkyl H's). FTIR cm^{-1}: 3073 (ν(=C-H)), 2962, 2924 and 2850 (ν(C-H)), 2198 (ν(C≡C)), 1603 (ν(C=C) vinylene linker), 1500 (ν(C=C) aromatic ring), 1464 (δ (CH$_2$)), 1203 (ν(C=C-O-C) aromatic-aliphatic).

P4 and P5 were synthesized under similar reaction conditions as described for P1 – P3. For P4, monomers Mc and M1 were employed while for P5; monomers Mc and M3 were employed. Both polycondensation reactions produced materials that appeared completely insoluble and could not be further characterized.

Synthesis of Small Molecule (SM)

Mb (190 mg, 0.14 mmol) and diethyl benzylphosphonate (79 mg, 0.34 mmol) were dissolved in dried toluene (15 ml) to give a greenish brown color while stirring vigorously under nitrogen and heating under reflux. Potassium-*tert*-butoxide (62 mg, 0.5 mmol) was added (and the reaction mixture was heated at reflux for 30 mins. After 30 mins toluene was added, heat removed and aqueous HCl (10 wt.%) was added. The purification process yielded a greenish material (170 mg,79 %). ^{1}H NMR (300 MHz, CDCl$_3$) δ 9.08 (d, *J* = 7.3 Hz, 2H), 8.92 – 8.78 (m, 2H), 8.27 (t, *J* = 7.7 Hz, 2H), 7.64 (d, *J* = 7.6 Hz, 4H), 7.56 - 7.18 (m, 16H), 4.37 (d, *J* = 5.2 Hz, 4H), 4.28 (t, *J* = 6.4 Hz, 4H), 4.15 (t, *J* = 6.2 Hz, 4H), 2.19 (m, 2H), 1.94 – 1.03 (m, 80H), 0.94 (d, *J* = 6.6 Hz, 12H), 0.83 (t, *J* = 6.2 Hz, 12H).

NMR spectra were measured in CDCl$_3$ with a Gemini 300 MHz spectrometer and Bruker Avance IIIHD 400 MHz Nanobay NMR spectrometer equipped with a 5 mm BBO. Gel-permeation chromatography (GPC) measurements in form of size exclusion chromatography

144

(SEC) were performed using a Pump Deltachrom (Watrex Comp.) with a Midas autosampler and two columns of MIXED-B LS PL gel, particle size 10 μm. An evaporative light scattering detector (PL-ELS-1000 from Polymer Laboratories) was used; THF was the mobile phase and polystyrene standards were used for calibration.

5.1.2 UV-Vis and Photoluminescence Measurements

The UV-Vis and photoluminescence measurements were conducted using a Perkin Elmer UV-Vis/NIR Lambda 1050 spectro and a PTi Photon Technology Intl. fluorometer, respectively. Polymer was dissolved in chlorobenzene ($1.0 * 10^{-5}$ M) for the solution measurements while 80 μL solution was spin-coated from a 10 mg/mL solution on pre-cleaned ITO coated glass substrate at a speed of 20 rps for film measurement.
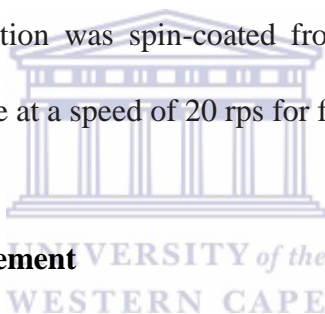
5.1.3 Electrochemical Measurement

The electrochemical properties in thin film which includes the redox potentials and the positions of the frontier orbitals of P1, P2 and P3 were investigated using cyclic voltammetry in acetonitrile with tetrabutylammonium hexafluorophosphate ($TBAPF_6$) as supporting electrolyte, a Ag/AgCl reference electrode, a platinum wire counter electrode and indium-doped tin oxide (ITO)-coated glass slides (15 Ω/sq, Xin Yan Tech. LTD) covered with a thin film of the polymer was used as working electrode (WE) at a scan rate of 50 mV/s. Experiments were set up in a glove box and recorded with a Jaissle Potentiostat-Galvanostat IMP 83 PC - 10. The potentials were measured at the position of the current onset. Prior to measurements, substrates were cleaned using the standard procedure for substrate cleaning as detailed below

145

Standard procedure for substrate cleaning:

- ✓ Wipe with kimwipe with isopropanol

- ✓ Clean in piranha solution

    Recipe for cleaning subatrates with piranha solution

    - • 300 mL H_2O + 5 mL NH_4OH solution (ultrasonicate at 80°C for 15 min)

    - • Add 2 mL H_2O_2 solution

    - • Untrasonicate at 80°C (bubbling) for 15 min

Substrate used: ITO glass substrate

    Size: 61.5 x 8.5 mm

Spin coating program

    16 rps 2 s   25 s

    33 rps 2 s   30 s

150 µL of each polymer sample was spin-coated from solution (10 mg/mL) in chlorobenzene and dried in air.

5.1.4   Infrared Spectroscopy, Stability, and Thickness Measurements

Fourier transform infrared spectroscopy (FTIR) was performed with Perkin Elmer ATR TWO FTIR Spectrometer at room temperature. Thermal gravimetric analysis (TGA) was analysed using Perkin Elmer TGA 7 from 20-600 at 10°C/min in nitrogen. The thickness of the films was characterized with Bruker DektakXT profilometer.

5.1.5   Photovoltaic Measurement

Indium-doped tin oxide (ITO)-coated glass slides (15 Ω/sq, Xin Yan Tech. LTD) (substrates) were pre-cut and cleaned before spin-coating, evaporation of top electrode and subsequent measurement. Below is the step-by-step procedure

Procedure for cutting and cleaning of substrates:

Cutting of substrates (1.5 x 6.4 mm)

Etching in HCl

Cutting into smaller sizes (1.5 x1.5 mm)

Substrates were cleaned using the standard procedure for substrate cleaning

Standard procedure for substrate cleaning (1.5 x 1.5 mm):

1. Acetone + 20 min ultrasonic bath [room temperature]

2. Isopropanol + 20 min ultrasonic bath [room temperature]

3. Dried with compressed N_2 gun

The above process is followed by plasma treatment and device fabrication as illustrated below:

ITO substrate $\rightarrow$ plasma oven treatment (plasma ETCH PE-50) 5 min, 50W O_2

Spin-coating of PEI (80 μL spincoated for each substrate)

Substrate/PEI treatment for 10 mins @ 105°C

Spin-coating of active layer (donor:acceptor) on substrate/PEI

Spin coating program

　　　20 rps 2 s   25 s

　　　33 rps 2 s   30 s

80 μL of each active layer spin-coated

Evaporation of top electrode (MoOx (0.1 KA) and Ag (1.0 KA)). Evaporation was achieved using Univex 350 Leybold instrument.

Measurement of current-voltage (*I-V*) curves and equivalent quantum efficiency (EQE):

Current voltage (*I-V*) curves of the devices were recorded in the dark and under illumination using a solar simulator. A "Gold sun" Sun simulator was used to record the current-voltage characteristics with LS02821 LOT Quantum Design at 100 mW/cm^2 Keithley output reader. All *I-V* characteristics measurements were carried out in nitrogen filled glovebox. External quantum efficiency (EQE) were measured with EG & G Instruments lock-in-amplifier, optical chopper – SEITEC Instruments LTD Muller Electronics Optics LXH100.

5.2   Results and Discussion
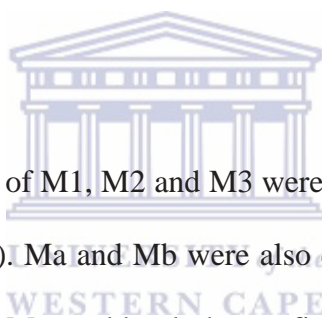
The chemical structure and purity of M1, M2 and M3 were confirmed by ^{1}H NMR, ^{13}C NMR and ^{31}P NMR (**Figure 5.3 – 5.11**). Ma and Mb were also confirmed using ^{1}H NMR and ^{13}C NMR (**Figure 5.12 - 5.15**), while Mc could only be confirmed using ^{1}H NMR (**Figure 5.16**) due to solubility issues. For the polymers P1, P2 and P3, ^{1}H NMR and FTIR spectroscopy were conducted (**Figure 5.17 – 5.19, 5.21 - 5.23**), while the small molecule SM was confirmed by ^{1}H NMR only (**Figure 5.20**).

5.2.1   Nuclear Magnetic Resonance (NMR) Spectroscopy

The NMR investigation of M1 – M3 confirms all the protons, carbon and phosphorous present in the compounds. The ^{1}H NMR **(Figure 5.3, 5.6, and 5.9)** reveal the protons in the two CH groups in the benzene ring of M1 – M3 in the region 6.92 – 6.85 ppm. In the region 4.04 – 6.85 ppm, the –CH$_2$ protons in the phosphonate end of the compounds was observed.

148

The -CH$_2$ protons directly linked to the oxygen in the alkyloxy side chain are seen in the region 3.91 – 3.73 ppm, the -CH$_2$ protons linking the benzene ring to the phosphonate are seen around 3.20 – 3.14 ppm; and the -CH next to the CH$_2$ attached to the oxygen ring (in the case of M1 and M3), all CH$_3$ and other CH$_2$ protons present in the compound appear in the region 1.86 – 0.63 ppm. The ^{13}C NMR **(Figure 5.4, 5.7, and 5.10)** reveal the carbons present in the compound while the ^{31}P NMR **(Figure 5.5, 5.8, and 5.11)** reveal just a signal confirming the presence of just one type of phosphorous present in the compound as expected.
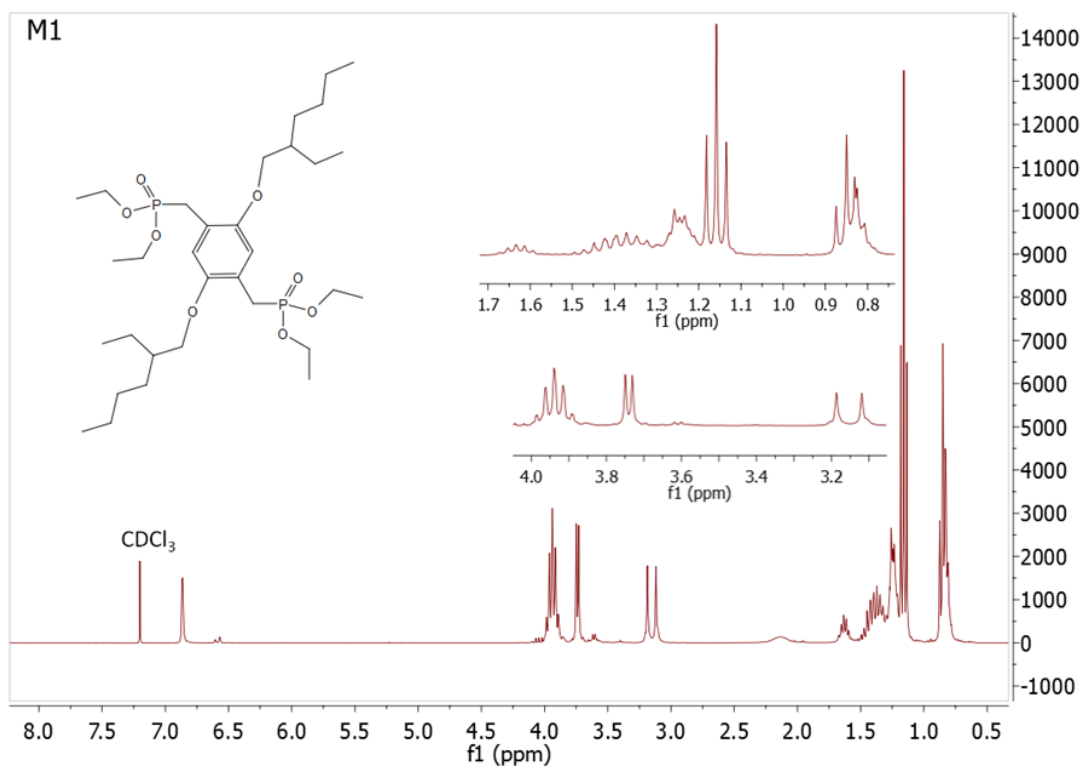
Figure 5.3: ^{1}H NMR signal of M1.
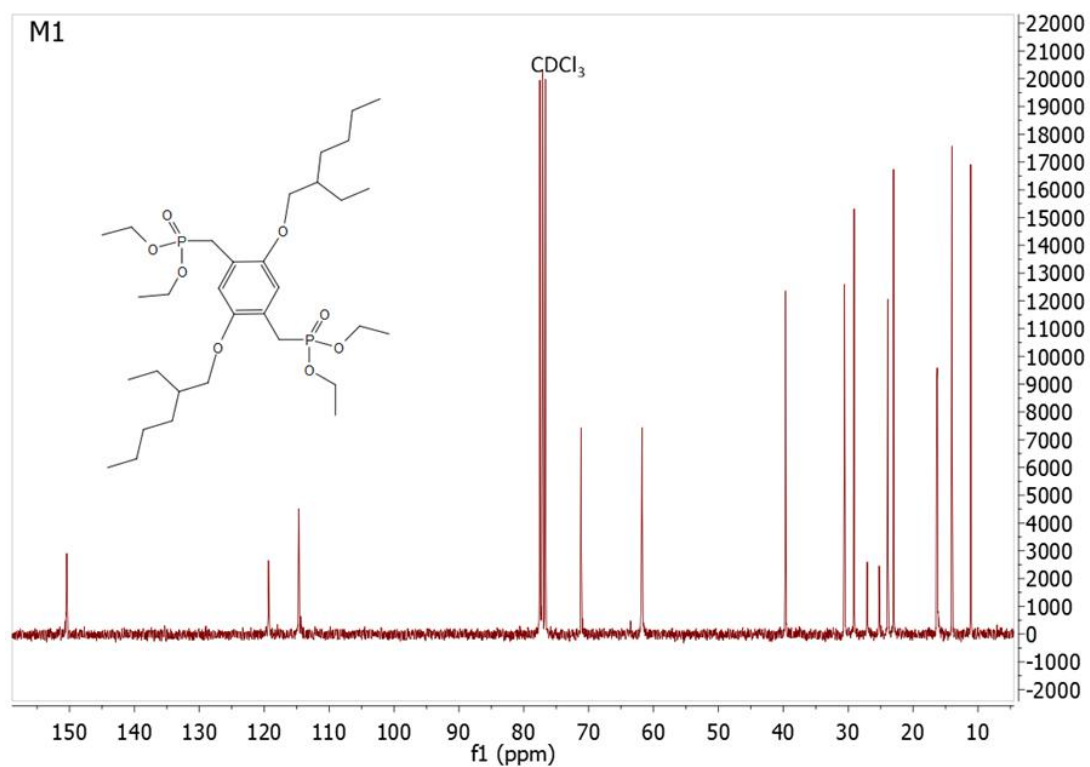
Figure 5.4: ^{13}C NMR signal of M1.
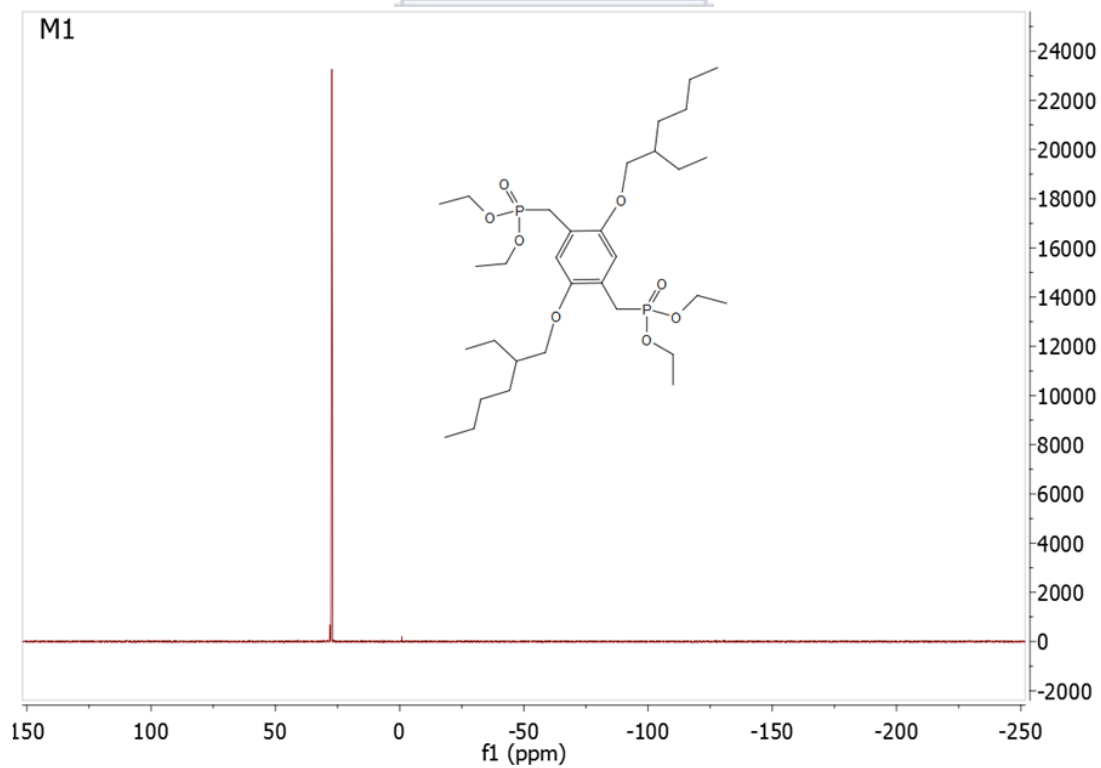
Figure 5.5: ^{31}P signal of M1.

150
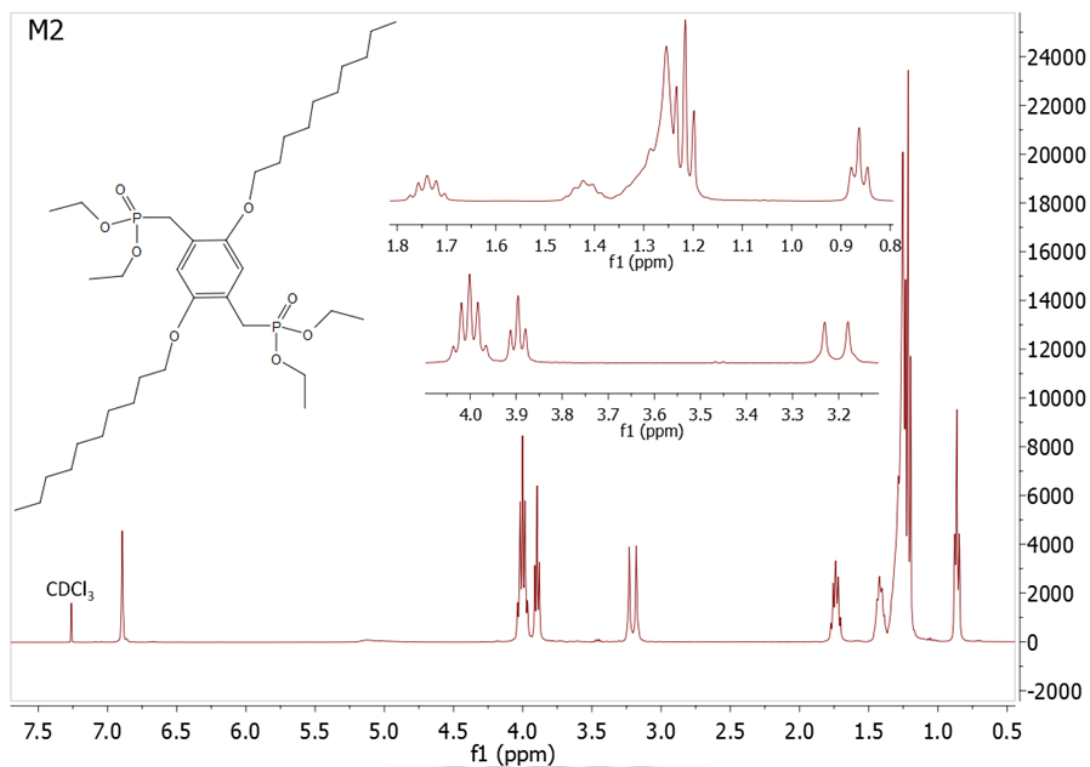
Figure 5.6: ^{1}H NMR signal of M2.
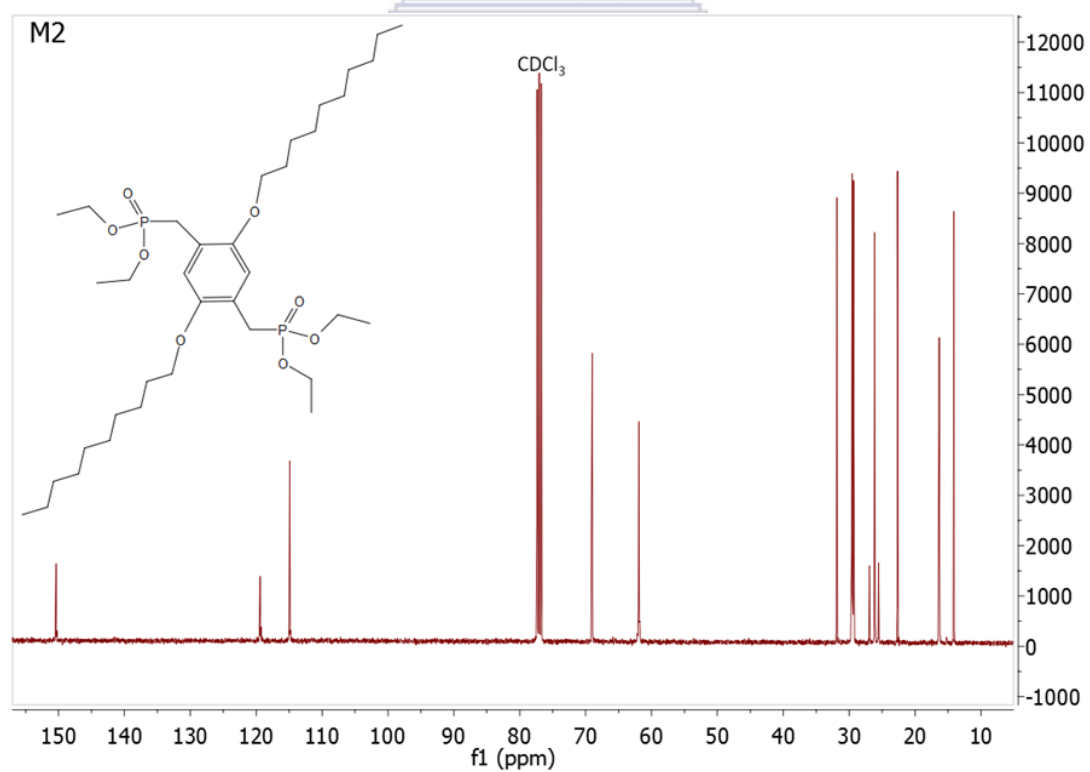
Figure 5.7: ^{13}C NMR signal of M2.

151
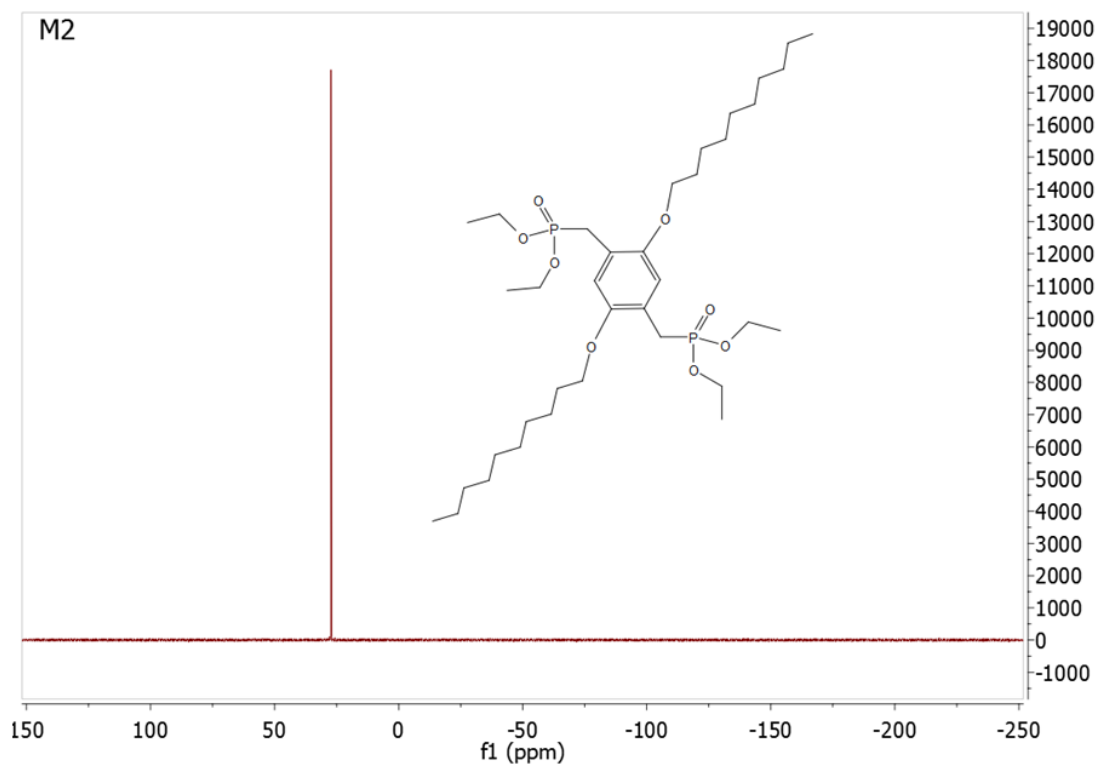
Figure 5.8: [31]P signal of M2.
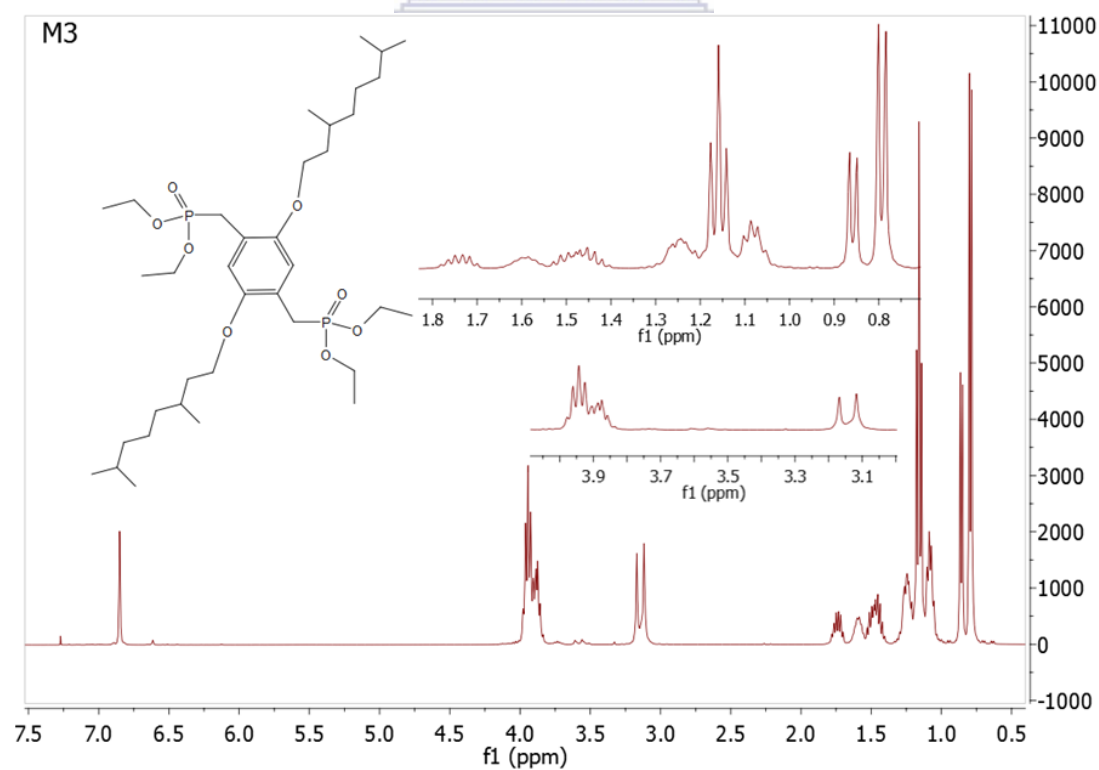
Figure 5.9: ^{1}H NMR signal of M3.

152
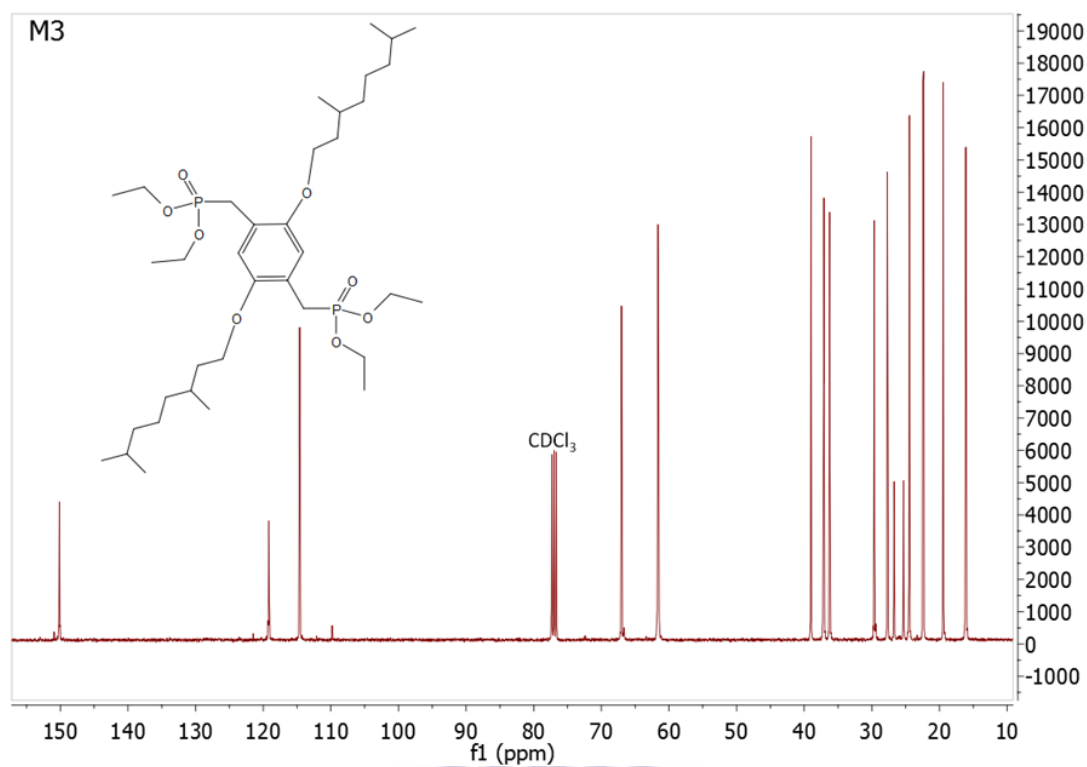
Figure 5.10: ^{13}C NMR signal of M3.
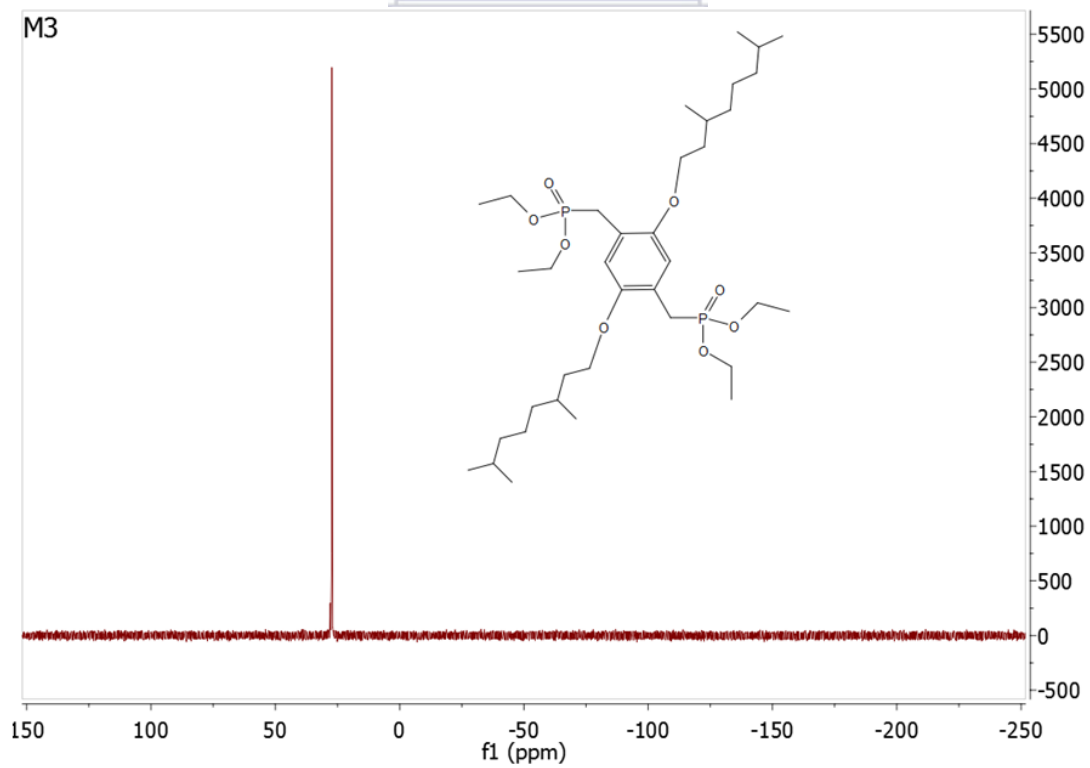
Figure 5.11: [31]P signal of M3.

153

For Ma – Mc, the ^{1}H signals **(Figure 5.12, 5.14, and 5.16)** in the range 10.49 – 10.44 ppm are attributed to the CHO aldehyde protons while the CH protons in the anthanthrone/anthanthrene unit appear in the range 8.94 – 7.09 ppm. The CH protons in the phenyl group attached to both ends of the anthanthrone/anthanthrene unit via the triple bond are seen in the 7.38 – 7.09 ppm region, while the CH_2 protons directly linked to the oxygen in the alkoxy side chain both in the phenyl group and in the anthanthrene unit are visible in the 4.92 – 3.49 ppm region; the CH (ethylhexyloxy side chain) and CH_2 (decyloxy side chain) protons next to the CH_2 protons directly linked to the oxygen of the alkoxy side chains are assigned to the signals in the range 2.36 – 1.68 ppm. All other CH_2 protons present in the compounds show signals in the range 1.68 – 1.03 ppm while the signals of all CH_3 protons are clearly visible in the 1.03 – 0.87 ppm range. The ^{13}C spectra of Ma and Mb has been schematically illustrated and explained as shown in **Figure 5.13 and 5.15** respectively.
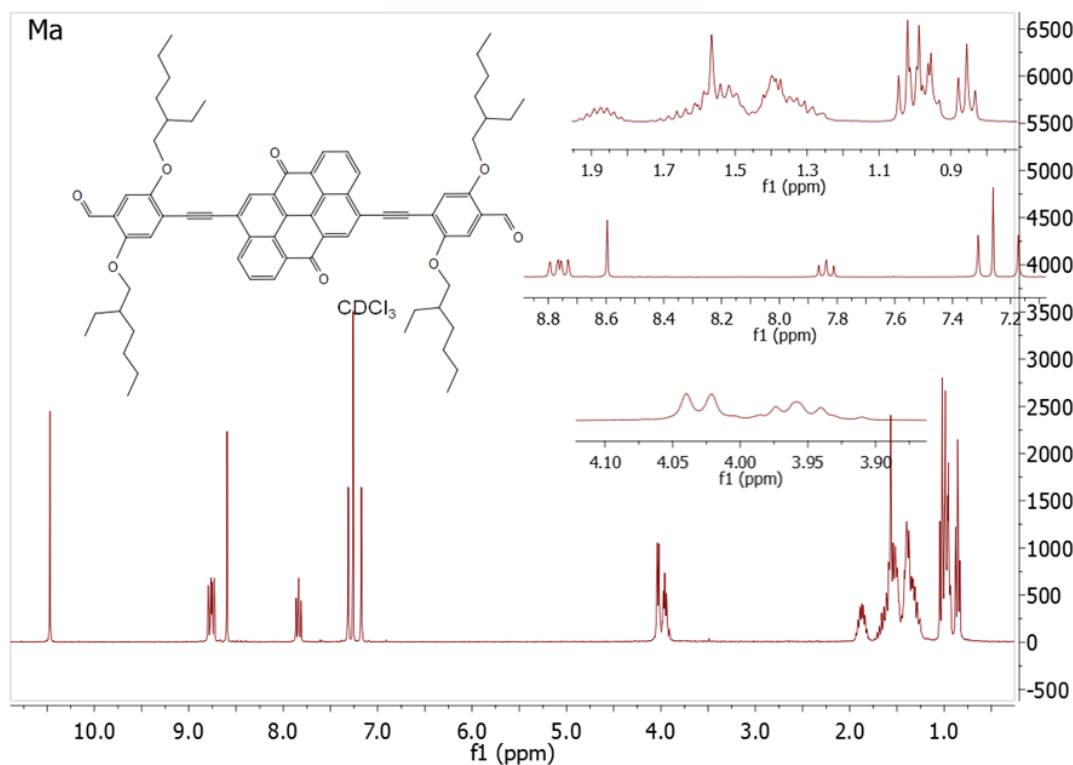
Figure 5.12: ^{1}H NMR signal of Ma.

154
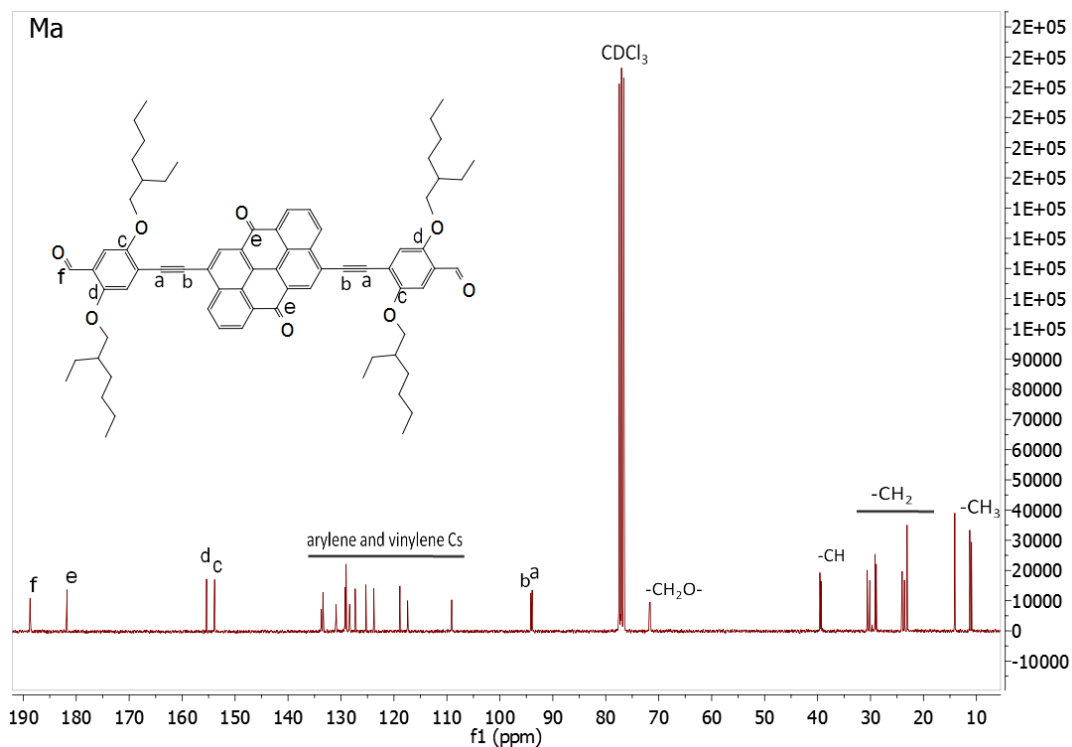
Figure 5.13: ^{13}C NMR signal of Ma.
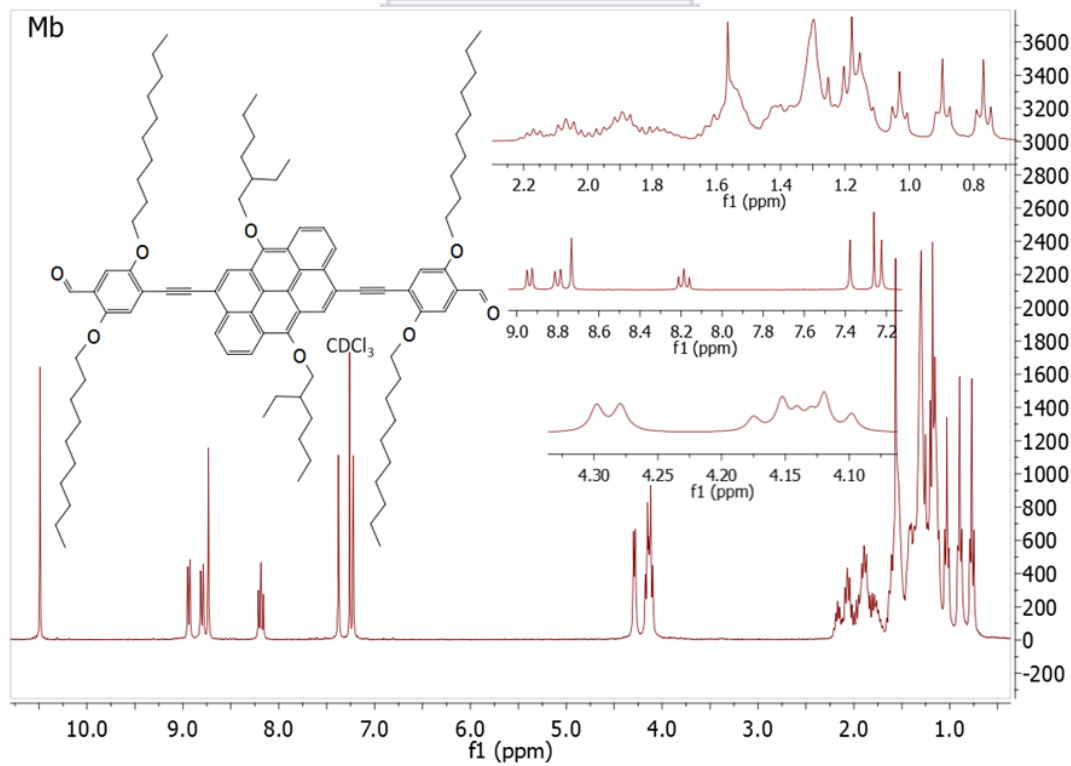
Figure 5.14: ^{1}H NMR signal of Mb.

155
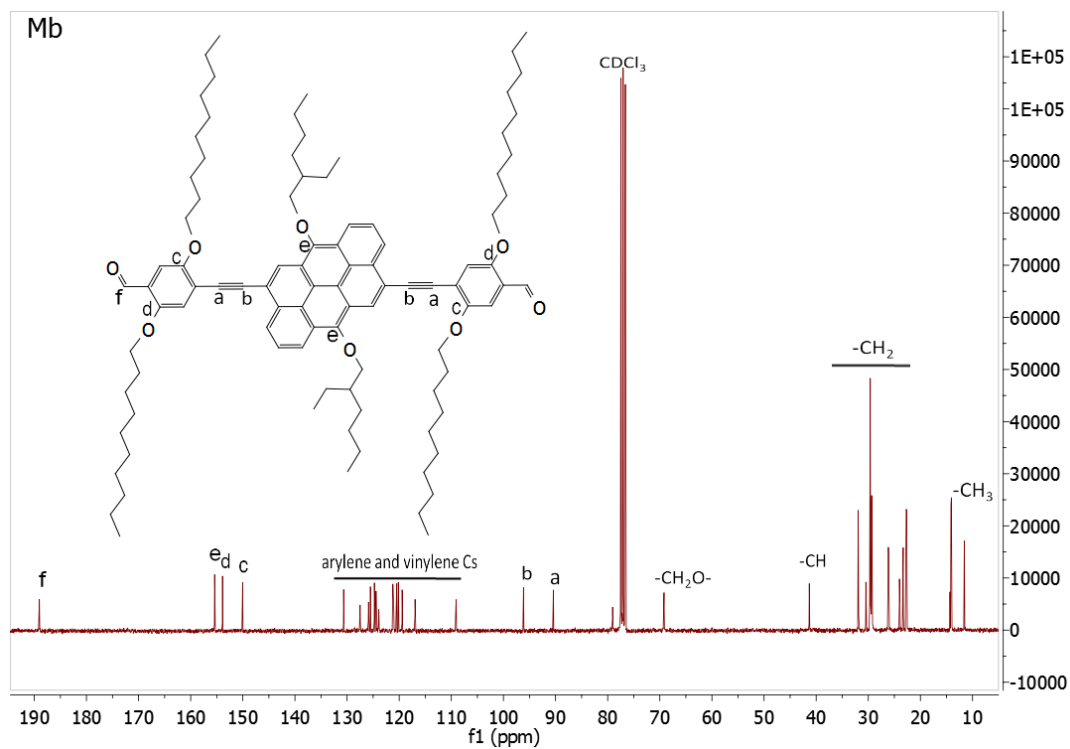
Figure 5.15: ^{13}C NMR signal of Mb.
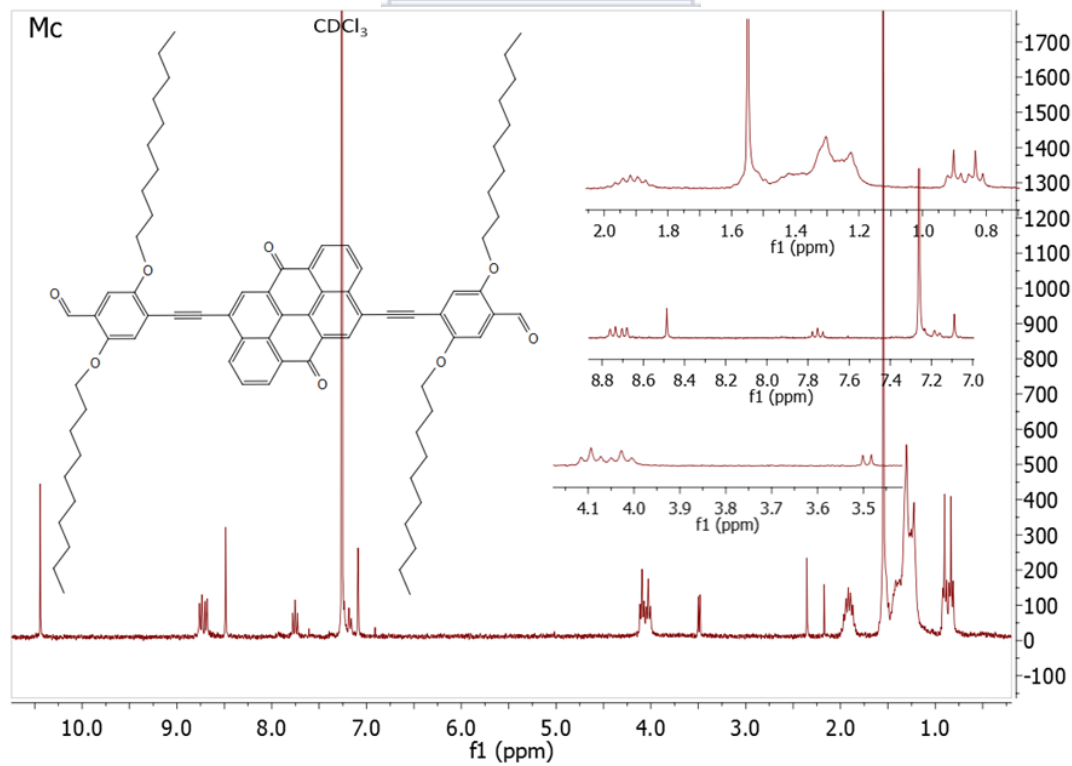
Figure 5.16: ^{1}H NMR signal of Mc.

156

While the 1H-NMR spectra of the polycondensation comonomers, bisphosphonates and dialdehydes, are well-resolved and show defined signals, the spectra of the HWE polycondensation products are characterized by distinct signal broadening and loss in resolution. As the depletion or absence of the characteristic signals for the reactive functionalities of the comonomers, CHO (~ 10.5 ppm) and CH2-P (3.5 ppm), this indicates the successful formation of polymeric species. The signals between 9.25 – 8.41 ppm in P1 are assigned to the protons of the anthanthrone core. Between 8.07 and 6.67 ppm arylene vinylene proton signals can be found. The signals in the region 4.37 – 3.20 ppm and 2.49 – 0.37 ppm are the protons of the alkyloxy side chains (**Figure 5.17**). The presence of a residual aldehyde signal in the ^{1}H-NMR spectrum of P1 (~ 10.5 ppm) suggests that the soluble fraction of P1 consists of low-molecular species with aldehyde end groups. **Figure 5.18 and 5.19** shows the ^{1}H NMR signals of P2 and P3 respectively. The broad NMR peaks between 9.05 - 8.22 ppm are ascribed to the anthanthrenylene protons, signals from 7.65 - 6.92 ppm are ascribed to the arylene vinylene protons, while the peaks in the region 4.61-3.28 ppm and 2.41 – 0.42 originates from the protons of the alkoxy side chains. In contrast to P1 the ^{1}H-NMR spectra of P2 and P3 do not show any sign of a residual aldehyde signal. The ^{1}H NMR of SM is shown in **Figure 5.20**.

Mc was applied in HWE polycondensation reactions with the bisphosphonate M1 and M3 to obtain the polymers P4 and P5, respectively. However, the materials obtained from this reaction showed no reasonable solubility in common solvents, which prevented further characterization. Despite P1, P4 and P5 possessing identical backbones based on anthanthrone units the presence of only branched 2-ethylhexyloxy side chains apparently granted partly solubility for P1 in common organic solvent. The linear decyloxy side chains in P4 and P5 appear much less efficient in promoting solubility. The significantly better

solubility of the polymers P2 and P3 can be apparently attributed to the presence of anthanthrene instead of anthanthrone building blocks in the polymer backbones. The repeating units of P2 and P3 are isomeric. Their structures only differ in the side chains, linear dodecyloxy and branched 3,7-dimethyloctyl)oxy, introduced by the different bisphosphonates, which were used in the respective polycondensation reaction. This was done in order to study the effect of various side chains on the polymer properties.
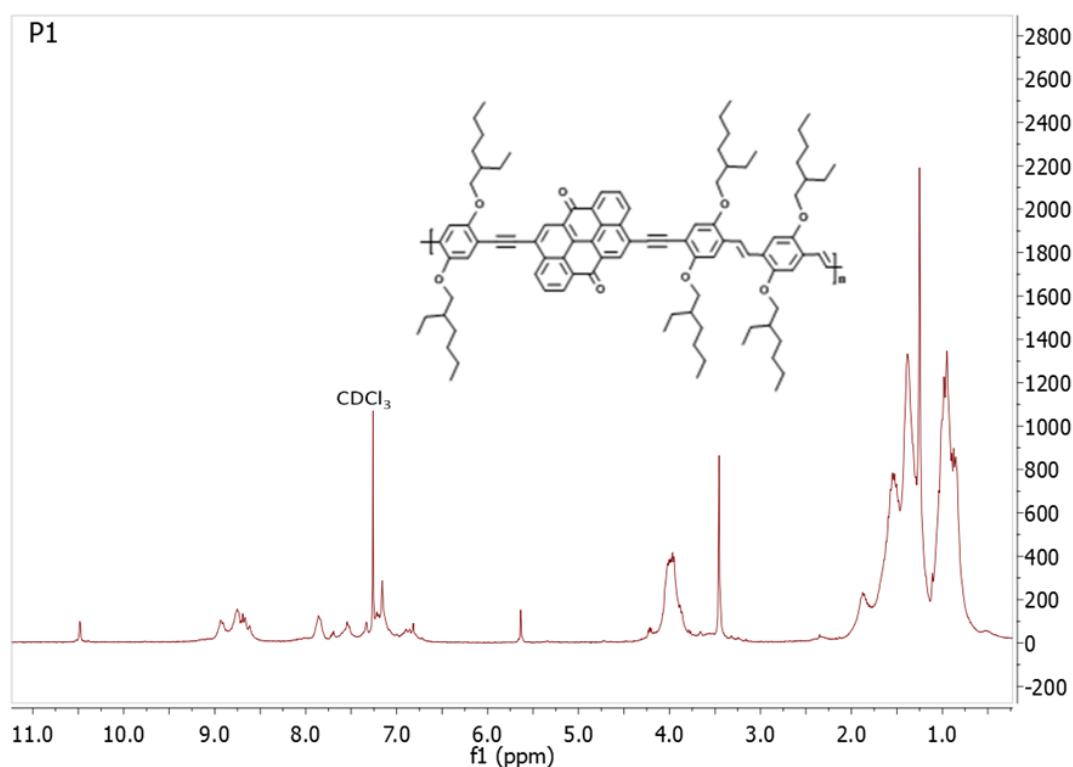
Figure 5.17: ^{1}H NMR signal of P1.
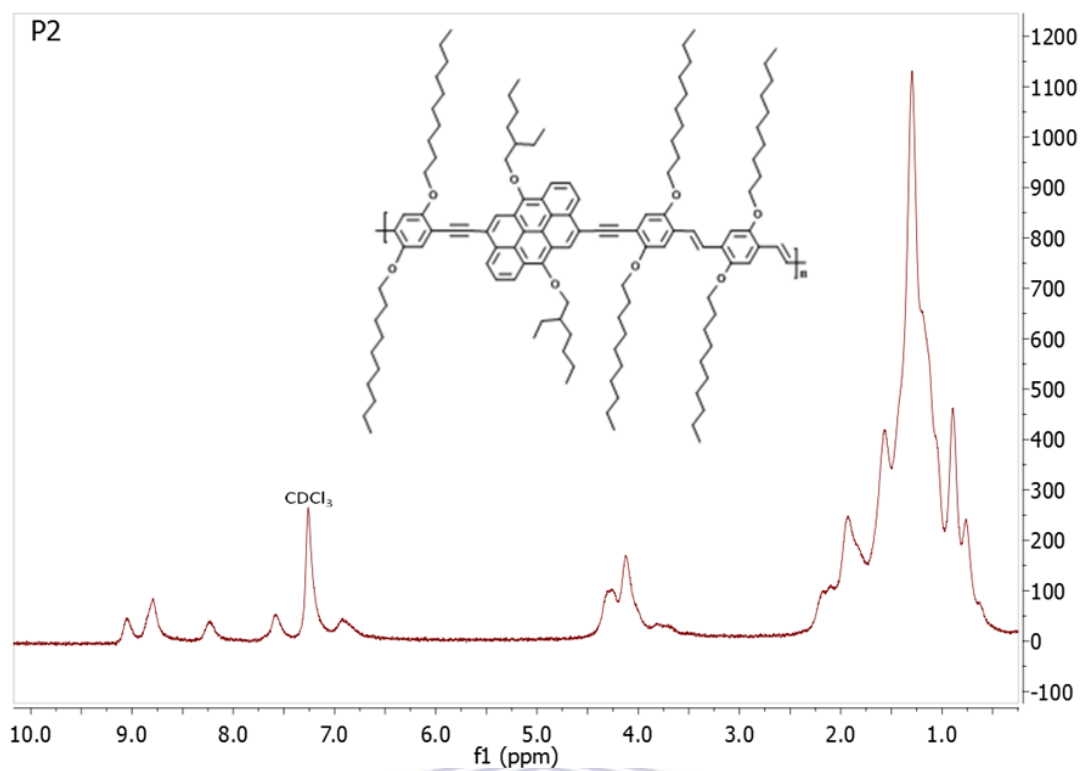
Figure 5.18: ^{1}H NMR signal of P2.
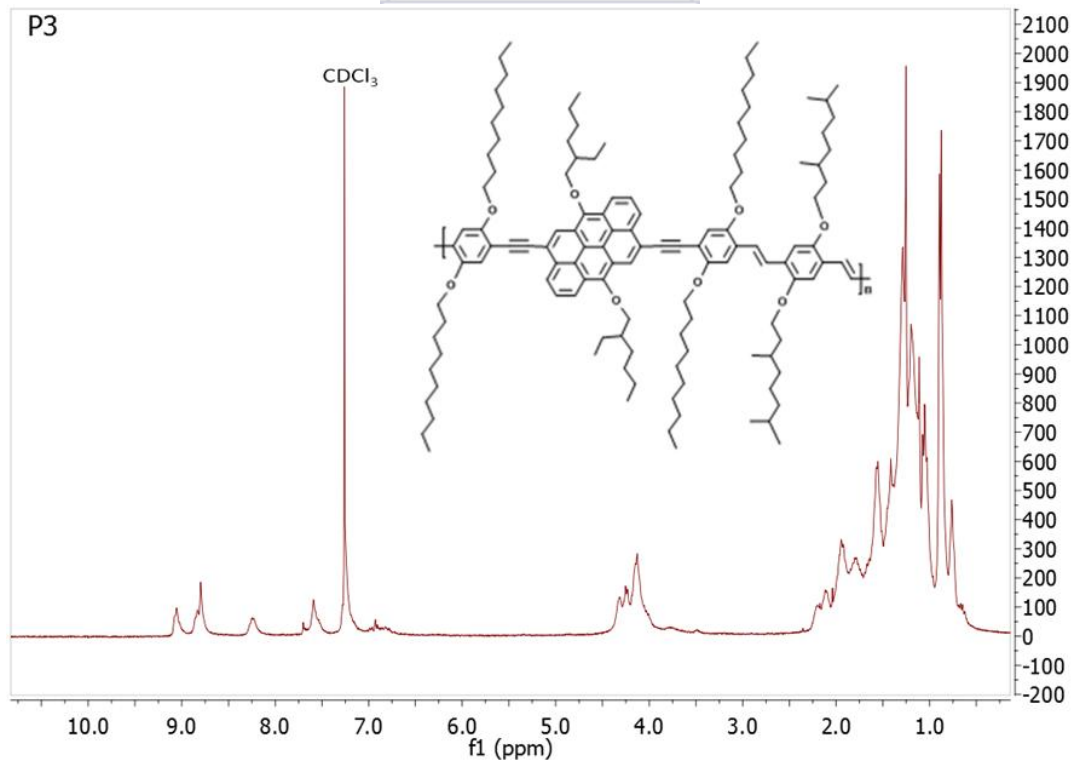
Figure 5.19: ^{1}H NMR signal of P3.
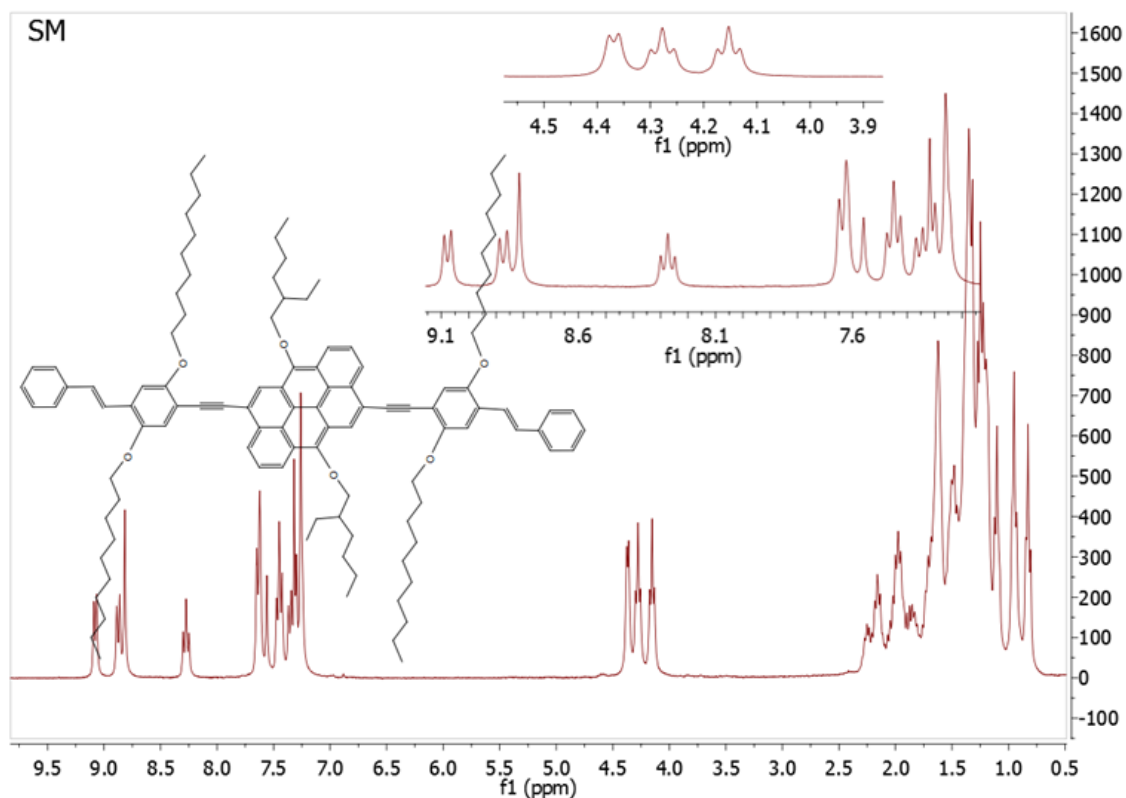
Figure 5.20: 1H NMR signal of SM.

5.2.2   Fourier Transform Infra Red (FTIR) Spectroscopy

The characteristic FTIR signals associated with molecule vibrations of P1, P2 and P3 appear around 3073-3064, 2962-2850, 2198-2180, 1659, 1603-1575, 1500, 1464, 1380 and 1203 cm^{-1} (**Figure 5.21 – 5.23**). The peaks between 3073-3064 cm^{-1} are attributed to the stretching vibrations of aromatic =C-H and unsaturated hydrocarbon (vinylene). Characteristic aliphatic -C-H stretching vibrations of all three polymers show high intensity signals around 2962-2850 cm^{-1} while the vibrational stretching of the ethynylene linker bond (-C≡C-) shows a weak signal situated around 2198-2180 cm^{-1} for all three polymers. These values confirm a di-substituted ethynylene linker bond. The characteristic stretching vibration associated to the ketone group (-C=O) of P1 is observed at 1659 cm^{-1}, and, as expected, this peak is completely absent in the spectra of P2 and P3. The signals around 1603-1575 cm^{-1} are

160

ascribed to vinylene linker bond stretching while the signals at 1500 cm^{-1} and 1203 – 1031 cm^{-1} stem from the stretching vibrations of aromatic -C=C- and aromatic-aliphatic -C=C-O-C- bonds, respectively. The band at 969 cm^{-1} and between 861 – 869 cm^{-1} stem from the vinylene double bonds.
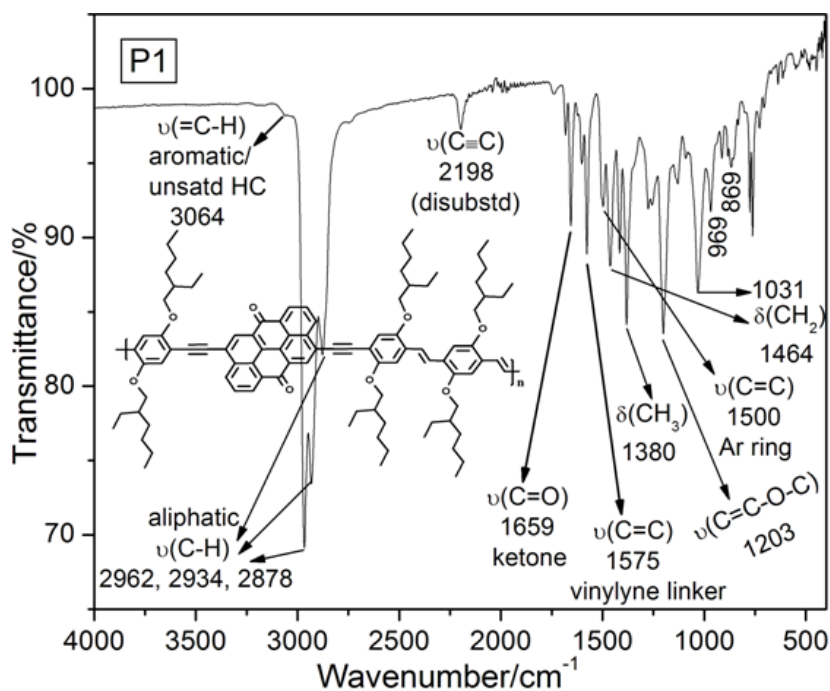
Figure 5.21: FTIR spectra of P1 with arrows marking the absorptions of functional group including olefinic C–H out-of-plane deformation (trans-CH=CH at 969 cm^{-1} and cis-CH=CH at 869 cm^{-1}).

161
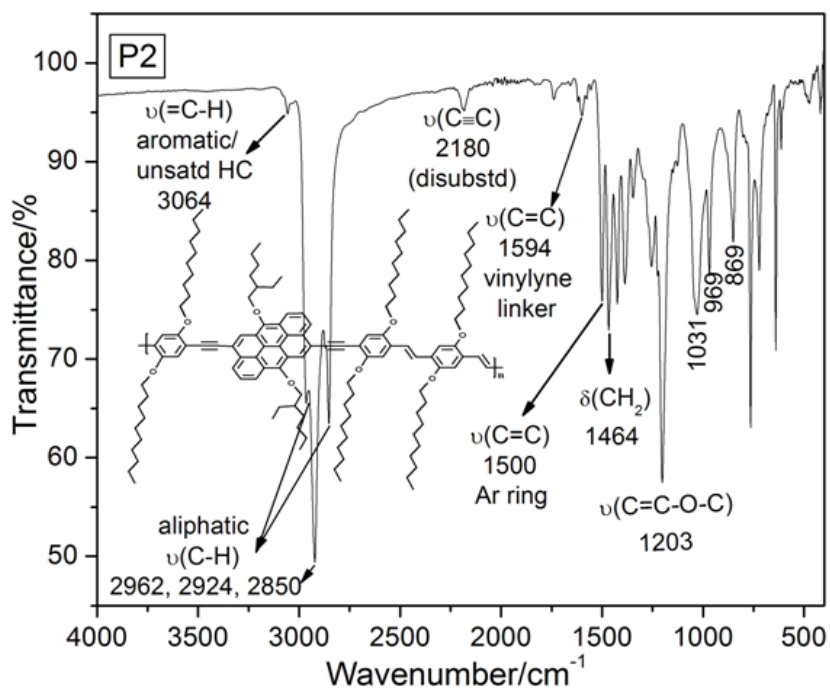
Figure 5.22: FTIR spectra of P2 with arrows marking the absorptions of functional group including olefinic C–H out-of-plane deformation (trans-CH=CH at 969 cm^{-1} and cis-CH=CH at 869 cm^{-1}).
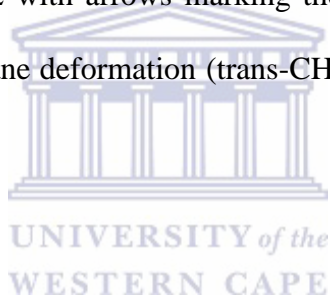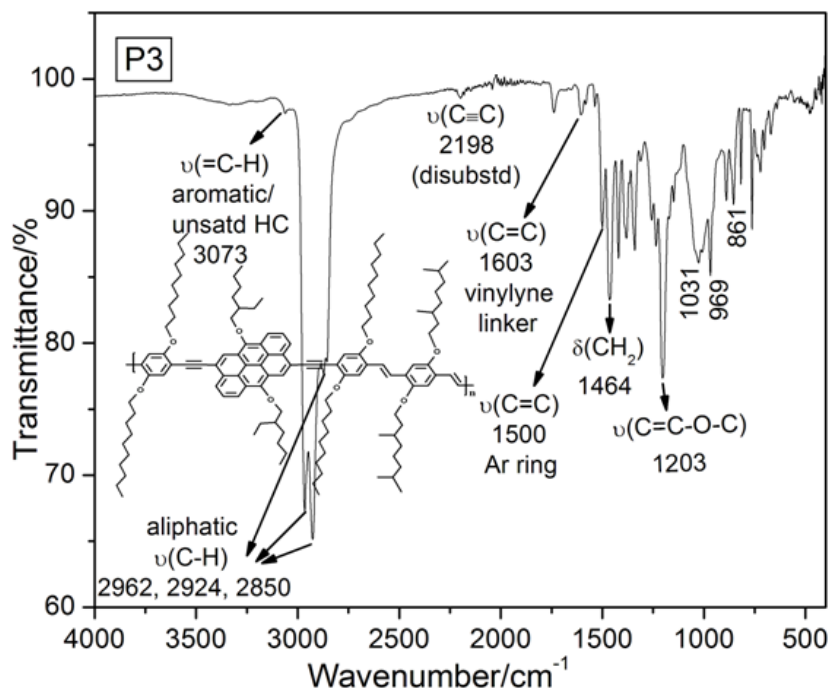
Figure 5.23: FTIR spectra of P3 with arrows marking the absorptions of functional group including olefinic C–H out-of-plane deformation (trans-CH=CH at 969 cm^{-1} and cis-CH=CH at 861 cm^{-1}).
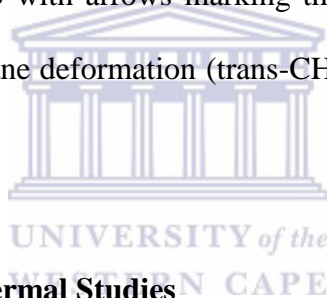
5.2.3   Molecular Mass and Thermal Studies

Results obtained from SEC (THF as eluent, polystyrene standards) and thermogravimetric analysis (TGA) are provided in **Table 5.1**. The molecular mass of the polymers P1, P2 and P3 were relatively low. The difficulties to prepare polymers of elevated molecular mass, that contain anthanthrone or anthanthrene building blocks, are apparent. The relatively low M_n value obtained for P1 can be attributed to the rapid precipitation from the reaction mixture during the polycondensation owing to their relatively poor solubility. Thermo-gravimetric analysis (TGA) gives indications of good thermal stability for all three polymers (P1, P2 and P3). A 5% weight loss is observed between 314 and 331°C (**Table 5.1** and **Figure. 5.24**).

163

Table 5.1: Molecular mass and thermal studies of P1, P2 and P3

Code	Oil Bath Temp.(°C)	Yield (%)	M_n (g/mol)	M_w (g/mol)	PDI	T_d (°C) @ 5% weight loss
P1	118	95	1,830	3,570	2	325
P2	118	*95	3,200	11,730	3.7	314
P3	118	*33	2,880	7,820	2.7	331
P3	111	*73	3,650	11,800	3.2	-

* Determined for the soluble fraction
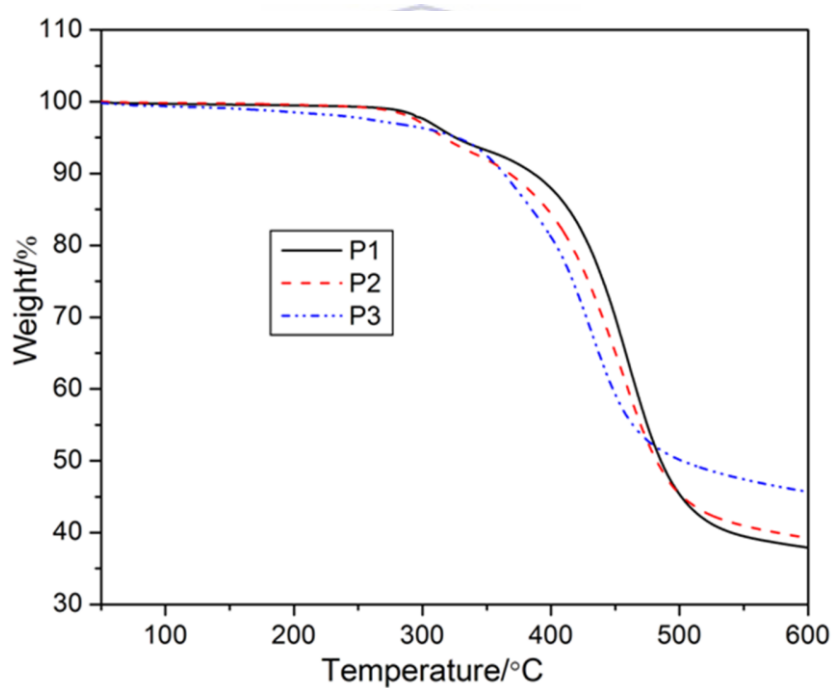
Figure 5.24: Thermo-gravimetric analysis curve of P1, P2 and P3.

5.2.4 Absorption and Emission Characterization

The optical characteristics of the polymers were investigated by UV–Vis absorption and photoluminescence spectroscopy both, in the solid state (thin films) and in solution at low concentration ($\sim 10^{-5}$ M). The absorption spectra of P1 are structured, exhibiting two well-defined peaks in solution (374, 567 nm) as well as in thin film (403, 586 nm) (**Figure 5.25**). The peak at higher energy can be ascribed to the π-π* transition of the polymer backbone and the lower energy band is ascribed to the carbonyl of the anthanthrone moiety.
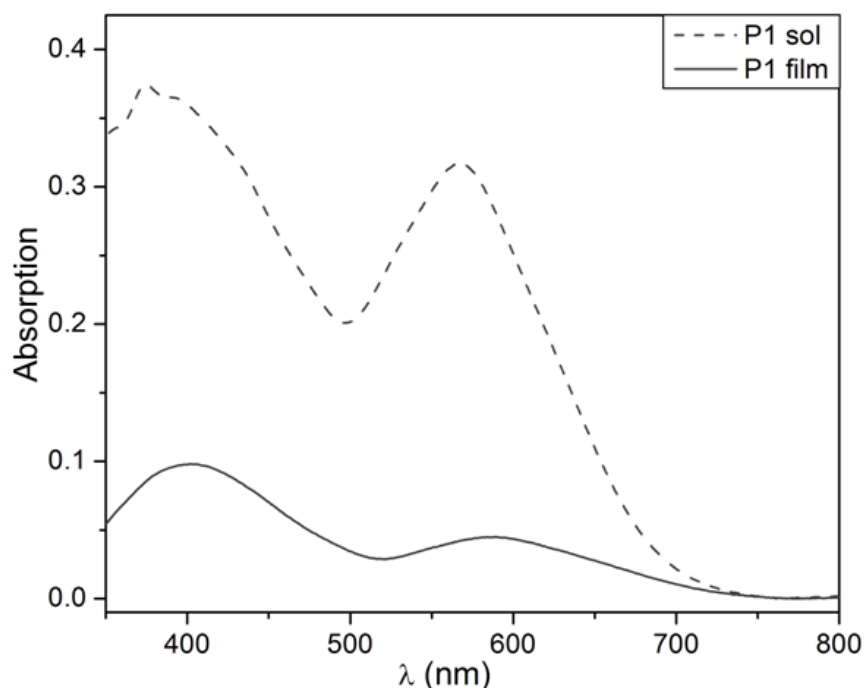
Figure 5.25: UV-Vis spectra of P1 in solution and film.

In the case of P2 and P3, the UV-Vis spectra showed vibronic peaks with absorptions around 481 nm and at 453 nm in both solution and thin film with a shoulder for the thin film samples at 519 nm for both polymers (**Figure 5.26**) as a result of an efficient internal charge transfer between the monomeric units. These vibronic peaks can also be attributed to the presence of

165

H- and *J*-aggregates in P2 and P3 in both, solution and thin film. The peaks at higher energy (453 nm) are attributed to *H*-aggregates while the peaks, which are further in the red (481 nm), are attributed to *J*-aggregates. The presence of both aggregates in the polymer reveals that some of the polymer units stack on each other (*H*-aggregates) while others lay side by side (*J*-aggregates). In both, solution and thin film, *J*-aggregates dominate and contribute more to the optical properties observed for the systems. The presence of these two peaks in the absorption spectrum also suggests structural ordering/semi-crystallinity in the polymer [30].

The onset of absorption allows the evaluation of the optical energy gaps of these organic semiconductors. In film (**Figure 5.26**), the absorption maxima and profiles resemble those recorded in solution. The optical band gaps of all three polymers reveal the same band gaps both in film and solution.
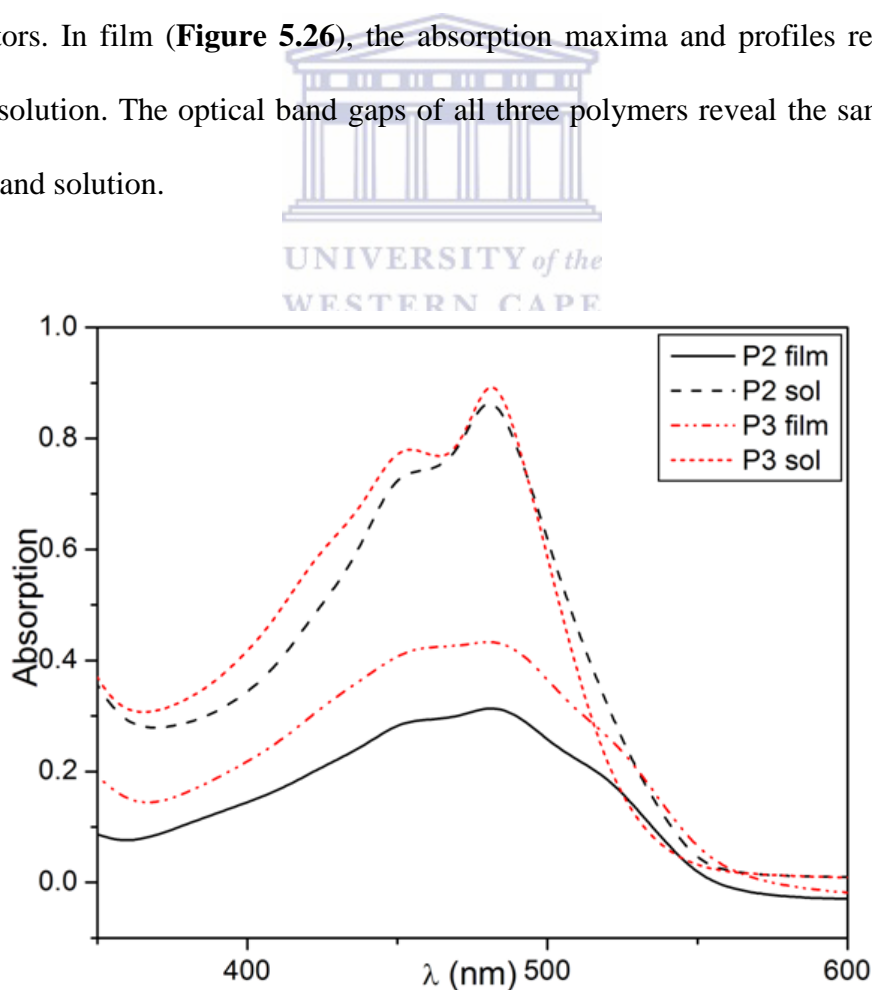
Figure 5.26: UV-Vis spectra of P2 and P3 in solution and film.

166

Anthanthrene small molecule (SM) was also synthesized, investigated and compared with its polymer "analogue" P2. SM exhibited both, in solution and in the solid state, fine vibronic bands, which are typical of fused conjugated systems. The spectra show three bands each with two sharp maxima at about 448 and 479 nm in solution, and, slightly shifted to red, at around 457 and 488 nm in thin film (**Figure 5.27**). The polymer (P2) exhibit red-shifted and broad optical response compared to the small molecule (SM) both, in solution and in film, confirming the extension of conjugation length via polymerization.
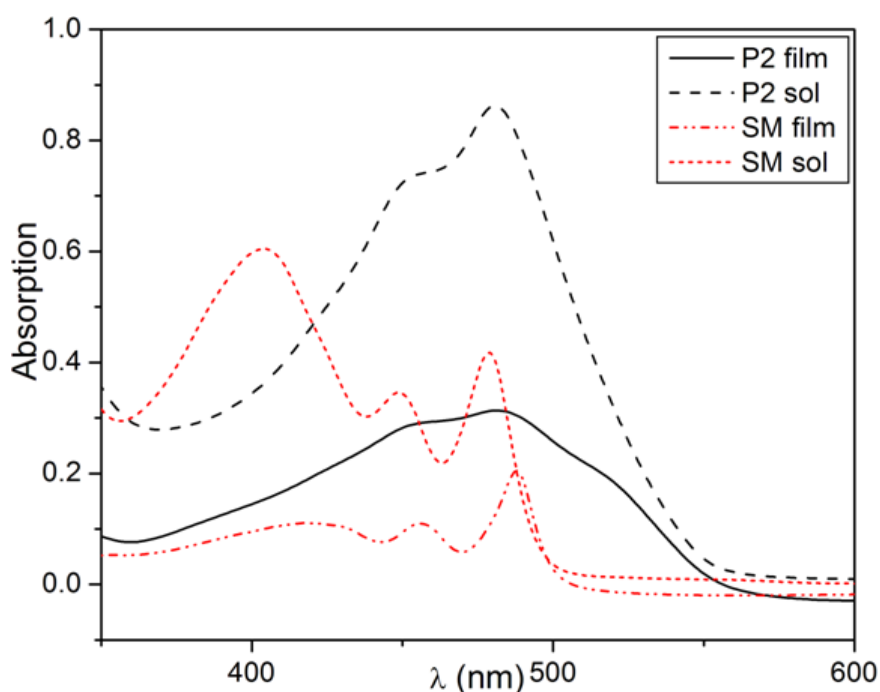
Figure 5.27: UV-Vis spectra of SM and its analogues polymer P2.

The photoluminescence (PL) of all three polymers was investigated. In solution, the emission spectrum of P1 gave a maximum at 611 nm (**Figure 5.28**). P1 displayed rather poor emitting characteristics and the recording of a PL spectrum in solid state was not possible. P2 and P3 were both excited at 450 nm. Both polymers exhibited highly similar fluorescence behaviour in solution showing a close to mirror-image-like impression of the absorption with a

167

maximum at 530 nm (**Figure 5.29**). This mirror-image-like appearance indicates planarity which further supports the structural ordering or semi-crystalline nature of both polymers as already indicated by the absorption study in film and solution. The fluorescence of P2-3 in thin film appeared red-shifted with a maximum at 587 and 597 nm, respectively (**Figure 5.30**). Both polymers seem moderately emissive with Stokes' shifts of 116 and 106 nm, respectively, in thin film, and 49 nm in solution. The maximum wavelength values in the solid state of the polymers P1, P2 and P3 is rather high and with relatively low band gap considering no strong donor–acceptor interactions occurs within the polymer backbone.
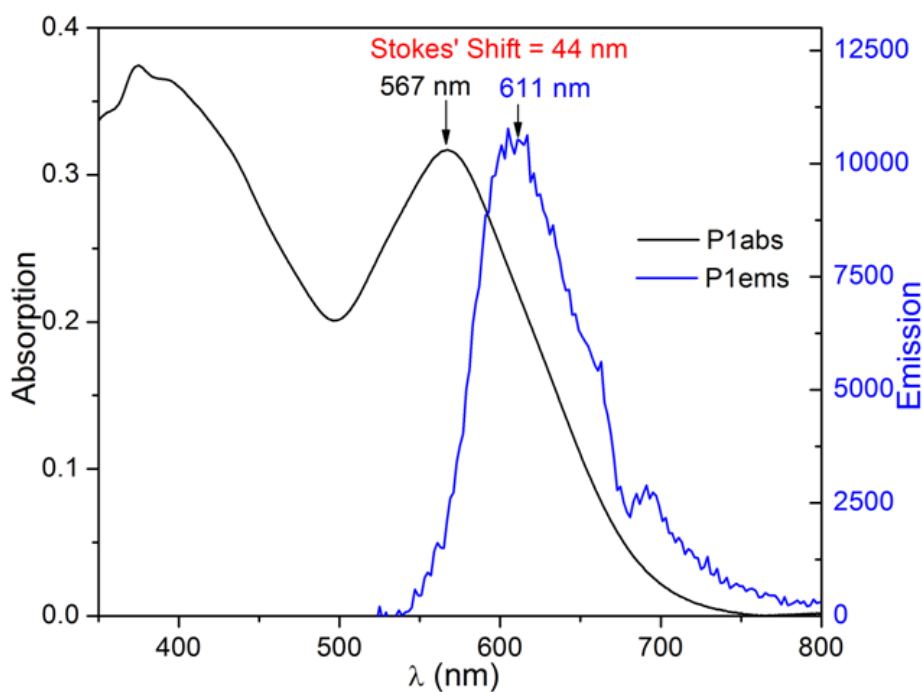
Figure 5.28: UV-Vis and photoluminescence spectra of P1 in solution.

168
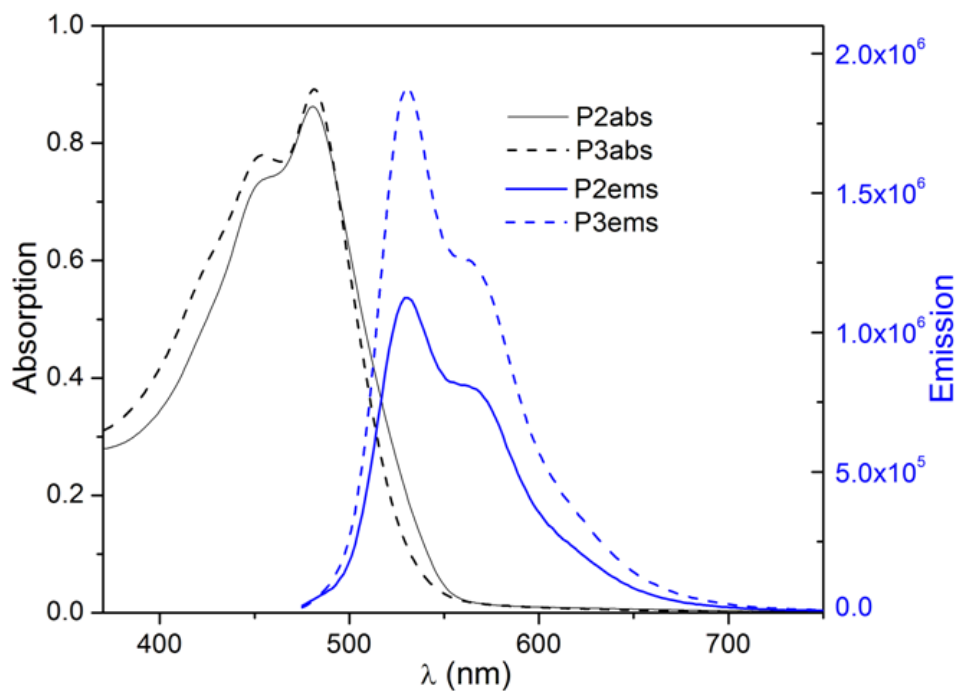
Figure 5.29: UV-Vis and photoluminescence spectra of P2 and P3 in solution.
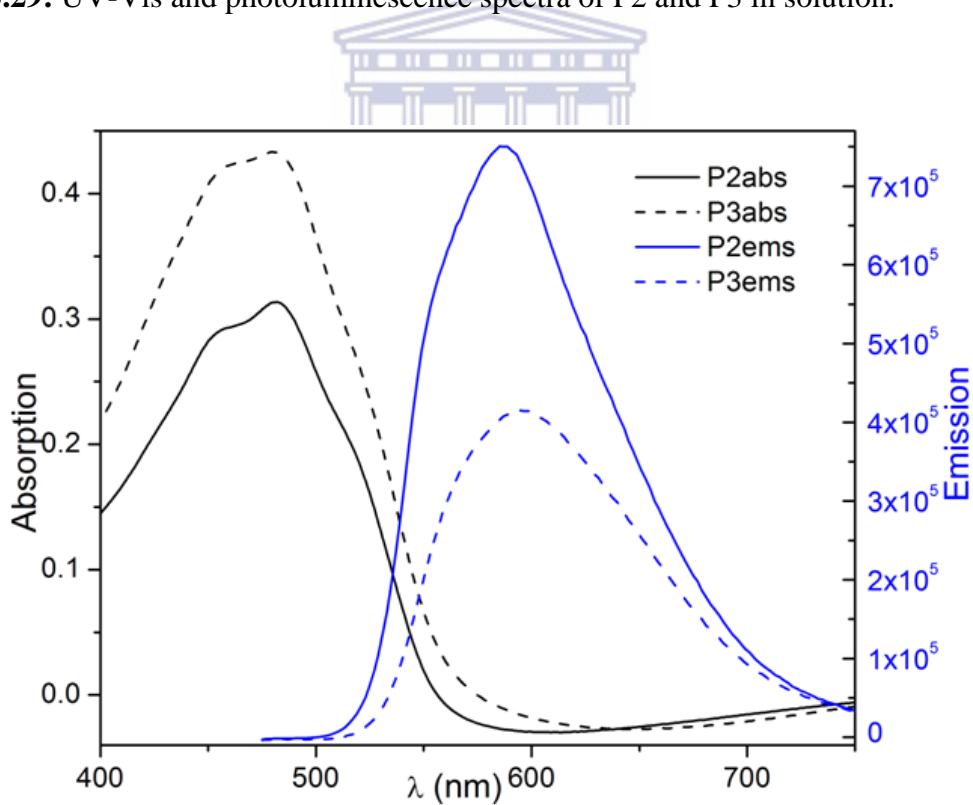
Figure 5.30: UV-Vis and photoluminescence spectra of P2 and P3 in film.

In the solution the photoluminescence of SM possesses rather high resemblance to the features observed for P2, however, hypsochromically shifted with a maximum at 496 nm and a pronounced shoulder at 532 nm (**Figure 5.31**). In film, the PL characteristics of SM are quite different from P2. Tow emission maxima at 496 and 549 nm (most intense) as well as two shoulders at 595 and 699 nm were observed (**Figure 5.32**). The emission shoulder of SM at 595 nm seems to correlate with the emission maximum of P2 (587 nm). This suggests that the optical properties of these materials are dominated by the anthanthrene unit and not the substituent; and this confirms why P2 and P3 show virtually the same absorption and emission response. **Table 5.2** summarizes the UV-Vis and photoluminescence properties of P1, P2, P3 and SM in solution and thin film.
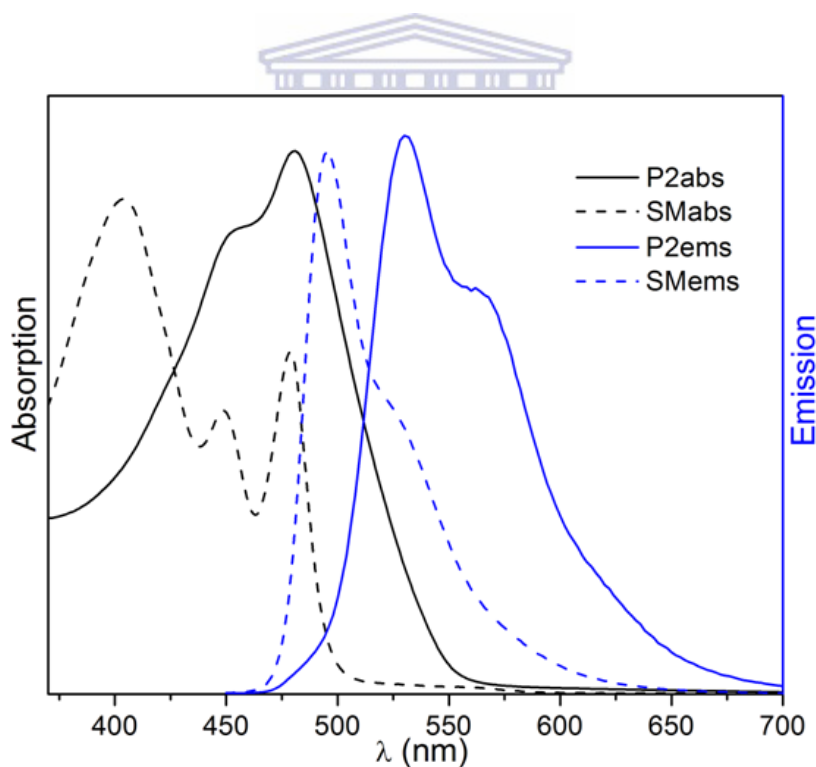
Figure 5.31: UV-Vis and photoluminescence spectra of SM and P2 in solution.

170
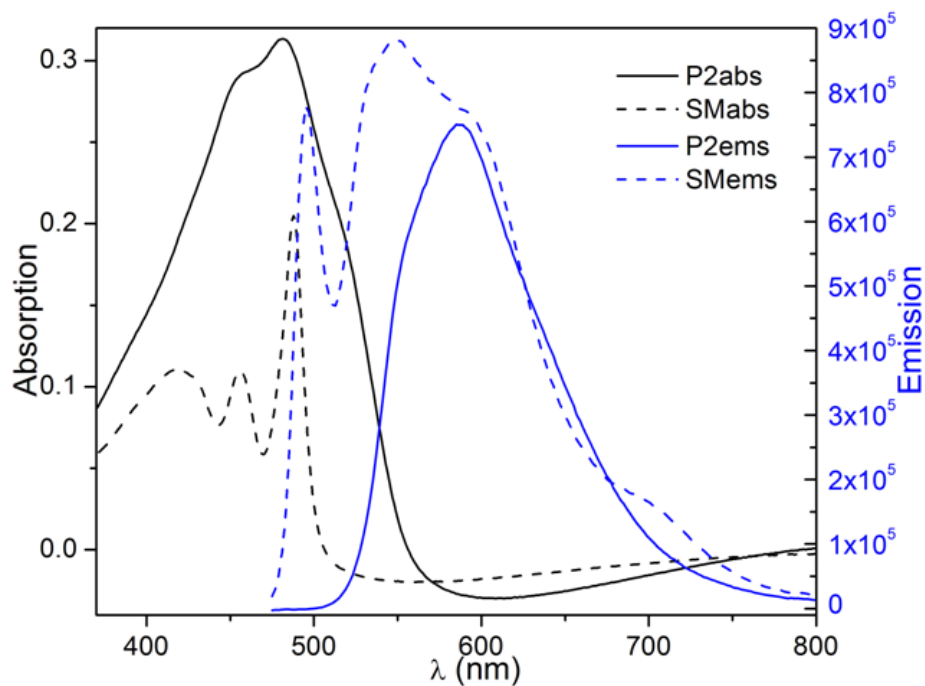
Figure 5.32: UV-Vis and photoluminescence spectra of SM and P2 in film.

Table 5.2: UV-Vis and photoluminescence properties of P1, P2, P3 and SM in solution and film (all experiments were conducted at ambient temperature)

Code	Solution					Film				
	λ_{max} (nm)	λ_{PL} (nm)	λ_{onset} (nm)	E_g^{opt} (eV)	Stokes Shift (nm)	λ_{max} (nm)	λ_{PL} (nm)	λ_{onset} (nm)	E_g^{opt} (eV)	Stokes Shift (nm)
P1	374, 567	611	752	1.6	44	403, 586	-	766	1.6	-
P2	453, 481,	530	572	2.2	49	453, 481	587	558	2.2	106
P3	453, 481	530	570	2.2	49	454, 481	597	575	2.2	116
SM	404, 449, 479	496, 532	536	2.3	-	423, 456, 488	549, 595, 699	507	2.5	-

$$E_g^{opt} = \frac{1240}{\lambda_{onset}}$$

5.2.5 Electrochemical Characterization

Figure 5.33 shows the voltammogram of P1 having five visible reduction peaks (-800, -1046, -1786, -1890 and -2200 mV (vs. Ag/AgCl))), the first two being reversible and well-defined, which is a typical characteristic for anthanthrone compounds [46-47]. The first and second reversed reduction (re-oxidation) peaks are similar in intensity and are located at -956 mV and -606 mV respectively versus Ag/AgCl. Four non-reversible oxidation peaks were

172

observed at 1079, 1183, 1649 and 2039 mV. Oxidation peaks recorded for the few anthanthrone based polymers that have been reported are largely influenced by the attached co-monomer [27]. The oxidative peaks in this study are likely to originate from structural elements besides the anthanthrone units - phenylene, ethynylene, vinylene.
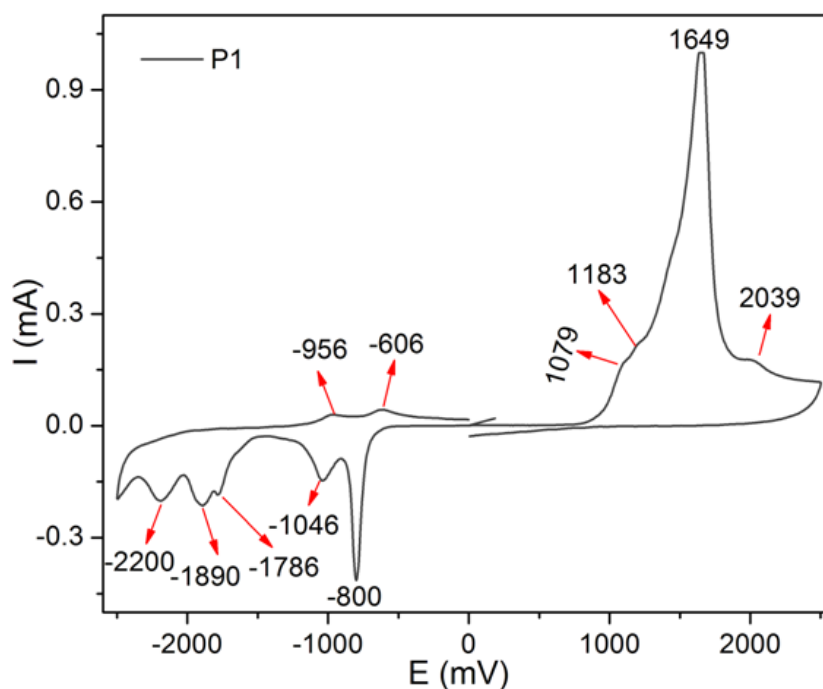
Figure 5.33: Cyclic voltammogram of P1 in $TBAPF_6$/acetonitrile vs Ag/AgCl at scan rate 50 mV/s.

For P2 and P3, the major difference in the voltammograms is in the reduction scan (**Figure 5.34**). Substitution of the decyloxy side chain by 3,7-dimethyloctyloxy side chains resulted in two and more negative reduction potentials (-2220 and -2427 mV) in P3. P2 showed a single and more positive reduction potential at -1977 mV. The kinetics probably involing difference in solubility and the side chain substitution negatively shifted the reduction potential by 243 mV in P2 to -2220 mV in P3. This response is indicative of good electronic communication

173

between the core and the side chains. Two reversed reduction (re-oxidation) signals are seen at -1714 and -1142 mV in P3 while only one is seen in P2 peaking at -1510 mV.

Similarly, the oxidation of P2 and P3 were studied. The existence of three distinct oxidation step was observed at 1096, 1359 and 1822 mV for P2; 1040, 1378 and 1732 mV for P3. A reversible peak at 1542 mV corresponding to the oxidation peak at 1822 mV was observed for P2 while no reversible oxidation peak is observed in P3. This observation can be attributed to the nature of the interaction of the different side chains of the phenyl group attached by a vinylene linker to the anthanthrene core in P2 and P3. Nevertheless, the small potential differences and variations had no distinct effect on the frontier orbitals of the polymers. The frontier orbitals of P2 and P3 appear to be strongly dominated by the anthanthrene core with HOMO (-5.3 eV) and LUMO (-3.0 eV) energy level of both polymers peaking at same value.

174
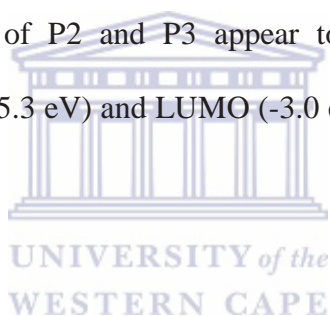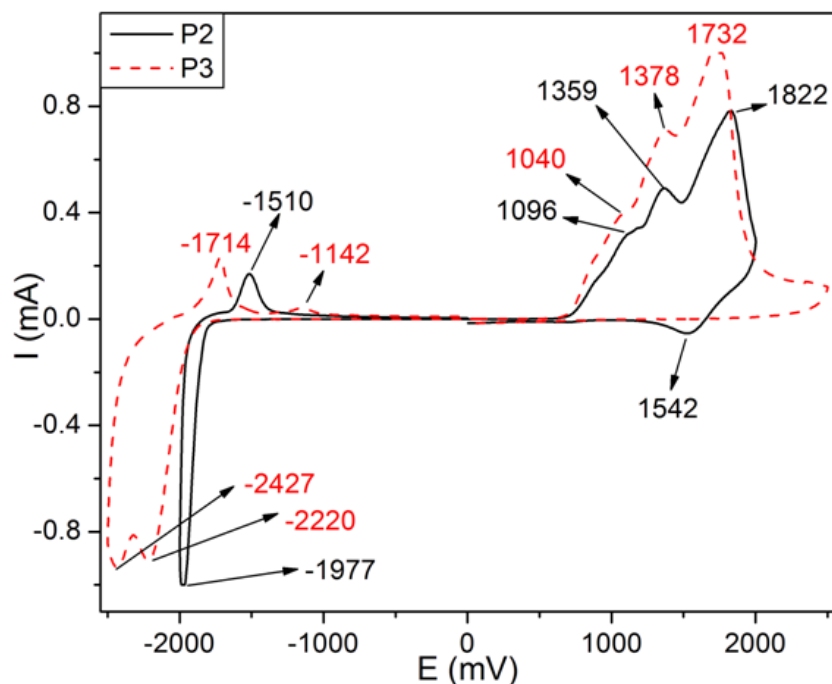
Figure 5.34: Cyclic voltammogram of P2 and P3 in TBAPF$_6$/acetonitrile vs Ag/AgCl at scan rate 50 mV/s.

The low band gap value, $E_g{}^{opt}$ = 1.6 eV and $E_g{}^{el}$ = 1.4 eV, obtained for P1 compared to P2 and P3, $E_g{}^{opt}$ = 2.2 eV and $E_g{}^{el}$ = 2.3 eV, can be attributed to the presence of the ketone group in the polymer backbone of P1. The HOMO (-5.3 eV) and LUMO (-3.0 eV) energy values of P2 and P3 are identical while that of P1 differ significantly (HOMO level at -5.5 eV and LUMO level at -4.1 eV). This suggests that the frontier orbitals are dominated by anthanthrone and anthanthrene, respectively. The deep LUMO level of P1 is attributed to the two electron-withdrawing keto groups present at the 6- and 12-positions of the anthanthrone unit.

The redox properties of SM are similar to the characteristics of the corresponding polymer P2, but with some potential shifts (**Figure 5.35**). The reduction peak of P2 at -1977 mV correlates with -1767 mV in SM, which shows another reduction peak at -2081 mV. The

reversed reduction peak of P2 observed at -1510 mV is seen around -1067 mV in SM. Oxidation peaks of P2 at 1096, 1359 and 1822 mV find their counterparts at 1041, 1216 and 1361 mV in the voltammogram of SM. The reverse oxidation peak observed at 1542 mV in P2 is absent in SM. This further confirms the initial statement that the reverse oxidation peak at 1542 mV in P2 emanates from the interaction of the decyloxy side chain of the phenyl group attached by a vinylene linker to the anthanthrene core in P2. Aside the shift in signal response of the SM in relation to its corresponding polymer P2, differences in signal intensity for the reduction, oxidation and re-oxidation signals, respectively, was also observed. All electrochemical experiments were conducted in a glove box at a scan rate of 50 mV/s. **Table 5.3** summarizes the electrochemical properties.
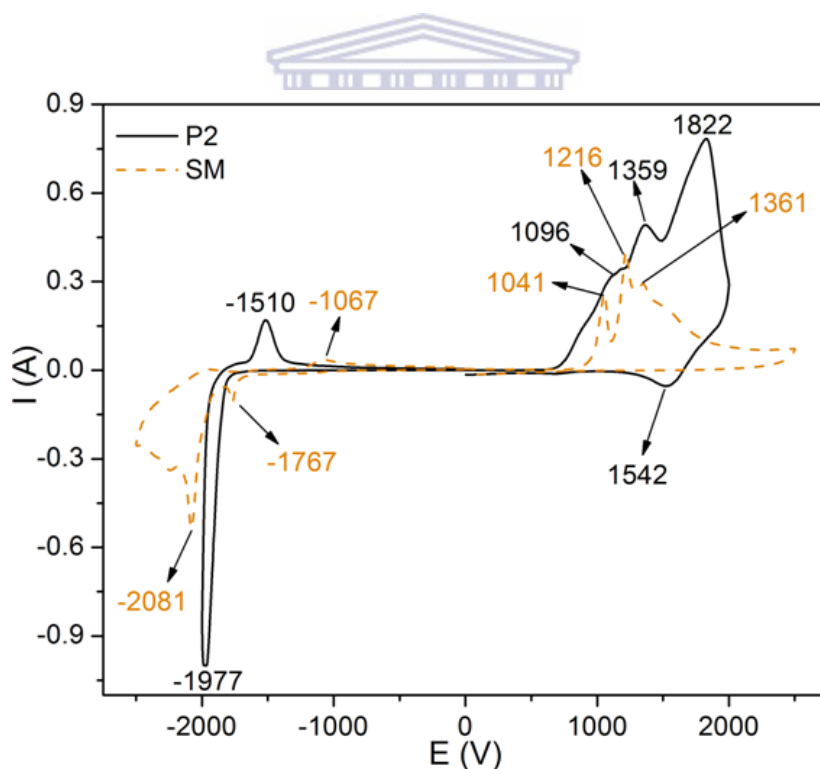
Figure 5.35: Cyclic voltammogram of SM and its corresponding polymer P2 in TBAPF$_6$/acetonitrile vs Ag/AgCl at scan rate 50 mV/s.

Table 5.3: Electrochemical properties of P1, P2 and P3 with onset absorption and optical band gap

Code	E_{onset}^{ox} (V)	E_{onset}^{red} (V)	HOMO (eV)	LUMO (eV)	E_g^{el} (eV)	λ_{onset} (nm)	E_g^{opt} (eV)
P1	0.8	0.6	-5.5	-4.1	1.4	766	1.6
P2	0.6	1.7	-5.3	-3.0	2.3	558	2.2
P3	0.6	1.7	-5.3	-3.0	2.3	575	2.2
SM	0.8	1.6	-5.4	-3.1	2.4	507	2.5

5.2.6 Photovoltaic Investigation

To investigate the performance of the new polymers P1 - P3 as absorbers in bulk heterojunction solar cell applications, devices with non-optimized configurations were fabricated. The *I-V* curves of organic photovoltaic (OPV) devices applying P1 – P3 with the architecture ITO/PEI/Polymer:PCBM(1:2)/MoO$_x$(10 nm)/Ag(100 nm) are shown in **Figure 5.36 – 5.37**. All three polymers show low efficiency with P2 having the highest efficiency of 1.17% among the three. The portion of energy in the form of sunlight that is converted into electricity via photovoltaics is termed the efficiency of an OPV device and can be estimated from *I-V* characteristics using the following mathematical expression:

$$\eta = \frac{FF.J_{sc}.V_{oc}}{P_i}$$

equation (5.1)

where η is the efficiency, *FF* is the fill factor, J_{sc} is the short-circuit current density, V_{oc} is the open-circuit voltage and P_{in} the incident light power. The higher efficiency realized with

177

P2 can be attributed to relatively high J_{sc} and *FF* (**Table 5.4**). The V_{oc} ideally correlates with the difference between the LUMO of the acceptor and the HOMO of the donor. The polymers P2 and P3 showed high resemblance in their V_{oc} values, 0.76 V for P2 and 0.78 V for P3. The value which was found for P1 is significantly higher, V_{oc} = 0.93 V. This approximately equal V_{oc} value for P2 and P3 can be traced back to their equal HOMO of -5.3 eV as observed from the electrochemical measurement since the same acceptor (PCBM) was employed for the photovoltaic investigation. P1 and P3 show low *FF* which is likely to be attributed to poor film morphologies and non-suitable layer thicknesses. The solubility of conducting polymers plays a major role in the film morphology. Poor solubility leads to poor film morphology and poor morphology leads to low *FF* which invariably lowers the efficiency. The solubility of conducting polymers plays a major role in the film morphology. Poor solubility leads to visually rather poor films apparently inducing low *FFs* which invariably lower the OPV device efficiency. Besides other characteristics, solubility, molecular mass, intermolecular interactions and charge carrier mobilities of conjugated semiconducting polymers can largely impact their photovoltaic properties [48-51] All three polymers showed rather poor solubility during device fabrications. The poor solubility seemed also to cause a poor miscibility with the electron acceptor PCBM which might partly explain the limited performance of the devices. For molecular mass, with the same reaction temperature of 118°C, P2 has the highest molecular weight (11, 730 g/mol), followed by P3 (7, 820 g/mol) and then P1 (3, 570 g/mol). The efficiency can also be seen to follow the trend P2>P3>P1. The rather poor photovoltaic response of the non-optimized devices using the investigated polymers might be a result of different parameters e.g. poor mobility of the generated charges, poor interface layers, poor film morphologies and too thin active layers due to low molecular masses and/or unfit spin coating recipe.
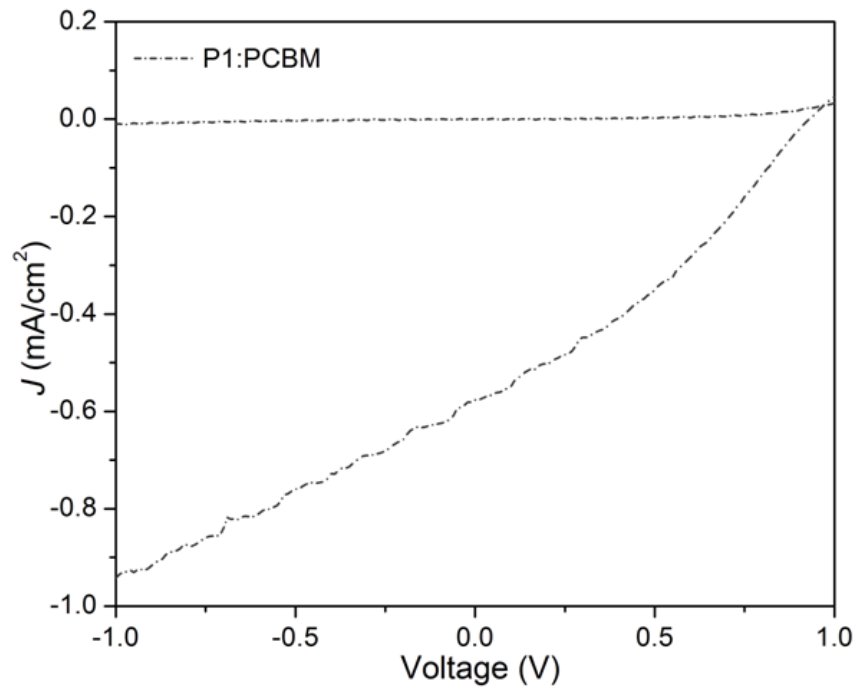
Figure 5.36: Current-voltage (*I-V*) curve of P1.
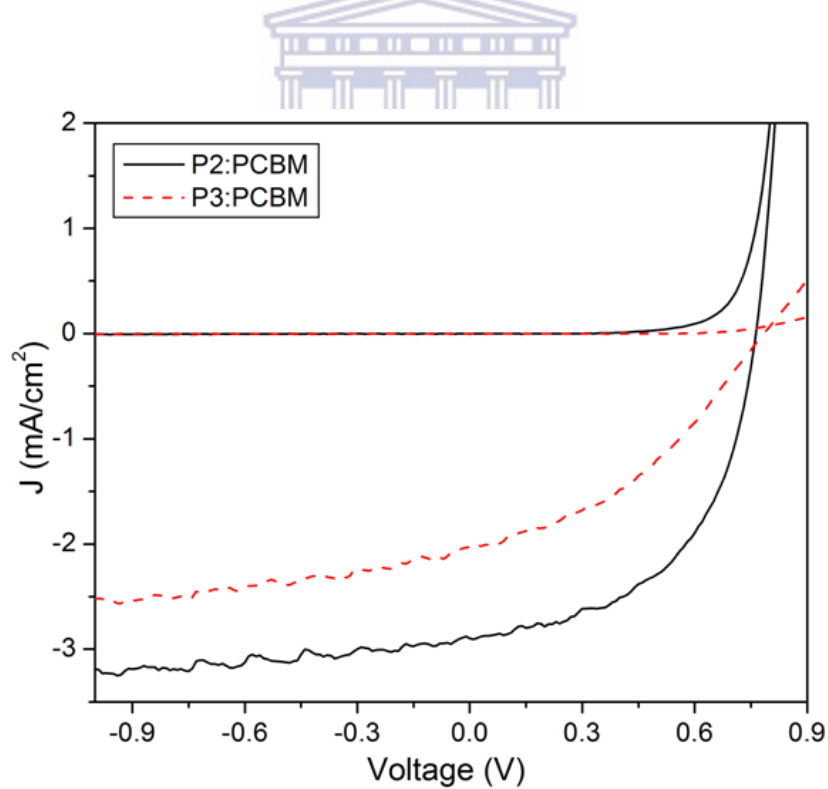
Figure 5.37: Current-voltage (*I-V*) curve of P2 and P3.

179

The external quantum efficiency (EQE) which is the measure of the efficiency of a cell to convert incident photons into free charge carriers was also investigated. It is mathematically defined as

$$EQE = 1240 \frac{J_{sc}}{\lambda_i P_i}$$
<div align="right">**equation (5.2)**</div>

where J_{sc} is the short-circuit current, λ_i is the incident light wavelength and P_{in} is the incident photon flux. Considering the linear correlation between EQE and J_{sc} (**equation 5.2**), the EQE value at each wavelength scales with the number of photo-generated free charge carriers. As a result, high EQE values can be achieved by the combined effect of efficient exciton generation in the bulk of the active blend layer, the dissociation into free charge carriers, and the charge transport to the respective electrode. The linear correlation between J_{sc} and EQE can be seen in P1 – P3 (**Figure 5.38**, **Table 5.4**). P2 having the highest J_{sc} shows the highest EQE, while P1, with the lowest J_{sc}, shows the lowest EQE value.
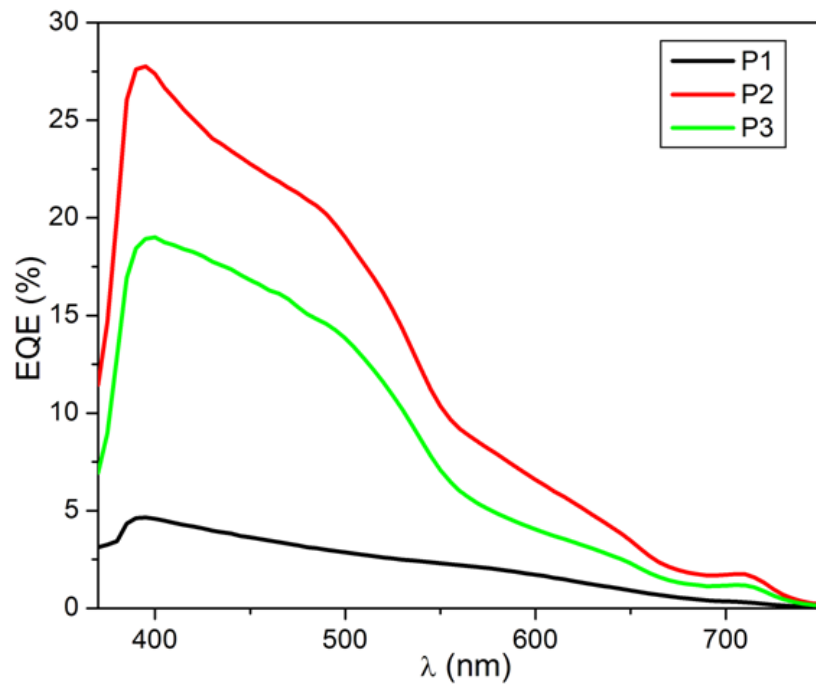
Figure 5.38: External quantum efficiency of P1, P2 and P3 with PCBM (1:2).

181

Table 5.4: Current Voltage (*I-V*) characteristics of devices based on P1, P2 and P3

Code	Bulk Thickness (nm)	J_{sc} [mA/cm^2]	V_{oc} [V]	*FF*	Eff %	Eff [%]EQE corrected	@ -2 V [mA/cm^2]	@ +2 V [mA/cm^2]
P1	92	0.58	0.93	0.33	0.18	0.12	-0.94	0.05
P2	104	2.90	0.76	0.53	1.17	0.89	-3.19	22.74
P3	134	2.02	0.78	0.39	0.61	0.46	-2.53	0.95

182
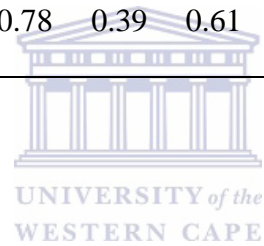
5.3   Conclusion

Polycyclic aromatic building blocks based on anthanthrone and anthanthrene, were incorporated for the first time into the backbone of poly(arylene ethynylene)-*alt*- poly(arylene vinylene)s (PAE-PAVs). The implementation of PACs such as anthanthrone into conjugated polymeric backbones with reasonable solubility and molecular masses is challenging. Using only branched 2-ethylhexyloxy side chains yielded a partly soluble PAE-PAV (P1) material. This was not possible with P4 and P5 with linear decyloxy side chains and this was already indicated by the good solubility of Ma and the rather poor solubility of Mc. The polycondensation reactions for P4 and P5 were based on a comonomer with linear decyloxy side chains (Mc), which apparently promoted the formation of only insoluble materials. Substitution of anthanthrone with anthanthrene units appears to be an efficient strategy to prepare polymers with reasonable solubility (P2 and P3). In P1 however, we were able to show the preparation of a polymer with soluble fractions with 4,10-linked anthanthrone building blocks and with an all-branched 2-ethylhexyloxy side chain configuration.

The synthesis of P1, P2 and P3 were confirmed by spectroscopic methods including NMR and FTIR. These polymers were studied in detail for their photo-physical properties and probed for organic photovoltaic applications. All three polymers show interesting photo-physical properties with P1 having the most intriguing absorption properties. The optical properties of P2 and P3 are highly similar. The frontier orbital energy levels were basically unaffected by using different side chains. However, the replacement of decyloxy side chains in P2 with 3,7-dimethyloctyloxy in P3 resulted in lower yield and decline of photovoltaic performance. The "transformation" of the anthanthrone's carbonyl groups into anthanthrene's alkyloxy substituents in the preparation of P2 and P3 impacted the photo-physical properties

183

significantly. In all cases (P1, P2 and P3), the properties of the polymers appear dominated by the polycyclic chromophore. Although these new polymers showed only low photovoltaic response in first tests, improvements in solubility and optimization of the device composition and architecture might yield significant enhancements of the photovoltaic performance.

5.4   References

[1]   A. P. H. J. Schenning and E. W. Meijer, "Supramolecular electronics; nanowires from self-assembled π-conjugated systems," *Chem. Commun.,* (**2005**) 3245 - 3258.

[2]   F. J. M. Hoeben, P. Jonkheijm, E. W. Meijer and A. P. H. J. Schenning, "About supramolecular assemblies of pi-conjugated systems," *Chem. Rev.,* 105 (**2005**) 1491 - 1546.

[3]   E. Moulin, J.-J. Cid and N. Giuseppone, "Advances in Supramolecular Electronics – From Randomly Self-Assembled Nanostructures to Addressable Self-Organized Interconnects " *Adv. Mater.,* 25 (**2013**) 477 - 487.

[4]   W. Pisula, X. Feng and K. Müllen, "Tuning the Columnar Organization of Discotic Polycyclic Aromatic Hydrocarbons," *Adv. Mater.,* 22 (**2010**) 3634 - 3649.

[5]   J. Mei, Y. Diao, A. L. Appleton, L. Fang and Z. Bao, "Integrated Materials Design of Organic Semiconductors for Field-Effect Transistors," *J. Am. Chem. Soc.,* 135 (**2013**) 6724 - 6746.

[6]   M. Ball, Y. Zhong, Y. Wu, C. Schenck, F. Ng, M. Steigerwald, S. Xiao and C. Nuckolls, "Contorted Polycyclic Aromatics " *Acc. Chem. Res.,* 48 (**2015**) 267 - 276.

[7]   Q. Ye and C. Chi, "Recent Highlights and Perspectives on Acene Based Molecules and Materials," *Chem. Mater.,* 26 (**2014**) 4046 - 4056.

[8]   G. E. Collis, "Designing small molecule polyaromatic p- and n-type semiconductor materials for organic electronics " *Proc. SPIE,* 9668 (**2015**) 96683O-1.

[9]   L. Schmidt-Mende, A. Fechtenkotter, K. Mullen, E. Moons, R. H. Friend and J. D. MacKenzie, "Self-organized discotic liquid crystals for high-efficiency organic photovoltaics," *Science,* 293 (**2001**) 1119 - 1122.

[10]   S. Laschat, A. Baro, N. Steinke, F. Giesselmann, C. Hagele, G. Scalia, R. Judele, E. Kapatsina, S. Sauer, A. Schreivogel and M. Tosoni, "Discotic Liquid Crystals: From Tailor-Made Synthesis to Plastic Electronics," *Angew. Chem., Int. Ed.,* 46 (**2007**) 4832 - 4887

[11]   W. W. H. Wong, T. B. Singh, D. Vak, W. Pisula, C. Yan, X. Feng, E. L. Williams, K. L. Chan, Q. Mao, D. J. Jones, C.-Q. Ma, K. Mullen, P. Bauerle and A. B. Holmes, "Solution Processable Fluorenyl Hexa-peri-hexabenzocoronenes in Organic Field-Effect Transistors and Solar Cells," *Adv. Funct. Mater,* 20 (**2010**) 927 - 938.

[12]   W. Pisula, X. Feng and K. Müllen, "Charge-Carrier Transporting Graphene-Type Molecules," *Chem. Mater.,* 23 (**2011**) 554 - 567.

[13]   Z. Zhang, T. Lei, Q. Yan, J. Pei and D. Zhao, "Electron-transporting PAHs with dual perylenediimides: syntheses and semiconductive characterizations," *Chem. Commun.,* 49 (**2013**) 2882 - 2884.

[14]   S. Xiao, S. J. Kang, S. Zhang, A. M. Scott, A. Moscatelli, N. J. Turro, M. L. Steigerwald, H. Li and C. Nuckolls, "Controlled doping in thin-film transistors of large contorted aromatic compounds," *Angew. Chem., Int. Ed.,* 52 (**2013**) 4558 - 4562.

[15]   B. He, H. Tian, Y. Geng, F. Wang and K. Müllen, "Facile Synthesis of 9,10-Diarylphenanthrenes and Poly(9,10-diarylphenanthrene)s," *Org. Lett.,* 10 (**2008**) 773 - 776.

185

[16]   S.-I. Kawano, C. Yang, M. Ribas, S. Baluschev, M. Baumgarten and K. Müllen, "Blue-Emitting Poly(2,7-pyrenylene)s: Synthesis and Optical Properties," *Macromolecules,* 41 (**2008**) 7933 - 7937.

[17]   M. Saleh, Y.-S. Park, M. Baumgarten, J.-J. Kim and K. Müllen, "Conjugated Triphenylene Polymers for Blue OLED Devices," *Macromol. Rapid Commun.,* 30 (**2009**) 1279 - 1283.

[18]   H. Chen, X. Hu and S.-C. Ng, "Synthesis and characterization of soluble conjugated polymers having pyrene moiety in the main chain," *J. Polym. Sci., Part A: Polym. Chem.,* 48 (**2010**) 5562 - 5569.

[19]   C.-E. Chou, D. Wang, M. Bagui, J. Hsu, S. Chakraborty and Z. Peng, "Syntheses and optical properties of triphenylene-containing conjugated polymers," *J. Lumin.,* 130 (**2010**) 986 - 994.

[20]   D. Lehnherr and R. R. Tykwinski, "Conjugated Oligomers and Polymers Based on Anthracene, Tetracene, Pentacene, Naphthodithiophene, and Anthradithiophene Building Blocks," *Aust. J. Chem.,* 64 (**2011**) 919 - 929.

[21]   H. Kim, N. Schulte, G. Zhou, K. Müllen and F. Laquai, "A High Gain and High Charge Carrier Mobility Indenofl uorene-Phenanthrene Copolymer for Light Amplifi cation and Organic Lasing," *Adv. Mater.,* 23 (**2011**) 894 - 897.

[22]   D. S. Yang, K. H. Kim, M. J. Cho, J.-I. Jin and D. H. Choi, "Donor–acceptor alternating π-conjugated polymers containing Di(thiophen-2-yl)pyrene and 2,5-Bis(2-octyldodecyl)pyrrolo[3,4-c]pyrrole-1,4(2H,5H)-dione for organic thin-film transistors," *J. Polym. Sci., Part A: Polym. Chem.,* 51 (**2013**) 1457 - 1467.

[23]   G. Li, C. Kang, C. Li, Z. Lu, J. Zhang, X. Gong, G. Zhao, H. Dong, W. Hu and Z. Bo, "Planar Conjugated Polymers Containing 9,10-Disubstituted Phenanthrene Units for Efficient Polymer Solar Cells," *Macromol., Rapid Commun.*, 35 (**2014**) 1142 - 1147.

[24]   A. C. Grimsdale and K. Müllen, "The Chemistry of Organic Nanomaterials," *Angew. Chem., Int. Ed.,* 44 (**2005**) 5592 - 5629.

[25]   Z. Sun, Q. Ye, C. Chi and J. Wu, "Low band gap polycyclic hydrocarbons: from closed-shell near infrared dyes and semiconductors to open-shell radicals," *Chem. Soc. Rev.,* 41 (**2012**) 7857 - 7889.

[26]   K. Hinkel, D. Cho, W. Pisula, M. Baumgarten and K. Müllen, "Alternating Donor-Acceptor Arrays from Hexa-peri-hexabenzocoronene and Benzothiadiazole: Synthesis, Optical Properties, and Self-Assembly," *Chem. Eur. J.,* 21 (**2015**) 86 - 90.

[27]   A. Lafleur-Lambert, J.-B. Giguère and J .-F. Morin, "Conjugated Polymers Based on 4,10-Bis(thiophen-2-yl)anthanthrone:Synthesis, Characterization, and Fluoride-Promoted Photoinduced Electron Transfer," *Macromolecules,* 48 (**2015**) 8376 - 8381.

[28]   A. Lafleur-Lambert, J.-B. Giguère and J.-F. Morin, "Anthanthrene as a large PAH building block for the synthesis of conjugated polymers," *Polym. Chem.,* 6 (**2015**) 4859 - 4863.

[29]   D. A. M. Egbe, B. Carbonnier, E. Birckner and U.-W. Grummt, "Arylene-ethynylene/arylene-vinylene copolymers: Synthesis and structure–property relationships," *Prog. Polym. Sci.,* 34 (**2009**) 1023 - 1067.

[30]   D. A. M. Egbe, S. Turk, S. Rathgeber, F. Kuhnlenz, R. Jadhav, A. Wild, E. Birckner, G. Adam, A. Pivrikas, V. Cimrova, G. Knor, N. S. Sariciftci and H. Hoppe, "Anthracene Based Conjugated Polymers: Correlation between π-π-Stacking Ability, Photophysical Properties, Charge Carrier Mobility, and Photovoltaic Performance," *Macromolecules,* 43 (**2010**) 1261 - 1269.

[31]   S. Günes, A. Wild, E. Cevik, A. Pivrikas, U. S.Schubert and D. A. M. Egbe, "Effect of shifting of aromatic rings on charge carrier mobility and photovoltaic response of

anthracene and thiophene-containing MEH-PPE-PPVs," *Solar Energy Materials & Solar Cells,* 94 (**2010**) 484 - 491.

[32]   D. K. Susarova, E. A. Khakina, P. A. Troshin, A. E. Goryachev, N. S. Sariciftci, V. F. Razumov and D. A. M. Egbe, "Photovoltaic performance of PPE-PPV copolymers: effect of the fullerene component," *J. Mater. Chem.,* 21 (**2011**) 2356 - 2361.

[33]   N. Tore, E. A. Parlak, Ö. Usluer, D. A. M. Egbe, S. E. San and P. Aydogan, "Effect of blend ratio on poly(p-phenylene-ethynylene)-alt-poly (p-phenylene-vinylene) polymer solar cell," *Solar Energy Materials & Solar Cells,* 104 (**2012**) 39 - 44.

[34]   C. Kästner, D. K. Susarova, R. Jadhav, C. Ulbricht, D. A. M. Egbe, S. Rathgeber, P. A. Troshin and H. Hoppe, "Morphology evaluation of a polymer–fullerene bulk heterojunction ensemble generated by the fullerene derivatization," *J. Mater. Chem.,* 22 (**2012**) 15987 - 15997.

[35]   P. A. Troshin, O. A. Mukhacheva, Ö. Usluer, A. E. Goryachev, A. V. Akkuratov, D. K. Susarova, N. N. Dremova, S. Rathgeber, N. S. Sariciftci, V. F. Razumov and D. A. M. Egbe, "Improved Photovoltaic Performance of PPV-Based Copolymers Using Optimized Fullerene-Based Counterparts," *Adv. Energy Mater.,* 3 (**2013**) 161 - 166.

[36]   M.A. Saidani, A. Benfredj, Z. Ben Hamed, S. Romdhane, C. Ulbricht, D. A. M. Egbe and H. Bouchriha, "Franck-Condon analysis of the photoluminescence spectra of atriple-bond containing polymer as a solution and as a thin film," *Synth. Met,* 184 (**2013**) 83 - 85.

[37]   J. Gasiorowski, S. Boudiba, K. Hingerl, C. Ulbricht, V. Fattori, F. Tinti, N. Camaioni, R. Menon, S. Schlager, L. Boudida, N. S. Sariciftci and D. A. M. Egbe, "Anthracene-Containing Conjugated Polymer Showing Four Optical Transitions Upon Doping: A Spectroscopic Study," *J. Polym. Sci., Part B: Polym. Phys.,* 52 (**2014**) 338 - 346.

188

[38] A. Kösemen, N. Tore, E. A. Parlak, Z. A. Kösemen, C. Ulbricht, Ö. Usluer, D. A. M. Egbe, Y. Yerli and S. E. San, "An efficient organic inverted solar cell with AnE-PVstat:PCBM active layer and V2O5/Al anode layer," *Solar Energy,* 99 (**2014**) 88 - 94.

[39] C. Kästner, D. A. M. Egbe and H. Hoppe, "Polymer aggregation control in polymer–fullerene bulk heterojunctions adapted from solution," *J. Mater. Chem. A,* 3 (**2015**) 395 - 403.

[40] L. Ding, D. A. M. Egbe and F. E. Karasz, "Photophysical and Optoelectronic Properties of Green-Emitting Alkoxy-Substituted PE/PV Hybrid Conjugated Polymers," *Macromolecules,* 37 (**2004**) 6124 - 6131.

[41] D. A. M. Egbe, L. H. Nguyen, B. Carbonnier, D. Mühlbacher and N. S. Sariciftci, "Thiophene-containing poly(arylene–ethynylene)-alt-poly(arylene–vinylene)s: Synthesis, characterisation and optical properties," *Polymer,* 46 (**2005**) 9585 - 9595.

[42] A. Wild, D. A. M. Egbe, E. Birckner, V. Cimrova, R. Baumann, U.-W. Grummt and U. S. Schubert, "Anthracene- and thiophene-containing MEH-PPE-PPVs: Synthesis and study of the effect of the aromatic ring position on the photophysical and electrochemical properties," *J. Polym. Sci. Part A: Polym. Chem.,* 47 (**2009**) 2243 - 2261.

[43] Ö. Usluer, C. Kästner, M. Abbas, C. Ulbricht, V. Cimrova, A. Wild, E. Birckner, N. Tekin, N. S. Sariciftci, H. Hoppe, S. Rathgeber and D. A. M. Egbe, "Charge Carrier Mobility, Photovoltaic, and Electroluminescent Properties of Anthracene-Based Conjugated Polymers Bearing Randomly Distributed " *J. Polym. Sci. Part A: Polym. Chem.,* 50 (**2012**) 3425 - 3436.

[44] D. A. M. Egbe, S. Sell, C. Ulbricht, E. Birckner and U.-W. Grummt, "Mixed Alkyl- and Alkoxy-Substituted Poly[(phenylene ethynylene)-alt-(phenylene vinylene)]

189

Hybrid Polymers: Synthesis and Photophysical Properties," *Macromol. Chem. Phys.,* 205 (**2004**) 2105 - 2115.

[45] D. A. M. Egbe, L. H. Nguyen, K. Schmidtke, A. Wild, C. Sieber, S. Günes and N. S. Sariciftci, "Combined effects of conjugation pattern and alkoxy side chains on the photovoltaic properties of thiophene- containing PPE-PPVs," *J. Polym. Sci. Part A Polym. Chem.,* 45 (**2007**) 1619 - 1631.

[46] J.-B. Giguère, Q. Verolet and J.-F.Morin, "4,10-Dibromoanthanthrone as a new building block for p-type, n-type, and ambipolar π-conjugated materials," *Chem. - Eur. J.,* 19 (**2013**) 372 - 381.

[47] J.-B. Giguère, J. Boismenu-Lavoie and J.-F. Morin, "Cruciform alkynylated anthanthrene derivatives: a structure-properties relationship case study," *J. Org. Chem.,* 79 (**2014**) 2404 - 2418.

[48] P. M. Beaujuge and J. M. J. Fréchet, "Molecular design and ordering effects in pi-functional materials for transistor and solar cell applications," *J. Am. Chem. Soc.,* 133 (**2011**) 20009 - 20029.

[49] J. B. Bijleveld, A. J. Zoombelt, S. G. J. Mathijssen, M. M. Wienk, M. Turbiez, D. M. de Leeuw and R. A. J. Janssen, "Poly(diketopyrrolopyrrole-terthiophene) for ambipolar logic and photovoltaics," *J. Am. Chem. Soc.,* 131 (**2009**) 16616 - 16617.

[50] M. Moroni, J. Le Moigne, T. A. Pham and J.-Y. Bigot, "Rigid Rod Conjugated Polymers for Nonlinear Optics. 3. Intramolecular H Bond Effects on Poly(phenyleneethynylene) Chains," *Macromolecules,* 30 (**1997**) 1964 - 1972.

[51] U. H. F. Bunz, "Poly(aryleneethynylene)s: Syntheses, Properties, Structures, and Applications," *Chem. Rev.,* 100 (**2000**) 1605 - 1644.

190

CHAPTER SIX

RESULTS AND DISCUSSION - Side Chain Engineering of Anthracene-Based Polymers: Applications in Photovoltaics

Abstract

The research on organic photovoltaic cells has attracted much attention in recent years as a result of the need and desire for renewable energy to replace dwindling non-renewable energy and expensive inorganic silicon based photovoltaic cells. Photovoltaic cells based on organic conjugated materials pose potential low-cost and light weight advantages over mainstream silicon based inorganic photovoltaic cells. In this contribution, the synthesis and characterization of ten anthracene-containing polymers based on poly(arylene ethynylene)-alt-(arylene vinylene) (PAE-PAV) backbone with different alkyloxy substituents is reported. Mixed linear and branched chain (SV1-SV6, and P7), solely branched (SV7-SV8) and solely linear (P6) alkyloxy side chains were grafted to the backbone in order to engineer their properties for photovoltaic applications. Their thermal, photo-physical, electroluminescent as well as their photovoltaic properties were investigated. Two types of device configuration based on bulk heterojunction architecture (normal and inverted) were made from these polymers. The efficiencies of the normal or regular configuration based on poly(3,4-ethylenedioxythiophene)-poly(styrenesulfonate) (PEDOT-PSS) ranged from 1.2 - 2.3% while efficiency up to 2.62% was obtained for inverted cells based on polyethylene imine (PEI). Open circuit voltage > 0.9 V (almost 1V) was obtained for SV1 - SV8 irrespective of the attached side chain and the device configuration (inverted or normal); while a remarkable

high fill factor (*FF*) of 0.67 was obtained for P7. The photovoltaic parameter was revealed to depend on the side chain as insulating or volume fraction ratio effect was observed in the photovoltaic response of polymers with longer alkyloxy side chain. The established correlation between the side chain engineering and photovoltaic response is a practical starting point for such polymers with potential for large-scale device fabrication.

6   Introduction

π-Conjugated semiconducting polymers have attracted significant interest since the pioneering works of A. G. McDiarmid, A. J. Heeger and H. Shirakawa [1-4]. Intensive development of electro-active and photo-active semiconducting conjugated polymers has been triggered due to their wide range of applications. Enormous progress has been made in the synthesis of π -conjugated polymers and in the fabrication and characterization of organic electronics like electroluminescent diodes based on polymers [5], organic field effect transistors (OFETs) [6] and organic photovoltaic (OPV) cells [7]. The necessity and crave to develop low-cost renewable energy sources has stimulated extensive research for efficient, flexible, cheap and lightweight photovoltaic devices based on organic semiconducting materials globally [8-14].

The morphology of photovoltaic device active layer (formed from semiconducting materials) plays a key role in the overall performance of the device. A number of methods such as annealing, solvent variation, use of additives [15] and incorporation of various alkyl and alkyloxy solubilizing side chains to tune the morphology of the active layer so as to improve device performance have been reported. Annealing of P3HT-PC$_{61}$BM based device for example significantly enhances the device performance compared to the un-annealed form

192

[16-19]. The use of chlorobenzene in place of toluene as the spin coating solvent has been reported to improve device performance [20]. In poly[2,6-(4,4-bis(2-ethylhexyl)-4H-cyclopenta[2,1-b;3,4-b0]-alt-4,7-(2,1,3-benzothiadiazole)](PCPDTBT)-PC$_{71}$BM(6,6-phenyl-C$_{71}$butyric acid methyl ester) bulk heterojunction solar cells, the use of octane-dithiol as processing additive for morphology control reportedly improved the efficiency from 2.8% to 5.5% [21]. The use of solubilizing alkyloxy side chains to tune the morphology of devices based on poly(arylene-ethynylene)-alt-poly(arylenevinylene)s (PAE-PAVs) have also been reported and proposed as a significant aspect to be considered for improvement in the performance of such devices [22-25].

Functionalization of conjugated materials by attachment of alkyl or alkyloxy side chains enhances the solubility of the resulting polymers and subsequent process-ability of the materials into thin/transparent films for various applications [22, 26]. This improves their quality as advanced materials in applications such as light-emitting diodes [27-28], field effect transistors [29-33], and photovoltaic cells [8, 12-13]. In addition to aiding solubility and subsequent process-ability of the polymers into thin films for various applications, the position and choice of side chain (linear, branched, chain length, alkyl, alkyloxy, etc.) can also significantly influence the molecular self assembly, packing motifs, optoelectronic and transport properties of the polymer [23, 34-46]. For instance, compared to their alkyloxy analogue, the absorption spectra of alkyl-substituted polymers are blue-shifted as a result of less electron-donating nature of alkyl groups and strong steric hindrance [47]. The attachment of alkyloxy side chains to the backbone of some phenylene-ethynylene-*alt*-phenylene-vinylene hybrid polymers lowered the optical band gap of the polymers, resulting in color tuning of the polymeric materials [48-54]. The influence of the position of side chains (alkyloxy and alkyl) on polymer backbone was extensively studied and evaluated for solar

193

cells by Livi *et al* [55]. The best characteristics were found for the polymer with alkyloxy side chains on the benzene ring with efficiency of 3.6% achieved. It is therefore important that for optimization of a polymer with a potential for large-scale device fabrication, determination of the best anchoring position for the side chains, type of side chains and length of side chains is the most rational starting point.

In this report a series of ten anthracene-containing PAE-PAV polymers of general constitutional unit: (-Ph-C≡C-Anthrc-C≡C-Ph-CH=CH-Ph-CH=CH-)$_n$ with varying side chains (**Figure 6.1b**) were synthesized through side chain engineering and investigated. Solely linear (P6) and solely branched (SV7 and SV8) as well as mixed linear and branched (SV1-SV6 and P7) alkyloxy side chains were grafted to the backbone. The nature and length of the side chains were varied in a systematic manner in order to tune the photo-physical properties and, thus, the photovoltaic performance. The thermal stability, photo-physical properties and subsequent photovoltaic behavior were investigated and discussed. In addition, the electroluminescence of a selected few of these polymers was investigated. The main aim of this study is to draw conclusions about the correlation between side chain substitution, the photo-physical properties and the photovoltaic performance.

We investigated two types of bulk heterojunction organic photovoltaic cell configurations. One based on normal cell with PEDOT:PSS layer (SV1-SV8, P6 and P7) and the other based on inverted cell with PEI layer (SV3, SV8, P6 and P7). For both types, (6,6)-phenyl-C$_{61}$-butyric acid methyl ester (PCBM) was employed as the n-type or acceptor material. The structure of this report therefore, will be, discussion on the side chain engineering and the effect on the photo-physical properties and organic electronics (photovoltaics and light emitting diodes); and then the effect of different photovoltaic cells (normal and inverted) on

194

the photovoltaic properties of selected polymers (P6, P7, SV3 and SV8) under comparative studies.
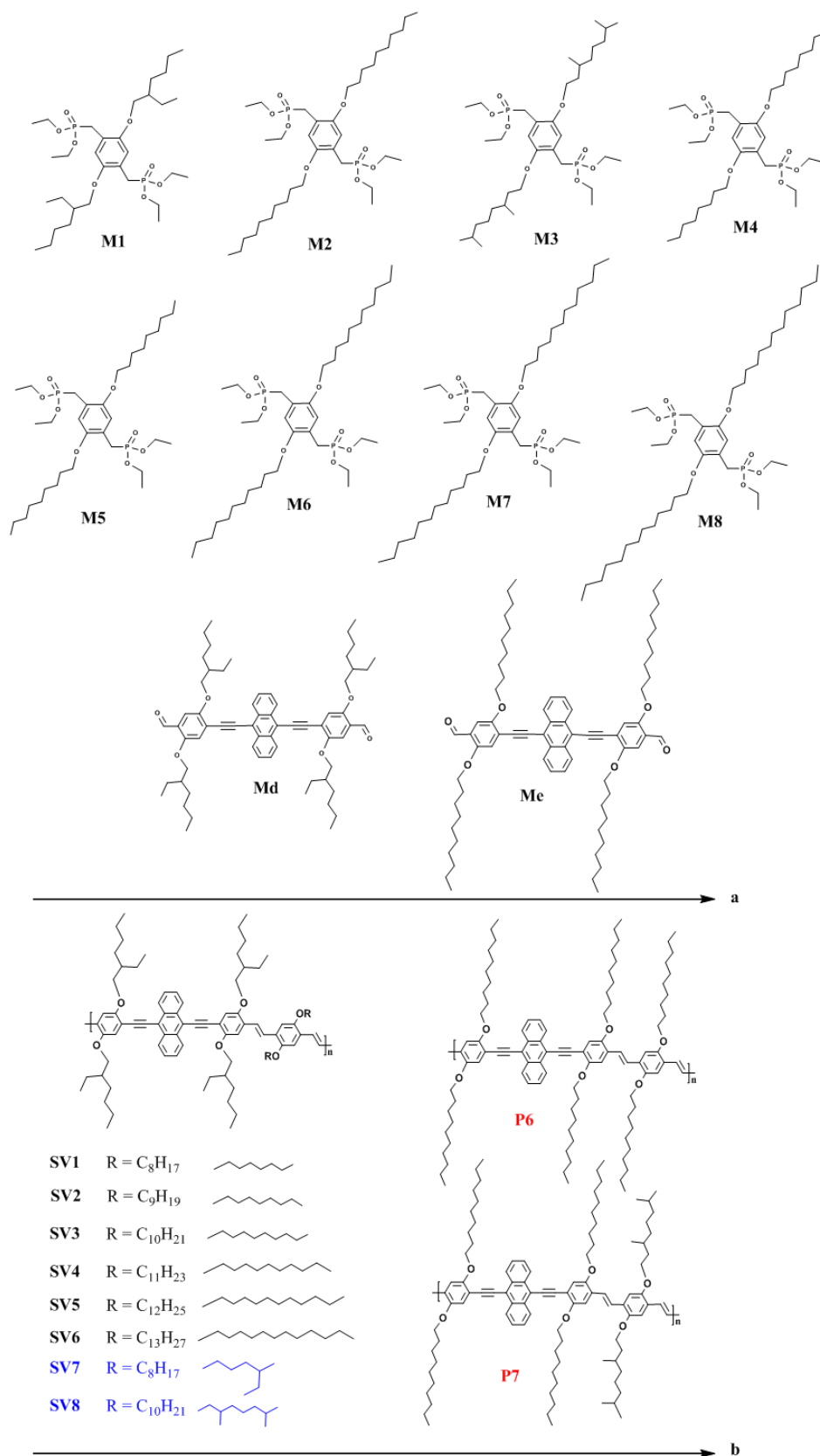
Figure 6.1: a) Monomers (M1 – M8, Md and Me), b) Polymers (SV1 – SV8, P6 and P7).

196
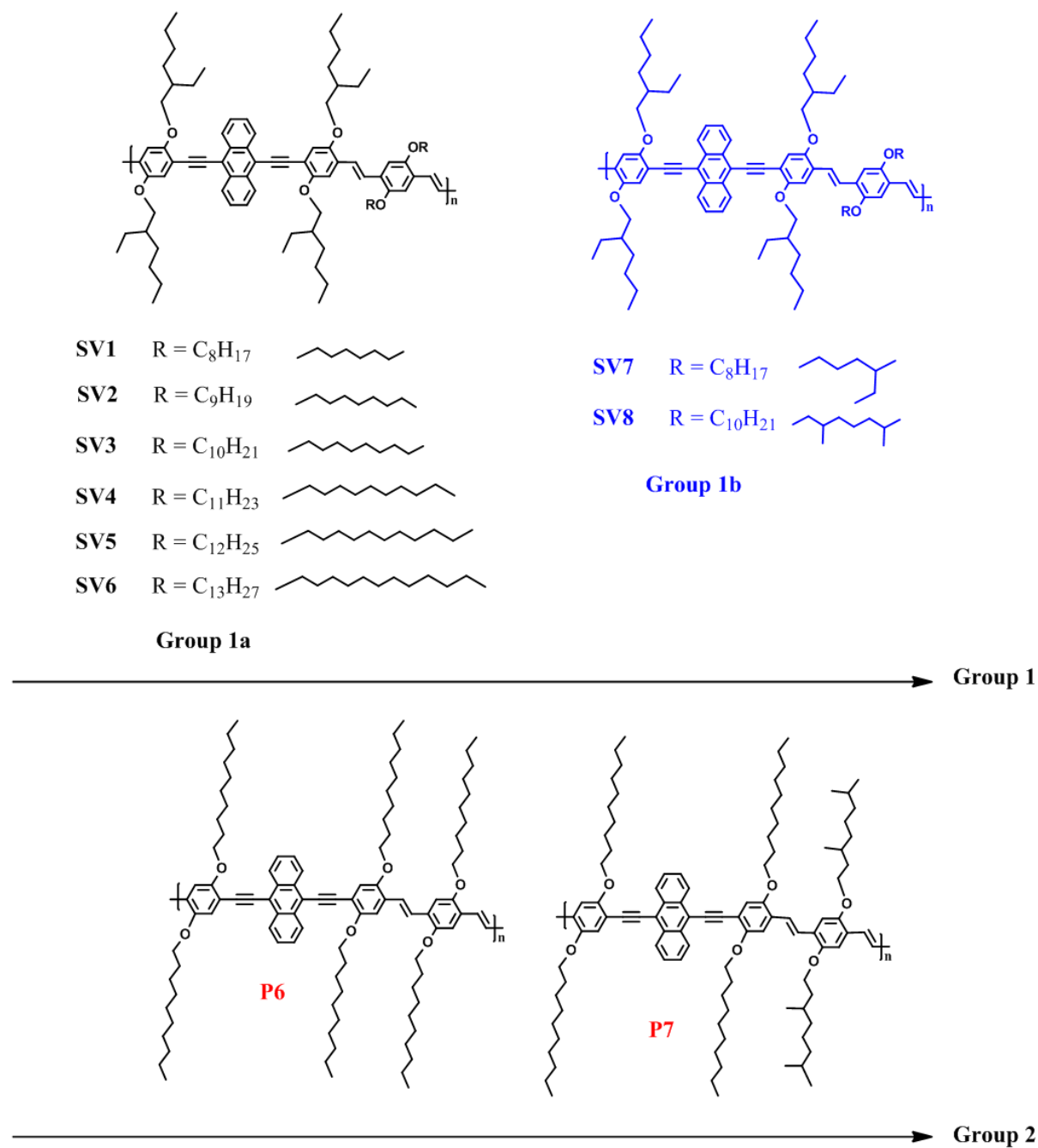
Figure 6.2: Classification of the polymers SV1 – SV8, P6 and P7.

197

6.1 Experimental

6.1.1 Materials

All starting materials and solvents were purchased from commercial suppliers (Sigma Aldrich, Merck, Alfa Aesar and VWR).

6.1.2 Instrumentation

All NMR spectra were measured in deuterated chloroform using a Gemini 300 MHz spectrometer and Bruker Avance IIIHD 400 MHz Nanobay NMR spectrometer equipped with a 5 mm BBO. For P6 and P7, Fourier transform infrared spectroscopy (FTIR) was performed with Perkin Elmer ATR TWO FTIR Spectrometer at room temperature. For SV1 – SV8, Thermo Scientific, Nicolet iS10 FTIR spectrometer equipped with a diamond crystal was used. Analyses were done between 650 and 4000 cm^{-1} wavenumbers and 64 scans were taken per sample at a resolution of 4 cm^{-1}. Data processing was done using the OMNIC software. Gel-permeation chromatography (GPC) measurements in form of size exclusion chromatography (SEC) were performed using a Pump Deltachrom (Watrex Comp.) with a Midas autosampler and two columns of MIXED-B LS PL gel, particle size 10 μm. An evaporative light scattering detector (PL-ELS-1000 from Polymer Laboratories) was used; THF was the mobile phase and polystyrene standards were used for calibration. The absorption measurements were carried out using a Perkin Elmer UV/Vis/NIR Lambda 1050 spectrometer. A PTi Photon Technology Intl. fluorometer and a Coherent GaN-based violet diode laser (Vioflame series) emitting at 405 nm were employed for photoluminescence measurements in solution and film respectively. The laser power on the sample was about 50

198

μW (spot diameter ca 1mm). Polymer was dissolved in chlorobenzene (~1.0 * 10^{-5} M) for the solution measurements while films were cast from a 10 mg/mL solution of chlorobenzene on pre-cleaned glass slides for film measurements. Cyclic voltammetry in acetonitrile with tetrabutylammonium hexafluorophosphates (TBAPF$_6$) as supporting electrolyte, a Ag/AgCl reference electrode, a platinum wire counter electrode and indium-doped tin oxide (ITO)-coated glass slides (15 Ω/sq, Xin Yan Tech. LTD) covered with a thin film of the polymer was used as working electrode (WE) at a scan rate of 50 mV/s. Experiments were set up in a glove box and recorded with a Jaissle Potentiostat-Galvanostat IMP 83 PC - 10. 150 μL of each polymer sample was spin-coated from solution (10 mg/mL) in chlorobenzene. For P6, P7 SV3 (batch1) and SV8 (batch1), thermal behavior was analysed using Perkin Elmer TGA 7 from 20-600 at 10°C/min in nitrogen. For SV1 – SV8, TGA Q500 at ramp 20°C/min to 600°C in nitrogen at a flow rate of 50 mL/min was employed. Atomic force microscopy images were recorded in tapping mode (Dimension V SPM, Veeco).
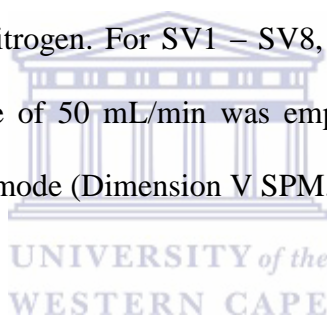
6.1.3 Organic bulk heterojunction solar cells fabrication

6.1.3.1 Solution preparation

The investigated photovoltaic devices were fabricated using two different forms of bulk-heterojunction architecture (normal and inverted). For all donor:acceptor devices, 1:2 blend solution was in 1 ml chlorobenzene. Solutions were stirred at 70°C overnight.

6.1.3.2 Substrate preparation

Indium tin oxide (ITO) glass slides were cut into 1.5 cm width using diamond cutter. Part of the cut ITO were covered with an adhesive tape and the uncovered part etched (ITO etched away) by immersion in hydrochloric acid to prevent short circuits. The adhesive tape protects the ITO in the covered region while the uncovered part is etched away. After etching, the substrates were rinsed with deionised water to remove the acid residue. The glass-ITO slides were then cut into 1.5 cm x 1.5 cm squares. The obtained squares were labelled in the top left corner in the non-conductive side (the side without ITO). The final cleaning process was done in an ultrasonic bath in acetone and iso-propanol each for 15 mins.

6.1.3.3 Device fabrication

Cleaned substrates were plasma treated by (plasma ETCH PE-50) for 5 min at 50 W O_2. Filtered poly (3,4-ethylenedioxythiophene)-poly(styrenesulphonate) (PEDOT-PSS) (a transparent, conductive polymer with high ductility) was then spun on each plasma treated substrate. The PEDOT-PSS was used to improve the extraction properties between the ITO and the active layer and to reduce the roughness of the ITO. PEDOT-PSS was gently wiped away from the etched part of the ITO using deionized water with a cotton bud to enhance contact with the electrode. The prepared donor:acceptor solution was spin coated on the PEDOT-PSS substrate and partly wiped away from the sample borders with toluene soaked cotton bud and de-ionized water. The samples were then transferred to a nitrogen-filled glovebox to dry. Finally, LiF and Al (top electrode) were thermally evaporated on the glass/ITO/PEDOT-PSS/polymer:PCBM substrate to complete the device fabrication. The device configuration in this case is represented as glass/ITO/PEDOT-

200

PSS/polymer:PCBM/LiF/Al. For the inverted cells, polyethylene imine (PEI) was used in place of PEDOT-PSS and the top electrode was MoOx/Ag. The device configuration is represented as glass/ITO/PEI/polymer:PCBM/MoOx/Ag.

6.1.3.4 Device characterisation

Current voltage (*I-V*) curves of the devices were recorded in the dark and under illumination using a solar simulator. A "Gold sun" Sun simulator was used to record the current-voltage characteristics with LS02821 LOT Quantum Design at 100 mW/cm^2 Keithley output reader. All *I-V* characteristics measurements were carried out in nitrogen filled glovebox. External quantum efficiency (EQE) were measured with EG & G Instruments lock-in-amplifier, optical chopper – SEITEC Instruments LTD Muller Electronics Optics LXH100. The thickness of the films was characterized with a Bruker DektakXT profilometer. The detailed step by step device fabrication and characterization for the top cells is given below
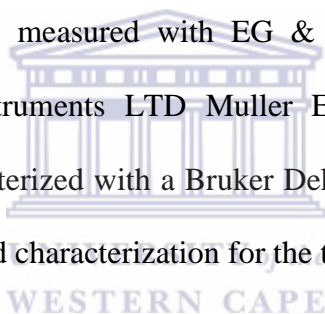
Normal Device

SV1 – SV8

Recipe:

Standard cutting & etching of Merck glass

Tap protecting, HCl conc. for 10 min

Standard cleaning of the samples:

1.) Acetone+ 15 min ultra sonic bath [RT],

2.) IPA+ 15 min ultra sonic bath [RT]

201

=> Compressed N_2 gun

Plasma treatment of the ITO substrate (Plasma ETCH PE50): 50 Watt, O_2, 5 min.

Spin coating of Clevios [pure, filtered 0.45 μm] (P VP AI 4083) on ITO glass

40 rps in 2 sec. for 2 sec. => 67 rps in 2 sec. for 30 sec. => END

Spin coating of polymer solution on PEDOT-PSS substrate

Solution at ~70 °C

Chlorobenzene p.a. [Aldrich]

Spin coating parameter for top cells of each sample

SV1 30 rps in 1 sec. for 5 sec. => 70 rps in 4 sec. for 20 sec. => END

SV2 30 rps in 1 sec. for 5 sec. => 70 rps in 4 sec. for 20 sec. => END

SV3 40 rps in 1 sec. for 5 sec. => 70 rps in 4 sec. for 20 sec. => END

SV4 25 rps in 1 sec. for 5 sec. => 70 rps in 4 sec. for 20 sec. => END

SV5 30 rps in 1 sec. for 5 sec. => 70 rps in 4 sec. for 20 sec. => END

SV6 20 rps in 1 sec. for 5 sec. => 70 rps in 4 sec. for 20 sec. => END

SV7 40 rps in 1 sec. for 5 sec. => 70 rps in 4 sec. for 20 sec. => END

SV8 30 rps in 1 sec. for 5 sec. => 70 rps in 4 sec. for 20 sec. => END

Contact cleaning with toluene and H_2O for all samples

=> Top electrode: 0.7 nm LiF / 111 nm Al evaporation

=> Measurement "Gold sun" Sun simulator ~ 100 mW/cm^2 [no mismatch factor for eff. data]

P6 and P7

Recipe:

Standard cutting & etching of Merck glass

Tap protecting, HCl conc. for 10 min

Standard cleaning of the samples:

1.) Acetone+ 15 min ultra sonic bath [RT],

2.) IPA+ 15 min ultra sonic bath [RT]

=> Compressed N_2 gun

Plasma treatment of the ITO substrate (Plasma ETCH PE50): 50 Watt, O_2, 5 min.

Spin coating of Clevios [pure, filtered 0.45 μm] (P VP AI 4083) on ITO glass

33 rps in 2 sec. for 2 sec. => 67 rps in 2 sec. for 30 sec. => END

Spin coating of polymer:PCBM on PEDOT

Solution: CB 1 % [Polymer] : 2 % (PCBM [Solenne, Lot#16-10-13])

Chlorobenzene p.a. [Aldrich]

25 rps in 2 sec. for 20 sec. => 33 rps in 2 sec. for 30 sec. => END

Contact cleaning with toluene & H_2O

=> Top electrode: 0.7 nm LiF / 100 nm Al

=> Measurement "Gold sun" Sun simulator ~ 100 mW/cm^2 [no mismatch factor for eff. data]

203

Inverted Device

P6 and P7; SV3 and SV8

Recipe:

Standard cutting & etching of Merck glass

Tap protecting, HCl conc. for 10 min

Standard cleaning of the samples:

1.) Acetone+ 15 min ultra sonic bath [RT],

2.) IPA+ 15 min ultra sonic bath [RT]

=> Compressed N_2 gun

Plasma treatment of the ITO substrate (Plasma ETCH PE50): 50 Watt, O_2, 5 min.

Spin coating of poly(ethyleneimine) (PEI) solution on ITO glass

33 rps in 2 sec. for 2 sec. => 67 rps in 2 sec. for 30 sec. => END

Spin coating of polymer:PCBM on PEI

Solution: CB 1 % [Polymer] : 2 % (PCBM [Solenne, Lot#16-10-13])

Chlorobenzene p.a. [Aldrich]

20 rps in 2 sec. for 25 sec. => 33 rps in 2 sec. for 30 sec. => END

Contact cleaning with toluene & H_2O

=> Top electrode: 0.1 KA MoOx / 1.0 KA Ag

=> Measurement "Gold sun" Sun simulator ~ 100 mW/cm^2 [no mismatch factor for efficiency data]

EQE measurement

Picture on the microscope

Thickness measurement with profilometer

204

6.1.4 Organic Light Emitting Diodes (OLEDs) Preparation and Characterization:

6.1.4.1 Fabrication

The OLEDs were fabricated with a device configuration of glass/ITO/PEI/polymer/MoOx/Ag. Pre-patterned indium tin oxide (ITO) coated glass substrates were sequentially cleaned with Hellmanex®, de-ionized water, acetone and iso-propanol in an ultrasonic bath. The cleaned substrates were plasma treated in oxygen plasma for five minutes prior to layer deposition. Polyethylene imine (PEI) and the polymer layers were sequentially deposited by blade-coating at 70°C substrate temperature (PEI: 0.27 mg/ml in n-butanol, polymer: 10 mg/ml in chlorobenzene). MoOx (10 nm) and the silver (100 nm) were deposited by vacuum evaporation. The area of one cell is about 0.24 cm².
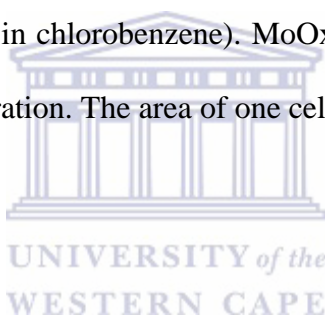
6.1.4.2 Characterization

Electroluminescence spectra of the OLEDs were measured using a Shamrock SR-303i monochromator and an Andor iDus Si-CCD detector. Different potentials were applied with a Keithley 2401 source meter. The applied voltages and the corresponding currents are listed in the graphs.

6.1.5   Synthesis

6.1.5.1 Monomer Synthesis

Synthesis of M1

A mixture of 1,4-bis(bromomethyl)-2,5-(2-ethylhexyloxy)benzene (15.2 g, 18.97 mmol) and excess triethylphosphite (9.47 g, 57 mmol) was stirred and heated slowly to 150±160°C; simultaneously. The evolving ethyl bromide was distilled off and after 4 h; vacuum was applied for 30 mins at 180°C to distil off excess triethylphosphite. The resulting oil was allowed to cool to room temperature to form pure oily substance (14.4 g, 83% yield). ^{1}H NMR (300 MHz, CDCl$_3$) δ/ppm: 6.92 (d, J = 1.6 Hz, 2H), 4.08 − 3.89 (m, 8H), 3.79 (d, J = 5.6 Hz, 4H), 3.15 (d, J = 20.1 Hz, 4H), 1.76 − 1.59 (m, 2H), 1.55 − 1.34 (m, 10H), 1.34 − 1.11 (m, 18H), 0.99 − 0.63 (m, 12H); ^{13}C NMR (75 MHz, CDCl$_3$) δ 150.43, 119.30, 114.50, 71.17, 61.8, 39.65, 30.58, 29.09, 27.06, 25.21, 23.89, 23.00, 16.30, 14.01, 11.12.

M2 − M8 were prepared under similar reaction conditions as described for M1

Synthesis of M2

A mixture of 1,4-bis(bromomethyl)-2,5-decyloxybenzene (3.37 g, 5.85 mmol) and an excess of triethylphosphite (3.0 g, 17.6 mmol) was stirred and heated slowly to 150-160°C, and the evolving ethyl bromide was distilled off simultaneously. The reaction went on for 4 h, after which vacuum was applied for 1 h at 180°C to distil off any excess of triethylphosphite left in the mixture. The resulting oil was allowed to cool to room temperature to form a white solid,

which was recrystallized from diethyl ether (30 ml) yielding a white powder (3.9 g, 97%). ^{1}H NMR (400 MHz, CDCl$_3$) δ 6.89 (s, 2H), 4.00 (m, 8H), 3.90 (t, *J* = 6.5 Hz, 4H), 3.20 (d, *J* = 20.3 Hz, 4H), 1.82 − 1.65 (m, 4H), 1.41 − 1.15 (m, 40H), 0.86 (t, *J* = 6.6 Hz, 6H); ^{13}C NMR (100 MHz, CDCl$_3$) δ 150.31, 119.28, 114.70, 68.89, 61.69, 31.89, 29.61, 29.56, 29.47, 29.44, 29.32, 26.92, 26.13, 25.54, 22.67, 16.38, 16.34, 16.31, 14.10.

Synthesis of M3

A mixture of 1,4-bis(bromomethyl)-2,5-(3,7-dimethyloctyloxy)benzene (5.1 g, 8.7 mmol) and excess triethylphosphite (4.4 g, 26.1 mmol) was stirred and heated slowly to 150±160°C, and the evolving ethyl bromide was concurrently distilled off. After 4 h, vacuum was applied for 30 min at 180°C to distil off any excess triethylphosphite still present in the mixture. The resulting oil was allowed to cool to room temperature to form a pure yellowish oil (5.73 g, 96% yield). ^{1}H NMR (400 MHz, CDCl$_3$) δ 6.85 (s, 2H), 4.07 − 3.79 (m, 12H), 3.14 (d, *J* = 20.4 Hz, 4H), 1.86 − 1.37 (m, 8H), 1.32 − 1.01 (m, 24H), 0.86 (d, *J* = Hz, 6H), 0.79 (d, *J* = 6.6 Hz, 12H); ^{13}C NMR (100 MHz, CDCl$_3$) δ 150.15, 119.18, 114.60, 67.01, 61.61, 38.99, 37.09, 36.23, 29.63, 27.72, 26.71, 25.32, 24.45, 22.45, 22.34, 19.44, 16.09.

Synthesis of M4

A mixture of 1,4-bis(bromomethyl)-2,5-octyloxybenzene (4.35 g, 8.36 mmol) and triethylphosphite (4.3 g, 25.9 mmol) were heated at 150°C for 4.25 h. Afterward the temperature was enhanced up to 170°C and the pressure reduced by using a membrane pump. After re-crystallization from diethyl ether a white material (4.25 g, 6.7 mmol) was obtained .Yield: 80.1%. ^{1}H NMR (300 MHz, CDCl$_3$) δ 6.90 (d, *J* = 1.4 Hz, 2H), 4.13 − 3.80 (m, 12H),

3.22 (d, J = 12.4 Hz, 4H), 1.85 − 1.61 (m, 4H), 1.52 − 1.09 (m, 32H), 0.87 (t, J = 6.6 Hz, 6H). ^{13}C NMR (75 MHz, CDCl$_3$) δ 150.84, 120.09, 115.11, 69.80, 63.2, 31.77, 29.60, 27.15, 26.06, 25.30, 22.61, 16.63, 14.04.

Synthesis of M5

A mixture of 1,4-bis(bromomethyl)-2,5-nonyloxybenzene (3.0 g, 5.47 mmol) and triethylphosphite (2.82g, 24.24 mmol) were stirred at 150°C for 4 h. Afterward the mixture was heated to 180°C and vacuum was applied to remove the excess of triethylphospite. The residue was worked up to give 2.86 g (4.31 mmol) of a white substance. Yield: 79%. ^{1}H NMR (300 MHz, CDCl$_3$) δ 6.90 (d, J = 1.3 Hz, 2H), 4.14 − 3.80 (m, 12H), 3.21 (d, J = 20.2 Hz, 4H), 1.83 − 1.62 (m, 4H), 1.33 (ddd, J = 19.9, 14.2, 6.9 Hz, 36H), 0.87 (t, J = 6.7 Hz, 6H). ^{13}C NMR (75 MHz, CDCl$_3$) δ 151.36, 120.60, 114.88, 68.95, 62.86, 31.84, 29.39, 27.12, 26.09, 25.27, 22.62, 16.58, 14.05.
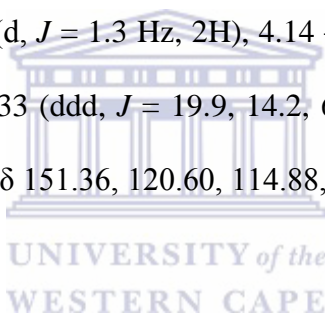
Synthesis of M6

A mixture of 1,4-bis(bromomethyl)-2,5-undecyloxybenzene (4.20 g, 6.95 mmol) and excess triethylphosphite (3.5 g, 20.9 mmol) was stirred and heated slowly to 150±160°C, and the evolving ethyl bromide was distilled off simultaneously. The reaction went on for 4 h, after which vacuum was applied for 1 h at 180°C to distil off any excess triethylphosphite left in the mixture. The resulting oil was allowed to cool to room temperature to form a white solid, which was re-crystallized from diethyl ether (30 ml) yielding (4.36 g, 87%) of pure substance. ^{1}H NMR (300 MHz, CDCl$_3$) δ 6.90 (d, J = 4.6 Hz, 2H), 4.12 − 3.81 (m, 12H), 3.21 (d, J = 20.2 Hz, 4H), 1.84 − 1.60 (m, 4H), 1.47 − 1.11 (m, 44H), 0.87 (t, J = 6.7 Hz, 6H). ^{13}C

208

NMR (75 MHz, CDCl$_3$) δ 150.37, 119.45, 114.90, 68.99, 61.82, 31.90, 29.94, 27.17, 26.12, 25.33, 22.66, 16.34, 14.08.

Synthesis of M7

A mixture of 1,4-bis(bromomethyl)-2,5-dodecyloxybenzene (5.60 g, 8.85 mmol) and excess triethylphosphite (4.5 g, 26.6 mmol) was stirred and heated slowly to 150±160°C, and the evolving ethyl bromide was distilled off simultaneously. The reaction went on for 4 h, after which vacuum was applied for 1 h at 180°C to distil off any excess triethylphosphite left in the mixture. The resulting oil was allowed to cool to room temperature to form a yellowish solid, which was re-crystallized from diethyl ether (30 ml) yielding (5.9 g, 89%) of white substance. ^{1}H NMR (300 MHz, CDCl$_3$) δ 6.90 (d, *J* = 1.4 Hz, 2H), 4.10 − 3.81 (m, 12H), 3.21 (d, *J* = 20.2 Hz, 4H), 1.83 − 1.63 (m, 4H), 1.32 (ddd, *J* = 16.8, 14.0, 6.4 Hz, 48H), 0.87 (t, *J* = 6.7 Hz, 6H). ^{13}C NMR (75 MHz, CDCl$_3$) δ 151.61,, 120.59, 114.81, 68.96, 63.40, 31.88, 29.90, 27.13, 26.10, 25.30, 22.65, 16.60, 14.07.

Synthesis of M8

A mixture of 1,4-bis(bromomethyl)-2,5-tridecyloxybenzene (2.42 g, 3.66 mmol) and excess triethylphosphite (1.9 g, 11.0 mmol) was stirred and heated slowly to 150±160°C, and the evolving ethyl bromide was distilled off simultaneously. The reaction went on for 4 h, after which vacuum was applied for 1 h at 180°C to distil off any excess triethylphosphite left in the mixture. The resulting oil was allowed to cool to room temperature to form a yellowish solid, which was re-crystallized from diethyl ether (30 ml) yielding (2.4 g, 85%) of white substance. ^{1}H NMR (300 MHz, CDCl$_3$) δ 6.88 (dd, *J* = 9.6, 2.0 Hz, 2H), 4.10 − 3.81 (m,

12H), 3.19 (t, J = 12.5 Hz, 4H), 1.85 – 1.63 (m, 4H), 1.32 (ddd, J = 17.6, 13.6, 6.1 Hz, 52H), 0.87 (t, J = 6.7 Hz, 6H). ^{13}C NMR (75 MHz, CDCl$_3$) δ 150.32, 120.45, 114.90, 68.98, 63.02, 31.88, 29.44, 27.16, 26.11, 25.31, 22.65, 16.62, 14.07.

Synthesis of Md

9,10-Dibromoanthracene (5.77 g, 0.0172 mols) was given to a degassed solution of 211 mL of diisopropylamine and 529 mL of toluene. Pd(PPh$_3$)$_4$ (0.81 g, 0.70 mmol), and CuI (0.13 g, 0.70 mmol) were added after 30 mins of stirring and degassing and the reaction was allowed to run under same condition for 1 h. 2,5-bis((2-ethylhexyl)oxy)-4-ethynylbenzaldehyde (13.55 g, 0.0350 mols) was dissolved in 50 mL of toluene and degassed for 30 mins. The degassed solution of 2,5-bis((2-ethylhexyl)oxy)-4-ethynylbenzaldehyde was added to the reaction mixture drop-wisely by means of a controlled dropping funnel. The reaction mixture was heated at 75°C for 24 h in a nitrogen atmosphere and monitored with TLC. 80 mL of toluene was added and heat removed while still stirring. After cooling to room temperature, the precipitated diisopropylammonium bromide was filtered off and the solvent was evaporated under vacuum. The residue was chromatographed on a silica gel column with hexane:dichloromethane (1:1) as eluent to yield a dark orange powder which was re-crystallized several times in methanol and 1% H$_2$O to yield (14.2 g, 87%) bright orange powder. ^{1}H NMR (300 MHz, CDCl$_3$) δ 10.52 (s, 2H), 8.93 – 8.67 (m, 4H), 7.78 – 7.56 (m, 4H), 7.44 (s, 2H), 7.33 (s, 2H), 4.21 – 3.90 (m, 8H), 2.08 – 1.75 (m, 4H), 1.75 – 1.14 (m, 32H), 0.92 (ddt, J = 39.4, 36.8, 7.3 Hz, 24H). ^{13}C NMR (75 MHz, CDCl$_3$) δ 189.09, 155.72, 154.07, 132.25, 127.48, 126.99, 125.18, 120.23, 118.89, 117.20, 109.39, 99.06, 94.37, 71.65, 39.55, 30.70, 30.31, 29.09, 24.07, 23.74, 23.05, 14.07, 11.28, 10.95.

Synthesis of Me

9,10-Dibromoanthracene (311 mg, 0.92 mmol) was given to a degassed solution of 15 mL of diisopropylamine and 35 mL of toluene. 30 mins later, Pd(PPh$_3$)$_4$ (43.6 mg, 0.0378 mmol), and CuI (7.2 mg, 0.0378 mmol) were added. Mixture was allowed to stir and degas for another 30 mins and thereafter, 2,5-bis((decyl)oxy)-4-ethynylbenzaldehyde (840 mg, 1.89 mmol) (in a solution of degassed toluene) was added drop-wisely. The reaction mixture was heated at 75°C for 24 h in a nitrogen atmosphere and monitored with TLC. After cooling to room temperature, the precipitated diisopropylammonium bromide was filtered off and the solvent was evaporated under vacuum. The residue was chromatographed on a silica gel column with toluene:hexane (1:1) as eluent to yield an orange solid which was re-crystallized in methanol to yield (550 mg g, 56%) shiny bright orange powder. ^{1}H NMR (300 MHz, CDCl$_3$) δ 10.50 (s, 2H), 8.82 (dd, J = 6.7, 3.2 Hz, 4H), 7.65 (dt, J = 13.8, 6.9 Hz, 4H), 7.40 (s, 2H), 7.29 (s, 2H), 4.16 (t, J = 6.5 Hz, 8H), 2.15 − 1.74 (m, 8H), 1.68 − 1.06 (m, 56H), 0.87 (dt, J = 13.6, 6.7 Hz, 12H). ^{13}C NMR (101 MHz, CDCl$_3$) δ 189.17, 155.61, 154.01, 132.27, 127.47, 126.95, 125.11, 120.21, 118.90, 117.00, 109.31, 99.08, 94.66, 69.39, 31.90, 29.45, 26.10, 22.69, 14.13.

6.1.5.2 Polymer Synthesis

Synthesis of SV1

Dialdehyde Md (1000 mg, 1.06 mmol) and bisphosphonate M4 (671 mg, 1.06 mmol) were dissolved in dried toluene (100 ml) to give a greenish light orange color while stirring vigorously under nitrogen and heating under reflux. The polycondensation was initiated by

addition of potassium-*tert*-butoxide (474 mg, 4.23 mmol) when a stable temperature was achieved and an instant color change to blackish deep orange was observed. After 80 mins benzaldehyde was added and the reaction allowed running for 10 mins. Toluene (80 ml) was added and the heating turned off. Reaction mixture was allowed to continue to stir for 10 mins and 10% HCl was added. Stirring continued until the entire mixture was completely dissolved. The organic layer was separated and extracted several times with distilled water until the water phase became neutral (pH = 6 – 7). A Dean-Stark apparatus was used to dry the organic layer. The hot (50-60°C) toluene solution was filtered; the filtrate was concentrated to the minimum by using a rotary evaporator and then precipitated in vigorously stirred cold methanol (250 ml). The polymer was extracted by Soxhlet extraction with methanol until a clear solution was observed around the thimble. The polymer was again dissolved in a small amount of toluene, re-precipitated in cold methanol and kept for 24 h under 4-8°C. It was thereafter filtered and allowed to dry under air. 790 mg (0.6058 mmol, with respect to the repeating unit) of dark red polymer was obtained. Yield: 56%. GPC (THF, polystyrene): M_w= 13,030 g/mol, M_n = 5,280 g/mol, PDI = 2.5. ^{1}H NMR (300 MHz, CDCl$_3$) δ 8.86, 7.60 and 7.05 – 6.68 (arylene and vinylene H´s); 4.31 – 3.45 (-CH$_2$O-); 2.16 – 0.51 (CH$_3$(CH$_2$)$_3$CH(CH$_2$CH$_3$)- and CH$_3$(CH$_2$)$_6$-).

SV2 – SV8 were prepared under similar reaction conditions as described for SV1

Synthesis of SV2

Dialdehyde Md (1000 mg, 1.06 mmol) and bisphosphonate M5 (701 mg, 1.06 mmol) were dissolved in dried toluene (100 ml) to give a greenish light orange color while stirring vigorously under nitrogen and heating under reflux. Potassium-*tert*-butoxide (474 mg, 4.23

212

mmol) was added (instant color change to greenish deep orange was observed); and the reaction mixture was heated at reflux for 80 mins. The polycondensations was quenched by addition of benzaldehyde, toluene and dilute HCl (10%). The organic layer was separated, extracted with distilled water until the water phase became neutral (pH = 6-7), dried by means of a Dean stark apparatus, filtered, concentrated and precipitated in cold methanol (250 ml). The polymer was extracted with methanol for 24 h, dissolved in 10 mL toluene and re-precipitated in methanol. The resulting brownish red fibrous polymer was filtered and dried in air to give 1320 mg (0.9910 mmol with respect to the repeating unit). Yield: 94%. GPC (THF, polystyrene): M_w= 27,500 g/mol, M_n = 6,900 g/mol, PDI = 4.0. ^{1}H NMR (300 MHz, CDCl$_3$) δ 8.84, 7.58 and 7.01 − 6.71 (arylene and vinylene H´s); 3.89 (-CH$_2$O-); 2.11 − 0.63 (CH$_3$(CH$_2$)$_3$CH(CH$_2$CH$_3$)- and CH$_3$(CH$_2$)$_7$-).

Synthesis of SV3

Dialdehyde Md (1000 mg, 1.06 mmol) and bisphosphonate M2 (730 mg, 1.06 mmol) were dissolved in dried toluene (90 ml) to give a greenish brown color while stirring vigorously under nitrogen and heating under reflux. The polycondensation was initiated by addition of potassium-*tert*-butoxide (474 mg, 4.23 mmol) when a stable temperature was achieved and an instant color change to brownish orange which became darker as the reaction progressed was observed. After reacting for 80 mins, benzaldehyde was added and mixture stirred for 10 mins; the heating was stopped and the mixture was diluted with toluene (80 ml), and aqueous HCl (10 wt.%, 20 ml) was added to quench the reaction. The organic phase was separated and washed several times with distilled water until the water phase became neutral. The organic layer was dried in a Dean-Stark apparatus. The solution was filtered, concentrated under vacuum, dissolved in 10 mL toluene and precipitated in methanol. The polymer was

213

filtered off and extracted for 24 h with methanol (Soxhlet extraction). After re-dissolving in toluene the polymer was once more precipitated in methanol and kept at 4-8°C for 24 h, filtered off and dried in air to yield brownish red fibers 1290 mg (0.9485 mmol with respect to the repeating unit). Yield: 90%. GPC (THF, polystyrene): M_w = 20,480 g/mol, M_n = 4,220 g/mol, PDI = 4.9. ^{1}H NMR (300 MHz, CDCl$_3$) δ 8.96 – 8.69, 7.80 – 7.42, and 7.02 – 6.71 (m, (arylene and vinylene H´s); 4.28 – 3.46 (CH$_2$O-); 2.20 – 0.55 (CH$_3$(CH$_2$)$_3$CH(CH$_2$CH$_3$)- and CH$_3$(CH$_2$)$_8$-).

Synthesis of SV4

Dialdehyde Md (1000 mg, 1.06 mmol) and bisphosphonate M6 (760 mg, 1.06 mmol) were dissolved in dried toluene (80 ml) to give a greenish brown color while stirring vigorously under nitrogen and heating under reflux. Potassium-*tert*-butoxide (474 mg, 4.23 mmol) was added (instant color change to brownish orange was observed); and the reaction mixture was heated at reflux for 80 mins. After this time benzaldehyde was added and mixture allowed stirring for 10 mins. Toluene (80 mL) was added and the reaction was quenched with aqueous HCl (10 wt.%). The organic phase was separated and extracted several times with distilled water until the water phase became neutral (pH = 6-7). The organic phase was dried in Dean-Stark apparatus. The resulting toluene solution was filtered, concentrated under vacuum to the minimum and precipitated in cold methanol. The polymer was extracted for 24 h with methanol, dissolved once more in toluene, and re-precipitated in methanol. The precipitate in methanol was kept at 4-8°C for 24 h, filtered and dried under air. A brownish red fiber of 1330 mg (0.9581 mmol with respect to the repeating unit) was obtained. Yield = 91%. GPC (THF, polystyrene): M_w = 26,430 g/mol, M_n = 10,050 g/mol, PDI = 2.6. ^{1}H NMR (300 MHz,

214

CDCl$_3$) δ 8.83, 7.76 – 7.44, and 7.02 – 6.68 (arylene and vinylene H´s); 4.23 – 3.49 (-CH$_2$O-); 2.10 – 0.57 (CH$_3$(CH$_2$)$_3$CH(CH$_2$CH$_3$)- and CH$_3$(CH$_2$)$_9$-).

Synthesis of SV5

The dialdehyde Md (1000 mg, 1.06 mmol) and bisphosphonate M7 (790 mg, 1.06 mmol) were dissolved in dried toluene (80 ml) to give a greenish brown color while stirring vigorously under nitrogen and heating under reflux. Potassium-*tert*-butoxide (474 mg, 4.23 mmol) was added (instant color change to brownish orange was observed); and the reaction mixture was heated at reflux for 80 mins. Benzaldehyde was added and 10 min later, toluene (80 mL) and aqueous HCl (10 wt %, 10 mL) were added to quench the reaction. The organic phase was separated and extracted several times with distilled water until the water phase became neutral (pH = 6−7). The organic layer was dried in a Dean−Stark apparatus. After filtration the toluene solution was concentrated under vacuum and precipitated in cold methanol. The precipitate was filtered and the polymer was extracted for 24 h with methanol (Soxhlet extraction), dissolved once more in toluene, and re-precipitated in cold methanol. Filtration and drying yielded a brownish red fibrous polymer (1390 mg (0.9815 mmol with respect to the repeating unit), 93 %). GPC (THF, polystyrene): M_w= 29,850 g/mol, M_n = 7,930 g/mol, PDI = 3.8. ^{1}H NMR (300 MHz, CDCl$_3$) δ 8.83, 7.79 – 7.41, and 6.84 (arylene and vinylene H´s); 4.30 – 3.46 (-CH$_2$O-); 2.13 – 0.57 (CH$_3$(CH$_2$)$_3$CH(CH$_2$CH$_3$)- and CH$_3$(CH$_2$)$_{10}$-).

Synthesis of SV6

Dialdehyde Md (1000 mg, 1.06 mmol) and bisphosphonate M8 (819 mg, 1.06 mmol) were dissolved in dried toluene (80 ml) to give a greenish brown color while stirring vigorously under nitrogen and heating under reflux. Potassium-*tert*-butoxide (474 mg, 4.23 mmol) was added (instant color change to deep brown orange was observed); and the reaction mixture was heated at reflux for 80 min. After 80 mins benzaldehyde was added. 10 mins later the heating was stopped and toluene (80 ml) and aqueous HCl (10 wt.%, 20 ml) were added. The work up yielded a brownish red fibrous polymer (1340 mg (0.9278 mmol with respect to the repeating unit), 89 %). GPC (THF, polystyrene): M_w= 21,720 g/mol, M_n = 9,770 g/mol, PDI = 2.2. ^{1}H NMR (300 MHz, CDCl$_3$) δ 8.83, 7.81 – 7.41, and 6.84 (arylene and vinylene H´s); 4.25 – 3.44 (-CH$_2$O-); 2.11 – 0.58 (CH$_3$(CH$_2$)$_3$CH(CH$_2$CH$_3$)- and CH$_3$(CH$_2$)$_{11}$-).

Synthesis of SV7

Dialdehyde Md (1000 mg, 1.06 mmol) and bisphosphonate M1 (671 mg, 1.06 mmol) were dissolved in dried toluene (80 ml) to give a greenish brown color while stirring vigorously under nitrogen and heating under reflux. Potassium-*tert*-butoxide (474 mg, 4.23 mmol) was added (instant color change to dark brown orange was observed); and the reaction mixture was heated at reflux for 80 mins. After 80 mins benzaldehyde was added and the mixture allowed stirring for 10 mins. Toluene was added, heat removed and aqueous HCl (10 wt.%) was added. The purification process yielded a brownish red polymer (1100 mg (0.8436 mmol with respect to the repeating unit), 80 %). GPC (THF, polystyrene): M_w= 15,870 g/mol, M_n = 6,720 g/mol, PDI = 2.4. ^{1}H NMR (300 MHz, CDCl$_3$) δ 8.83, 7.59 and 7.05 – 6.66 (arylene and vinylene H´s); 4.30 – 3.37 (-CH$_2$O-); 2.19 – 0.49 (CH$_3$(CH$_2$)$_3$CH(CH$_2$CH$_3$)-).

216

Synthesis of SV8

For SV8, Md (1000 mg, 1.06 mmol) and bisphosphonate M3 (730 mg, 1.06 mmol) were dissolved in dried toluene (80 ml) to give a greenish brown color while stirring vigorously under nitrogen and heating under reflux. Potassium-*tert*-butoxide (474 mg, 4.23 mmol) was added (instant color change to dark brown orange was observed); and the reaction mixture was heated at reflux for 80 mins. After 80 mins benzaldehyde was added and the mixture allowed stirring for 10 mins. Toluene was added, heat removed and aqueous HCl (10 wt.%) was added. The purification process yielded a brownish red fibrous polymer (1300 mg (0.9558 mmol with respect to the repeating unit), 90 %). GPC (THF, polystyrene): M_w= 26,720 g/mol, M_n = 11,820 g/mol, PDI = 2.3. ^{1}H NMR (300 MHz, CDCl$_3$) δ 8.83, 7.78 – 7.42, and 6.88 (arylene and vinylene H´s); 4.25 – 3.48 (-CH$_2$O-); 2.12 – 0.50 (CH$_3$(CH$_2$)$_3$CH(CH$_2$CH$_3$)- and CH$_3$CH(CH$_3$)(CH$_2$)$_3$CH(CH$_3$)(CH$_2$)-).

The polymer P6 and P7 were prepared using dialdehyde Me

Synthesis of P6

Dialdehyde Me (260 mg, 0.25 mmol), M2 (170 mg, 0.25 mmol) and dried toluene (25 ml) were mixed under nitrogen and heating under reflux. Potassium-*tert*-butoxide (110 mg, 0.98 mmol) was thereafter added. After 60 mins, benzaldehyde was added. 10 mins later, toluene (30 ml) and dilute hydrochloric acid were added. The organic layer was washed with water, dried, filtered, concentrated and precipitated. The polymer was extracted for 24 h(Soxhlet extraction), dissolved, re-precipitated and dried to give 320 mg (0.2173 mmol with respect to the repeating unit) of dark red polymer. Yield: 85%. GPC (THF, polystyrene): M_w= 13,430

217

g/mol, M_n = 6,070 g/mol, PDI = 2.2. ^{1}H NMR (300 MHz, CDCl$_3$) δ 8.86, 7.58 and 7.02 – 6.72 (arylene and vinylene H´s); 4.37 – 3.56 (-CH$_2$O-); 2.22 – 0.65 (CH$_3$(CH$_2$)$_8$-).

Synthesis of P7

Dialdehyde Me (110 mg, 0.10 mmol), M3 (72 mg, 0.10 mmol), dried toluene (20 ml) and potassium-*tert*-butoxide (47 mg, 0.42 mmol) were mixed under nitrogen and heating under reflux. After 60 mins, benzaldehyde was added. 10 mins later, toluene (30 ml) and dilute hydrochloric acid were added. The organic layer was washed with water, dried, filtered, concentrated and precipitated. The polymer was extracted for 24 h (Soxhlet extraction), dissolved, re-precipitated and dried to give 130 mg (0.0883 mmol with respect to the repeating unit) of dark red polymer. Yield: 89%. GPC (THF, polystyrene): M_w= 28,430 g/mol, M_n = 11,720 g/mol, PDI = 2.4. ^{1}H NMR (300 MHz, CDCl$_3$) δ 8.86, 7.77 – 7.43, and 6.89 (arylene and vinylene H´s); 4.42 – 3.57 (-CH$_2$O-); 2.23 – 0.59 (CH$_3$(CH$_2$)$_8$- and CH$_3$CH(CH$_3$)(CH$_2$)$_3$CH(CH$_3$)(CH$_2$)-).

6.2   Results and Discussion

6.2.1   Synthesis and Material Verification/Confirmation

The polymers were synthesized through the Horner-Wadsworth-Emmons (HWE) olefination reaction of dialdehydes with bisphosphonate esters. The choice of HWE reaction over other cross coupling reactions like Suzuki, Sonogashira, Heck or Stille for polycondensation stems from its high rate of reaction, low structural defects and high yields [48]. For instance, the high possibility of side reactions such as the oxidative Glaser coupling (diyne formation) in

218

Sonogashira reaction can result in structural defect. Furthermore, these cross-coupling reactions require long reaction times and the indispensable application of metal catalyst in these reactions makes their purification steps more demanding. All polycondensation reactions in this report were performed within 80 mins reaction time with good yields.

In order to employ this reaction for the polymer synthesis, their respective bisphosphonates (**M1 - M8**) and dialdehydes (**Md - Me**) (**Figure 6.1a**) were preliminarily synthesized according to the multi-step reaction steps described in the experimental section of **Chapter 5, Figure 5.2**. In brief, the synthesis of the bisphosphonates (**M1 - M8**) involved a sequence of Williamson etherification or dialkylation of hydroquinone, dibromomethylation and Michealis−Arbuzov reaction. The dialdehydes (**Md and Me**) were also synthesized in several steps. Starting with dialkylation of hydroquinone (Williamson synthesis), followed by dibromination of the dialkylated hydroquinone to give 2,5-dialkyloxy-1,4-dibromobenzene. This product then undergoes a four step reaction of formylation, palladium catalyzed Sonogashira cross-coupling reaction with trimethylsilylacetylene, the deprotection of the acetylene units, and finally, another Sonogashira reaction of the deprotected acetylene unit with a dibromoanthracene to give bright orange colored dialdehyes alongside some diyne dialdehyde [56]. The materials were purified by column chromatography and/or re-crystallization and purity confirmed by NMR spectroscopy. The synthetic steps of the monomers (**M1 - M8**, **Md** and **Me**) and NMR confirmation are detailed in experimental section under synthesis. All ten polymers were synthesized by reacting dialdehyde with corresponding bisphosphonate. The chemical structures of the monomers (**M1 – M8**, **Md** and **Me**) and polymers (SV1 – SV8, P6 and P7) were confirmed by NMR (in CDCl$_3$) and FTIR spectroscopy.

6.2.1.1 Nuclear Magnetic Resonance (NMR) Spectroscopy

The NMR spectra of the synthesized intermediates and polycondensation monomers are characterized by well resolved and defined signals. The NMR investigation of **M1 – M8** confirmed all the protons (**Figure 6.3**), carbon (**Figure 6.4 – 6.6**) and phosphorous (**Figure 6.7**) present in the compounds. The ^{1}H NMR of **M1 – M8** reveal the protons in the two -CH groups in the benzene ring in the region 6.92 – 6.85 ppm, the -CH$_2$ protons in the phosphonate end of the compounds and those directly linked to the oxygen in the alkyloxy side chains in the region 4.14 – 3.74 ppm, the -CH$_2$ protons linking the benzene ring to the phosphonate are seen around 3.22 – 3.14 ppm; and the -CH next to the -CH$_2$ attached to the oxygen ring (in the case of M1 and M3), all -CH$_3$ and other -CH$_2$ protons present in the compound appear in the region 1.86 – 0.63 ppm. The ^{13}C NMR reveal the carbons present in the compound while the ^{31}P NMR reveal just a signal confirming the presence of just one type of phosphorous present in the compound as expected.

220
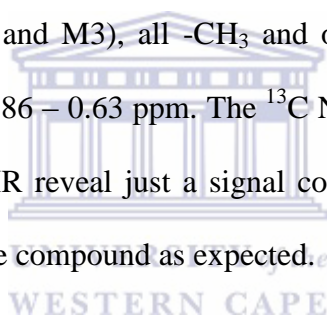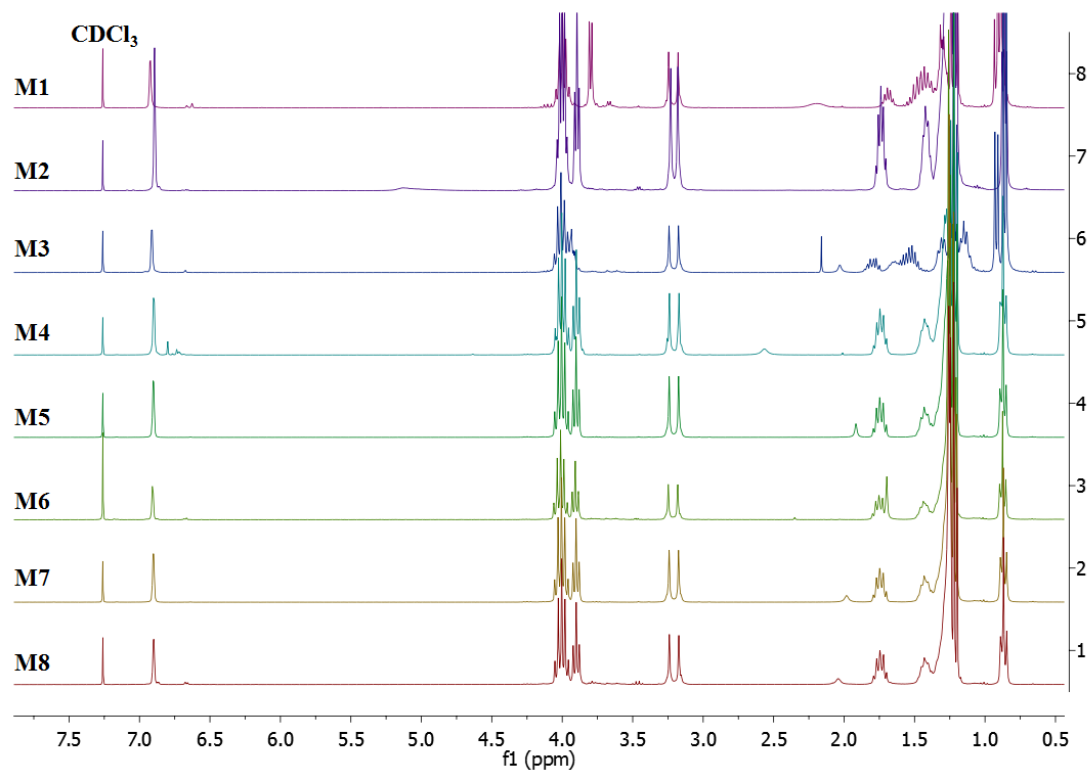
Figure 6.3: ^{1}H NMR of M1 – M8.
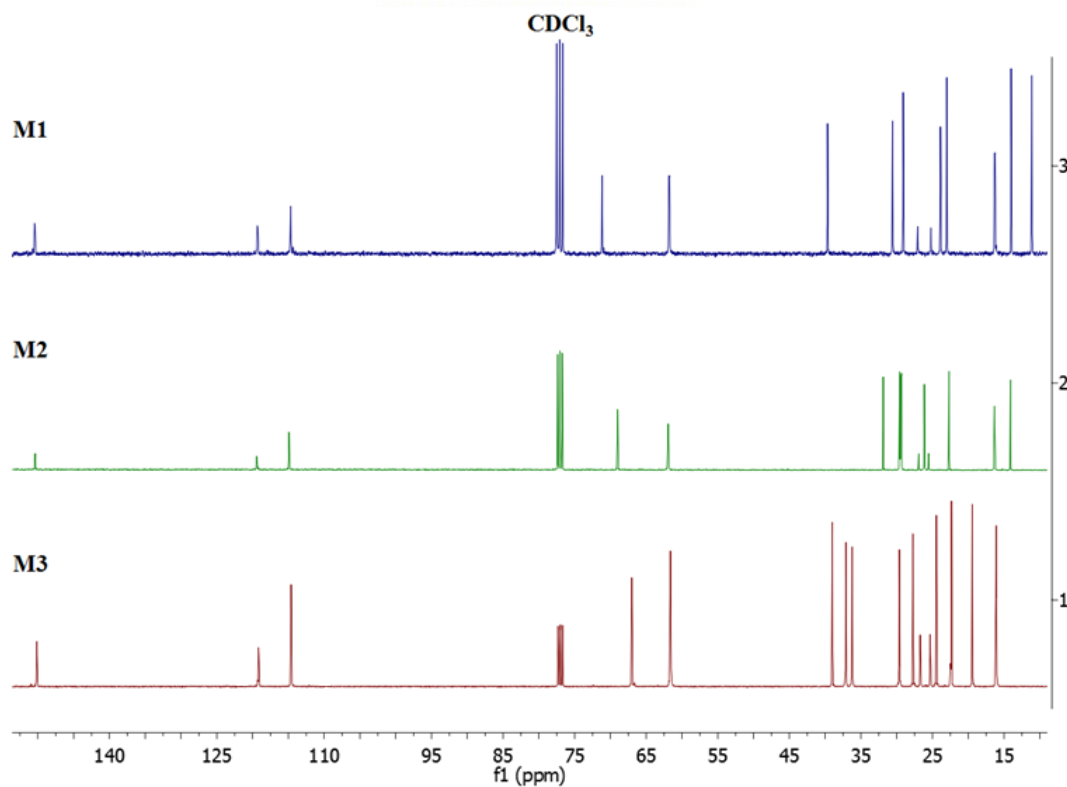
Figure 6.4: ^{13}C NMR of M1 – M3.

221
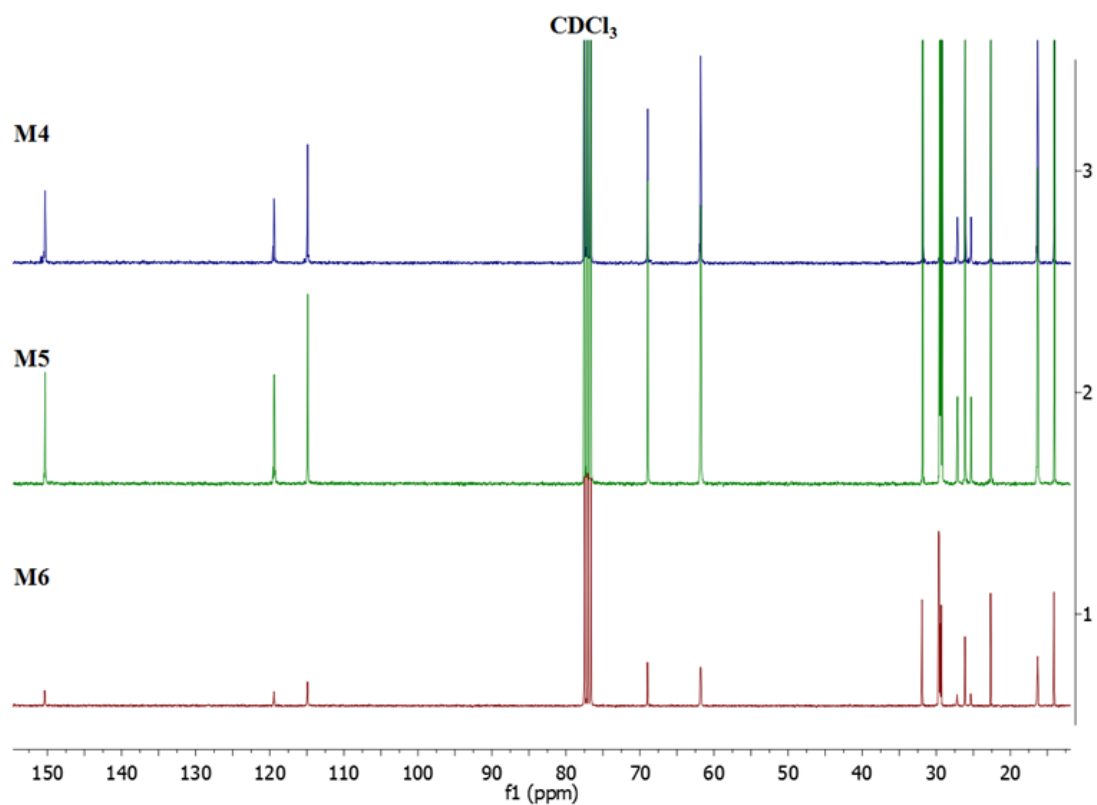
Figure 6.5: ^{13}C NMR of M4 – M6.
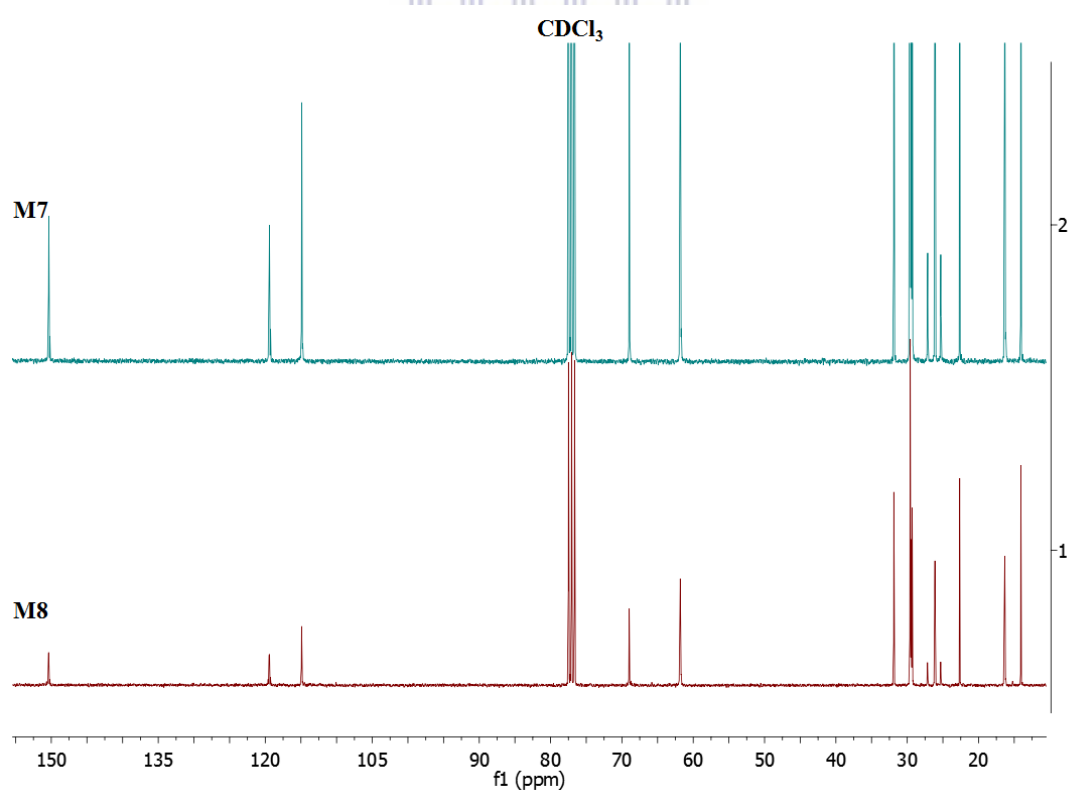
Figure 6.6: ^{13}C NMR of M7 – M8.

222
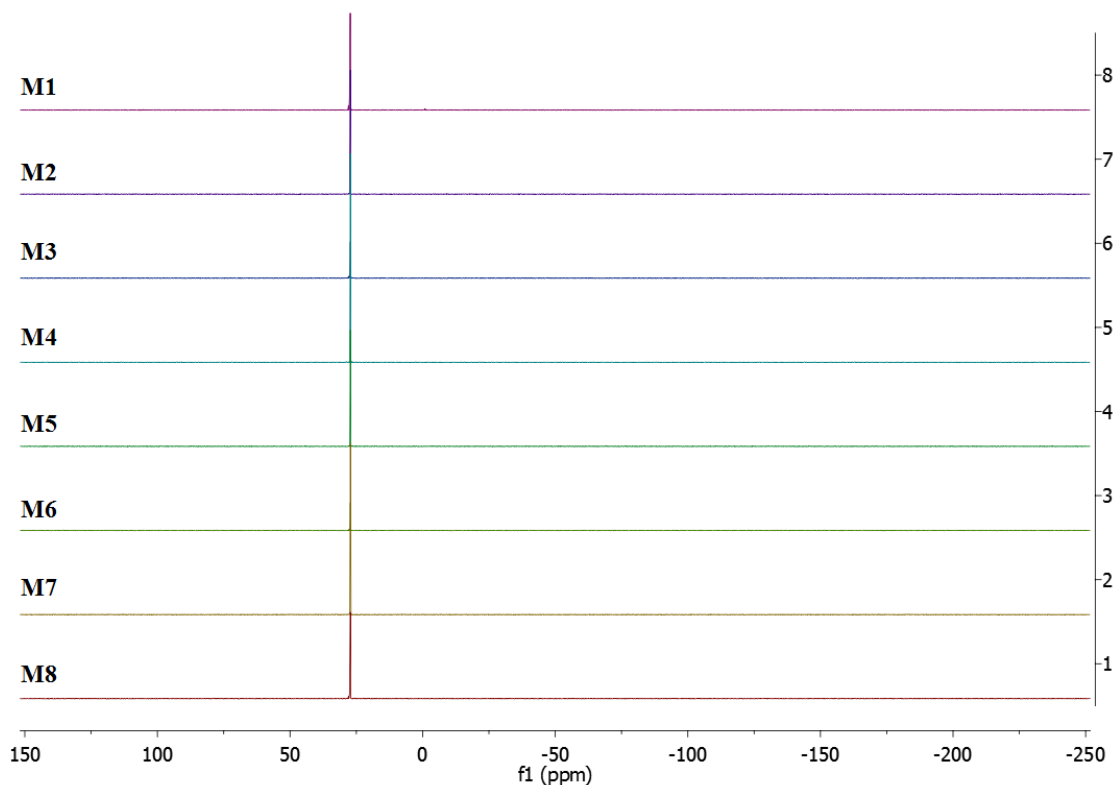
Figure 6.7: ^{31}P NMR of M1 – M8.

For **Md** and **Me**, the ^{1}H NMR signals (**Figure 6.8**) in the range 10.52 – 10.50 ppm are attributed to the -CHO protons while the -CH protons in the anthracene unit and those in the phenyl group attached to both ends of the anthracene unit via the triple bond appear in the range 8.93 – 7.29 ppm. The -CH$_2$ protons directly linked to the oxygen in the alkyloxy side chain in the phenyl group are visible in the 4.21 – 3.90 ppm region; the -CH (from 2-ethylhexyloxy side chain in the case of **Md**) and -CH$_2$ (decyloxy side chain in the case of **Me**) protons next to the -CH$_2$ protons directly linked to the oxygen of the alkyloxy side chains are assigned to the signals in the range 2.15 – 1.74 ppm. All other -CH$_2$ protons present in the compounds show signals in the range 1.75 – 1.06 ppm while the signals of all -CH$_3$ protons are obvious in the 0.92 – 0.87 ppm range.

223
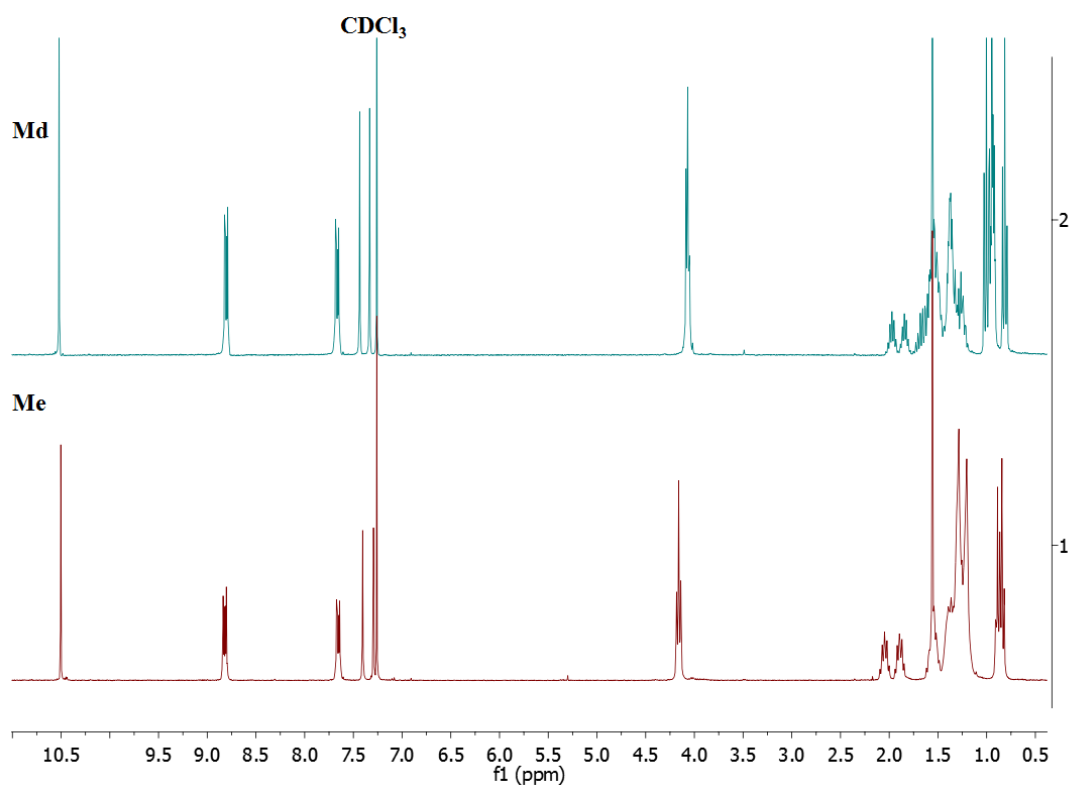
Figure 6.8: ^{1}H NMR of Md and Me.

The ^{13}C NMR spectra of **Md** and **Me** are, according to their structure, nearly the same and the spectra is schematically interpreted as shown in **Figure 6.9** and **6.10** respectively. The signal around 189 ppm denoted as **e** in the spectra is attributed to the –CHO carbon while the signals in the region 155.72 – 109.31 ppm are assigned to the aromatic and vinylenic carbons; the peaks from those of the triple bond carbons denoted **a**, **b** in the spectrum appeared between 99.08 and 94.37 ppm. The signals of the alkyloxy side chains are seen to arise between 71.65 and 10.95 ppm. As expected, a –CH bond carbon signal was detected for **Md** but absent in **Me**.
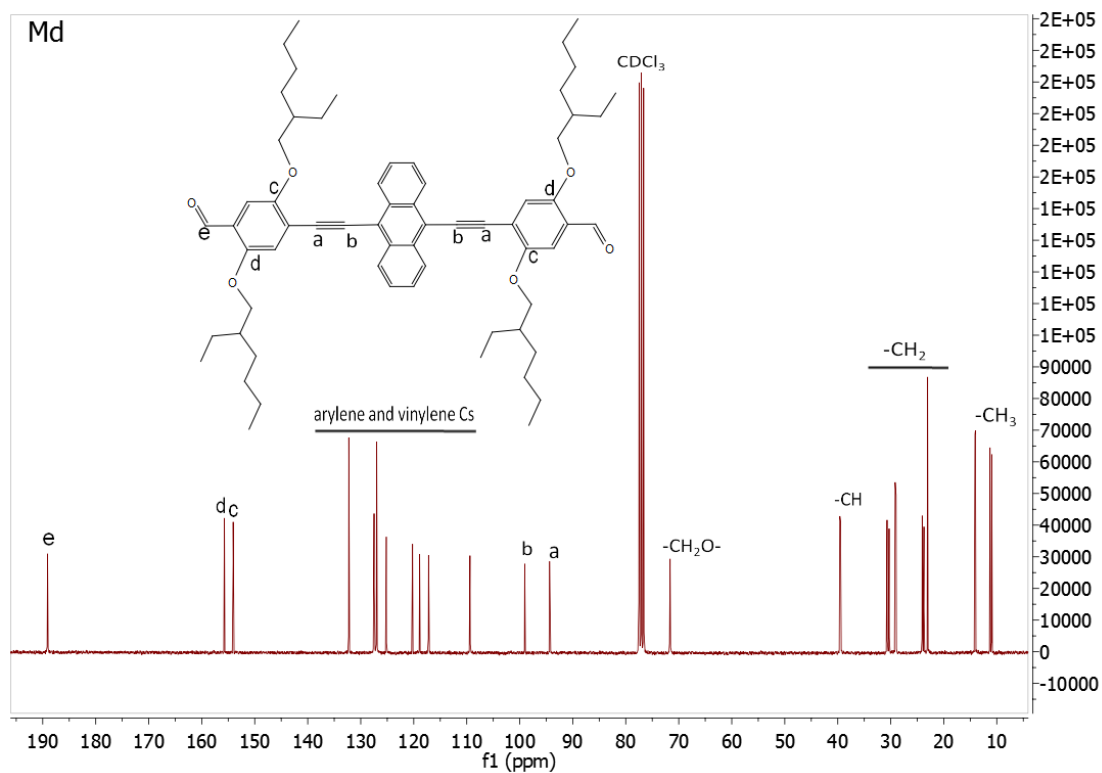
Figure 6.9: ^{13}C NMR of Md.
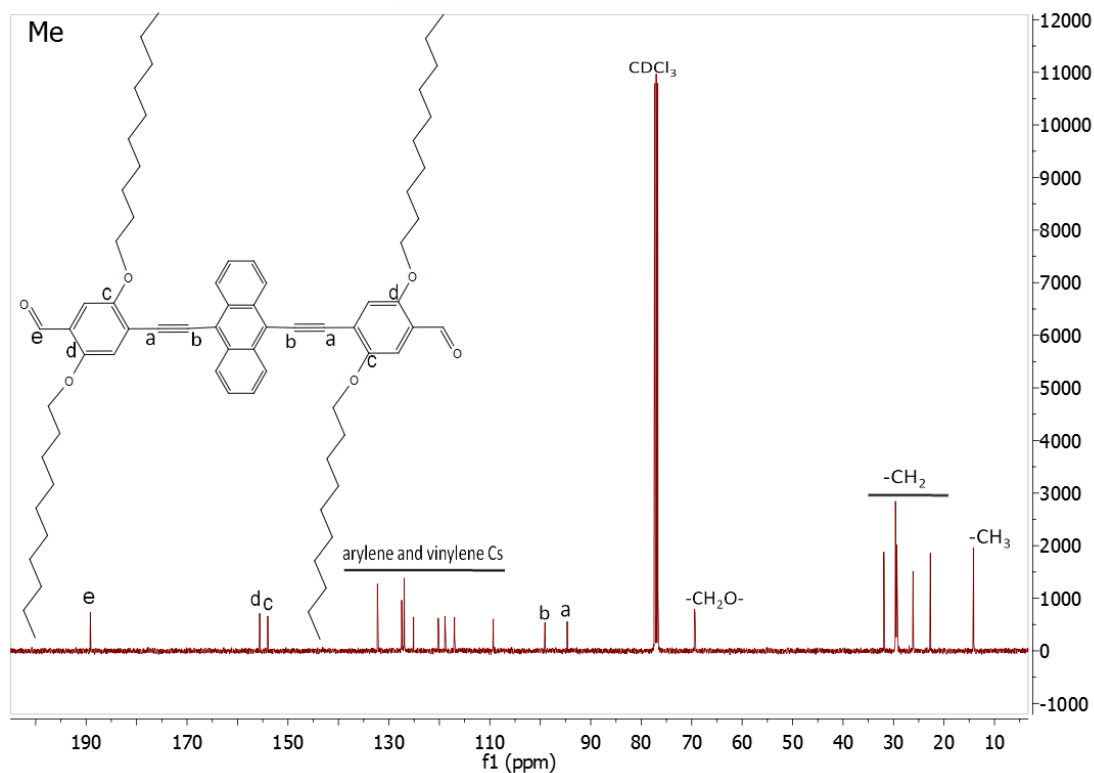
Figure 6.10: ^{13}C NMR of Me.

225

^{1}H NMR confirmed the structure and purity of the synthesized polymers (**SV1 – SV8, P6 and P7**) and their signals were compared with those of their dialdehyde monomers (**Figure 6.11 and 6.12**). The broad NMR signals in the down-field region 8.96 – 6.66 ppm are ascribed to the arylene and vinylene protons, while the signals in the region 4.42 - 0.49 ppm originate from the protons of the alkyloxy side chains. Although the ^{1}H NMR signals of the polymers SV1-SV8 and P6-P7 are broad and non-specific, they show a similarity to the signals of the corresponding monomer dialdehyde with regards to the region where the signals are observed; except that characteristic signals of the polycondensation monomers (dialdehyde, ~10.5 ppm (−CHO); bisphosphonate, ~3.2 ppm (-H_2CP)) are completely absent. These are clear indications of the formation of polymer material from the corresponding monomers. The presence of the signals marked **x** and **y** in **Figure 6.11 and 6.12** suggests the presence of a *cis* configuration [57]. The spectrum therefore suggests a *trans* (*E*) and *cis* (*Z*) configuration in all polymers due to the presence of signals or peaks indicating the presence of vinylenic double bonds with a *cis* (*Z*) configuration.

226
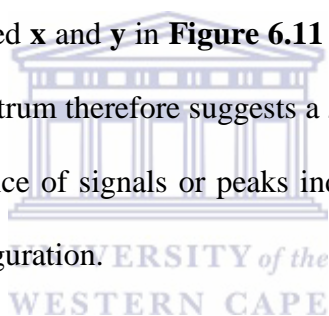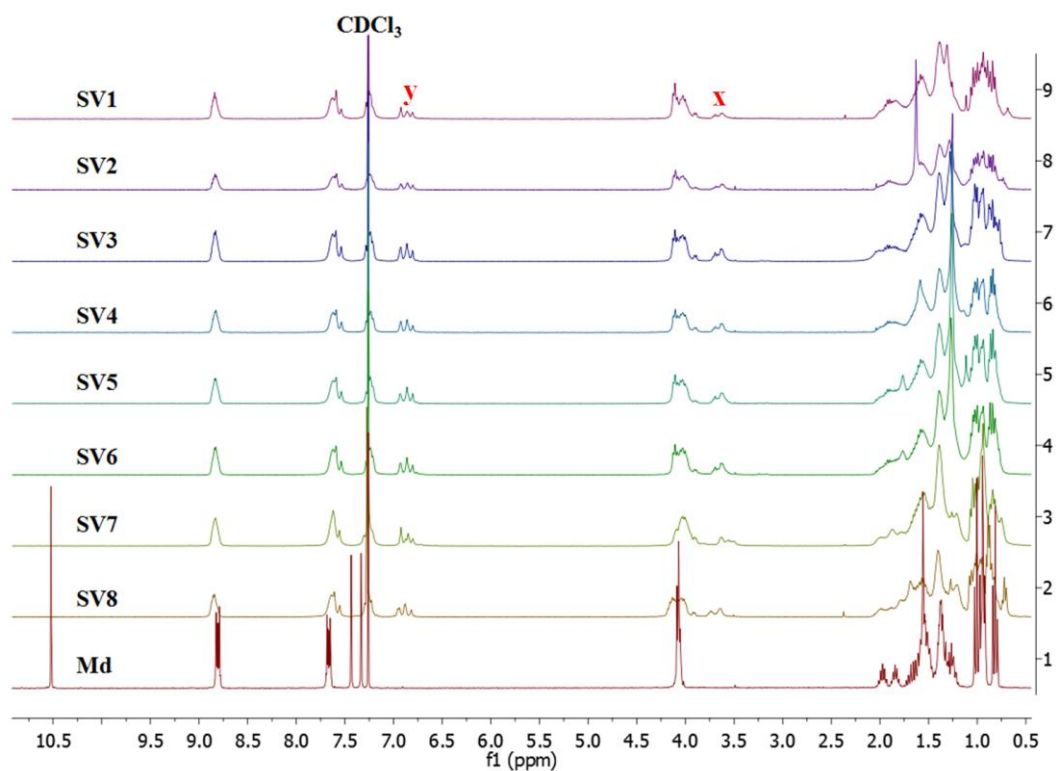
Figure 6.11: ^{1}H NMR of SV1 – SV8 with their corresponding dialdehyde Md.
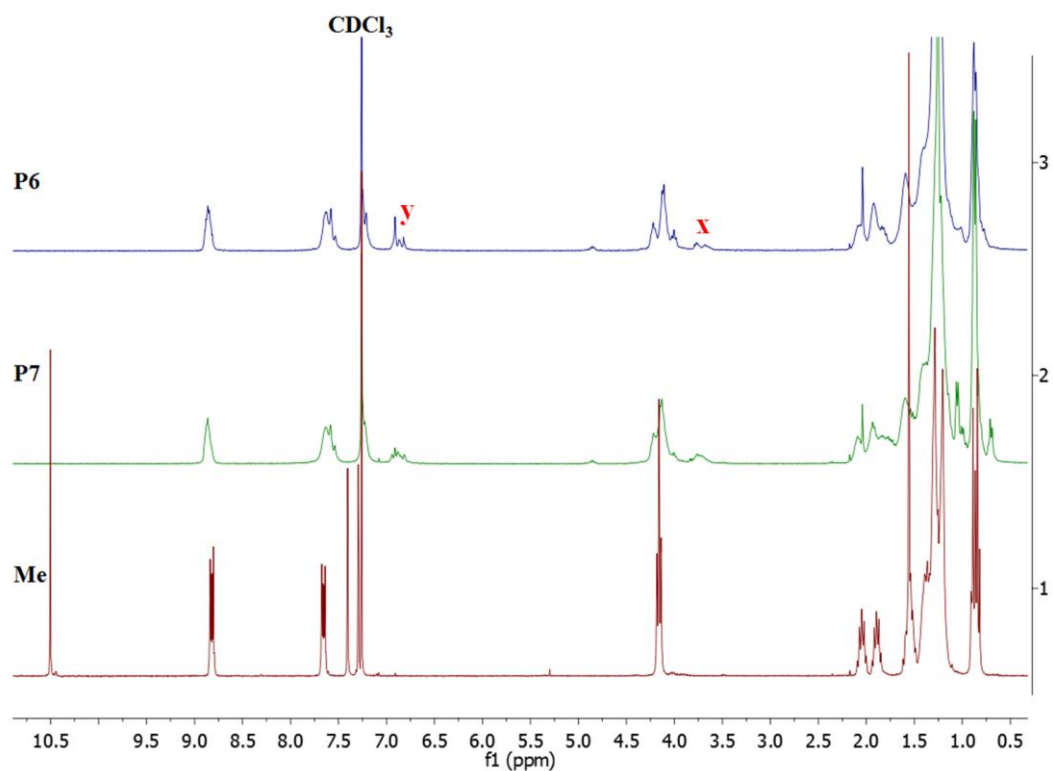
Figure 6.12: ^{1}H NMR of P6 and P7 with their corresponding dialdehyde Me.

227

6.2.1.2 Fourier Transform Infra Red (FTIR) Spectroscopy

For further investigation and verification of the polymer structure, infrared spectroscopic measurements were performed. **Figure 6.13 and 6.14** depicts the IR spectra of SV1 - SV8 and P6 - P7 respectively. The characteristic FTIR signals associated with molecule vibrations of SV1 – SV8, P6 and P7 investigated appear around 3067 - 3056, 2972-2857, 2187 - 2183, 1604 - 1603, 1509 - 1508, 1466, 1204 - 1202, 1035 - 1032, 971 - 961, and 869 - 867 cm^{-1}. The very weak band in the range of 3067 – 3056 cm^{-1} are attributed to the stretching vibrations of aromatic =C-H and of arylene and vinylene vibrations. Very strong characteristic aliphatic -C-H stretching vibrations signals emerge in the region 2972 - 2857 cm^{-1}. Weak signal situated in the range 2187 - 2183 cm^{-1} are observed for the vibrational stretching of the disubstituted ethynylene linker bond (-C≡C-). The signals around 1604 – 1603 cm^{-1} originate from vinylenic vibrations while the signals at 1509 - 1508 cm^{-1} stem from the stretching vibrations of aromatic -C=C- bonds. Strong signals at 1204 - 1202 cm^{-1} and medium signals at 1035 - 1032 cm^{-1} are ascribed to alkyloxy functionalities or aromatic-aliphatic -C=C-O-C- bonds. The band at 971 - 961 cm^{-1} and 869 - 867 cm^{-1} stem from the vinylene double bonds with *trans* (*E*) and *cis* (*Z*) configuration respectively [57-58].

228
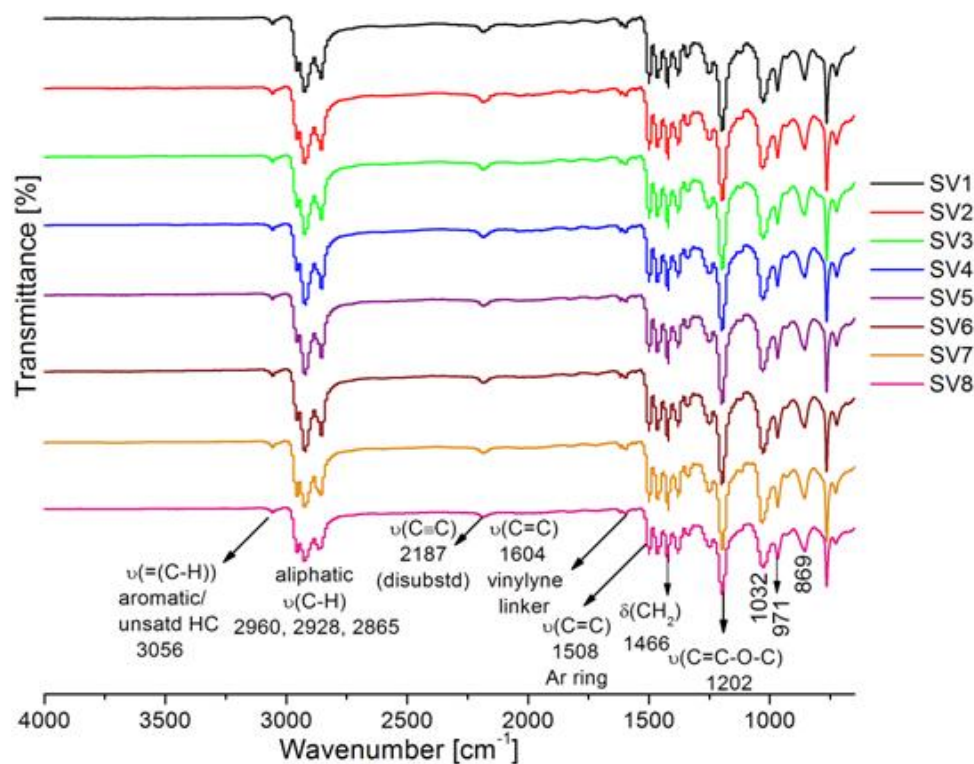
Figure 6.13: Stacked FTIR spectra of SV1 − SV8 with arrows marking the absorptions of functional group signals including olefinic -C–H out-of-plane deformation (*trans*-CH=CH at 971 cm^{-1} and *cis*-CH=CH at 869 cm^{-1}).

229
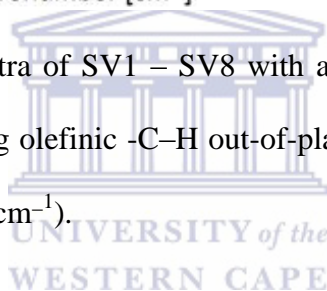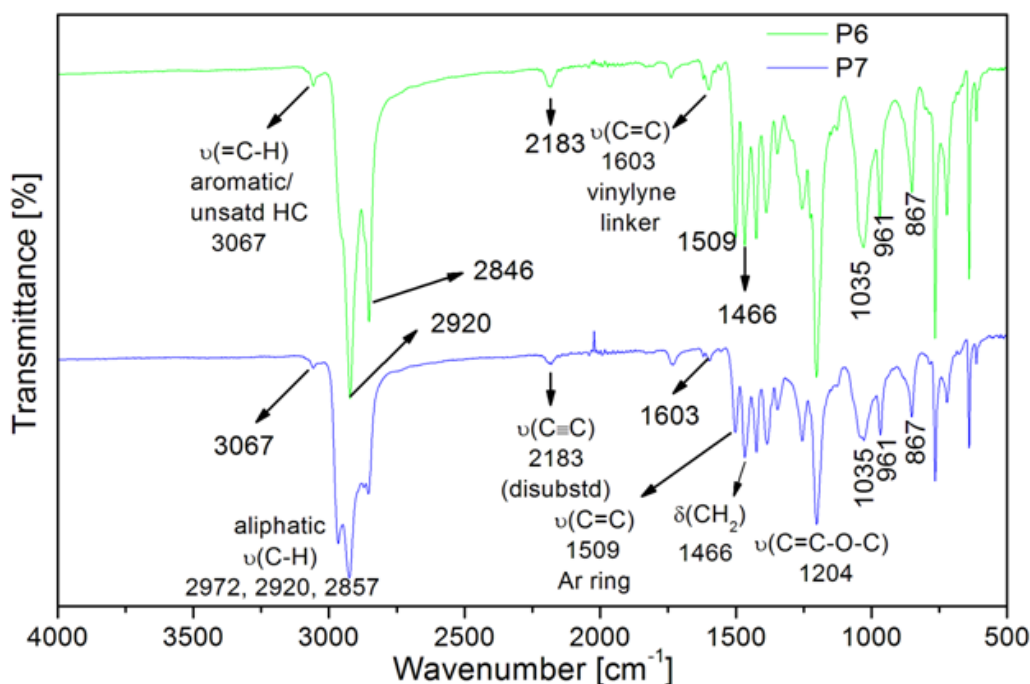
Figure 6.14: Stacked FTIR spectra of P6 and P7 with arrows marking the absorptions of functional group signals including olefinic -C–H out-of-plane deformation (*trans*-CH=CH at 961 cm^{-1} and *cis*-CH=CH at 867 cm^{-1}).
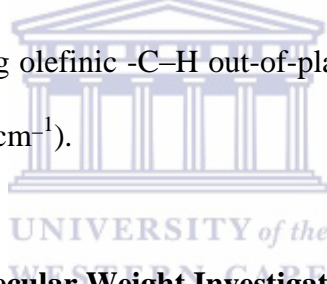
6.3   Thermal Studies and Molecular Weight Investigation

The thermal stability of the polymers was investigated by thermo-gravimetric analysis (TGA) and the results are depicted in **Figure 6.15** and **6.16**. All the polymers reveal excellent and reliable thermal stability for photovoltaic cells and other organic electronic applications with their thermal decomposition temperatures at 5% weight loss in the range 344 – 392°C. Gel permeation chromatography (GPC) analysis revealed the polymers to have polydispersity indices (PDI), M_w/M_n, between 2.2 and 4.9 except for SV8 (batch1). A reasonably low polydispersity index is required for defined properties in polymers for photovoltaic applications [9]. Data from GPC (polystyrene standards, THF as eluent), reaction times,

230

yields and thermal responses (temperatures at 5% weight loss ($T_{5\%}$), 10% weight loss, ($T_{10\%}$)) are given in **Table 6.1**.
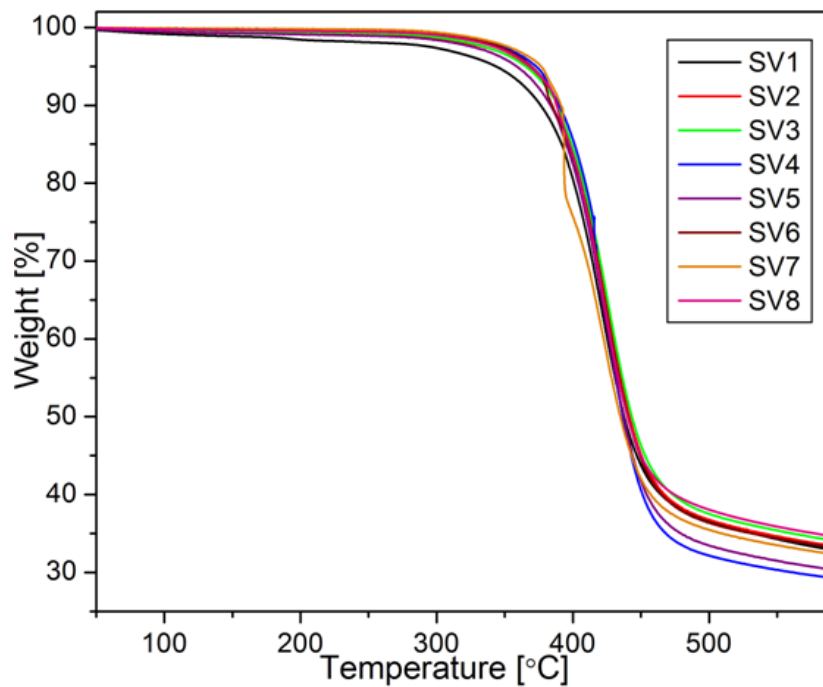
Figure 6.15: Thermo-gravimetric analysis plot of SV1 – SV8.

231
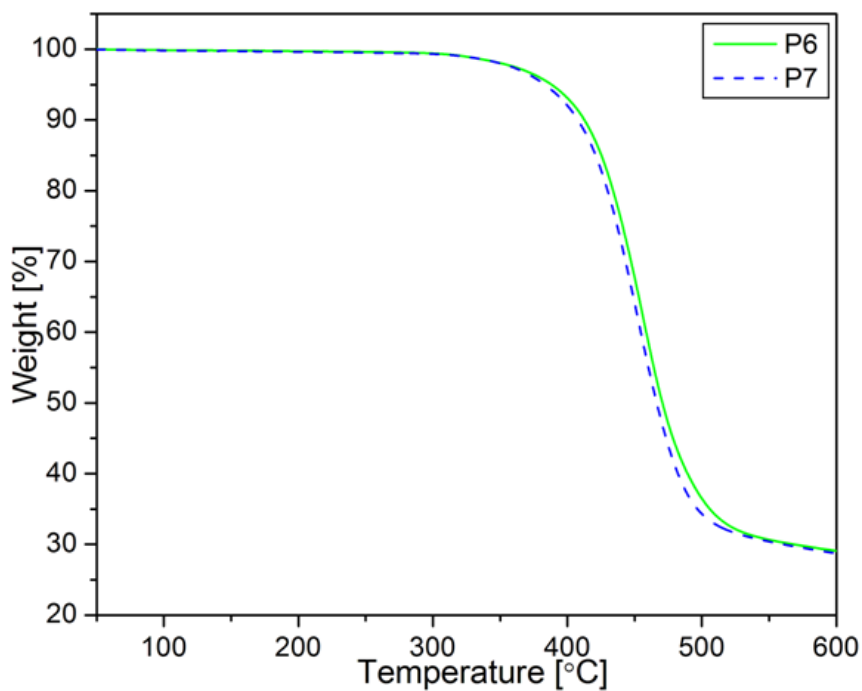
Figure 6.16: Thermo-gravimetric analysis plot of P6 and P7.

232

Table 6.1: Data from GPC (polystyrene standards, THF as eluent), reaction times, yields and thermal responses of SV1 – SV8, P6 and P7

Code	Reaction Temp.(°C)	Yield (%)	M_n (g/mol)	M_w (g/mol)	PDI	DP	T_d (°C) 5% weight loss	T_d (°C) 10% weight loss
SV1	118	56	5,280	13,030	2.5	4	344	377
SV2	118	94	6,900	27,500	4.0	5	367	389
SV3	118	90	4,220	20,480	4.9	3	367	388
SV4	118	91	10,050	26,430	2.6	7	374	391
SV5	118	93	7,930	29,850	3.8	6	358	384
SV6	118	89	9,770	21,670	2.2	7	372	384
SV7	118	80	6,720	15,870	2.4	5	375	391
SV8	118	90	11,820	26,720	2.3	9	368	388
SV3 (batch 1)	115	99	14,660	36,060	2.5	11	392	411
SV8 (batch 1)	115	67	3,500	26,170	7.5	3	367	393
P6	115	85	6,070	13,430	2.2	4	389	413
P7	115	89	11,720	28,430	2.4	8	385	410

PDI = polydispersity index, DP = degree of polymerization, $T_{5\%, 10\%}$ = decomposition temperatures at 5% and 10% weight loss, respectively. PDI = M_w/M_n, and degree of polymerization (DP) = M_n/M_{rp}. M_w = weight average molecular weight, M_n = number average molecular weight and M_{rp} = molecular weight of polymer repeat unit.

233

6.4   Photo-physical Properties

The photo-physical properties of the polymers were investigated in chlorobenzene solution as well as in thin films spin-coated from chlorobenzene solution. Results include the wavelength at the absorption maximum (λ_{abs}), the onset absorption (λ_{onset}), the optical band gap energy (E_g^{opt}) calculated using $1240/\lambda_{onset}$, the wavelength at the emission maximum (λ_{PL}) as well as the Stokes' shift both in solution and in film.

In dilute chlorobenzene solution (**Figure 6.17**), the absorption bands of all the polymers are broad and less structured with a shoulder around 520 – 524 nm and main peak in the range 542 – 547 nm corresponding to the absorption of the $\pi - \pi^*$ transition of the conjugated backbone. The polymer shoulders vary from polymer to polymer; possibly influenced by the attached side chain but with no defined trend. SV2 and SV3 show more pronounced shoulder (**Figure 6.18 (expanded region of solution spectra)**) compared to other **Group 1** polymers as described in **Figure 6.2**. The photoluminescence (PL) emission spectra in chlorobenzene solution (**Figure 6.17**) show an improved structure with sharp peaks compared to the absorption with emission maxima located around 586 nm for all the polymers and shoulder peaked around 634 – 639 nm reflecting the vibronic structure of the polymers. The absorption behavior in solution can be attributed to the flexibility of the molecules in the ground while the emission behavior can be ascribed to enhanced conjugation and the reduced flexibility in the emitting excited state. The vibronic structure can also be associated with their chain planarity. Although the PL emission is better structured compared to the absorption, there is no clear trend in the PL emission and absorption with variation in side chain. Similar absorption and emission behavior irrespective of the side chains were observed.

234
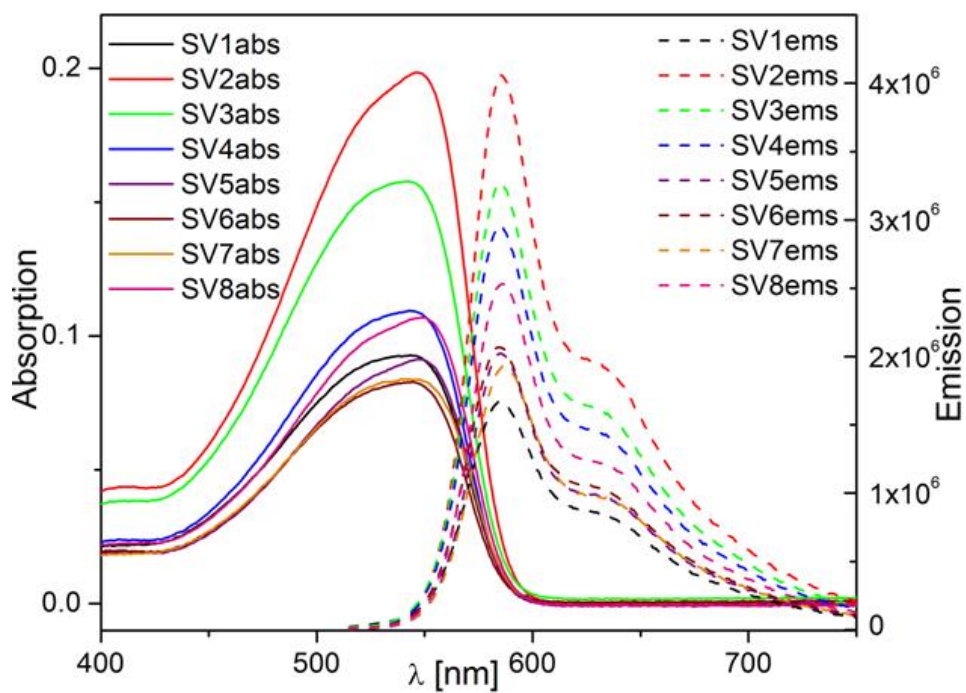
Figure 6.17: UV-Vis and photoluminescence spectra of SV1 – SV8 in solution.

Figure 6.18: Expanded region of UV-Vis spectra of SV1 – SV8 in solution.

235
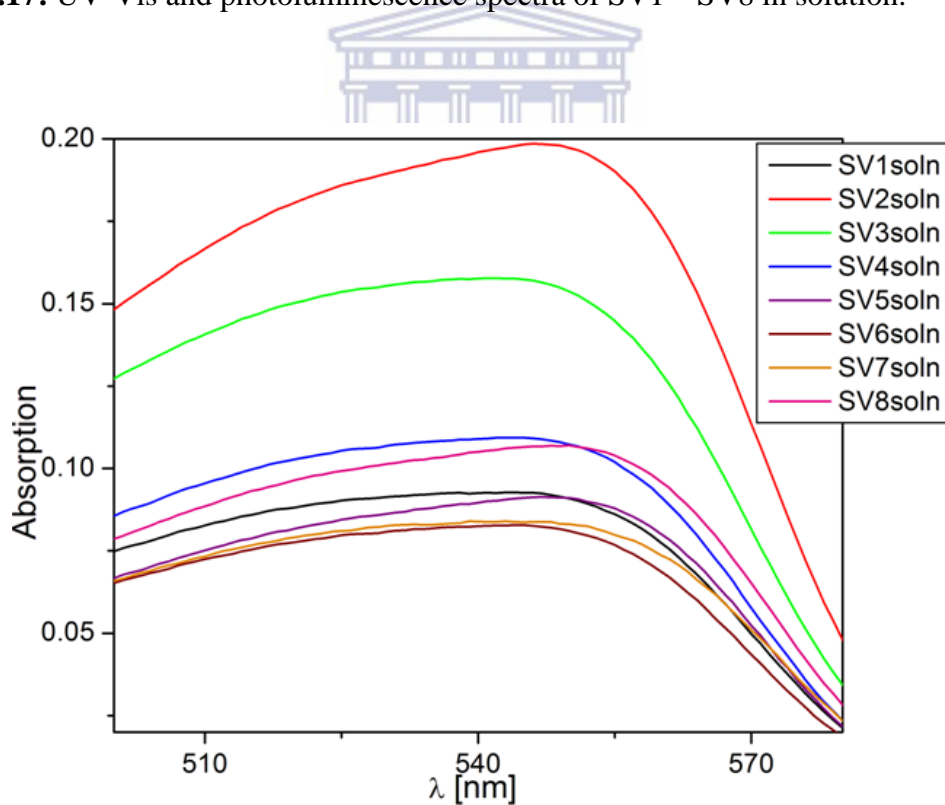
Transparent thin films of the polymers were doctor bladed from a chlorobenzene solution. Compared with the spectra of the solutions, the absorption spectra of the thin films are slightly broader possessing vibronic peaks toward longer wavelengths (**Figure 6.19**). This can be attributed to intermolecular interaction and enhanced planarization of the conjugated backbone in the ground state in thin film. The optical band gap of the polymers was evaluated from both solution and thin-film absorption edge. The band gap in solution for SV1 − SV8 was 2.1 eV while this value reduced to 1.9 eV for SV2, SV4 and SV8; and 2.0 eV for others in thin film. Contrary to the less-structured form of the solution absorption of the polymers, the solid state absorption in the form of thin film are well structured with two well resolved peaks of varying degree except for SV3 and SV7 which have second peaks that are not well resolved.
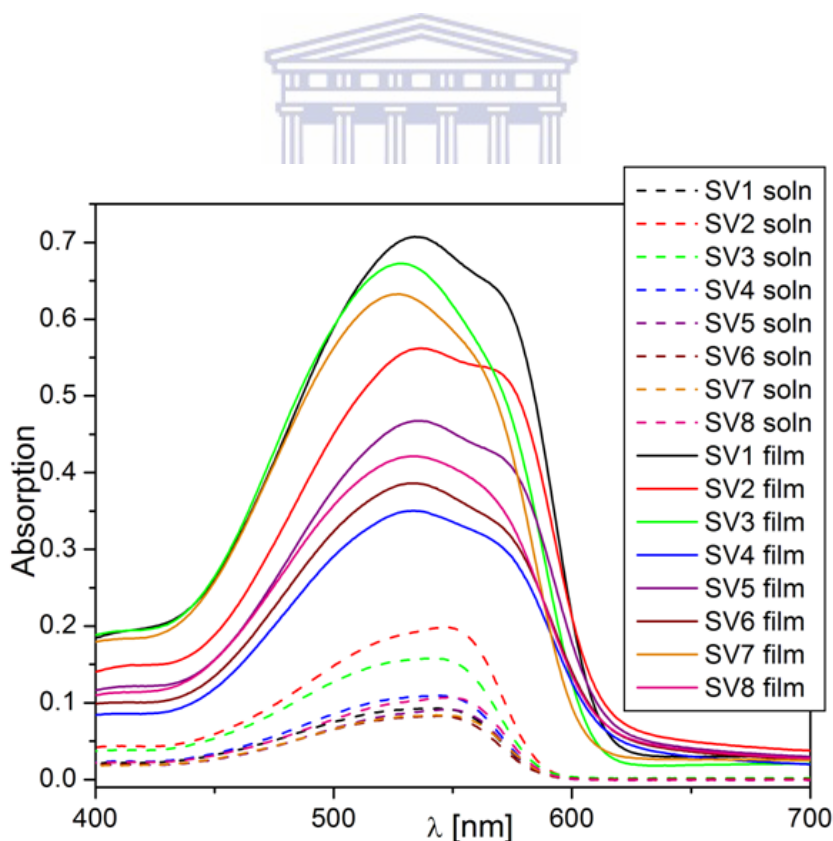
Figure 6.19: UV-Vis spectra of SV1 − SV8 in solution and film.

236

Figure 6.20 shows the thin film absorption and emission spectra of polymers SV1 – SV8. Two absorption peaks located around 527 – 537 nm and 559 – 571 nm respectively are observed. In principle, the absorption at higher wavelength can be attributed to *J*-aggregate and the absorption at lower wavelength ascribed to *H*-aggregate. The amount of both aggregate varies from polymer to polymer as the degree of resolution of the second peak varies from polymer to polymer but with no straightforward dependence on the attached side chain. **Figure 6.21** shows the expanded absorption spectra of measurement in film which reveals clearly the varying degree of resolution or intensity of the second absorption peak of all **Group 1** polymers with SV3, SV7 and SV8 having the least resolution and hypsochromically shifted compared to SV1, SV2 and SV5 with the best degrees of resolution. This observation can be related to a number of possibilities like the influence of side chain on the intermolecular interactions on the conjugated backbone, molecular weight, the ratio of *cis-trans* configuration present in the polymer, slight variation in reaction temperature or film thickness. To completely probe into this behaviour, an X-ray investigation and thickness study of all polymers will be worthwhile.

237
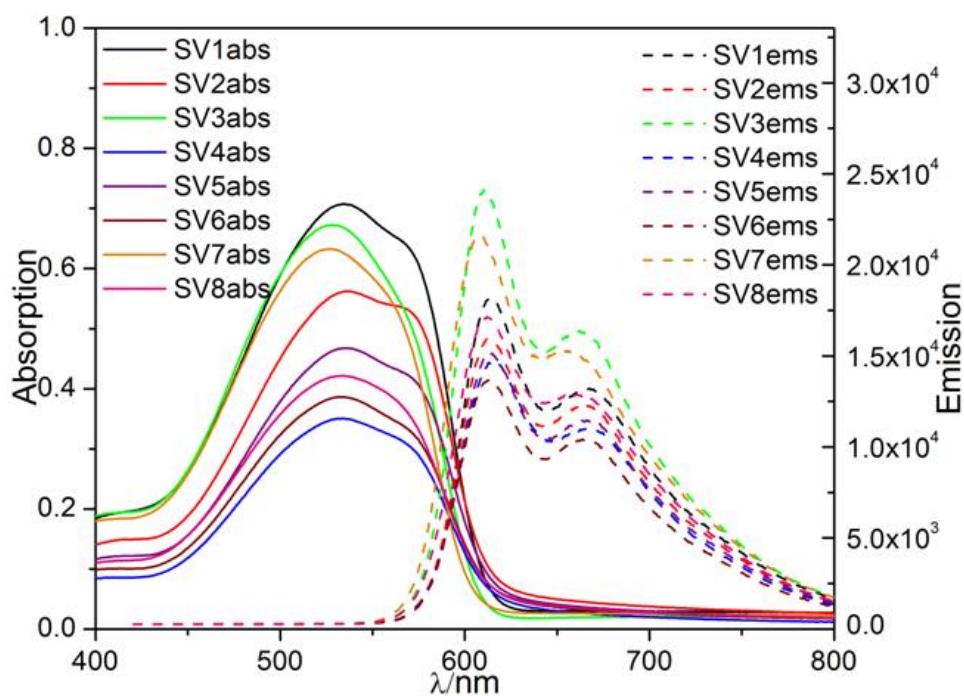
Figure 6.20: UV-Vis and photoluminescence spectra of SV1 – SV8 in film.
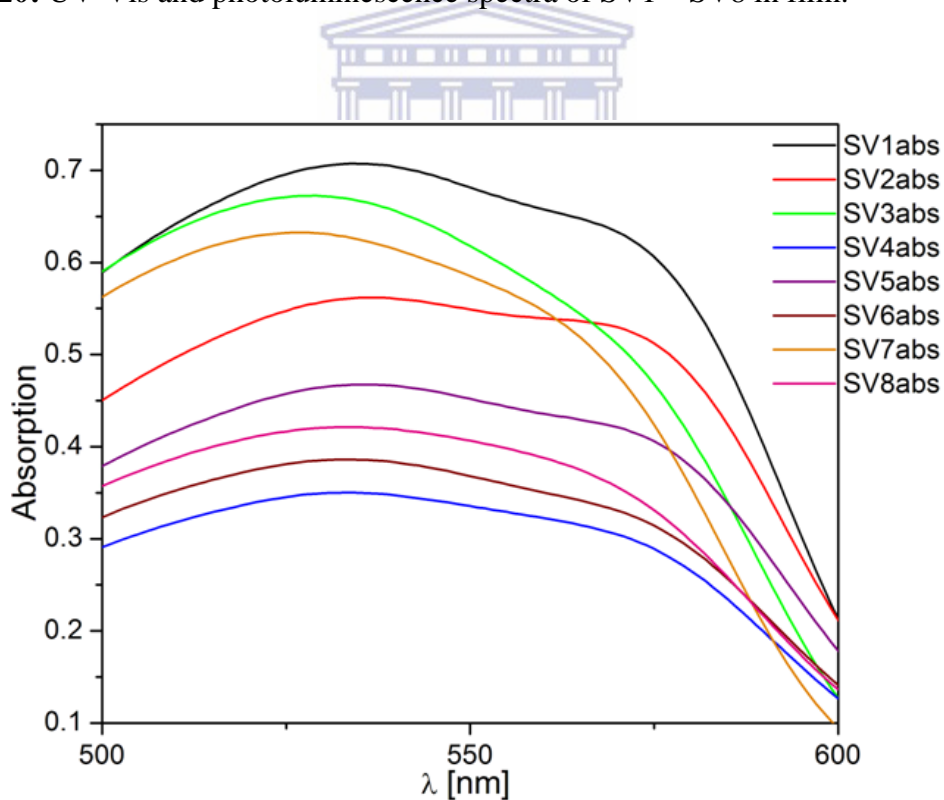
Figure 6.21: Expanded region of UV-Vis spectra of SV1 – SV8 in film.

238

Well structured emission spectra consisting of two sharp peaks in the range of 608 - 615nm (first peak) and 653 - 667 nm (second peak) were observed in thin films. The PL emission spectra are similar in shape compared to that in solution but with a bathochromic shift and enhancement in the shoulder observed in solution. In film, the shoulder observed around 586 nm became more intense and transformed to a peak at around 653 – 667 nm. All the polymers show two well resolved and intense emission peaks compared to their solution emission as a result of enhanced planarization in the singlet excited state, S_1 [59]. This also explains the red shift of the absorption spectra in thin films relative to the solutions. The most pronounced or intense emission spectra are observed for SV3 and SV7 (**Figure 6.20 and Figure 6.22 (expanded region**)). All other polymers exhibit a hypsochromic (blue-shift) emission compared to SV3 and SV7. An orange color emission was detected from the polymer films, and the solutions exhibited a lighter orange color emission. The photo-physical data of the polymers in dilute chlorobenzene solution and in thin film doctor bladed from chlorobenzene are summarized in **Table 6.2**. Emission spectra were recorded at 500 nm excitation wavelength in solution while spectra in film were recorded at 550 nm for polymers SV1 – SV8.

239
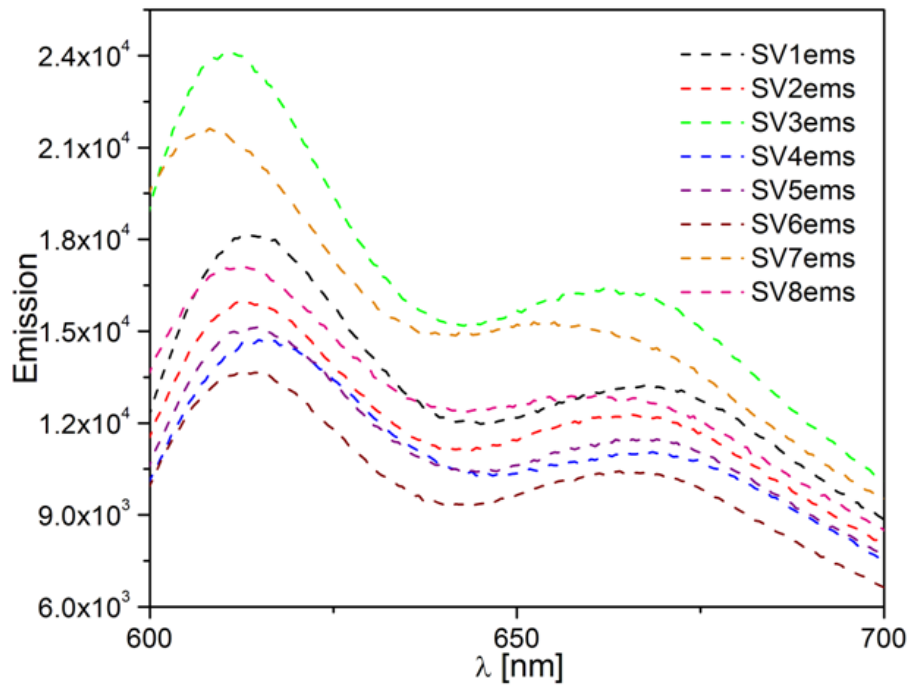
Figure 6.22: Expanded region of photoluminescence spectra of SV1 – SV8 in film.

240

Table 6.2: Photo-physical data of the polymers in dilute chlorobenzene solution and in thin film casted from chlorobenzene

	Solution					Film				
Code	λ_{abs} (nm)	λ_{PL} (nm)	λ_{onset} (nm)	E_g^{opt} (eV)	Stokes Shift (nm)	λ_{abs} (nm)	λ_{PL} (nm)	λ_{onset} (nm)	E_g^{opt} (eV)	Stokes Shift (nm)
SV1	*524, 542	586, *635	598	2.1	44	535, 569	613, 667	628	2.0	44
SV2	*521, 547	586, *635	600	2.1	39	537, 568	613, 665	642	1.9	45
SV3	*520, 543	585, *634	598	2.1	42	529, 565	611, 662	623	2.0	46
SV4	*521, 543	585, *634	598	2.1	42	533, 566	615, 667	643	1.9	49
SV5	*524, 548	586, *635	600	2.1	38	537, 571	613, 667	634	2.0	42
SV6	*520, 545	585, *634	597	2.1	40	534, 568	613, 665	634	2.0	45
SV7	*520, 543	586, *635	598	2.1	43	527, 559	608, 653	621	2.0	49
SV8	*523, 548	586, *639	600	2.1	38	534, 561	611, 660	621	2.0	50
P6	*494, 540, *600	588, *639	644	1.9	48	*506, 545, 582	619, 665	648	1.9	37
P7	526, 555	589, *640	621	2.0	34	548, 581	624, 671	637	1.9	43

*Shoulder, $E_g^{opt} = \dfrac{1240}{\lambda_{onset}}$

241

6.5   Photovoltaic Investigation

Photovoltaic devices based on glass/ITO/PEDOT:PSS/polymer:PCBM/LiF/Al with polymer:PCBM weight ratio 1:2 were prepared and investigated for polymers SV1 – SV8 and the observed energy conversion efficiencies ranged from η = 1.2% to 2.3%. The current-voltage (*I-V*) measurements are depicted in **Figure 6.23** and **Table 6.3** summarizes the photovoltaic parameters obtained from the current-voltage (*I-V*) measurements for all polymer:PCBM blends. In general, the devices can be grouped into two classes of mixed linear and branched side chain polymers (SV1 - SV6, class 1) and solely branched side chain polymers (SV7 - SV8, class 2). For the first class, the efficiency rose from 1.8 – 2.3% (SV1 – SV3) and then began to drop to 1.6 (SV4), and finally down to 1.2 (SV6). The lowest energy conversion efficiencies were obtained for SV6. This can be attributed to the effect of side chain volume ratio. As linear side chain length increases, the concentration of the absorbing conjugated species per volume unit is diluted thereby leading to reduction in the amount of photons absorbed, increased phase separation, increase in resistance against charge transfer between donor and acceptor and subsequently poor photovoltaic performance [60]. On the other hand, SV7 and SV8 with branched side chain all over the polymer backbone followed a different trend with almost similar efficiency (SV8, 1.9%; SV7, 1.8%).

242
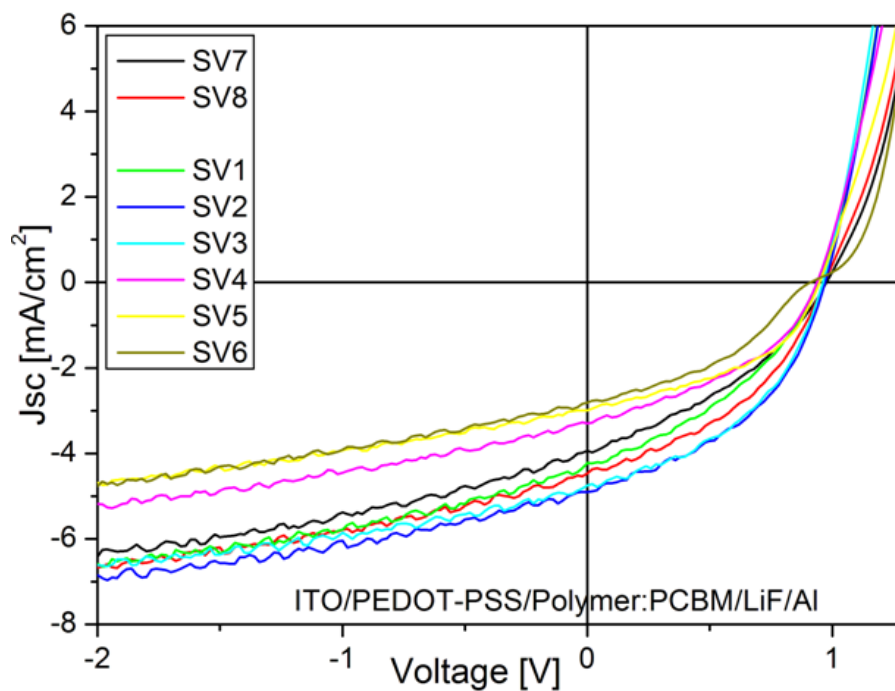
Figure 6.23: The current-voltage (*I–V*) characteristics of polymer (SV1 – SV8):PCBM (1:2) blend devices on PEDOT:PSS configuration under 100 mW/cm^2.

243
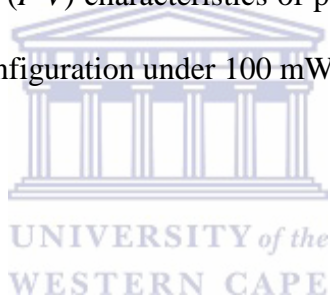
Table 6.3: Photovoltaic parameters obtained from current-voltage (*I-V*) measurements for all polymer:PCBM (1:2) blends

Code	Weight of Polymer (mg)	Weight of PCBM (mg)	Chlorobenzene (μL)	Bulk Thickness (nm)	Optical Density of Bulk	J_{sc} [mA/cm^2]	V_{oc} [V]	*FF*	Eff %	@ -0.1 V [mA/cm^2]	@ +1 V [mA/cm^2]
SV1	10.2	20.4	850	155	0.36	4.55	0.97	0.41	1.8	-4.73	0.69
SV2	13.0	26.1	1,084	154	0.38	4.90	0.97	0.45	2.1	-5.03	0.83
SV3	10.4	21.0	867	166	0.37	5.06	0.96	0.47	2.3	-5.08	1.1
SV4	12.9	25.8	1,074	162	0.40	3.81	0.95	0.43	1.6	-3.94	1.39
SV5	10.5	21.1	875	162	0.40	3.17	0.95	0.47	1.4	-3.27	1.07
SV6	10.0	20.0	833	157	0.38	2.90	0.95	0.42	1.2	-2.99	0.23
SV7	10.4	20.9	867	164	0.36	4.15	0.99	0.38	1.6	-4.27	0.21
SV8	11.9	21.7	992	145	0.37	4.51	0.97	0.44	1.9	-4.61	0.55

244

Nevertheless, the devices of polymers SV1 – SV8 show similar morphology under the microscope (**Figure 6.24**) and no significant impact on the V_{oc} with increase in chain length as all polymers reveal a V_{oc} value above 0.9 V. It has been shown with poly(*p*-phenylene ethynylene)-*alt*-poly(*p*-phenylene vinylene)s (PPE-PPV) based polymers that the open circuit voltage, V_{oc}, increases with decreasing side chain density [23]. In the report, polymers bearing longer dodecyloxy or decyloxy side groups lead to low V_{oc} values around 0.65 V. Polymers decorated with octyloxy and/or 2-ethylhexyloxy-groups, yielded V_{oc} values of approximately 0.80 V; whereas polymers having the lowest side chain density due to grafting of methyloxy groups demonstrated the highest V_{oc} (~ 0.90 V) [60]. In this report however, regardless of the side chain, the V_{oc} of the investigated polymer was almost 1 V. This suggests that the V_{oc} is influenced by the backbone and not the side chains. All devices measured showed relatively low fill factor (*FF*). This can be attributed to poor film morphology and unbalanced charge transport between donor and acceptor.

UNIVERSITY *of the*

WESTERN CAPE

245
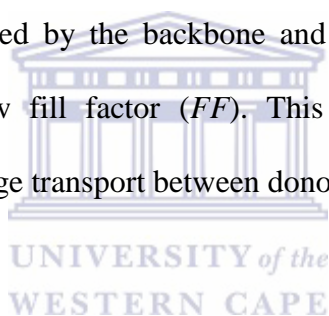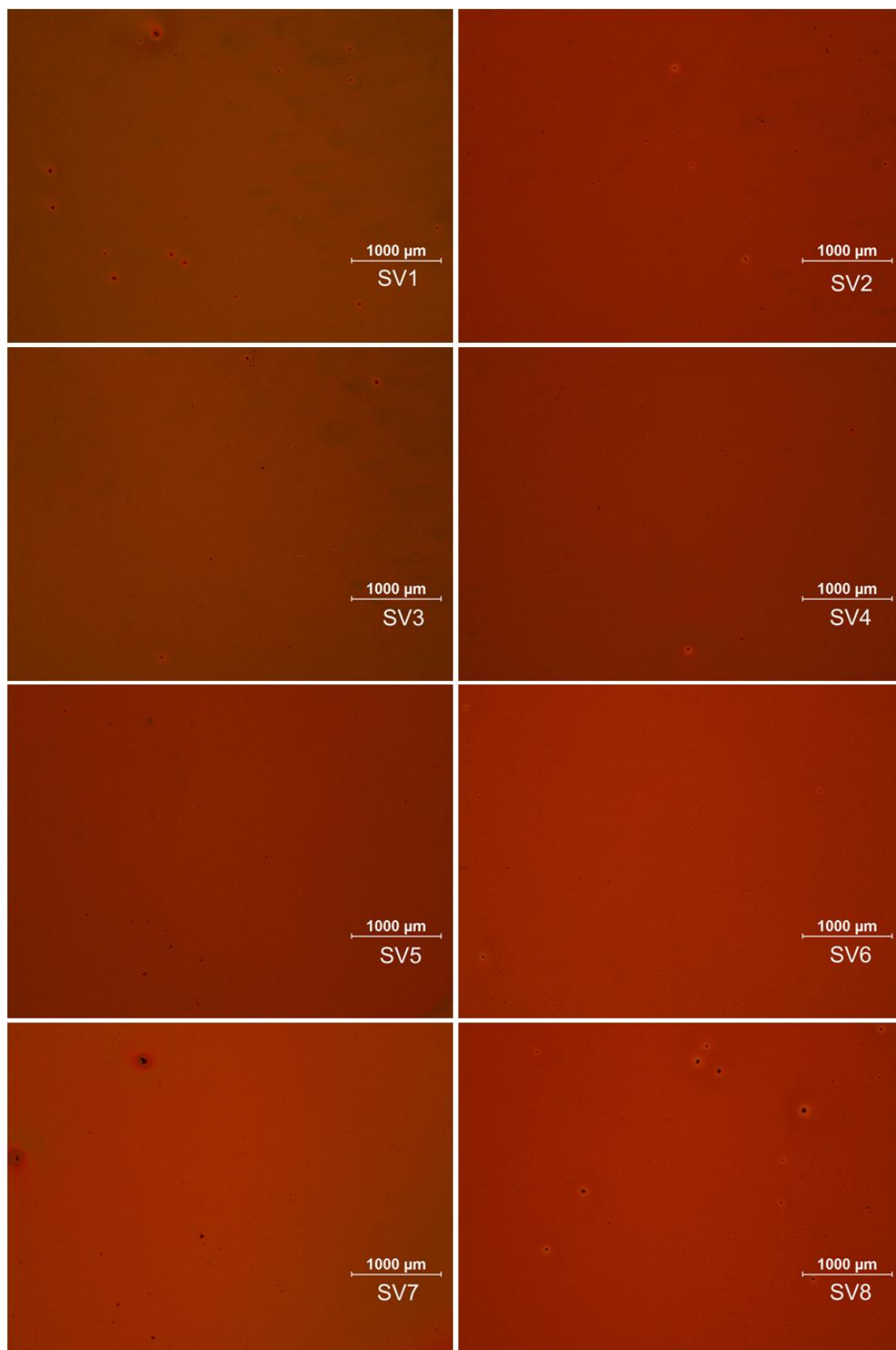
Figure 6.24: Optical microscopy images of polymer (SV1 – SV8):PCBM (1:2) blend devices on PEDOT:PSS configuration.

Table 6.4 shows a comparison of the photo-physical and photovoltaic response of SV1 and SV7 with previous report of same polymers reported as AnE-PV*ba* and AnE-PV*bb* respectively [60]. The previous report shows similar optical band gap with SV1 and SV7 respectively but with higher molecular weights. However, SV1 and SV7 gave better photovoltaic response than those reported for AnE-PV*ba* and AnE-PV*bb*. Improvement in photovoltaic response may be ascribed to the differences in molecular weights as well as in the experimental conditions and processes.

247

Table 6.4: Comparison of the optical, electrochemical and photovoltaic response of SV1 and SV7 with previous report of same polymers reported as AnE-PV*ba* and AnE-PV*bb* respectively

Code	Yield (%)	M_n (g/mol)	M_w (g/mol)	PDI	DP	λ_{abs} (nm)	λ_{PL} (nm)	E_g^{opt} (eV)	J_{sc} [mA/cm^2]	V_{oc} [V]	*FF*	Eff %	Ref
SV1	56	5,280	13,030	2.5	4	535, 569	613, 667	2.1	4.55	0.97	0.41	1.8	This work
SV7	80	6,900	27,500	4.0	5	527, 559	608, 653	2.0	4.15	0.99	0.38	1.6	This work
AnE-PV*ba* (SV1)	53	25,500	77,800	3.05	20	504	605	1.95	3.44	0.93	0.35	1.11	[60]
AnE-PV*bb* (SV7)	94	15,800	47,200	2.98	13	527	600	2.02	4.22	0.83	0.35	1.22	[60]

The equivalent quantum efficiencies (EQE) of SV1 – SV8 (**Figure 6.25**) reveal a good correlation with the short circuit current as shown in **Table 6.3**. The EQE intensity increased with increasing short circuit current of the polymers. SV3 with the highest short circuit current (5.06 mA/cm^2) has the highest quantum efficiency of almost 35% while SV6 with the lowest current of 2.90 mA/cm^2 has the lowest quantum efficiency of less than 20%.
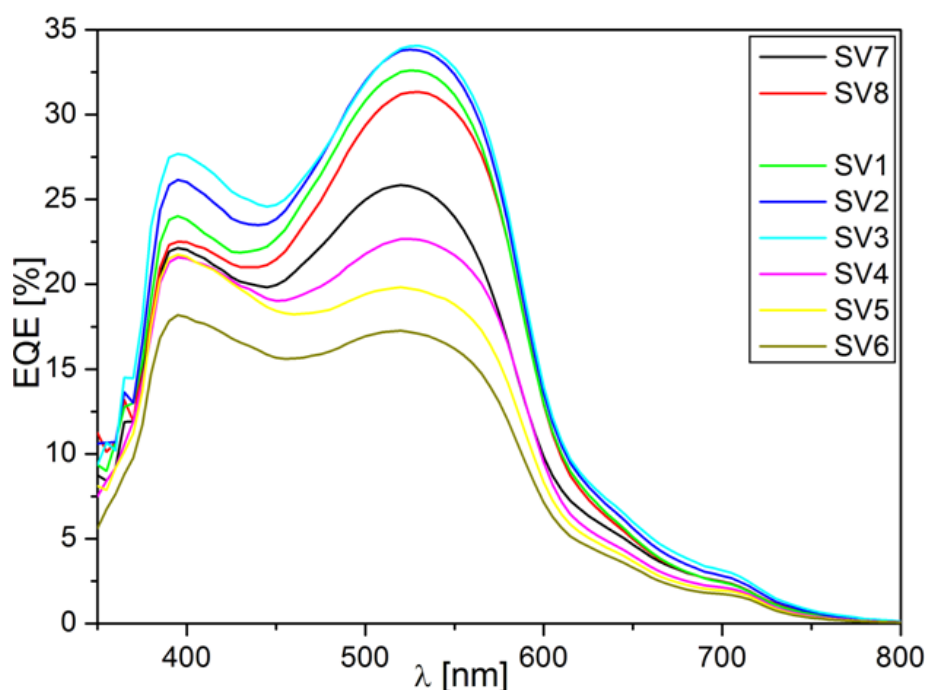
Figure 6.25: Equivalent quantum efficiencies of (SV1 – SV8):PCBM (1:2) blend devices on PEDOT:PSS configuration.

The device performance of the polymers SV1 – SV8 were evaluated and analyzed in more detail with **Figure 6.26 – 6.28** comparing the V_{oc}, the J_{sc} and the efficiency of the different polymers. All polymers show a high open circuit voltage over 0.9 V.
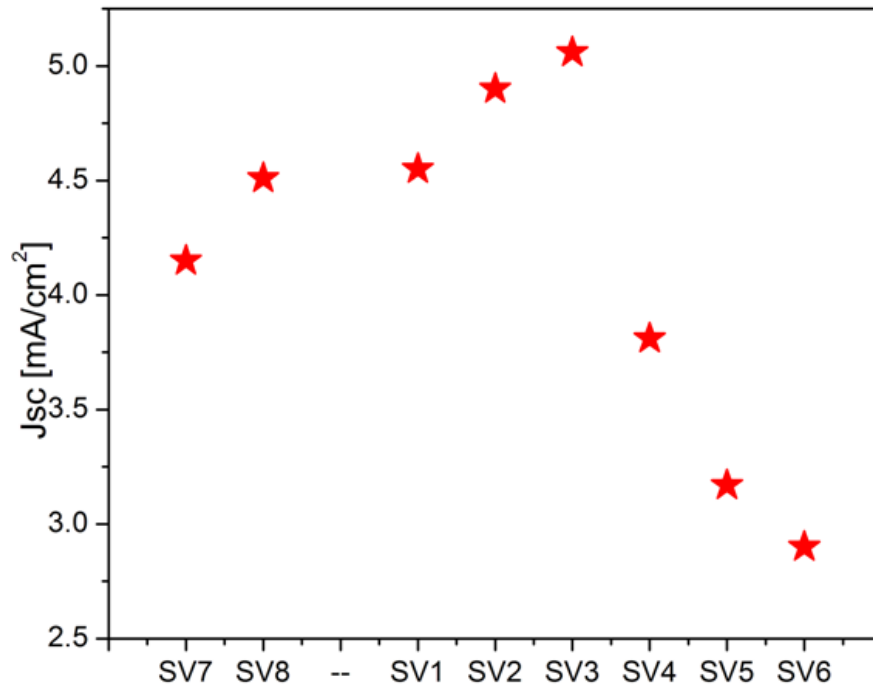
Figure 6.26: Comparative plot of short circuit current (J_{sc}) against polymers (SV1 – SV8): PCBM blend devices on PEDOT:PSS configuration.
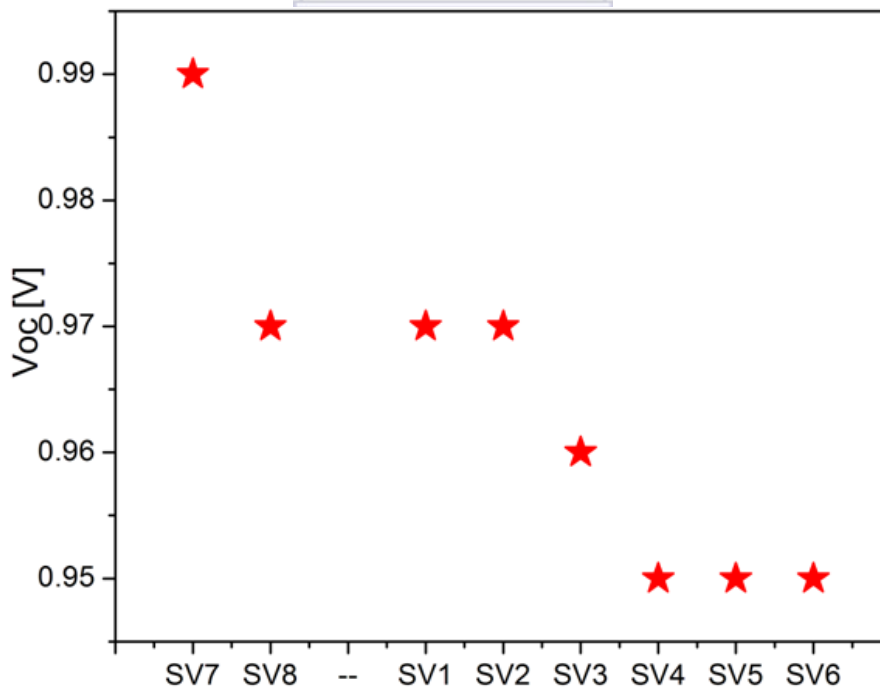
Figure 6.27: Comparative plot of open circuit voltage (V_{oc}) against polymers (SV1 – SV8): PCBM blend devices on PEDOT:PSS configuration.

250
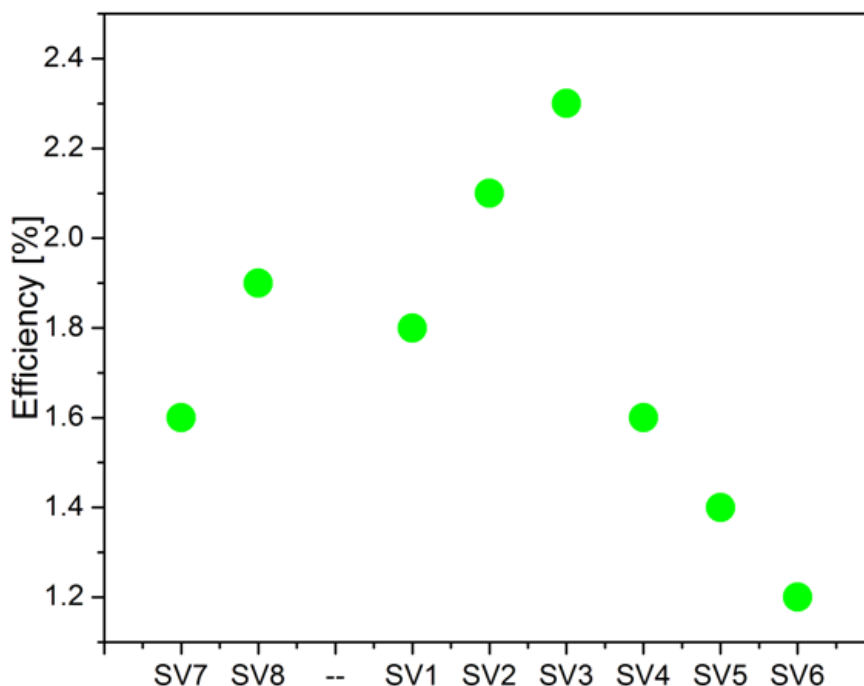
Figure 6.28: Comparative plot of obtained efficiency against polymers (SV1 – SV8): PCBM blend devices on PEDOT:PSS configuration.

6.6   Comparative Studies of SV3, SV8, P6 and P7

Polymer SV3 and SV8 reported in this section are polymers with same structure as SV3 and SV8 polymers described in previous section but were synthesized in a separate batch with reaction conditions as those of **P6** and **P7**. They are regarded in this study as **SV3 (batch 1)** and **SV8 (batch 1).**

6.6.1   Photo-physics

Figure 6.29 depicts the absorption and emission spectra of **SV3 (batch 1)**, **SV8 (batch 1)**, **P6** and **P7** in dilute chlorobenzene solution. In solution, polymers bearing solely linear decyloxy side chains (**P6**), branched 3,7-dimethyloctyloxy side chains with linear decyloxy side chains

251

(**P7**) and those incorporating 2-ethylhexyloxy side chains with linear decyloxy side chains **SV3 (batch 1)** and 3,7-dimethyloctyloxy side chains **SV8 (batch 1)** show distinct behavior. The absorption spectra of **P6** exhibit shoulders around 494 and 600 nm. The shoulder at 600 nm is ascribed to the formation of aggregates already in dilute medium and similar to the behavior of AnE-PV*ad* (solely linear octyloxy and decyloxy side chain polymer) in previous report [60]. The aggregate formation in AnE-PV*ad* was further confirmed by recording temperature dependent measurement in toluene and the shoulder gradually disappeared upon temperature increase from 20 - 80°C [60]. For polymer **P7** which has a similar backbone and side chain with **P6** except for the replacement of two of the six decyloxy side chains by 3,7-dimethyloctyloxy, this shoulders were completely absent resulting in a hypsochromic shift of **P7** relative to **P6**. The absorption spectrum of **P7** is quite similar to those of **SV3 (batch 1)** and **SV8 (batch 1)** except for a slight bathochromic shift of **P7**. Polymer **P7** and **SV8 (batch 1)** shows structured solution absorption with two peaks. **P6** on the other hand exhibit a structure- less behaviour with a peak and two shoulders. The onset absorption of **SV3 (batch 1)** and **SV8 (batch 1)** (603 nm) bearing bulky 2-ethylhexyloxy side chains close to the anthracene unit is hypsochromically shifted relative to **P6** (644 nm) and **P7** (621 nm) bearing linear decyloxy side chains in same region. This hypsochromic shift is attributed to the high sensitivity of the anthracene moiety to steric hindrances in its neighborhood [60-63].

252
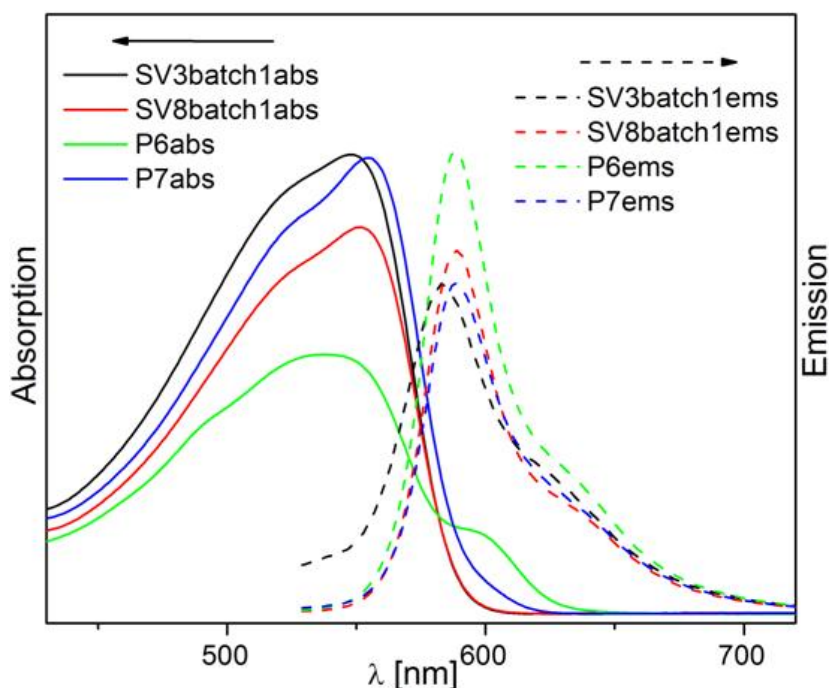
Figure 6.29: UV-Vis and photoluminescence spectra of SV3 (batch1), SV8 (batch1), P6 and P7 in solution.

In spite of the differences in the absorptive behaviour of the polymers in solution which resulted in band gap between 1.9 and 2.1 eV, the main emission peaks for all polymers in solution reveal no significant differences as shown in **Figure 6.29** (**SV3 (batch 1)**, 583 nm; **SV8 (batch 1)**, 588 nm; **P6**, 588 nm; and **P7**, 589 nm).

In thin film however, the absorption of **P6** and **P7** are quite similar with well defined peaks (**Figure 6.30**). Well resolved absorption spectra consisting of two peaks around 619, 665 nm and 624, 671 nm were recorded for **P6** and **P7** respectively. The emergence of these well resolved peaks especially for **P6** which was almost amorphous in solution is evidence of improved ordering or semi-crystallinic nature in thin film [60]. This accounts for the bathochromic shift in absorption spectra both in solution and film of **P6** and **P7** polymers relative to that of **SV3 (batch1)** and **SV8 (batch 1)**. The polymer **P6** show the same optical

253

band gap (1.9 eV) both in solution and film; **P7** show a band gap of 2.0 eV in solution and 1.9 eV in film while 2.03 eV in solution and 2.0 eV in thin film was obtained for **SV3 (batch 1)** and **SV8 (batch 1)**. The lower band gaps values obtained for thin film absorptions as compared to the solution absorptions is due to enhanced planarization and intermolecular interactions in the films. The thin film emission of all four polymers shows similar shape comparable to their emission in solution. However, the thin film emission spectra of **SV3 (batch 1)** and **SV8 (batch 1)** show a slight shift to shorter wavelength compared to **P6** and **P7**.
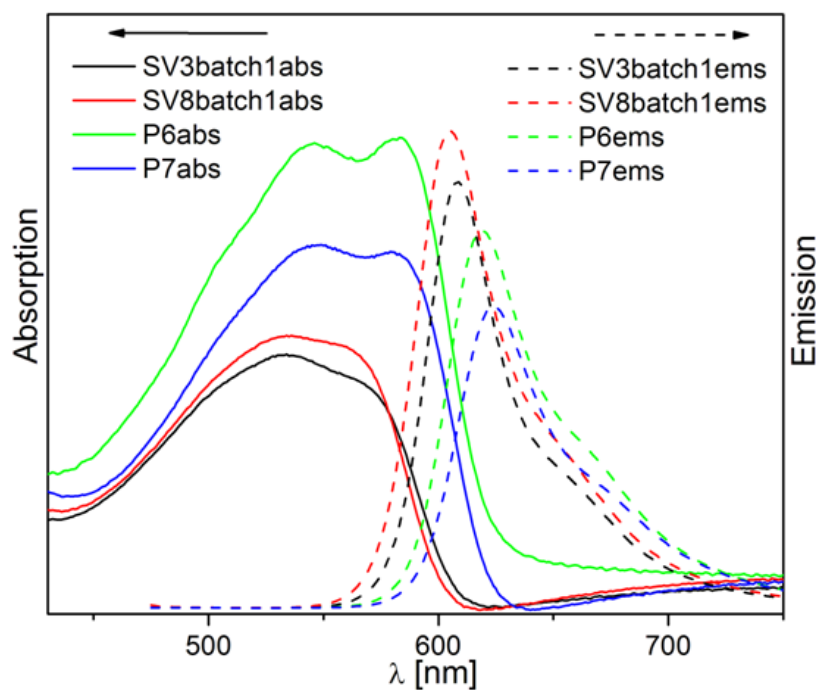
Figure 6.30: UV-Vis and photoluminescence spectra of SV3 (batch1), SV8 (batch1), P6 and P7 in film.

6.6.2 Electrochemical Studies of SV3, SV8, P6 and P7 (SV3 and SV8 data were recorded from batch 1)

The electrochemical behavior of the polymers **SV3**, **SV8**, **P6** and **P7** were investigated by cyclic voltammetry (CV) and **Figure 6.31 – 6.34** shows their electrochemical responses. Measurements were performed on thin polymer films spin-coated from chlorobenzene solutions at a scan rate of 50 mV/s. All polymers exhibited quasi reversibility in their reductive scan and exhibited an electrochromic change of color upon reduction and oxidation. **SV3** and **SV8** are anodically shifted in the oxidative voltammetric response, covers a wider potential window and with more re-oxidative peaks relative to **P6** and **P7** (**Figure 6.31**).
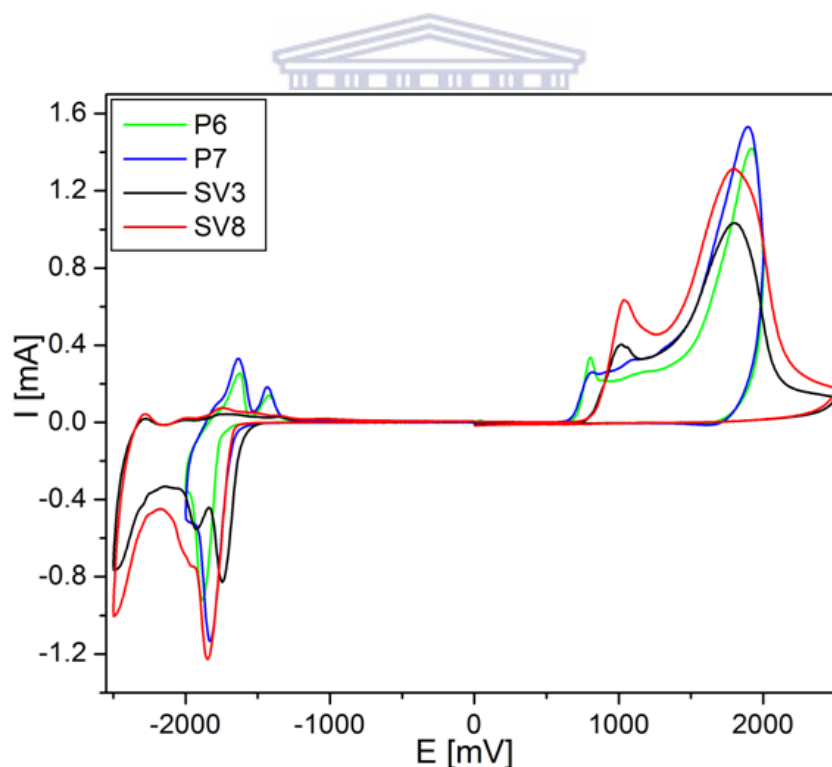
Figure 6.31: Cyclic voltammetric responses of polymer SV3, SV8, P6 and P7 films coated on ITO in TBAPF$_6$/acetonitrile supporting electrolyte/solvent system at 50 mV/s. SV3 and SV8 data were recorded from batch 1.

255

The shift in the reductive scan did not follow a particular order as **SV3** is more anodically shifted followed by **P7**, **SV8** and then **P6**. **SV3** and **SV8** (**Figure 6.32**) have similar oxidative peak at 1805 mV, reductive peak at -2500 mV and similar re-oxidative peaks at -2278 and -1051 mV (vs. Ag/AgCl). For the dissimilar peaks, the **SV3** oxidative peak at 1014 mV is cathodically shifted by 27 mV relative to the oxidative peak of **SV8** at 1041 mV while the reductive peaks at -1748 and -1929 mV are anodically shifted compared to -1850 and -1976 mV reductive peaks of **SV8**. There are five re-oxidative peaks (-2278 mV, -1994, -1723, -1363 and -1051 mV (vs. Ag/AgCl)) of **SV3** and six (-2278, -1984, -1747, -1491, -1358 and -1051 mV (vs. Ag/AgCl)) for **SV8** (**Figure 6.33 (expanded region)**). The re-oxidative peak of **SV3** at -1994 mV is cathodically shifted relative to its counterpart -1984 mV of **SV8** while all other re-oxidative peaks apart from the similar ones are anodically shifted. The major difference in these two polymers is obviously observed in the re-oxidative peak where **SV3** has five peaks and **SV8** has six peaks.
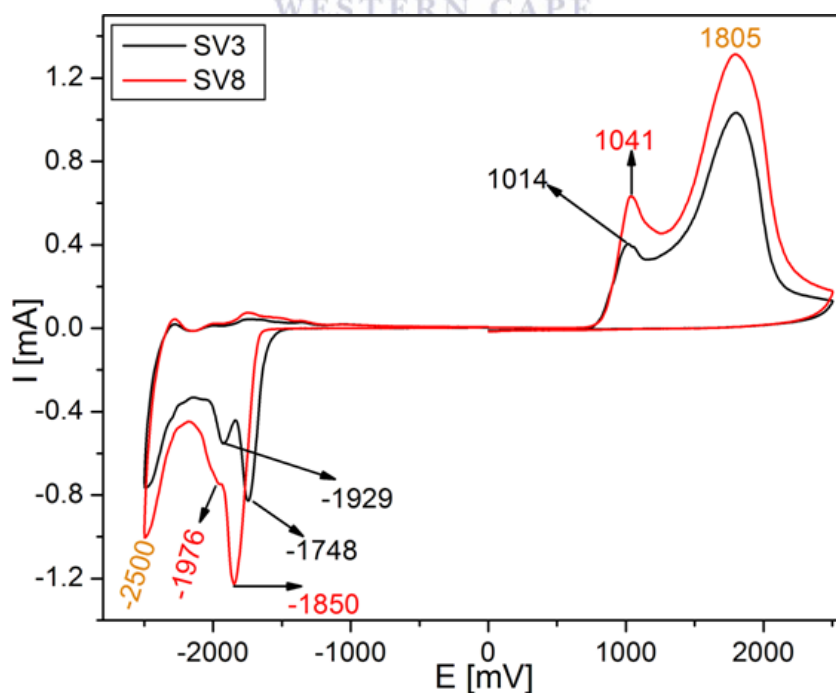
Figure 6.32: Cyclic voltammetric responses of polymer SV3 and SV8 films with peak labels.

256
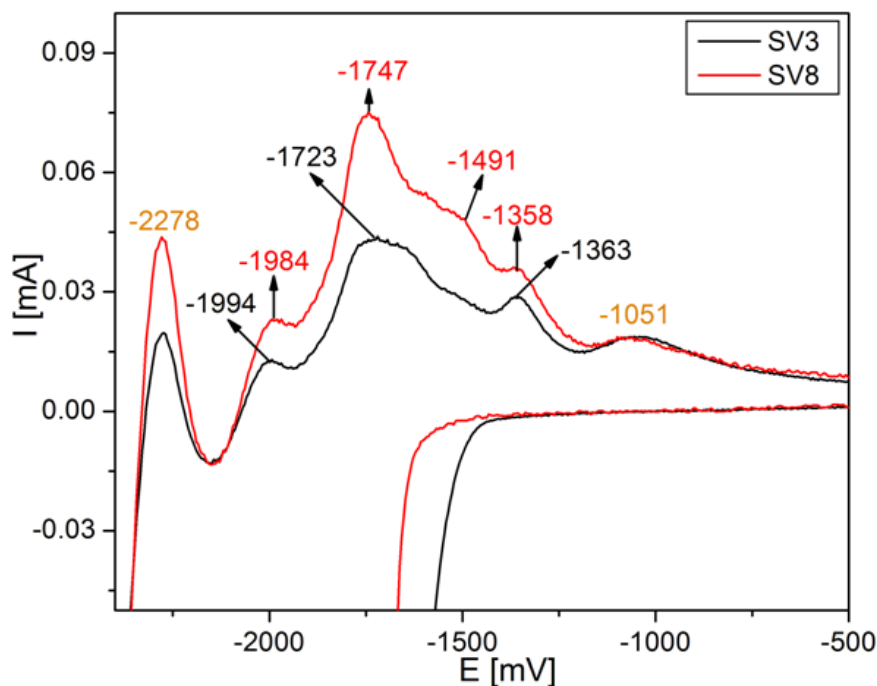
Figure 6.33: Electrochemical responses of SV3 and SV8 (expanded re-oxidation region).

Considering **P6** and **P7 (Figure 6.34)**, **P6** is anodically shifted in the oxidative and re-oxidative scan response except in the reductive response where it is cathodically shifted. In the oxidative scan, two non-reversible peaks at 809 and 1186 mV are observed for **P6** while three non-reversible peaks at 809, 1092 and 1296 mV are observed for **P7**. Two quasi reductive peaks as well are recorded for **P6** (-2006 and -1893 mV) and **P7** (-2006 and -1830 mV) with reverse or re-oxidative peaks observed for **P6** (-1620 and -1422 mV) and **P7** (-1803, -1631 and -1432 mV (vs. Ag/AgCl)). They both have similar oxidative peak at 809 mV and reductive peak at -2006 mV. The **P6** oxidative peak at 1186 mV corresponds to the **P7** oxidative peak at 1092 mV accounting for an oxidative anodic shift of 94 mV for **P6**. The major difference observed in the voltammetric response of **P6** and **P7** are observed in the oxidative and re-oxidative response where **P7** have three peaks in both cases and **P6** has just two. Therefore, the different alkyloxy side chains attached to the phenyl of **Group 2** (**Figure 6.2**) (decyloxy for **P6** and 3,7-dimethyloctyloxyl for **P7**) has an influence on the oxidative

257

scan. However, this difference has no significant influence on the HOMO and the electrochemical band gap. The highest occupied molecular orbital is presumed to be influenced by the alkyloxy side chains in the neighborhood of the anthracene moiety as the onset oxidation of **SV3** and **SV8** is anodically shifted relative to **P6** and **P7**.
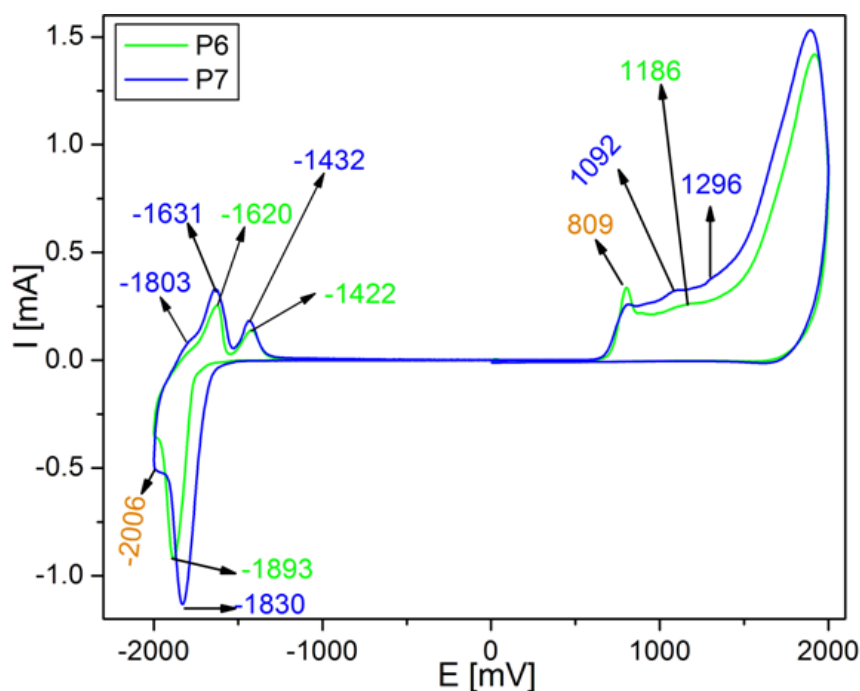
Figure 6.34: Electrochemical responses of P6 and P7 films with peak labels.

The HOMO and LUMO energy levels were estimated from the onset of first oxidation and reduction potentials respectively. The electrochemical data including the onset oxidation and reduction, HOMO, LUMO and electrochemical band gap are summarized in **Table 6.5**. **SV3** and **SV8** possess deeper HOMO of -5.47 eV compared to **P6** (-5.39 eV) and **P7** (-5.37 eV). Apart from **SV3** with LUMO energy of -3.21 eV, the other polymers (**SV8, P6 and P7**) exhibit similar LUMO energy level in the range -3.06 to -3.10 eV. It can therefore be concluded that the main electrochemistry of **SV3, SV8, P6** and **P7** polymers investigated lies on both the anthracene moiety, the attached alkyloxy side chains in the anthracene

neighborhood and those attached to the phenyl group linked to the anthracene neighborhood by a vinylene bond. **Table 6.5** also shows a comparison of the electrochemical and optical band gap. The electrochemical band gaps are quite higher than those recorded from the absorption studies (optical band gap). This difference can be attributed to the insulating nature of the highly dense alkyloxy shell around the conjugated backbone which impedes the transfer of charges [23, 42, 61, 64]. It can also be as a result of variations in the thickness of the films employed for optical and electrochemical investigation which may result in associated backbone planarity [24].

Table 6.5: Electrochemical data including the electrochemical and optical band gap of SV3, SV8, P6 and P7. SV3 and SV8 data were recorded from batch 1.

Code	$E_{\text{onset}}^{\text{ox}}$ (V)	$E_{\text{onset}}^{\text{red}}$ (V)	HOMO (eV)	LUMO (eV)	E_{g}^{el} (eV)	$E_{\text{g}}^{\text{opt}}$ (eV)	ΔE_{g} (eV)
SV3	0.77	-1.49	-5.47	-3.21	2.3	2.0	0.3
SV8	0.77	-1.64	-5.47	-3.06	2.4	2.0	0.4
P6	0.69	-1.63	-5.39	-3.07	2.3	1.9	0.4
P7	0.67	-1.60	-5.37	-3.10	2.3	1.9	0.4

6.6.3   Photovoltaic and Morphological Investigation of SV3, SV8, P6 and P7 (SV3 and SV8 data were recorded from batch 1)

6.6.3.1 Photovoltaic Comparison

Devices based on inverted configuration (ITO/PEI/polymer:PCBM/MoOx/Ag) and devices based on normal or regular configuration (ITO/PEDOT-PSS/polymer:PCBM/LiF/Al) were investigated for **SV3, SV8, P6** and **P7**. The *I-V* curves from the measurement are depicted in **Figure 6.35 – 6.36** and the photovoltaic parameters recorded in **Table 6.6**. For the inverted configuration, **P6** showed the highest efficiency of 2.62%. For same polymer investigated in normal or regular configuration, the efficiency dropped to 1.46%. The next recorded high efficiency polymer for inverted device is **SV3**. Efficiency of 2.43% was recorded and this efficiency dropped to 1.29% for same polymer **SV3** in a regular device configuration. However, for **P7**, the efficiency increased from 2.11% in inverted device to 2.49% in regular device due to the improved fill factor from 0.59 in inverted device to 0.67 in regular device; and current from 4.57 to 4.88 mA/cm^2. The very low efficiency (0.55%) recorded for **SV8** in inverted device configuration may most likely be due to the layer thickness (320 nm) which is the highest in the recorded set.

260
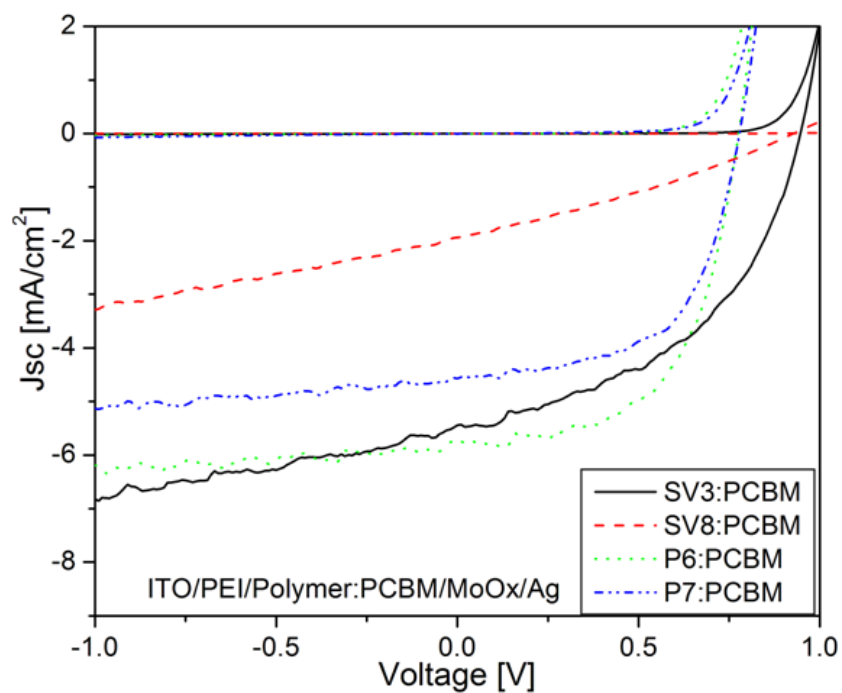
Figure 6.35: The current–voltage (*I–V*) characteristics of the inverted devices based on polymer (SV3, SV8, P6 and P7): PCBM (1:2) blend under 100 mW/cm^2. SV3 and SV8 data were recorded from batch 1.

261
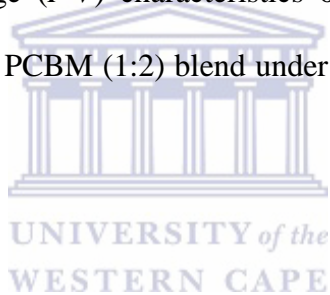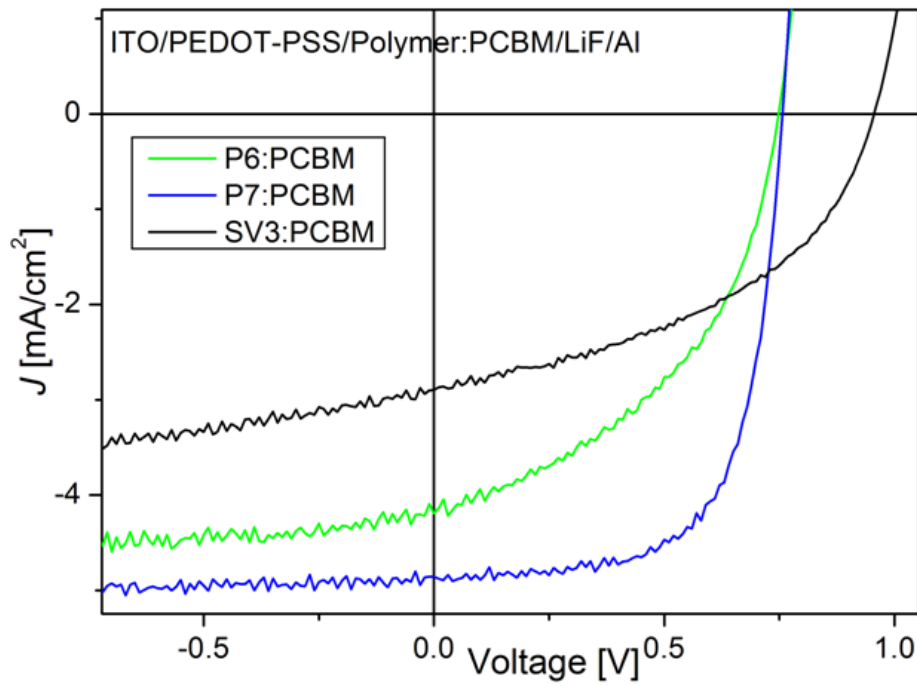
Figure 6.36: The current-voltage (*I–V*) characteristics of the normal or regular devices based on polymer (SV3, P6 and P7): PCBM (1:2) blend under 100 mW/cm^2. SV3 data was recorded from batch 1.

262
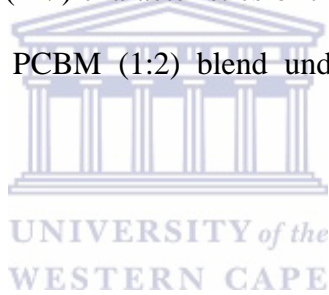
Table 6.6: Photovoltaic parameters of SV3, SV8, P6 and P7 on inverted and normal device configurations. SV3

and SV8 data were recorded from batch 1

ITO/PEI/polymer:PCBM/MoOx/Ag									
Code	M_w (g/mol)	PDI	Bulk Thickness (nm)	J_{sc} [mA/cm^2]	V_{oc} [V]	*FF*	Eff %	@ -2 V [mA/cm^2]	@ +2 V [mA/cm^2]
SV3 (batch 1)	36,060	2.5	75	5.44	0.95	0.47	2.43	-6.82	1.95
SV8 (batch 1)	26,170	7.5	320	1.94	0.93	0.30	0.55	-3.29	0.23
P6	13,430	2.2	150	5.74	0.78	0.59	2.62	-6.19	15.41
P7	28,430	2.4	143	4.57	0.78	0.59	2.11	-5.13	14.44

ITO/PEDOT:PSS/polymer:PCBM/LiF/Al									
Code	M_w (g/mol)	PDI	Bulk Thickness (nm)	J_{sc} [mA/cm^2]	V_{oc} [V]	*FF*	Eff %	@ -2 V [mA/cm^2]	@ +2 V [mA/cm^2]
SV3 (batch 1)	36,060	2.5	120	2.89	0.96	0.47	1.29	-3.96	125
P6	13,430	2.2	185	4.20	0.74	0.46	1.46	-4.52	380
P7	28,430	2.4	185	4.88	0.76	0.67	2.49	-5.05	44

263

From the comparative study, considering **SV3**, **P6** and **P7**, the inverted devices gave improved efficiency except for **P7**. The first conclusion that can be drawn from this comparative study is that the inverted devices are more efficient than the regular devices. In principle, inverted devices tend to be more efficient than normal or regular devices as they possess intrinsic active layer vertical phase separation [65-66] and minimal absorbance losses. Secondly, irrespective of the configuration type, the **SV3** and **SV8** type polymers have a high V_{oc} of almost 1 V and **SV3** has a fill factor (*FF*) of 0.47. However, **P6** and **P7** class of polymers have a better fill factor especially for **P7** which has a remarkably high fill factor of almost 70%. This improvement is ascribed to the enhancement of the charge carrier mobility and live time product. The electrical performance of **P7** made it possible to make devices with reasonable active layer thicknesses beyond 180 nm. An important observation in this study is the different film forming ability between **SV3/SV8** and **P6/P7**. Using the same solvent and spin coating parameters, **SV3** resulted in thinner layers compared to **P6** and **P7** irrespective of the device configuration type. **SV8** on the other hand showed a thicker layer compared to **P6** and **P7** under the same solvent and spin coating parameters. This can naturally be attributed to differences in molecular weights. However, considering the fact that the molecular weight of **SV3** (36,060 g/mol) is higher than that of **SV8** (26,170 g/mol), higher than that of **P7** (28,430 g/mol) and **P6** (13,430 g/mol) (**Table 6.6**), and no particular trend is observed for weight versus thicknesses, this attribution will be misleading. The only ideal explanation in this case will be that the chosen fabrication conditions are disadvantageous for **SV3/SV8** polymers type.

The external quantum efficiency (**Figure 6.37**) of the inverted configuration devices shows a linear correlation with J_{sc} (**Table 6.6**). **P6** device with the highest J_{sc} (5.74 mA/cm^2) has the highest external quantum efficiency intensity followed by **SV3** (5.44 mA/cm2), **P7** (4.57

mA/cm^2) and **SV8** (1.94 mA/cm^2). The higher the J_{sc}, the higher the intensity of the external quantum efficiency as expected. Nonetheless, the absorbance range (450-640 nm) of the polymers is a limiting factor for better external quantum efficiency especially for the regular bulk heterojunction device architecture.
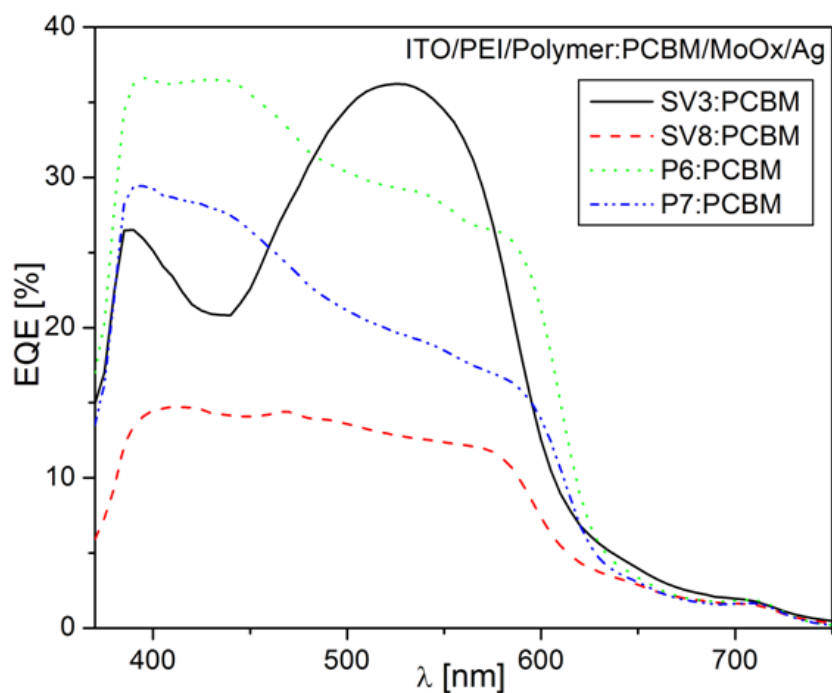
Figure 6.37: External quantum efficiency of the inverted devices based on polymer (SV3, SV8, P6 and P7): PCBM (1:2) blend. SV3 and SV8 data were recorded from batch 1.

6.6.3.2 Morphological Studies

The morphological differences between the devices with ITO/PEI/polymer:PCBM/MoOx/Ag configuration were investigated by atomic force microscopy (AFM) measurements in order to probe into the photoactive layers. The AFM measurement reveals that the polymers have oval-grain structures (**Figure 6.38**). The film of **SV3** with branched and bulky 2-ethylhexyloxy side chains in the anthracene neighborhood and linear decyloxy side chain on

265

the vinylene linked phenyl group reveal bundles of small oval-like grain structures. **SV8** with the same backbone as **SV3** around the anthracene neighbourhood but with a 3,7-dimethyloctyloxy replacing the decyloxy of **SV3** has bigger oval-like grains compared to **SV3**. For polymers **P6** and **P7** with decyloxy side chain around the anthracene neighborhood, the image is in close resemblance with the class of **SV3** and **SV8** except that **P7** has much bigger oval-like grain structure while that of **P6** is not completely structured or defined. This might be responsible for the high V_{oc} (above 0.9 V) of the **SV3** and **SV8** class of polymers compared to the V_{oc} of **P6** and **P7** (less than 0.8 V).
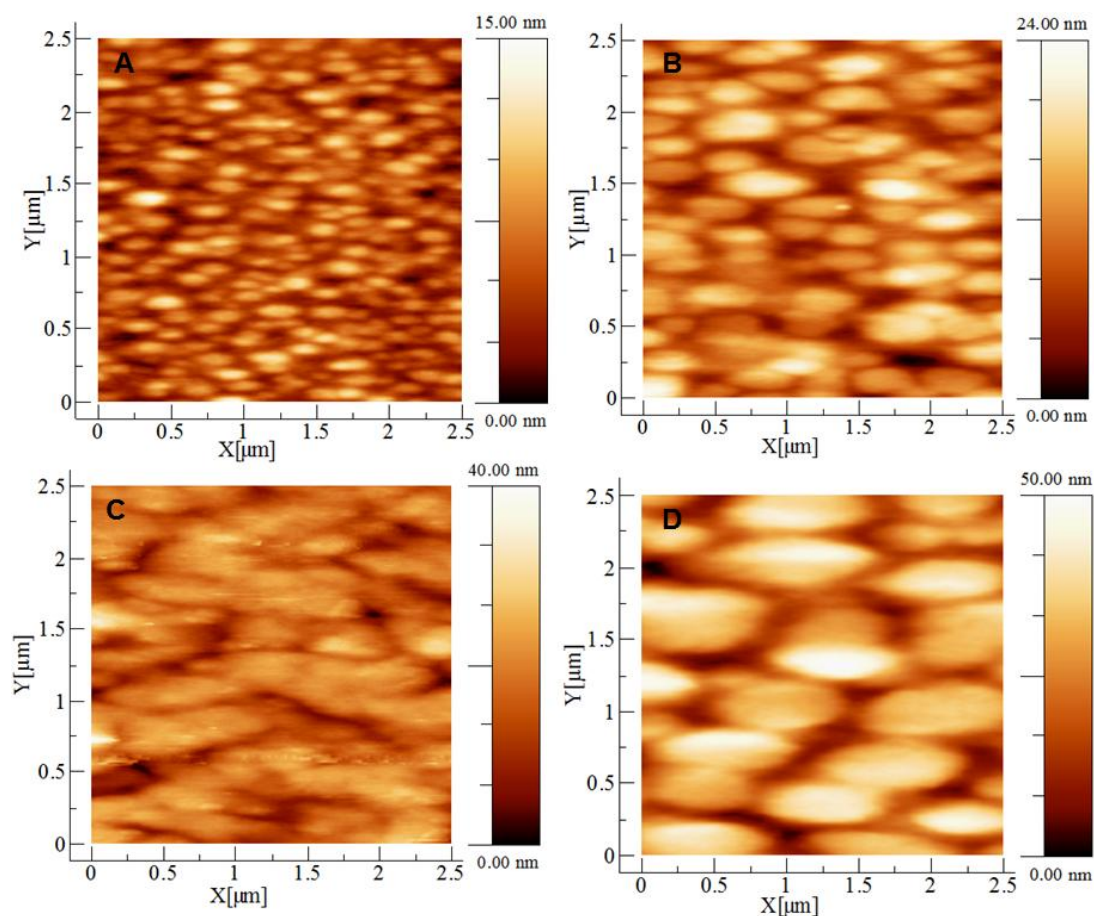
Figure 6.38: AFM images of SV3, SV8, P6 and P7 on ITO/PEI/polymer:PCBM/MoOx/Ag device configuration. A) SV3, B) SV8, C) P6, and D) P7. SV3 and SV8 devices were recorded from batch 1.

266

6.6.4 Electroluminescence Investigations of Selected Polymers

Organic light-emitting devices (OLEDs) of the configuration ITO/PEI/polymer/MoOx/Ag with a hole-injecting electrode formed by ITO covered with a polyethylene imine (PEI) and an electron-injecting electrode of molybdenum oxide covered with silver (MoOx/Ag) were prepared for preliminary investigation of the electroluminescence properties of selected few of the polymers. The electroluminescent (EL) spectra of the OLEDs are shown in **Figure 6.39 and 6.40**. The electroluminescence spectra are similar in shape to their corresponding thin film photoluminescence spectra. This similarity can be attributed to emission from identical singlet excited states S_1 in both cases. From the spectra, we see the devices light up at very low voltages hinting a nicely low turn-on-voltage for the devices. The emissions are stable with EL spectra exhibiting the same shape over a broad voltage range; and the intensity of the emission is varied by the applied voltage. Irrespective of the attached side chains, an orange color emission was observed but with slight variation in shades. Comparing the selected polymers investigated for OLED application, all the polymers emit in the same wavelength region but with different shape (**Figure 6.41**). The investigated polymers can therefore be used as emitters and are useful for the design of OLEDs.
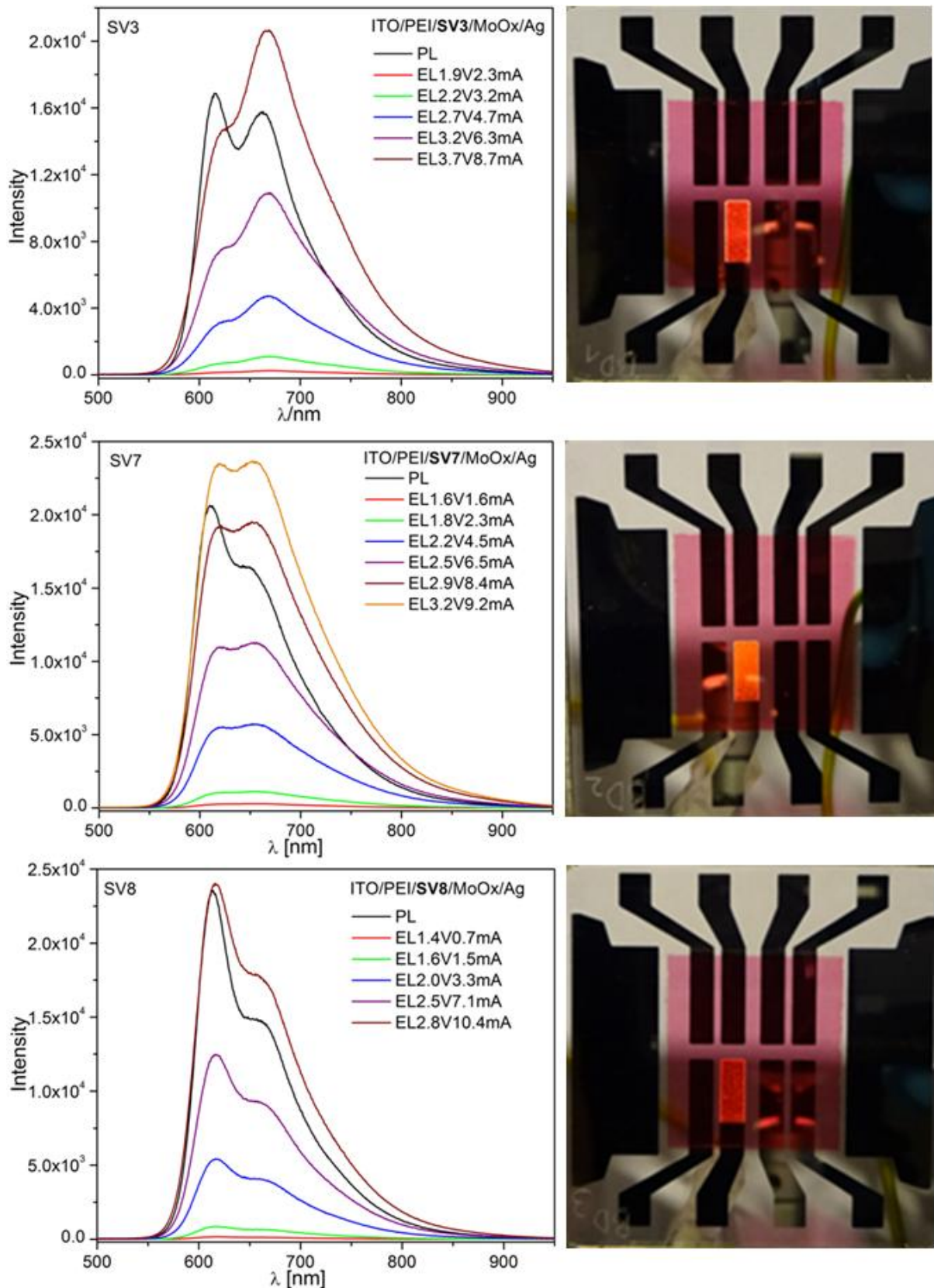
Figure 6.39: Electroluminescence of SV3, SV7 and SV8 measured on ITO/PEI/polymer/MoOx/Ag revealing voltage dependence intensity.

268
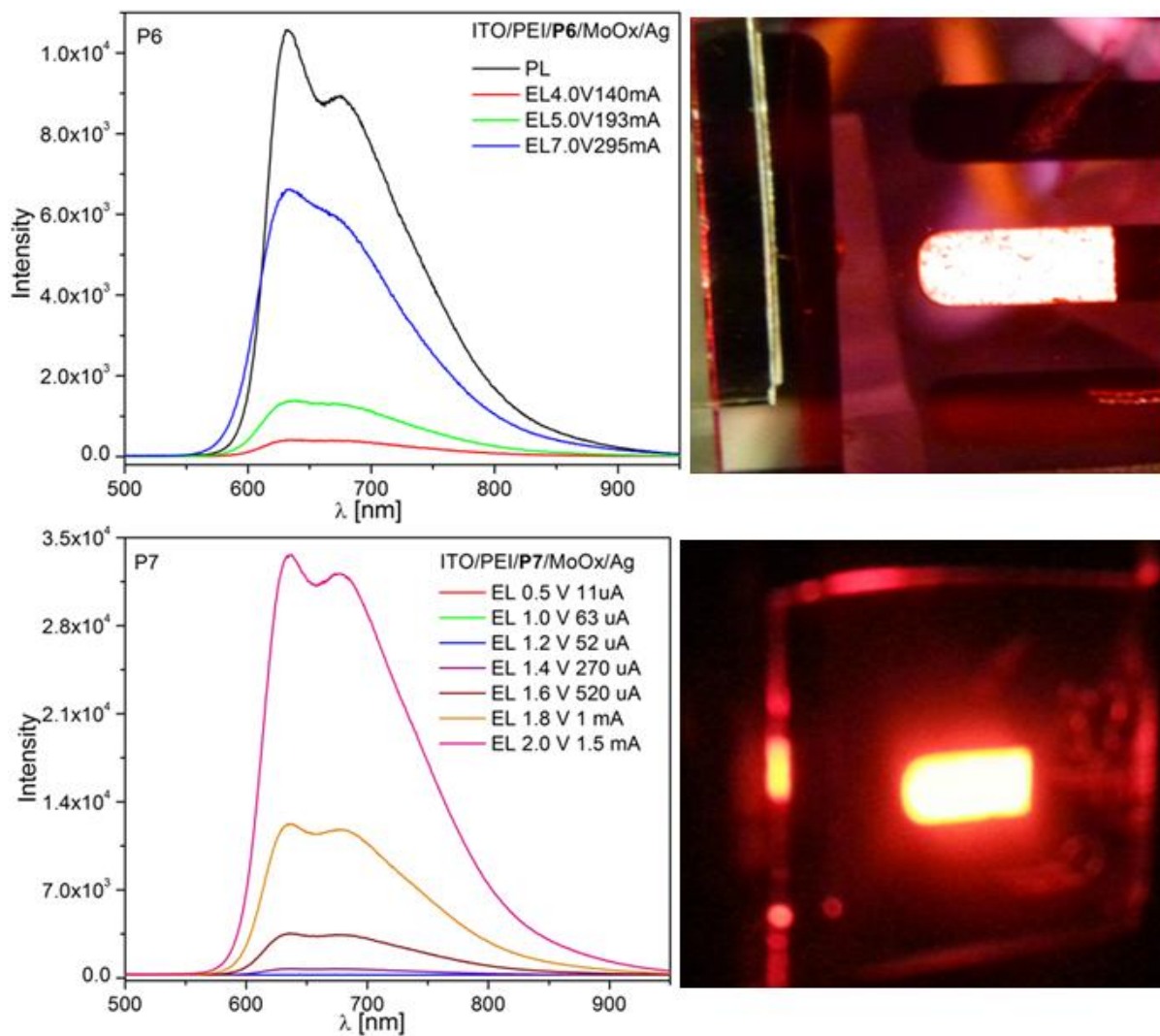
Figure 6.40: Electroluminescence of P6 and P7 measured on ITO/PEI/polymer/MoOx/Ag revealing voltage dependence intensity.
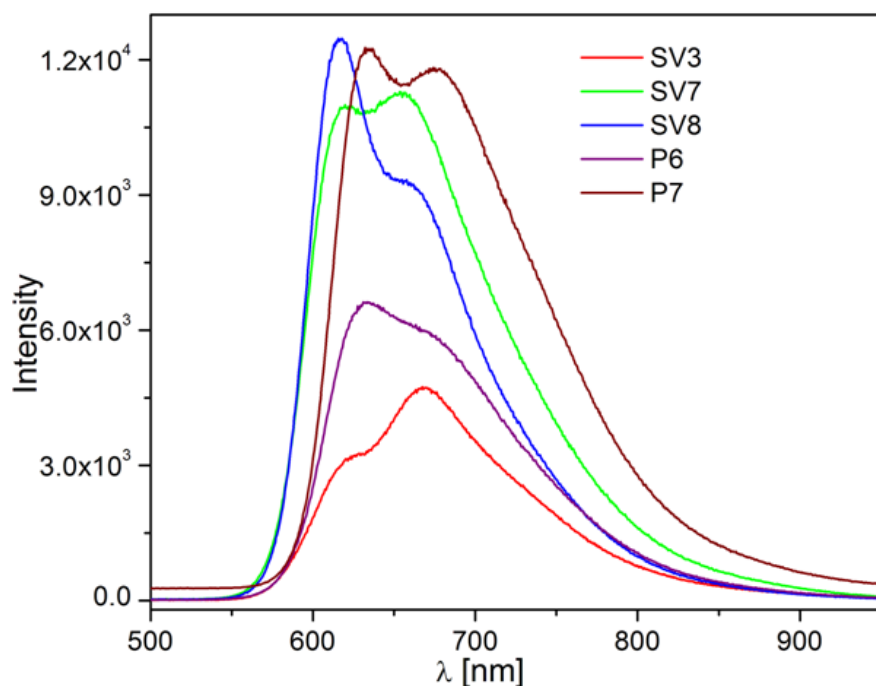
Figure 6.41: Electroluminescence of SV3, SV7, SV8, P6 and P7 measured on ITO/PEI/polymer/MoOx/Ag revealing the wavelength emission region of the investigated polymers.
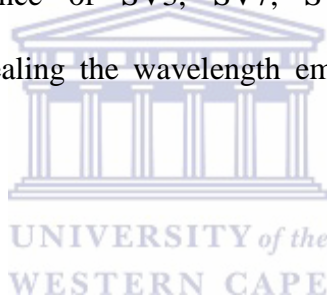
6.7   Conclusion

Ten anthracene-containing polymers with varying side chain have been synthesized by Horner Wadsworth Emmons' polycondensationn reactions and were characterized by NMR, FTIR, UV-Vis and photoluminescence spectroscopy, electrochemistry and thermo-gravimetric analysis. It was observed that the type, nature and number of attached side chain in the polymeric backbone have minimal influence on the photo-physical properties of the polymers. All SV based polymers exhibit identical absorptive and emissive behavior in dilute solution and film. However, the relative intensities of the emission spectra are polymer-specific. The optical responses of these polymers suggest that to a large extent, the

270

conjugated system determines the optical properties both in dilute solution and in film regardless of the side chains.

Photovoltaic investigation of these polymers reveal 2.49% efficiency recorded for photovoltaic devices based on regular configuration while efficiency of up to 2.62% was recorded for the inverted configuration. Very high open circuit voltage of almost 1 V was obtained for SV1 - SV8 irrespective of the attached side chain and the device configuration (inverted or normal); while a high fill factor (*FF*) was observed for P6 and P7 with P7 having a remarkable *FF* of almost 70%. The photovoltaic parameters reveal a dependence on side chain resulting from volume fraction ratio effect in the photovoltaic response of polymer with longer alkyloxy side chain. The efficiencies reported in this work do not represent the maximum attainable efficiencies of devices with these polymers. Optimization of device is necessary and important in this case. For instance, the low *FF* of the SV1 – SV8 polymers can be addressed by optimization of the donor:acceptor ratio and layer thickness. In addition to the recorded photovoltaic properties, the polymers can operate as emitters in organic light-emitting diode (OLEDs) and are useful for the design of OLEDs.

271

6.8 References

[1] G. Hadziioannou and P. F. van Hutten, "Semiconducting Polymers: Chemistry, Physics and Engineering," *1st ed. Wiley-VCH: Weinheim, Germany,* (**2000**)

[2] H. Shirakawa, E. J. Louis, A. G. MacDiarmid, C. K. Chiang and A. J. Heeger, "Synthesis of electrically conducting organic polymers: halogen derivatives of polyacetylene, (CH)x," *J. Chem. Soc., Chem. Commun.,* (**1977**) 578 - 580.

[3] C. K. Chiang, C. B. Fincher Jr., Y. W. Park, A. J. Heeger, H. Shirakawa, E. J. Louis, S. C. Gau and A. G. MacDiarmid, "Electrical Conductivity in Doped Polyacetylene," *Phys. Rev. Lett.,* 39 (**1977**) 1098 - 1101.

[4] C. K. Chiang, M. A. Druy, S. C. Gau, A. J. Heeger, E. Louis, A. G. MacDiarmid, Y. W. Park and S. Shirakawa, "Synthesis of highly conducting derivatives of polyacetylene," *J. Am. Chem. Soc.,* 100 (**1978**) 1013 - 1015.

[5] P. Raghunath, M. Ananth Reddy, C. Gouri, K. Bhanuprakash and V. Jayathirtha Rao, "Electronic properties of anthracene derivatives for blue light emitting electroluminescent layers in organic light emitting diodes: a density functional theory study," *Phys. Chem. A,* 110 (**2006**) 1152 - 1159.

[6] L.-L. Chua, J. Zaumseil, J.-F. Chang, E. C.-W. Ou, P. K.-H. Ho, H. Sirringhaus and R. H. Friend, "General observation of n-type field-effect behaviour in organic semiconductors," *Nature,* 434 (**2005**) 194 - 199.

[7] S. Günes, H. Neugebauer and N. S. Sariciftci, "Conjugated Polymer-Based Organic Solar Cells," *Chem. Rev.,* 107 (**2007**) 1324 - 1338.

[8] C. J. Brabec, N. S. Sariciftci and J. C. Hummelen, "Plastic Solar Cells," *Adv. Funct. Mater.,* 11 (**2001**) 15 - 26.

272

[9]   P. Schilinsky, U. Asawapirom, U. Scherf, M. Biele and C. J. Brabec, "Influence of the Molecular Weight of Poly(3-hexylthiophene) on the Performance of Bulk Heterojunction Solar Cells," *Chem. Mater.,* 17 (**2005**) 2175 - 2180.

[10]   F. C. Krebs, "Fabrication and processing of polymer solar cells. A review of printing and coating techniques," *Solar Energy Material & Solar Cells,* 93 (**2009**) 394 - 412.

[11]   L.-M. Chen, Z. Hong, G. Li and Y. Yang, "Recent progress in polymer solar cells: manipulation of polymer: fullerene morphology and the formation of efficient inverted polymer solar cells," *Adv. Mater.,* 21 (**2009**) 1434 - 1449.

[12]   H. Hoppe and N. S. Sariciftci, "Organic solar cells: an overview," *J. Mater. Res.,* 19 (**2004**) 1924 - 1945.

[13]   C. Winder and N. S. Sariciftci, "Low bandgap polymers for photon harvesting in bulk heterojunction solar cells," *J. Mater. Chem.,* 14 (**2004**) 1077 - 1086.

[14]   Y. J. Cheng, S. H. Yang and C. S. Hsu, "Synthesis of conjugated polymers for organic solar cell applications," *Chem. Rev.,* 109 (**2009**) 5868 - 5923.

[15]   Y. Yao, J. Hou, Z. Xu, G. Li and Y. Yang, "Effects of Solvent Mixtures on the Nanoscale Phase Separation in Polymer Solar Cells," *Adv. Funct. Mater,* 18 (**2008**) 1783 - 1789.

[16]   S. E. Shaheen, C. J. Brabec, N. S. Sariciftci, F. Padinger, T. Fromherz and J. C. Hummelen, "2.5% efficient organic plastic solar cells," *Appl. Phys. Lett.,* 78 (**2001**) 841 - 843.

[17]   D. Chirvase, J. Parisi, J. C. Hummelen and V. Dyakonov, "Influence of nanomorphology on the photovoltaic action of polymer? fullerene composites," *Nanotechnology,* 15 (**2004**) 1317 - 1323.

[18]   T. Erb, U. Zhokhavets, G. Gobsch, S. Raleva, B. Stühn, P. Schilinsky, C. Waldauf and C. J. Brabec, "Correlation Between Structural and Optical Properties of

273

Composite Polymer/Fullerene Films for Organic Solar Cells," *Adv. Funct. Mater.,* 15 (**2005**) 1193 - 1196.

[19]   F. Zhang, K. G. Jespersen, C. Björström, M. Svensson, M. R. Andersson, V. Sundström, K. Magnusson, E. Moons, A. Yartsev and O. Inganäs, "Influence of Solvent Mixing on the Morphology and Performance of Solar Cells Based on Polyfluorene Copolymer/Fullerene Blends," *Adv. Funct. Mater.,* 16 (**2006**) 667 - 674.

[20]   H. Hoppe and N. S. Sariciftci, "Morphology of polymer/fullerene bulk heterojunction solar cells," *J. Mater. Chem.,* 16 (**2006**) 45 - 61.

[21]   J. Peet, J. Y. Kim, N. E. Coates, W. L. Ma, D. Moses, A. J. Heeger and G. C. Bazan, "Efficiency enhancement in low-bandgap polymer solar cells by processing with alkane dithiols," *Nat. Mater.,* 6 (**2007**) 497 - 500.

[22]   U. H. F. Bunz, "Poly(aryleneethynylene)s: Syntheses, Properties, Structures, and Applications," *Chem. Rev.,* 100 (**2000**) 1605 - 1644.

[23]   D. A. M. Egbe, L. H. Nguyen, H. Hoppe, D. Muhlbacher and N. S. Sariciftci, "Side Chain Influence on Electrochemical and Photovoltaic Properties of Yne-Containing Poly(phenylene vinylene)s," *Macromol. Rapid Commun.,* 26 (**2005**) 1389 - 1394.

[24]   D. A. M. Egbe, L. H. Nguyen, K. Schmidtke, A. Wild, C. Sieber, S. Günes and N. S. Sariciftci, "Combined fffects of conjugation pattern and alkoxy side chains on the photovoltaic properties of thiophene- containing PPE-PPVs," *J. Polym. Sci. Part A Polym. Chem.,* 45 (**2007**) 1619 - 1631.

[25]   D. A. M. Egbe, B. Carbonnier, E. Birckner and U.-W. Grummt, "Arylene-ethynylene/arylene-vinylene copolymers: Synthesis and structure–property relationships," *Prog. Polym. Sci.,* 34 (**2009**) 1023 - 1067.

274

[26]   M. Moroni, J. Le Moigne, T. A. Pham and J.-Y. Bigot, "Rigid Rod Conjugated Polymers for Nonlinear Optics. 3. Intramolecular H Bond Effects on Poly(phenyleneethynylene) Chains," *Macromolecules,* 30 (**1997**) 1964 - 1972.

[27]   J. H. Burroughes, D. D. C. Bradley, A. R. Brown, R. N. Marks, K. Mackay, R. H. Friend, P. L. Burn and A. B. Holmes, "Light-emitting diodes based on conjugated polymers," *Nature,* 347 (**1990**) 539 - 541.

[28]   X. Yang, D. Neher, D. Hertel and T. K. Däubler, "Highly Efficient Single-Layer Polymer Electrophosphorescent Devices," *Adv. Mater.,* 16 (**2004**) 161 - 166

[29]   G. Horowitz, "Organic Field-Effect Transistors," *Adv. Mater.,* 10 (**1998**) 365 - 377

[30]   G. Horowitz, "Field-effect transistors based on short organic molecules," *J. Mater. Chem.,* 9 (**1999**) 2021 - 2026.

[31]   F. Wurthner, "Plastic Transistors Reach Maturity for Mass Applications in Microelectronics," *Angew. Chem. Int. Ed.,* 40 (**2001**) 1037 - 1039.

[32]   F. C. Krebs and M. Jørgensen, "High Carrier Mobility in a Series of New Semiconducting PPV-Type Polymers," *Macromolecules,* 36 (**2003**) 4374 - 4384.

[33]   M. Jørgensen and F. C. Krebs, "Stepwise Unidirectional Synthesis of Oligo Phenylene Vinylenes with a Series of Monomers. Use in Plastic Solar Cells," *J. Org. Chem.,* 70 (**2005**) 6004 - 6017.

[34]   Y. Liu, M. S. Liu and A. K-Y. Jen, "Synthesis and characterization of a novel and highly efficient light-emitting polymer," *Acta Polymerica,* 50 (**1999**) 105 - 108.

[35]   E. Tekin, H. Wijlaars, E. Holder, D. A. M. Egbe and U. S. Schubert, "Film thickness dependency of the emission colors of PPE–PPVs in inkjet printed libraries " *J. Mater. Chem.,* 16 (**2006**) 4294 - 4298.

[36] D. A. M. Egbe, E. Tekin, E. Birckner, A. Pivrikas, N. S. Sariciftci and U. S. Schubert, "Effect of Styryl Side Groups on the Photophysical Properties and Hole Mobility of PPE−PPV Systems," *Macromolecules,* 44 (**2007**) 7786 - 7794.

[37] C. D. Dimitrakopoulos and D. J. Mascaro, "Organic thin-film transistors: a review of recent advances," *IBM J. Res. Dev.,* 45 (**2001**) 11 - 27.

[38] F. Padinger, R. S. Rittberger and N. S. Sariciftci, "Effects of Postproduction Treatment on Plastic Solar Cells," *Adv. Funct. Mater.,* 13 (**2003**) 85 - 88.

[39] D. G. Colak, I. Cianga, L. Cianga and Y. Yagci, "Synthesis and self-assembly of fluorene-vinylene alternating copolymers in "Hairy-Rod" architecture: side chain – mediated tuning of conformation, microstructure and photophysical properties," *Designed Monomers and Polymers,* 19 (**2016**) 508 - 534.

[40] F. Cacialli, P. Samorì and C. Silva, "Supramolecular architectures," *Mater. Today,* 7 (**2004**) 24 - 32.

[41] S. C. Rasmussen, B. D. Straw and J. E. Hutchison, "Tuning the extent of conjugation in processable polythiophenes through control of side chain density and regioregularity," *ACS Symp. Series,* 735 (**1999**) 347 - 366.

[42] Z.-K. Chen, W. Huang, L.-H. Wang, E.-T. Kang, B. J. Chen, C. S. Lee and S. T. Lee, "A Family of Electroluminescent Silyl-Substituted Poly(p-phenylenevinylene)s: Synthesis, Characterization, and Structure−Property Relationships," *Macromolecules,* 33 (**2000**) 9015 - 9025.

[43] A. Bolognesi, W. Porzio, A. Provasoli, C. Botta, A. Comotti, P. Sozzani and R. Simonutti, "Structural and Thermal Behavior of Poly-(3-octylthiophene): a DSC, 13C MAS NMR, XRD, Photoluminescence, and Raman Scattering Study," *Macromol. Chem. Phys.,* 202 (**2001**) 2586 - 2591.

276

[44] Z. Wu, S. Wu and Y. Liang, "Monolayer Behavior and LB Film Structure of Poly(2-methoxy-5-(n-hexadecyloxy)-p-phenylene vinylene)," *Langmuir,* 17 (**2001**) 7267 - 7273.

[45] J. Eldo and A. Ajayaghosh, "New Low Band Gap Polymers: Control of Optical and Electronic Properties in near Infrared Absorbing π-Conjugated Polysquaraines," *Chem. Mater.,* 14 (**2002**) 410 - 418.

[46] C.-K. Shin and H. Lee, "Effect of alkyl side-chain length and solvent on the luminescent characteristics of poly(3-n-alkylthiophene)," *Synth. Met.,* 140 (**2004**) 177 - 181.

[47] Z. Bao, W. K. Chan and L. Yu, "Exploration of the Stille Coupling Reaction for the Syntheses of Functional Polymers " *J . Am. Chem. Soc,* 117 (**1995**) 12426 - 12435

[48] D. A. M. Egbe, H. Tillmann, E. Birckner and E. Klemm, "Synthesis and Properties of Novel Well-Defined Alternating PPE/PPV Copolymers," *Macromol. Chem. Phys.,* 202 (**2001**) 2712 - 2726.

[49] D. A. M. Egbe, C. P. Roll, E. Birckner, U.-W. Grummt, R. Stockmann and E. Klemm, "Side Chain Effects in Hybrid PPV/PPE Polymers," *Macromolecules,* 35 (**2002**) 3825 - 3837.

[50] D. A. M. Egbe, Bader Cornelia, J. Nowotny, W. Gunther and E. Klemm, "Investigation of the Photophysical and Electrochemical Properties of Alkoxy-Substituted Arylene-Ethynylene/Arylene-Vinylene Hybrid Polymers," *Macromolecules,* 36 (**2003**) 5459 - 5469.

[51] D. A. M. Egbe, C. Bader, E. Klemm, L. Ding, F. E. Karasz, U.-W. Grummt and E. Birckner, "Influence of the conjugation pattern on the photophysical properties of alkoxy-substituted PE/PV hybrid polymers," *Macromolecules,* 36 (**2003**) 9303 - 9312.

[52]   D. A. M. Egbe, B. Carbonnier, L. Ding, D. Mühlbacher, E. Birckner, T. Pakula, F. E. Karasz and U.-W. Grummt, "Supramolecular Ordering, Thermal Behavior, and Photophysical, Electrochemical, and Electroluminescent Properties of Alkoxy-Substituted Yne-Containing Poly(phenylene-vinylene)s," *Macromolecules,* 37 (**2004**) 7451 - 7463.

[53]   L. Ding, D. A. M. Egbe and F. E. Karasz, "Photophysical and Optoelectronic Properties of Green-Emitting Alkoxy-Substituted PE/PV Hybrid Conjugated Polymers," *Macromolecules,* 37 (**2004**) 6124 - 6131.

[54]   L. Ding, Z. Lu, D. A. M. Egbe and F. E. Karasz, "Structure-Morphology-Electroluminescence Relationship for Hybrid Conjugated Polymers," *Macromolecules,* 37 (**2004**) 10031 - 10035.

[55]   F. Livi, N. K. Zawacka, D. Angmo, M. Jørgensen, F. C. Krebs and E. Bundgaard, "Influence of Side Chain Position on the Electrical Properties of Organic Solar Cells Based on Dithienylbenzothiadiazole-altphenylene Conjugated Polymers," *Macromolecules,* 48 (**2015**) 3481 - 3492.

[56]   N. Bouguerra, A. Růžička, C. Ulbricht, C. Enengl, S. Enengl, V. Pokorná, D. Výprachtický, E. Tordin, R. Aitout, V. r. Cimrová and D. A. M. Egbe, "Synthesis and photophysical and electroluminescent properties of poly(1,4-phenylene−ethynylene)-alt-poly(1,4-phenylene−vinylene)s with various dissymmetric substitution of alkoxy side chains," *Macromolecules,* 49 (**2016**) 455 - 464.

[57]   F. Wang, F. He, Z. Q. Xie, Y. P. Li, M. Hanif, M. Li and Y. Ma, "Poly(p-phenylene vinylene) Derivatives with Different Contents of cis-Olefins and their Effect on the Optical Properties," *Macromol. Chem. Phys.,* 209 (**2008**) 1381 - 1388.

[58]   J. Coates, "Interpretation of Infrared Spectra, A Practical Approach," *Encyclopedia of Analytical Chemistry,* DOI: 10.1002/9780470027318.a5606 (**2006**)

278

[59] D. A. M. Egbe, B. Carbonnier, E. L. Paul, D. Muhlbacher, T. Kietzke, E. Birckner, D. Neher, U.-W. Grummt and T. Pakula, "Diyne-Containing PPVs: Solid-State Properties and Comparison of Their Photophysical and Electrochemical Properties with Those of Their Yne-Containing Counterparts," *Macromolecules,* 38 (**2005**) 6269 - 6275.

[60] D. A. M. Egbe, S. Turk, S. Rathgeber, F. Kuhnlenz, R. Jadhav, A. Wild, E. Birckner, G. Adam, A. Pivrikas, V. Cimrova, G. Knor, N. S. Sariciftci and H. Hoppe, "Anthracene Based Conjugated Polymers: Correlation between π-π-Stacking Ability, Photophysical Properties, Charge Carrier Mobility, and Photovoltaic Performance," *Macromolecules,* 43 (**2010**) 1261 - 1269.

[61] R. O. Garay, H. Naarmann and K. Mullen, "Synthesis and characterization of poly(1,4-anthrylenevinylene)," *Macromolecules,* 27 (**1994**) 1922 - 1927.

[62] A. Wild, D. A. M. Egbe, E. Birckner, V. Cimrova, R. Baumann, U.-W. Grummt and U. S. Schubert, "Anthracene- and Thiophene-Containing MEH-PPE-PPVs: Synthesis and Study of the Effect of the Aromatic Ring Position on the Photophysical and Electrochemical Properties," *J. Polym. Sci. Part A: Polym. Chem.,* 47 (**2009**) 2243 - 2261.

[63] J. A. Mikroyannidis, M. M. Stylianakis, P. Balraju, P. Suresh and G. D. Sharma, "Novel p-Phenylenevinylene Compounds Containing Thiophene or Anthracene Moieties and Cyano−Vinylene Bonds for Photovoltaic Applications," *ACS Appl. Mater. Interfaces,* 1 (**2009**) 1711 - 1718.

[64] T. Yamamoto and B.-L. Lee, "New Soluble, Coplanar Poly(naphthalene-2,6-diyl)-Type π-Conjugated Polymer, Poly(pyrimido[5,4-d]pyrimidine-2,6-diyl), with Nitrogen Atoms at All of the o-Positions. Synthesis, Solid Structure, Optical

Properties, Self-Assembling Phenomena, and Redox Behavior," *Macromolecules,* 35 (**2002**) 2993 - 2999.

[65]   L.-M. Chen, Z. Hong, G. Li and Y. Yang, "Recent Progress in Polymer Solar Cells: Manipulation of Polymer:Fullerene Morphology and the Formation of Efficient Inverted Polymer Solar Cells," *Adv. Mater.,* 21 (**2009**) 1434 - 1449.

[66]   F. Zhang, X. Xu, W. Tang, J. Zhang, Z. Zhuo, J. Wang, J. Wan, Z. Xu and Y. Wang, "Recent development of the inverted configuration organic solar cells," *Solar Energy Material & Solar Cells,* 95 (**2011**) 1785 - 1799.

UNIVERSITY *of the*

WESTERN CAPE

CHAPTER SEVEN

RESULTS AND DISCUSSION - Novel 5-(Benzo[b]thiophene-3-yl)pyridinealdehyde (BTPA) Functionalization Framework For Modulating Fullerene Electronics

Abstract

Fullerenes are interesting n-type materials with phenyl-C_{61}-butyric-acid-methyl-ester (PCBM) appearing to be the only soluble fullerene derivative that has found application especially in solar cell. The use of PCBM as acceptor for a variety of polymers with different optoelectronics property has limited the progress of organic solar cells. Study of suitable fullerene derivatives for different polymers is essential to enhance device performance. In this study, the properties of fullerene C_{60} was modulated with a synthesized novel organic compound, 5-(benzo[b]thiophene-3-yl)pyridinealdehyde, to form processable and stable 3-(benzo[b]thiophene-3yl)-5-fulleropyrrolidinepyridine. The electrochemical and photo-physical properties of this derivative and PCBM were studied. PCBM and BTFP exhibited about the same first reduction potential (-0.61 and -0.62 V, respectively), with a lowest occupied molecular orbital (LUMO) energy level of 0.47 eV in both cases. BTFP showed a broad and structured absorption with three major peaks and a shoulder covering a wider range of the spectrum compared to PCBM with two major peaks and a shoulder in chloroform. The absorption maximum of BTFP was observed at 290 nm while that of PCBM was seen at 260 nm. Despite the similar LUMO (0.47 eV) observed for BTFP and PCBM, their luminescence quenching of poly[(9,9-di-*n*-octylfluorenyl-2,7-diyl)-*alt*-(benzo[2,1,3]thiadiazol-4,8-diyl)]

281

(F8BT) and poly[(9,9-dioctylfluorenyl-2,7-diyl)-*co*-bithiophene](F8T2); and preliminary photovoltaic response with poly(3-hexylthiophene) (P3HT) differ. A relatively poor photovoltaic response was observed for cells with BTFP as acceptor. Although PCBM gave better photovoltaic response with P3HT, the structured strong absorption and bathochromic shift in the maximum wavelength of BTFP compared to that of PCBM in chloroform may contribute to light absorption of a suitable donor thereby improving device efficiency. The stability of BTPF allows for easy handling coupled with ambient temperature process-ability and long shelf life.

7   Introduction

The uniqueness of closed cage, nearly spherical C_{60} and related fullerene molecules has attracted considerable attention. The icosahedral symmetry [1] and numerous possibilities of functionalization allow to modulate their optoelectronic properties [2-5], giving an idea of the unabated interest in these intriguing carbon allotropes. The chemistry of fullerenes is that of electron-poor olefins, with sp^2 carbon atoms constrained into a pyramidalized geometry. Moreover, multiple double bonds are available on the carbon backbone, making multiple functionalization [6] an interesting route towards new functional materials. This has led to a wide variety of novel compounds with finely tuneable features that have found applications as catalysts [7-8], anti-oxidants [9], in sensors [10] and solar cells [2, 11]. The functionalization of fullerenes does not only modify their properties, but converts them into more processable forms, as pristine C_{60} is only sparsely soluble in most solvents making it intractable. Indeed, the quest for soluble fullerenes was (and still is) one of the main driving forces in the field of covalent modification of carbon nanostructures. Phenyl-C_{61}-butyric-acid-methyl-ester ([60]PCBM), a fullerene derivative, is an effective solution processable n-

type organic semiconductor which is commonly blended with p-type conjugated polymers to make photovoltaic (PV) cells. However, due to the dependence of photovoltaic properties on frontier orbital energy levels of donor and acceptor materials, the application of PCBM to all donor polymers irrespective of their optoelectronic properties leads to untrue photovoltaic properties of such devices. For instance, the report by Susarova *et al* [12] compared the photovoltaic responses of two polymers with PCBM and other functionalized fullerenes and observed that PCBM gave just moderate efficiencies in combination with the polymers while the best photovoltaic performances were obtained with a blend of each polymer with specific fullerene derivatives possessing suitable molecular structures. The report by Kastner *et al* [13] has also shown PCBM not to be the most compatible fullerene derivative for AnE-PV$_{stat}$ polymers. The result of a series of fullerene derivatives investigated for AnE-PV$_{stat}$ showed the best efficiency for the polymer and a fullerene derivative bearing an ethyl ester residue, with efficiency of up to 4.8% and fill factor (*FF*) of up to 72%. Another report showed the photovoltaic investigation of an anthracene based co-polymer in combination with twelve different fullerene derivatives including PCBM. The best photovoltaic parameters were obtained for a fullerene derivative with an attached thiophene unit and an n-buthyl side chain. Short circuit current (J_{sc} (8.3 mA/cm^2)), open circuit voltage (V_{oc} (0.77 V)) and fill factor (*FF* (0.61)) was obtained for the polymer with the fullerene derivative while J_{sc} (2.3 mA/cm^2), V_{oc} (0.79 V) and *FF* (0.46) was obtained for PCBM in the same study [14].

Out of all the chemical routes for fullerene functionalization, cycloaddition reactions are the most popular [15-18]. Herein, we describe a fulleropyrrolidine [19], 3-(benzo[b]thiophene-3yl)-5-fulleropyrrolidinepyridine (BTFP), that is obtained from C$_{60}$ by 1,3-dipolar cycloaddition of the azomethine ylide that forms when 5-(benzo[b]thiophene-3-yl)pyridinealdehyde (BTPA)is reacted with sarcosine. Besides the structural characterization

283

of BTFP, we report its electrochemical and spectroscopic properties, in order to assess its potential as an electron-acceptor material for solar energy harvesting. The solar energy harvesting performances of blends of BTFP with two electron-donating polymers, poly[(9,9-di-*n*-octylfluorenyl-2,7-diyl)-*alt*-(benzo[2,1,3]thiadiazol-4,8-diyl)] (F8BT) and poly[(9,9-dioctylfluorenyl-2,7-diyl)-*co*-bithiophene](F8T2), were evaluated in comparison with benchmark acceptor material phenyl C_{61} butyric acid methyl ester (PCBM).

7.1   Materials, Instruments and Methods

All starting materials (benzo[*b*]thien-3-ylboronic acid, 5-Bromo-3-pyridinecarboxaldehyde, tetrakis(triphenylphosphine) palladium(0), triphenyl phosphine, potassium carbonate, sarcosine), tetrabutylammonium hexafluorophosphate (TBAPF$_6$) and solvents were purchased from Sigma Aldrich and used as received. Fullerene C_{60} was purchased from Bulky USA and used as received. P3HT used for photovoltaic evaluation was supplied by Rieke, PCBM by Solenne and ITO substrate was provided by Xin Yan Technology LTD, 15 Ω/sq ITO coated glass (XY15S) surface finish-polish, thickness 1x1 mm. Tetrabutylammonium hexafluorophosphate (TBAPF$_6$) was used in the electrochemical experiments as purchased from Sigma-Aldrich. Thin layer chromatography (TLC) and column chromatography were performed using a Polygram SilG/UV254 (TLC plates) and silica gel MN 60 (70–230 mesh) by Macherey-Nagel. FTIR spectra were recorded for 5-(benzo[b]thiophene-3-yl)pyridinealdehyde (BTPA) using a NEXUS 870 FTIR (Thermo Nicolet) spectrophotometer at room temperature and humid free atmosphere by making KBr pellets while spectra was recorded for 3-(benzo[b]thiophene-3yl)-5-fulleropyrrolidinepyridine (BTFP) using FTIR Spectrometer (UATR TWO), Perkin Elmer. ^{1}H (500 MHz) NMR spectra of a solution of BTPA and BTFP were recorded on a Bruker AMX-500 spectrometer. All other NMR data

284

were acquired on a Bruker Avance IIIHD 400 MHz Nanobay NMR spectrometer equipped with a 5 mm BBO. Data were acquired in dimethyl sulfoxide-d6 and 1,2-dichlorobenzene-d4. Mass spectroscopy analysis of BTPA was carried out using a Waters Synapt G2 QTOF mass spectrometer, by injecting the ESI probe into a stream of acetonitrile. BTFP MS fingerprint was recorded using a 4800 MALDI-TOF/TOFt Plus Analyzer (Applied Biosystems, Foster City, CA, USA) and 2′,4′,6′-Trihydroxyacetophenone monohydrate as the matrix. The mass spectrum was obtained in the reflectron/delayed extraction mode at an accelerating voltage of 5 kV. Thermo-gravimetric analysis (TGA) was carried out with a Q5000IR TGA (TA Instruments) by heating at 10°C/min rate under nitrogen atmosphere. Morphology of the pristine fullerene C_{60} and the novel materials were obtained with Auriga high resolution-scanning electron microscopy while the details about the internal composition were analyzed with Auriga high resolution-transmission electron microscopy. Atomic force microscopy images were recorded with Nanosurf Easyscan 2. The absorption spectra of BTPA and BTFP solutions were measured using a Nicolet Evolution 100 UV–visible spectrometer (Thermo Electron). Photoluminescence quenching was monitored by NanoLog *i*HR320 at ambient temperature. Cyclic voltammetric (CV) measurements were carried out using a BASi Epsilon potentiostat equipped with a standard three-electrode configuration. Typically, a three electrode cell equipped with a glassy carbon working electrode, an Ag/AgCl reference electrode, and a Pt wire counter electrode was employed. The measurements were carried out in a 4:1 1,2-dichlorobenzene:acetonitrile mixture, with 0.1 M tetrabutyl ammonium hexafluorophosphate (TBAF$_6$P) as the supporting electrolyte under an argon atmosphere. The working electrode was 3 mm in diameter. Both the counter and the reference electrode were separated from the working electrode by ~0.5 cm. Formal potential values correspond to (E_{pc} + E_{pa})/2 from CV and the electrochemical onsets were determined at the position where the current starts to differ from the baseline.

Device for photovoltaic characterization were fabricated according to the procedure below

Procedure for cutting and cleaning of substrates:

Cutting of substrates (1.5 x 6.4 mm)

Substrates etched in HCl

Cut into small sizes (1.5 x1.5 mm)

Substrates were cleaned using the standard procedure for substrate cleaning

Standard procedure for substrate cleaning (1.5 x 1.5 mm):

1. Acetone + 20 min ultrasonic bath [RT]

2. Isopropanol + 20 min ultrasonic bath [RT]

3. Dried with compressed N_2 gun

ITO substrate → plasma oven treatment (plasma ETCH PE-50) 5 min, 50 W O_2

Spin-coating of PEI (80 μL spincoated for each substrate)

Substrate/PEI treatment for 10 mins @ 105°C

Spin-coating of active layer (Donor:Acceptor) on substrate/PEI

Spin coating program

15 rps 2 s   25 s

33 rps 2 s   30 s

80 μL of each sample spincoated

Annealing @ 110°C for 5 min

Evaporation of top electrode (MoOx (10 nm) and Ag (100 nm))

Measurement of current-voltage (*I-V*) curves

Device microscopic images were capture by Nikon ECLIPSE LV100ND, *I-V* curves were measured using LS0821 LOT Quantum design measured @ 100 mW/cm^2 KEITHLEY output reader. External quantum efficiency (EQE) was measured using EG & G INSTRUMENTS

LOCK-IN AMPLIFIER; chopper: optical chopper – SEITEC INSTRUMENTS LTD
MULLER ELECTRONICS OPTICS LXH100.

7.2   Synthesis of Materials

7.2.1   Synthesis of 5-(Benzo[b]thiophene-3-yl)pyridinealdehyde (BTPA)

In a 50 ml round bottom flask, equipped with magnetic bar and a bubble condenser topped
with a calcium chloride trap, 5-Bromo-3-pyridinecarboxaldehyde (0.20 g, 1.1 mmol) was
dissolved in a 4:1 dimethoxyethane:water mixture (20 ml). Tetrakis(triphenylphosphine)
palladium(0) (0.13 g, 0.11 mmol, 0.1 eq), potassium carbonate (0.53 g, 3.8 mmol) and
triphenyl phosphine (0.14 g, 0.055 mmol, 0.05 eq) were added to the mixture rapidly under
vigorous stirring. Subsequently, (benzo[*b*]thien-3-ylboronic acid (0.23 g, 1.3 mmol, 1.2 eq)
was added after 20 mins to the activated reaction mixture. The mixture was heated at 65°C
with an oil bath under stirring for 24 h and monitored by TLC. After refluxing for 24 h, the
crude mixture (deep green color) was cooled down to room temperature and concentrated to
remove dimethoxyethane. Thereafter, it was dissolved in 100 mL dichloromethane and
transferred into a separation funnel. The organic phase was collected and washed with
deionized water (5 x 50 ml) to a pH of ca 7. The combined organic phase was washed with
celite to remove the palladium catalyst, dried over sodium sulphate and concentrated at
reduced pressure. The crude obtained was assessed by TLC and purified by column
chromatography (SiO$_2$, petroleum ether/ethyl acetate 3:1, R$_f$ 0.38) and gave the target BTPA
(0.15 g, 57%) as a bright yellow solid. Using the same reaction condition, and chloro(2-
dicyclohexylphosphino-2′,4′,6′-triisopropyl-1,1′-biphenyl)[2-(2′-amino-1,1′-
biphenyl)]palladium(II) as catalyst, a yield of 86% was obtained.

287

^{1}H NMR (400 MHz, DMSO-d6): δ = 7.487 (m, 2H), 7.926 (m, 1H), 8.472 (t, J = 2.0 Hz, 1H), 9.115 (m, 2H), 10.222 (s, 1H). ^{13}C NMR (100 MHz, DMSOd6): δ = 122.0, 123.4, 124.9, 125.1, 127.1, 131.2, 131.5, 132.3, 13.6, 136.7, 140.1, 149.7, 153.6, 192.5.

ESI-MS: *m/z* calcd for $C_{14}H_9NOS$: 240 [*M*+*H*$^+$]; found 240 [*M*+*H*$^+$].

UV-Vis (dichloromethane): λ (nm) 238, 264, 282, 294, 303, 443.

FTIR (KBr) ν cm^{-1}: 1650, 1696, 2874, 3094.

7.2.2   Synthesis of 3-(Benzo[b]thiophene-3yl)-5-fulleropyrrolidinepyridine (BTFP)

In a 50 ml round bottom flask, fullerene (C_{60}) (0.19 g, 0.00027 mol) was dissolved in chlorobenzene in nitrogen under dark (25 ml) and refluxed with vigorous stirring. Afterwards, a solution of the BTPA (0.13 g, 0.0005 mol, 1.9 eq) and a solution of finely ground *N*-methyl glycine (0.70 g, 0.0007 mol, 2.6 eq), each in 2 mL chlorobenzene was added to the refluxing solution under vigorous stirring. The reaction mixture was monitored under this condition every 5 mins by TLC and stopped after 25 mins. The crude mixture was cooled down to room temperature and concentrated under reduced pressure to give a dark brown substance. The obtained brownish crude was dissolved in toluene, assessed by TLC and purified by column chromatography on silica gel (elution gradient from toluene (R_f = 0.9) to toluene:ethyl acetate 9.5: 0.5 (R_f = 0.39)). The product was washed with methanol:toluene 9:1 once and 100% methanol for six times and centrifuged after each wash to remove the non-fullerene by-products. The obtained product was dried under vacuum to give the target BTFP in a 35% yield.

^{1}H NMR (500 MHz, CDCl$_3$/CS$_2$) δ 8.86 (t, *J* = 100.9 Hz, 3H), 7.92 (d, *J* = 8.0 Hz, 1H), 7.61 − 7.50 (m, 2H), 7.50 − 7.28 (m, 2H), 5.14 (s, 1H), 5.05 (d, *J* = 9.5 Hz, 1H), 4.37 (d, *J* = 9.5 Hz, 1H), 2.86 (s, 3H). ^{13}C NMR (101 MHz, 1,2-DCB) δ 154.03, 151.48, 150.55, 147.83,

145.21, 145.15, 144.25, 144.13, 144.08, 143.99, 143.82, 143.49, 143.45, 143.17, 143.03, 142.64, 142.37, 142.32, 142.21, 141.09, 140.91, 140.57, 140.49, 140.46, 140.37, 140.22, 140.17, 140.08, 140.03, 139.97, 139.88, 139.71, 139.62, 139.47, 138.84, 138.19, 138.11, 138.00, 137.63, 135.85, 135.46, 134.23, 133.74, 132.18, 130.92, 130.39, 128.29, 128.03, 127.78, 125.44, 125.19, 124.95, 122.97, 122.82, 122.73, 121.06, 120.35, 74.93, 67.92, 66.95, 37.73.

MALDI TOF/TOFt m/z calcd for $C_{66}H_{14}N_2S$: 986.337; found 986.917.

UV-Vis (dichloromethane): λ (nm) 259, 306, 325, 430; (chloroform): 247, 289, 307, 328[*], and 431. FTIR (KBr) ν cm^{-1}: 527, 577, 1183, 1426, 2949.

[*]shoulder

289

7.3   Results and Discussion

7.3.1   Spectroscopic Studies

7.3.1.1 Nuclear Magnetic Resonance Spectroscopy of BTPA and BTFP

The synthetic route leading to the preparation of BTPA and BTFP is shown in **Figure 7.1** and **7.2**.
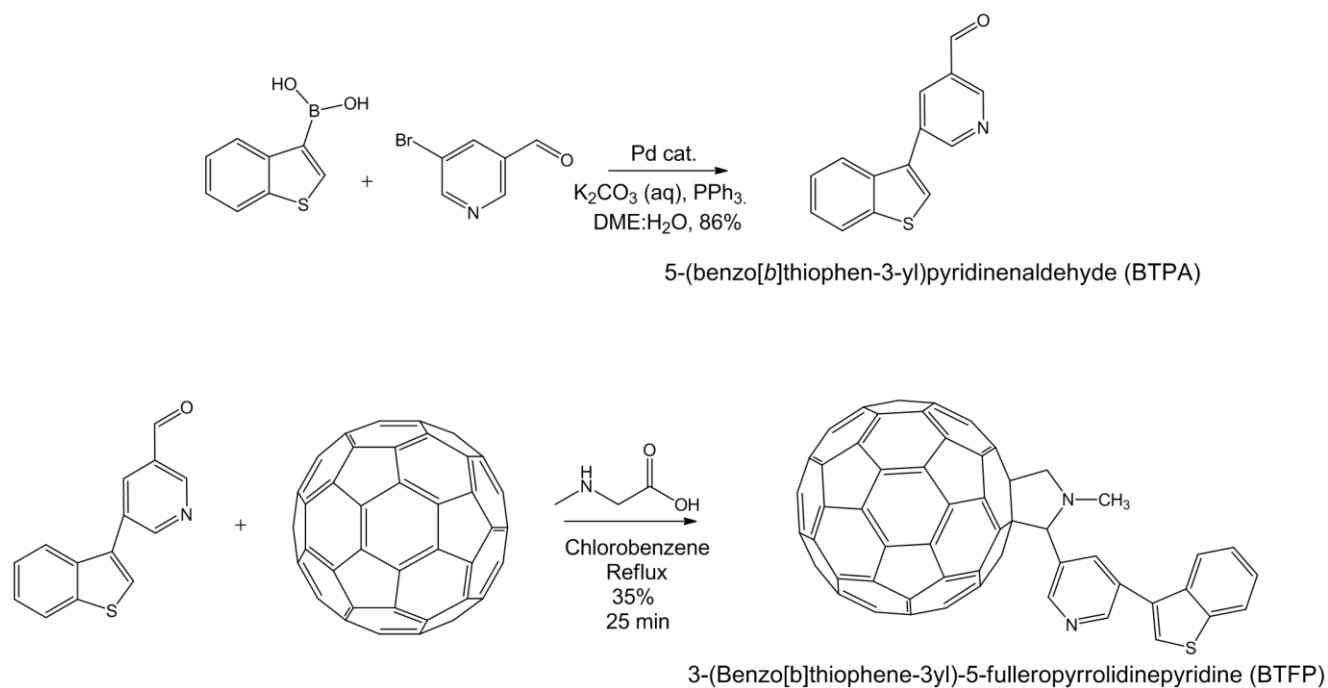
Figure 7.1: Schematic of the synthesis of BTPA and BTFP.

290
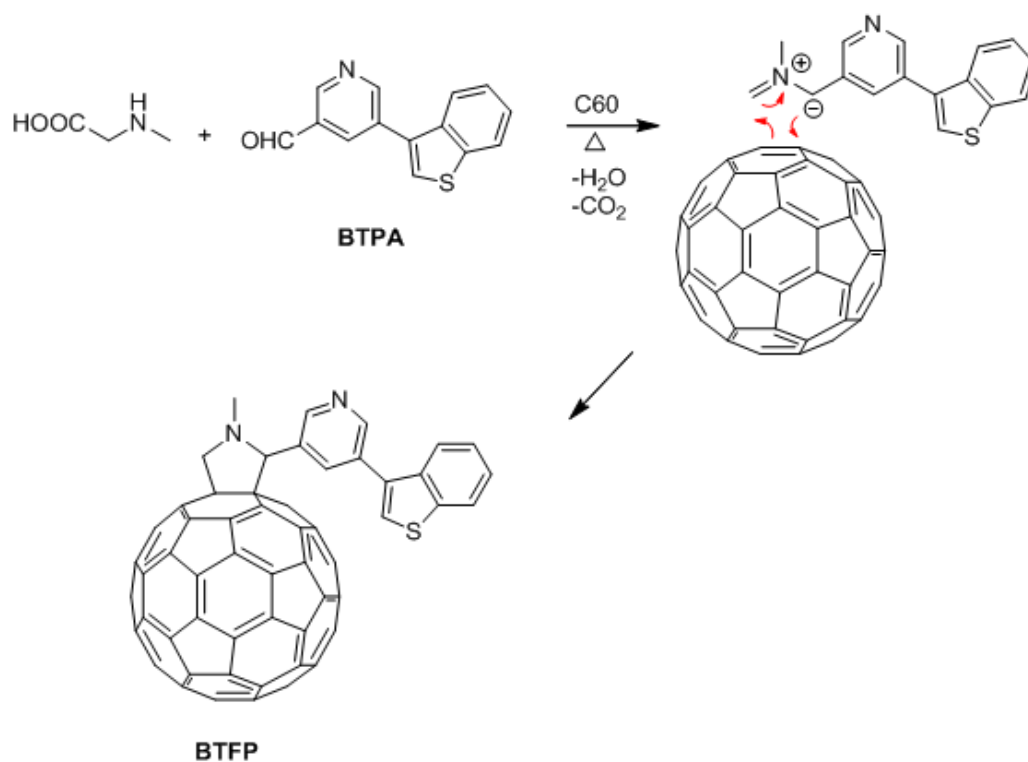
Figure 7.2: Mechanism for the synthesis of BTFP.

The products were characterized by NMR, UV-Vis, PL, TEM and SEM/EDS. For BTPA, ^{1}H-NMR in DMSO-d6 confirmed the presence of aldehyde at 10.2 ppm (**Figure 7.3 and 7.4**), while ^{13}C-NMR showed 14 signals as expected in the proposed structure (**Figure 7.5 and 7.6**). The coupling of BTPA as shown in **Figure 7.6** is represented structurally in **Figure 7.7** and the data analysis is given in **Table 7.1**. The product is bright yellow, stable and soluble in common organic solvents. The ^{13}C-NMR spectrum of BTFP show the loss of the aldehyde peak (at 188ppm) of BTPA, along with the splitting of the C_{60} signal (141 ppm), into 10 signals in the 140 - 145 region due to the breaking of the spherical symmetry of starting material (**Figure 7.8**). The result shows a shift and slight distortion of the geometry of BTFP in relation to C_{60} and BTPA. DEPT data (**Figure 7.9**) shows the signals for the *N*-methyl glycine analogue. It shows that we have an *N*-CH$_3$ (at 37.9 ppm), a -CH$_2$ (at 68.3 ppm) and a

291

–CH signal (at 79.3 ppm) which is due to the linkage between the glycine and the BTPA (where the BTPA contributed the C).
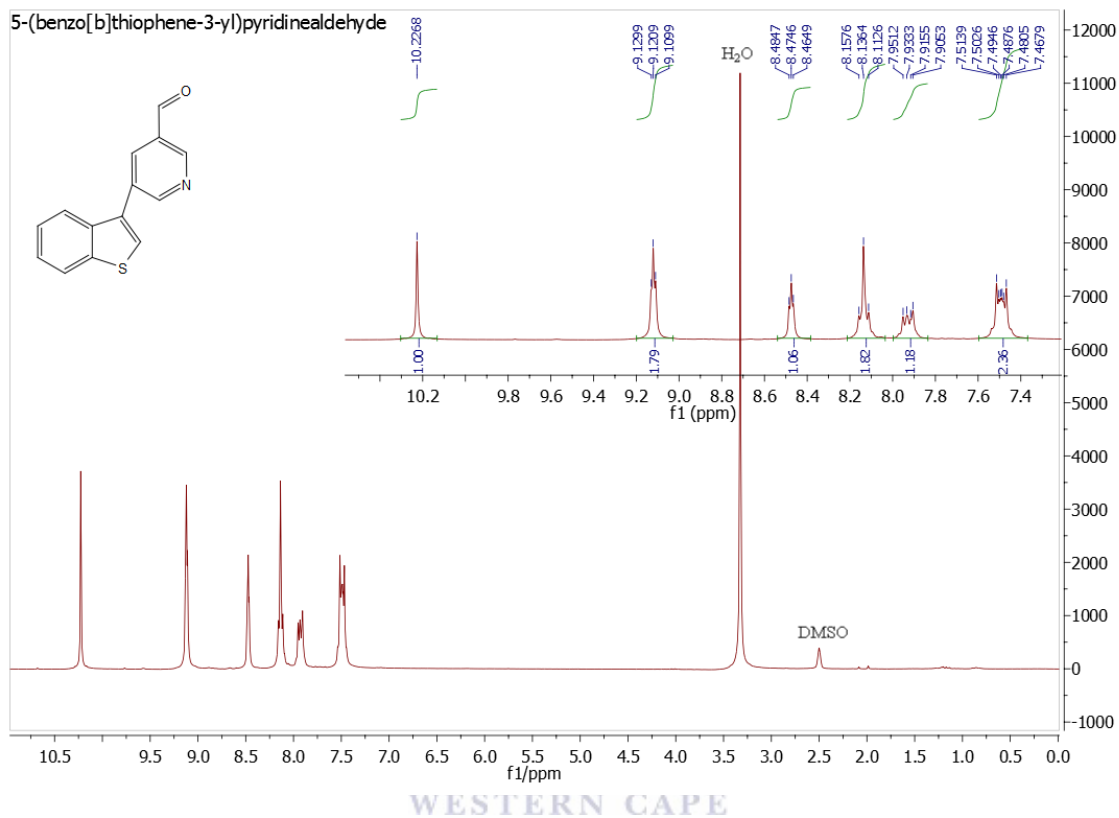
Figure 7.3: ^{1}H NMR (500 MHz, DMSO-d6) of 5-(Benzo[b]thiophene-3-yl) pyridinealdehyde (BTPA). Inset show the expanded region.

292
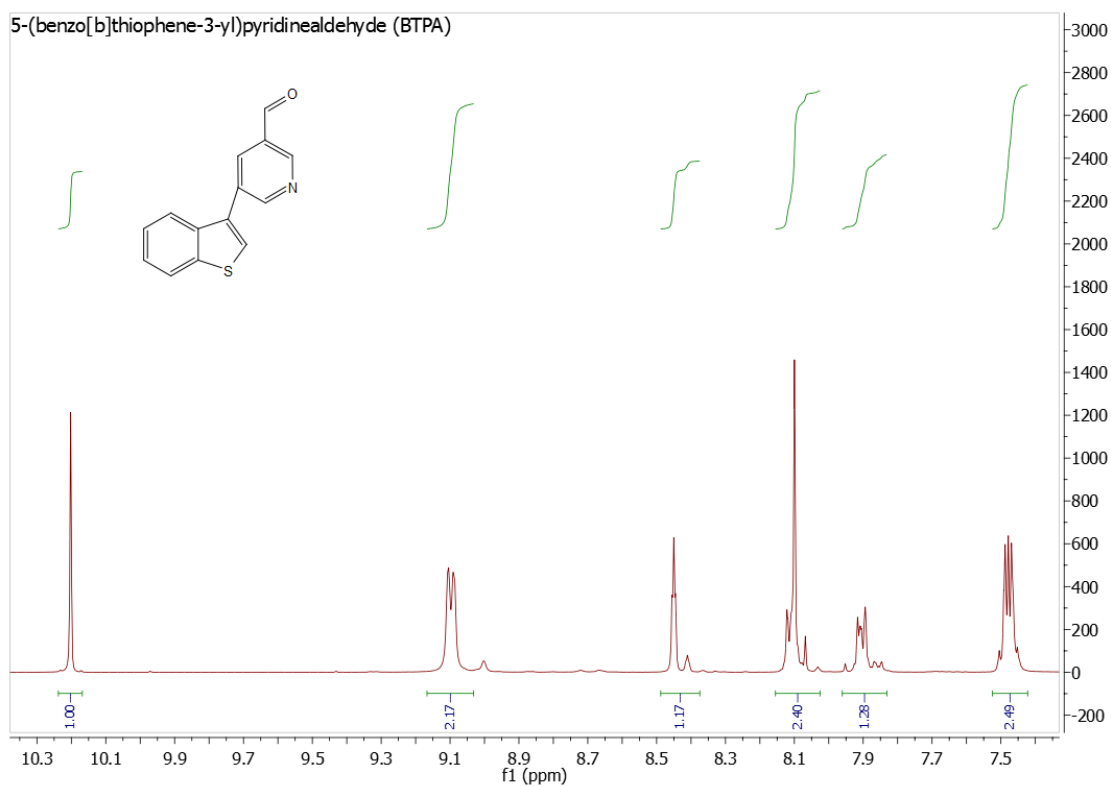
Figure 7.4: ^{1}H NMR (400 MHz, DMSO-d6) of 5-(Benzo[b]thiophene-3-yl) pyridinealdehyde (BTPA).
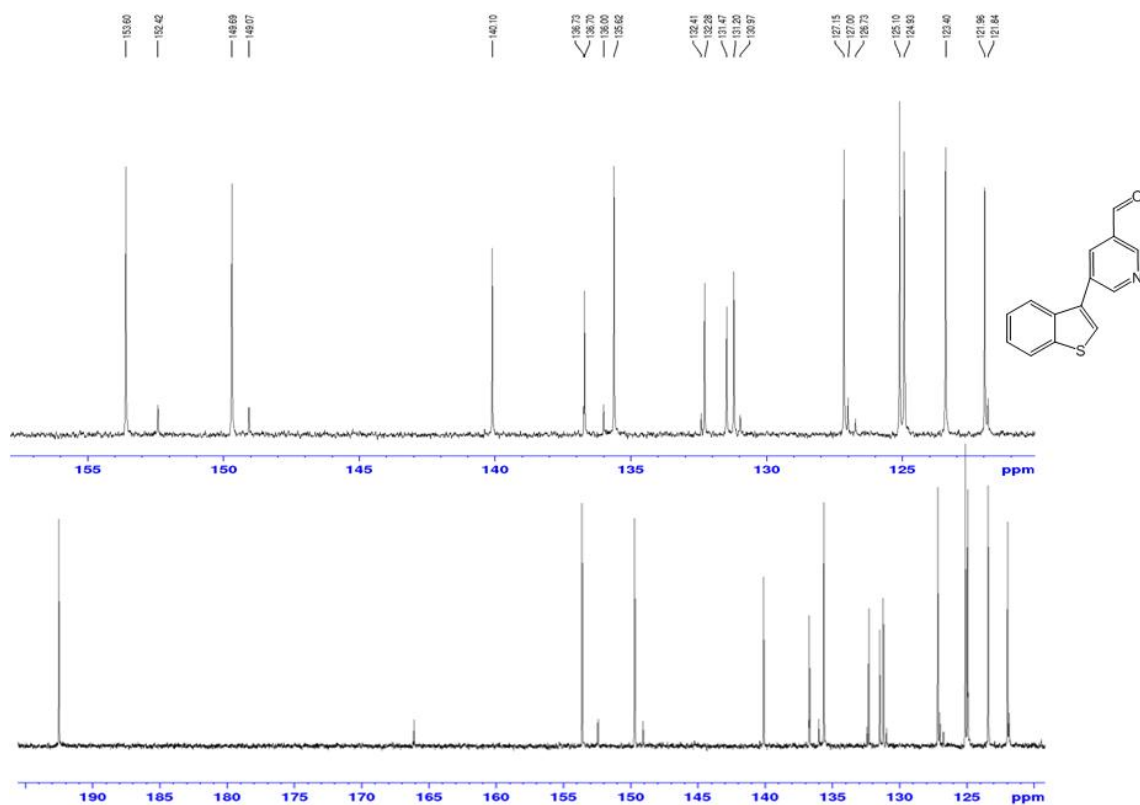
Figure 7.5: ^{13}C NMR (100 MHz, DMSO-d6) of 5-(Benzo[b]thiophene-3-yl) pyridinealdehyde (BTPA). Top spectrum shows the expanded region.

294
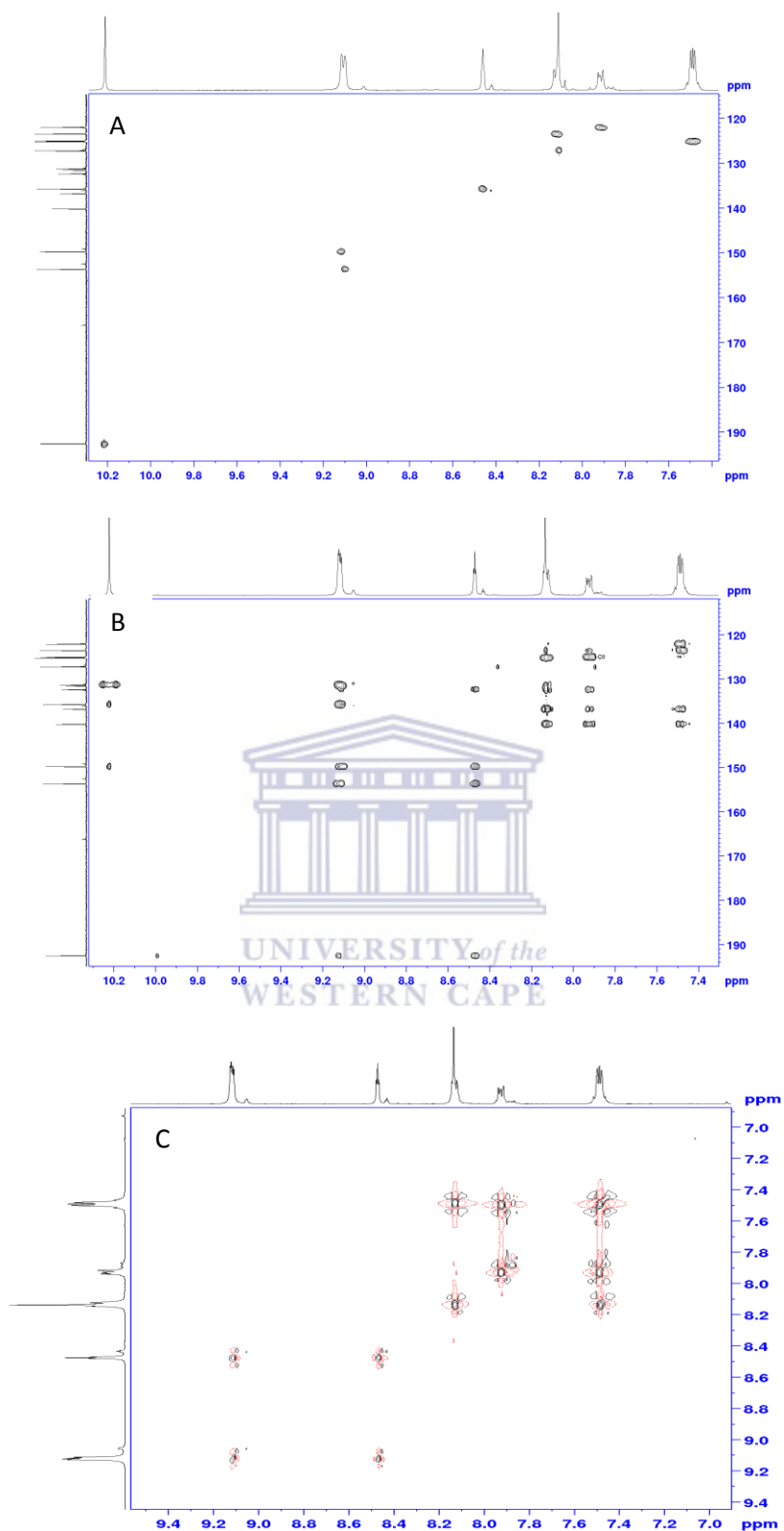
Figure 7.6: DOSY spectra of 5-(Benzo[b]thiophene-3-yl) pyridinealdehyde (BTPA) (a) HSQC, (b) sel HMBC and (c) COSY.

295
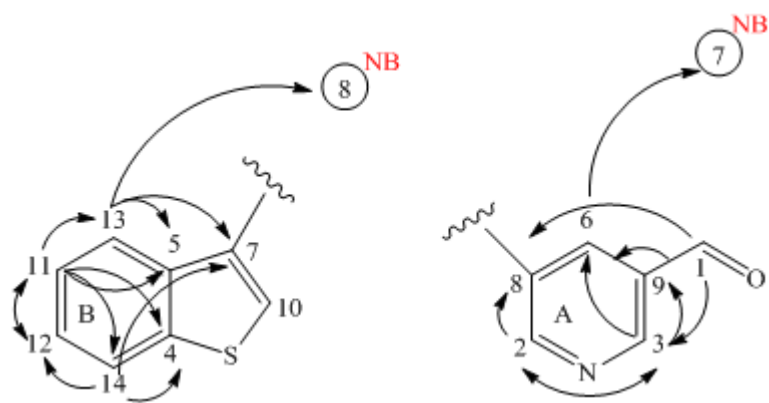
Figure 7.7: Schematic of BTPA structure showing NMR correlation of the pyridine part (A) and the Benzo[b]thiophene part (B).

Table 7.1: NMR spectra data analysis of 5-(Benzo[b]thiophene-3-yl)pyridinealdehyde (BTPA)

S/N	^{13}C (mult)	^{1}H (mult, J, int)	COSY	HMBC (sel)
1.	192.5 (d)	10.222 (s, 1H)		C-3, C-6, C-8
2.	153.6 (d)	9.101 (m, 1H[*])	H-6 (lr)	C-8, C-3
3.	149.7 (d)	9.114 (m, 1H[*])	H-6 (lr)	C-2, C-9, C-6
4.	140.1 (s)	-		
5.	136.7 (s)	-		
6.	135.6 (d)	8.472 (t, J = 2.0 Hz, 1H)	H-2/H-3	C-1, C-7, C-3, C-2
7.	132.3 (s)	-		
8.	131.5 (s)	-		
9.	131.2 (s)	-		
10.	127.1 (d)	8.134 (m, 1H[*])		
11.	125.1 (d)	7.487 (m, 1H[*])	H-14, H-11/H-12	C-4, C-5, C-12 (*lr*), C-13, C-14 (*lr*)
12.	124.9 (d)	7.487 (m, 1H[*])	H-14, H-11/H-12	C-4, C-5, C-11 (*lr*), C-13, C-14 (*lr*)
13.	123.4 (d)	8.121 (m (*br*), 1H[*])	H-11/H-12	C-4, C-5, C-7, C-8
14.	122.0 (d)	7.926 (m, 1H[*])	H-11/H-12	C-12, C-7, C-5 (*lr*), C-4

[*]: Overlap ^{1}H signals. In some cases we were able to differentiate the 2D correlations

lr: long range correlation, *br*: broad range correlation
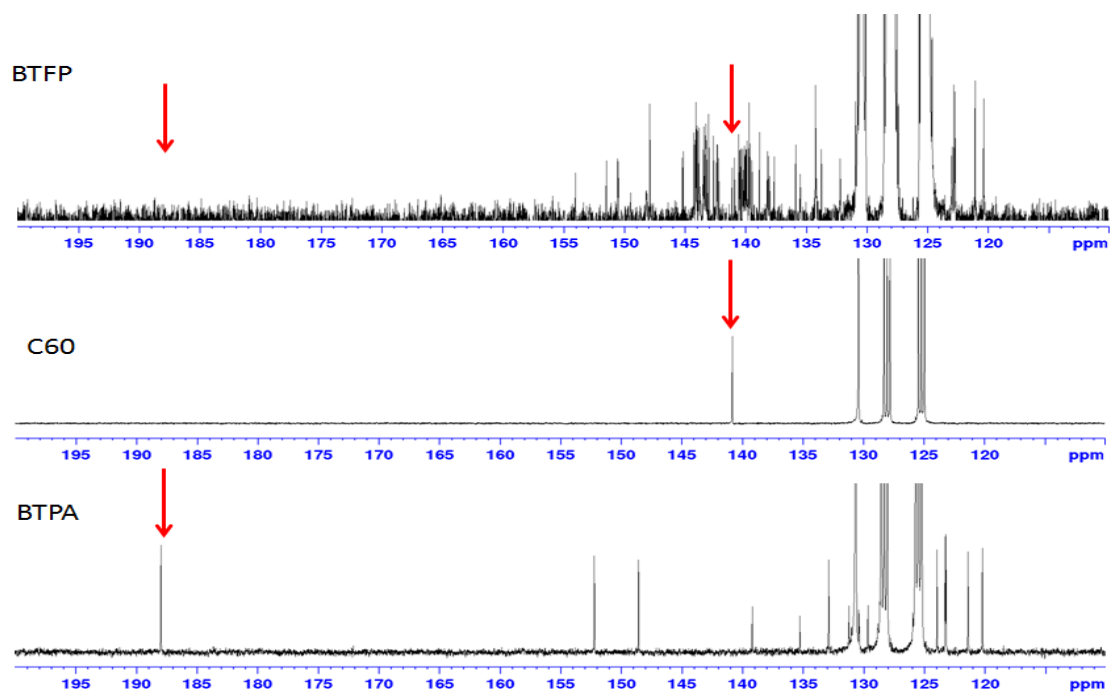
Figure 7.8: ^{13}C NMR (100 MHz, 1, 2-DCB-d4) of BTPA, C$_{60}$ and BTFP.
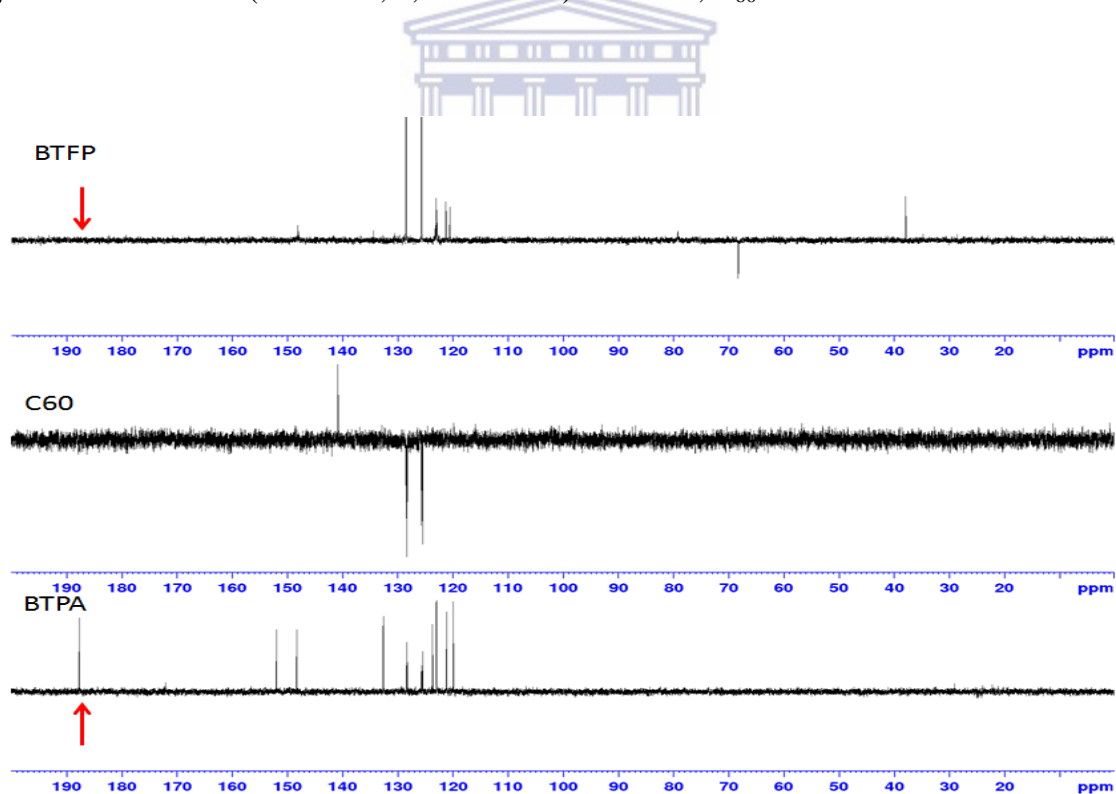
Figure 7.9: DEPT signal of BTPA, C$_{60}$ and BTFP.

298

The ^{1}H NMR data also shows the loss of the aldehyde signal when forming the conjugate (**Figure 7.10**). ^{1}H NMR spectra show the -CH$_2$ protons of the pyrrolidine ring as two doublets (J= 9.6 Hz) at 4.37 and 5.05 ppm respectively and a -CH proton singlet at 5.14 ppm (**Figure 7.11**) and a slight shift in signal of BTFP in relation to C$_{60}$ and BTPA (**Figure 7.12**). Protons of the methyl group (-CH$_3$) attached to the nitrogen atom of the pyrrolidine ring, appear as a singlet around 2.86 ppm.
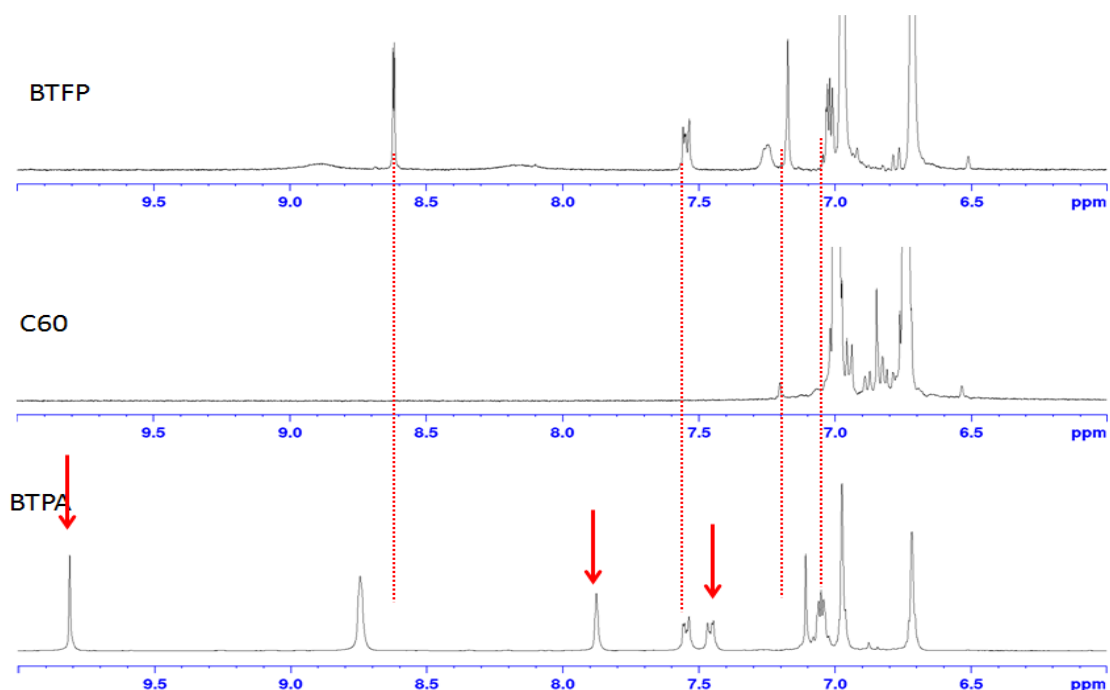
Figure 7.10: ^{1}H NMR (400 MHz, 1,2-DCB-d4) of BTPA, C$_{60}$ and BTFP.

299
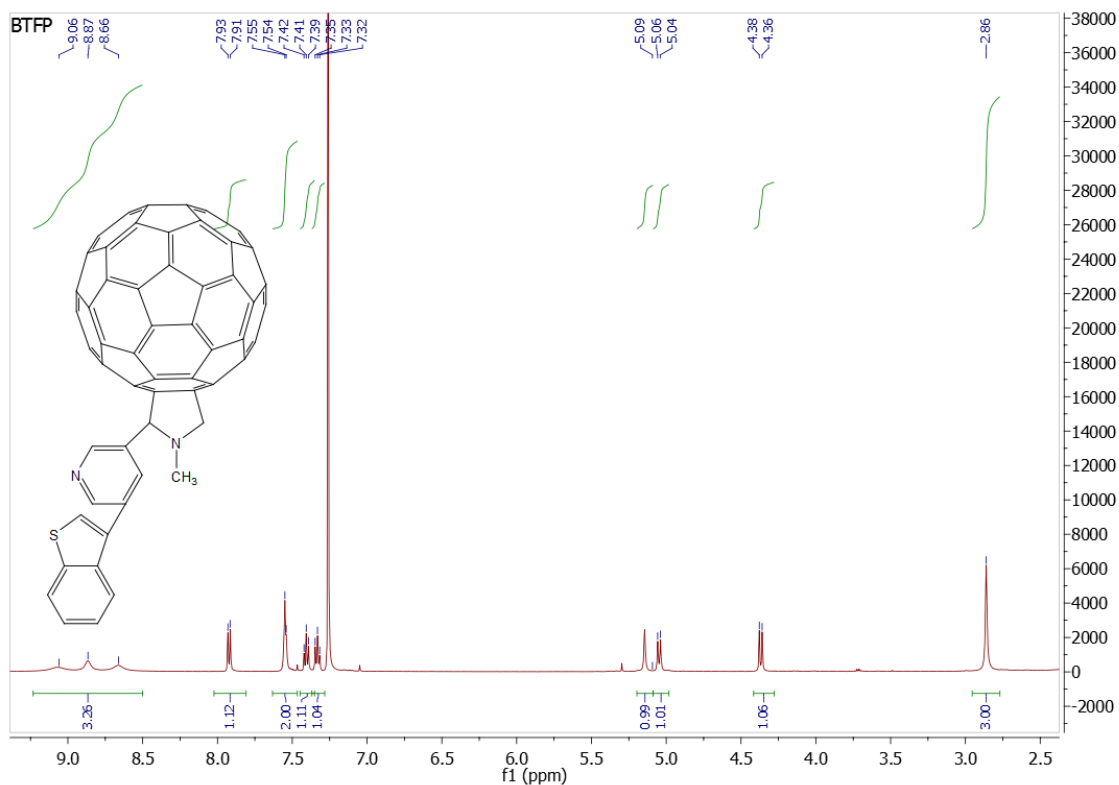
Figure 7.11: ^{1}H NMR (500 MHz, CDCl$_3$/CS$_2$) showing -CH$_3$, -CH$_2$ and -CH signals of the pyrrolidine ring of BTPF. The region between 2.6 and 5.2 ppm of the spectrum highlights the presence of the protons of the pyrrolidine ring. The signals between 6.5 and 8.8 ppm are ascribed to the protons of the organic framework attached to the C$_{60}$.
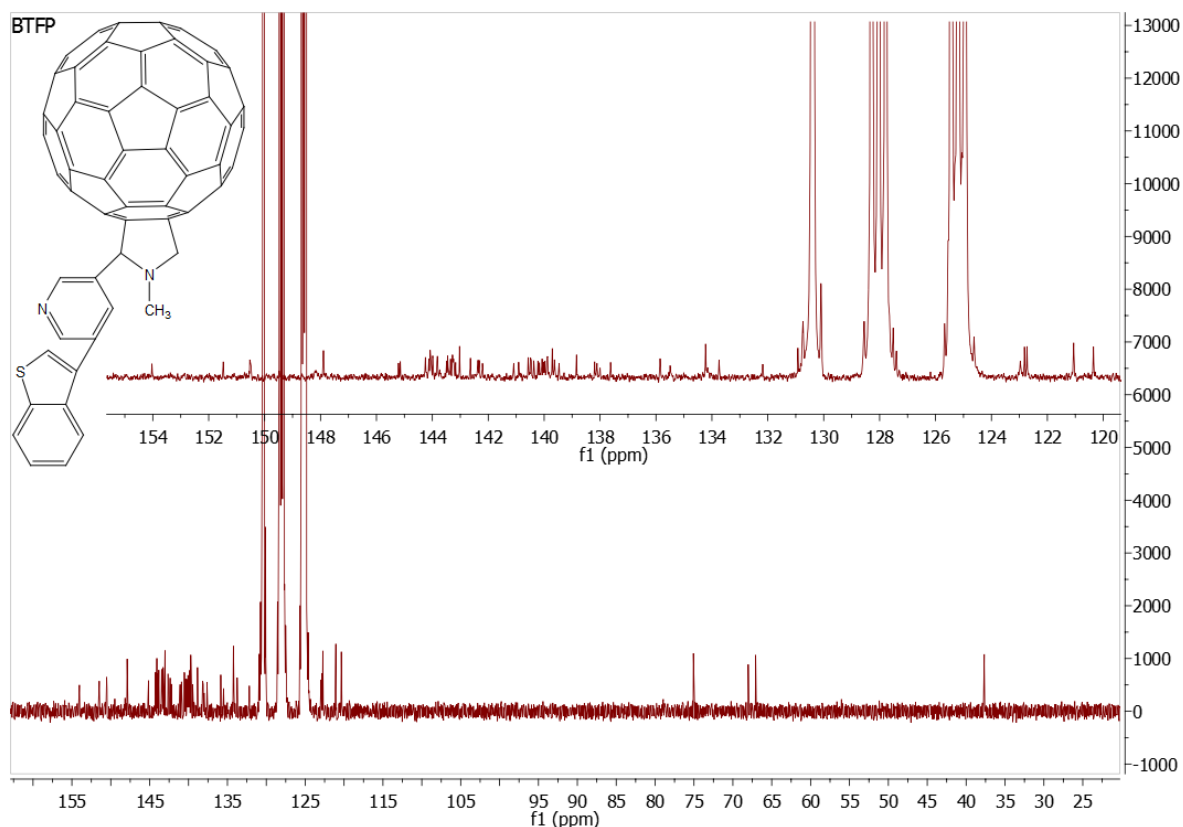
Figure 7.12: ^{13}C NMR (100 MHz, 1,2-DCB) of BTPF.
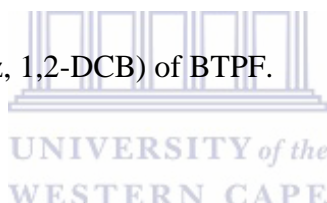
7.3.1.2 Fourier Transform Infra Red (FTIR) and Mass Spectroscopy (MS) of BTPA and BTFP

FTIR of BTPA (**Figure 7.13**), confirms the presence of the pyridine ring and the carbonyl group with stretching frequencies at 1650 and 1696 cm^{-1}, respectively. BTFP, on the contrary, did not yield any signal for the carbonyl group, while pyridine signals are still present, albeit weak (**Figure 7.14**), hinting at the success of the cycloaddition reaction. Prominent fullerene C$_{60}$ IR-active peaks at 527 and 577 cm^{-1} modes associated with the primary radial motion of the carbon atoms; and 1,184, 1,426 cm^{-1} modes associated with the tangential motion of the carbon atoms [7, 20] were also observed in BTFP. Mass

301

spectroscopy confirmed the product BTPA at m/z = 240.04 and m/z = 258.05, corresponding

to the hydrated product [M+H$_2$O] (**Figure 7.15**).
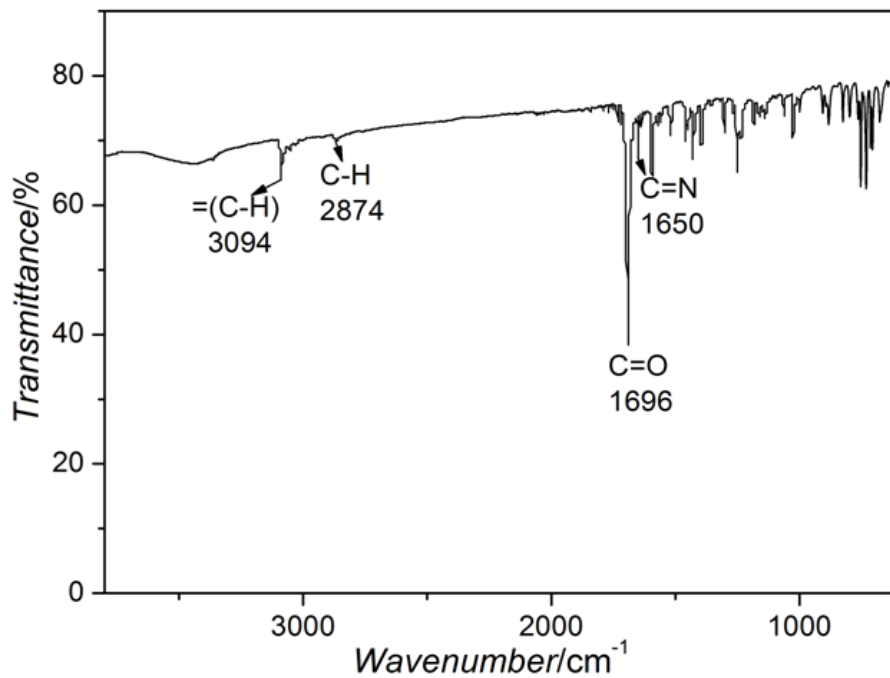
Figure 7.13: FTIR of 5-(Benzo[b]thiophene-3-yl) pyridinealdehyde (BTPA).

302
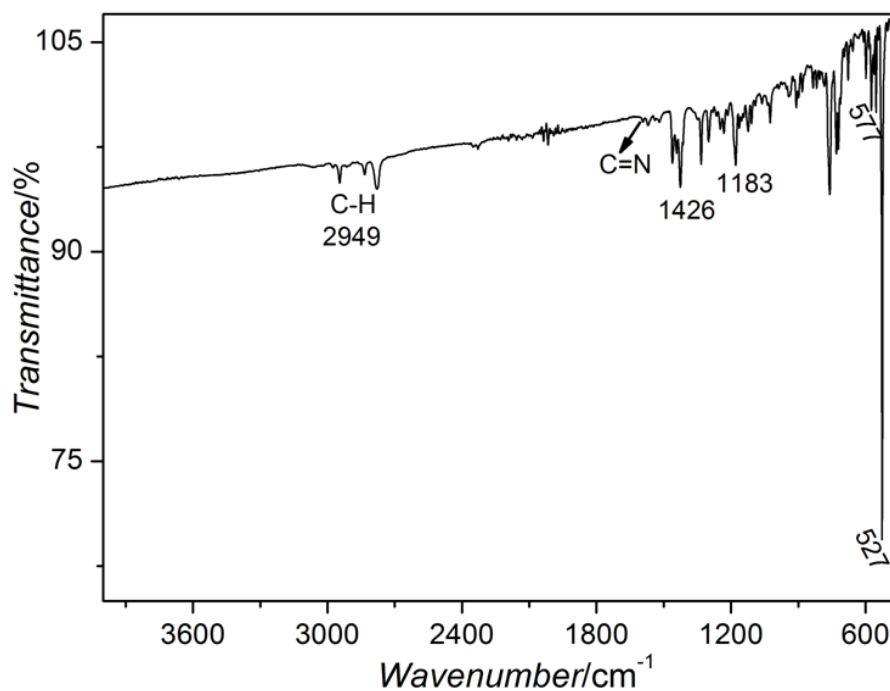
Figure 7.14: FTIR Spectroscopy of 3-(Benzo[b]thiophene-3yl)-5-fulleropyrrolidinepyridine (BTFP).
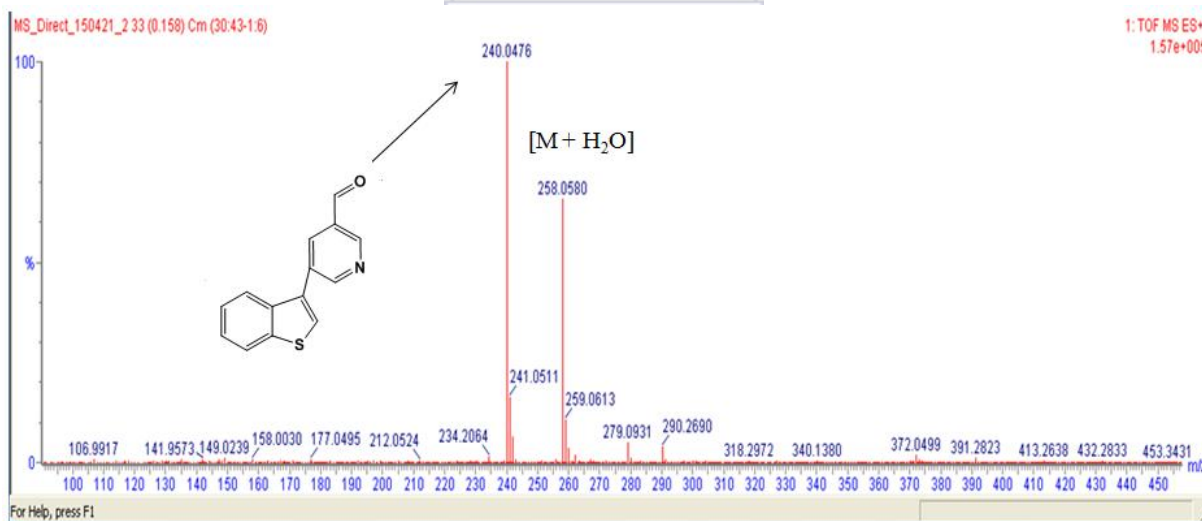
Figure 7.15: ESI-MS of 5-(Benzo[b]thiophene-3-yl) pyridinealdehyde (BTPA). Source: ESI positive, cone voltage 15 V, Lock mass: leucine encephalin.

303

Molecular weight of BTFP was confirmed using MALDI-TOF (**Figure 7.16**). A mass of 986.917 g/mol was found and this is exactly similar to the calculated mass of 986.337 g/mol. The themogravimetric analysis of BTFP under nitrogen atmosphere (heating rate: 10°C/min shows a 1% weight loss at about 248°C and a first steep of 5% weight loss at 340°C (**Figure 7.17**). This first steep can be attributed to the thermal decomposition of the attachment on C_{60}. The second steep weight loss observed at about 470°C is attributed to the thermal decomposition of the fullerene cage [21]. The 1% weight loss at 248°C demonstrates an excellent thermal stability for BTFP.
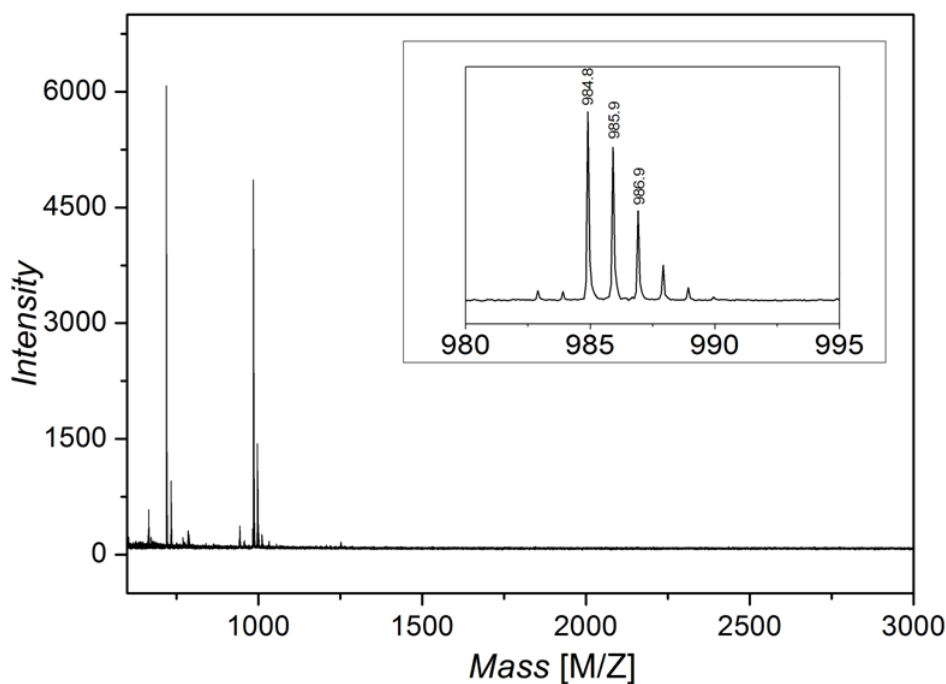
Figure 7.16: MALDI TOF mass spectra of 3-(Benzo[b]thiophene-3-yl)-5-fulleropyrrolidine pyridine (BTFP) using 2′,4′,6′-Trihydroxyacetophenone monohydrate as matrix. Inset show the expanded region. Calculated mass = 986.337 g/mol; Found mass = 986.917 g/mol.
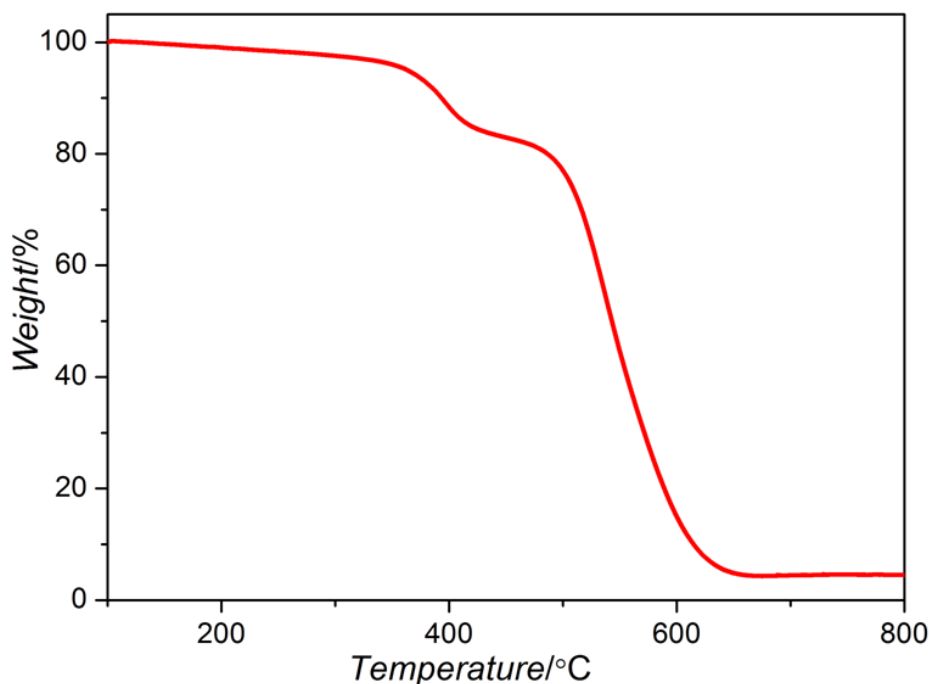
Figure 7.17: Themogravimetric analysis of BTFP under nitrogen atmosphere (heating rate: 10°C/min.

7.3.1.3 UV-Vis and Photoluminescence Spectroscopy of Donor (F8BT and F8T2) and Acceptors (PCBM and BTFP)

The UV-Vis spectrum of BTPA (**Figure 7.18**) is dominated by the $\pi \rightarrow \pi*$ transition. The absorption spectra of BTFP in dichloromethane and chloroform are shown in **Figure 7.19 a and b**, respectively, and compared to PCBM. Similar to PCBM, the electronic spectra of BTFP is dominated by the $\pi \rightarrow \pi*$ transitions with strong absorption in the UV region which corresponds to the allowed electronic transition in the fullerene core [22]. In dichloromethane, the two spectra show analogous absorptions, except for the rise of a peak ("peak a") at ca 310 nm for BTFP. The situation changed in chloroform. BTFP showed a broad and structured absorption with three major peaks located at 290 and 307 nm, and a shoulder at 329 nm covering a wider range of the spectrum compared to PCBM with two major

305

peaks and a shoulder in chloroform. The absorption maximum of BTFP was observed at 290 nm while that of PCBM was seen at 260 nm. This structure and bathochromic effect in the maximum wavelength of BTFP is believed to be influenced by the grafted benzo[b]thiophene-3-yl)pyridine. The absorptions of BTFP in dichloromethane located at 256, 310 and 430 nm show typical features characteristic of a mono-fulleropyrrolidine derivative [23-24]. The extremely sharp peak around 432 nm for BTFP and PCBM in both dichloromethane and chloroform are typical for fullerene derivatives with [6,6]-bridged carbons [25-26].

To investigate the electron accepting properties of BTFP, the photoluminescence (PL) spectra of different donor-acceptor blends was assayed. For donors, we employed poly[(9,9-di-*n*-octylfluorenyl-2,7-diyl)-*alt*-(benzo[2,1,3]thiadiazol-4,8-diyl)]   (F8BT)   and   poly[(9,9-dioctylfluorenyl-2,7-diyl)-*co*-bithiophene](F8T2). BTFP was used as acceptor and was compared to benchmark material, PCBM. The PL responses of the F8BT and F8T2 samples blended with PCBM and BTFP were measured at an excitation wavelength of 450 and 458 nm for blends based on F8BT and F8T2 respectively. PL quenching is described by the ratio of the emission intensity of the polymer/fullerene blend normalized over the emission intensity of the pristine polymer. The PL quenching of both acceptors differs as can be seen in **Figures 7.19 c-d** (**inset**). Although PCBM showed a better quenching ability in the case of the investigated polymers, the structured strong absorption and bathochromic shift in the maximum wavelength of BTFP compared to that of PCBM in chloroform may contribute to light absorption of a suitable donor thereby enhancing efficiency.
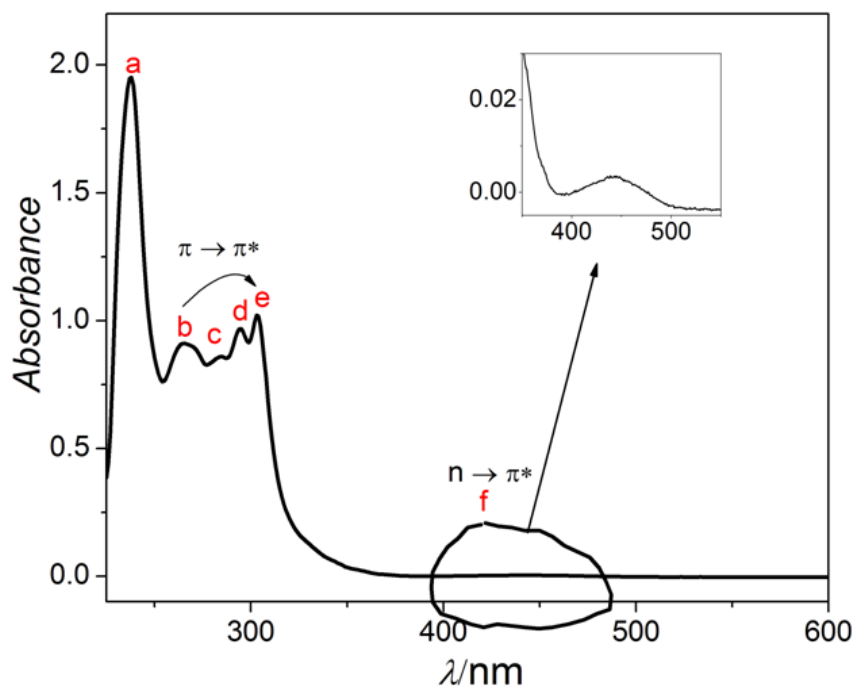
Figure 7.18: UV-Vis spectrum of BTPA in dichloromethane. Inset is the visible region absorption.
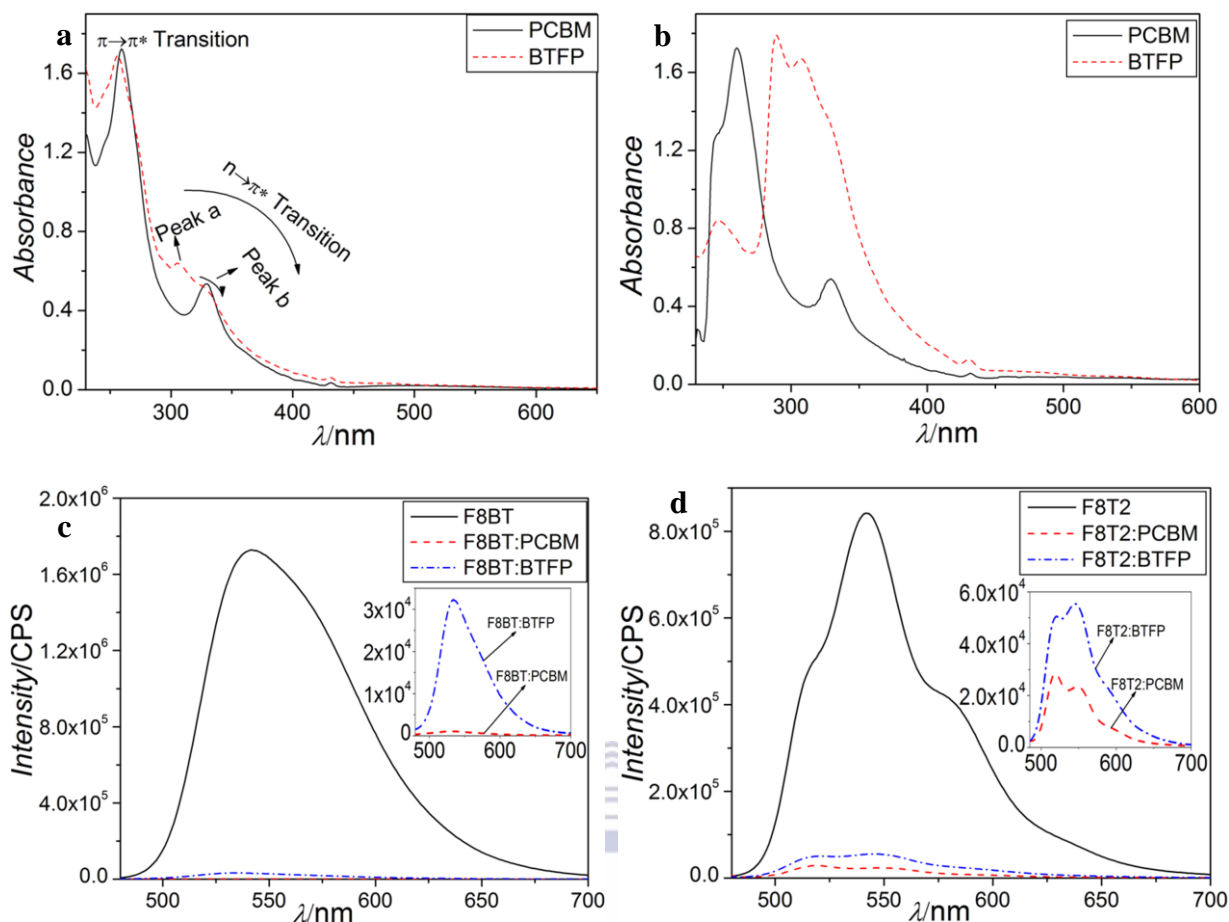
Figure 7.19: UV-Vis of BTFP and PCBM in (a) Dichloromethane and (b) Chloroform. The PL quenching spectra of (c) F8BT and (d) F8T2 (the acceptors are PCBM and BTFP).

7.3.2   Microscopic Studies

Figure 7.20 shows the morphology of BTPA crystals observed by scanning electron microscopy (SEM). The product shows a needle-like morphology and its energy dispersive spectroscopy (EDS) spectrum analysis (**Figure 7.21**) is compatible with the structure of the compound. EDS analysis of BTFP (**Figure 7.22**) also corresponds with the structure with 93.72% C, 5.18% N and 1.1% S. Furthermore, a comparison between the morphologies of molecular crystals of fullerene C_{60}, BTPA and BTFP is made using SEM and transmission electron microscopy (TEM) in **Figure 7.23 and 7.24** respectively.
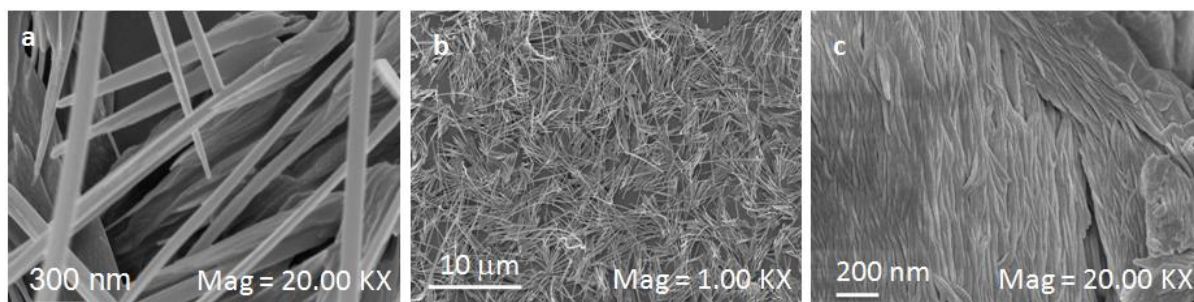
Figure 7.20: High resolution SEM images of (a) BTPA thin film at 20000 magnification, (b) BTPA thin film at 1000 magnification and (c) BTPA solid/powder sample.
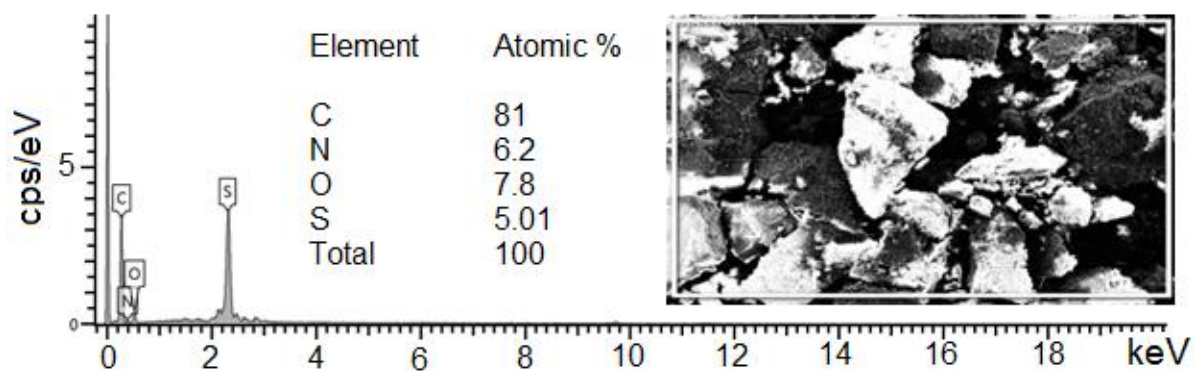
Figure 7.21: EDS spectra of 5-(Benzo[b]thiophene-3-yl) pyridinealdehyde (BTPA).
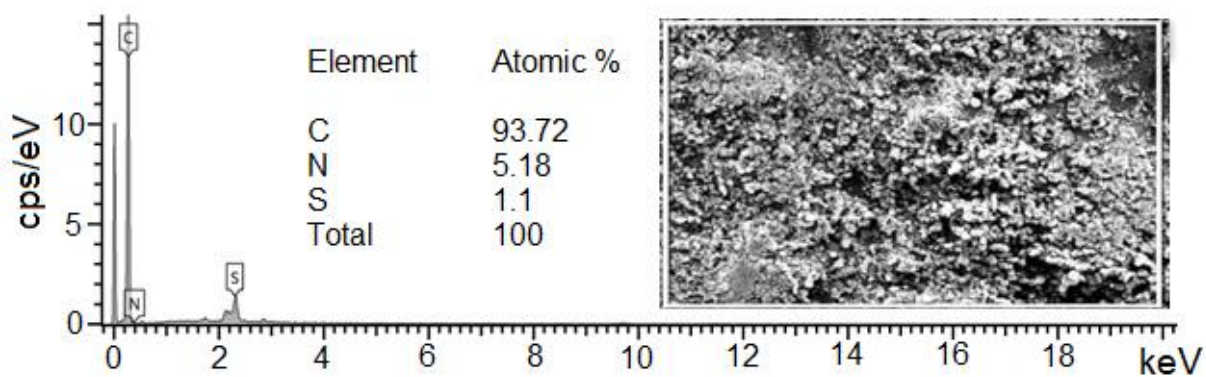
Figure 7.22: EDS spectra of 3-(Benzo[b]thiophene-3yl)-5-fulleropyrrolidinepyridine (BTFP).
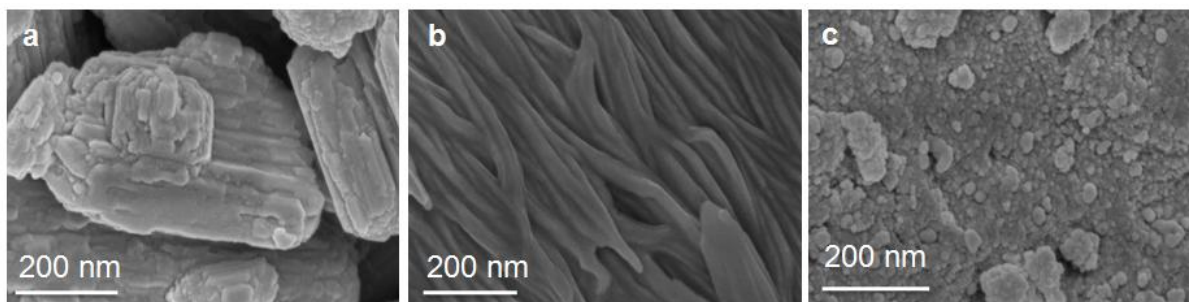
Figure 7.23: High resolution SEM images of (a) fullerene C_{60}, (b) BTPA and (c) BTFP at 50000 magnification.
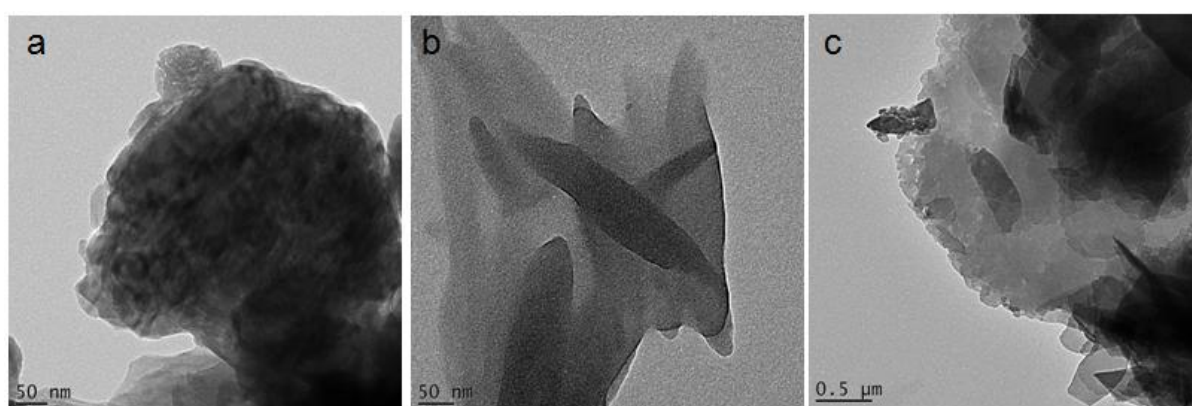
Figure 7.24: High resolution TEM images of (a) fullerene C_{60}, (b) BTPA and (c) BTFP.

7.3.3 Electroanalysis of BTFP and PCBM

The redox behavior of BTFP with that of the parent C_{60} and PCBM was determined by cyclic voltammetry (CV) under identical conditions. The CVs (**Figure 7.25**) showed 4 reversible reduction waves (**a-d** in the range -2.2 to 0 V vs Ag/AgCl) corresponding to the reduction of the fullerene cage. As shown in **Table 7.2**, the CVs of PCBM and BTFP showed a cathodic shift in all well defined reduction waves in comparison to C_{60}. Both systems show identical cathodic shift for reduction potentials **a** and **b** while **c** showed a slight difference. The voltammogram showed a comparable first reduction wave for PCBM and BTFP with

310

distinctive difference in comparison to C_{60}. The first reduction wave is indicative of the electron acceptor strength of the compounds. C_{60} (± 0.50 V) appeared to be a better electron acceptor than PCBM (± 0.61 V) and BTFP (± 0.62 V), while there is the possibility of electron transfer with PCBM and BTFP due to the cathodic shifts.
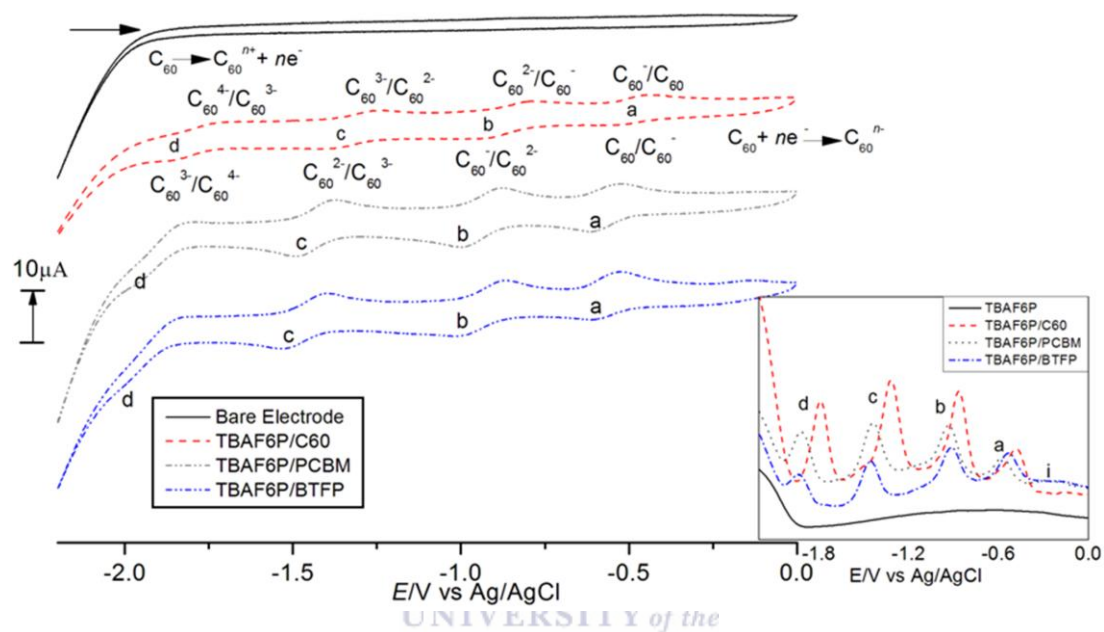
Figure 7.25: CV of C_{60}, PCBM and BTFP in TBAPF$_6$ with a GCE at 50 mV/s. Inset) Square wave voltammetry

Table 7.2: Cathodic shifts of PCBM and BTFP in relation to reduction potentials of C_{60}

	Cathodic Shift				
	a	**b**	**c**	$E_{\text{red}}^{\text{on}}$ **(V)**	**LUMO (eV)**
C_{60}				0.29	4.11
PCBM	0.22	0.10	0.15	-0.47	3.93
BTFP	0.22	0.10	0.22	-0.47	3.93

Experimental conditions: V vs. Ag/AgCl; TBAPF$_6$ (0.1 M) as supporting electrolyte; 1, 2-DCB:MeCN (4:1) as solvent; 100 mV/s; GCE as working electrode.

311

The Square wave voltammetry (SWV) on the other hand revealed 5 peak potentials for C_{60}, PCBM and BTFP (**Figure 7.25 (inset)**). These peak potentials and their relative cathodic shifts are well defined in the SWV using Pt as the working electrode (**Figure 7.26**). The SWV better resolved **d** and revealed a new peak **i** in C_{60}, PCBM and BTFP. The onset reduction potentials E_{red}^{on} were estimated at the potential at which the current response begins to deviate from the baseline, recording -0.47 for both PCBM and BTFP. From the E_{red}^{on}, the LUMO energy levels were calculated according to the equation $-(E_{red}^{on} + 4.4)$ eV [27]. The result shows both PCBM and BTFP to be energetically identical.

Several works on the electrochemical properties and behaviour of C_{60} with 3 to 6-electron reduction depending on the solvent, supporting electrolyte and temperature of reaction have been reported (**Table 7.3**). These studies show that the choice of solvent, supporting electrolyte, temperature and a host of other factors has a profound effect on the value of the reduction potential of fullerenes. Therefore, one should compare the relative differences in those potentials, rather than evaluate their absolute values.

312
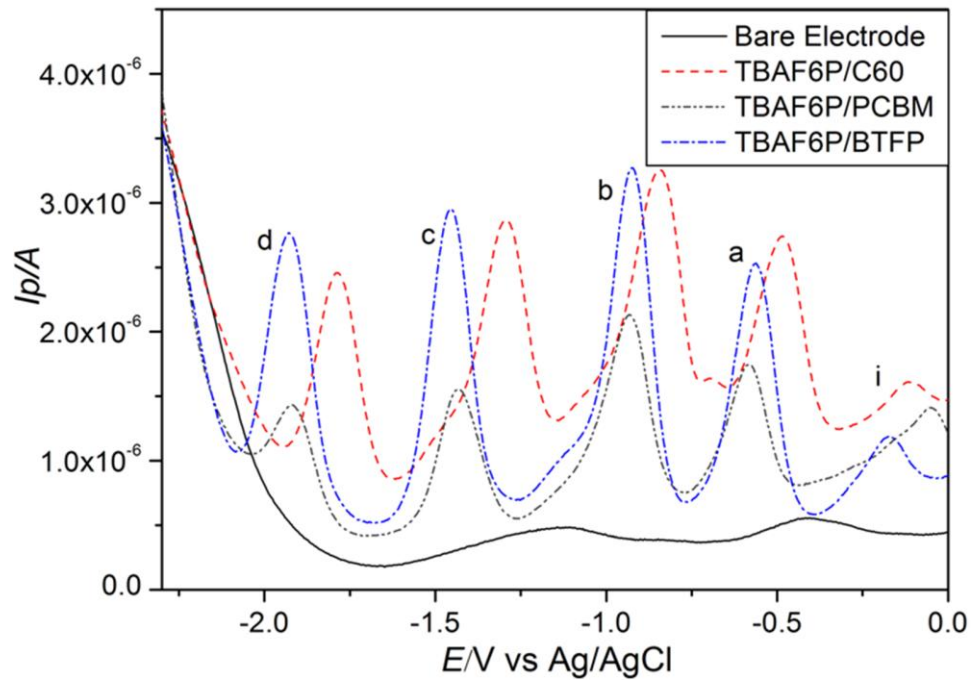
Figure 7.26: Square wave voltammetry of PtE, C_{60}, PCBM and BTFP. Conditions are as in

Figure 7.25.

313

Table 7.3: Redox potentials of several reports on C_{60}

E_1 (V)	E_2 (V)	E_3 (V)	E_4 (V)	E_5 (V)	E_6 (V)	Solvent	Supporting Electrolyte	Temp. °C	Ref. Electrode	Scan Rate (mV/s)	Ref.
-0.40	-0.76	-1.25	-	-	-	ODCB	TBNBF$_4$	RT	Ag/AgCl	100	[28]
-0.21	-0.81	-1.39	-	-	-	THF	TBNBF$_4$	RT	Ag/AgCl	100	[28]
-0.33	-0.73	-1.22	-	-	-	CH$_2$Cl$_2$	TBNBF$_4$	RT	Ag/AgCl	100	[28]
-0.33	-0.82	-1.25	-	-	-	PhCN	TBNBF$_4$	RT	Ag/AgCl	100	[28]
-0.44	-0.82	-1.25	-1.72	-	-	CH$_2$Cl$_2$	TBNBF$_4$		SCE	2000	[29]
-0.98	-1.37	-1.87	-2.35	-2.85	-3.26	MeCN:Tol 1:5.4	TBAPF$_6$	-10		100	[30-31]
-0.34	-0.76	-1.28	-	-	-	Pyridine	(TBA)ClO$_4$	RT	SCE	100	[32]
-0.49	-0.88	-1.33	-	-	-	CH$_2$Cl$_2$	(TBA)ClO$_4$	RT	SCE	100	[32]
-0.26	-0.72	-1.31	-1.85	-	-	DMF	(TBA)ClO$_4$	RT	SCE	100	[32]
-0.60	-1.01	-1.46	-	-	-	ODCB:MeCN 4:1	TBNPF$_6$	RT	Ag/AgCl	100	[33]
-0.50	-0.88	-1.34	-1.80	-	-	ODCB:MeCN 4:1	TBAPF$_6$	RT	Ag/AgCl	100	This work

314

7.3.4 Photovoltaic Application Response of BTFP

The new material was processed as acceptor combined with poly(3-hexylthiophene) (P3HT) and investigated as a potential electron accepting material for organic solar cells. The bulk heterojunction photovoltaic device is constructed in a configuration of ITO/PEI/Donor:Acceptor/MoOx/Ag. P3HT in combination with BTFP and PCBM was selected as the active layer components where P3HT served as the donor and BTFP and PCBM individually served as the acceptors. The photovoltaic responses of the device from different solvents and conditions are given in **Figure 7.27, 7.28 and 7.29** with the external quantum efficiency given in **Figure 7.28 and 7.29.**

The photocurrent characteristics (*I-V* curve) measured under white light illumination of intensity 100 mW/cm^2 and EQE of the device with the best response for P3HT:BTFP and P3HT:PCBM were compared as depicted in **Figure 7.27** and **Figure 7.29** respectively. The short-circuit current (J_{sc}), open-circuit voltage (V_{oc}), fill factor (*FF*) and power conversion efficiency (η) of each device were extracted from their respective current-voltage (*I–V*) curves and summarized in **Table 7.4**. A relatively poor photovoltaic response was observed for cells with BTFP as acceptor. This can be attributed to the poor solubility of BTFP which leads to inaccurate ratio of P3HT:BTFP and inability to form a proper bulk heterojunction layer. The inability to form a proper bulk heterojunction layer in principle will lead to inefficient exciton generation and thereby lowering the efficiency of the device. Microscopic images (**Figure 7.30**) also confirm immiscibility of the P3HT:BTFP in the active layer, thereby resulting in poor film forming ability and making bulk heterojunction layer impossible. However, the mobility of BTFP may be comparable to that of PCBM. The injection current measured in devices gives information about the mobility of the acceptor.

315

High injection current equals good mobility. Devices made from BTFP acceptor show good injection current. Therefore, improvement in the solubility of BTFP will most likely improve the photovoltaic properties. As can be seen from the microscopic images and **Table 7.4**, the efficiency of devices made from P3HT:BTFP improved with improvement in the active layer film.
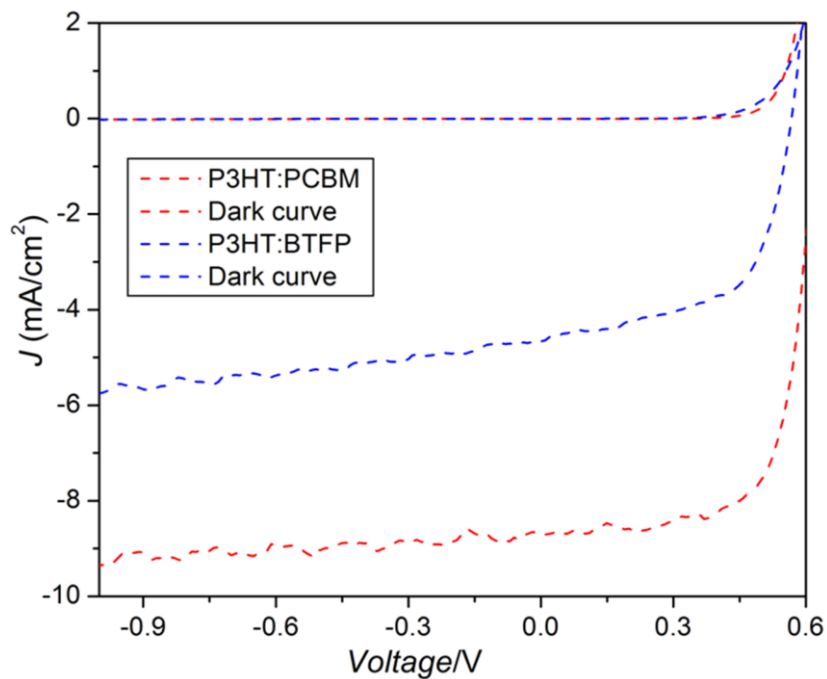
Figure 7.27: Current-voltage (*I–V*) curves of P3HT:PCBM and P3HT:BTFP.
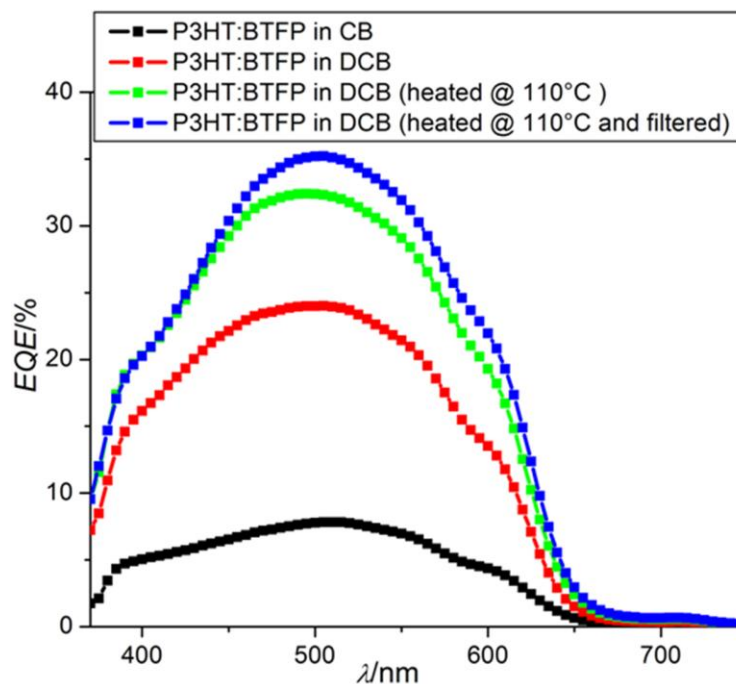
Figure 7.28: External quantum efficiency (EQE) of P3HT:BTFP @ different solvents and conditions.
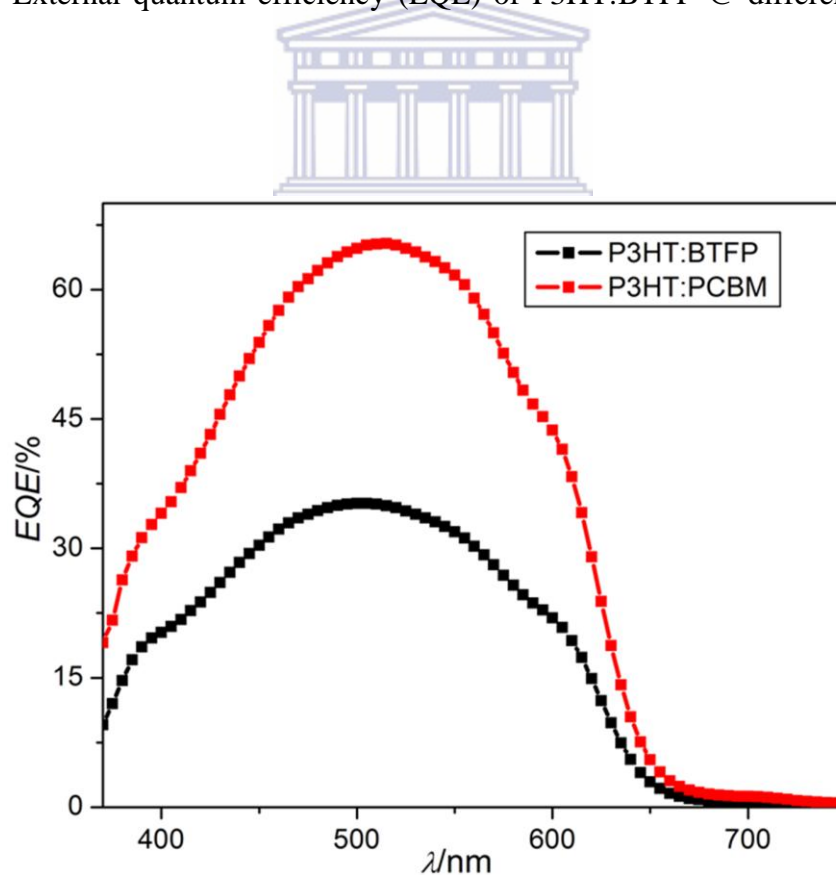
Figure 7.29: External quantum efficiency (EQE) of P3HT:PCBM and P3HT:BTFP.

317
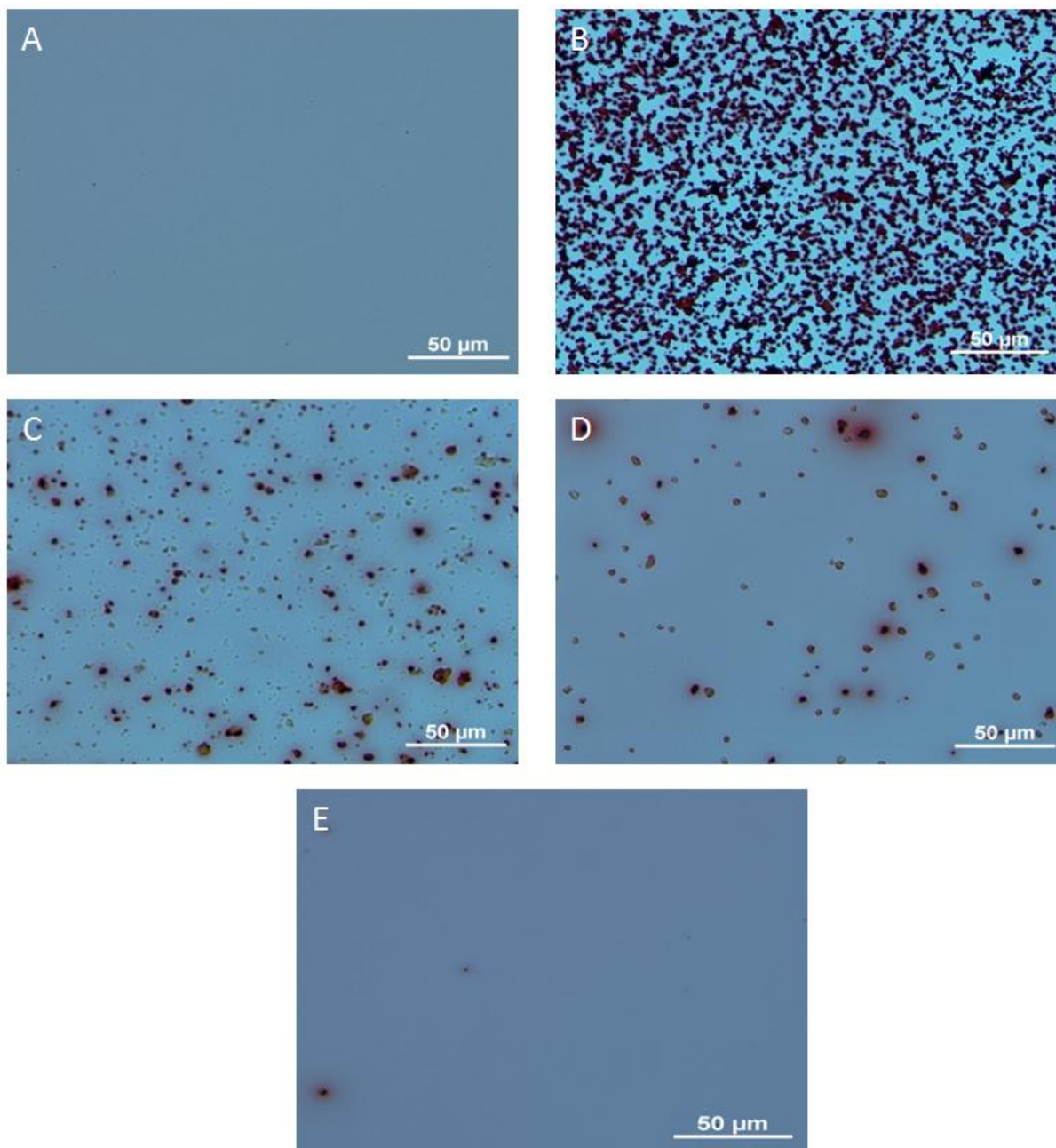
Figure 7.30: A) P3HT:PCBM in CB; B) P3HT:BTFP in CB, C) P3HT:BTFP in DCB, D) P3HT:BTFP in DCB (solution heated @ 110°C for 2 h), E) P3HT:BTFP in DCB (solution heated @ 110°C for 2 h and filtered. Filter made by Whatmann, membrane-PTFE, size-0.45 μm).

318

Table 7.4: Photovoltaic responses of P3HT:PCBM and P3HT:BTFP in different solvents and conditions

Name	I_{sc} As meas	J_{sc} [mA/cm²]	V_{oc} [V]	*FF*	Eff [%]	Eff [%] EQE corrected	-2 [mA/cm²]	+2 [mA/cm²]
P3HT:BTFP in CB	0.09476	1.5794	0.30	0.37	0.17	0.10	-1.827415	5.57
P3HT:BTFP in DCB	0.28439	2.9624	0.54	0.51	0.82	0.79	-3.408733	148.64
P3HT:BTFP in DCB (soln. heated @ 110°C	0.21742	3.6236	0.58	0.52	1.10	1.17	-4.584863	186.00
P3HT:BTFP in DCB (soln. heated @ 110°C and filtered)	0.27963	4.6605	0.57	0.59	1.57	1.42	-5.751600	231.16
P3HT:PCBM in CB	0.71598	8.5236	0.62	0.71	3.76	3.48	-9.479476	1190.56

319

7.4 Conclusion

In conclusion, a novel organic compound (BTPA), with nano-structured morphology was synthesized and applied for an extremely rapid functionalization of C_{60} to obtain process-able fullerene derivative (BTFP). BTPA was used to improve C_{60} to obtain properties comparable to those of PCBM. The study showed that PCBM and BTFP exhibit about the same first reduction potential in (0.1 M) $TBABF_6$ supporting electrolyte (-0.61 and -0.62 V, respectively), with a LUMO of 0.47 eV in both cases. This makes BTFP energetically PCBM-like. However, they differ in their luminescence properties and this may have positive influence on suitable donor for photovoltaics. Although the solubility of this material needs to be improved, it shows a promise for electronic applications and may contribute to the development of new technologies. Works on improving the solubility is underway and achieving this will make BTFP compete with PCBM with an advantage of cost and ease of synthesis.

320
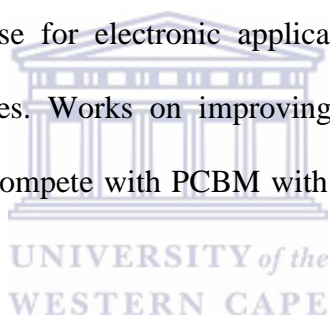
7.5   References

[1]   M. Bodner, J. Patera and M. Szajewska, "Breaking of Icosahedral Symmetry: C60 to C70," *PLoS One,* 9 (**2014**) 1-5.

[2]   Y. Liu, X. Du, J. Cao, W. Zhang, S. Chen, Z. Xiao, X. Cai, Q. Zuo and L. Ding, "Facile syntheses of N-alkylaziridino[60]fullerenes and their application in polymer solar cells," *Synth. Met.,* 162 (**2012**) 1271 - 1278.

[3]   K. Lewandowska, B. Barszcz, A. Graja, A. Biadasz, B. Bursa, D. Wróbel, S.-T. Kim, T.-D. Kim and K.-S. Lee, "Molecular orientation in self-assembled layers of two functionalized fullerenes—Role of bromine atom at the end of alkyl chain," *Synth. Met.,* 162 (**2012**) 2134 – 2137.

[4]   M. Lehmann and M. Hîgel, "A Perfect Match: Fullerene Guests in Star-Shaped Oligophenylenevinylene Mesogens," *Angew. Chem. Int. Ed. 2015, 54, 4110–4114; Angew. Chem.,* 127 (**2015**) 4183–4187.

[5]   L. Moreira, J. Calbo, B. M. Illescas, J. Arago, I. Nierengarten, B. Delavaux-Nicot, E. Orti, N. Martin and J.-F. Nierengarten, "Metal-Atom Impact on the Self-Assembly of Cup-and-Ball Metalloporphyrin–Fullerene Conjugates," *Angew. Chem. Int. Ed.,* 54 (**2015**) 1255 –1260.

[6]   M. Anafcheh and R. Ghafouri, "Mono- and multiply-functionalized fullerene derivatives through 1,3-dipolar cycloadditions: A DFT study," *Phys. E,* 56 (**2014**) 351–356.

[7]   H. Veisi, R. Masti, D. Kordestani, M. Safaei and O. Sahin, "Functionalization of fullerene (C60) with metformine to immobilized palladium as a novel heterogeneous and reusable nanocatalyst in the Suzuki–Miyaura coupling reaction at room temperature," *J. Mol. Catal. A: Chem.,* 385 (**2014**) 61–67.

321

[8] X. Zhang, Q. Wang, L.-H. Zou and J.-W. You, "Facile fabrication of titanium dioxide/fullerene nanocomposite and its enhanced visible photocatalytic activity," *J. Col. Interf. Sci,* 466 (**2016**) 56 - 61.

[9] J. Vávrová, M. Řezáčová and J. Pejchal, "Fullerene nanoparticles and their anti-oxidative effects: a comparison to other radioprotective agents " *J. Appl. Biomed.,* 10 (**2012**) 1-8.

[10] Y.-F. Gao, T. Yang, X.-L. Yang, Y.-S. Zhang, B.-L. Xiao, J. Hong, N. Sheibani, H. Ghourchian, T. Hong and A. A. Moosavi-Movahedi, "Direct electrochemistry of glucose oxidase and glucose biosensing on a hydroxyl fullerenes modified glassy carbon electrode," *Biosens. Bioelectron.,* 60 (**2014**) 30–34.

[11] S. Urnikaite, T. Malinauskas, V. Gaidelis, R. Maldzius, V. Jankauskas and V. Getautis, "Solution processable C60 fullerene-hydrazone dyads for optoelectronics," *Carbon,* 49 (**2011**) 320 - 325.

[12] D. K. Susarova, E. A. Khakina, P. A. Troshin, A. E. Goryachev, N. S. Sariciftci, V. F. Razumov and D. A. M. Egbe, "Photovoltaic performance of PPE-PPV copolymers: effect of the fullerene component," *J. Mater. Chem.,* 21 (**2011**) 2356 - 2361.

[13] C. Kastner, C. Ulbricht, D. A. M. Egbe and H. Hoppe, "Polymer BHJ Solar Cell Performance Tuning by C_{60} Fullerene Derivative Alkyl Side-Chain Length," *J. Polym. Sci. Part B: Polym. Phys.,* 50 (**2012**) 1562 - 1566.

[14] P. A. Troshin, O. A. Mukhacheva, A. E. Goryachev, N. N. Dremova, D. Voylov, C. Ulbricht, D. A. M. Egbe, N. S. Sariciftcic and V. F. Razumova, "Material structure–composite morphology–photovoltaic performance relationship for organic bulk heterojunction solar cells," *Chem. Commun.,* 48 (**2012**) 9477 - 9479.

322

[15] F.-F. Li, J. R. Pinzón, B. Q. Mercado, M. M. Olmstead, A. L. Balch and L. Echegoyen, "[2+ 2] Cycloaddition Reaction to Sc3N@ I h-C80. The Formation of Very Stable [5, 6]-and [6, 6]-Adducts," *J. Am. Chem. Soc.,* 133 (**2011**) 1563-1571.

[16] E. E. Maroto, A. d. Cozar, S. Filippone, A. Martin-Domenech, M. Suarez, F. P. Cossio and N. Martin, "Hierarchical Selectivity in Fullerenes: Site-, Regio-, Diastereo-, and Enantiocontrol of the 1,3-Dipolar Cycloaddition to C70," *Angew. Chem.,* 123 (**2011**) 6184 –6188.

[17] J. Marco-Martinez, V. Marcos, S. Reboredo, S. Filippone and N. Martin, "Asymmetric Organocatalysis in Fullerenes Chemistry: Enantioselective Phosphine-catalyzed Cycloaddition of Allenoates onto C60," *Angew. Chem. Int. Ed.,* 52 (**2013**) 5115 –5119.

[18] S. Sato, Y. Maeda, J.-D. Guo, M. Yamada, N. Mizorogi, S. Nagase and T. Akasaka, "Mechanistic Study of the Diels−Alder Reaction of Paramagnetic Endohedral Metallofullerene: Reaction of La@C82 with 1,2,3,4,5-Pentamethylcyclopentadiene," *J. Am. Chem. Soc.,* 135 (**2013**) 5582−5587.

[19] M. Maggini, G. Scorrano and M. Prato, "Addition of Azomethine Ylides to C_{60}: Synthesis,Characterization, and Functionalization of Fullerene Pyrrolidine," *J. Am. Chem. Soc.,* 115 (**1993**) 9798-9799.

[20] S. Iglesias-Groth, F. Cataldo and A. Manchado, "Infrared spectroscopy and integrated molar absorptivity of C60 and C70 fullerenes at extreme temperatures," *Mon. Not. R. Astron. Soc.,* doi:10.1111/j.1365-2966.2011.18124.x (**2011**)

[21] I. J. Ramírez-Calera, V. Meza-Laguna, T. Y. Gromovoy, M. I. Chávez-Uribe, V. A. Basiuk and E. V. Basiuk, "Solvent-free functionalization of fullerene C_{60} and pristine multi-walled carbon nanotubes with aromatic amines," *Appl. Surf. Sci.,* 328 (**2015**) 45-62.

[22] K. Kordatos, T. D. Ros, M. Prato, R. V. Bensasson and S. Leach, "Absorption spectra of the mono-adduct and eight bis-adduct regioisomers of pyrrolidine derivatives of C60," *Chem. Phys.,* 293 (**2003**) 263 - 280.

[23] P. Zhang, Z. X. Guo and S. Lv, "Synthesis and aggregation properties of amphiphilic mono and bisadducts of fullerene in aqueous solution," *Chin. Chem. Lett.,* 19 (**2008**) 1039 - 1042.

[24] A. Parveen, V. Sughanya and S. Nagarajan, "Quenching of fluorescence in C60 fulleropyrrolidines by chloroform," *Spectrochimica Acta, Part A: Molecular and Biomolecular Spectroscopy* 152 (**2016**) 77 - 81.

[25] J. P. Hare, H. W. Kroto and R. Taylor, "Preparation and UV/Visible Spectra of Fullerenes C_{60} and C_{70}," *Chem. Phys. Lett.,* 177 (**1991**) 394 - 398.

[26] S. Das, F. Herrmann-Westendorf, F. H. Schacher, E. Täuscher, U. Ritter, B. Dietzek and M. Presselt, "Controlling Electronic Transitions in Fullerene van der Waals Aggregates via Supramolecular Assembly," *ACS Appl. Mater. Interf.,* 8 (**2016**) 21512 - 21521.

[27] S. Admassie, O. Inganas, W. Mammo, E. Perzon and M. R. Andersson, "Electrochemical and optical studies of the band gaps of alternating polyfluorene copolymers," *Synth. Met.,* 156 (**2006**) 614 - 623.

[28] P. M. Allemand, A. Koch, F. Wudl, Y. Rubin, F. Diederich, M. M. Alvarez, S. J. Anz and R. L. Whetten, "Two Different Fullerenes Have the Same Cyclic Voltammetry," *J . Am. Chem. Soc,* 113 (**1991**) 1050 - 1051.

[29] D. Dubois and K. M. Kadish, "Spctroelectrochemical Study of the C_{60} and C_{70} Fullerenes and Their Mono-, Di-, Tri-, and Tetraanions," *J . Am. Chem. Soc,* 113 (**1991**) 4364 - 4366.

324

[30] Q. Xie, E. Ptrez-Cordero and L. Echegoyen, "Electrochemical Detection of C_{60}^{6-} and C_{70}^{6-}: Enhanced Stability of Fullerides in Solution," *J. Am. Chem. Soc.,* 114 (**1992**) 3978 - 3980.

[31] L. Echegoyen, Q. Xie and E. Ptrez-Cordero, "Reducing supermolecules to "pseudo-atoms" and anions: Cryptatium species and C_{60}," *Pure & Appl. Chem.,* 65 (**1993**) 441 - 446.

[32] D. Dubois, G. Moninot, W. Kutner, M. T. Jones and K. M. Kadish, "Electroreductlon of Buckminsterfullerene, CeO, in Aprotlc Solvents: Solvent, Supporting Electrolyte, and Temperature Effects," *J. Phys. Chem.,* 96 (**1992**) 7137 - 7145.

[33] C. J. Brabec, A. Cravino, D. Meissner, N. S. Sariciftci, T. Fromherz, M. T. Rispens, L. Sanchez and J. C. Hummelen, "Origin of the Open Circuit Voltage of Plastic Solar Cells," *Adv. Funct. Mater.,* 11 (**2001**) 374 - 380.

UNIVERSITY *of the*

WESTERN CAPE

325
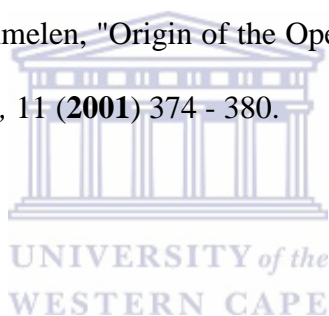
CHAPTER EIGHT

RESULTS AND DISCUSSION - Photoluminescence quenching of poly(octylfluorenylbenzothiadiazole) luminophore by n-type cobalt (II) salicylaldimine metallodendrimer

Abstract

Cobalt (II) salicylaldimine metallodendrimer (Co-PPI) which combines a strong absorption over a broad range in the vis-NIR region with good electrical characteristics was explored as a potential novel electron-accepting material for organic solar cells. The non-fullerene acceptor exhibited efficient light absorption, exciton dissociation and charge transportation characteristics when blended with poly[(9,9-di-*n*-octylfluorenyl-2,7-diyl)-*alt*-(benzo[2,1,3]thiadiazol-4,8-diyl)] (F8BT) as donor material for bulk heterojunction organic solar cell. Co-PPI was found to be an excellent quencher of F8BT with a photoluminescence quenching of almost 100% achieved. It (Co-PPI) exhibited more red-shifted absorption bands with a vis-NIR absorption in the region 600-750 nm, and better miscibility with the donor polymer, F8BT, when compared to the traditional fullerene-based acceptor, [6,6]-phenyl C_{61} butyric acid methyl ester (PCBM), which is characterized by relatively poor absorption in the visible region. The morphology and size distribution of Co-PPI were confirmed by atomic force microscopy (AFM) and scanning electron microscopy (SEM) analysis with the SEM analysis further buttressing the photoluminescence quenching. These properties of Co-PPI make it a very promising 'ideal' acceptor material for organic solar cell. The kinetics and potential of poly[(9,9-di-*n*-octylfluorenyl-2,7-diyl)-*alt*-(benzo[2,1,3]thiadiazol-4,8-diyl)]

326

(F8BT) as a donor material for organic solar cell fabrication was also investigated in this study by electrochemical methods.

8   Introduction

Solution processed conjugated polymers have gained increased attraction and acceptance for application in optoelectronic devices like organic field effect transistors, organic light emitting diodes and organic solar cells. This is due to their low cost of manufacturing, ease of processing, room temperature fabrication, flexibility of chemical tailoring to obtain desired properties e.g. tuning of band gap, mechanical flexibility, light weight, semi-transparent and ultrathin characteristics [1-2]. The field of donor-acceptor organic solar cells has witnessed the development and interrogation of numerous new functional donor polymers with a few of them demonstrating promising power conversion efficiencies [3-6]. To further improve polymer-based device performance, researchers have improved on device fabrication, film morphology control and pursued novel donor polymers of lower band gaps tuned to capture as much of the solar spectrum as possible thereby potentially attaining higher efficiency [2, 7]; but the same acceptor material (fullerene based acceptors) are being continuously used and this has continually resulted in getting almost the same result with different donor materials. For high performance organic solar cells (OSCs), electron acceptors are as important as electron donors. As important as they are, no much attention has been given to their development as have been done for donors. Fullerene based acceptors are the most widely used in bulk heterojunction organic solar cells (BHJ OSCs) with [6,6]-Phenyl C_{61} butyric acid methyl ester (PCBM) being the conventional acceptor. Although, derivatives of fullerene have many advantages as acceptors in BHJ OSCs, their relatively poor absorption in the visible region [8-9], restricts further improvement of their device performance. The

327

potential lack of morphological stability and high cost of production of fullerene derivatives will likely hinder the future commercialization of OSCs based on functionalized fullerene acceptors [10]. It is therefore imperative to develop and study non-fullerene-based acceptors that will retain the attractive properties of fullerene as well as overcome their drawbacks. Organic solar cells based on non-fullerene acceptors (all polymer solar cells) have shown promising efficiencies rising from ca 0.1 to over 5% [10-16]. Although a few other materials like carbon nanotubes based materials have been applied as acceptors with suitable donors but their use is challenging. The review by Bruno and group [17] highlights the associated challenges with the synthesis, purification, functionalization and device integration of carbon nanotubes; making it difficult to rely on them as suitable acceptor for enhanced photovoltaic cell fabrication. In the quest for more suitable materials, we have investigated a unique class of compound - dendrimers.
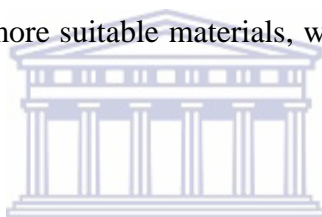
Dendrimers are an intriguing class of materials with a wide range of applications. Functionalization of the periphery of dendrimers can result in p- or n-type materials. p-Type conjugated dendrimers have been extensively studied while there is only a few report on the n-type dendrimers [18]. Their metal complexes - metallodendrimers, are metal-containing macromolecules having well-defined molecular architecture emanating from a central core with metals on the periphery or encapsulated within the architecture. These macromolecules proposed to produce lasting effects on many areas of chemistry due to their role in the development of useful molecular composites [19-20] have found specific applications in medicinal chemistry [21-25], host-guest chemistry, catalysis [26-29], and recently, biosensors [30-31] and optoelectronics [32-35].

The photo-physical and electrochemical properties of Cobalt (II) salicylaldimine metallodendrimer (Co-PPI) were investigated in this report and compared with those of traditional PCBM fullerene based acceptor. Both acceptors were individually applied in the photoluminescence quenching of donor polymer poly[(9,9-di-*n*-octylfluorenyl-2,7-diyl)-*alt*-(benzo[2,1,3]thiadiazol-4,8-diyl)] (F8BT). Co-PPI revealed a great impact on exciton dissociation, and charge transportation when blended with donor polymer (F8BT). The UV-Visible absorption spectroscopy revealed more light absorption, a vis-NIR region absorption and better miscibility with the donor polymer F8BT when compared to the traditional fullerene-based PCBM acceptor. The nature of the functional groups and modes of vibrations present in both acceptors were studied by Fourier transform infrared (FTIR) spectroscopy and the morphology was studied by atomic force microscopy (AFM) and high resolution scanning electron microscopy (HR-SEM). The kinetics of polymer/solution and metal/polymer interfaces of the donor F8BT was electrochemically studied employing the Butler-Volmer formulation for electrode kinetics.
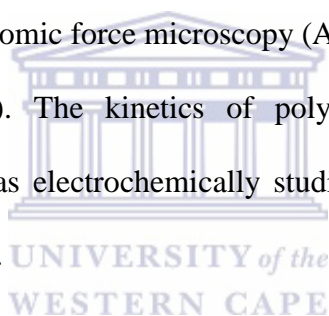
8.1   Experimental

Poly[(9,9-di-*n*-octylfluorenyl-2,7-diyl)-*alt*-(benzo[2,1,3]thiadiazol-4,8-diyl)]   (F8BT)   and [6,6]-phenyl C_{61} butyric acid methyl ester (PCBM) were purchased from Sigma Aldrich. Cobalt (II) salicylaldimine metallodendrimer (Co-PPI) was synthesized [36]. Spectroscopic measurements: A Nicolet Evolution 100 UV–Visible spectrometer (Thermo Electron) was used for UV–Visible absorption measurements of samples. Photoluminescence quenching was monitored by NanoLog *i*HR320 at ambient temperature. Fourier transform infrared spectroscopy (FTIR) was performed with Perkin Elmer ATR TWO FTIR Spectrometer. Thin films of the polymer and blend of donor-acceptor were prepared by drop-coating onto pre-

329

cleaned glass slides from dichloromethane solutions and dried under argon prior to measurement. The morphology of the films was obtained with Auriga high resolution-scanning electron microscopy.

Electrochemical measurements: Cyclic and square wave voltammetric measurements were carried out using a BASi Epsilon potentiostat equipped with a standard three-electrode configuration. Typically, a three electrode cell equipped with a glassy carbon working electrode, an Ag/AgCl reference electrode, and a Pt wire counter electrode was employed. The measurements were done in anhydrous acetonitrile/dichloromethane with 0.1 M tetrabutyl ammonium hexafluorophosphate (TBAF$_6$P) as the supporting electrolyte under an argon atmosphere. The electrochemical onsets were determined at the position where the current starts to differ from the baseline. Electrochemical impedance spectroscopy (EIS) measurements were performed on GC/F8BT electrode with an IM6ex electrochemical workstation (BAS-Zahner, Germany) and Thales software was used for experimental control and data collection in the frequency range of 100 kHz to 100 mHz at sinusoidal voltage perturbation of 10 mV amplitude. Spectra were obtained at several dc potentials (-1.016 to -0.516 V) in solutions containing 0.1 M TBAF$_6$P supporting electrolyte in acetonitrile/10% v/v dichloromethane and fitted to equivalent electrical circuits using the complex non-linear least square (CNLS) program. All experiments were performed under argon at room temperature.

330

8.2 Results and Discussion

The chemical structures of Co-PPI, PCBM and F8BT studied in this report are shown in
Figure 8.1
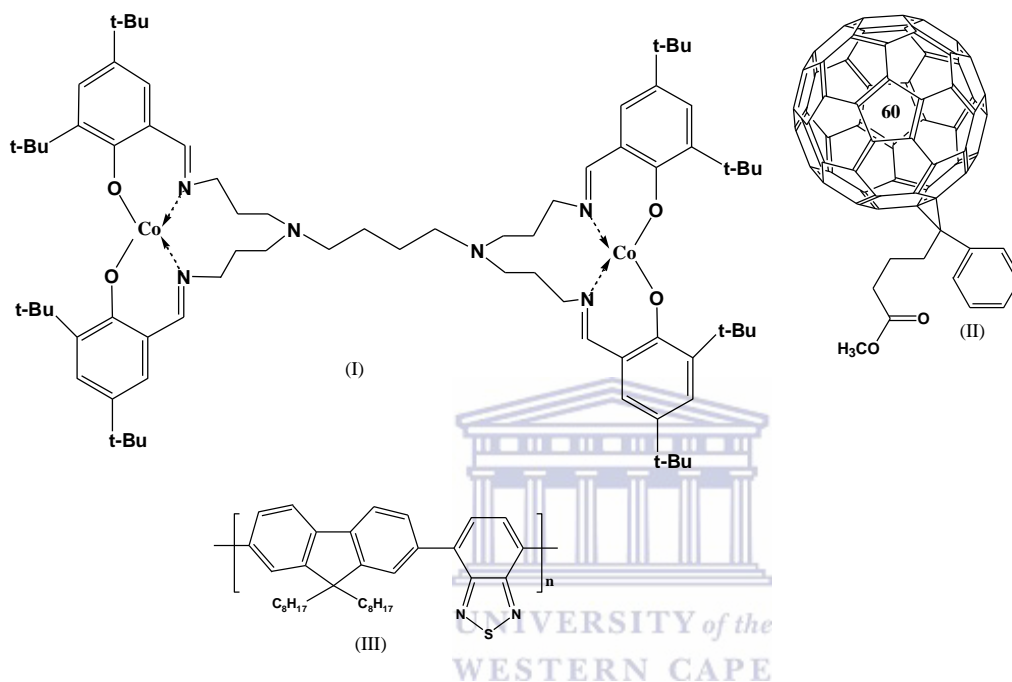
Figure 8.1: Chemical structures of (I) Co-PPI, (II) PCBM and (III) F8BT.

8.2.1 Spectroscopic Studies

8.2.1.1 Fourier Transform Infra Red (FTIR) Spectroscopy of Co-PPI and PCBM

Information regarding the nature of the functional groups present in the Co-PPI and PCBM
was obtained by FTIR spectroscopy (**Figure 8.2**). Infrared spectra of the coordinated
salicylaldimine metallodendrimer and fullerene based molecule were obtained in the
powdered form with distinct ν(C=N), ν(Co-O), ν(C-O), and ν(C=O) bands (**Table 8.1**). The
band due to ν(C-O) was observed in the region 1350-1100 cm^{-1} in both materials (Co-PPI and

331

PCBM) studied; although Co-PPI shows ν(C-O) band at higher frequency ~ 1318 cm^{-1} relative to PCBM. The ability of fullerenes to act as electron acceptor is intrinsic and not specifically due to the modification or functionalization. The ability of Co-PPI on the other hand may be due to the presence of ν(C-O) band believed to play a major role in the deactivating/electron withdrawing effect of the material.
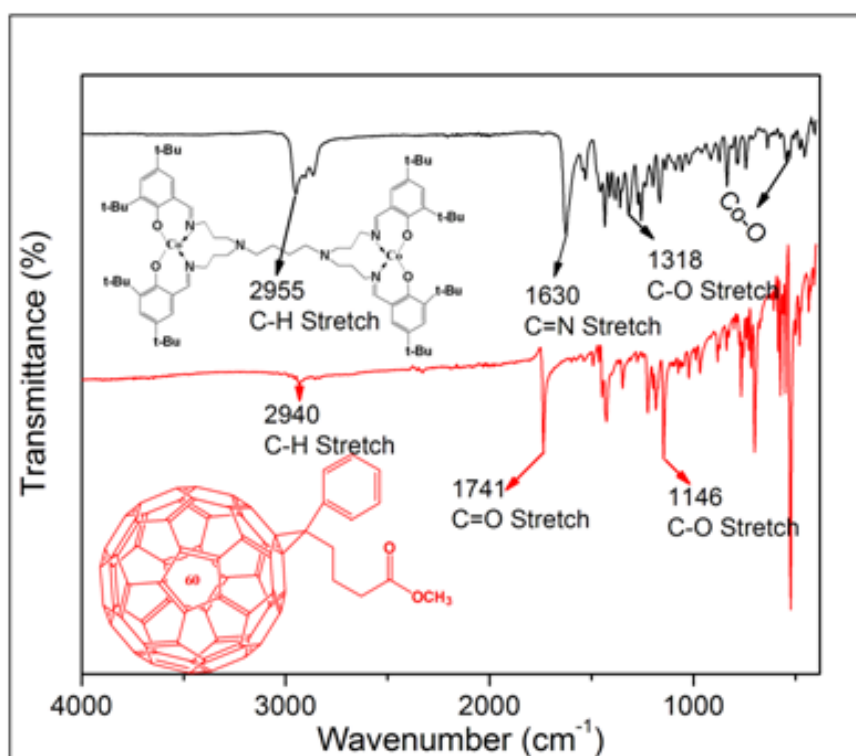
Figure 8.2: FTIR spectra of Co-PPI and PCBM.

332

Table 8.1: FTIR Spectra Analysis of Co-PPI and PCBM

Origin	Group Frequency (cm⁻)		Vibrational Mode
	Co-PPI	PCBM	
C-H	2955	2940	C-H Stretch
C-O	1318	1146	C-O Stretch
C=N	1630	-	C=N Stretch
C=O	-	1741	C=O Stretch

8.2.1.2 UV-Vis Spectroscopy of the Donor and Acceptors Studied

The UV-Vis spectra for the investigated materials were obtained in dichloromethane (solution and film) and the absorption peaks and transitions observed for the complexes are shown in **Table 8.2**. The spectra of the investigated Co-PPI metallodendrimer show two main broad bands (**Figure 8.3**) with maximum absorption at 235-239 nm associated with the intra-ligand $\pi \rightarrow \pi^*$ transitions and 359-361 nm associated with metal to ligand charge transfer (MLCT) transitions [36].
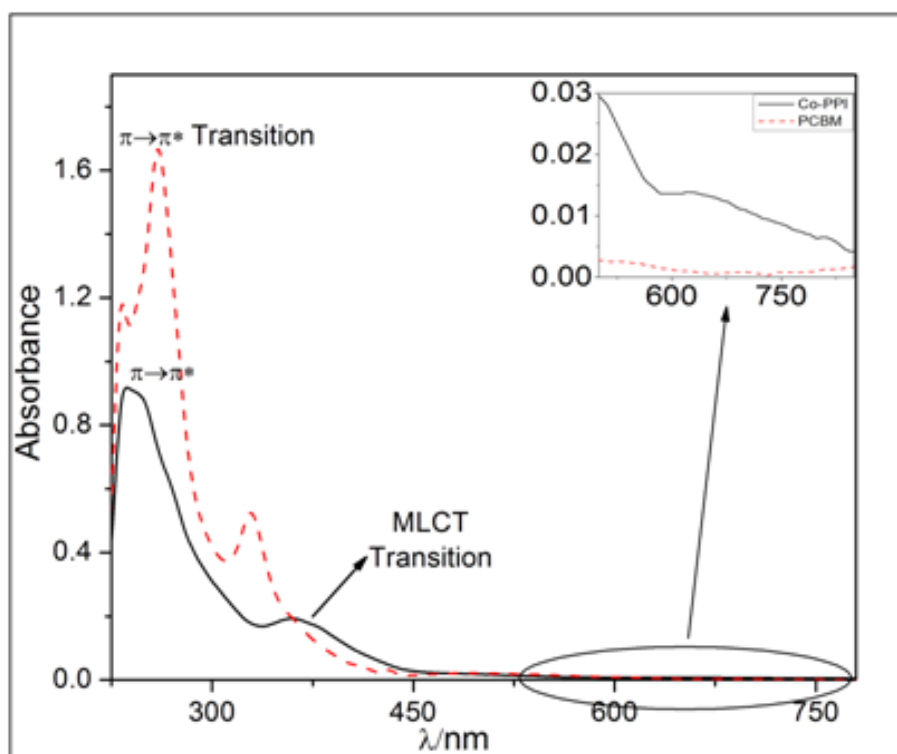
Figure 8.3: UV-Vis spectra of Co-PPI and PCBM in dichloromethane solution.
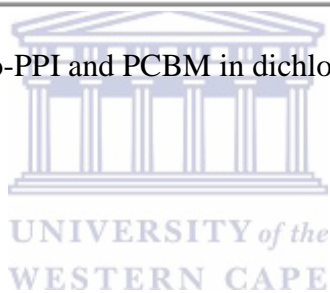
Table 8.2: UV-Vis spectra analysis of the donor and acceptors studied (solution and film)

Complex	Solution		Film		Transition
	λ_{max} (nm)	λ_{onset} (nm)	λ_{max} (nm)	λ_{onset} (nm)	
Co-PPI	237,359	457	-	-	$\pi \rightarrow \pi^*$ MLCT
PCBM	230, 260, 329	438	-	-	$\pi \rightarrow \pi^*$
F8BT:Co-PPI	236, 310, 339[a], 449	526	252, 315[a], 326, 339[a], 465	543	ICT
F8BT:PCBM	233, 258, 327, 449	515	263, 332, 463	538	ICT

[a]: Shoulder

An important optical feature of Co-PPI is the third broad absorption (**Figure 8.3** inset) present in the Vis-NIR region 600-750 nm. Traditional fullerene based acceptors are characterized with weak absorption in the low wavelength area of the visible region [8] and this limits their contribution to light harvesting in solar photovoltaic conversion. The presence of this broad and Vis-NIR region absorption in Co-PPI suggests it as an acceptor with the potential of contributing to light harvesting in organic solar cell. This third absorption reveals a good match of Co-PPI with the solar spectrum (an important property for solar photovoltaic materials) which will enhance a good interaction with a suitable donor. In essence, in addition to serving as an electron acceptor, it can also contribute to the harvest of light, leading to improvement of the absorption capability of the donor material involved and

335

thereby enhancing efficiency. This is evident in the spectra acquired for the mixture of the donor-acceptor material in the solid state in the form of thin film at room temperature (**Figure 8.4**). From the spectra, we observe an improved light harvesting in the F8BT:Co-PPI compared to the F8BT:PCBM as evident in the onset absorption wavelength. A bathochromic shift in the film absorption of F8BT:Co-PPI relative to F8BT:PCBM is presumed to be due to improved light absorption of the donor with the contribution of the metallodendrimer.

UNIVERSITY *of the*
WESTERN CAPE

336
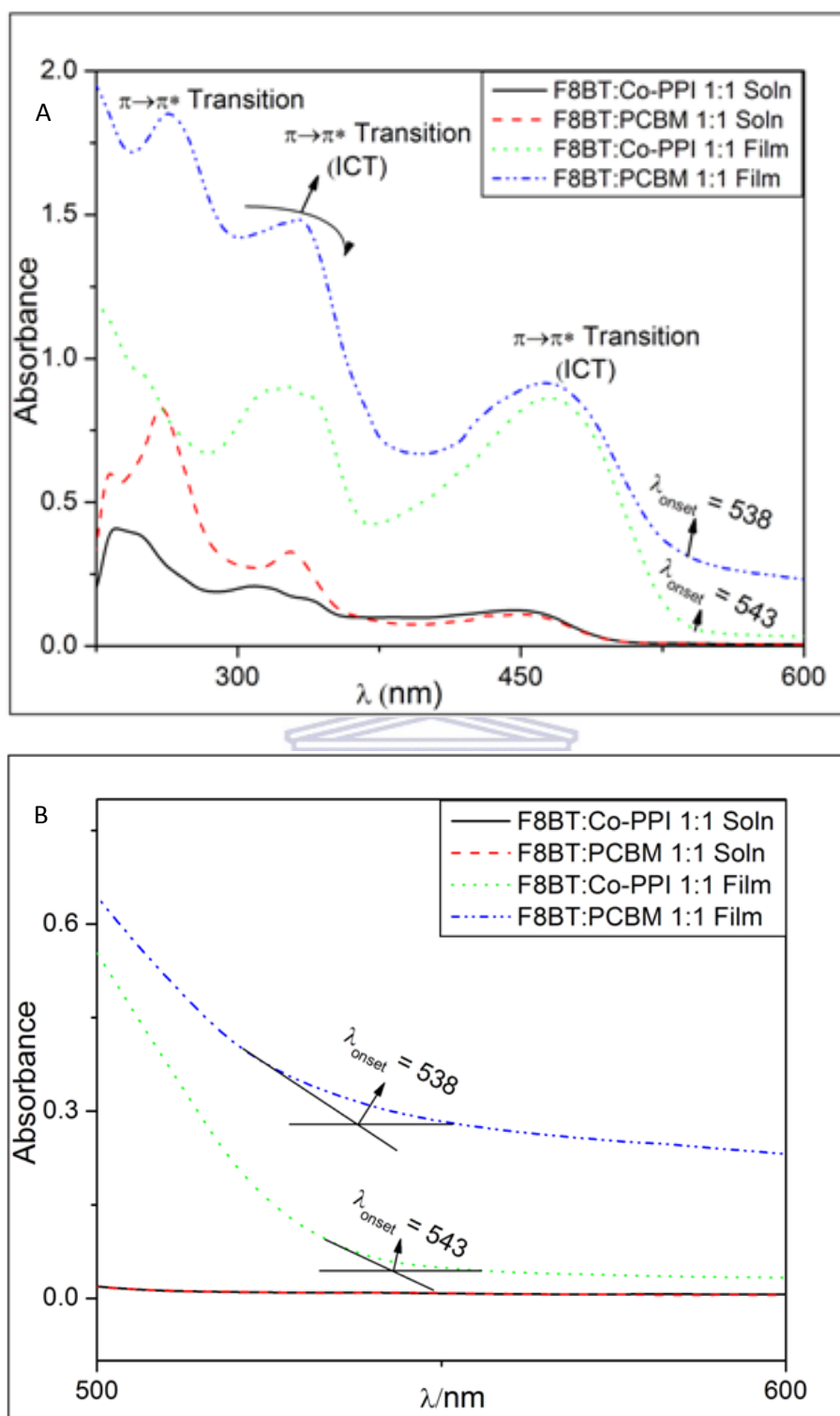
Figure 8.4: UV-Vis spectra of donor (F8BT) and acceptor (Co-PPI, PCBM) in a 1:1 ratio in

dichloromethane solution and film. (A) 225 nm to 600 nm and (B) 500 nm to 600 nm.

337

The transitions observed correspond to those of charge transfer behaviour. The entire shift in film absorption of both donor-acceptor (F8BT:Co-PPI and F8BT:PCBM) materials compared to their solution response is attributed to symmetric molecular structure of the donor and the inter-molecular charge transfer (ICT) interaction between the donor and the acceptor which enhance inter-chain stacking in polymers [37-38], improves charge transport and light harvesting.

8.2.1.3 Photoluminescence Spectroscopy of Materials Studied

The photoluminescence spectra of pure F8BT and its blend with Co-PPI and PCBM respectively when excited at a wavelength of 450 nm are shown in **Figure 8.5**. Photoluminescence quenching studies were carried out to examine the exciton behaviour. At the excited wavelength of 450 nm, 96.6% of the donor F8BT was quenched in F8BT:Co-PPI blend and 97.29% was quenched in F8BT:PCBM blend; indicating excellent degree of exciton splitting and charge transfer in both systems.
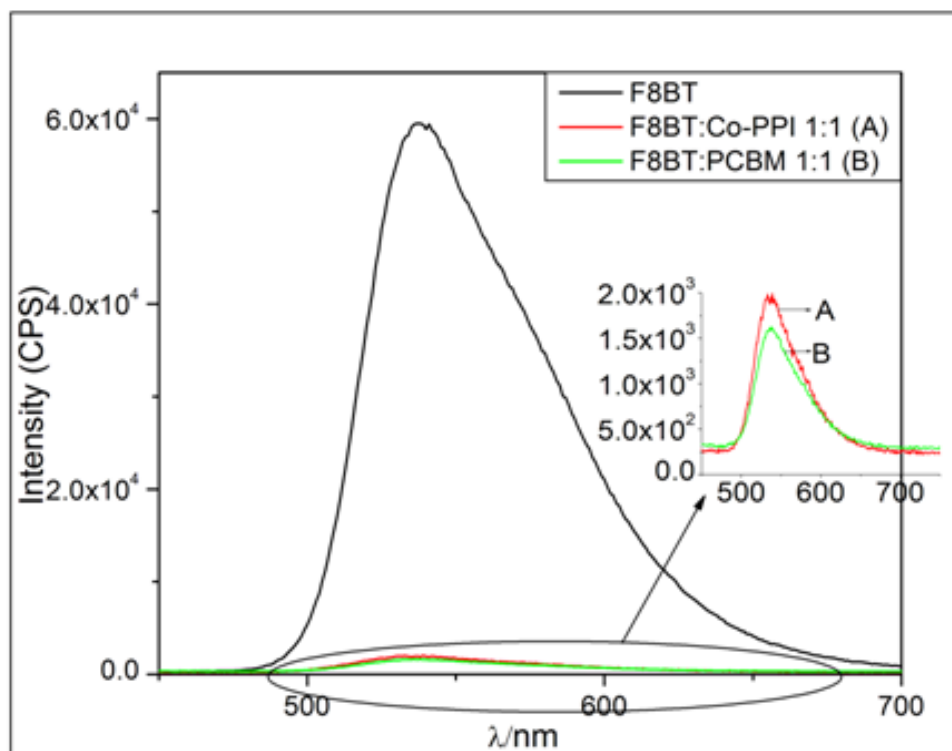
Figure 8.5: Photoluminescence quenching of donor F8BT.

Photoluminescence quenching amongst other uses is used as an indicator of how well excitons can diffuse to a donor-acceptor interface and split into free charges. It is governed by photo-induced charge transfer and resonance energy transfer between species in the excited and ground states respectively. Energy transfer depends on inter-molecular distance and the overlap of the absorption spectra of the acceptor and emission spectra of the donor [39-40]. The quenching in F8BT:Co-PPI is believed to be due to charge transfer and not resonance energy transfer since the optical absorption spectra of the Co-PPI do not overlap with the F8BT emission spectrum. The 1:1 blend of F8BT:Co-PPI shows an almost complete photoluminescence quenching which indicates that charge transfer is efficiently carried out in the system [41]. Co-PPI has good solubility in common organic solvents like dichloromethane and tetrahydrofuran. This aided intimate mixing of the Co-PPI with F8BT

339

resulting in generation of excitons within angstroms of the donor-acceptor interface and an almost complete photoluminescence quenching.

8.2.2   Microscopic Studies

The microstructure (**Figure 8.6**) of the blends of donor-acceptor films prepared from dichloromethane on glass substrates were captured using resolution scanning electron microscopy (HR-SEM). **Figure 8.6a** shows a sample with surface composed of holes. This was also confirmed by atomic force microscopy (AFM) analysis of the films prepared in different solvents (**Figure 8.7**). AFM images of the films prepared from same solvent (dichloromethane) were taken and they show no morphological differences in comparison to the SEM images. The response in dichloromethane and chloroform reveals the presence of intrinsic holes in F8BT with chloroform revealing more holes, confirming that the electron beam has no effect in the holes present in the SEM morphology. The histogram of morphologies shown in **Figure 8.6** shows the size distribution and central location of the material. From the histogram we see that the sizes of the pure F8BT range majorly from 2100 – 2800 nm, F8BT:Co-PPI films range majorly from 800 – 1600 while that of F8BT:PCBM falls within the range of 400 – 1200 nm. We observe from the histogram that the donor holes become smaller on introduction of the acceptor. The smaller the holes are, the easier the separation of the charges (exciton). In principle, the ease of charge separation results in enhanced quenching of the donor signal by the acceptor. This further explains the 96.6% and 97.29% quenching of the donor F8BT observed in F8BT:Co-PPI and F8BT:PCBM respectively in the photoluminescence study.
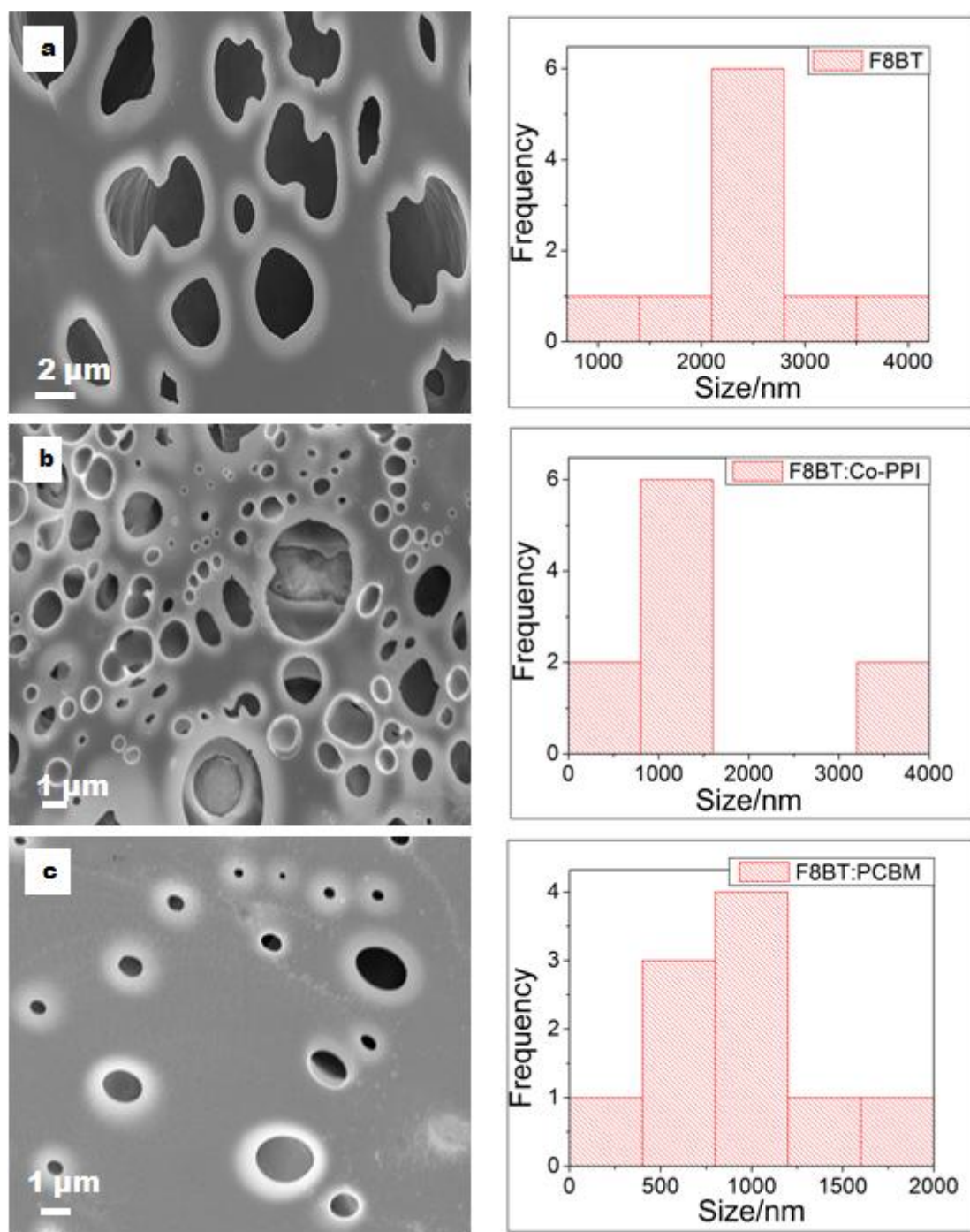
Figure 8.6: High resolution scanning electron microscope images of (a) F8BT at 5000 magnification, (b) F8BT:Co-PPI at 5000 magnification and (c) F8BT:PCBM at 5000 magnification films prepared in dichloromethane.

341
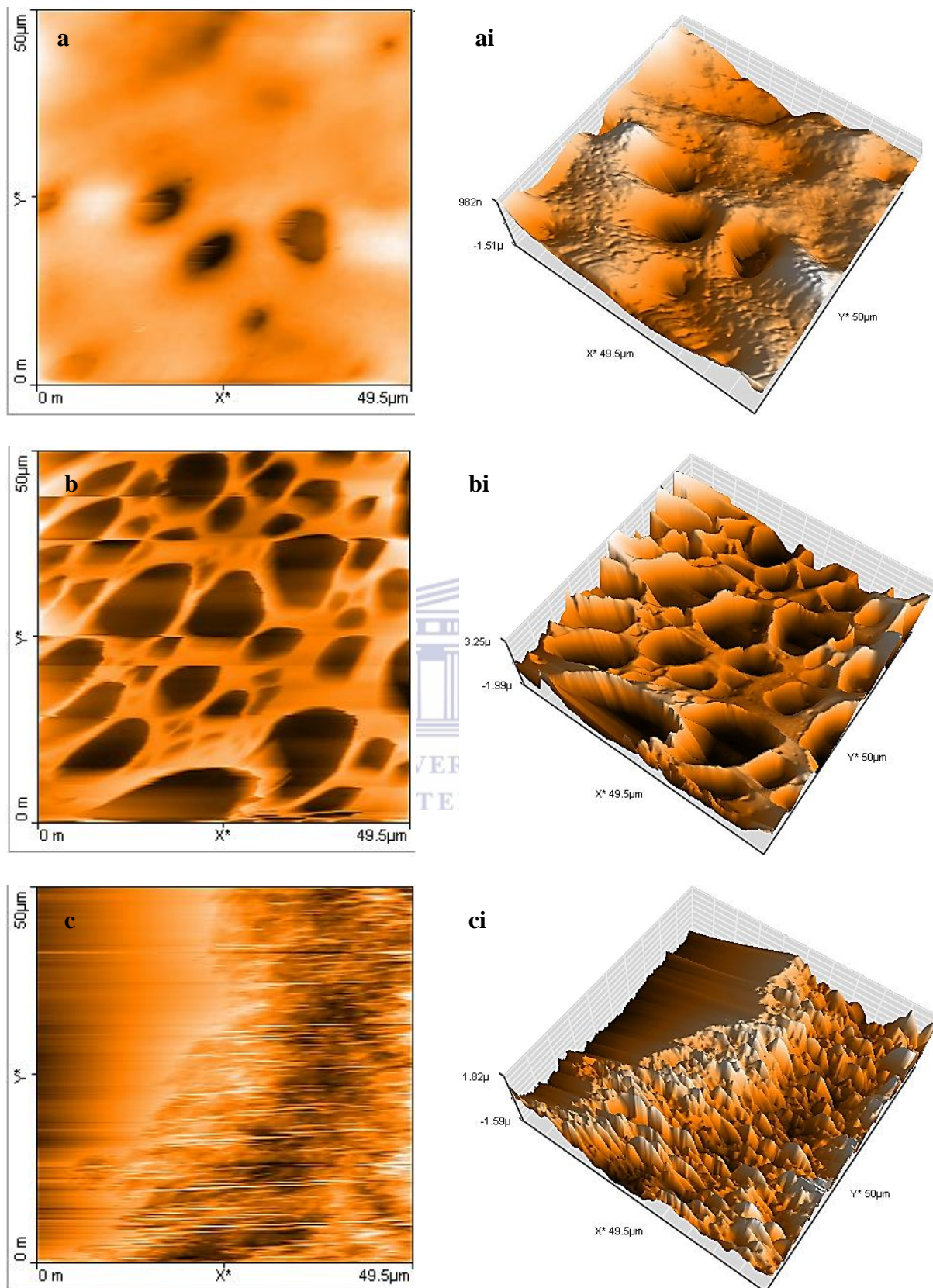
Figure 8.7: (a) AFM (2D, 3D) images of F8BT films prepared at room temperature in (a, ai) dichloromethane, (b, bi) chloroform and (c, ci) tetrahydrofuran.

342

8.2.3 Electroanalysis of F8BT and Co-PPI films

Using the linear correlation between the ionization potential and oxidation potential and also the electron affinity and reduction potential derived by Bredas and co-workers [42] on the basis of a comprehensive comparison between the valence effective Hamiltonian (VEH) theoretical results and experimental electrochemical data, the electrochemical band gap of the donor F8BTwas calculated using the following correlations (**equation 8.1 – 8.3**) given as

$$I_p = -\left(E_{onset}^{ox} + 4.4\right) eV \qquad\qquad \textbf{equation (8.1)}$$

$$E_a = -\left(E_{onset}^{red} + 4.4\right) eV \qquad\qquad \textbf{equation (8.2)}$$

$$\text{And } E_g^{el} = I_p - E_a \qquad\qquad \textbf{equation (8.3)}$$

where E_{onset}^{ox} and E_{onset}^{red} are onset oxidation and reduction potentials (determined at the position where the current starts to differ from the baseline) versus the Ag/AgCl reference electrode. The cyclic voltammetric (CV) response of F8BT films obtained from the F8BT film modified glassy carbon electrode (GCE) is shown in **Figure 8.8**. F8BT film was cycled within the electrode potential range from -1850 to +1850 mV at scan rate 50 mV/s. The voltammogram shows the presence of three distinct peaks labelled a-c with a pair of well resolved peaks in the potential range -1850 to -500 mV with peak electrode potentials at -1.37 V and -1.60 V (peaks a and b) and peak c at ca 1.15 V. It also shows two oxidation and one reduction peaks at -0.68 V, -0.43 V and -0.78 V (vs. Ag/AgCl) as shown in the voltammogram B. The response was used to estimate the ionization potential and electron affinity from the onset oxidative and onset reductive potentials of the polymer films respectively using equations 8.1 and 8.2. The electrochemical band gap was estimated to be

343

2.2 eV from the ionization potential and electron affinity. The result reveals a deep HOMO energy level of -5.4 eV and a relatively high band gap of 2.2 eV. The electrochemical response and calculated band gap is comparable to the electrochemical response and band gaps of other polyfluorene based donor copolymers [43-44].
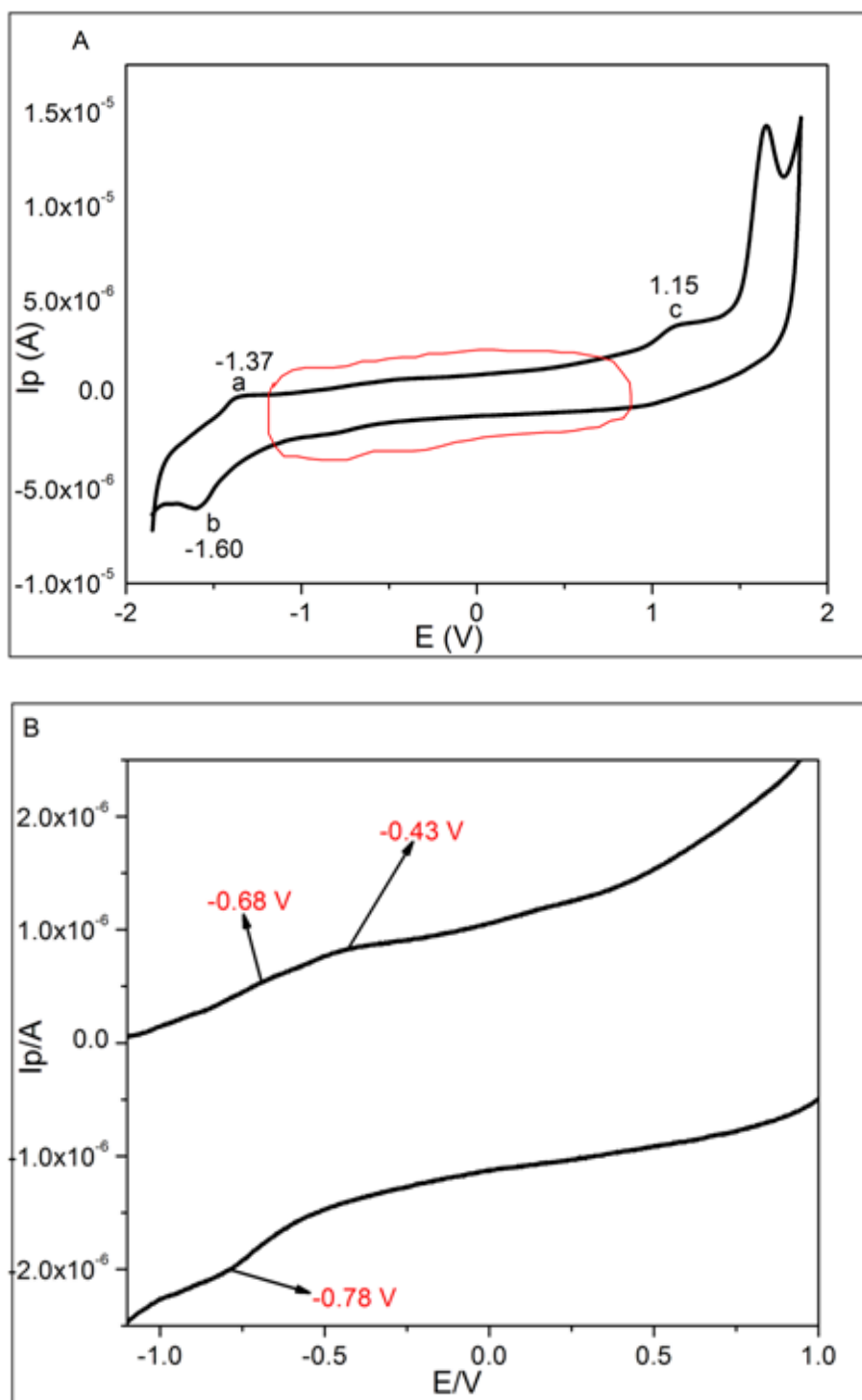
Figure 8.8: Cyclic voltammograms of F8BT films coated on a GCE in TBAPF$_6$/AcN/DCM supporting electrolyte/solvent system at 50 mV/s, plotted for (A) from -2 V to +2 V and (B) from -1.1 V to +1.0 V.

The redox behaviour of Co-PPI in TBAPF$_6$/AcN/DCM supporting electrolyte/solvent system at 50 mV/s were investigated and measured under inert conditions by cyclic and square wave voltammetry. Co-PPI exhibits reversible reduction and oxidation potentials in the potential range -0.7 to 1.3 V vs Ag/Ag+ (**Figure 8.9**). The LUMO energy level was estimated to be -4.3 eV from the onset reduction potential which is indicative of the electron acceptor strength of the material. This value is comparable to the LUMO of an 'ideal acceptor' pegged at -4.2 eV for an 'ideal donor' HOMO of -5.4 eV [38] for the required enhanced efficiency for organic photovoltaic cell. From energetic considerations therefore, Co-PPI (LUMO energy level estimated at -4.3 eV) is a good acceptor for F8BT donor (HOMO energy level estimated at -5.4 eV).
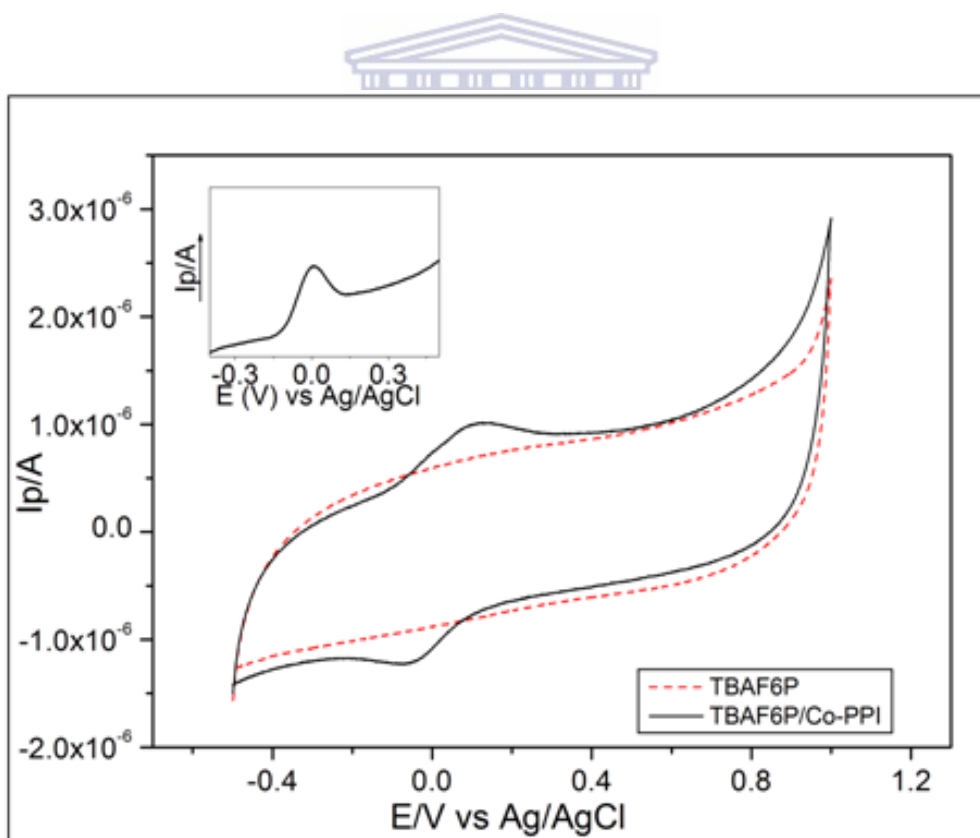
Figure 8.9: Cyclic voltammograms of GCE and GCE/Co-PPI in TBAPF$_6$/AcN/DCM vs. Ag/AgCl. (Inset) The corresponding square wave voltammogram for GCE/Co-PPI.

346

8.2.4   Capacitive Behaviour and Kinetics of F8BT

Electrochemical impedance spectroscopy (EIS) finds applications in electrode kinetics, interface transfer mechanism investigation and the characterization of semiconductors and organic films. The kinetics and mechanisms of charge transfer and ion transport in polymer film/solution interface can be studied from the reliance of EIS parameters of the conducting polymer system on the applied potential. EIS was therefore performed to monitor the electrochemical behaviour of the donor F8BT. The Bode plot (**Figure 8.10a**) shows the electronics of the donor F8BT. The spectra was taken at the formal potential (-0.7 V) of the well defined redox peak of the voltammograms shown in **Figure 8.8**. The spectra presented in the form log |Z| and phase angle against log f enables equal representation of all experimental data over the entire frequency range. The plot recorded in the frequency range between 100 KHz and 100 mHz contains only one near capacitive behaviour denoted by a phase angle which closely approaches -60° and with an electrode impedance with two shoulders or bends indicating solution resistance and the presence of charge transfer resistance. Owing to the microscopic roughness of the electrode surface, slow adsorption of ions and surface inhomogeneity which makes it practically impossible for the barrier film (double layer) to exhibit the theoretically expected phase angle of -90°, the double layer capacitance was modelled/expressed using the distributive constant phase element (CPE) (**Figure 8.10b**). Thales software was used for experimental control, data collection and determination of the equivalent circuits.

The impedance of CPE is defined by $Z_{CPE} = \left[T(jw)^p \right]^{-1}$ where T and p are independent parameters and $0 \leq p \leq 1$ [45]. Depending on the system behaviour (capacitive, resistive or

347

infinite Warburg), the value of p relates to a non-uniform current distribution as a result of surface inhomogeneity. The studied system revealed a p value 0.8; a close to an ideal capacitive system.
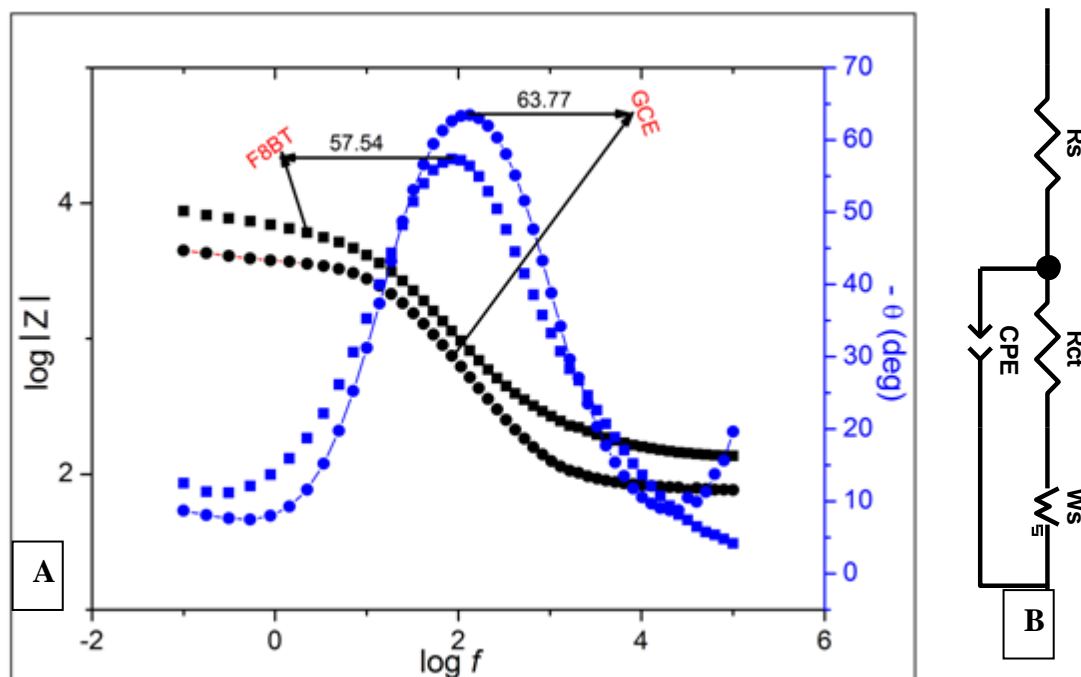
Figure 8.10: (A) Bode plots for the EIS of F8BT in 0.1 M TBAPF$_6$/AcN/10% v/v DCM and (B) the corresponding quivalent circuit; where R$_s$, is the solution resistance, R$_{ct}$, the charge transfer resistance, CPE is the constant phase element and Ws is the Warburg impedance.

The kinetics of electron transfer was also studied from the data obtained for F8BT film at a.c frequency varying from 100 KHz to 100 mHz in the electrode potential regions corresponding to the electro-activity in 0.1 M TBAPF$_6$/AcN/DCM solution according to the Butler-Volmer formulation for electrode kinetics (**equations 8.4, 8.5 and 8.6**) [46].

$$I_o = nFA k_o c_o \exp\left[\dfrac{\alpha nF\left(E_{dc} - E^{o'}\right)}{(RT)}\right] \qquad \textbf{equation (8.4)}$$

348

$$R_{ct} = \frac{RT}{nF\, I_o}$$

equation (8.5)

$$k_o = \frac{RT}{\left\{ n^2 F^2 R_{ct} A C_o \exp\left[\frac{-\alpha nF\left(E_{dc} - E^{o'}\right)}{(RT)} \right] \right\}}$$

equation (8.6)

where I_o is the exchange current, k_o is the standard rate constant, C_o is concentration, E_{dc} is dc potential, $E^{o'}$ is the formal redox potential, α is the transfer coefficient and other symbols having their usual standard electrochemical significance.

Figure 8.11a shows a series of Nyquist plots for the impedance data obtained at a few selected potentials. They reveal three characteristic parts (a semicircle, a capacitive response and a Warburg region). Increase in the anodic electrode potential is accompanied by a significant decrease in the diameter of the semicircle in the studied range. The semicircle corresponds to a parallel resistance-capacitance circuit element as shown in the fitted circuit element **(Figure 8.10b).**
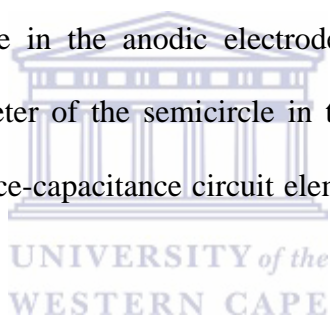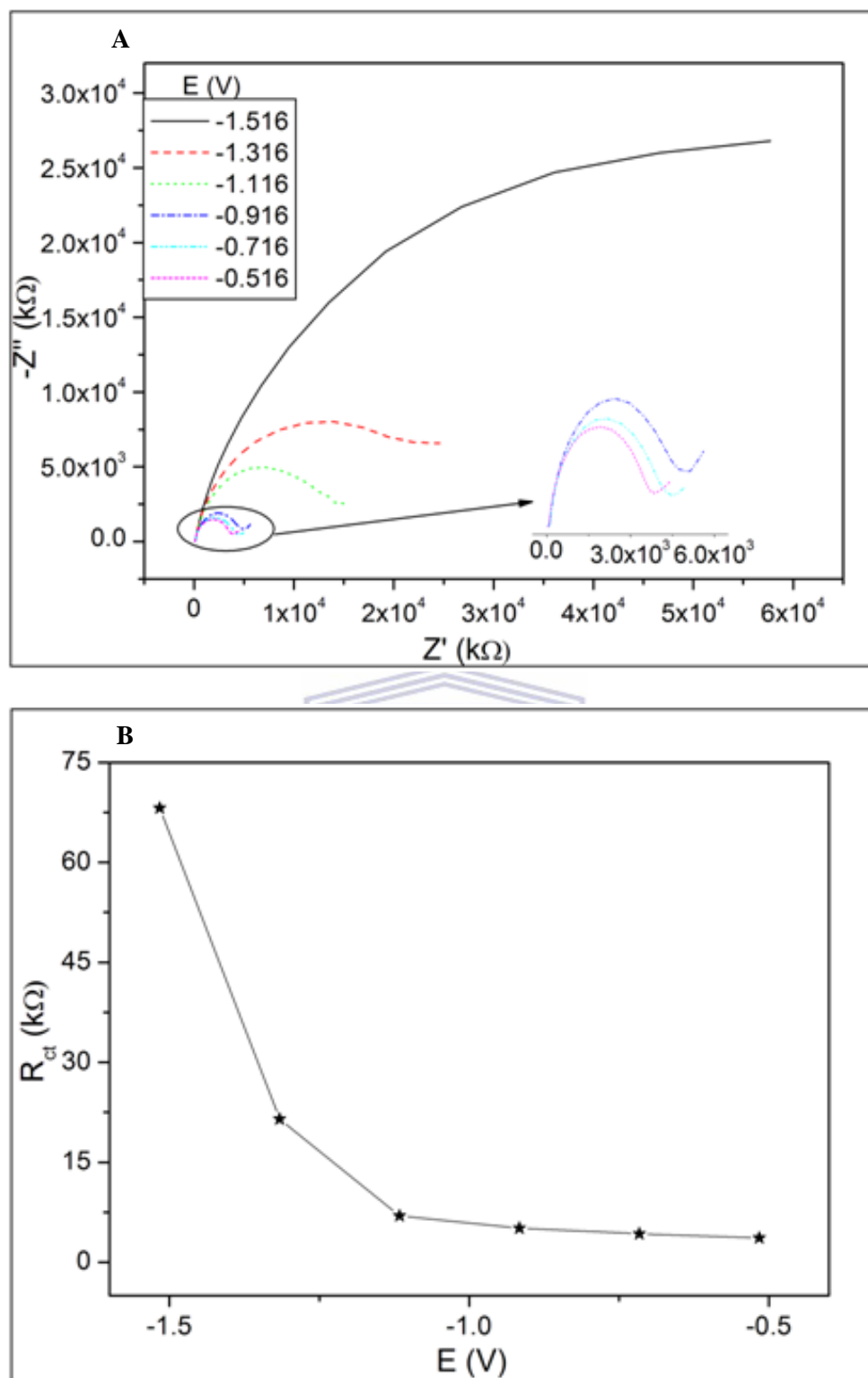
Figure 8.11: (A) Potential dependence Nyquist plots for (A) the EIS of F8BT film in 0.1 M TBAPF$_6$/AcN/10% v/v DCM and (B) the corresponding Rct values.

The charge transfer resistance R_{ct} indicating the kinetic resistance to charge transfer at the polymer/solution interface or electron transfer at the electrode/polymer interface were plotted as a function of the electrode potentials studied (**Figure 8.11b**). The plot reveals an exponential increase in R_{ct} upon decreasing potential, indicating that the electron transfer follows the Butler-Volmer formulation for electrode kinetics [47-48]. k_o and I_o are very important parameters in kinetic studies and they are directly proportional. A large value i.e k_o ≥ 2.0 x 10^{-4} ms^{-1} indicates a reversible system [49]. These parameters were estimated to ascertain the conductive behaviour of F8BT on the kinetics of the supporting electrolyte. The investigation of the conductive behaviour of F8BT is important since bulk heterojunction organic solar cells require the use of organic semiconductors for solar energy conversion. The response revealed a large k_o ($2(\pm0.2)$ x 10^{-2} cms^{-1}) and I_o ($8.9(\pm1.2)$ x 10^{-6} A) - (reversible system) for the first three responses from the more positive applied potential; while the less positive potential began to drift towards quasi-reversible behaviour. The response further shows the dependence of the heterogeneous electrochemical rate on the potential (**Table 8.3**) as described by the Butler-Volmer formulation.

Table 8.3: Kinetic parameters obtained with the Butler-Volmer equation

E/V	R_{ct}/kΩ	I_o x 10^{-6}/A	k_o x 10^{-2}/cm s^{-1}
-0.516	3.649	10	2.0
-0.716	4.274	9.0	2.0
-0.916	5.111	7.7	1.5
-1.116	6.963	5.6	1.1
-1.316	21.490	1.8	0.4
-1.516	68.150	0.6	0.1
Average (first 3 values)		8.9	1.8
SDEV (first 3 values)		1.2	0.2

8.3   Conclusion

Co-PPI was explored for its potential as acceptor for OSCs. Blends of an electron donor F8BT, electron acceptor PCBM and potential acceptor Co-PPI respectively were studied by spectroscopic and microscopic methods. The optical response in the form of UV-Vis revealed a broad absorption band in the Co-PPI in the Vis-NIR region and a bathochromic shift in its blend with F8BT relative to PCBM blend. This response shows that Co-PPI better match the electromagnetic spectrum and better compliments the donor, leading to a good interaction between the Co-PPI as acceptor and the F8BT donor. A virtually 100% Photoluminescence quenching was achieved. Co-PPI has been demonstrated in this study as a promising acceptor material for the active layer of BHJ OSCs. It revealed a good exciton generation, dissociation and charge transfer properties in the photoluminescence study upon blending with F8BT as a donor. The blend of Co-PPI and donor F8BT provided ideal characteristics for BHJ OSC

352

acceptor materials, e.g. broad light absorption and good miscibility. Another interesting property of Co-PPI is its air stability. The stability of Co-PPI in air gives room for easy handling, room temperature processability and long shelf life. These properties are important for materials used for solar cell device fabrication. To the best of our knowledge, this material has not been studied/applied for organic solar cell fabrication. Its Vis-NIR region absorption is a property that is capable of enhancing the property of a suitable donor, thereby improving efficiency. The kinetic investigation of the donor F8BT reveals (i) a potential-dependence of the kinetics of the electrode process that is in good agreement with the Butler-Volmer formulation for electrode kinetics and (ii) an almost ideal capacitive system.

UNIVERSITY *of the*
WESTERN CAPE

8.4 References

[1] F. C. Krebs, T. Tromholt and M. Jørgensen, "Upscaling of polymer solar cell fabrication using full roll-to-roll processing," *Nanoscale,* 2 (**2010**) 873 - 886.

[2] M. Jørgensen, K. Norrman, S. A. Gevorgyan, T. Tromholt, B. Andreasen and F. C. Krebs, "Stability of Polymer Solar Cells," *Adv. Mater.,* 24 (**2012**) 580 - 612.

[3] L. Dou, J. You, J. Yang, C.-C. Chen, Y. He, S. Murase, T. Moriarty, K. Emery, G. Li and Y. Yang, "Tandem polymer solar cells featuring a spectrally matched low-bandgap polymer," *Nat. Photon.,* 6 (**2012**) 180 - 185.

[4] Z. He, C. Zhong, S. Su, M. Xu, H. Wu and Y. Cao, "Enhanced power-conversion efficiency in polymer solar cells using an inverted device structure," *Nat. Photon.,* 6 (**2012**) 591 - 595.

[5] Z. He, C. Zhon, X. Huang, W.-Y. Wong, H. Wu, L. Chen, S. Su and Y. Cao, "Simultaneous Enhancement of Open-Circuit Voltage, Short-Circuit Current Density, and Fill Factor in Polymer Solar Cells," *Adv. Mater.,* 23 (**2011**) 4636 - 4643.

[6] J. You, L. Dou, K. Yoshimura, T. Kato, K. Ohya, T. Moriarty, K. Emery, C.-C. Chen, J. Gao, G. Li and Y. Yang, "A polymer tandem solar cell with 10.6% power conversion efficiency," *Nat. Commun.,* 4 (**2013**) 1 - 10.

[7] W. Zixuan, Z. Fujun, W. Jin, X. Xiaowei, W. Jian, L. Yang and X. Zheng, "Organic photovoltaic cells: Novel organic semiconducting materials and molecular arrangement engineering," *Chin. Sci. Bull.,* 57 (**2012**) 4143 - 4152.

[8] Y. He, H.-Y. Chen, J. Hou and Y. Li, "Indene-C_{60} Bisadduct: A New Acceptor for High-Performance Polymer Solar Cells," *J. Am. Chem. Soc.,* 132 (**2010**) 1377 – 1382.

[9] J. T. Bloking, X. Han, A. T. Higgs, J. P. Kastrop, L. Pandey, J. E. Norton, C. Risko, C. E. Chen, J.-L. Brédas, M. D. McGehee and A. Sellinger, "Solution-Processed

354

Organic Solar Cells with Power Conversion Efficiencies of 2.5% using Benzothiadiazole/Imide-Based Acceptors " *Chem. Mater.,* 23 (**2011**) 5484 - 5490.

[10]   Y. Zhou, T. Kurosawa, W. Ma, Y. Guo, L. Fang, K. Vandewal, Y. Diao, C. Wang, Q. Yan, J. Reinspach, J. Mei, A. L. Appleton, G. I. Koleilat, Y. Gao, S. C. B. Mannsfeld, A. Salleo, H. Ade, D. Zhao and Z. Bao, "High performance all-polymer solar cell via polymer side-chain engineering," *Adv. Mater.,* 26 (**2014**) 3767 - 3772.

[11]   C. Luo, X. Meng, L. Han, S. Sun, T. Lin, J. Suna, H. Peng and J. Chu, "n-Type pyromellitic diimide-benzodithiophene-containingconjugated polymers for all-polymer solar cells with highopen-circuit voltage," *Synth. Met.,* 196 (**2014**) 110 - 116.

[12]   W. Liu, R. Tkachov, H. Komber, V. Senkovskyy, M. Schubert, Z. Wei, A. Facchetti, D. Neher and A. Kiriy, "Chain-growth polycondensation of perylene diimide-based copolymers: a new route to regio-regular perylene diimide-based acceptors for all-polymer solar cells and n-type transistors," *Polym. Chem.,* 5 (**2014**) 3404 - 3411.

[13]   W. Li, W. S. C. Roelofs, M. Turbiez, M. M. Wienk and R. A. J. Janssen, "Polymer Solar Cells with Diketopyrrolopyrrole Conjugated Polymers as the Electron Donor and Electron Acceptor," *Adv. Mater.,* 26 (**2014**) 3304 - 3309.

[14]   Y. Lin, Y. Wang, J. Wang, J. Hou, Y. Li, D. Zhu and X. Zhan, "A Star-Shaped Perylene Diimide Electron Acceptor for High-Performance Organic Solar Cells," *Adv. Mater.,* 26 (**2014**) 5137–5142.

[15]   C. Mu, P. Liu, W. Ma, K. Jiang, J. Zhao, K. Zhang, Z. Chen, Z. Wei, Y. Yi, J. Wang, S. Yang, F. Huang, A. Facchetti, H. Ade and H. Yan, "High-efficiency all-polymer solar cells based on a pair of crystalline low-bandgap polymers," *Adv. Mater.,* 26 (**2014**) 7224 - 7230.

[16]   C. Lee, H. Kang, W. Lee, T. Kim, K.-H. Kim, H. Y. Woo, C. Wang and B. J. Kim, "High-Performance All-Polymer Solar Cells Via Side-Chain Engineering of the

Polymer Acceptor: The Importance of the Polymer Packing Structure and the Nanoscale Blend Morphology," *Adv. Mater.,* 27 (**2015**) 2466 - 2471.

[17]   S. Cataldo, P. Salice, E. Menna and B. Pignataro, "Carbon nanotubes and organic solar cells," *Energy Environ. Sci.,* 5 (**2015**) 5919 - 5940.

[18]   J. Y. Kwon, N. J. Singh, H. N. Kim, S. K. Kim, S. K. Kim and J. Yoon, "Fluorescent GTP-sensing in aqueous solution of physiological pH," *J. Am. Chem. Soc.,* 126 (**2004**) 8892 - 8893.

[19]   C. Gorman, "Metallodendrimers: Structural Diversity and Functional Behavior," *Adv. Mater.,* 10 (**1998**) 295 - 309.

[20]   G. R. Newkome, E. He and C. N. Moorefield, "Suprasupermolecules with novel properties: metallodendrimers," *Chem. Rev.,* 99 (**1999**) 1689 - 1746.

[21]   N. Farrell, "Polynuclear platinum drugs," *Met. Ions Biol. Syst.,* 42 (**2004**) 251 - 296.

[22]   P. Govender, B. Therrien and G. S. Smith, "Bio-Metallodendrimers – Emerging Strategies in Metal-Based Drug Design," *Eur. J. Inorg. Chem.,* 2012 (**2012**) 2853 - 2862.

[23]   R. Payne, P. Govender, B. Therrien, C. M. Clavel, P. J. Dyson and G. S. Smith, "Neutral and cationic multinuclear half-sandwich rhodium and iridium complexes coordinated to poly (propyleneimine) dendritic scaffolds: Synthesis and cytotoxicity," *J. Organomet. Chem.,* 729 (**2013**) 20 - 27.

[24]   C. J. Backlund, B. V. Worley and M. H. Schoenfisch, "Anti-biofilm action of nitric oxide-releasing alkyl-modified poly(amidoamine) dendrimers against Streptococcus mutans," *Acta Biomaterialia,* 29 (**2016**) 198 - 205.

[25]   S. Rajabnezhad, L. Casettari, J. K. W. Lam, A. Nomani, M. R. Torkamani, G. F. Palmieri, M. R. Rajabnejad and M. A. Darbandi, "Pulmonary delivery of rifampicin

microspheres using lower generation polyamidoamine dendrimers as a carrier," *Powder Technology,* 291 (**2016**) 366 - 374.

[26]   R. Malgas, S. F. Mapolie, S. O. Ojwach, G. S. Smith and J. Darkwa, "The application of novel dendritic nickel catalysts in the oligomerization of ethylene," *Catal. Commun.,* 9 (**2008**) 1612 - 1617.

[27]   R. Malgas-Enus, S. F. Mapolie and G. S. Smith, "Norbornene polymerization using multinuclear nickel catalysts based on a polypropyleneimine dendrimer scaffold," *J. Organomet. Chem.,* 693 (**2008**) 2279 - 2286.

[28]   R. Malgas-Enus and S. F. Mapolie, "Nickel metallodendrimers as catalyst precursors in the tandem oligomerization of ethylene and Friedel–Crafts alkylation of its olefinic products," *Inorg. Chim. Acta,* 409 (**2014**) 96 - 105.

[29]   A.-M. Caminade, A. Ouali, R. Laurent, C.-O. Turrin and J.-P. Majoral, "Coordination chemistry with phosphorus dendrimers. Applications as catalysts, for materials, and in biology," *Coord. Chem. Rev.,* 308 (**2016**) 478 - 497.

[30]   O. A. Arotiba, A. Ignaszak, R. Malgas, A. Al-Ahmed, P. G. Baker, S. F. Mapolie and E. I. Iwuoha, "An electrochemical DNA biosensor developed on novel multinuclear nickel (II) salicylaldimine metallodendrimer platform," *Electrochimica Acta,* 53 (**2007**) 1689 - 1696.

[31]   Y.-H. Tang, A. Ya-Ting Huang, P.-Y. Chen, H.-T. Chen and C.-L. Kao, "Metallodendrimers and dendrimer nanocomposites," *Current Pharmaceutical Design,* 17 (**2011**) 2308 - 2330.

[32]   S.-H. Hwang, C. N. Moorefield and G. R. Newkome, "Dendritic macromolecules for organic light-emitting diodes," *Chem. Soc. Rev.,* 37 (**2008**) 2543 - 2557.

[33]   D. Astruc, E. Boisselier and C. Ornelas, "Dendrimers Designed for Functions: From Physical, Photophysical, and Supramolecular Properties to Applications in Sensing,

357

Catalysis, Molecular Electronics, Photonics, and Nanomedicine," *Chem. Rev.,* 110 (**2010**) 1857 - 1959.

[34]   G. A. Nemnes and S. Iftimie, "Charge localization effects and transport in dendritic nanostructuresfor photovoltaic applications," *Appl. Surf. Sci.,* 352 (**2015**) 158 - 162.

[35]   T. Zhang, D.-Q. Xu, J.-M. Chen, P. Zhang and X.-C. Wang, "Synthesis and characterization of carbazole-based dendrimers as bipolar host materials for green phosphorescent organic light emitting diodes," *Chin. Chem. Lett.,* dx.doi.org/10.1016/j.cclet.2015.12.028 (**2016**)

[36]   S. F. Mapolie and J. L. van Wyk, "Synthesis and characterization of dendritic salicylaldimine complexes of copper and cobalt and their use as catalyst precursors in the aerobic hydroxylation of phenol," *Inorganic Chimica Acta,* 394 (**2013**) 649 - 655.

[37]   Y. Kim, S. Cook, S. M. Tuladhar, S. A. Choulis, J. Nelson, J. R. Durrant, D. D. C. Bradley, M. Giles, I. McCulloch, C.-S. Ha and M. Ree, "A strong regioregularity effect in self-organizing conjugated polymer films and high-efficiency polythiophene:fullerene solar cells," *Nat. Mater.,* 5 (**2006**) 197 - 203.

[38]   H. Zhou, L. Yang, S. Stoneking and W. You, "A Weak Donor-Strong Acceptor Strategy to Design Ideal Polymers for Organic Solar Cells," *Appl. Mater. Interf.,* 2 (**2010**) 1377 - 1383.

[39]   P. Suresh, S. K. Sharma, M. S. Roy and G. D. Sharma, "Photocurrent mechanism and photovoltaic properties of photo-electrochemical device based on PPAT and PPAT:TY blend," *Synth. Met.,* 159 (**2009**) 52 - 61.

[40]   S. A. Zapunidy, D. S. Martyanov, E. M. Nechvolodova, M. V. Tsikalova, Y. N. Novikov and D. Y. Paraschu, "Approaches to low-bandgap polymer solar cells: Using polymer charge-transfer complexes and fullerene metallocomplexes," *Pure Appl. Chem. ,* 80 (**2008**) 2151 - 2161.

358

[41]   S. Chatterjee, S. Banerjee and P. Banerji, "New polymer acceptor for solar cells application," *Synth. Met.,* 162 (**2012**) 566 - 572.

[42]   J. L. Bredas, R. Silbey, D. S. Boudreaux and R. R. Chance, "Chain-length dependence of electronic and electrochemical properties of conjugated systems: polyacetylene, polyphenylene, polythiophene, and polypyrrole," *J. Am. Chem. Soc.,* 105 (**1983**) 6555 - 6559.

[43]   S. Admassie, O. Inganas, W. Mammo, E. Perzon and M. R. Andersson, "Electrochemical and optical studies of the band gaps of alternating polyfluorene copolymers," *Synth. Met.,* 156 (**2006**) 614 - 623.

[44]   Y. Zhang, Y. Xiao, Y. Xie, L. Zhu, D. Shi and C. Cheng, "Fluorene-centered perylene monoimides as potential non-fullerene acceptor in organic solar cells," *Org. Electron.,* 21 (**2015**) 184–191.

[45]   A. Iwan, E. Schab-Balcerzak, K. P. Korona, S. Grankowska and M. Kamińska, "Investigation of optical and electrical properties of new aromatic polyazomethine with thiophene and cardo moieties toward application in organic solar cells," *Synth. Met.,* 185–186 (**2013**) 17 - 24.

[46]   J. Bobacka, M. Grzeszczuk and A. Ivaska, "Electron transfer at conducting polymer film electrodes: mechanism and kinetics of ferrocene oxidation at poly(3-octylthiophene)," *J. Electroanal. Chem.,* 427 (**1997**) 63 - 69.

[47]   E. G. Tolstopyatova, S. N. Sazonova, V. V. Malev and V. V. Kondratiev, "Electrochemical impedance spectroscopy of poly(3-methylthiophene) and poly(3-octylthiophene) film electrodes," *Electrochimical Acta,* 50 (**2005**) 1565 - 1571.

[48]   S. H. Cho, H. J. Lee, Y. Ko and S.-M. Park, "Electrochemistry of Conductive Polymers 47: Effects of Solubilizers on 3,4-Ethylenedixoythiophene Oxidation in

Aqueous Media and Properties of Resulting Films," *J. Phys. Chem. C,* 115 (**2011**) 6545 - 6553.

[49] P. Zanello, "Inorganic Electrochemistry: Theory, Practice, and Application," *Royal Society of Chemistry ISBN 0-85404-661-5,* 615 (**2003**).

CHAPTER NINE
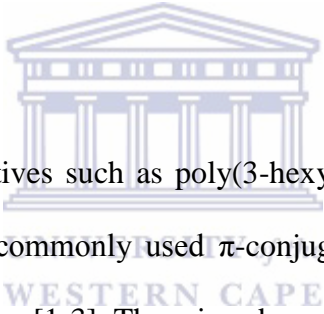
RESULTS AND DISCUSSION - Enhancing the Properties of Poly(Arylene Ethynylene)-*alt*-Poly(Arylene Vinylene)s (PAE-PAV) Polymers Based on Anthanthrone And Its Derivatives by Backbone Modification

Abstract
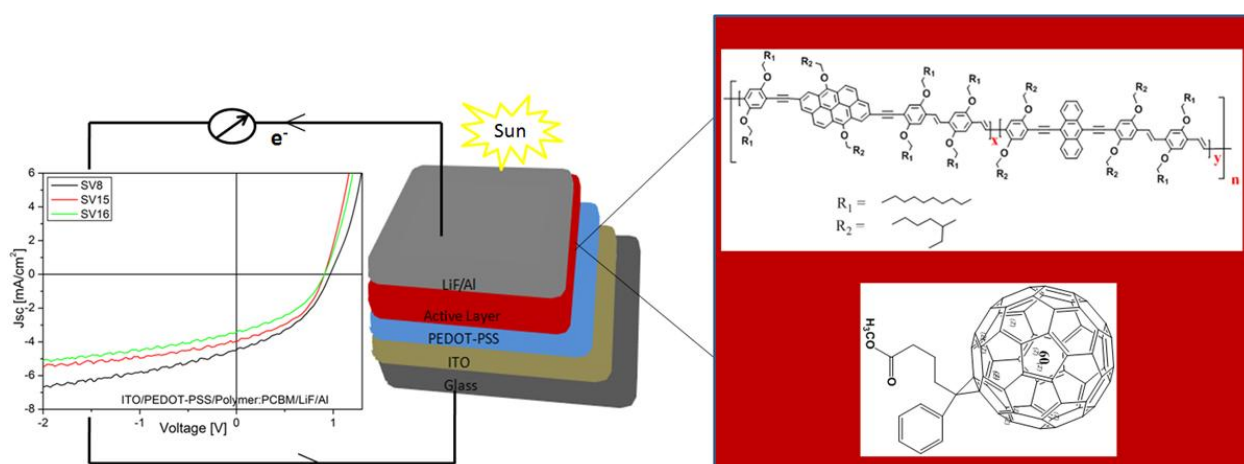
The design of advanced new generation conjugated materials with improved properties for photovoltaic applications has been the focus of research in recent years. This work reports on novel anthanthrone/anthracene and anthanthrene/anthracene co-polymers as p-type conjugated semiconductors in organic photovoltaics. Polycondensation reactions of luminophoric dialdehydes and bisphosphonate esters gave a class of novel π-conjugated co-polymers (SV9 – SV16) with well-defined structure confirmed by nuclear magnetic resonance and infrared spectroscopy. Polymers that are thermo-stable, with improved solubility and good film forming ability were obtained. The presence of anthracene

361

component together with the grafted alkyloxy side chains enhanced the solubility and process-ability of the co-polymers. The polymers are good photoconductors with interesting photo-physical properties in solution and films. The photo-physical and photovoltaic parameters greatly depend on the ratio of the components of the co-polymers and the nature of the grafted side chains. Photovoltaic devices with blends of SV15 and [6,6]-Phenyl C_{61} butyric acid methyl ester (PCBM) in 1:2 ratio gave J_{sc} of 3.97 mA/cm^2 and V_{oc} of 0.92 V corresponding to power conversion efficiency of 1.7%. This study reveals the potential of co-polymerization of anthanthrone or its derivative with anthracene as a useful method of improving the properties of anthanthrone based polymers for photovoltaic applications.

9   Introduction

At present, polythiophene derivatives such as poly(3-hexylthiophene) (P3HT) and poly (3-octylthiophene) (P3OT) are the commonly used π-conjugated polymers for fabrication of organic photovoltaic (OPV) devices [1-3]. There is a demand for the design of advanced new generation conjugated materials in the form of homo or co-polymers with better absorption and transport properties for photovoltaic applications. A number of π-conjugated materials with promising photovoltaic properties have been reported [4-8]. Improvement in the photovoltaic responses of these materials or development of new polymers with improvement in the efficiency of laboratory-type solar cells is necessary to advance this field of research.

A good understanding of the relationship between chemical structure and morphology of a polymer with its optical response is key to understanding how organic electronics (photovoltaic cells, light emitting diodes and field effect transistors) works [9-10]. Light emission, output yield in light emitting diodes and efficiency of photovoltaic cells [11-14]

362

can be tuned chemically through the linking of monomers in copolymerization or by physical mixing and subsequent co-precipitation [15]. In co-polymer synthesis, it is important to take into consideration intrinsic properties of each monomer in order to get a co-polymer with good properties for electronic devices. Properties like low band gap, good solubility in common organic solvents, inter and intra chain interactions are important for polymers for organic electronic applications.

In this report, two types of polycyclic aromatic compounds (anthanthrone/anthracene or anthanthrene/anthracene) in an alternating poly(arylene ethynylene)-alt-(arylene vinylene) (PAE-PAV) backbone were employed for co-polymerization. Anthracenes have been shown as attractive soluble polymer building blocks with high thermal and device stability [16]. They possess high fluorescence quantum yield and their emission can be tuned during polymerization by the incorporation of other arylene-building blocks [17]. The good photoconductive behavior, high fluorescence quantum yields in thin films and high absorption coefficients around 100 000 M^{-1} cm^{-1} of anthracene based polymers make them ideal for design of organic electronic devices [18] and they have been investigated [19-21] and used in light emitting diodes [22] transistors [23] and photovoltaic cells [24]. Anthanthrones on the other hand are polycyclic aromatic compounds with extended conjugation and symmetric structures used as pigments and vat dyes. Their large conjugated planar structure facilitates intermolecular interactions with good optical response and their extended π-conjugation is believed to be an advantage in photovoltaics. However, they have been rarely studied as building blocks for organic semiconductors; except the recent report by Morin group [25-26]. To the best of my knowledge, anthanthrone and its derivative (anthanthrene) were incorporated for the first time into the backbone of poly(arylene ethynylene)-*alt*-poly(arylene vinylene)s (PAE-PAV) in the course of this work as reported in

Chapter 5 of this report. The polymers show interesting optoelectronic properties with the un-substituted anthanthrone polymer (P1) having the most intriguing absorption properties. However, the polymers show poor photovoltaic responses which is attributed to their poor solubility. To optimize device performance, the advantage offered by the solubility of anthracene coupled with the good optical response of anthanthrone and its derivative (anthanthrene) were exploited to make co-polymers (SV9 – SV16) with different ratios as shown in **Figure 9.1 – 9.3** from monomers M1 – M3, Ma, Mb and Md (**Figure 9.1**). The photo-physical and photovoltaic performances of the co-polymers employed as donors with respect to i) the type of constituent (anthanthrone/anthracene or anthanthrene/anthracene), ii) the ratio of constituent and iii) the side chains were evaluated and compared to their corresponding homo-polymers P1 (an all anthanthrone polymer), P2 (an all anthanthrene polymer) and SV7 (an all anthracene polymer) (**Figure 9.2 – 9.3**).
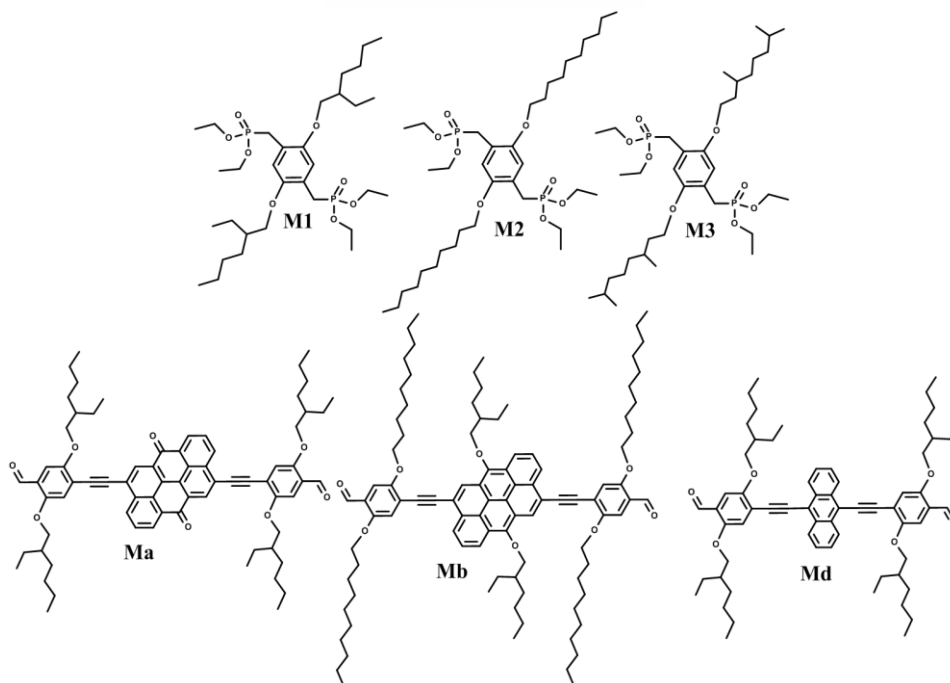
Figure 9.1: Synthesized monomers.
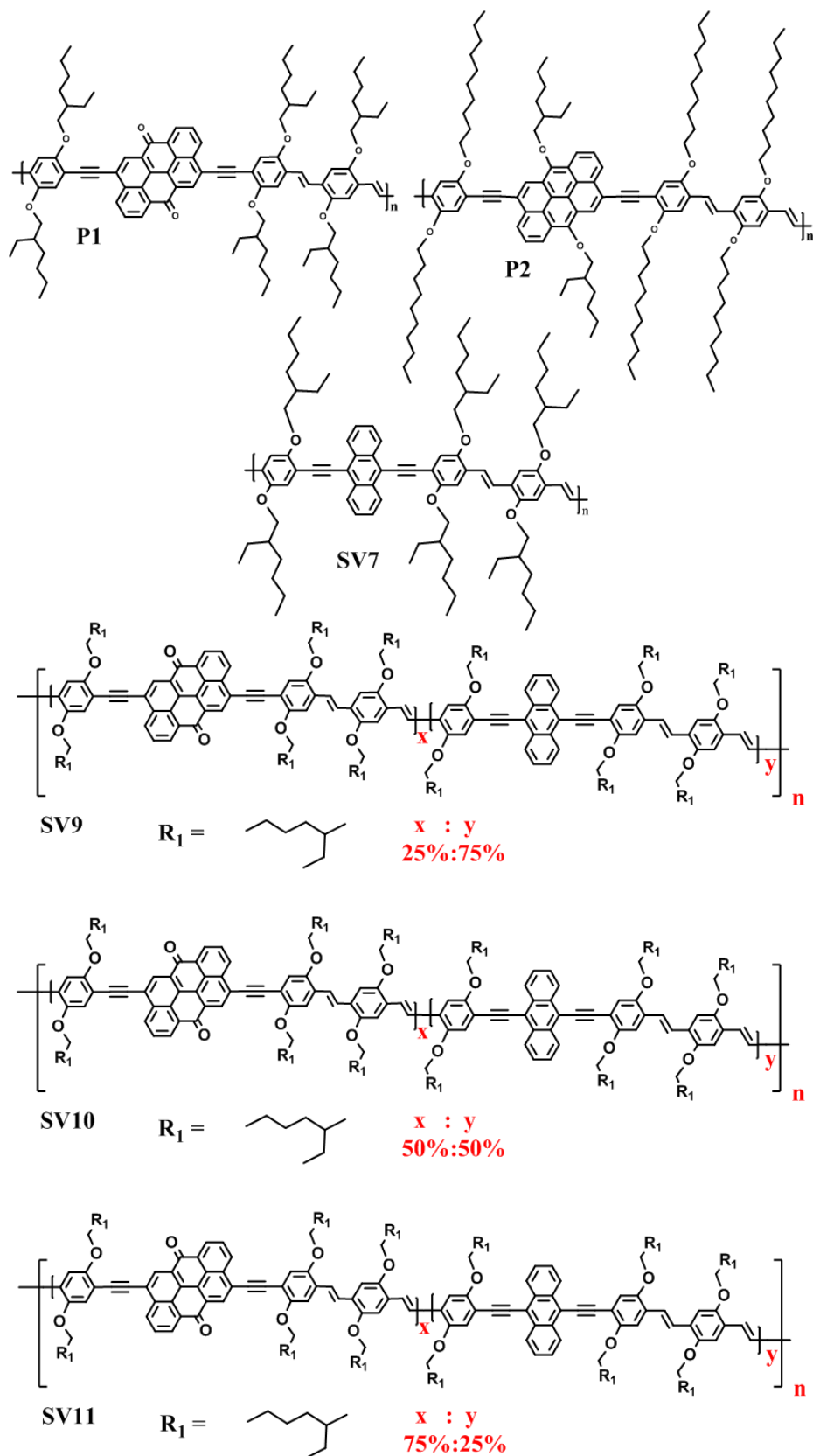
Figure 9.2: Synthesized homo-polymers P1, P2 and SV7; and co-polymers SV9 – SV11.
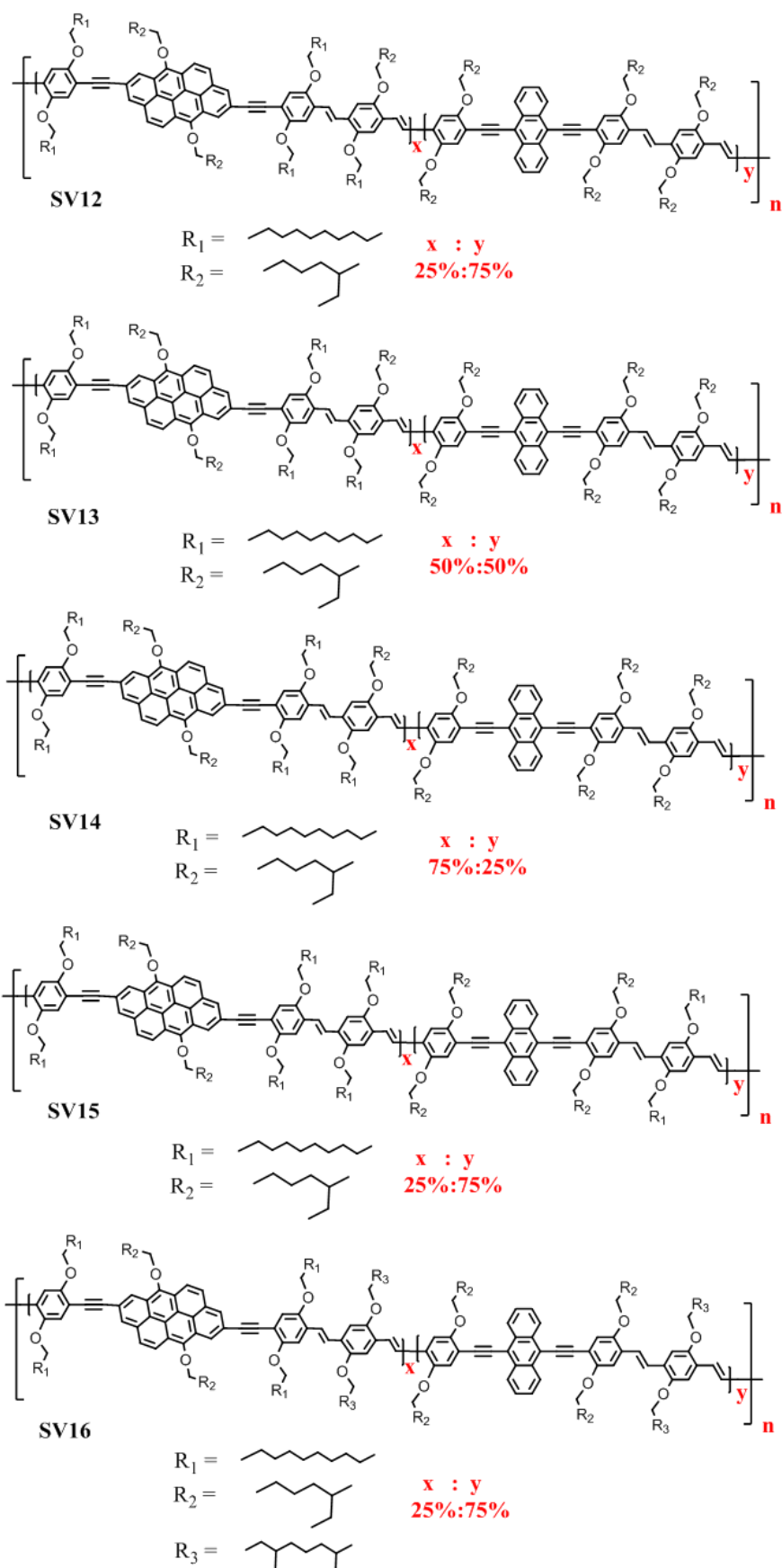
Figure 9.3: Synthesized co-polymers SV12 – SV16.

366

9.1 Experimental

9.1.1 Materials

All starting materials and solvents were purchased from commercial suppliers (Sigma Aldrich, Merck, Alfa Aesar and VWR).

9.1.2 Instrumentation

All NMR spectra were measured in deuterated chloroform using a Gemini 300 MHz spectrometer and Bruker Avance IIIHD 400 MHz Nanobay NMR spectrometer equipped with a 5 mm BBO using tetramethylsilane as internal standard. Gel permeation chromatography (GPC) measurements in the form of size exclusion chromatography (SEC) were performed using a Pump Deltachrom (Watrex Comp.) with a Midas autosampler and two columns of MIXED-B LS PL gel, particle size 10 μm. An evaporative light scattering detector (PL-ELS-1000 from Polymer Laboratories) was used; THF was the mobile phase and polystyrene standards were used for calibration. The solution and solid state absorption spectra were recorded using an ultra-violet-visible spectrophotometer (Perkin-Elmer Lambda 1050), while a PTi Photon Technology Intl. fluorometer was employed for emission measurements in solution. For the photoluminescence measurements in thin film, a Coherent GaN-based violet diode laser (Vioflame series) emitting at 405 nm was employed. The laser power on the sample was about 50 µW (spot diameter ~ 1mm). Polymer was dissolved in chlorobenzene ($\sim 1.0 * 10^{-5}$ M) for the solution measurements while films were cast from a 10 mg/mL solution of chlorobenzene on pre-cleaned glass slides for film measurements. Fourier transform infrared spectroscopy (FTIR) was performed with Thermo Scientific, Nicolet iS10

367

FTIR spectrometer equipped with a diamond crystal. Analyses were done between 650 and 4000 cm^{-1} wavenumbers and 64 scans were taken per sample at a resolution of 4 cm^{-1}. Data processing was done using the OMNIC software. Thermal behavior was analysed using TGA Q500 at ramp 20°C/min to 600°C in nitrogen at a flow rate of 50 mL/min.

9.1.3 Organic bulk heterojunction solar cells fabrication

9.1.3.1 Solution preparation

The investigated photovoltaic devices were fabricated using the regular or normal configuration of bulk-heterojunction architecture. For all donor:acceptor devices, 1:2 blend solution was in 1 ml chlorobenzene. Solutions were stirred at 70°C overnight.
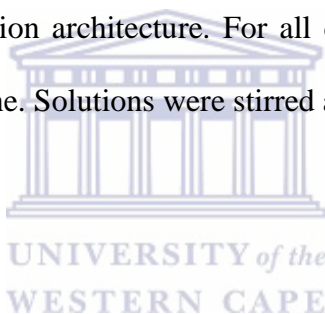
9.1.3.2 Substrate preparation

Indium tin oxide (ITO) glass slides were cut into 1.5 cm width using diamond cutter. Part of the cut ITO were covered with tape and the uncovered part etched (ITO etched away) by immersion in hydrochloric acid to prevent short circuits. The tape used is an adhesive tape that covers only the parts of glass-ITO slides where the ITO coating should remain. After etching, the substrates were rinsed with deionised water to remove the acid residue. The glass-ITO slides were then cut into 1.5 cm x 1.5 cm squares. The obtained squares were labelled in the top left corner in the non-conductive side (the side without ITO). The final cleaning process was done in an ultrasonic bath for 15 minutes in acetone and iso-propanol respectively.

368

9.1.3.3 Device fabrication

Cleaned substrates were plasma treated by (plasma ETCH PE-50) 5 min, 50 W O_2. Filtered poly (3,4-ethylenedioxythiophene)-poly(styrenesulphonate) (PEDOT-PSS) (a transparent, conductive polymer with high ductility) was then spun on each plasma treated substrate. The PEDOT-PSS was used to improve the extraction properties between the ITO and the active layer and to reduce the roughness of the ITO. PEDOT-PSS was gently wiped away from the etched part of the ITO using de-ionized water with a cotton bud to enhance contact with the electrode. The prepared donor:acceptor solution was spin coated on the PEDOT-PSS. The samples were then transferred to a nitrogen-filled glovebox to dry. Finally, LiF and Al (top electrode) were thermally evaporated on the glass/ITO/PEDOT-PSS/polymer:PCBM substrate to complete the device fabrication. The final device configuration is represented as glass/ITO/PEDOT-PSS/polymer:PCBM/LiF/Al.
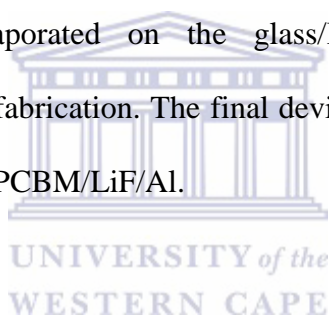
9.1.3.4 Device characterization

Current voltage (*I-V*) curves of the devices were recorded in the dark and under illumination using a solar simulator. A "Gold sun" Sun simulator was used to record the current-voltage characteristics with LS02821 LOT Quantum Design at 100 mW/cm^2 Keithley output reader. All *I-V* characteristics measurements were carried out in nitrogen filled glovebox. External quantum efficiency (EQE) were measured with EG & G Instruments lock-in-amplifier, optical chopper – SEITEC Instruments LTD Muller Electronics Optics LXH100. The thickness of the films was characterized with a Bruker DektakXT profilometer. The detailed step-by-step device fabrication and characterization method of the top cells is given below:

369

SV7 –SV16

Recipe:

Standard cutting & etching of Merck glass

Tap protecting, HCl conc. for 10 min

Standard cleaning of the samples:

1.) Acetone+ 15 min ultra sonic bath [RT],

2.) IPA+ 15 min ultra sonic bath [RT]

=> Compressed N_2 gun

Plasma treatment of the ITO substrate (Plasma ETCH PE50): 50 Watt, O_2, 5 min.

Spin coating of Clevios [pure, filtered 0.45 μm] (P VP AI 4083) on ITO glass

40 rps in 2 sec. for 2 sec. => 67 rps in 2 sec. for 30 sec. => END

Spin coating of polymer solution on PEDOT

Solution at ~70 °C

Chlorobenzene p.a. [Aldrich]

Spin coating parameter for top cells of each sample

SV7 40 rps in 1 sec. for 5 sec. => 70 rps in 4 sec. for 20 sec. => END

SV9 13 rps in 1 sec. for 5 sec. => 70 rps in 4 sec. for 20 sec. => END

SV10 20 rps in 2 sec. for 5 sec. => 70 rps in 4 sec. for 20 sec. => END

SV11 13 rps in 2 sec. for 5 sec. => 70 rps in 4 sec. for 20 sec. => END

SV12 20 rps in 2 sec. for 5 sec. => 70 rps in 4 sec. for 20 sec. => END

SV13 20 rps in 1 sec. for 5 sec. => 70 rps in 4 sec. for 20 sec. => END

SV14 30 rps in 1 sec. for 5 sec. => 70 rps in 4 sec. for 20 sec. => END

SV15 30 rps in 1 sec. for 5 sec. => 70 rps in 4 sec. for 20 sec. => END

SV16 20 rps in 1 sec. for 5 sec. => 70 rps in 4 sec. for 20 sec. => END

370

contact cleaning with toluene and H_2O for all samples

=> Top electrode: 0.7 nm LiF / 111 nm Al evaporation

=> Measurement "Gold sun" Sun simulator ~ 100 mW/cm^2 [no mismatch factor for eff. data]
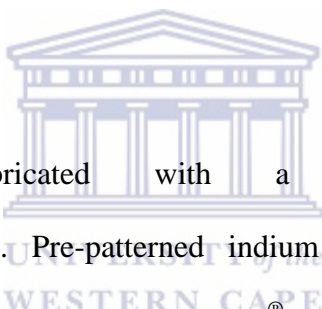
EQE measurement

Picture on the microscope

Thickness measurement with profilometer

9.1.4 Organic Light Emitting Diodes (OLEDs) Preparation and Characterization

9.1.4.1 Fabrication

The OLEDs were fabricated with a device configuration of glass/ITO/PEI/polymer/MoOx/Ag. Pre-patterned indium tin oxide (ITO) coated glass substrates were sequentially cleaned with Hellmanex®, de-ionized water, acetone and iso-propanol in an ultrasonic bath. The cleaned substrates were plasma treated in oxygen plasma for five minutes prior to layer deposition. Polyethylene imine (PEI) and the polymer layers were sequentially deposited by blade-coating at 70°C substrate temperature (PEI: 0.27 mg/ml in n-butanol, polymer: 10 mg/ml in chlorobenzene). MoOx (10 nm) and the silver (100 nm) were deposited by vacuum evaporation and the area of one cell is about 0.24 cm².

9.1.4.2 Characterization

Electroluminescence spectra of the OLEDs were measured using a Shamrock SR-303i monochromator and an Andor iDus Si-CCD detector. Different potentials were applied with a

371

Keithley 2401 source meter. The applied voltages and the corresponding currents are listed in the graphs.

9.1.5   Synthesis

9.1.5.1 Monomer Synthesis

Synthesis of M1

A mixture of 1,4-bis(bromomethyl)-2,5-(2-ethylhexyloxy)benzene (15.2 g, 18.97 mmol) and excess triethylphosphite (9.47 g, 57 mmol) was stirred and heated slowly to 150±160°C; simultaneously, the evolving ethyl bromide was distilled off. After 4 h, vacuum was applied for 30 mins at 180°C to distil off excess triethylphosphite. The resulting oil was allowed to cool to room temperature to form pure oily substance (14.4 g, 83% yield). ^{1}H NMR (300 MHz, CDCl$_3$) δ/ppm: 6.92 (d, J = 1.6 Hz, 2H), 4.08 − 3.89 (m, 8H), 3.79 (d, J = 5.6 Hz, 4H), 3.15 (d, J = 20.1 Hz, 4H), 1.76 − 1.59 (m, 2H), 1.55 − 1.34 (m, 10H), 1.34 − 1.11 (m, 18H), 0.99 − 0.63 (m, 12H); ^{13}C NMR (75 MHz, CDCl$_3$) δ 150.43, 119.30, 114.50, 71.17, 61.8, 39.65, 30.58, 29.09, 27.06, 25.21, 23.89, 23.00, 16.30, 14.01, 11.12.

M2 and M3 were prepared under similar reaction conditions as described for M1

Synthesis of M2

A mixture of 1,4-bis(bromomethyl)-2,5-decyloxybenzene (3.37 g, 5.85 mmol) and excess triethylphosphite (3.0 g, 17.6 mmol) was stirred and heated slowly to 150±160°C, and the

372

evolving ethyl bromide was distilled off simultaneously. The reaction went on for 4 h, after which vacuum was applied for 1 h at 180°C to distil off any excess triethylphosphite left in the mixture. The resulting oil was allowed to cool to room temperature to form a white solid, which was recrystallized from diethyl ether (30 ml) yielding (3.9 g, 97%) of pure substance. ^{1}H NMR (400 MHz, CDCl$_3$) δ 6.89 (s, 2H), 4.00 (m, 8H), 3.90 (t, *J* = 6.5 Hz, 4H), 3.20 (d, *J* = 20.3 Hz, 4H), 1.82 – 1.65 (m, 4H), 1.41 – 1.15 (m, 40H), 0.86 (t, *J* = 6.6 Hz, 6H); ^{13}C NMR (100 MHz, CDCl$_3$) δ 150.31, 119.28, 114.70, 68.89, 61.69, 31.89, 29.61, 29.56, 29.47, 29.44, 29.32, 26.92, 26.13, 25.54, 22.67, 16.38, 16.34, 16.31, 14.10.

Synthesis of M3

A mixture of 1,4-bis(bromomethyl)-2,5-(3,7-dimethyloctyloxy)benzene (5.1 g, 8.7 mmol) and excess triethylphosphite (4.4 g, 26.1 mmol) was stirred and heated slowly to 150±160°C, and the evolving ethyl bromide was concurrently distilled off. After 4 h, vacuum was applied for 30 min at 180°C to distil off any excess triethylphosphite still present in the mixture. The resulting oil was allowed to cool to room temperature to form a pure yellowish oil (5.73 g, 96% yield). ^{1}H NMR (400 MHz, CDCl$_3$) δ 6.85 (s, 2H), 4.07 – 3.79 (m, 12H), 3.14 (d, *J* = 20.4 Hz, 4H), 1.86 – 1.37 (m, 8H), 1.32 – 1.01 (m, 24H), 0.86 (d, *J* = Hz, 6H), 0.79 (d, *J* = 6.6 Hz, 12H); ^{13}C NMR (100 MHz, CDCl$_3$) δ 150.15, 119.18, 114.60, 67.01, 61.61, 38.99, 37.09, 36.23, 29.63, 27.72, 26.71, 25.32, 24.45, 22.45, 22.34, 19.44, 16.09.

Synthesis of Ma

4,10-Dibromoanthanthrone (2000 mg, 4.31 mmol) was given to a degassed solution of 67 mL of diisopropylamine and 167 mL of tetrahydrofuran. 30 mins later, Pd(PPh$_3$)$_4$ (221.4 mg,

373

0.192 mmol), and CuI (36.5 mg, 0.192 mmol) were added. Mixture was allowed to stir and degas for another 30 mins and thereafter, 2,5-bis((2-ethylhexyl)oxy)-4-ethynylbenzaldehyde (3700 mg, 9.60 mmol) (in a solution of degassed THF) was added drop-wisely. The reaction mixture was heated at 60°C for 72 h in a nitrogen atmosphere and monitored with TLC. 50 mL of toluene was thereafter added and heat removed while still stirring. After cooling to room temperature, the mixture was re-precipitated in cold methanol and refrigerated for 4 h. The mixture was filtered, re-dissolved in toluene and concentrated under vacuum. The residue was chromatographed on a silica gel column with toluene as eluent to yield 1200 mg (26%) of a purplish black substance. ^{1}H NMR (300 MHz, CDCl$_3$) δ 10.47 (s, 2H), 8.87 – 8.66 (m, 4H), 8.60 (s, 2H), 7.95 – 7.73 (m, 2H), 7.32 (s, 2H), 7,17 (s, 2H), 4.17 – 3.82 (m, 8H), 2.03 – 1.73 (m, 4H), 1.73 – 1.16 (m, 32H), 1.1 – 0.8 (m,24H); ^{13}C NMR (100 MHz, CDCl$_3$) δ 188.98, 182.12, 155.49, 154.07, 134.07, 133.74, 131.28, 129.53, 129.30, 128.63, 127.60, 125.45, 124.11, 119.09, 117.49, 109.36, 94.20, 93.96, 71.72, 71.65, 39.57, 39.48, 30.65, 30.34, 29.71, 29.14, 29.01, 24.04, 23.77, 23.11, 23.08, 14.13, 14.07, 11.26, 11.06.

Mb and Md were prepared under similar reaction conditions as described for Ma

Synthesis of Mb

4,10-Dibromo-6,12-ethylhexyloxylanthanthrene (2100 mg, 3.00 mmol) was given to a degassed solution of 47 mL of diisopropylamine and 117 mL of toluene. Pd(PPh$_3$)$_4$ (140.6 mg, 0.122 mmol), and CuI (23.2 mg, 0.122 mmol) were added after 30 mins of stirring and degassing and the reaction was allowed to run under same condition for 1 h. 2,5-bis(decyloxy)-4-ethynylbenzaldehyde (2961 mg, 6.70 mmol) was dissolved in 30 mL of toluene and degassed for 30 mins. The degassed solution of 2,5-bis(decyloxy)-4-

374

ethynylbenzaldehyde was added drop-wisely to the reaction mixture. The reaction mixture was heated at 70-80°C for 24 h in a nitrogen atmosphere and monitored with TLC. 50 mL of toluene was added and heat removed while still stirring. After cooling to room temperature, the precipitated diisopropylammonium bromide was filtered off and the solvent was evaporated under vacuum. The residue was chromatographed on a silica gel column with toluene:hexane (4:1) as eluent. 3200 mg (75% yield) of a greenish substance was obtained. ^{1}H NMR (300 MHz, CDCl$_3$) δ 10.49 (s, 2H), 8.94 (d, J = 7.4 Hz, 2H), 8.80 (d, J = 8.1 Hz, 2H), 8.73 (s, 2H), 8.19 (m, 2H), 7.38 (s, 2H), 7.22 (s, 2H), 4.29 (d, J = 5.5 Hz, 4H), 4.21 – 4.07 (m, 8H), 2.23 – 1.68 (m, 10H), 1.68 – 1.08 (m, 78H), 1.03 (t, J = 7.0 Hz, 6H), 0.90 (t, J = 6.6 Hz, 6H), 0.77 (t, J = 6.7 Hz, 6H); ^{13}C NMR (100 MHz, CDCl$_3$) δ 189.13, 155.51, 153.95, 150.13, 130.72, 127.58, 125.98, 125.61, 124.88, 124.52, 123.95, 121.27, 120.54, 120.22, 119.50, 117.12, 109.28, 96.16, 90.48, 69.26, 59.55, 41.30, 38.17, 31.94, 31.86, 31.26, 30.48, 29.70, 29.62, 29.46, 29.32, 26.12, 24.03, 23.31, 22.72, 22.58, 14.32, 14.15, 14.05, 11.56.

Synthesis of Md

9,10-Dibromoanthracene (5.77 g, 0.0172 mols) was given to a degassed solution of 211 mL of diisopropylamine and 529 mL of toluene. Pd(PPh$_3$)$_4$ (0.81 g, 0.70 mmol), and CuI (0.13 g, 0.70 mmol) were added after 30 mins of stirring and degassing and the reaction was allowed to run under same condition for 1 h. 2,5-bis((2-ethylhexyl)oxy)-4-ethynylbenzaldehyde (13.55 g, 0.0350 mols) was dissolved in 50 mL of toluene and degassed for 30 mins. The degassed solution of 2,5-bis((2-ethylhexyl)oxy)-4-ethynylbenzaldehyde was added to the reaction mixture drop-wisely by means of a controlled dropping funnel. The reaction mixture was heated at 75°C for 24 h in a nitrogen atmosphere and monitored with TLC. 80 mL of

375

toluene was added and heat removed while still stirring. After cooling to room temperature, the precipitated diisopropylammonium bromide was filtered off and the solvent was evaporated under vacuum. The residue was chromatographed on a silica gel column with hexane:dichloromethane (1:1) as eluent to yield a dark orange powder which was re-crystallized several times in methanol and 1% H_2O to yield (14.2 g, 87%) bright orange powder. ^1H NMR (300 MHz, $CDCl_3$) δ 10.52 (s, 2H), 8.93 − 8.67 (m, 4H), 7.78 − 7.56 (m, 4H), 7.44 (s, 2H), 7.33 (s, 2H), 4.21 − 3.90 (m, 8H), 2.08 − 1.75 (m, 4H), 1.75 − 1.14 (m, 32H), 0.92 (ddt, J = 39.4, 36.8, 7.3 Hz, 24H). ^{13}C NMR (75 MHz, $CDCl_3$) δ 189.09, 155.72, 154.07, 132.25, 127.48, 126.99, 125.18, 120.23, 118.89, 117.20, 109.39, 99.06, 94.37, 71.65, 39.55, 30.70, 30.31, 29.09, 24.07, 23.74, 23.05, 14.07, 11.28, 10.95.

9.1.5.2 Polymer Synthesis

Synthesis of P1

For the synthesis of P1, a solution of Ma (150 mg, 0.14 mmol) and M1 (89 mg, 0.14 mmol) in dry toluene (12 mL) was mechanically stirred and heated under nitrogen to reflux. The polymerization was initiated by the addition of potassium *tert*-butoxide (63 mg, 0.56 mmol) and an instant color change from deep pink to black was observed. Reaction mixture was stirred for 45 min and additional toluene (100 mL) was added. The reaction was quenched with aqueous HCl (10%, 10 mL). The organic phase was separated and washed with de-ionized water until a pH of ~ 7 was obtained. Residual water was removed from the mixture by heating to reflux in a Dean Stark apparatus. The obtained solution was concentrated under reduced pressure using a rotary evaporator. The resulting concentrated solution was precipitated in cold methanol and kept in the refrigerator for 24 h. After 24 h the precipitate

was filtered off in a Soxhlet thimble and transferred into a Soxhlet extractor. Extraction was done using methanol to remove oligomers and any impurity. The extraction continued until the extract became colorless. The polymer was re-dissolved in toluene, re-precipitated in cold methanol and stored in the refrigerator. After 24 h, it was filtered and dried under air to obtain 190 mg (95% yield) of black partially soluble polymeric material. GPC (THF as eluent; polystyrene as standard): Mn 1,830 g/mol, Mw 3,570 g/mol, PDI 2. ^{1}H NMR (300 MHz, CDCl$_3$) δ 10.48 (s), 9.25 – 8.41 (m, anthanthronylene H's), 8.07 – 6.67 (m, arylene vinylene H's), 4.37 – 3.20 (m, -CH2O-), 2.49 – 0.37 (m, alkyl H's). FTIR cm^{-1}: 3064 (ν(=C-H)), 2962, 2934 and 2878 (ν(C-H)), 2198 (ν(C≡C)), 1659 (ν(C=O)), 1575 (ν(C=C) vinylene linker), 1500 (ν(C=C) aromatic ring), 1464 (δ (CH$_2$)), 1380 (δ (CH$_3$)), 1203 (ν(C=C-O-C) aromatic-aliphatic).

P2, SV7, SV9 – SV16 were prepared under similar reaction conditions as described for P1

Synthesis of P2

A solution of Mb (170 mg, 0.12 mmol) and M2 (83 mg, 0.12 mmol) in dry toluene (12 mL) was mechanically stirred and heated under nitrogen to reflux. Potassium *tert*-butoxide (54 mg, 0.48 mmol) was added at a stable temperature to initiate the reaction. A color change from bright to dark green was observed. The reaction mixture was stirred for 80 min. Thereafter, toluene (100 mL) was added, and the reaction was quenched with aqueous HCl (10%, 10 mL) to neutralize the potassium tert-butoxide. Mixture was cooled to room temperature; the organic phase separated and washed with de-ionized water until a pH of ~ 7 was obtained. Residual water was removed from the mixture by heating to reflux in a Dean Stark apparatus. The obtained solution was concentrated under reduced pressure using a

rotary evaporator. The resulting concentrated solution was precipitated in cold methanol and kept in the refrigerator for 24 h. After 24 h the precipitate was filtered off and transferred into a Soxhlet extractor, and extracted using methanol. The polymer was re-dissolved in chloroform and re-precipitated in cold methanol. It was filtered and dried after 24 h to obtain 220 mg (95% yield) of brownish green polymeric material. GPC (THF as eluent; polystyrene as standard): Mn 3,200 g/mol, Mw 11,730 g/mol, PDI 3.7. ^{1}H NMR (300 MHz, CDCl$_3$) δ 9.05 - 8.22 (anthanthrenylene H's), 7.58 - 6.92 (arylene vinylene H's), 4.28- 3.28 (m, -CH$_2$O-), 2.41 – 0.42 (m, alkyl H's). FTIR cm^{-1}: 3064 (ν(=C-H)), 2962, 2924 and 2850 (ν(C-H)), 2180 (ν(C≡C)), 1594 (ν(C=C) vinylene linker), 1500 (ν(C=C) aromatic ring), 1464 (δ (CH$_2$)), 1203 (ν(C=C-O-C) aromatic-aliphatic).

Synthesis of SV7

Dialdehyde Md (1000 mg, 1.06 mmol) and bisphosphonate M1 (671 mg, 1.06 mmol) were dissolved in dried toluene (80 ml) to give a greenish brown color while stirring vigorously under nitrogen and heating under reflux. Potassium-*tert*-butoxide (474 mg, 4.23 mmol) was added (instant color change to dark brown orange was observed); and the reaction mixture was heated at reflux for 80 mins. After 80 mins benzaldehyde was added and the mixture allowed stirring for 10 mins. Toluene was added, heat removed and aqueous HCl (10 wt.%) was added. The purification process yielded a brownish red polymer (1100 mg (0.8436 mmol with respect to the repeating unit), 80 %). GPC (THF, polystyrene): M_w= 15,870 g/mol, M_n = 6,720 g/mol, PDI = 2.4. ^{1}H NMR (300 MHz, CDCl$_3$) δ 8.83, 7.59 and 7.05 – 6.66 (arylene and vinylene H´s); 4.30 – 3.37 (-CH$_2$O-); 2.19 – 0.49 (CH$_3$(CH$_2$)$_3$CH(CH$_2$CH$_3$)-).

Synthesis of SV9

Dialdehydes Ma (313.4 mg, 0.26 mmol), Md (750 mg, 0.79 mmol) and bisphosphonate M1 (670 mg, 1.06 mmol) were dissolved in dried toluene (120 mL) to give a reddish brown orange color while stirring vigorously under nitrogen and heating under reflux. The polycondensation was initiated by addition of potassium-*tert*-butoxide (473.8 mg, 4.22 mmol) when a stable temperature was achieved and an instant color change to black was observed. After 60 mins benzaldehyde was added and the reaction allowed running for 10 mins. Toluene (50 ml) was added and the heating turned off. Reaction mixture was allowed to continue to stir at room temperature for 10 mins and 10% HCl was added. Stirring continued for about 20 min to dissolve part of the reaction mixture. The organic layer was separated and extracted several times with distilled water until the water phase became neutral (pH = 6 - 7). A Dean-Stark apparatus was used to dry the organic layer. The hot (50-60°C) toluene solution was filtered; the filtrate was concentrated to the minimum by using a rotary evaporator and then precipitated in vigorously stirred cold methanol (250 ml). The polymer was extracted by Soxhlet extraction with hot methanol until a clear solution was observed around the thimble. The polymer was again dissolved in a small amount of toluene, re-precipitated in cold methanol and kept for 24 h under 4 - 8°C. It was thereafter filtered and allowed to dry under air to obtain 1.1 g (47%) of soluble black fibrous polymer. GPC (THF): M_w 13,550 g/mol, M_n 3,590 g/mol, PDI 3.8. ^{1}H NMR (300 MHz, CDCl$_3$) δ 8.98 (d, *J* = 8.5 Hz, 1H), 8.78 (d, *J* = 25.3 Hz, 7H), 7.90 (d, *J* = 7.4 Hz, 1H), 7.58 (d, *J* = 19.7 Hz, 9H), 7.04 – 6.68 (m, 5H), 4.23 – 3.73 (m, 18H), 3.73 – 3.39 (m, 5H), 2.11 – 0.56 (m, 172H).

379

Synthesis of SV10

Dialdehydes Ma (351.1 mg, 0.30 mmol), Md (280 mg, 0.30 mmol) and bisphosphonate M1 (375.3 mg, 0.59 mmol) were dissolved in dried toluene (80 mL) to give a brownish orange color while stirring vigorously under nitrogen and heating under reflux. Potassium-*tert*-butoxide (265.4 mg, 2.36 mmol) was added (instant color change to black was observed); and the reaction mixture was heated at reflux for 60 mins. Benzaldehyde was added and 10 min later, toluene (50 mL) and aqueous HCl (10 wt. %, 10 mL) were added to quench the reaction. The organic phase was separated and extracted several times with distilled water until the water phase became neutral (pH 6 - 7). The organic layer was dried in a Dean-Stark apparatus. The resulting hot toluene mixture was filtered to remove the insoluble part. The filtrate was evaporated under vacuum and precipitated in cold methanol (250 mL). The precipitate was filtered and the polymer was extracted with a Soxhlet extractor using hot methanol until a clear methanol solution was observed in the thimble. Polymer was re-dissolved in toluene (20 mL) and re-precipitated in cold methanol, stored at 4 - 8°C for 24 h, filtered and dried under air. 350 mg (26%) of soluble black fibrous polymer was obtained. GPC (THF): M_w 4,710 g/mol, M_n 1,850 g/mol, PDI 2.5. ^{1}H NMR (300 MHz, CDCl$_3$) δ 8.99 (s, 1H), 8.79 (d, J = 20.0 Hz, 8H), 7.92 (s, 2H), 7.58 (d, J = 17.9 Hz, 10H), 7.02 − 6.74 (m, 7H), 4.21 − 3.73 (m, 23H), 3.55 (d, J = 38.1 Hz, 7H), 2.10 − 0.50 (m, 250H).

Synthesis of SV11

Dialdehydes Ma (519.1 mg, 0.44 mmol), Md (138 mg, 0.15 mmol) and bisphosphonate M1 (369.9 mg, 0.58 mmol) were dissolved in dried toluene (80 mL) to give a brownish orange color while stirring vigorously under nitrogen and heating under reflux. Potassium-*tert*-

380

butoxide (261.6 mg, 2.33 mmol) was added (instant color change to black was observed); and the reaction mixture was heated at reflux for 60 mins. Afterwards, benzaldehyde was added and 10 min later, toluene (80 mL) and aqueous HCl (10 wt. %, 10 mL) were added to quench the reaction. The organic phase was separated and extracted several times with distilled water until the water phase became neutral (pH 6 - 7). The organic layer was dried in a Dean-Stark apparatus. The resulting toluene mixture was filtered to remove the insoluble part. The soluble part was evaporated under vacuum and precipitated in cold methanol (250 mL). The polymer was extracted with a Soxhlet extractor using hot methanol until a clear methanol solution was observed in the thimble. Polymer was re-dissolved in toluene (20 mL) and re-precipitated in methanol, stored at 4 - 8°C for 24 h, filtered and dried under air. Only 130 mg (10%) of poorly soluble black material was obtained. The main part of the product was insoluble. GPC (THF): M_w 4,390 g/mol, M_n 1,170 g/mol, PDI 3.8. ^{1}H NMR (300 MHz, CDCl$_3$) δ 9.00 (s, 1H), 8.82 (s, 11H), 7.91 (s, 2H), 7.61 (s, 10H), 6.98 – 6.62 (m, 9H), 3.99 (s, 30H), 3.56 (d, J = 38.9 Hz, 9H), 2.09 – 0.48 (m, 465H).
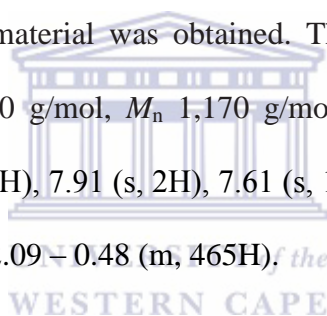
Synthesis of SV12

Dialdehyde Mb (248.7 mg, 0.18 mmol), Md (500 mg, 0.53 mmol), and bisphosphonate M1 (446.7 mg, 0.70 mmol) were dissolved in dried toluene (80 mL) to give a greenish dark brown green color while stirring vigorously under nitrogen and heating under reflux. The polycondensation was initiated by addition of potassium-*tert*-butoxide (315.8 mg, 2.81 mmol) when a stable temperature was achieved and an instant color change to dark brown orange was observed. The reaction mixture was heated at reflux for 80 min. After reacting for 80 mins, benzaldehyde was added and mixture stirred for 10 mins; the heating was stopped and the mixture was diluted with toluene (50 ml), and aqueous HCl (10 wt. %, 20 ml) was

381

added to quench the reaction. The organic layer was dried in a Dean-Stark apparatus. The solution was filtered, concentrated under vacuum, dissolved in 10 mL toluene and precipitated in methanol. The polymer was filtered off and extracted for 24 h with methanol (Soxhlet extraction). After re-dissolving in toluene the polymer was once more precipitated in methanol and kept at 4 - 8°C for 24 h, filtered and dried under air to obtain 880 mg of soluble deep brownish fibrous polymer (48% yield). GPC (THF): M_w 15,280 g/mol, M_n 6,230 g/mol, PDI 2.5. ^{1}H NMR (300 MHz, CDCl$_3$) δ 9.03 (d, J = 7.6 Hz, 1H), 8.94 – 8.70 (m, 8H), 8.34 – 8.11 (m, 1H), 7.59 (d, J = 19.7 Hz, 10H), 7.04 – 6.58 (m, 6H), 4.45 – 3.75 (m, 21H), 3.75 – 3.37 (m, 5H), 2.28 – 0.53 (m, 203H).

Synthesis of SV13

Dialdehyde Mb (447.8 mg, 0.32 mmol), Md (300 mg, 0.32 mmol), and bisphosphonate M1 (402.1 mg, 0.63 mmol) were dissolved in dried toluene (80 mL) to give a dirty green orange color while stirring vigorously under nitrogen and heating under reflux. Potassium *tert*-butoxide (284.3 mg, 2.53 mmol) (instant color change to dirty green orange was observed); and the reaction mixture was heated at reflux for 80 min. The polycondensations was quenched by addition of benzaldehyde, toluene and dilute HCl (10%). The organic layer was separated, extracted with distilled water until the water phase became neutral (pH = 6 - 7), dried by means of a Dean stark apparatus, filtered at room temperature, concentrated and precipitated in cold methanol (250 ml). The polymer was extracted with methanol for 24 h, dissolved in 10 mL toluene and re-precipitated in methanol. The resulting blackish brown fibrous polymer was filtered and dried in air to obtain 880 mg (53% yield). GPC (THF): M_w 16,020 g/mol, M_n 6,340 g/mol, PDI 2.5. ^{1}H NMR (300 MHz, CDCl$_3$) δ 9.05 (t, J = 9.7 Hz,

1H), 8.95 – 8.68 (m, 4H), 8.35 – 8.08 (m, 1H), 7.59 (d, J = 17.9 Hz, 4H), 7.03 – 6.66 (m, 3H), 4.47 – 3.73 (m, 12H), 3.73 – 3.40 (m, 2H), 2.28 – 0.54 (m, 114H).
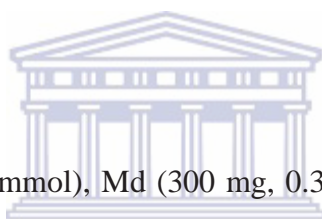
Synthesis of SV14

Dialdehyde Mb (448.0 mg, 0.32 mmol), Md (100 mg, 0.11 mmol), and bisphosphonate M1 (268.1 mg, 0.42 mmol) were dissolved in dried toluene (80 mL) to give a deep green color while stirring vigorously under nitrogen and heating under reflux. Potassium *tert*-butoxide (189.6 mg, 1.69 mmol) (gradual color change to deep dirty green orange was observed); and the reaction mixture was heated at reflux for 80 min. Afterwards, benzaldehyde (2 mL) was added and 10 min later, toluene (80 mL) and aqueous HCl (10 wt. %, 10 mL) were added to quench the reaction. The organic phase was separated and extracted several times with distilled water until the water phase became neutral (pH 6 - 7). The organic layer was dried in a Dean-Stark apparatus and the resulting toluene mixture was filtered to remove any solid impurity or insoluble part. No insolubility was observed. The filtrate was concentrated under vacuum and precipitated in cold methanol (250 mL). The polymer was extracted with a Soxhlet extractor using hot methanol until a clear methanol solution was observed in the thimble. Polymer was re-dissolved in toluene (20 mL) and re-precipitated in methanol, stored at 4 - 8°C for 24 h, filtered and dried under air to obtain a deep red fibrous material 530 mg (48% yield). GPC (THF): M_w 14,750 g/mol, M_n 7,090 g/mol, PDI 2.1. ^{1}H NMR (300 MHz, CDCl$_3$) δ 9.05 (dd, J = 12.1, 7.1 Hz, 1H), 8.94 – 8.67 (m, 2H), 8.36 – 8.07 (m, 1H), 7.75 – 7.41 (m, 2H), 7.03 – 6.63 (m, 2H), 4.52 – 3.70 (m, 8H), 3.53 (d, J = 26.0 Hz, 1H), 2.34 – 0.57 (m, 78H).

Synthesis of SV15

Dialdehyde Mb (198.9 mg, 0.14 mmol), Md (400 mg, 0.42 mmol), and bisphosphonate M2 (388.9 mg, 0.56 mmol) were dissolved in dried toluene (80 mL) to give a greenish brown color while stirring vigorously under nitrogen and heating under reflux. Potassium *tert*-butoxide (252.7 mg, 2.25 mmol) (instant color change to brownish orange was observed); and the reaction mixture was heated at reflux for 80 min. Benzaldehyde was added and 10 min later, toluene (80 mL) and aqueous HCl (10 wt. %, 10 mL) were added to quench the reaction. The organic phase was separated and extracted several times with distilled water until the water phase became neutral (pH = 6 - 7). The organic layer was dried in a Dean−Stark apparatus. After filtration, the toluene solution was concentrated under vacuum and precipitated in cold methanol. The precipitate was filtered and the polymer was extracted for 24 h with methanol (Soxhlet extraction), dissolved once more in toluene, and re-precipitated in cold methanol. Filtration and drying yielded a brownish red fibrous polymer of 760 mg (50% yield). GPC (THF): M_w 34,720 g/mol, M_n 9,280 g/mol, PDI 3.7. ^{1}H NMR (300 MHz, CDCl$_3$) δ 9.03 (s, 1H), 8.82 (s, 5H), 8.23 (s, 1H), 7.79 − 7.42 (m, 6H), 6.86 (t, J = 19.0 Hz, 4H), 3.94 (dt, J = 51.8, 41.2 Hz, 16H), 2.29 − 0.53 (m, 130H).

Synthesis of SV16

For SV16, dialdehyde Mb (174.2 mg, 0.12 mmol), Md (350 mg, 0.37 mmol), and bisphosphonate M3 (340.4 mg, 0.49 mmol) were dissolved in dried toluene (80 mL) to give a greenish brown color while stirring vigorously under nitrogen and heating under reflux. Potassium *tert*-butoxide (252.7 mg, 2.25 mmol) (instant color change to brownish orange was observed); and the reaction mixture was heated at reflux for 80 min. After 80 mins

384

benzaldehyde was added and the mixture allowed stirring for 10 mins. Toluene was added, heat removed and aqueous HCl (10 wt. %) was added. The purification process yielded a soluble brownish red fibrous polymer of 630 mg (47% yield). GPC (THF): M_w 26,290 g/mol, M_n 9,230 g/mol, PDI 2.8. ^{1}H NMR (300 MHz, CDCl$_3$) δ 9.05 (s, 1H), 8.83 (d, J = 3.7 Hz, 7H), 8.23 (s, 1H), 7.57 (d, J = 17.0 Hz, 10H), 7.06 – 6.69 (m, 5H), 4.42 – 3.46 (m, 25H), 2.24 – 0.50 (m, 214H).

9.2   Results and Discussion

9.2.1   Synthesis and Material Verification/Confirmation

9.2.1.1 Synthesis of the Monomers

The preliminary synthesis of the monomers (bisphosphonate esters (**M1** – **M3**) and luminophoric dialdehydes (**Ma**, **Mb** and **Md**)) (**Figure 9.1**) are essential steps to the synthesis of the polymers (**Figure 9.2 and 9.3**) going by the Horner-Wadsworth-Emmons olefination reaction. The monomer syntheses were achieved through a series of reactions. The bisphosphonate esters were synthesized starting with the O-alkylation of hydroquinone with the corresponding alkyl bromides, dibromomethylation of the alkyloxy derivative using NaBr/H$_2$SO$_4$ and paraformaldehyde; the dibromomethyl derivatives were finally converted to the corresponding bisphosphonate esters by the Michealis-Arbuzov reaction. The conjugated luminophoric dialdehydes were synthesized through the Sonogashira Pd-catalyzed cross-coupling reaction of the corresponding 2,5-bis(alkyloxy)-4-ethynylbenzaldehyde. **M1** and **M3** were obtained as viscous brown and yellow oil respectively while **M2** was obtained as a white solid. **Ma**, **Mb** and **Md** were obtained as purple, green and orange solids respectively.

385

9.2.1.2 Synthesis of the Polymers

All homo and co-polymers reported in this study were obtained through the Horner-Wadsworth-Emmons (HWE) polycondensation reaction of the corresponding dialdehydes and bisphosphonates in dry toluene solution in the presence of an excess of potassium *tert*-butoxide [18, 27-33]. The dialdehydes are synthesized with the ethynyl motifs embedded while the vinylene constituent is introduced during the polycondensation. Reacting the anthanthrone/anthanthrene/anthracene dialdehydes (**Ma**, **Mb** and/**Md**) with the phenyl based bisphosphonates (**M1**, **M2** or **M3**), homo or co-polymers with identical conjugation backbone but varying ratio and/or diverse combinations and distributions of side chains were realized.

The Horner-Wadsworth-Emmons polycondensation reaction of Ma, Md and M1 to give SV9 – SV11 under the same reaction conditions as for the synthesis of all alkyloxy-substituted hybrid polymers led to partially insoluble materials which were then filtered to separate the soluble part. This resulted in low yield soluble portion of these polymers (SV9 (47%), SV10 (26%) and SV11 (10%). It is worthy of note that the yields of polymerization were estimated from the soluble fraction obtained after filtration and purification. Thus, the low yields obtained for SV10 and SV11 is a result of their relatively poor solubility. The main part of SV11 was insoluble thus lowering the yield of the desirable soluble product. SV12 – SV16 were obtained at an average yield of 50%. SV9 – SV11 were obtained as black fibrous materials except for SV11 which was not fibrous; SV12 was obtained as deep brownish fibrous material, SV13 as blackish brown fibrous material, SV14 as deep red fibrous material, while SV15 and SV16 were obtained as brownish red fibrous materials. The chemical structures were confirmed by NMR and FTIR spectroscopy.

9.2.1.3 Nuclear Magnetic Resonance Spectroscopic Investigation

The NMR of the monomers and polymers were measured in deuterated chloroform. For the bisphosphonate monomers (M1, M2 and M3), the ^{1}H NMR (**Figure 9.4)** reveal the protons in the two -CH groups in the benzene rings in the downfield region 6.92 – 6.85 ppm, the -CH$_2$ protons in the phosphonate end of the compounds and those directly linked to the oxygen in the alkyloxy side chain are seen in the region 4.04 – 3.73 ppm, the -CH$_2$ protons linking the benzene ring to the phosphonate are seen around 3.20 – 3.14 ppm; and the -CH next to the -CH$_2$ attached to the oxygen ring (in the case of M1 and M3), all -CH$_3$ and other -CH$_2$ protons present in the compound appear in the up-field region 1.86 – 0.63 ppm.
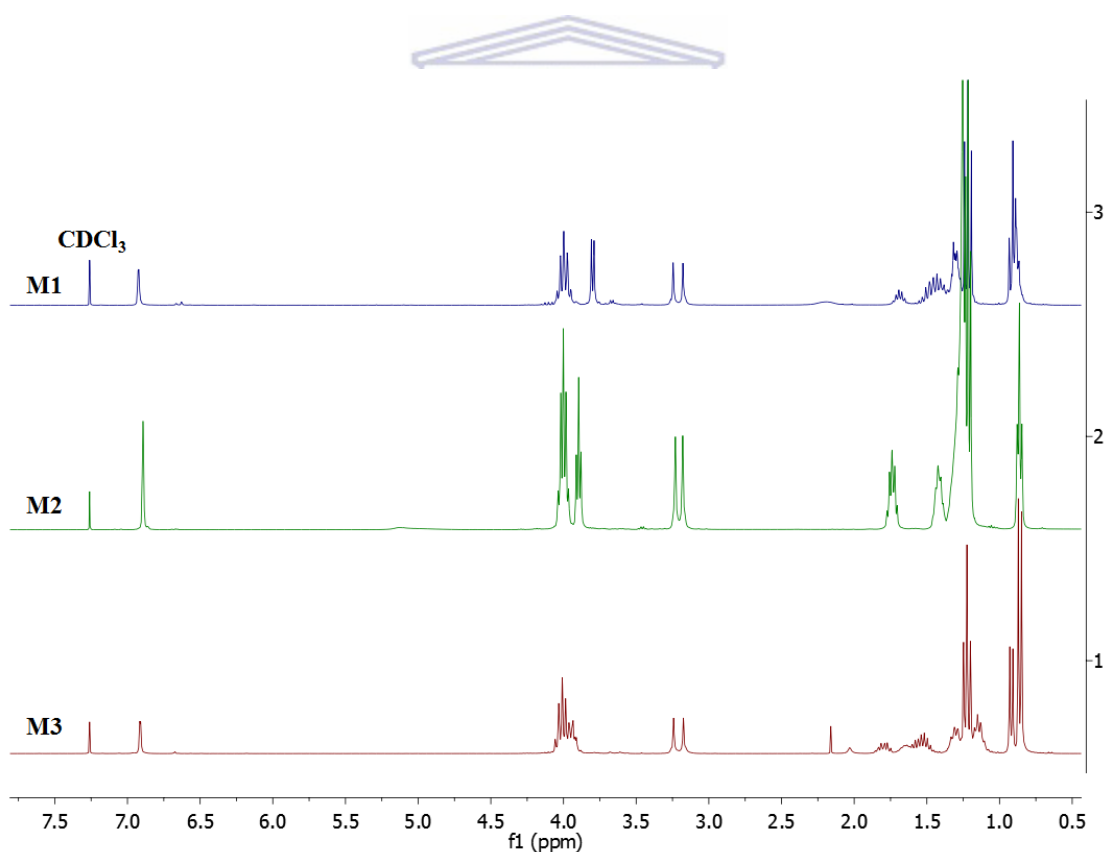
Figure 9.4: ^{1}H NMR of M1 – M3.

The ^{13}C NMR (**Figure 9.5**) reveal the carbons present in the compound while the ^{31}P NMR (**Figure 9.6**) reveal just a signal confirming the presence of just one type of phosphorous present in the compound as expected.
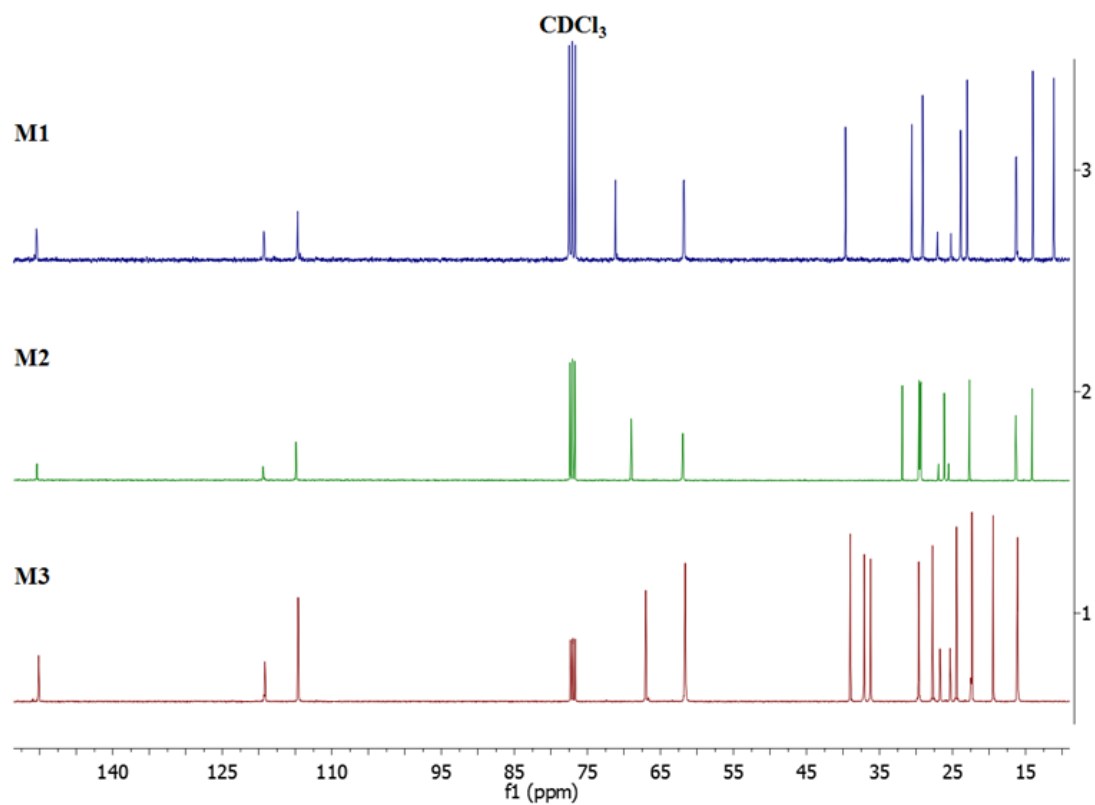
Figure 9.5: ^{13}C NMR of M1 – M3.

388
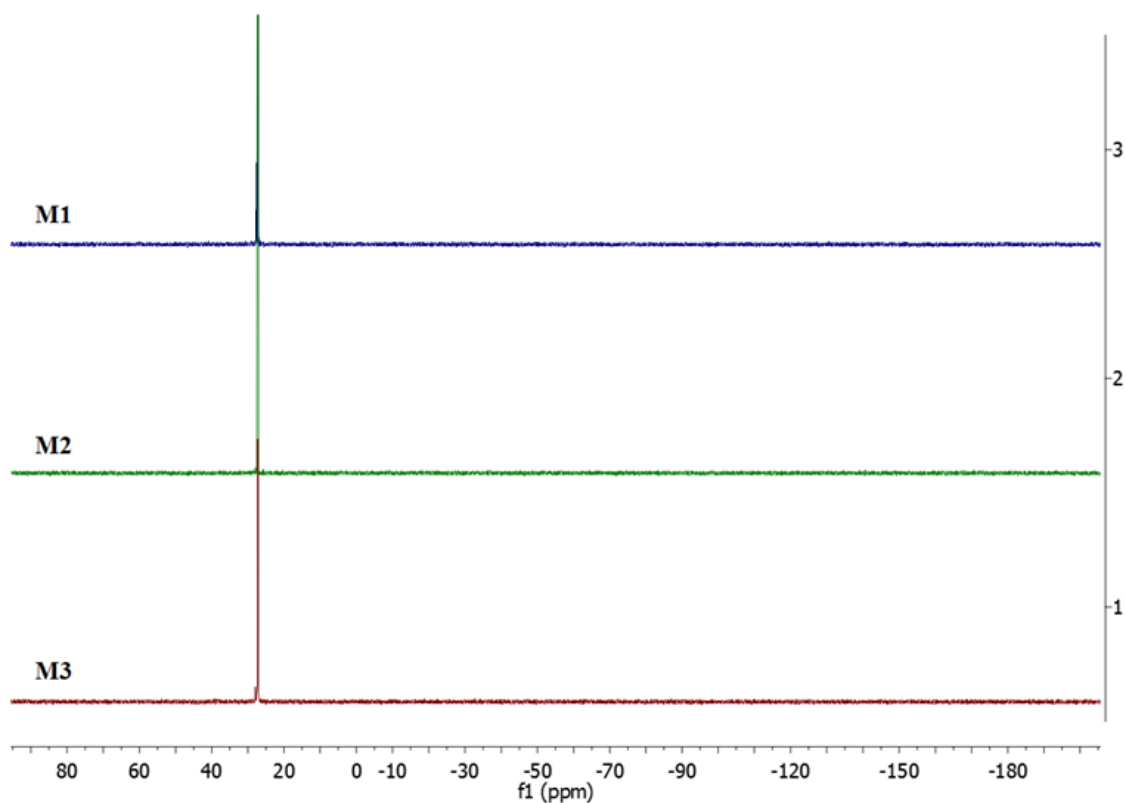
Figure 9.6: ^{31}P NMR of M1 – M3.

Figure 9.7 depicts the ^{1}H NMR while **Figure 9.8 – 9.10** depicts the ^{13}C NMR spectra of the dialdehyde monomers (**Ma, Mb and Md**) in deuterated chloroform. All the signals could be readily assigned to their corresponding carbons and are schematically illustrated.

389
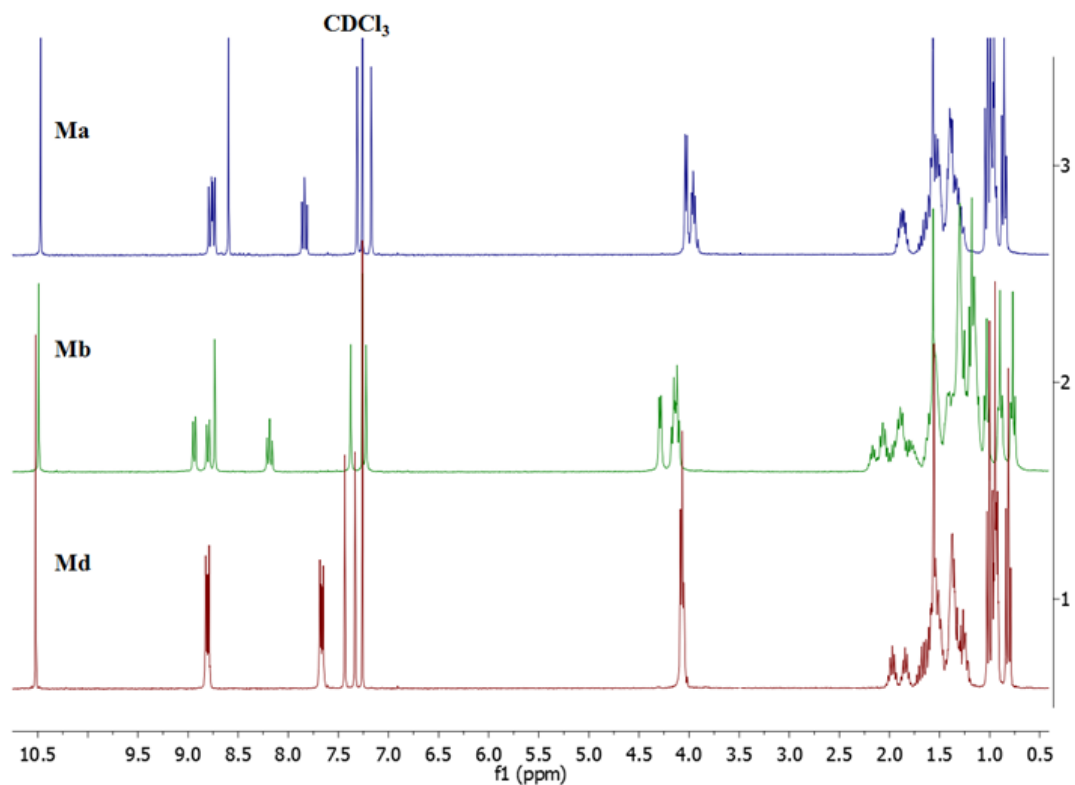
Figure 9.7: ^{1}H NMR of Ma, Mb and Md.
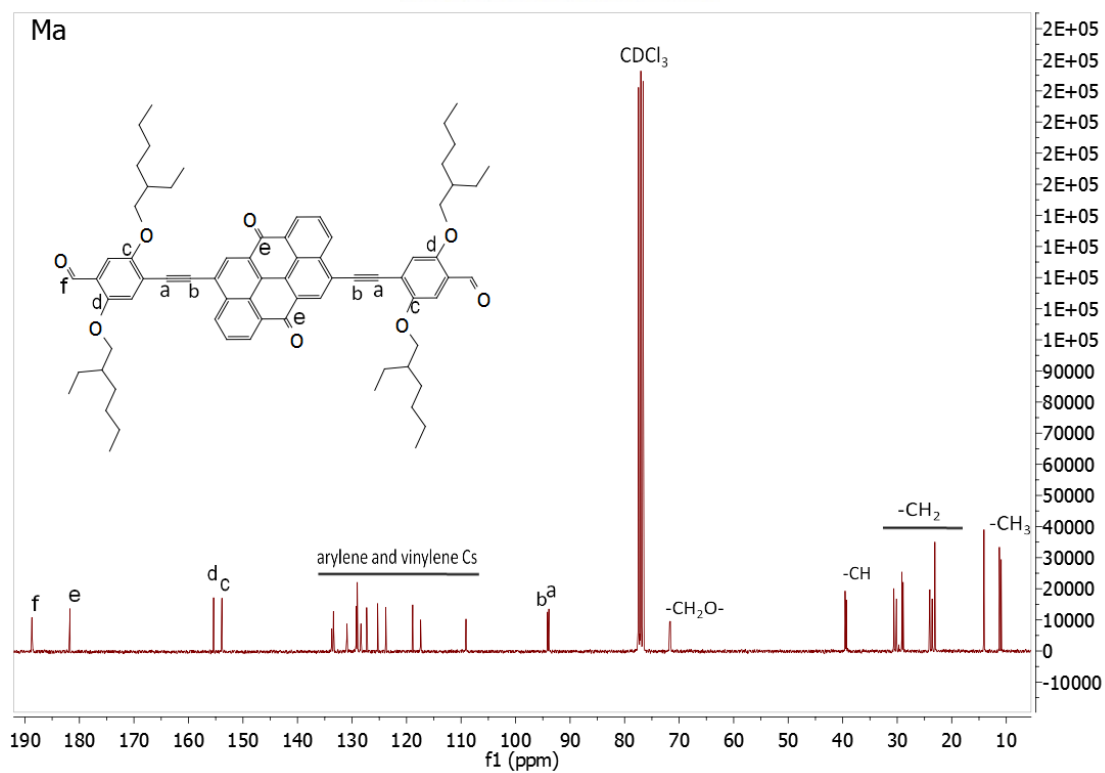
Figure 9.8: ^{13}C NMR of Ma.

390
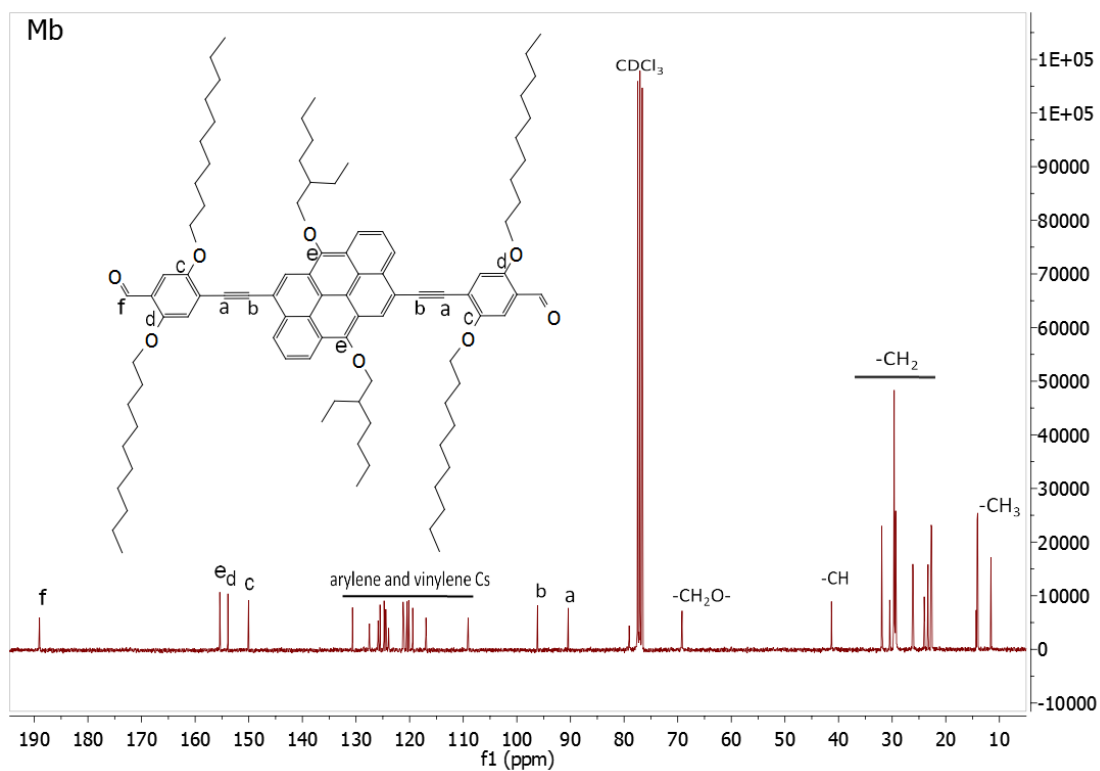
Figure 9.9: ^{13}C NMR of Mb.
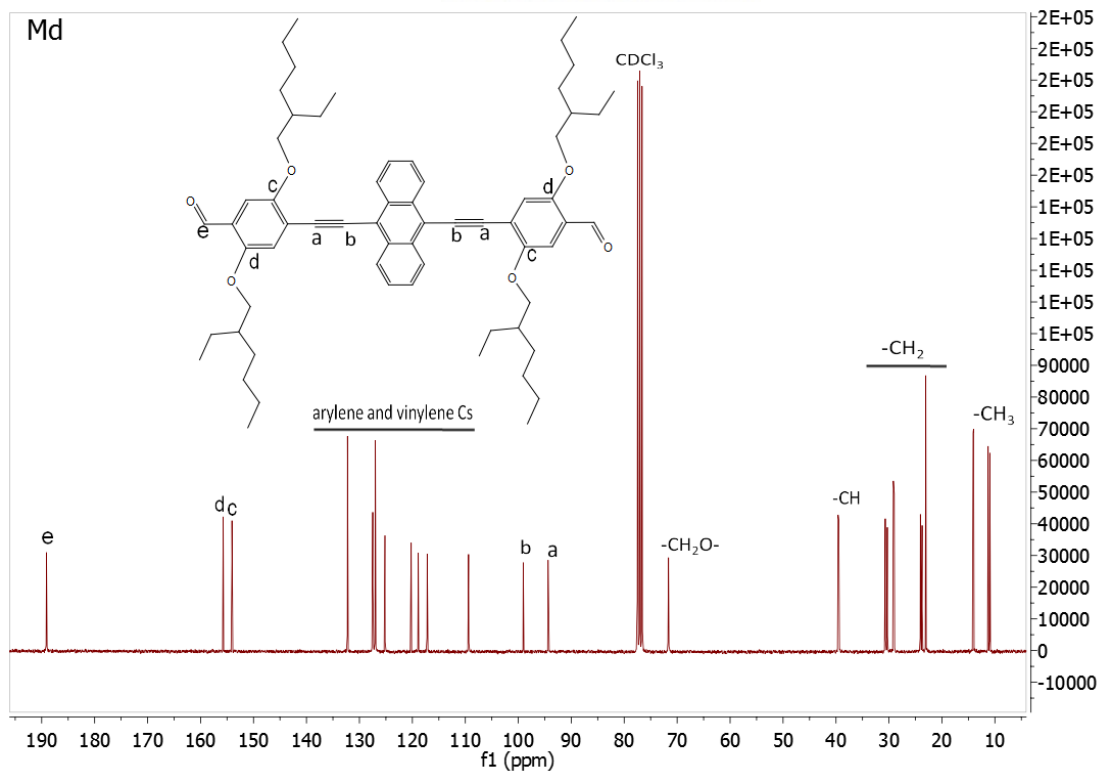
Figure 9.10: ^{13}C NMR of Md.

391

^{1}H NMR spectroscopy was employed to confirm structure and purity of the polymers and their signals were compared with those of their corresponding dialdehyde monomers (**Figure 9.11 – 9.12**). The broad NMR signals in the down-field region 9.05 – 6.58 ppm are ascribed to the arylene and vinylene protons, while the signals in the region 4.52- 0.48 ppm originate from the protons of the alkyloxy side chains. The signals are broad and non-specific but show a similarity to their corresponding dialdehydes in the observed signal region. However, the characteristic signals of the polycondensation monomers (dialdehyde, ~10.5 ppm (−CHO); bisphosphonate, ~3.2 ppm (-H$_2$CP)) are completely absent, giving clear indications of the formation of polymer material from the corresponding monomers.
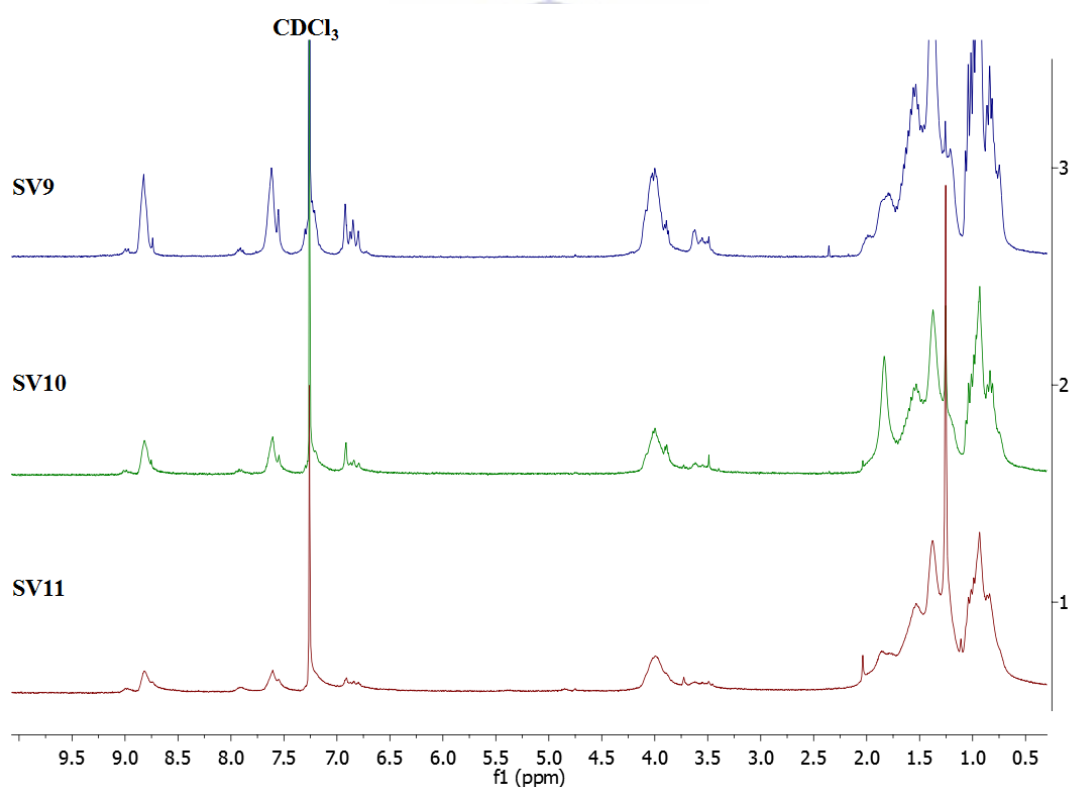
Figure 9.11: ^{1}H NMR of SV9 – SV11.
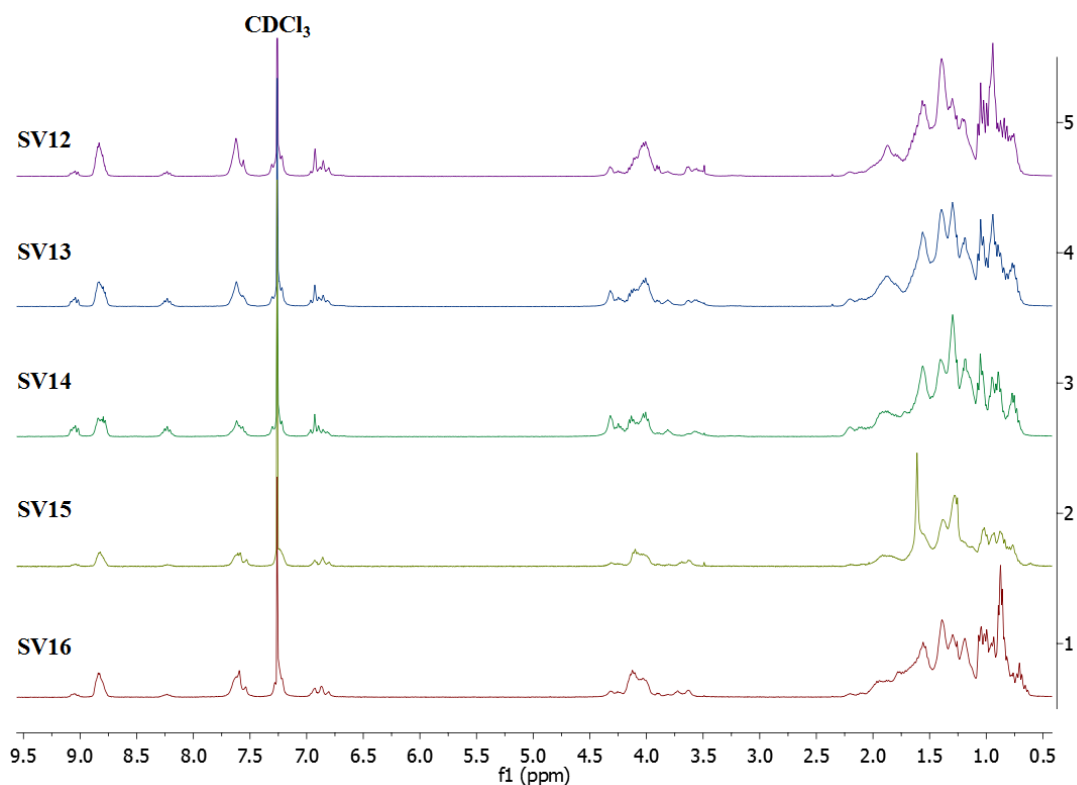
Figure 9.12: ^{1}H NMR of SV12 – SV16.

The spectrum suggests a trans (*E*) and cis (*Z*) configuration in all polymers due to the presence of signals or peaks (**x** and **y** in **Figure 9.13**) indicating the presence of vinylenic double bonds with a cis (*Z*) configuration [34]. The influence of anthanthrone and its derivative in their respective co-polymers with anthracene is observed in the aromatic down-field region. Comparing SV7, SV9 and SV12 with their corresponding dialdehydes (**Figure 9.13**), the signals at around 8.98 ppm (labelled **a**) and 7.90 ppm (labelled **b**) are ascribed solely to the anthanthrone component of the co-polymer SV9; and, the signals at around 9.03 ppm (labelled **c**) and that around 8.34 ppm (labelled **d**) ascribed solely to the anthanthrene component of the co-polymer SV12; while all other signals emanate from a contribution of the components (anthanthrone/anthracene or anthanthrene/anthracene together with the alkyloxy side chains) present in the co-polymers.

393
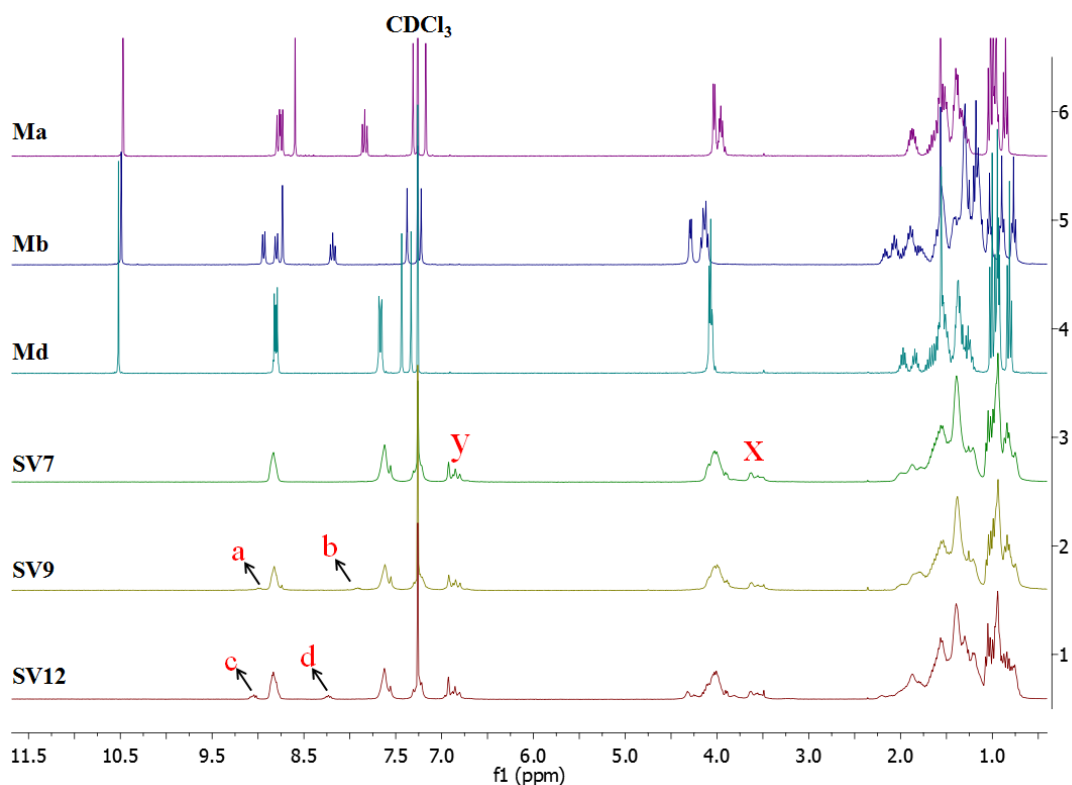
Figure 9.13: ^{1}H NMR of SV7, SV9 and SV12 with their corresponding dialdehydes.
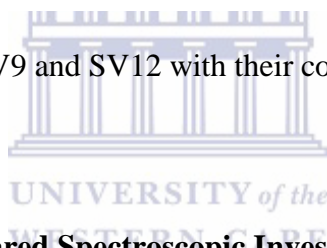
9.2.1.4 Fourier Transform Infrared Spectroscopic Investigation

Figure 9.14 shows the infrared spectra of SV7, SV9 – SV16. The characteristic FTIR signals associated with molecule vibrations of the investigated polymers appear around 3056, 2960-2865, 2187, 1656, 1604, 1508, 1466, 1202, 1032, 971, and 869 cm^{-1}. The very weak band around of 3056 cm^{-1} is attributed to the stretching vibrations of aromatic =C-H and of arylene and vinylene vibrations. Very strong characteristic aliphatic -C-H stretching vibrations signals are observed in the region 2960 - 2865 cm^{-1}. The spectra show weak signal situated in the region 2187 cm^{-1}. This signal arises from the vibrational stretching of the disubstituted ethynylene linker bond (-C≡C-). The signals around 1604 cm^{-1} originate from vinylenic vibrations while the signals at 1508 cm^{-1} stem from the stretching vibrations of aromatic -

394

C=C- bonds. Strong signals at 1202 cm^{-1} and medium signals at 1032 cm^{-1} are ascribed to alkyloxy functionalities or aromatic-aliphatic -C=C-O-C- bonds. The band at 971 and 869 confirms the trans (*E*) and cis (*Z*) configuration of the vinylene double bonds present in the polymers. The lack of -CHO as an end group which was initially confirmed by ^{1}H NMR is also confirmed by FTIR as no terminal aldehyde function is observed. The characteristic stretching vibration associated with the ketone group (-C=O) of SV9 and SV10 is observed at 1656 cm^{-1}. This signal is absent in all other polymers investigated as shown in **Figure 9.14**.
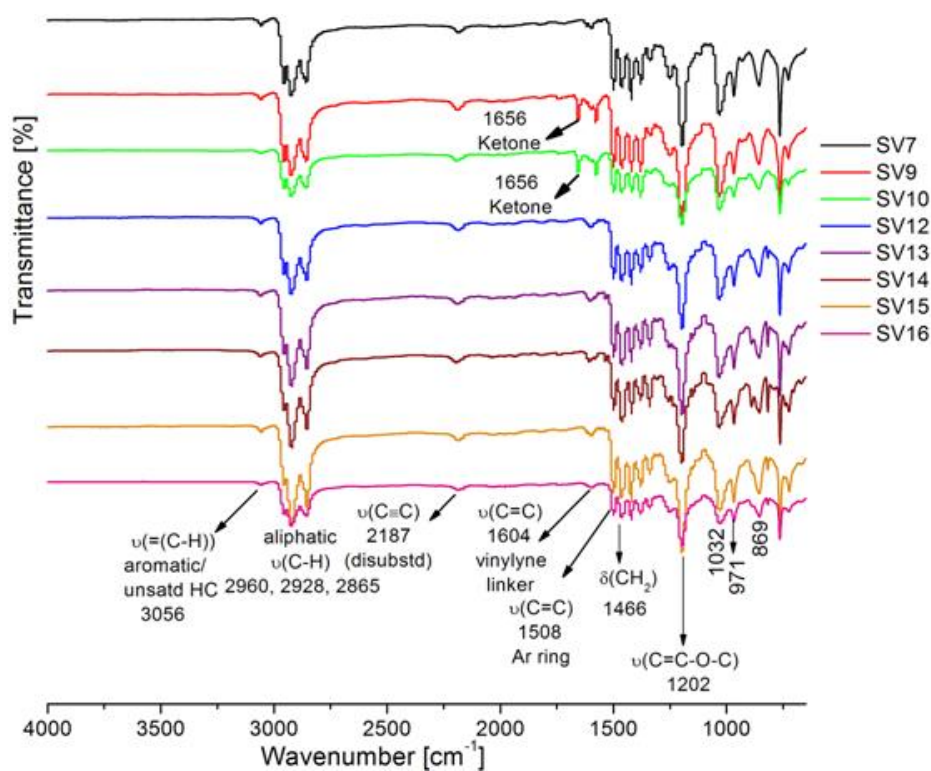
Figure 9.14: Stacked FTIR spectra of investigated polymers with arrows marking the absorptions of functional group signals including olefinic -C–H out-of-plane deformation (*trans*-CH=CH at 971 cm$^{–1}$ and *cis*-CH=CH at 869 cm$^{–1}$).

9.2.1.5 Thermal Stability and Molecular Weight Investigation

Thermo-gravimetric analysis and gel permeation chromatography measurements were performed to determine the decomposition temperature and molecular weights of the polymers. Thermal analysis conducted at ambient temperature at a heating rate of 20°C/min indicates high thermal stability of the polymers (**Figure 9.15**). Thermal decomposition above 300°C where recorded at approximately 5% weight-loss for all polymers except SV10. The molecular weights of the co-polymers were determined by gel permeation chromatography (GPC) measurements in the form of size exclusion chromatography (SEC) using THF as eluent and polystyrene as the standard. The GPC analysis revealed polymers with polydispersity index between 2.4 and 3.8. The decomposition temperatures taken at 5 and 10% and results obtained from GPC measurements as well as yields of the materials are provided in **Table 9.1**.
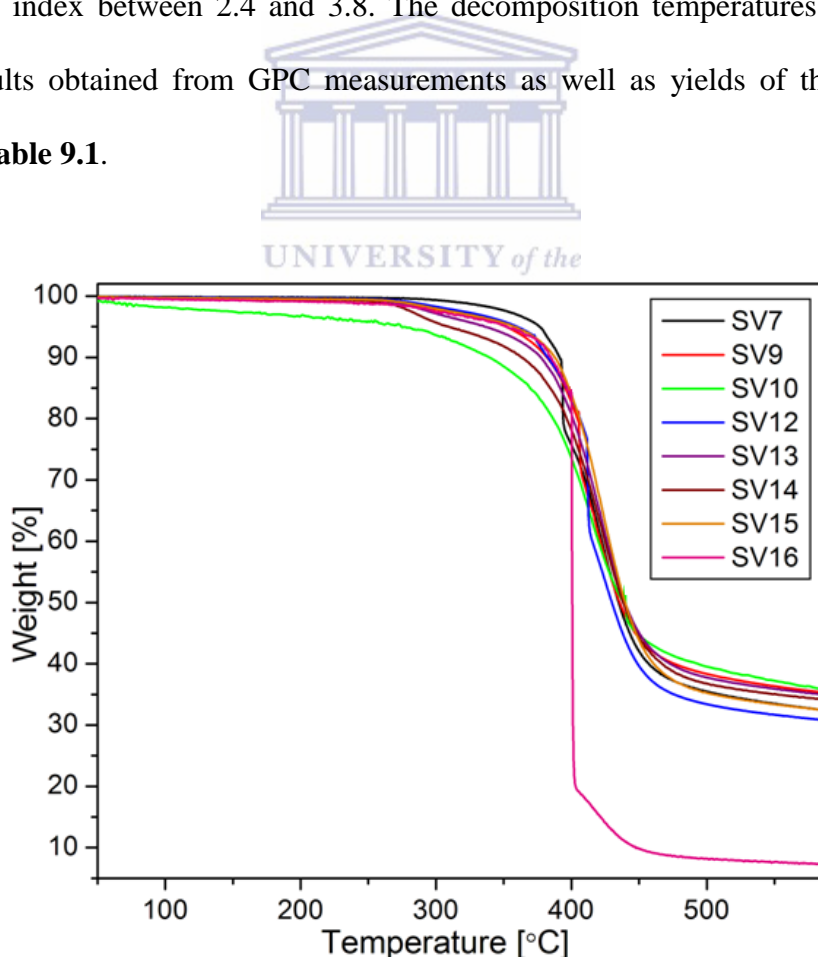
Figure 9.15: Thermo-gravimetric analysis.

Table 9.1: Data from GPC (polystyrene standards, THF as eluent), yields and thermal responses

Code	Yield (%)	M_n (g/mol)	M_w (g/mol)	PDI	T_d (°C) 5% weight loss	T_d (°C) 10% weight loss
SV7	80	6,720	15,870	2.4	375	391
SV9	47	3,590	13,550	3.8	351	384
SV10	26	1,850	4,710	2.5	281	341
SV12	48	6,230	15,280	2.5	362	382
SV13	53	6,340	16,020	2.5	339	377
SV14	48	7,090	14,750	2.1	316	367
SV15	50	9,280	34,720	3.7	360	388
SV16	47	9,230	26,290	2.8	360	386

9.2.2 Properties

The polymers are soluble in common organic solvents and have good film forming ability except for SV11 whose poor solubility does not allow the forming of good films.

397

9.2.2.1 Photo-physical Properties

The photo-physical properties of the homo and co-polymers were studied by UV-Vis absorption and photoluminescence in chlorobenzene solution and film. All emission data were obtained by exciting at the wavelength of the main absorption band.

Copolymers containing 25%, 50% and 75% of anthanthrone/anthracene units (SV9 – SV11) showed absorption spectra influenced by the combination of the anthracene and anthanthrone absorptive properties in solution and in film (**Figure 9.16**).

Figure 9.16: UV-Vis spectra comparing co-polymers SV9 – SV11 with homo-polymers P1 and SV7 in solution and film.

The co-polymers show the absorption of anthracene which spans from 430 – 615 nm, and also shows the region covering up to 720 nm from the anthanthrone component. Maximum

398

wavelength of absorption of anthracene was observed in the range 526 – 537 nm and maximum wavelength of absorption of anthanthrone was observed in the range 621 – 623 nm for SV10 and SV11. For SV9, the anthanthrone absorption was not really visible as the signal in the anthanthrone region is almost flat. In thin films however, the absorption of the co-polymers including SV9 was dominated by their anthracene and anthanthrone components with a slight red shift compared to the solution response. The contribution from anthanthrone in the co-polymers reduced the optical band gap to 1.7 eV compared to SV7 (all anthracene containing polymer) with a band gap of 2.0 eV.

The emission of SV9 – SV11 in solution is identical to and overlaps that of SV7 while they are blue-shifted compared to P1 (an all anthanthrone containing polymer) (**Figure 9.17**). Emission peak around 586 nm and a shoulder around 635 nm overlapping the emission peak of SV7 in solution were observed for SV9 – SV11. The emission of the co-polymers in solution can therefore be said to be majorly influenced by the anthracene part of the co-polymer. Interestingly, the emission spectra of the co-polymers in thin films show well defined emission peak emitting only the anthanthrone contribution (**Figure 9.18**); and as the anthanthrone content in the co-polymer increased, the emission shifts to longer wavelengths (SV9 (777 nm) < SV10 (781 nm) < SV11 (796 nm)). It is obvious that the emission in thin film originates mainly from that of the anthanthrone component present in the co-polymer. In solution, the emission of SV9 – SV11 overlaps that of SV7 while in thin film; their emission is red-shifted compared to SV7. This confirms that the emission of SV9 – SV11 observed in solution is solely or majorly from the anthracene component while in thin film, the emission emanates from the anthanthrone component. This unique behavior may be ascribed to different chromophores dominating in different forms of the polymers.

399
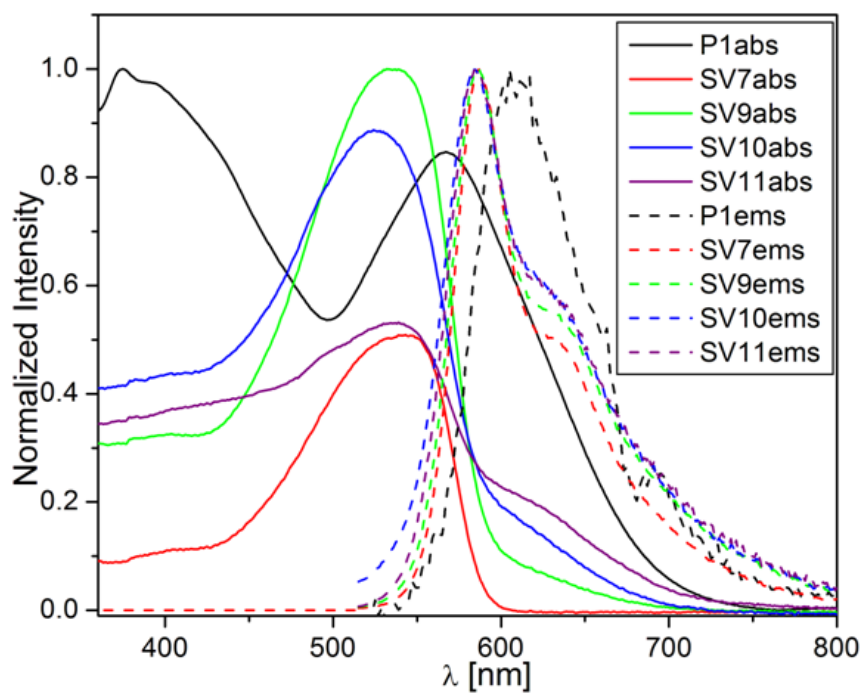
Figure 9.17: UV-Vis and photoluminescence spectra comparing co-polymers SV9 – SV11 with homo-polymers P1 and SV7 in solution.
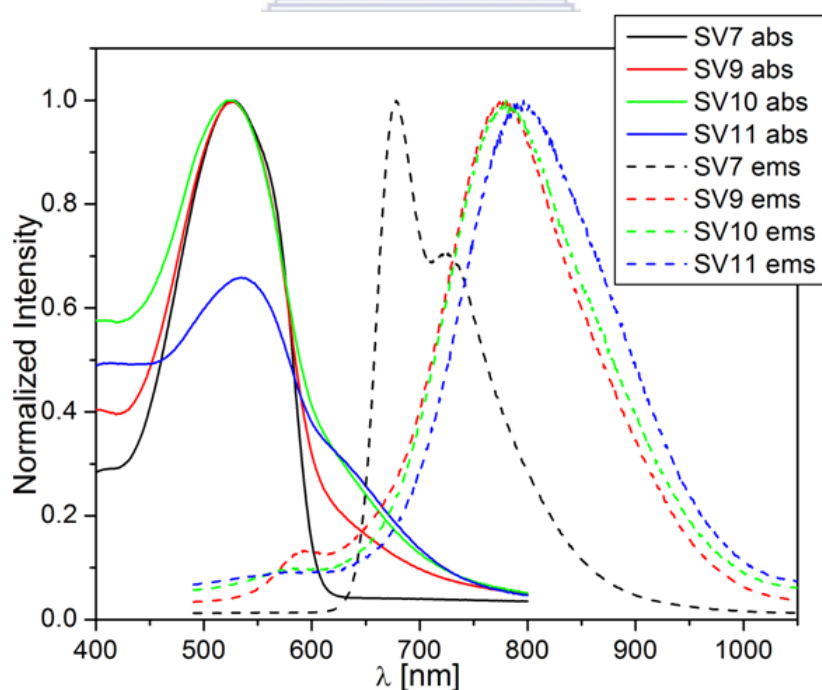
Figure 9.18: UV-Vis and photoluminescence spectra comparing co-polymers SV9 – SV11 with homo-polymer SV7 in thin film.

400

Component ratio (anthanthrene/anthracene) and side group dependent absorption; and component ratio dependent emission was obtained for co-polymers SV12 – SV16. The absorption spectra in solution and in thin film are shown in **Figure 9.19**. In solution, the absorption spectra are blue-shifted with increase in anthanthrene content in the co-polymer. Co-polymers SV13 and SV14 show vibronic absorption signals while broad absorption bands were observed for SV12, SV15 and SV16. The main absorption peak of SV12, SV15 and SV16 appears as a shoulder in SV13 and SV14. This absorption peak is the peak of anthracene as observed in SV7 (all anthracene containing polymer) and completely absent in P2 (all anthanthrene containing polymer). The shoulder in SV13 (50% anthracene component) is more pronounced than that in SV14 (25% anthracene component). The higher the anthracene component in the co-polymer, the more pronounced the shoulder which then becomes a peak at higher % anthracene component. The absorption of SV12, SV15 and SV16 (co-polymers with 25% anthracene component and varying side chains) is in the same spectra region as that of SV7 and red-shifted compared to those of P2, SV13 and SV14 in their main absorption peak. Nevertheless, SV12, SV13, SV14, SV15 and SV16 all have comparable onset absorption with SV7 resulting in an optical band of 2.1 eV for SV7, SV12, SV13 and SV14; 2.0 eV for SV15 and SV16.
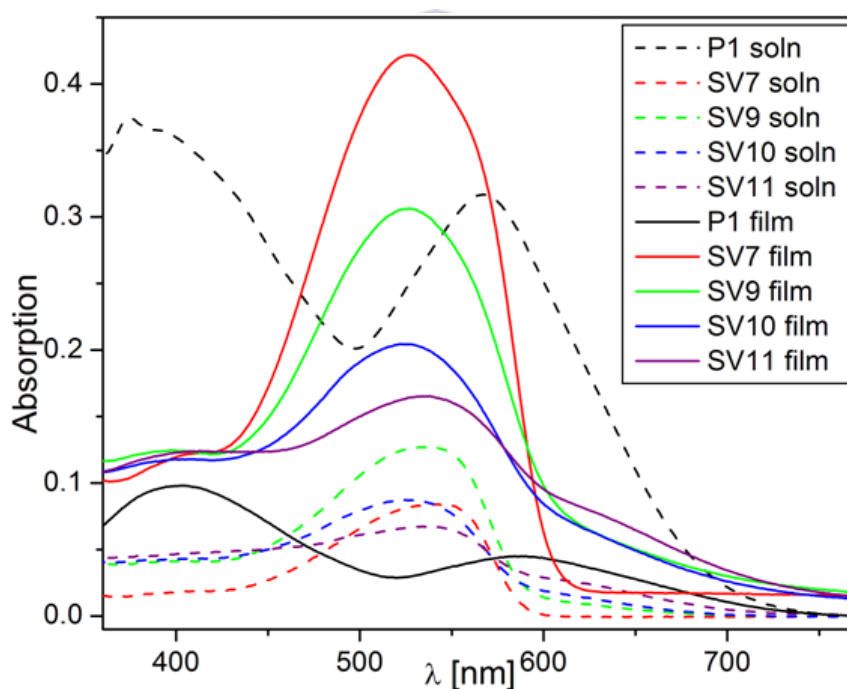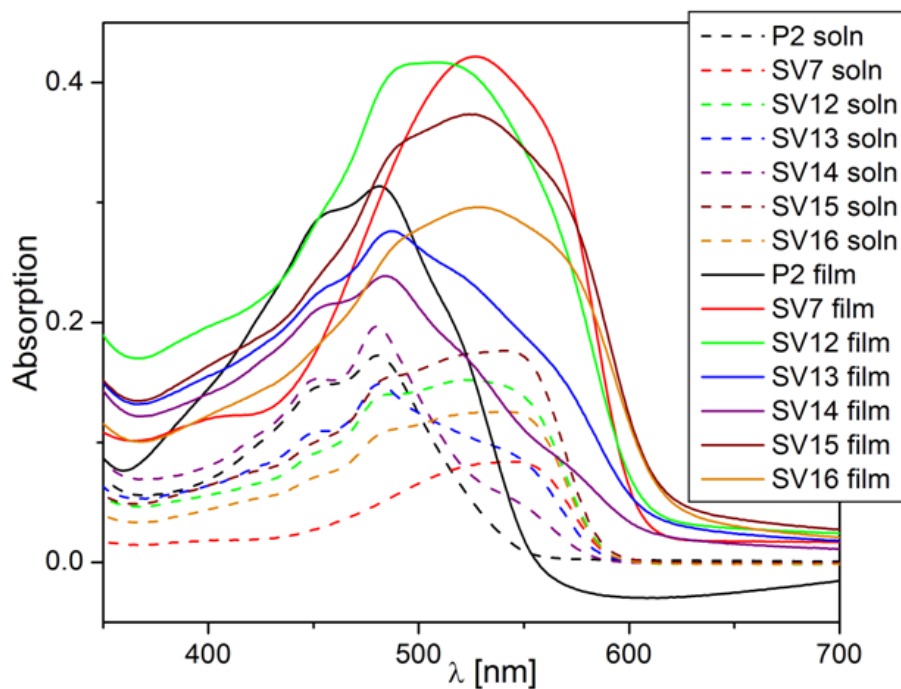
Figure 9.19: UV-Vis spectra comparing co-polymers SV12 – SV16 with homo-polymers P2 and SV7 in solution and film.

The thin film absorption follows the same pattern as that of the solution except that they are red shifted due to planarization in thin films. The absorption of SV12 – SV16 vary depending on the grafted side chain as well as the ratio of anthracene and anthanthrene component present in the co-polymer. Like in solution, the main absorption peak of SV13 and SV14 show a narrow band comparable to that of P2 while the absorption of SV12, SV15 and SV16 show broad bands comparable to that of SV7. The absorption spectra of SV13 and SV14 show more structured peaks with two maximums at around 451 – 453 nm and 481 nm and a shoulder at 545 – 548 nm. SV15 and SV16 like in solution, absorb in the same region as SV7. The absorption of SV12 in this case covers a broader region covering the absorption range of both P2 and SV7. Co-polymers with 75% anthracene and 25% anthanthrene but with different phenyl bisphosphonates (SV12, SV15 and SV16) are bathochromically shifted and with broad absorption band compared to SV13 and SV14 with increased anthanthrene ratio.

402

They absorb in the region of absorption of SV7 and their absorption is almost uninfluenced by the side chain of the attached phenyl bisphosphonate as the shape of their absorption band is very similar. The broader absorption peaks of these group of co-polymers suggests that there are more energy levels corresponding to the π - π* transition for the co-polymers with higher anthracene component ratio than those with higher or equal anthanthrene component ratio. In spite of these differences in the value and shape of the absorption peak, the onset absorption of all the polymers except P2 lies in the same region resulting in a band gap between 1.9 and 2.0 eV.

Despite the variation in absorption of SV12 – SV16 in solution and thin film, similar emission spectra were observed for these co-polymers. For emission in solution (**Figure 9.20**), a main peak and a shoulder is observed for all polymers. The co-polymers with 75 % and 50% anthracene component (SV12, SV13, SV15 and SV16) are red shifted compared to SV7 (all anthracene containing polymer) while SV14 with 75% anthanthrene is blue shifted and overlaps the emission of P2 (an all anthanthrene containing polymer). Main emission peaks are observed in the range 581 – 586 nm with a shoulder in the range 626 – 636 nm.
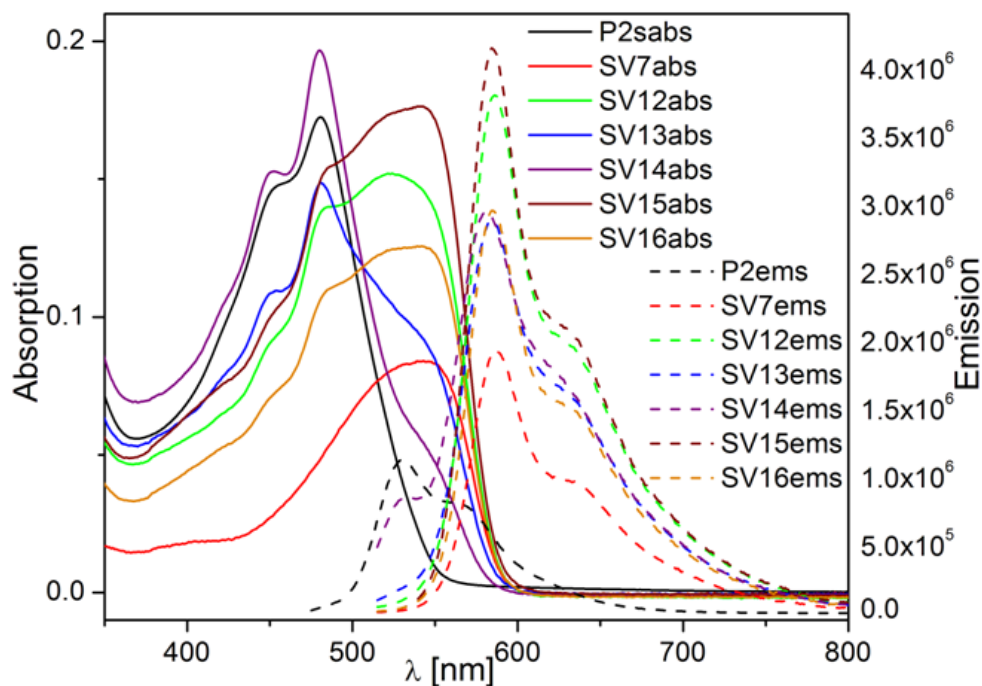
Figure 9.20: UV-Vis and photoluminescence spectra comparing co-polymers SV12 – SV16 with homo-polymers P2 and SV7 in solution.

The emission spectra of SV12 - SV16 are similar both in film and solution in terms of shape but the emission in film are red-shifted and with the shoulder observed in solution emerging as a peak in film (**Figure 9.21**). All the polymers show well structured vibronic emission spectra similar in shape to and in the same spectra region as that of SV7; with an intense peak in the range of 604 – 615 nm and the less intense peak at longer wavelength in the region 651 – 669 nm proving they all emit from the same excited chromophores. The observed shoulder in solution emerged as a second peak in thin film with red-shifted emission. This fine structure (splitting of the emission spectra into two well resolved peaks) observed for the emission spectra both in solution and in thin film and the variation or absence of similarity (mirror image) between absorption and emission spectra, is ascribed to vibronic coupling of the excitons [35]. The emission peaks of SV13 overlap that of SV7 at 608 nm and 653 nm for

404

the first and second peaks respectively. The thin film emission of all the co-polymers is red-shifted compared to that of P2.
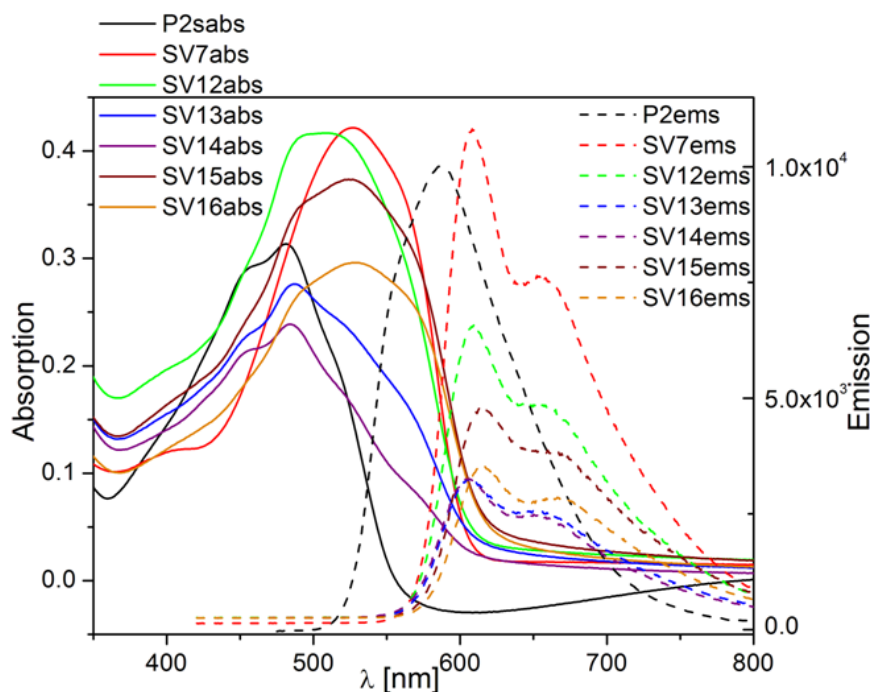
Figure 9.21: UV-Vis and photoluminescence spectra comparing co-polymers SV12 – SV16 with homo-polymers P2 and SV7 in thin film.

Although the emission bands of SV12 – SV16 are all sharp and the overlap of the emission and absorption spectra is quite narrow, it is important to draw attention to the slight influence of side chain variation observed for the thin film emission of SV12, SV15 and SV16 (co-polymers with 75% anthracene and 25% anthanthrene but vary in the side chain of the attached phenyl bisphosphonates). It is observed that the overlapping area of the film samples slightly increases in the order SV12>SV15>SV16 due to the broadening of the absorption spectra in this order. It is also worthy of note that the emission spectra of SV14 which has 75% anthanthrene is a mirror image of the absorption. This can be ascribed to chain planarization induced by the anthanthrene component and it is an indication that the

405

conformational relaxation is not important for both and their decays take place from lumophores with similar geometry.

The optical bandgap of SV9 – SV16 ranged from 1.7 – 2.1 eV in solution and film. The photo-physical spectra and data confirm that the structure (linear or branched side chains) and ratio of components have a significant influence on the ground and excited state properties of the co-polymers both in solution and film. Very large Stokes shifts were observed for SV9 (250 nm), SV10 (256 nm) and SV11 (259 nm) in film. This indicates excimer formation or aggregation in the solid state [36]. The Stokes shift of anthanthrone or its derivative is so strong that it was impossible to prevent it in the co-polymerization with anthracene. P2, SV12 – SV14 also show large Stokes shift (101 – 120 nm); the higher the ratio of anthanthrene in the co-polymer, the higher the Stokes shift. However, those of SV9 – SV11 are the largest for the polymers under study. The ratio of anthanthrone in the co-polymer did not show any influence on the Stokes shift in solution but a huge influence was observed in film. We assume that the pronounced tendency to aggregate is due to the carbonyl group present in the anthanthrone component. The photo-physical responses including the maximum absorption (λ_{abs}), the onset absorption (λ_{onset}), optical band gap energy (E_g^{opt}) calculated using $1240/\lambda_{onset}$, wavelength at emission maximum (λ_{PL}) as well as the Stokes' shift both in solution and in film are summarized in **Table 9.2**.

406

Table 9.2: Photo-physical data of the polymers in dilute chlorobenzene solution and in thin film spin-coated from chlorobenzene

	Solution					Film		*Shoulder, $E_g^{opt} = 1240/\lambda_{onset}$		
Code	λ_{abs} (nm)	λ_{PL} (nm)	λ_{onset} (nm)	E_g^{opt} (eV)	Stokes Shift (nm)	λ_{abs} (nm)	λ_{PL} (nm)	λ_{onset} (nm)	E_g^{opt} (eV)	Stokes Shift (nm)
P1	374, 567	611	752	1.6	44	403, 586	-	766	1.6	-
P2	453, 481,	530	572	2.2	49	453, 481	587	558	2.2	106
SV7	*520, 543	586, *635	598	2.1	43	527, 559	608, 653	621	2.0	49
SV9	537	586, *635	701	1.8	49	527, 638	777	710	1.7	250
SV10	526, 623	585, *633	723	1.7	59	525, 638	781	725	1.7	256
SV11	537, 621	586, *637	737	1.7	49	537, 643	796	728	1.7	259
SV12	449, 481, 522	586, *634	603	2.1	64	*491, 509	610, 657	623	2.0	101
SV13	453, 481, *545	585, *635	598	2.1	104	454, 488	608, 653	622	2.0	120
SV14	451, 481, *548	581, *626	592	2.1	111	457, 485	604, 651	623	2.0	119
SV15	449, 485, 542	585, *634	608	2.0	43	*493, 524	615, 662	641	1.9	91
SV16	447, 483, 542	585, *636	610	2.0	43	*497, 529	615, 669	644	1.9	86

407

9.2.2.2 Photovoltaic Properties

To investigate the photovoltaic performance of the polymers, solar cell devices were fabricated and tested on a regular device configuration of glass/ITO/PEDOT-PSS/polymer:PCBM/LiF/Al. The polymer:PCBM active layers were spin-coated from dichlorobenzene solutions in a 1:2 ratio for all devices. **Figure 9.22 – 9.23** shows the *I-V* curves of the fabricated solar cells. The co-polymers SV12 – SV16 revealed generally the best photovoltaic parameters in this study (**Figure 9.22**).
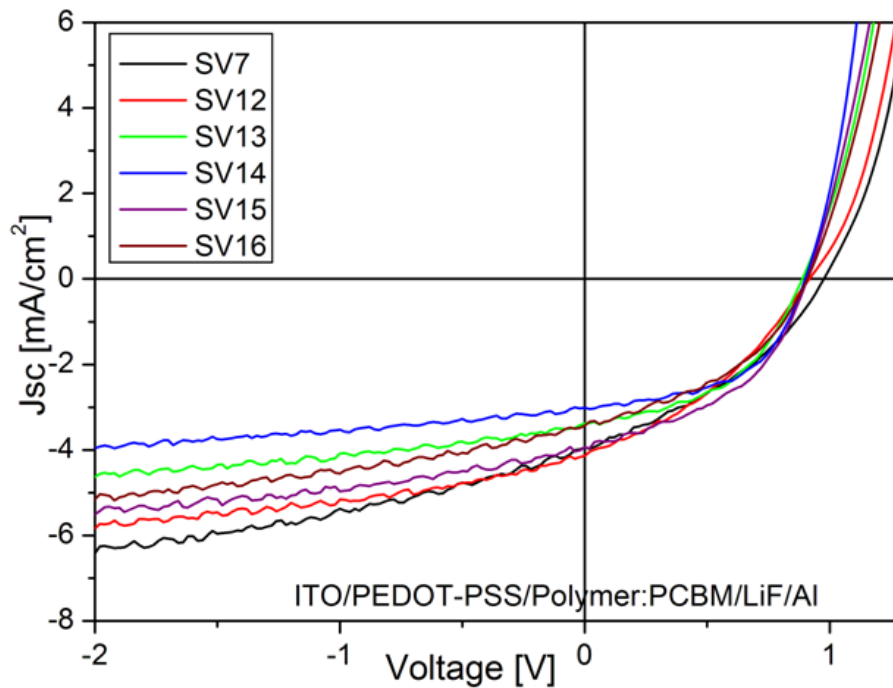
Figure 9.22: The current-voltage (*I–V*) characteristics of (homo-polymer SV7 and co-polymers SV12 – SV16):PCBM (1:2) blend devices on PEDOT:PSS configuration under 100 mW/cm^2.

408
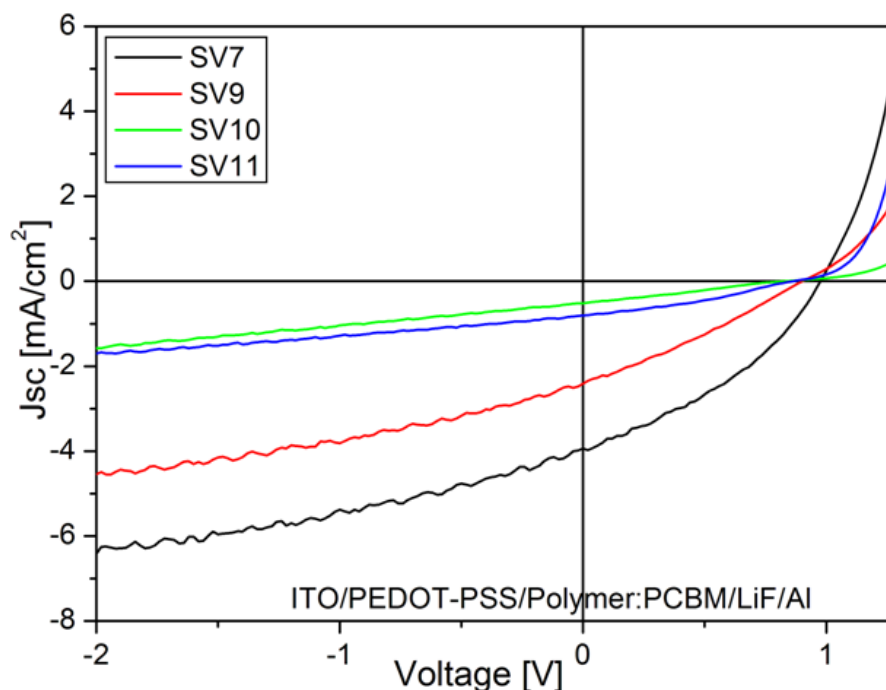
Figure 9.23: The current-voltage (*I–V*) characteristics of (homo-polymer SV7 and co-polymers SV9 – SV11):PCBM (1:2) blend devices on PEDOT:PSS configuration under 100 mW/cm^2.
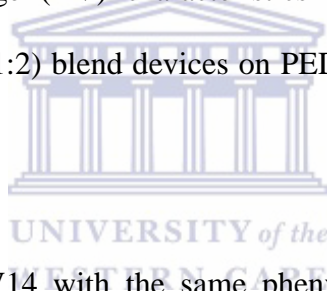
For the co-polymer SV12 – SV14 with the same phenyl bisphosphonate side chain (2-ethylhexyloxy phenyl), the short circuit current (J_{sc}) was observed to decrease from SV12 – SV14 with SV12 (4.53 mA/cm^2)>SV13 (3.50 mA/cm^2)>SV14 (3.01 mA/cm^2). Reverse order was however observed for the fill factor (*FF*) with SV12 (0.39)<SV13 (0.47)<SV14 (0.54). Going by the photovoltaic parameters of SV7 (an all anthracene based polymer with 2-ethylhexyloxy side chain phenyl bisphosphonate), the J_{sc} of the co-polymers SV12 – SV14 can be attributed to contribution of the anthracene component to the co-polymer while the relatively good *FF* is obviously a contribution from the anthanthrene component. This assertion is further buttressed from the fact that SV14 with the highest *FF* is a combination of 75% anthanthrene and 25% anthracene. In addition to the influence of the ratio of each component in the co-polymer on the photovoltaic performance, it can be ascertained that the

409

photovoltaic parameters are also side chain dependent. Comparing the co-polymers SV12, SV15 and SV16 (co-polymers with 75% anthracene and 25% anthanthrene) with varying side chain ((SV12; 2-ethylhexyloxy side chain phenyl bisphosphonate), (SV15; decyloxy side chain phenyl bisphosphonate) and (SV16; 3,7-dimethyloctyloxy side chain phenyl bisphosphonate)), the photovoltaic parameters are seen to be slightly influenced by the grafted side chain. For instance, the J_{sc} of SV12 (4.53 mA/cm^2) with bulky 2-ethylhexyl side chain in the phenyl group connected to the co-polymer by a vinylene bond is higher than that of SV15 (4.00 mA/cm^2) with a linear decyloxy side chain in the same phenyl position as SV12, while that of SV16 (3.87 mA/cm^2) with 3,7-dimethyloctyloxy is lower than that of SV15. In this group, SV15 exhibits the highest *FF* (0.47) while SV12 exhibits the highest J_{sc} (4.53 mA/cm^2). The *FF* of SV16 (0.42) is next to that of SV15 but it gave the least J_{sc} (3.87 mA/cm^2) in this group. SV9 – SV11 show low J_{sc} and relatively low *FF* (**Figure 9.23**). Overall best efficiency was observed for SV15 with an efficiency of 1.7%. **Table 9.3** shows the complete set of photovoltaic parameters under AM1.5 illumination for the best solar cell device of each polymer:PCBM blend.

410

Table 9.3: The complete set of photovoltaic parameters under AM1.5 illumination for the best solar cell device of each polymer:PCBM (1:2) blend

Code	Weight of Polymer (mg)	Weight of PCBM (mg)	Chlorobenzene (μL)	Bulk Thickness (nm)	Optical Density of Bulk	J_{sc} [mA/cm^2]	V_{oc} [V]	*FF*	Eff %	@ -0.1 V [mA/cm^2]	@ +1 V [mA/cm^2]
SV7	10.4	20.9	867	164	0.36	4.15	0.99	0.38	1.6	-4.27	0.21
SV9	10.2	20.4	850	176	0.37	2.69	0.92	0.32	0.8	-2.88	0.37
SV10	10.3	20.6	858	180	0.30	0.58	0.90	0.28	0.1	-0.60	0.05
SV11	11.1	22.3	925	199	-	0.93	0.90	0.34	0.3	-0.97	0.16
SV12	10.3	20.6	858	206	0.34	4.53	0.92	0.39	1.6	-4.71	0.96
SV13	13.6	27.4	1,134	160	0.38	3.50	0.91	0.47	1.5	-3.79	1.28
SV14	11.7	23.4	975	143	0.34	3.01	0.90	0.54	1.5	-3.09	2.6
SV15	10.3	20.6	858	182	0.39	4.00	0.92	0.47	1.7	-4.08	2.03
SV16	11.4	22.8	950	179	0.38	3.87	0.91	0.42	1.5	-4.04	1.73

411

It is obvious that the component ratio and type of side chain has no distinct influence on the open-circuit voltage (V_{oc}) of all investigated polymers. The V_{oc} of the investigated devices were found to be high for all co-polymers irrespective of the type and ratio of components or nature of the grafted alkyloxy side chain. In general, high V_{oc} of over 0.9 V were obtained for all investigated polymers including the co-polymers SV12 – SV16 (co-polymers containing anthanthrene) as against the less than 0.8 V reported for anthanthrene small molecule devices [37] and the PAE-PAV based anthanthrene polymers reported in **Chapter 5** of this study. The comparative plots of J_{sc}, V_{oc}, *FF* and efficiency against the investigated polymers are shown in **Figure 9.24 – 9.27**, while the morphology of the films investigated by optical microscopy is shown in **Figure 9.28**.

Figure 9.24: Comparative plot of short circuit current (J_{sc}) against (homo-polymer SV7 and co-polymers (SV9 – SV16):PCBM (1:2) blend devices on PEDOT:PSS configuration.

412

Figure 9.25: Comparative plot of open circuit voltage (V_{oc}) against (homo-polymer SV7 and co-polymers (SV9 – SV16):PCBM (1:2) blend devices on PEDOT:PSS configuration.

Figure 9.26: Comparative plot of fill factor (*FF*) against (homo-polymer SV7 and co-polymers (SV9 – SV16):PCBM (1:2) blend devices on PEDOT:PSS configuration.
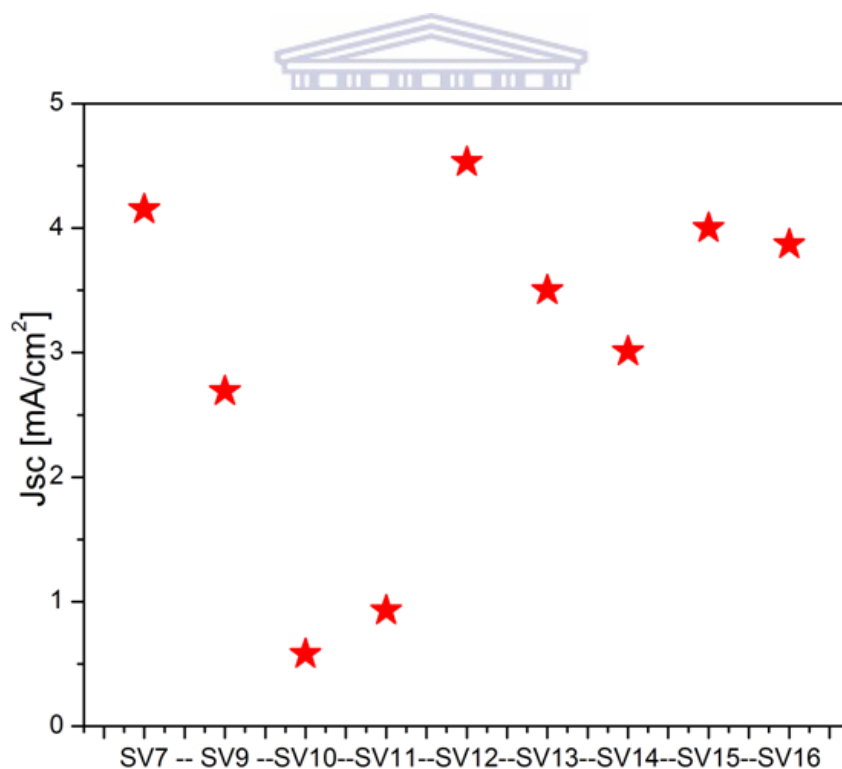
413

Figure 9.27: Comparative plot of device efficiency against (homo-polymer SV7 and co-polymers (SV9 – SV16):PCBM (1:2) blend devices on PEDOT:PSS configuration.
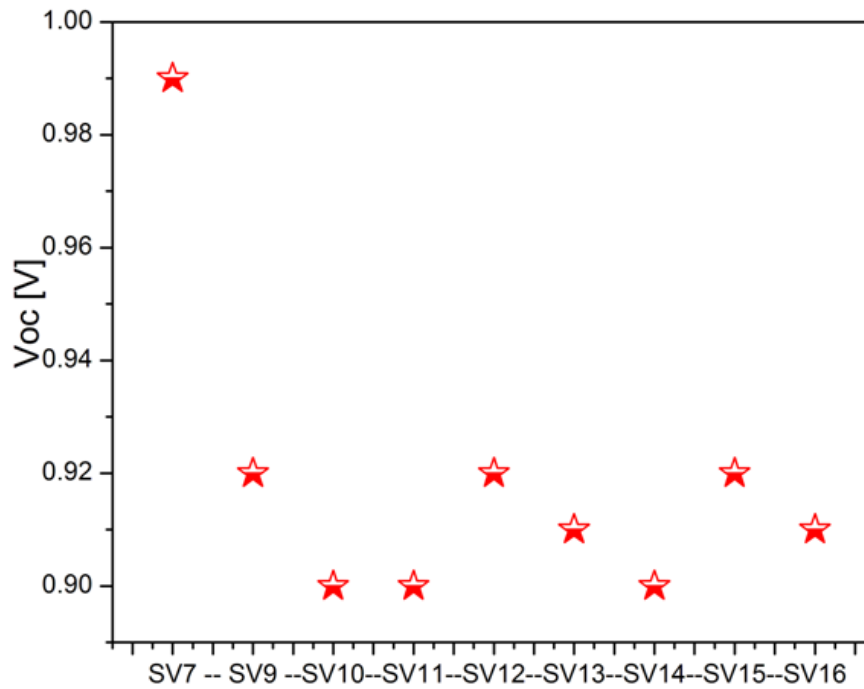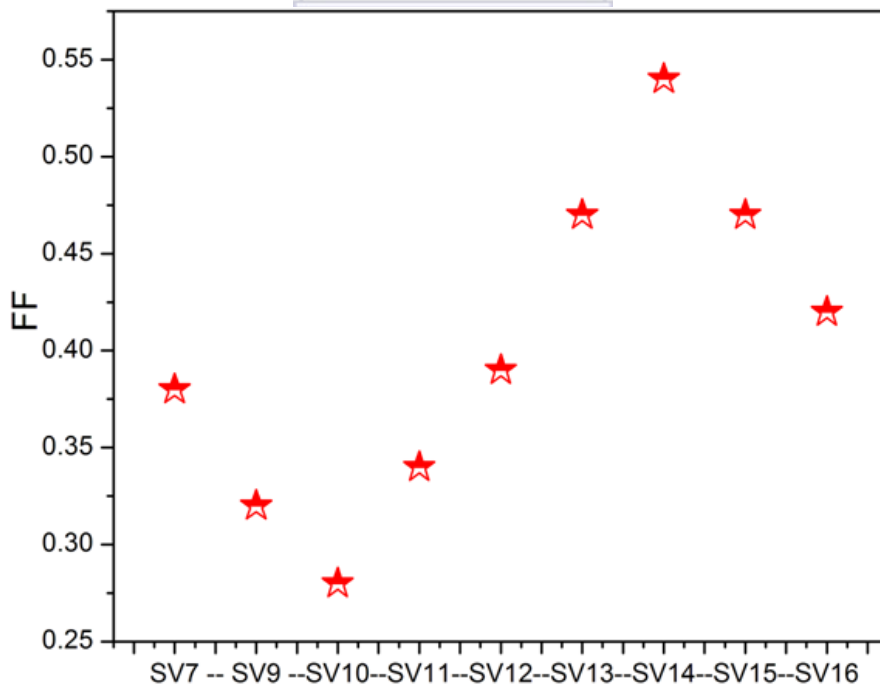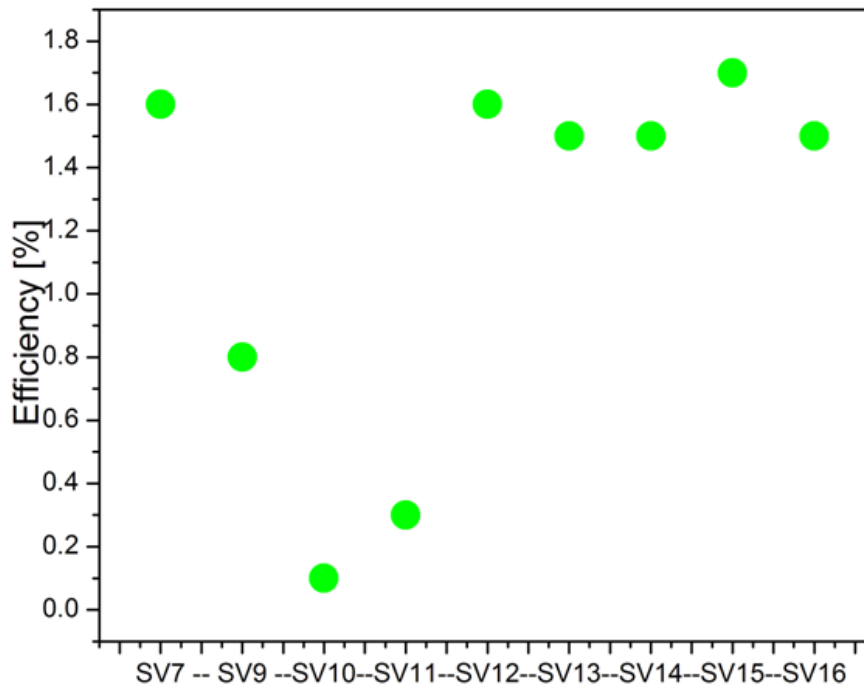
414
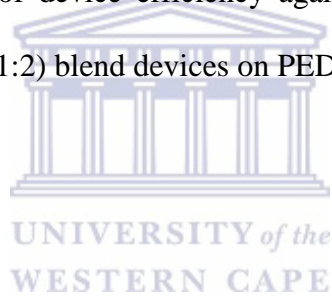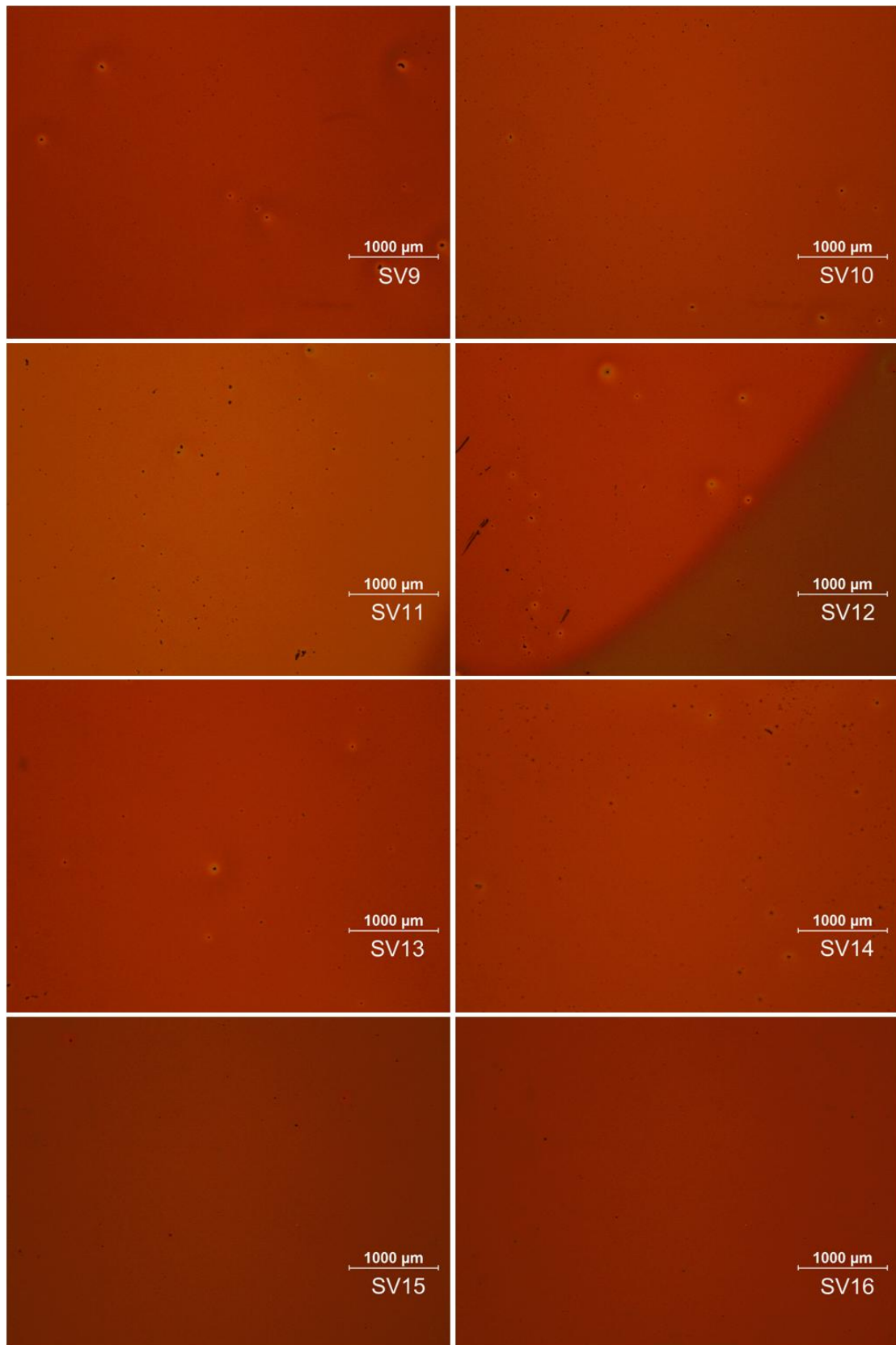
Figure 9.28: Optical microscopy images of co-polymers (SV9 – SV16):PCBM (1:2) blend devices on PEDOT:PSS configuration.

415

9.2.2.3 External Quantum Efficiency (EQE)

External quantum efficiency (EQE) measurements of the best devices were carried out to further assess the photoelectrical behavior of the polymers. The EQE reveals the percentage of photons that create charges at a given wavelength that reach the electrodes. **Figure 9.29 and 9.30** shows the EQE of SV7, SV9 – SV16. The spectra lie over a wide range of wavelengths (400 – 750 nm) in agreement with the absorption spectra and with two maximum photo-current contributions around 395 and 525 nm for all polymers investigated. For the maximum around 525 nm, the percentage EQE defined response is in accordance with the photovoltaic performance in terms of the short circuit current (J_{sc}). The intensity or strength of the EQE signal of each polymer clearly correlates with the achieved short-circuits currents. The higher the J_{sc}, the higher the EQE for all the polymers (**Figure 9.29 and Table 9.3**). SV12 for example, show EQE higher than that of SV7 in the 525 nm range despite having the same efficiency of 1.6%. This is due to the higher J_{sc} generated by SV12 (4.53 mA/cm^2) compared to SV7 (4.15 mA/cm^2). The signals or maximum around 395 nm and the shoulder around 710 nm emanate from PCBM. The EQE response of SV9 – SV11 are also in accordance with the output current with SV9>SV11>SV10 (**Figure 9.30 and Table 9.3**). Between 400 and 500nm, a flat response is observed for the co-polymers (SV9 – SV16) while a deep downward peak is observed for SV7. This contribution emanates from the anthanthrone and anthanthrene components in their respective co-polymers.

416
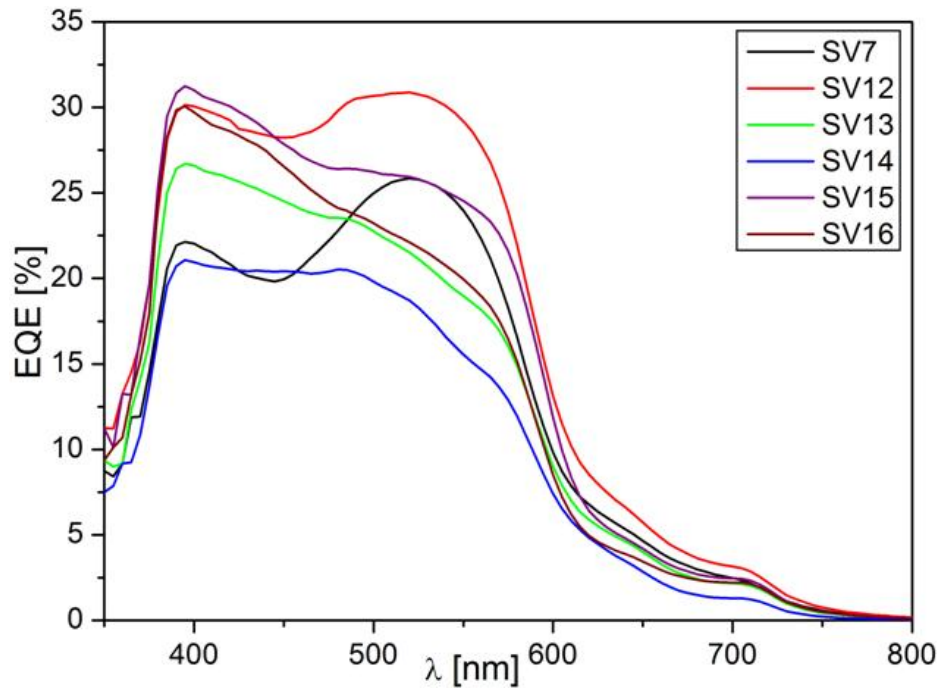
Figure 9.29: Equivalent quantum efficiencies of (homo-polymer SV7 and co-polymers (SV12 – SV16):PCBM (1:2) blend devices on PEDOT:PSS configuration.
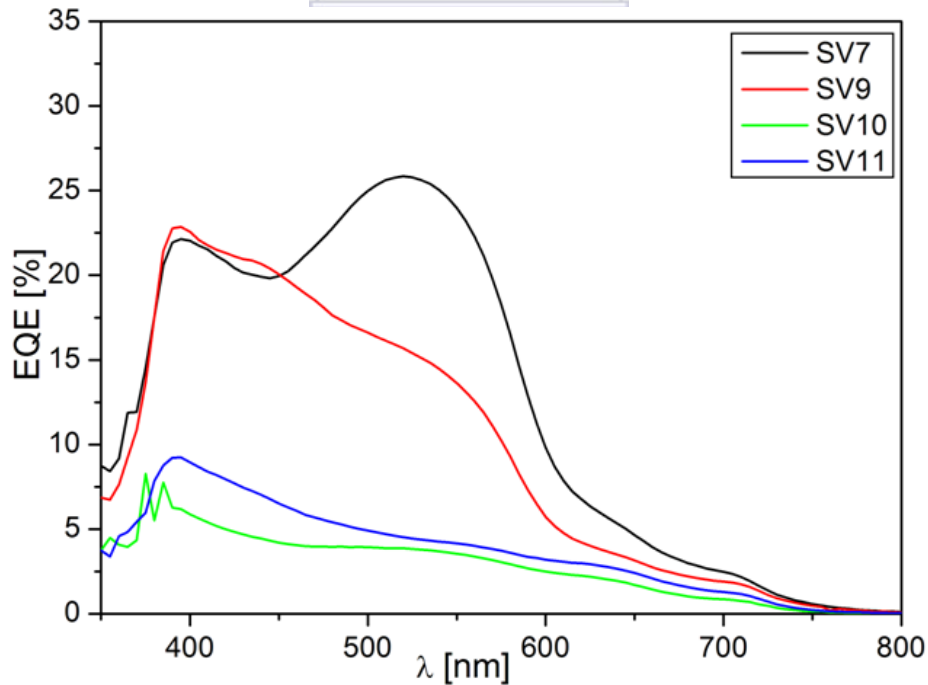
Figure 9.30: Equivalent quantum efficiencies of (homo-polymer SV7 and co-polymers (SV9 – SV11):PCBM (1:2) blend devices on PEDOT:PSS configuration.

417

Going by the ratio of anthracene to anthanthrone and the solubility issues associated with anthanthrone, one would expect to have a better photovoltaic response for SV10 than SV11. Strangely, however, this was not the case. One would also assume that the ratio of the anthanthrone component in the co-polymer may not actually be accurate as a result of the solubility issues which may compromise the actual ratio; resulting in the strange photovoltaic behavior of SV10 and SV11. In order to further confirm the ratio, the NMR spectra were investigated to get an idea of the ratio of the components of the co-polymers. To achieve this, the NMR spectra of P1, SV7 and SV9 – SV11 were investigated following the spectra integration (**Figure 9.31 – 9.36**) and equations (**equation 9.1 - 9.4**).

Comparing the spectra of P1, SV7, SV10 and the dialdehydes, the alkyl and alkyloxy signals located in the up field region of the NMR spectra show similar responses and integration in all polymers as expected. The ratio of anthanthrone component in the co-polymers can therefore be estimated from the aromatic signal region of the NMR spectra where only anthanthrone and anthracene signals excluding the phenyl signals are observed (**Figure 9.31 – 9.33**).

418

I = signal contribution from anthanthrone and anthracene

J = signal contribution from only anthanthrone
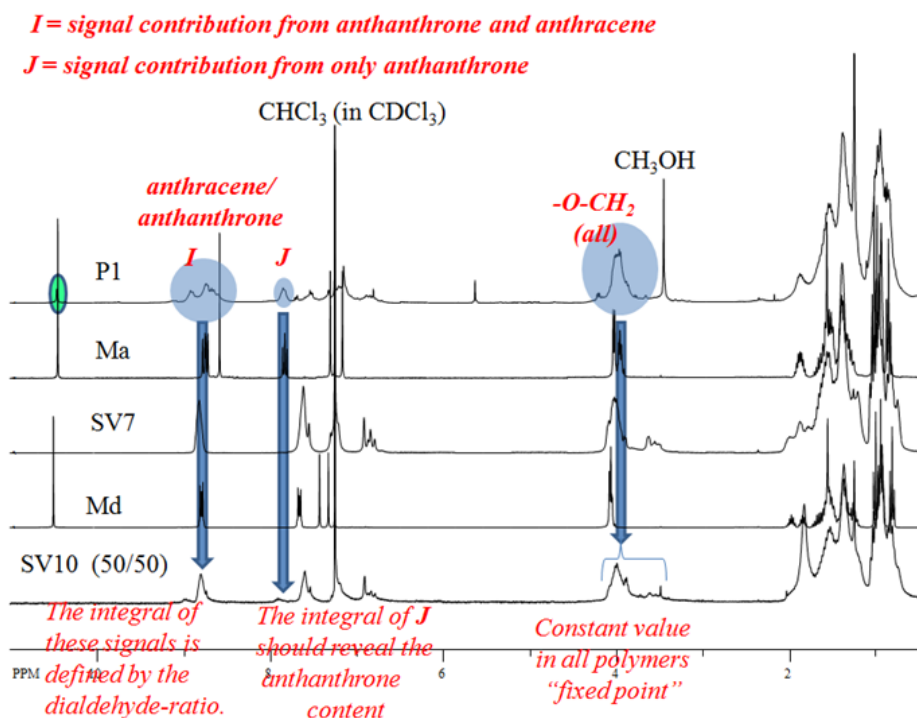
Figure 9.31: Full range ^{1}H NMR comparing P1, SV7, SV10 with their corresponding dialdehydes.
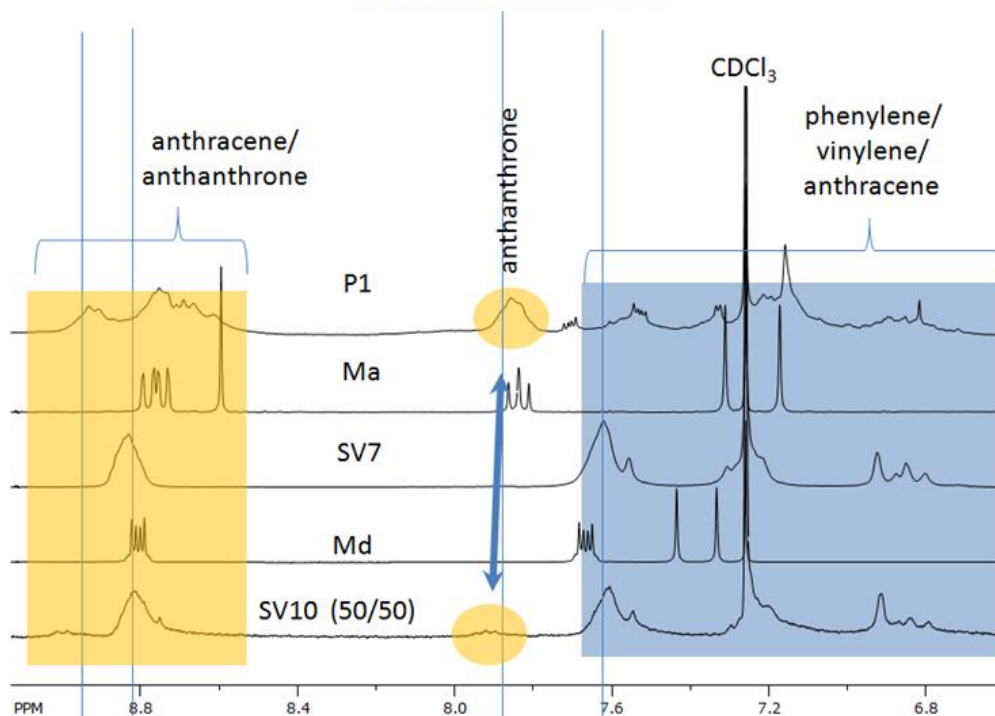
Figure 9.32: Aromatic region or down-field ^{1}H NMR comparing P1, SV7, SV10 with their corresponding dialdehydes.

419
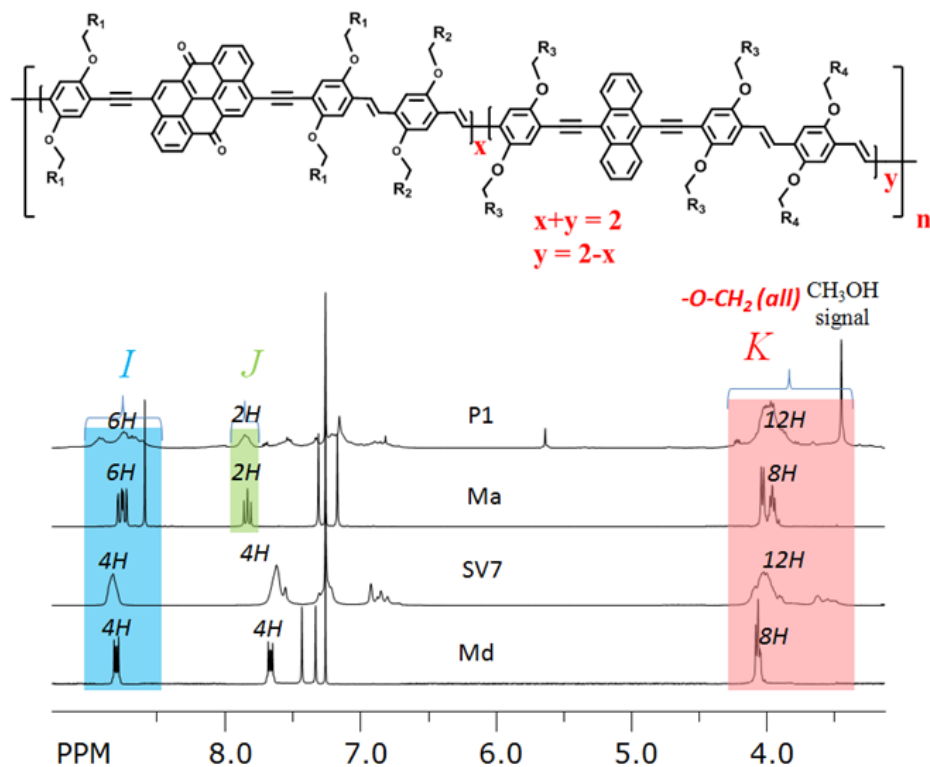
Figure 9.33: Aromatic region or down-field ^{1}H NMR comparing P1, SV7, SV10 with their corresponding dialdehydes and revealing the *I* and *J* regions of interest.
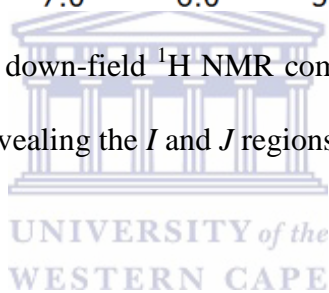
Considering **Figure 9.33**,

$$x + y = 2$$

$$y = 2 - x \qquad\qquad \textbf{equation 9.1}$$

$$I = y + 4H_{\text{anthracene}} + x * 6H_{\text{anthanthrone}}$$

$$x * 6H_{\text{anthanthrone}} = I - \left(y + 4H_{\text{anthracene}}\right)$$

$$x = \frac{I - \left(y + 4H_{\text{anthracene}}\right)}{6H_{\text{anthanthrone}}}$$

$$x = \frac{I - \left(y + 4H\right)}{6H} \qquad\qquad \textbf{equation 9.2}$$

$$J = x * 2H_{\text{anthanthrone}}$$

420

$$x = \frac{J}{2H_{\text{anthanthrone}}}$$

$$x = \frac{J}{2H} \qquad \qquad \textbf{equation 9.3}$$

Inserting **equation 9.3** into **equation 9.2**, we have

$$\frac{J}{2H} = \frac{I - (y + 4H)}{6H}$$

Cross-multiplying, we have

$$\frac{6H * J}{2H} = I - (y + 4H)$$

$$3J = I - (y + 4)$$

Rearranging, we have

$$y + 4 = I - 3J$$

Therefore

$$y = \frac{(I - 3J)}{4} \qquad \qquad \textbf{equation 9.4}$$

Inserting the integrated values of *I* and *J* in the NMR spectra into **equation 9.4**, the ratio of x:y in the copolymers were estimated. x:y were estimated to be approximately 0.5:1.5 for polymer SV9; 1:1 for polymer SV10 and 1.5:0.5 for polymer SV11 (**Figure 9.34, 9.35 and 9.36** respectively). These values match the anthanthrone/anthracene ratios represented by these polymers; thereby ruling out the assumption of inaccurate ratio due to insolubility of anthanthrone.

421
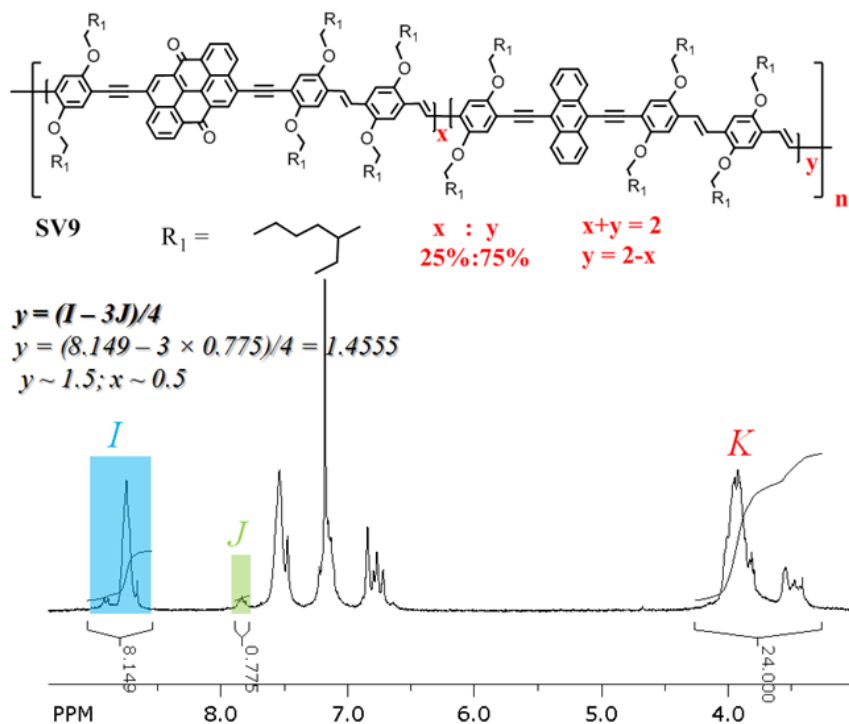
Figure 9.34: Aromatic region or down-field ^{1}H NMR of SV9 revealing the integration of the *I* and *J* regions of interest.
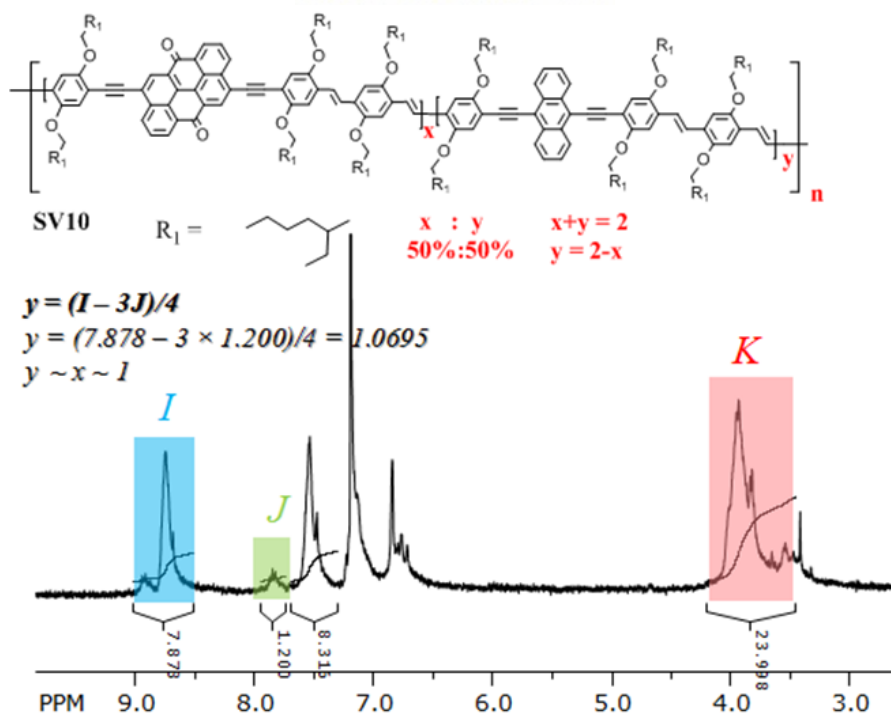
Figure 9.35: Aromatic region or down-field ^{1}H NMR of SV10 revealing the integration of the *I* and *J* regions of interest.

422
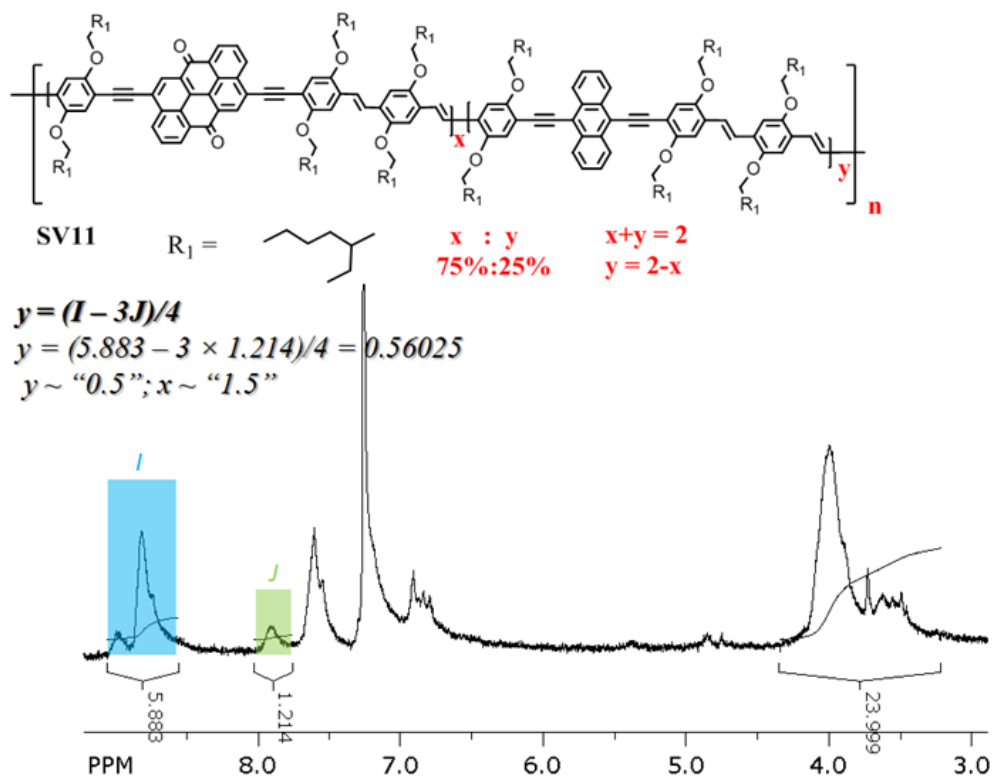
Figure 9.36: Aromatic region or down-field ^{1}H NMR of SV11 revealing the integration of the *I* and *J* regions of interest.
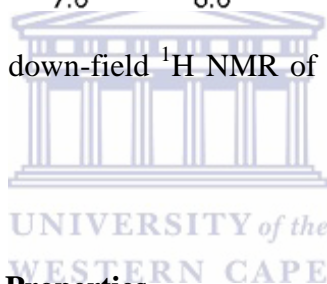
9.2.2.4 Electroluminescent (EL) Properties

A preliminary investigation of two of the co-polymers (SV12 and SV15) and their corresponding homo-polymers (P2 and SV7) for their electroluminescence behavior was conducted on an ITO/PEI/polymer/MoOx/Ag device configuration. The polymers served as emissive layers in the device. The EL spectra as depicted in **Figure 9.37** show similarities with those of the photoluminescence of the corresponding polymer films. This similarity can be attributed to emission from identical singlet excited states S_1 in both cases. However, the photoluminescence spectrum of P2 is blue-shifted compared to the electroluminescence spectra. From the EL spectra, we see the devices light up at very low voltages hinting a nicely low turn-on-voltage for the devices. The emissions are stable with EL spectra exhibiting the

423

same shape over a broad voltage range; and the intensity of the emission is varied by the applied voltage. They therefore form good light emitting diodes. Orange color emission was observed for the co-polymers as shown in the image. Comparing the electroluminescence of co-polymers SV12 and SV15 with their corresponding homo-polymer P1 and SV7, all the polymers emit in the same wavelength region but with different shape (**Figure 9.38**).

424
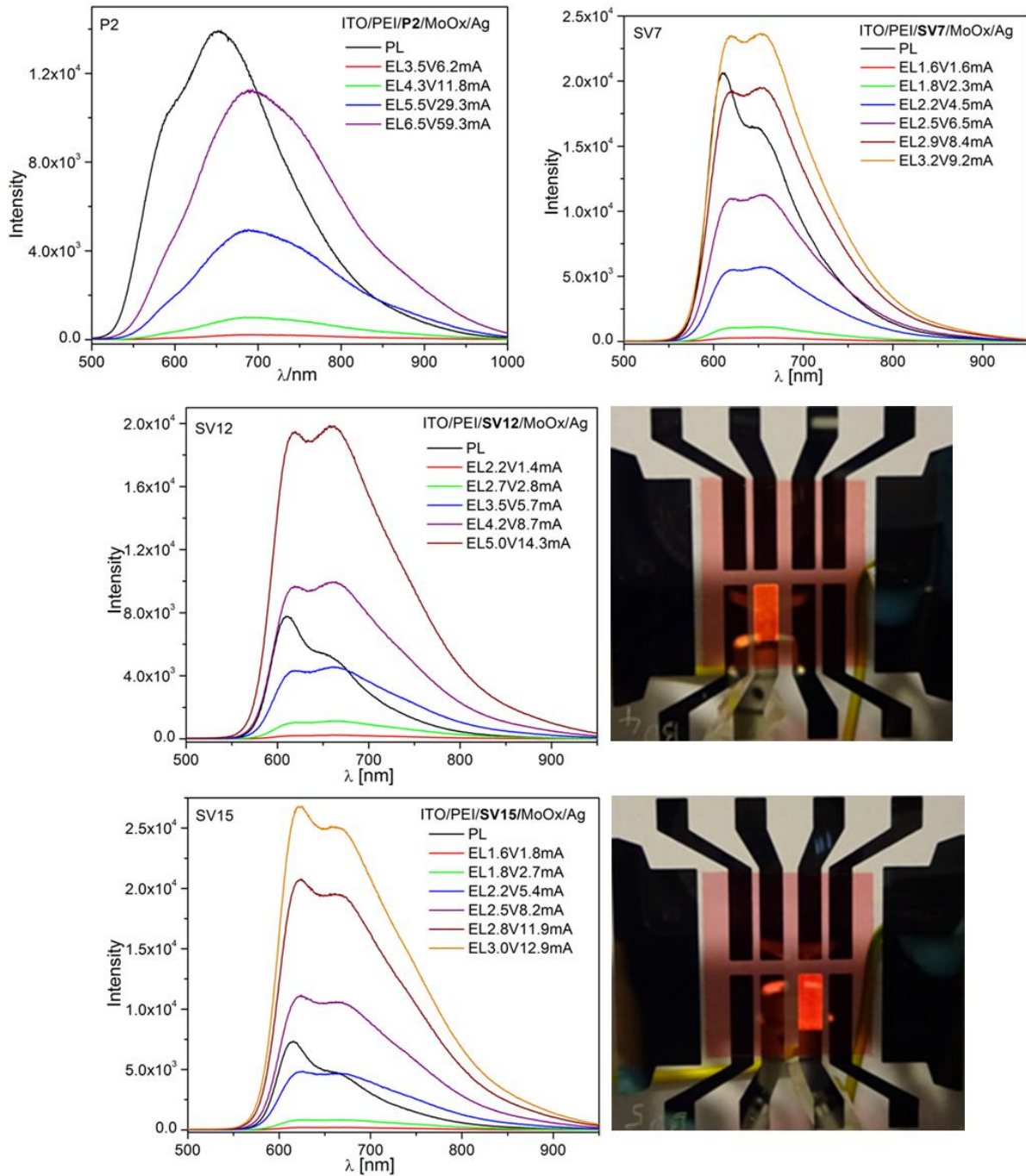
Figure 9.37: Electroluminescence of P2, SV7, SV12 and SV15 measured on ITO/PEI/polymer/MoOx/Ag revealing voltage dependence intensity.

425
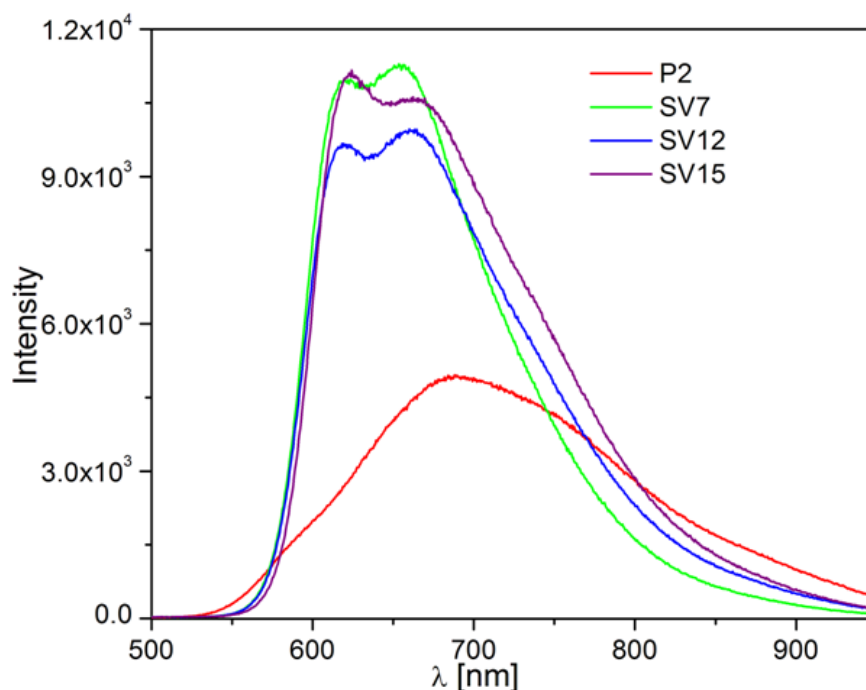
Figure 9.38: Electroluminescence of P2, SV7, SV12 and SV15 measured on ITO/PEI/polymer/MoOx/Ag revealing the wavelength emission region of the investigated polymers.
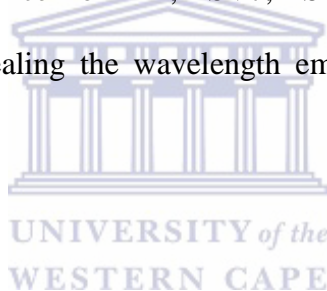
9.3   Conclusion

This report has shown the successful synthesis and investigation of novel anthanthrone/anthracene and anthanthrene/anthracene co-polymers as p-type semiconductors in organic electronics. Improvement in the solubility and process-ability of anthanthrone and its derivative based polymers was achieved through the co-polymerization of anthracene component and anthanthrone or its derivative to give co-polymers SV9 – SV16. The photo-physical behavior of the co-polymers depends on the grafted side chain and ratio of each component making up the co-polymer. Solar cells fabricated from these polymers were found to show quite different photovoltaic behaviors. The photovoltaic responses of anthanthrene/anthracene co-polymers (SV12 – SV16) on blending with PCBM are promising

426

for photovoltaic applications. Although anthracene improved the solubility and process-ability of anthanthrone polymers, the photovoltaic properties of SV10 and SV11 are not impressive. However, the obtained photovoltaic results are not the maximum for these polymers. An enhancement of the photovoltaic parameters is possible through morphological optimisation and post-production treatments of the polymer-PCBM blends.

427

9.4   References

[1]   T. Erb, S. Raleva, U. Zhokhavets, G. Gobsch, B. Stuhn, M. Spode and O. Ambacher, "Structural and optical properties of both pure poly(3-octylthiophene)(P3OT) and P3OT/fullerene Films," *Thin Solid Films,* 450 (**2004**) 97 - 100.

[2]   C. N. Hoth, P. Schilinsky, S. A. Choulis and C. J. Brabec, "Printing highly efficient organic solar cells," *Nano Lett.,* 8 (**2008**) 2806 - 2813.

[3]   J. A. Hauch, P. Schilinsky, S. A. Choulis, R. Childer, M. Biele and C. J. Brabec, "Flexible organic P3HT:PCBM bulk heterojunction modules with more than 1 year out door lifetime," *Solar Energy Material & Solar Cells,* 92 (**2008**) 727 - 731.

[4]   S. Roquet, A. Cravino, P. Leriche, O. Alévêque, P. Frère and J. Roncali, "Triphenylamine−Thienylenevinylene Hybrid Systems with Internal Charge Transfer as Donor Materials for Heterojunction Solar Cells," *J. Am. Chem. Soc.,* 128 (**2006**) 3459 - 3466.

[5]   J. Chen and Y. Cao, "Development of Novel Conjugated Donor Polymers for High-Efficiency Bulk-Heterojunction Photovoltaic Devices," *Acc. Chem. Res.,* 42 (**2009**) 1709 - 1718.

[6]   W.-Y. Wong, "Metallopolyyne Polymers as New Functional Materials for Photovoltaic and Solar Cell Applications," *Macromol. Chem. Phys.,* 209 (**2007**) 14 - 24

[7]   H.-Y. Chen, J. Hou, S. Zhang, Y. Liang, G. Yang, Y. Yang, L. Yu, Y. Wu and G. Li, "Polymer solar cells with enhanced open-circuit voltage and efficiency," *Nat. Photonics,* 3 (**2009**) 649 - 653.

[8]   N. B. Kolhe, S. Shinde, B. Saibal and S. K. Asha, "Novel Approaches in the Design of Donor-Acceptor Oligomeric and Polymeric Materials for Photovoltaic

428

Applications: D/A Blend versus Self-assembly of D/A by Covalent or Non-Covalent Interaction," *Org. Photonics Photovolt.,* 3 (**2015**) 71 - 100.

[9]   J. F. de-Deus, G. C. Faria, E. T. Iamazaki, R. M. Faria, T. D. Z. Atvars and L. Akcelrud, "Polyfluorene based blends for white light emission," *Org. Electron.,* 12 (**2011**) 1493 - 1504.

[10]   A. M. Assaka, B. Hu, J. Mays, E. T. Iamazaki, T. D. Z. Atvars and L. Akcelrud, "The effect of complexation with platinum in polyfluorene derivatives: A photo- and electro-luminescence study," *J. Lumin.,* 131 (**2011**) 710 - 720.

[11]   L. Akcelrud, "Electroluminescent polymers," *Prog. Polym. Sci.,* 28 (**2003**) 875 - 962.

[12]   A. Cirpan, L. Ding and F. E. Karasz, "Efficient Light Emitting Diodes from Polyfluorene Copolymer Blends," *Synth. Met.,* 150 (**2005**) 195 - 198.

[13]   J. N. de-Freitas, A. Pivrikas, B. F. Nowacki, L. C. Akcelrud, N. S. Sariciftci and A. F. Nogueira, "Investigation of new PPV-type polymeric materials containing fluorene and thiophene units and their application in organic solar cells," *Synth. Met.,* 160 (**2010**) 1654 - 1661.

[14]   B. Nowacki, I. R. Grova, R. A. Domingues, G. C. Faria, T. D. Z. Atvars and L. Akcelrud, "Photo- and electroluminescence in a series of PPV type terpolymers containing fluorene, thiophene and phenylene units," *J. Photochem. Photobio. A: Chem.,* 237 (**2012**) 71 - 79.

[15]   B. Nowacki, E. Iamazaki, A. Cirpan, F. Karasz, T. D. Z. Atvars and L. Akcelrud, "Highly efficient polymer blends from a polyfluorene derivative and PVK for LEDs," *Polymer,* 50 (**2009**) 6057 - 6064.

[16]   J.-W. Park, P. Kang, H. Park, H.-Y. Oh, J.-H. Yang, Y.-H. Kim and S.-K. Kwon, "Synthesis and properties of blue-light-emitting anthracene derivative with diphenylamino-fluorene," *Dyes Pigment,* 85 (**2010**) 93 - 98.

[17]   J. Sun, J. Chen, J. Zou, S. Ren, H. Zhong, D. Zeng, J. Du, E. Xu and Q. Fang, "π-Conjugated poly(anthracene-alt-fluorene)s with X-shaped repeating units: New blue-light emitting polymers," *Polymer,* 49 (**2008**) 2282 - 2287.

[18]   D. A. M. Egbe, Bader Cornelia, J. Nowotny, W. Gunther and E. Klemm, "Investigation of the Photophysical and Electrochemical Properties of Alkoxy-Substituted Arylene-Ethynylene/Arylene-Vinylene Hybrid Polymers," *Macromolecules,* 36 (**2003**) 5459 - 5469.

[19]   H. Meng, F. Sun, M. B. Goldfinger, F. Gao, D. J. Londono, W. J. Marshal, G. S. Blackman, K. D. Dobbs and D. E. Keys, "2,6-Bis[2-(4-pentylphenyl)vinyl]anthracene:a stable and high charge mobility organic semiconductor with densely packed crystal structure," *J. Am. Chem. Soc.,* 128 (**2006**) 9304 - 9305.

[20]   E. Gondek, I. V. Kityk and A. Danel, "Some anthracene derivatives with N,N-dimethylamine moieties as materials for photovoltaic devices," *Mater. Chem. Phys.,* 112 (**2008**) 301 - 304.

[21]   R. B. Chaâbane, N. Jaballah, M. Benzarti-Ghédira, A. Chaieb, M. Majdoub and H. B. Ouada, "Synthesis and thin films characterization of new anthracene-core molecules for opto-electronic applications," *Physica B,* 404 (**2009**) 1912 - 1916.

[22]   P. Raghunath, M. Ananth Reddy, C. Gouri, K. Bhanuprakash and V. Jayathirtha Rao, "Electronic properties of anthracene derivatives for blue light emitting electroluminescent layers in organic light emitting diodes: a density functional theory study," *Phys. Chem. A,* 110 (**2006**) 1152 - 1159.

[23]   Y. Li, T.-H. Kim, Q. Zhao, E.-K. Kim, S.-H. Han, Y.-H. Kim, J. Jang and S.-K. Kwon, "Synthesis and Characterization of a Novel Polymer Based on Anthracene

Moiety for Organic Thin Film Transistor," *J. Polym. Sci. Part A Polym. Chem.,* 46 (**2008**) 5115 - 5122.

[24]   L. Valentini, D. Bagnis, A. Marrocchi, M. Seri, A. Taticchi and J. M. Kenny, "Novel Anthracene-Core Molecule for the Development of Efficient PCBM-Based Solar Cells," *Chem. Mater.,* 20 (**2008**) 32 - 34.

[25]   J.-B. Giguère and J.-F. Morin, "Synthesis and Optoelectronic Properties of 6,12-Bis(amino)anthanthrene Derivatives," *J. Org. Chem.,* 78 (**2013**) 12769 - 12778.

[26]   J.-B. Giguère, J. Boismenu-Lavoie and J.-F. Morin, "Cruciform Alkynylated Anthanthrene Derivatives: A Structure–Properties Relationship Case Study," *J. Org. Chem.,* 79 (**2014**) 2404 - 2418.

[27]   D. A. M. Egbe, H. Tillmann, E. Birckner and E. Klemm, "Synthesis and Properties of Novel Well-Defined Alternating PPE/PPV Copolymers," *Macromol. Chem. Phys.,* 202 (**2001**) 2712 - 2726.

[28]   D. A. M. Egbe, C. P. Roll, E. Birckner, U.-W. Grummt, R. Stockmann and E. Klemm, "Side Chain Effects in Hybrid PPV/PPE Polymers," *Macromolecules,* 35 (**2002**) 3825 - 3837.

[29]   D. A. M. Egbe, B. Carbonnier, L. Ding, D. Mühlbacher, E. Birckner, T. Pakula, F. E. Karasz and U.-W. Grummt, "Supramolecular Ordering, Thermal Behavior, and Photophysical, Electrochemical, and Electroluminescent Properties of Alkoxy-Substituted Yne-Containing Poly(phenylene-vinylene)s," *Macromolecules,* 37 (**2004**) 7451 - 7463.

[30]   H. Hoppe, D. A. M. Egbe, D. Mühlbacher and N. S. Sariciftci, "Photovoltaic action of conjugated polymer/fullerene bulk heterojunction solar cells using novel PPE-PPV copolymers," *J. Mater. Chem.,* 14 (**2004**) 3462 - 3467.

[31]   D. A. M. Egbe, L. H. Nguyen, H. Hoppe, D. Muhlbacher and N. S. Sariciftci, "Side Chain Influence on Electrochemical and Photovoltaic Properties of Yne-Containing Poly(phenylene vinylene)s," *Macromol. Rapid Commun.,* 26 (**2005**) 1389 - 1394.

[32]   A. Wild, D. A. M. Egbe, E. Birckner, V. Cimrova, R. Baumann, U.-W. Grummt and U. S. Schubert, "Anthracene- and Thiophene-Containing MEH-PPE-PPVs: Synthesis and Study of the Effect of the Aromatic Ring Position on the Photophysical and Electrochemical Properties," *J. Polym. Sci. Part A: Polym. Chem.,* 47 (**2009**) 2243 - 2261.

[33]   D. A. M. Egbe, S. Turk, S. Rathgeber, F. Kuhnlenz, R. Jadhav, A. Wild, E. Birckner, G. Adam, A. Pivrikas, V. Cimrova, G. Knor, N. S. Sariciftci and H. Hoppe, "Anthracene Based Conjugated Polymers: Correlation between π-π-Stacking Ability, Photophysical Properties, Charge Carrier Mobility, and Photovoltaic Performance," *Macromolecules,* 43 (**2010**) 1261 - 1269.

[34]   F. Wang, F. He, Z. Q. Xie, Y. P. Li, M. Hanif, M. Li and Y. Ma, "Poly(p-phenylene vinylene) Derivatives with Different Contents of cis-Olefins and their Effect on the Optical Properties," *Macromol. Chem. Phys.,* 209 (**2008**) 1381 - 1388.

[35]   W. Y. Huang, W. Gao, T. K. Kwei and Y. Okamoto, "Synthesis and Characterization of Poly(alkyl-substituted p-phenylene ethynylene)s," *Macromolecules,* 34 (**2001**) 1570 - 1578.

[36]   J. A. Mikroyannidis, V. P. Barberis, D. Vyprachticky and V. Cimrova´, "Simple Synthesis, Photophysics, and Electroluminescent Properties of Poly[2,7-bis(4-tert-butylstyryl)fluorene-9,9-diyl-alt-alkane-α,ω-diyl]," *J. Polym. Sci. Part A Polym. Chem.,* 45 (**2006**) 809 - 821.

432

[37]   J.-B. Giguère, N. S. Sariciftci and J.-F. Morin, "Polycyclic anthanthrene small molecules: semiconductors for organic field-effect transistors and solar cells applications," *J. Mater. Chem. C,* 3 (**2015**) 601 - 606.

UNIVERSITY *of the*

WESTERN CAPE

CHAPTER TEN

CONCLUSION AND RECOMMENDATION

10   Summary of Findings

This work has shown the synthesis and investigation of a series of anthracene, anthanthrone and anthanthrene homo and co-polymers (SV1 – SV16, P6 and P7) with varying side chains as p-type semiconductors for organic photovoltaic cells and organic light emitting diodes. All investigated polymers show interesting optoelectronic properties with the anthanthrone based polymers (P1, SV9 – SV11) having the most intriguing absorption properties. Two device configurations (regular and inverted) were employed for the investigation of the photovoltaic properties. For the anthracene based homo-polymers (SV1 – SV8, P6 and P7), the photovoltaic parameters reveal a dependence on the grafted alkyloxy side chains. An influence of the grafted alkyloxy side chains in the arylene vinylene end of the homo-polymers SV1 – SV8 on the photovoltaic parameters was observed. As the length of the side chain in this region increased, the short circuit current decreased, resulting in decrease in efficiency. Comparing SV1 – SV8 with P6 – P7, the major influence of the grafted alkyloxy side chain on the photovoltaic parameters as confirmed by the absorption property was observed in the alkyloxy side chains in the neighborhood of the anthracene moiety in the polymer backbone. SV1 – SV8 with bulky 2-ethylhexyl side chains in the neighborhood of the anthracene moiety are observed to be hypsochromically shifted relative to P6 and P7 with linear decyloxy side chain in same region due to the high sensitivity of the anthracene moiety to steric hindrances in its neighborhood [1-4]. The grafted decyloxy side chain in P6 and P7 enhanced their charge carrier mobility and live time product. Remarkably high open circuit

voltage of almost 1 V was obtained for SV1 – SV8 irrespective of the attached side chain and the device configuration (inverted or normal). The devices have good leak currents, however; low fill factors resulting from low series resistances were observed for this group of polymers. P6 and P7 on the other hand exhibit high fill factor relative to SV1 – SV8 irrespective of device configuration type. P7 recorded a striking fill factor of 0.67. Photovoltaic efficiency of up to 2.49% was recorded for photovoltaic devices based on regular configuration while efficiency of up to 2.62% was recorded for the inverted configuration.

Furthermore, polycyclic aromatic compounds (PACs) based on anthanthrone and anthanthrene were incorporated for the first time into the backbone of poly(arylene ethynylene)-*alt*-poly(arylene vinylene)s (PAE-PAV). As a result of the challenge of solubility and complex synthetic route, these materials which are promising for organic electronics have not attracted much research interest. However, an improved solubility by the incorporation of solubilizing alkyloxy side chains in the aromatic ring of these materials and also through co-polymerization has been shown in this work. The preparation of soluble and process-able π-conjugated ethynylene containing polymers from 4,10-dibromoanthanthrone and its derivative with the incorporation of alkyloxy side chains and also through co-polymerization resulting in homo (P1, P2 and P3) and co-polymers (SV9 – SV16) was shown. Solubility of the co-polymers was enhanced through the incorporation of anthracene component and the grafting of linear and branched alkyloxy side groups. The photo-physical behavior of the co-polymers depends on the grafted side group and ratio of each component making up the co-polymer. Devices fabricated from the co-polymers using bulk heterojunction device architecture show quite improved behavior compared to the homo-polymers. For the co-polymer SV9 similar to homo-polymer P1, the short circuit current was

435

improved from 0.58 mA/cm^2 in P1 to 2.69 mA/cm^2 in SV9, and efficiency 0.18% recorded in P1 was improved to 0.8% in SV9. The short circuit current (2.90 mA/cm^2), open circuit voltage (0.76 V) and efficiency (1.17%) reported for homo-polymer P2 was increased to 4.00 mA/cm^2, 0.92 V and 1.7% respectively in co-polymer SV15. In addition to the recorded photovoltaic properties, the polymers can operate as emitters in organic light-emitting diode (OLEDs) and are useful for the design of OLEDs.

Also in this study, two new acceptors (fullerene (3-(benzo[b]thiophene-3yl)-5-fulleropyrrolidinepyridine (BTFP) based) and non-fullerene (cobalt (II) salicylaldimine metallodendrimer (Co-PPI)) based) were synthesized, investigated and compared to traditional [6,6]-phenyl C$_{61}$ butyric acid methyl ester (PCBM) as potential acceptors for organic photovoltaic devices. The engineering of pristine fullerene C$_{60}$ to obtain properties comparable to those of PCBM through modification by a novel nano-structured organic compound 5-(benzo[b]thiophene-3-yl)pyridinealdehyde (BTPA), to form solution process-able and stable 3-(benzo[b]thiophene-3yl)-5-fulleropyrrolidinepyridine (BTFP) was shown. The obtained BTFP is energetically PCBM-like and shows a promise for electronic applications. BTFP may contribute to the development of new technologies and compete with PCBM with an advantage of cost and ease of synthesis. Co-PPI explored for its potential as acceptor for organic solar cells revealed a good exciton generation, dissociation and charge transfer properties in the photoluminescence study upon blending with poly[(9,9-di-*n*-octylfluorenyl-2,7-diyl)-*alt*-(benzo[2,1,3]thiadiazol-4,8-diyl)] (F8BT) as a donor. The blend of Co-PPI and donor F8BT provided ideal characteristics for bulk heterojunction organic photovoltaic cell acceptor materials, e.g. broad light absorption and good miscibility. An interesting property of both investigated acceptors (BTFP and Co-PPI) is their air stability.

Their stability gives room for easy handling, room temperature process-ability and long shelf life.

10.1 Research Breakthrough

Anthanthrone and its derivatives can be said to be important materials for donor polymers for solar energy conversion because of their extended π-conjugation and good optical responses. One will therefore expect a myriad of application of this group of materials in the field of photovoltaic cells. However, the contrary is observed. The keyword search "*anthanthrone based polymers for photovoltaic applications*" returned no journal on any research work based on this subject matter. The keyword "*anthanthrene based polymers for photovoltaic applications*" returned similar result. Due to the challenge of synthesizing large PACs based polymers, the intriguing properties of these materials have not been explored in photovoltaic application. The dearth of literature in this subject matter is an index of the relevance of this work. This research has successfully shown the incorporation of PACs into the backbone of PAE-PAV to give polymers with impressive un-optimized photovoltaic responses. It has unveiled the possibilities of applications of PACs based on anthanthrone and anthanthrene for photovoltaic applications. This study is believed to be capable of introducing anthanthrone and its derivatives based polymers as alluring donor materials in the photovoltaic market. In addition, apart from fullerenes which are effective and promising acceptors for solar photovoltaic energy conversion, this work indicates the possibility of incorporation of dendritic materials as acceptor materials for photovoltaic investigation. In the few applications of dendritic materials for photovoltaics, they have only been analysed as donor materials [5-10]. No report of their investigation as acceptor. This research work has therefore opened a new field of research for photovoltaic donor and acceptor materials.

437

10.2 Conclusion

This thesis describes a number of new, exciting and promising materials for organic photovoltaic cells. It explored and uncovered ways of engineering and enhancing the potentials of donor and acceptor materials for organic photovoltaic applications. Improvement in solubility, photo-physical and photovoltaic parameters was achieved. However, the photovoltaic results obtained in this study are not optimal for these classes of materials. They do not represent the maximum attainable efficiencies of devices with these polymers. Further material and device optimization is required to fully explore them. Optimization of device is possible through morphological optimization and post-production treatments of the polymer-PCBM blends. For instance, the low fill factors recorded for most of the polymers in this work can be addressed by optimization of the donor:acceptor ratio and layer thickness.
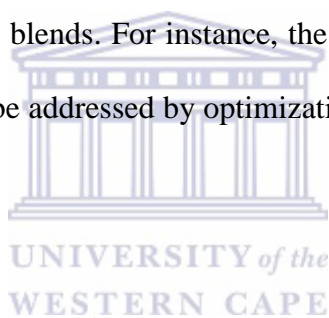
10.3 Future Work and Recommendation

1. Detailed quantitative and qualitative investigations of the photo-physical and photovoltaic properties of the polymer and co-polymers SV1 – SV16, P6 and P7 through X-ray investigation and mobility studies will be worthwhile.

2. Varying the ratio of PCBM to polymer, device engineering such as solvent annealing and thermal annealing which usually have different influence on the photo-physical and photovoltaic properties of the material is recommended.

3. Investigation of other electrodes in place of LiF/Al in the device configuration.

438

4. Furthermore, it is obvious that despite the good optical properties of anthanthrone, its photovoltaic properties are far from being enhanced. Under the same reaction conditions as in the case of SV12 – SV16, SV9 – SV11 were relatively insoluble and with relatively low yield. To achieve optimum photovoltaic properties from anthanthrone, the solubility challenge should be addressed. Ways to further improve the solubility and yield of anthanthrone based homo and co-polymers should be sort after.

5. Also, the solubility of the novel acceptor BTFP synthesized and reported in this study should be improved for better photovoltaic performance.

6. The metallodendrimer Co-PPI should be applied with suitable donor for device fabrication.
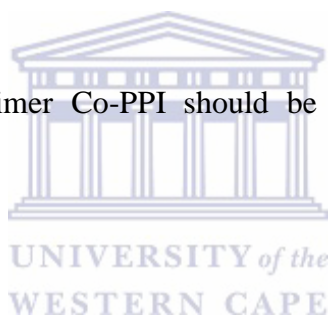
10.4 References

[1]   R. O. Garay, H. Naarmann and K. Mullen, "Synthesis and characterization of poly(1,4-anthrylenevinylene)," *Macromolecules,* 27 (**1994**) 1922 - 1927.

[2]   A. Wild, D. A. M. Egbe, E. Birckner, V. Cimrova, R. Baumann, U.-W. Grummt and U. S. Schubert, "Anthracene- and Thiophene-Containing MEH-PPE-PPVs: Synthesis and Study of the Effect of the Aromatic Ring Position on the Photophysical and Electrochemical Properties," *J. Polym. Sci. Part A: Polym. Chem.,* 47 (**2009**) 2243 - 2261.

[3]   J. A. Mikroyannidis, M. M. Stylianakis, P. Balraju, P. Suresh and G. D. Sharma, "Novel p-Phenylenevinylene Compounds Containing Thiophene or Anthracene Moieties and Cyano−Vinylene Bonds for Photovoltaic Applications," *ACS Appl. Mater. Interfaces,* 1 (**2009**) 1711 - 1718.

[4]   D. A. M. Egbe, S. Turk, S. Rathgeber, F. Kuhnlenz, R. Jadhav, A. Wild, E. Birckner, G. Adam, A. Pivrikas, V. Cimrova, G. Knor, N. S. Sariciftci and H. Hoppe, "Anthracene Based Conjugated Polymers: Correlation between π-π-Stacking Ability, Photophysical Properties, Charge Carrier Mobility, and Photovoltaic Performance," *Macromolecules,* 43 (**2010**) 1261 - 1269.

[5]   M. Lor, J. Thielemans, L. Viaene, M. Cotlet, J. Hofkens, T. Weil, C. Hampel, K. Müllen, J. W. Verhoeven, M. Van-Der-Auweraer and F. C. De-Schryver, "Photoinduced electron transfer in a rigid first generation triphenylamine core dendrimer substituted with a peryleneimide acceptor," *J. Am. Chem. Soc.,* 124 (**2002**) 9918 - 9925.

[6]   M. Braun, S. Atalick, D. M. Guldi, H. Lanig, M. Brettreich, S. Burghardt, M. Hatzimarinaki, E. Ravanelli, M. Prato, R. van-Eldik and A. Hirsch, "Electrostatic

440

Complexation and Photoinduced Electron Transfer between Zn-Cytochrome c and Polyanionic Fullerene Dendrimers," *Chem. Eur. J.,* 9 (**2003**) 3867 – 3875.

[7]   R. de-Bettignies, Y. Nicolas, P. Blanchard, E. Levillain, J. M. Nunzi and J. Roncali, "Planairzed Star-Shaped Oligothiophenes as a New Class of Organic Semiconductors for Heterojunction Solar Cells," *Adv. Mater.,* 15 (**2003**) 1939 – 1943.

[8]   T. Hasobe, Y. Kashiwagi, M. A. Absalom, J. Sly, K. Hosomizu, M. J. Crossley, H. Imahori, P. V. Kamat and S. Fukuzumi, "Supramolecular Photovoltaic Cells Using Porphyrin Dendrimers and Fullerene," *AdV. Mater.,* 16 (**2004**) 975 – 979.

[9]   N. Kopidakis, W. J. Mitchell, J.-v.-d. Lagemaat, D. S. Ginley, G. Rumbles, S. E. Shaheen and W. L. Rance, "Bulk heterojunction organic photovoltaic devices based on phenyl-cored thiophene dendrimers," *Appl. Phys. Lett.,* 89 (**2006**) 103524.

[10]   X. Sun, Y. Zhou, W. Wu, Y. Liu, W. Tian, G. Yu, W. Qiu, S. Chen and D. Zhu, "X-Shaped Oligothiophenes as a New Class of Electron Donors for Bulk-Heterojunction Solar Cells," *J. Phys. Chem. B,* 110 (**2006**) 7702 – 7707.
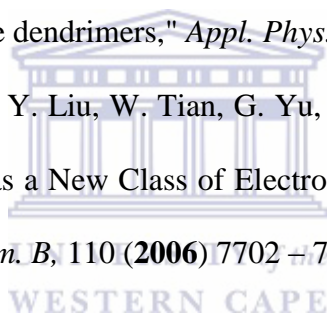
APPENDIX

ACS Publications
Most Trusted. Most Cited. Most Read.

Title: Synthesis and Optoelectronic Properties of 6,12-Bis(amino)anthanthrene Derivatives

Author: Jean-Benoît Giguère, Jean-François Morin

Publication: The Journal of Organic Chemistry

Publisher: American Chemical Society

Date: Dec 1, 2013

Copyright © 2013, American Chemical Society

Logged in as:
Suru Vivian John
Account #:
3001017879

LOGOUT

PERMISSION/LICENSE IS GRANTED FOR YOUR ORDER AT NO CHARGE

This type of permission/license, instead of the standard Terms & Conditions, is sent to you because no fee is being charged for your order. Please note the following:

- Permission is granted for your request in both print and electronic formats, and translations.
- If figures and/or tables were requested, they may be adapted or used in part.
- Please print this page for your records and send a copy of it to your publisher/graduate school.
- Appropriate credit for the requested material should be given as follows: "Reprinted (adapted) with permission from (COMPLETE REFERENCE CITATION). Copyright (YEAR) American Chemical Society." Insert appropriate information in place of the capitalized words.
- One-time permission is granted only for the use specified in your request. No additional uses are granted (such as derivative works or other editions). For any other uses, please submit a new request.

If credit is given to another source for the material you requested, permission must be obtained from that source.

Copyright Permission for **Figure 2.2**

License Number	3880180931222
License date	
Licensed Content Publisher	Royal Society of Chemistry
Licensed Content Publication	Polymer Chemistry
Licensed Content Title	Anthanthrene as a large PAH building block for the synthesis of conjugated polymers
Licensed Content Author	Antoine Lafleur-Lambert,Jean-Benoît Giguère,Jean-Francois Morin
Licensed Content Date	May 22, 2015
Licensed Content Volume	6
Licensed Content Issue	27
Type of Use	Thesis/Dissertation
Requestor type	academic/educational
Portion	figures/tables/images
Number of figures/tables/images	1
Format	print and electronic
Distribution quantity	50000
Will you be translating?	yes
Number of languages	5
Order reference number	
Languages	English
Title of the thesis/dissertation	Donor Polymers for Photovoltaic Applications
Expected completion date	Sep 2016
Estimated size	400

Copyright Permission for **Figure 2.5**

443

Copyright Clearance Center

RightsLink®

Home | Account Info | Help

ACS Publications
Most Trusted. Most Cited. Most Read.

Title: Investigation of the Photophysical and Electrochemical Properties of Alkoxy-Substituted Arylene–Ethynylene/Arylene–Vinylene Hybrid Polymers

Author: Daniel Ayuk Mbi Egbe, Bader Cornelia, Jürgen Nowotny, et al

Publication: Macromolecules

Publisher: American Chemical Society

Date: Jul 1, 2003

Copyright © 2003, American Chemical Society

Logged in as:
Suru Vivian John
Account #:
3001017879

LOGOUT

Copyright Permission for **Figure 2.7**

This Agreement between Suru Vivian John ("You") and John Wiley and Sons ("John Wiley and Sons") consists of your license details and the terms and conditions provided by John Wiley and Sons and Copyright Clearance Center.

License Number	3880190891775
License date	
Licensed Content Publisher	John Wiley and Sons
Licensed Content Publication	Journal of Polymer Science Part A: Polymer Chemistry
Licensed Content Title	Anthracene- and thiophene-containing MEH-PPE-PPVs: Synthesis and study of the effect of the aromatic ring position on the photophysical and electrochemical properties
Licensed Content Author	Andreas Wild,Daniel A. M. Egbe,Eckhard Birckner,Vera Cimrová,Reinhard Baumann,Ulrich-Walter Grummt,Ulrich S. Schubert
Licensed Content Date	Mar 25, 2009
Licensed Content Pages	19
Type of use	Dissertation/Thesis
Requestor type	University/Academic
Format	Print and electronic
Portion	Figure/table
Number of figures/tables	2
Original Wiley figure/table number(s)	Figure 4b and Figure 5b
Will you be translating?	Yes, including English rights
Number of languages	5
Languages	English
Title of your thesis / dissertation	Donor Polymers for Photovoltaic Applications
Expected completion date	Sep 2016
Expected size (number of	400

Copyright Permission for **Figure 2.8**

445

This Agreement between Suru Vivian John ("You") and John Wiley and Sons ("John Wiley and Sons") consists of your license details and the terms and conditions provided by John Wiley and Sons and Copyright Clearance Center.

License Number	3877850715823
License date	
Licensed Content Publisher	John Wiley and Sons
Licensed Content Publication	Journal of Applied Polymer Science
Licensed Content Title	Dynamic quenching of 5-(2'-ethyl-hexyloxy)-p-phenylene vinylene (MEH-PPV) by charge transfer to a C60 derivative in solution
Licensed Content Author	Jian Wang,Deli Wang,Daniel Moses,Alan J. Heeger
Licensed Content Date	Sep 20, 2001
Licensed Content Pages	5
Type of use	Dissertation/Thesis
Requestor type	University/Academic
Format	Print and electronic
Portion	Figure/table
Number of figures/tables	1
Original Wiley figure/table number(s)	Figure 1
Will you be translating?	Yes, including English rights
Number of languages	5
Languages	English
Title of your thesis / dissertation	Donor Polymers for Photovoltaic Applications
Expected completion date	Sep 2016
Expected size (number of pages)	400

Copyright Permission for **Figure 3.2**

446

This Agreement between ("You") and Elsevier ("Elsevier") consists of your order details and the terms and conditions provided by Elsevier and Copyright Clearance Center.

Order Number	501146895
Order date	May 28, 2016
Licensed Content Publisher	Elsevier
Licensed Content Publication	Synthetic Metals
Licensed Content Title	Excited state electron transfer reactions of ProtoporphyrinIX with fullerene
Licensed Content Author	A. Kathiravan
Licensed Content Date	August 2014
Licensed Content Volume	194
Licensed Content Issue	n/a
Start Page	77
End Page	81
Type of Use	reuse in a thesis/dissertation
Intended publisher of new work	other
Portion	figures/tables/illustrations
Number of figures/tables /illustrations	1
Format	both print and electronic
Are you the author of this Elsevier article?	No
Will you be translating?	Yes
Number of languages	5
Languages	English
Order reference number	
Original figure numbers	Figure 5

Copyright Permission for **Figure 3.3**

447

This Agreement between Suru Vivian John ("You") and Springer ("Springer") consists of your license details and the terms and conditions provided by Springer and Copyright Clearance Center.

License Number	3881521454883
License date	
Licensed Content Publisher	Springer
Licensed Content Publication	Springer eBook
Licensed Content Title	Quenching of Fluorescence
Licensed Content Author	
Licensed Content Date	Jan 1, 2006
Type of Use	Thesis/Dissertation
Portion	Figures/tables/illustrations
Number of figures/tables /illustrations	1
Author of this Springer article	No
Order reference number	
Original figure numbers	Figure 8.1
Title of your thesis / dissertation	Donor Polymers for Photovoltaic Applications
Expected completion date	Sep 2016
Estimated size(pages)	400
Requestor Location	Suru Vivian John SensorLab, Dept. of Chemistry University of the Western Cape Bellville Cape Town, Western Cape 7535 South Africa Attn: Suru Vivian John

Copyright Permission for **Figure 3.4**

448

This Agreement between Suru Vivian John ("You") and Elsevier ("Elsevier") consists of your license details and the terms and conditions provided by Elsevier and Copyright Clearance Center.

License Number	3878270850175
License date	
Licensed Content Publisher	Elsevier
Licensed Content Publication	Journal of Luminescence
Licensed Content Title	Supramolecular interactions of meso-tetra-2-chlorophenylporphyrin with fullerenes: A luminescence study
Licensed Content Author	Tandrima Chaudhuri,Sukhendu Nath,Subrata Chattopadhyay,Manas Banerjee,Sandip K. Nayak
Licensed Content Date	March 2010
Licensed Content Volume	130
Licensed Content Issue	3
Start Page	507
End Page	511
Type of Use	reuse in a thesis/dissertation
Intended publisher of new work	other
Portion	figures/tables/illustrations
Number of figures/tables /illustrations	2
Format	both print and electronic
Are you the author of this Elsevier article?	No
Will you be translating?	Yes
Number of languages	5
Languages	English

Copyright Permission for **Figure 3.5** and **3.6**

449

This Agreement between Suru Vivian John ("You") and John Wiley and Sons ("John Wiley and Sons") consists of your license details and the terms and conditions provided by John Wiley and Sons and Copyright Clearance Center.

License Number	3878281229848
License date	
Licensed Content Publisher	John Wiley and Sons
Licensed Content Publication	Advanced Functional Materials
Licensed Content Title	Nanoscale Morphology of Conjugated Polymer/Fullerene-Based Bulk- Heterojunction Solar Cells
Licensed Content Author	H. Hoppe,M. Niggemann,C. Winder,J. Kraut,R. Hiesgen,A. Hinsch,D. Meissner,N. S. Sariciftci
Licensed Content Date	Oct 18, 2004
Licensed Content Pages	7
Type of use	Dissertation/Thesis
Requestor type	University/Academic
Format	Print and electronic
Portion	Figure/table
Number of figures/tables	2
Original Wiley figure/table number(s)	Figure 3 and Figure 8
Will you be translating?	Yes, including English rights
Number of languages	5
Languages	English
Title of your thesis / dissertation	Donor Polymers for Photovoltaic Applications
Expected completion date	Sep 2016
Expected size (number of pages)	400

Copyright Permission for **Figure 3.9** and **3.10**

This Agreement between Suru Vivian John ("You") and Elsevier ("Elsevier") consists of your license details and the terms and conditions provided by Elsevier and Copyright Clearance Center.

License Number	3878290487399
License date	
Licensed Content Publisher	Elsevier
Licensed Content Publication	Dyes and Pigments
Licensed Content Title	D–A–D low band gap molecule containing triphenylamine and benzoxadiazole/benzothiadiazole units: Synthesis and photophysical properties
Licensed Content Author	Shaohang Zeng,Lunxiang Yin,Xueying Jiang,Yanqin Li,Kechang Li
Licensed Content Date	November 2012
Licensed Content Volume	95
Licensed Content Issue	2
Start Page	229
End Page	235
Type of Use	reuse in a thesis/dissertation
Intended publisher of new work	other
Portion	figures/tables/illustrations
Number of figures/tables /illustrations	1
Format	both print and electronic
Are you the author of this Elsevier article?	No
Will you be translating?	Yes
Number of languages	5
Languages	English

Copyright Permission for **Figure 3.11**

451